Control of quantum processes by designed external fields

Stéphane Guérin

Université de Bourgogne

Habilitation à Diriger des Recherches

présentée par

Stéphane GUERIN

Control of quantum processes by designed external fields

Soutenue le **jeudi 11 Mai 2006**,

devant la commission d'examen composée de :

O. Atabek	Directeur de Recherches (Université Paris-Sud, Orsay)	Rapporteur
T. Seideman	Professeur (Northwestern University, Evanston, USA)	Rapporteur
B.W. Shore	Chercheur (Universität Kaiserslautern, Germany)	Rapporteur
K. Bergmann	Professeur (Universität Kaiserslautern, Germany)	Examinateur
H.R. Jauslin	Professeur (Université de Bourgogne)	Examinateur
B. Lavorel	Directeur de Recherches (Université de Bourgogne)	Examinateur
G. Millot	Professeur (Université de Bourgogne)	Examinateur

Laboratoire de Physique de l'Université de Bourgogne
CNRS-UMR 5027
BP 47870 - 21078 Dijon - France

Remerciements

Je remercie tout particulièrement Hans Jauslin pour m'avoir guidé et soutenu patiemment.

Je remercie les étudiants en thèse, Sylvain Thomas, Nicolas Sangouard, Mahdi Amniat-Talab et Xavier Lacour, ainsi qu'Arnaud Rouzée, qui ont contribué efficacement à ce travail.

Je remercie également les membres de l'équipe expérimentale, Olivier Faucher, Edouard Hertz et Bruno Lavorel, qui m'ont beaucoup apporté.

Je remercie mes autres proches collaborateurs, David Daems, Arne Keller, Dominique Sugny, et Leonid Yatsenko, avec qui je prends un grand plaisir à travailler.

Je remercie aussi les rapporteurs Osman Atabek, Tamar Seideman et Bruce Shore pour leur lecture critique de ce travail.

Je remercie enfin Klaas Bergmann et Guy Millot pour avoir accepté d'être membres du jury.

Contents

Introduction

The control of quantum processes and the manipulation of quantum systems are very challenging tasks with important applications in a large variety of domains: in atomic, molecular and condensed matter physics, in optics, in information processing, communication and computation through the development of quantum algorithms, and in chemistry with perspectives of selective control of chemical reactions. External fields can be used to manipulate the internal level structure of the quantum systems in terms of both level position and population transfer. This allows one to control their external degrees of freedom, for instance to trap them, and to couple individual quantum systems to each other.

For this goal, laser sources yielding pulses of high intensity, short duration and controllable frequencies have been developed. Another source of electromagnetic fields that opens new possibilities of control are quantum cavity fields with strong coupling and low losses. A good model for both types of fields, for instance to analyze the exchange of photons with atoms and molecules, is the single mode harmonic oscillator. The bottom of its spectrum is mainly involved for the cavity field, and can be ignored for the laser field because of the very large number of photons available. More recently, a third type of pulsed electric fields (of zero mean frequency), known as half-cycle pulses, have been produced with applications to orientation of molecules.

An essential ingredient for quantum information is to both manipulate the internal states of a single atom (for instance with a laser field), and at the same time to couple a few atoms (for instance by the use of a cavity field). It is thus essential to formulate in a unified way a theory incorporating the laser and cavity couplings, in order to describe e.g. the exchange of photons between laser fields and cavities.

In this manuscript, we focus on one hand on processes induced by adiabatic passage, since they have very desirable properties of robustness with respect to an imperfect knowledge of the parameters of the interacting field and the quantum system itself. On the other hand, we analyze processes by ultra-short pulses inducing sudden effects. They are particularly interesting for the generation of postpulse wave-packets involving many bare states to control external degrees of freedom, such as the rotation of molecules.

We first formulate in a technical and self-consistent way the theoretical tools of analysis with a global approach: the adiabatic Floquet theory, the construction of effective Hamiltonians adapted for adiabatic passage with laser and cavity fields, and propagators appropriate for sudden dynamics. Such tools allow us to first analyze elementary control processes in simplified models. The construction of effective Hamiltonians is developed in a systematic way and allows us to construct more involved models for moderate field intensities (i.e. up to $10^{13} - 10^{14}$ W/cm^2).

We are next in position to apply these tools in three domains of control: The selective population transfer in atoms and molecules, the manipulation of their external degrees of freedom, and quantum information processing by adiabatic passage.

Some of our proposals have been implemented experimentally, such as the complete population transfer by bichromatic fields [154, 155], and the dynamical alternation of alignment [126].

This manuscript is organized into four main parts.

In the first and second parts, we develop the tools of analysis, which are the adiabatic Floquet theory, and the construction of effective Hamiltonians, with examples for atoms and molecules. The adiabatic Floquet theory has the key advantage that it can describe the exchange of photons between the laser and atoms and molecules. The analysis gets simplified, and can be conducted with the use of geometric and topological pictures that allow us to solve

the Schrödinger equation in a global way, i.e. for a whole set of parameters.

The second part deals in particular with the construction of effective Hamiltonians useful for adiabatic processes and of propagators for sudden dynamics with ultrashort pulses.

Parts three and four are devoted to applications of these tools for the control of processes in atoms and molecules by external fields.

In part three, we analyze the control by laser fields of selective population transfer, as well as its relation with the control of external degrees of atoms and molecules. The analysis consists first in identifying an internal target state that has the required property, for instance of deflection, of vibrational localization (e.g. through tunneling), of rotational localization (alignment), ... Then one constructs processes that populate the selected target state.

Part four deals with quantum information by adiabatic passage, where we use both laser and cavity fields. We propose different processes to achieve entanglement, photon Fock states, and quantum logic gates.

Part I

Adiabatic Floquet theory

The aim of parts I and II is to present in a self-contained way a set of theoretical tools that allow one to analyze the quantum dynamics of atoms or molecules driven by laser pulses, and to determine pulse designs that lead to specific effects. We have reviewed most of these tools in [1]. In particular we discuss processes to control the internal excitation of states, like electronic states or vibrational and rotational states of molecules. The idea is to design the characteristics of the laser pulse in such a way that if initially the molecule is in a given state, at the end of the pulse the population will be completely transferred to a selected target state, which can be an eigenstate or a superposition of them. The parameters of a single pulse that can be designed are the peak intensity, the shape of the pulse envelope, the carrier frequency and the chirp, which is a slow variation of the carrier frequency during the pulse. Furthermore one can use sequences of two or several pulses of different characteristics, acting simultaneously or with a well-defined delay. An important condition for the successful implementation of a control process is that it should be robust with respect to variations or imprecisions in the values of the parameters. For instance, the usual resonant $\pi-$pulse technique is not robust for a complete transfer, since it is achieved only for precise values of the total pulse area that interacts with the molecule, which is very difficult to fix in an experimental setup. A different approach that yields much more robust results is based on adiabatic passage. The analysis that we present here yields an explanation of the principles on which this robustness is based.

The models for the control processes start with the Schrödinger equation for the molecule in interaction with a laser field that is either treated as a classical or as a quantized electromagnetic field. In Chapter 1 we describe the Floquet formalism, and show how it can be used to establish the relation between the semi-classical model and a quantized representation that allows one to describe explicitly the exchange of photons. The molecule in interaction with the photon field is described by a time independent Floquet Hamiltonian, which is essentially equivalent to the time dependent semi-classical Hamiltonian. The analysis of the effect of the coupling with the field can thus be done by methods of stationary perturbation theory, instead of the time-dependent one used in the semi-classical description, as shown in part II. In Chapter 2 we describe the main ideas of adiabatic dynamics and combine it with the Floquet approach. The essential idea is that if some parameters like the pulse envelope or the frequency vary sufficiently slowly compared with the other characteristic times of the system, the time evolution will follow instantaneous eigenstates of the Floquet Hamiltonian. The analysis of adiabatic dynamics is thus reduced to the determination of eigenvalues and eigenvectors of Floquet Hamiltonians, as a function of the parameters of the pulse. In Chapter 3 we describe how the possible transfers of population by adiabatic passage are determined by the topology of the eigenenergy surfaces defined by varying the parameters of the pulses. The topology is in turn determined by resonances and quasi-resonances. This topological aspect is the basis of the robustness of the adiabatic transfer. An important conclusion of this analysis is that in the adiabatic regime the final result of the process is determined almost exclusively by the resonances of the Floquet Hamiltonian. The perturbative corrections lead only to small deformations of the path in Hilbert space that is followed while the pulse is in interaction, but they do not change the target state that is reached at the end.
The different aspects of this approach are illustrated with some simple examples in the corresponding sections.

We analyze the influence of the number of oscillations in a pulse on the adiabatic Floquet theory, considering the limiting case of pulses with only a few carrier oscillations. We show that the appearance of multiphoton resonances due to the broadening of the spectrum constitutes the main limitation of the adiabatic regime.

Chapter 1

Floquet theory

The Floquet theory can be seen from two different points of view. In the fist one, the Floquet formalism is just a mathematically convenient tool that allows one to transform the Schrödinger equation with a time-dependent Hamiltonian into an equivalent equation with a time-independent Hamiltonian. This new equation is defined on an enlarged Hilbert space. The time dependence has been substituted by the introduction of one auxiliary dynamical variable for each laser frequency.

The second point of view consists in constructing the Floquet representation starting from a model in which both the molecule and the field are quantized.

The initial photon state can be a number state (with a not well defined phase) or a linear combination of number states, for instance a coherent state. We formulate the construction of coherent states in the Floquet theory and show that choosing one as the initial photon state allows one to recover the usual semi-classical time dependent Schrödinger equation, with a classical field of a well defined phase (see Section 1.3).

This Floquet approach provides a physical interpretation of the dynamics in terms of photons in interaction with the molecule, which is in close analogy to the theory of dressed states in a cavity (see Section 1.4).

The formalism is developed for the case of an interacting field of a single frequency. It can be easily extended to the multifrequency case as shown in Section 1.5.

Another approach to determine the spectrum of the quasienergy operator, which uses directly the evolution operator in the original space, is shown in Section 1.6.

We finally discuss some extensions of the Floquet theory to nonperiodic perturbation in Section 1.7.

1.1 Floquet formalism from the semi-classical point of view

In the semi-classical model the molecule is treated quantum mechanically whereas the field is represented classically. We consider the simplest case of a dipole coupling. The formalism is easily extended to other types of couplings. The time dependence of the periodic Hamiltonian is introduced through the time evolution of the initial phase $\theta + \omega t$ of the field of amplitude $\mathcal{E}$ and frequency ω [2, 3, 4, 5, 6, 7]. The semiclassical Hamiltonian can be e.g. written as

$$H = H\left(x, \theta + \omega t\right) = H_0(x) - \mu(x)\mathcal{E}\cos(\theta + \omega t), \tag{1.1}$$

where x symbolizes the degrees of freedom of the atom or molecule, $\mu(x)$ is its dipole moment and $H_0(x)$ the Hamiltonian of the free molecule. The semi-classical Schrödinger equation

$$i\hbar\frac{\partial}{\partial t}\phi = H\left(x, \theta + \omega t\right)\phi, \qquad \phi \in \mathcal{H} \tag{1.2}$$

is defined on a Hilbert space $\mathcal{H}$, which can be of infinite dimension (e.g. the space of square-integrable functions $\mathcal{H} = L_2(\mathbb{R}^n,\ d^n x)$, where n is the number of the degrees of freedom of the molecule) or of finite dimension (e.g. in N-level models $\mathcal{H} = \mathbb{C}^N$). The initial phase θ appears as a parameter. One can think of Eq. (1.2) as a family of equations parameterized by the angle θ. We denote the corresponding family of propagators by $U(t, t_0; \theta)$, which describe the time evolution of arbitrary initial conditions $\phi(t_0)$:

$$\phi(t) = U(t, t_0; \theta)\phi(t_0), \tag{1.3}$$

and satisfy

$$i\hbar\frac{\partial}{\partial t}U\left(t, t_0; \theta\right) = H\left(\theta + \omega t\right)U\left(t, t_0; \theta\right), \quad U\left(t, t; \theta\right) = \mathbb{1}_{\mathcal{H}}. \tag{1.4}$$

The Floquet Hamiltonian K, also called quasienergy operator, is constructed as follows: We define an enlarged Hilbert space

$$\mathcal{K} := \mathcal{H} \otimes \mathcal{L}, \tag{1.5}$$

where $\mathcal{L} := L_2(\mathbb{S}^1, d\theta/2\pi)$ denotes the space of square integrable functions on the circle $\mathbb{S}^1$ of length 2π, with a scalar product

$$\langle \xi_1 \mid \xi_2 \rangle_{\mathcal{L}} := \int_{\mathbb{S}^1} \frac{d\theta}{2\pi}\, \xi_1^*(\theta)\xi_2(\theta). \tag{1.6}$$

This space is generated by the orthonormal basis $\{e^{ik\theta}\}$, $\quad k \in \mathbb{Z}$ (i.e. all integers). On the enlarged Hilbert space $\mathcal{K}$ the Floquet Hamiltonian is defined as

$$K = -i\hbar\omega\frac{\partial}{\partial\theta} + H\left(\theta\right). \tag{1.7}$$

In this expression $H\left(\theta\right)$ is just the semiclassical Hamiltonian (1.1) but with the phase $\theta + \omega t$ taken at the (fixed) initial value θ corresponding to $t = 0$. The usefulness of the Floquet Hamiltonian comes from the fact that it is time independent and that the dynamics it defines on $\mathcal{K}$ is essentially equivalent with the one of (1.2). This can be formulated as follows. The Floquet Hamiltonian K defines a time evolution in $\mathcal{K}$ through the equation

$$i\hbar\frac{\partial}{\partial t}\psi = K\psi, \qquad \psi \in \mathcal{K} = \mathcal{H} \otimes \mathcal{L}. \tag{1.8}$$

This time evolution can be expressed in terms of a propagator $U_K(t, t_0)$ characterized by

$$i\hbar\frac{\partial}{\partial t}U_K(t, t_0) = KU_K(t, t_0), \qquad U_K(t, t) = \mathbb{1}_{\mathcal{K}}, \tag{1.9}$$

where $\mathbb{1}_{\mathcal{K}}$ is the identity operator in $\mathcal{K}$, i.e. $\psi(t) = U_K(t, t_0)\psi(t_0)$. Since K is time independent, the propagator can be written as

$$U_K(t, t_0, \theta) = U_K(t - t_0, \theta) = e^{-iK(t-t_0)/\hbar}. \tag{1.10}$$

In order to establish a relation between U and U_K we define the following phase translation operator $\mathcal{T}_{\omega t}$ which acts on $\xi \in \mathcal{L}$, by

$$\mathcal{T}_{\omega t}\, \xi\, (\theta) = \xi\, (\theta + \omega t) \tag{1.11}$$

and can be expressed as

$$\mathcal{T}_{\omega t} = e^{\omega t \partial/\partial\theta}. \tag{1.12}$$

We first lift the family of operators $U(t, t_0; \theta)$ (defined on $\mathcal{H}$) into an operator acting on the enlarged space $\mathcal{K}$ by treating the dependence on θ as a multiplication operator. This operator is unitary in $\mathcal{K}$. The relation between U and U_K can then be expressed by

$$\mathcal{T}_{-\omega t}\, U\, (t, t_0; \theta)\; \mathcal{T}_{\omega t_0} = U_K(t - t_0, \theta) \equiv e^{-iK(t-t_0)/\hbar} \tag{1.13}$$

The proof of this relation is given in Appendix A in a more general setting. It implies that if $\psi(t, x, \theta)$ is a solution of (1.8) then we can obtain a solution of (1.2) by $\phi(t, x) = \mathcal{T}_{\omega t}\psi(t, x, \theta) = \psi(t, x, \theta + \omega t)$.

The fact that K is time independent opens the possibility to work with eigenfunction expansions. We consider the case in which K has pure point spectrum, i.e. no continuum. This is always the case for N-level models with periodic time dependent fields. Further remarks on other cases are given in Appendix B.

First we lift the initial condition $\phi(t_0)$ for (1.2) to the enlarged space $\mathcal{K}$ by taking $\phi(t_0) \otimes 1_{\mathcal{L}}$. This form reflects the fact that the initial condition is the same for the whole family of equations (1.2), i.e. it does not depend on the phase θ. With the eigenvalues and eigenvectors of

$$K\psi_\nu = \lambda_\nu \psi_\nu, \tag{1.14}$$

using the inverse of (1.13), the time evolution can be expressed by the eigenfunction expansion

$$\begin{aligned} \phi(t) &= U(t, t_0\ ;\ \theta)\phi(t_0) \\ &= \mathcal{T}_{\omega t} e^{-iK(t-t_0)/\hbar} \mathcal{T}_{-\omega t_0} \phi(t_0) \otimes 1_{\mathcal{L}} \\ &= \sum_\nu c_\nu e^{-i\lambda_\nu (t-t_0)/\hbar} \psi_\nu(x, \theta + \omega t), \end{aligned} \tag{1.15}$$

where the coefficients c_ν are determined by the scalar product

$$c_\nu = \langle \psi_\nu, \phi(t_0) \otimes 1 \rangle_{\mathcal{K}} = \langle \bar{\psi_\nu}, \phi(t_0) \otimes 1 \rangle_{\mathcal{H}}, \tag{1.16}$$

where the subindices $\mathcal{K}$ and $\mathcal{H}$ specify to which space the scalar product corresponds, and $\bar{\psi_\nu} := \int_{\mathbb{S}^1} d\theta/2\pi\ \psi_\nu(\theta)$ is the average of $\psi_\nu(\theta)$ over the phase, or equivalently, its constant Fourier component.
Thus, the determination of the Floquet eigenvectors and eigenvalues allows one to solve the dynamics of the semiclassical model.

The Floquet eigenelements have a periodic structure: $\psi_\nu \equiv \psi_{n,k} = \psi_{n,0} e^{ik\theta}$ and $\lambda_\nu \equiv \lambda_{n,k} = \lambda_{n,0} + k\hbar\omega$, where the index n refers to the molecule's Hilbert space $\mathcal{H}$ (i.e. $n = 1, \cdots, N$ if $\mathcal{H} = \mathbb{C}^N$), and k are all positive or negative integers. This allows one to classify the Floquet eigenstates in families labeled by n. The individual members within one family are distinguished by the index k.

The eigenfunction expansion can be simplified using only one representative of each family (e.g. the one with $k = 0$):

$$\phi(t) = \sum_n \tilde{c}_n(\theta) e^{-i\lambda_{n,0}(t-t_0)/\hbar} \psi_{n,0}(x, \theta + \omega t) \tag{1.17}$$

with

$$\tilde{c}_n(\theta) := \langle \psi_{n,0}(\theta), \phi(t_0) \rangle_{\mathcal{H}} \tag{1.18}$$

The coefficients $\tilde{c}_n(\theta + \omega t)$ are functions of θ, and become thus time dependent.

1.2 Floquet theory from quantized cavity dressed states

Although in the semi-classical model the only dynamical variables are those of the molecule, and that the extended Hilbert space $\mathcal{K} = \mathcal{H} \otimes \mathcal{L}$ and the Floquet Hamiltonian K can be thought as only mathematically convenient techniques to analyse the dynamics, it was clear from the first work of Shirley [2] that the enlarged Hilbert space should be related to photons. This relation was made explicit by Bialynicki-Birula [8, 9] and completed in [10]. The construction starts with a quantized photon field in a cavity of finite volume in interaction with the molecule. The limit of infinite volume with constant photon density leads to the Floquet Hamiltonian, which describes the interaction of the molecule with a quantized laser field propagating in free space. The construction presented below is taken from [10], where further details and mathematical precisions can be found.

We consider a quantized photon field in a cavity of volume V, of single frequency ω and polarized in the $\vec{e}$ direction, described by the Hamiltonian H_{L}, in interaction with a molecule characterized by the Hamiltonian H_{M}. For simplicity we consider the simplest situation of a dipole interaction described by the Hamiltonian [11, 12]

$$H_{\mathrm{ML}} = H_{\mathrm{M}} + H_{\mathrm{L}} + H_{\mathrm{int}} \tag{1.19}$$

with

$$H_{\mathrm{L}} = \hbar\omega a^\dagger a, \tag{1.20a}$$
$$H_{\mathrm{int}} = -\mu \otimes \mathcal{E}_V \left(a + a^\dagger\right), \tag{1.20b}$$

and $\mu = \vec{\mu} \cdot \vec{e}$, where $\vec{\mu}$ is the dipole moment of the molecule. The mode of the laser with frequency ω is described by the number operator of a harmonic oscillator, which can be expressed in terms of the annihilation and creation operators a, $a^\dagger$. They act on the Fock space $\mathcal{F}$ generated by the stationary states $|\, n \,\rangle$, $n = 0, 1, 2, \ldots$ of the harmonic oscillator. The coupling constant is given by

$$\mathcal{E}_V = \sqrt{\frac{\hbar\omega}{2\varepsilon_0 V}}, \tag{1.21}$$

where ε_0 is the permeability of the vacuum. The states of the coupled system evolve in the Hilbert space

$$\mathcal{H}_{\mathrm{ML}} = \mathcal{H} \otimes \mathcal{F}, \tag{1.22}$$

where we call $\mathcal{H}$ the Hilbert space of the molecule and $\mathcal{F}$ the Hilbert space of the photons.

We will establish a precise relation between dressed states in a cavity and the Floquet formalism. We show that the Floquet Hamiltonian K can be obtained exactly from the dressed

Hamiltonian in a cavity in the limit of infinite cavity volume and large number of photons: K represents *the Hamiltonian of the molecule interacting in free space with a field containing a large number of photons*. We establish the physical interpretation of the operator

$$N_{\mathrm{r}} = -i\frac{\partial}{\partial\theta} \tag{1.23}$$

in the limit of large number of photons as the *relative photon number operator*. It characterizes the relative photon number of the field with respect to the average $\bar{n}$. The variation of the average of N_{r} in the Floquet formalism gives the number of photons gained or lost (depending on the sign) by the field.

We remark that, with the cavity dressed state model (1.19), the field intensity does not appear explicitly. It depends on the average number of photons contained in the initial state of the field. The connection between this model and the Floquet formulation is given by the following property: Since the radiation is not confined in a cavity, but propagates and interacts with the molecule in free space, we have to take the limit

$V \to \infty$ *(infinite cavity volume),*

$\bar{n} \to \infty$ *(large photon number average),*

$\rho = \bar{n}/V = \mathrm{const}$ *(constant photon density).*

In this limit, the Hamiltonian H_{ML} *is identical, up to an additive constant, to the Floquet Hamiltonian* K

$$H_{\mathrm{ML}} - \hbar\omega\bar{n} \longrightarrow -i\hbar\omega\frac{\partial}{\partial\theta} + H_0 - \mu\mathcal{E}\cos\theta \equiv K, \tag{1.24}$$

where

$$\mathcal{E} = \sqrt{\frac{2\rho\hbar\omega}{\varepsilon_0}}. \tag{1.25}$$

To show this relation, we use the phase representation of H_{LM}, as formulated by Bialynicki-Birula [8, 9, 13, 14]. We construct an isomorphism between the Fock space and the space $\mathcal{L}_{\bar{n},\theta}$ defined as a subspace of $\mathcal{L} = L_2\left(\mathbb{S}^1, \frac{d\theta}{2\pi}\right)$, generated by the basis functions $\left\{|\, e^{ik\theta}\,\rangle;\ -\bar{n} \le k < +\infty\right\}$:

$$|\, n\,\rangle \in \mathcal{F} \qquad \longleftrightarrow \qquad |\, e^{ik\theta}\,\rangle \in \mathcal{L}_{\bar{n},\theta} \text{ with } \bar{n} + k = n, \quad \text{i.e. } k \in [-\bar{n}, \infty). \tag{1.26}$$

In the limit $\bar{n} \to \infty$ we obtain the whole space

$$\mathcal{L}_{\bar{n},\theta} \overset{\bar{n}\to\infty}{\longrightarrow} \mathcal{L}, \quad \text{and} \quad \mathcal{H}_{\mathrm{LM}} \overset{\bar{n}\to\infty}{\longrightarrow} \mathcal{K} = \mathcal{H} \otimes \mathcal{L}. \tag{1.27}$$

By this isomorphism, the creation, annihilation and photon number operators ($a^\dagger$, a and N) have a corresponding representation acting on $\mathcal{L}_{\bar{n},\theta}$, which we denote respectively $a^\dagger_{\bar{n},\theta}$, $a_{\bar{n},\theta}$ and $N_{\bar{n},\theta}$:

$$a^\dagger\,|\, n\,\rangle = \sqrt{n+1}\,|\, n+1\,\rangle \qquad \longleftrightarrow \qquad a^\dagger_{\bar{n},\theta} = \sqrt{\bar{n} - i\frac{\partial}{\partial\theta}}\; e^{i\theta}\, P_{\bar{n}}, \tag{1.28a}$$

$$a\,|\, n\,\rangle = \sqrt{n}\,|\, n-1\,\rangle \qquad \longleftrightarrow \qquad a_{\bar{n},\theta} = e^{-i\theta}\sqrt{\bar{n} - i\frac{\partial}{\partial\theta}}\, P_{\bar{n}}, \tag{1.28b}$$

$$N\,|\, n\,\rangle = a^\dagger a\,|\, n\,\rangle = n\,|\, n\,\rangle \qquad \longleftrightarrow \qquad N_{\bar{n},\theta} = \left(\bar{n} - i\frac{\partial}{\partial\theta}\right) P_{\bar{n}}, \tag{1.28c}$$

where $P_{\bar{n}} = \sum_{k=-\bar{n}}^{\infty} |\, e^{ik\theta} \,\rangle\langle\, e^{ik\theta} \,|$ is the projector on $\mathcal{L}_{\bar{n},\theta}$. The operator in the coupling term becomes

$$a_{\bar{n},\theta} + a^{\dagger}_{\bar{n},\theta} = P_{\bar{n}} \left(e^{-i\theta} \sqrt{\bar{n} - i\frac{\partial}{\partial\theta}} + \sqrt{\bar{n} - i\frac{\partial}{\partial\theta}}\, e^{i\theta} \right) P_{\bar{n}}, \tag{1.29}$$

and the Hamiltonian reads

$$H^{(\bar{n})}_{\mathrm{LM}} = H_0(x) \otimes P_{\bar{n}} + \mathbb{1}_{\mathcal{H}} \otimes \hbar\omega N_{\bar{n},\theta} - \mu(x) \otimes \mathcal{E}_V \left(a_{\bar{n},\theta} + a^{\dagger}_{\bar{n},\theta} \right). \tag{1.30}$$

We remark that this is an exact correspondence, which is just a precise expression of Dirac's transformation formalism of quantum mechanics [15, 16]. The explicit writing of the projector $P_{\bar{n}}$ in (1.28) is motivated by the fact that in this way the operators $H_0(x) \otimes P_{\bar{n}}$, $N_{\bar{n},\theta}, a_{\bar{n},\theta}$, $a^{\dagger}_{\bar{n},\theta}$ and $H^{(\bar{n})}_{\mathrm{LM}}$ are also well defined in the total space $\mathcal{L} = L_2(\mathbb{S}^1, d\theta/2\pi)$, and the discussion of the limit $\bar{n} \to \infty$ becomes conceptually clearer.

In [8, 9] the formal hypothesis

$$-i\frac{\partial}{\partial\theta} \ll \bar{n} \tag{1.31}$$

is invoked to approximate

$$\sqrt{\bar{n} - i\frac{\partial}{\partial\theta}} = \sqrt{\bar{n}} \sqrt{1 - \frac{i}{\bar{n}}\frac{\partial}{\partial\theta}} = \sqrt{\bar{n}} + \mathcal{O}\left(\frac{1}{\sqrt{\bar{n}}}\right),$$

which leads to

$$(a_{\bar{n},\theta} + a^{\dagger}_{\bar{n},\theta})/\sqrt{\bar{n}} \overset{\bar{n}\to\infty}{\longrightarrow} \left(e^{-i\theta} + e^{i\theta}\right) = 2\cos\theta. \tag{1.32}$$

In the limit $V \to \infty$, $\bar{n} \to \infty$, keeping the photon density $\rho = \bar{n}/V$ constant, we obtain the interaction term

$$\mathcal{E}_V \left(a_{\bar{n},\theta} + a^{\dagger}_{\bar{n},\theta} \right) \longrightarrow \sqrt{\frac{2\rho\hbar\omega}{\varepsilon_0}} \cos\theta. \tag{1.33}$$

Introducing the laser intensity per unit surface I

$$I = \frac{1}{2}\varepsilon_0 c \mathcal{E}^2 = \hbar\omega\Phi_{\mathrm{ph}} \tag{1.34}$$

with the photon velocity c, the field amplitude $\mathcal{E}$ and the photon flow $\Phi_{\mathrm{ph}} = \bar{n}c/V$, allows one to identify the interaction constant of equation (1.33) with $\mathcal{E}$ of Eq. (1.24) as $\mathcal{E} = \sqrt{2\rho\hbar\omega/\varepsilon_0}$. We obtain thus the Floquet Hamiltonian K of equation (1.24).

The formal hypothesis (1.31) must be interpreted in relation with the functions on which $-i\partial/\partial\theta$ acts. The statement is that if all the states $\left\{ |\, e^{ik\theta} \,\rangle \right\}$ that are relevant in the dynamics are such that $|k| \ll \bar{n}$, i.e. if only few photons are exchanged between light and matter compared to the average photon number $\bar{n}$ contained in the laser field, then *the coupled Hamiltonian* $H^{(\bar{n})}_{\mathrm{LM}}$ *can be identified with the Floquet Hamiltonian* K.

One can give a more precise formulation of this construction, based on the dynamics of the coupled system. Since $H^{(\bar{n})}_{\mathrm{LM}}$ and K are both well defined on $\mathcal{H} \otimes \mathcal{L}$, we can compare the time evolutions generated by the two Hamiltonians of any initial state $\psi_0 \in \mathcal{H} \otimes \mathcal{L}$: *For N-level models ($\mathcal{H} = \mathbb{C}^N$), given any initial state $\psi_0 \in \mathcal{H} \otimes \mathcal{L}$, the limit of the cavity dressed state dynamics is identical to the Floquet dynamics*:

$$\lim_{\substack{V,\bar{n}\to\infty \\ V/\bar{n}=\rho}} e^{-i(H^{(\bar{n})}_{\mathrm{LM}}/\hbar - \bar{n}\omega)t} \psi_0 = e^{-iKt/\hbar}\psi_0. \tag{1.35}$$

The proof of this statement is given in [10].

1.3 Connection with the semiclassical formulation: interaction representation and coherent states

From the formulation of the Floquet formalism given above, we can establish the precise connection between the dynamics in the enlarged space $\mathcal{K}$ defined by the Floquet Hamiltonian K, and the one defined by the semiclassical Hamiltonian in $\mathcal{H}$ with a classical description of the electric field:
The Schrödinger equation of the Floquet Hamiltonian in $\mathcal{K}$, where θ is a dynamical variable, is equivalent, in an interaction representation, to the semiclassical Schrödinger equation in $\mathcal{H}$, where θ is considered as a parameter corresponding to the fixed initial phase. The dynamics of the two models are identical if the initial photon state in the Floquet representation is a coherent state.

1.3.1 Interaction representation

The Schrödinger equation of the Floquet Hamiltonian in $\mathcal{K}$

$$i\hbar\frac{\partial}{\partial t}\psi(t) = K\psi(t) \tag{1.36}$$

can be expressed equivalently in an interaction representation defined by the unitary transformation

$$\phi(t) = U_{0\mathrm{r}}^{\dagger}(t)\psi(t), \tag{1.37}$$

where

$$U_{0\mathrm{r}}(t) = e^{-\omega t\partial/\partial\theta} \equiv \mathcal{T}_{-\omega t} \tag{1.38}$$

is the free photon field propagator, which is just the translation operator (1.12) used in the Floquet construction of Section 1.1. Using equation (1.13), we obtain

$$\begin{aligned}\phi(t) &= \mathcal{T}_{\omega t}\psi(t) = \mathcal{T}_{\omega t}\, U_K(t-t_0,\theta)\, \mathcal{T}_{-\omega t_0}\phi(t_0) \\ &= U(t,t_0;\theta)\phi(t_0),\end{aligned}$$

and the evolution equation in this representation becomes

$$i\hbar\frac{\partial}{\partial t}\phi(t) = H(\theta+\omega t)\phi(t), \tag{1.39}$$

where we have still $\phi(t) \in \mathcal{K}$, i.e. $H(\theta+\omega t)$ is still interpreted as an operator acting on the enlarged Hilbert space $\mathcal{K}$, which with respect to the variable θ is a multiplication operator.

Although this equation looks formally like the semiclassical Schrödinger equation (1.2), we emphasize that it is still different since it is defined in the enlarged Hilbert space $\mathcal{K}$ and the phase θ does not have a definite value, since it is a dynamical variable on the same footing as x. In order to recover the semiclassical equation from (1.39) we have to reduce it to an equation defined in the Hilbert space $\mathcal{H}$. From a mathematical point of view, this can be done by fixing a particular value of θ, as we did in Section 1.1. Physically this can be achieved, as we show in the following, by choosing the initial condition of the photon field as a coherent state.

1.3.2 Coherent states

The coherent states of the photon field can be defined as the eigenvectors of the annihilation operator

$$a\,|\,\alpha\,\rangle = \alpha\,|\,\alpha\,\rangle, \qquad \alpha = |\alpha| e^{-i\theta_0}. \tag{1.40}$$

In the usual Fock number state representation they are given, up to a phase factor, by

$$|\,\alpha\,\rangle = e^{-|\alpha|^2/2} \sum_{n=0}^{\infty} \frac{\alpha^n}{\sqrt{n!}}\,|\,n\,\rangle. \tag{1.41}$$

In the phase representation they can be written as

$$\begin{aligned} \Phi_{\theta_0}^{(\bar{n})}(\theta) &= e^{i\zeta} e^{-|\alpha|^2/2} \sum_{n=0}^{\infty} \frac{\alpha^n}{\sqrt{n!}}\, e^{i(n-\bar{n})\theta} \\ &= e^{-|\alpha|^2/2} \sum_{n=0}^{\infty} \frac{|\alpha|^n}{\sqrt{n!}}\, e^{i(n-\bar{n})(\theta-\theta_0)} \end{aligned} \tag{1.42}$$

(where ζ is an arbitrary constant phase that we have chosen as $\zeta = \bar{n}\theta_0$). In order to obtain the representation of coherent states in Floquet theory we have to take $|\alpha| = \sqrt{\bar{n}}$, since the average photon number in a coherent state is given by $|\alpha|^2$, and then apply the limit $\bar{n} \to \infty$. In Appendix B we show that in this limit the coherent states are represented by a generalized function $\Phi_{\theta_0}(\theta)$, which is real, and depends on $\theta - \theta_0$, where $\theta_0 \in \mathbb{S}^1$ is a fixed angle, and

$$\left(\Phi_{\theta_0}(\theta)\right)^2 = 2\pi\delta(\theta - \theta_0). \tag{1.43}$$

1.3.3 Expectation values for general initial states of the photon field

For a general initial condition of the photon field $\xi(\theta) \in \mathcal{L}$, we first remark that the evolution of the initial condition (that we take here at $t = t_0 = 0$) $\phi(x) \otimes \xi(\theta)$ can be obtained from the one of the initial condition $\phi(x) \otimes 1$ (where the constant function $1 \equiv e^{i(k=0)\theta}$ is the relative number state of zero photons):

$$\begin{aligned} U_K(t,\theta)\ (\phi(x) \otimes \xi(\theta)) &= \mathcal{T}_{-\omega t} U(t,0;\theta)\ (\phi(x) \otimes \xi(\theta)) \\ &= \xi(\theta - \omega t)\, U(t,0;\theta - \omega t)\, (\phi(x) \otimes 1) \\ &= \xi(\theta - \omega t)\, U_K(t,\theta)\, (\phi(x) \otimes 1) \end{aligned} \tag{1.44}$$

(since $U(t,0;\theta)$ is a multiplication operator with respect to θ).

As a consequence, for any observable $M(\theta) : \mathcal{K} \to \mathcal{K}$ that with respect to θ is a multiplication operator, using Eq. (1.13), we can write the expectation value as

$$\begin{aligned} \langle M \rangle(t) &:= \langle\, \phi \otimes \xi\,|\, U_K^\dagger(t,\theta)\, M(\theta)\, U_K(t,\theta)\,|\, \phi \otimes \xi\,\rangle_{\mathcal{K}} \\ &= \int_0^{2\pi} \frac{d\theta}{2\pi}\, |\xi(\theta)|^2 \langle\, \phi\,|\, U^\dagger(t,0;\theta) M(\theta + \omega t) U(t,0;\theta)\,|\, \phi\,\rangle_{\mathcal{H}} \\ &= \int_0^{2\pi} \frac{d\theta}{2\pi}\, |\xi(\theta)|^2 \langle\, \phi(t;\theta)\,|\, M(\theta + \omega t)\,|\, \phi(t;\theta)\,\rangle_{\mathcal{H}}, \end{aligned} \tag{1.45}$$

where we denote by $\phi(t;\theta) \equiv U(t,0;\theta)\phi$ the semiclassical evolution with initial phase θ of the initial condition $\phi \in \mathcal{H}$.
In particular, for an observable A of the molecule (i.e. $A \otimes \mathbb{1}_{\mathcal{L}}$) we have

$$\langle A\rangle(t) = \int_0^{2\pi} \frac{d\theta}{2\pi} |\xi(\theta)|^2 \langle\, \phi(t;\theta) \,|\, A \,|\, \phi(t;\theta) \,\rangle_{\mathcal{H}}. \tag{1.46}$$

1.3.4 Expectation values on coherent states; relation with the semiclassical model

We have stated that we can recover the evolution of the semi-classical model from the Floquet evolution in the interaction representation by taking initial states in which the photon field is in a coherent state. This can be formulated more precisely by the following statements:

If we take an initial condition of the form $\psi(t=0) = \phi(x) \otimes \Phi_{\theta_0}(\theta)$, then

i) If $A : \mathcal{H} \to \mathcal{H}$ is an observable of the molecule, then according to Eqs. (1.46) and (1.43)

$$\langle A\rangle(t) = \langle\, \phi(t;\theta_0) \,|\, A \,|\, \phi(t;\theta_0) \,\rangle_{\mathcal{H}}. \tag{1.47}$$

The last expression is the expectation value calculated with the semiclassical model with initial phase θ_0. We conclude thus that, *if one considers only observables of the molecule, the Floquet evolution with a coherent state in the initial condition is equivalent to the semiclassical model.*
We remark that a somewhat related construction, linking the evolution from cavity dressed states directly to the semi-classical model (i.e. without the intermediate level of Floquet states as we do here) was established in [17].

ii) More generally, if $M(\theta) : \mathcal{K} \to \mathcal{K}$ is an observable that with respect to θ is a multiplication operator, continuous in θ, then taking for θ a particular value θ_0 defines a family of operators $M(\theta_0) : \mathcal{H} \to \mathcal{H}$, parametrized by θ_0. Then, according to Eqs. (1.45) and (1.43)

$$\langle M\rangle(t) = \langle\, \phi(t;\theta_0) \,|\, M(\theta_0 + \omega t) \,|\, \phi(t;\theta_0) \,\rangle_{\mathcal{H}}. \tag{1.48}$$

It was remarked in References [2, 8] that in the semiclassical model, if the initial phase θ_0 is not known, one can take a statistical average over the initial phases, with uniform distribution:

$$\overline{A_{\mathrm{sc}}}(t) := \int_0^{2\pi} \frac{d\theta_0}{2\pi} \langle\, \phi(t;\theta_0) \,|\, A \,|\, \phi(t;\theta_0) \,\rangle_{\mathcal{H}}. \tag{1.49}$$

From the discussion above, this coincides with the expectation value $\langle A\rangle(t)$ calculated with the evolution in the Floquet picture of an initial condition of the photon field that is a photon number eigenstate $e^{ik\theta}$ (with arbitrary k), that is $\langle A\rangle(t) = \int_0^{2\pi} \frac{d\theta_0}{2\pi} \langle\, \phi(t;\theta_0) \,|\, A \,|\, \phi(t;\theta_0) \,\rangle_{\mathcal{H}}$ according to Eq. (1.46). We have seen on the other hand that the semiclassical evolution with an initial phase θ_0 corresponds, in the Floquet picture, to a coherent state initial condition for the photon field.
This property is quite remarkable: *In the large photon number regime the coherent quantum average on a number state gives the same result as the incoherent statistical average over coherent states.*

1.4 Emission and absorption of photons in Floquet theory

1.4.1 Exchanges of photons in Floquet theory

In Floquet theory the exchange of photons can be analyzed from the temporal variation of the relative photon number. In experiments, one measures for instance the difference in intensity of the laser pulse before and after the interaction with the molecules. Denoting the initial condition (at $t = t_0 = 0$) by $\phi(x) \otimes \xi(\theta)$, we describe the exchange of photons by

$$\delta\langle N\rangle(t) := \left\langle \phi\otimes\xi \;\middle|\; U_K^\dagger(t)\left(-i\frac{\partial}{\partial\theta}\right)U_K(t) \;\middle|\; \phi\otimes\xi\right\rangle_{\mathcal{K}} - \left\langle \phi\otimes\xi \;\middle|\; -i\frac{\partial}{\partial\theta} \;\middle|\; \phi\otimes\xi\right\rangle_{\mathcal{K}} \tag{1.50}$$

and we show below that

$$\delta\langle N\rangle(t) = \int_0^{2\pi}\frac{d\theta}{2\pi\hbar\omega}\,|\xi(\theta)|^2\Big[\,\langle\,\phi\,|\,H(\theta)\,|\,\phi\,\rangle_{\mathcal{H}} - \langle\,\phi(t;\theta)\,|\,H(\theta+\omega t)\,|\,\phi(t;\theta)\,\rangle_{\mathcal{H}}\,\Big]. \tag{1.51}$$

In particular, if the photon field is initially in a photon number eigenstate $|e^{ik\theta}\,\rangle$,

$$\delta\langle N\rangle(t) = \int_0^{2\pi}\frac{d\theta}{2\pi\hbar\omega}\Big[\,\langle\,\phi\,|\,H(\theta)\,|\,\phi\,\rangle_{\mathcal{H}} - \langle\,\phi(t;\theta)\,|\,H(\theta+\omega t)\,|\,\phi(t;\theta)\,\rangle_{\mathcal{H}}\,\Big]. \tag{1.52}$$

We remark that $\delta\langle N\rangle(t)$ is independent of the particular k we take, in accordance with the interpretation as relative photon number.
If the photon field is initially in a coherent state $\Phi_{\theta_0}(\theta) = (2\pi)^{1/2}\delta_{1/2}(\theta-\theta_0)$, then

$$\delta\langle N\rangle_{\rm cs}(t) = \frac{1}{\hbar\omega}\Big[\,\langle\,\phi\,|\,H(\theta_0)\,|\,\phi\,\rangle_{\mathcal{H}} - \langle\,\phi(t;\theta_0)\,|\,H(\theta_0+\omega t)\,|\,\phi(t;\theta_0)\,\rangle_{\mathcal{H}}\,\Big]. \tag{1.53}$$

Again, if the precise initial phase θ_0 of the coherent state is not known, one can take the (incoherent) statistical average over all phases θ_0:

$$\begin{aligned}\overline{\delta\langle N\rangle_{\rm cs}}(t) &= \int_0^{2\pi}\frac{d\theta_0}{2\pi}\,\delta\langle N\rangle_{\rm cs}(t)\\ &= \int_0^{2\pi}\frac{d\theta_0}{2\pi\hbar\omega}\Big[\,\langle\,\phi\,|\,H(\theta_0)\,|\,\phi\,\rangle_{\mathcal{H}} - \langle\,\phi(t;\theta_0)\,|\,H(\theta_0+\omega t)\,|\,\phi(t;\theta_0)\,\rangle_{\mathcal{H}}\,\Big].\end{aligned} \tag{1.54}$$

This incoherent statistical average over the phases also gives exactly the same result as the coherent average (1.52) in a photon number state.

We can obtain these relations as follows: Using the definition of the quasi-energy operator (1.7), we can express $\delta\langle N\rangle(t)$ in terms of quantities that do not involve the derivative $-i\partial/\partial\theta$:

$$\begin{aligned}\delta\langle N\rangle(t) &= \left\langle \phi\otimes\xi \;\middle|\; U_K^\dagger(t)\,\frac{K}{\hbar\omega}\,U_K(t) \;\middle|\; \phi\otimes\xi\right\rangle_{\mathcal{K}}\\ &\quad -\left\langle \phi\otimes\xi \;\middle|\; U_K^\dagger(t)\,\frac{H(\theta)}{\hbar\omega}\,U_K(t) \;\middle|\; \phi\otimes\xi\right\rangle_{\mathcal{K}} - \left\langle \phi\otimes\xi \;\middle|\; -i\frac{\partial}{\partial\theta} \;\middle|\; \phi\otimes\xi\right\rangle_{\mathcal{K}}.\end{aligned} \tag{1.55}$$

Using the fact that $[K, U_K] = 0$, $U_K^\dagger U_K = \mathbb{1}$ and equation (1.7), we can write

$$\delta\langle N\rangle(t) = \left\langle \phi\otimes\xi \;\middle|\; \frac{H(\theta)}{\hbar\omega} \;\middle|\; \phi\otimes\xi\right\rangle_{\mathcal{K}} - \left\langle \phi\otimes\xi \;\middle|\; U_K^\dagger(t)\,\frac{H(\theta)}{\hbar\omega}\,U_K(t) \;\middle|\; \phi\otimes\xi\right\rangle_{\mathcal{K}}, \tag{1.56}$$

and since

$$\begin{aligned} U_K^\dagger(t,\theta)\, H(\theta)\, U_K(t,\theta) &= U^\dagger(t,0;\theta)\mathcal{T}_{\omega t}\, H(\theta)\, \mathcal{T}_{-\omega t} U(t,0;\theta) \\ &= U^\dagger(t,0;\theta)\, H(\theta+\omega t)\, U(t,0;\theta), \end{aligned} \tag{1.57}$$

we obtain equation (1.51).

We can also get more precise information on the probability $P(L,t)$ that L photons are exchanged: If at time $t=0$ the photon field is in a photon number eigenstate $e^{ik\theta}$ and $\psi(t=0)=\psi_0=\phi\otimes e^{ik\theta}$, then the probability that a measurement performed at time t yields that L photons have been exchanged, is given by

$$\begin{aligned} P(L,t) &= \Big\langle U_K(t)\psi_0 \,\Big|\, \Big[\, \mathbb{1}_{\mathcal{H}} \otimes |\, e^{i(L+k)\theta}\,\rangle\langle\, e^{i(L+k)\theta}\,| \,\Big] \,\Big|\, U_K(t)\psi_0 \Big\rangle_{\mathcal{K}} \\ &= \sum_n \Big| \Big\langle \phi_n \otimes e^{i(k+L)\theta} \,\Big|\, U_K(t)\left(\phi\otimes e^{ik\theta}\right)\Big\rangle_{\mathcal{K}} \Big|^2, \end{aligned} \tag{1.58}$$

where $\{\phi_n\}$ is an arbitrary basis of $\mathcal{H}$.

1.4.2 Invariance with respect to the choice of the origin of the relative photon number

Due to the relative character of the number operator $-i\partial/\partial\theta$, all the physical predictions of the Floquet model must be invariant with respect to a global translation of the relative photon numbers. We show that this is indeed the case for the properties discussed above.
The probability $P(L,t)$ is independent of the particular initial photon number state chosen, i.e. it is independent of k since:

$$U_K(t)\Big(\phi\otimes e^{ik\theta}\Big) = U(t,0;\theta-\omega t)\Big(\phi\otimes e^{ik(\theta-\omega t)}\Big) \tag{1.59}$$

and thus

$$P(L,t) = \sum_n \Big| \Big\langle \phi_n \otimes e^{iL\theta} \,\Big|\, U_K(t)\,(\phi\otimes 1)\Big\rangle_{\mathcal{K}} \Big|^2. \tag{1.60}$$

For the average number of exchanged photons $\delta\langle N\rangle(t)$ it is straightforward to verify that one obtains the same result for the choice of any initial condition of the photon field of the form

$$\xi = \sum_k c_k\, e^{i(k+m)\theta}, \quad \text{with arbitrary translation } m. \tag{1.61}$$

1.4.3 Number of exchanged photons in adiabatic passage with coherent states

In adiabatic passage processes with pulsed lasers, as we will discuss in the forthcoming sections, one often encounters the following particular situation: If the initial condition of the photon field were a number state, i.e.

$$\psi_i = \phi_i(x)\otimes e^{ik\theta}, \tag{1.62}$$

then at the end of the pulse, the final state would be

$$\psi_f = \phi_f(x)\otimes e^{i(k-m)\theta}, \tag{1.63}$$

i.e the photon field would be again in a well-defined number state, and one can state that m photons had been adsorbed, since according to Eq. (1.60) $P(L,t_f) = \delta_{L,-m}$. Since k is the relative number of photons, if these relations are satisfied for one choice of the initial k they are also satisfied for all other choices of $k \in \mathbb{Z}$. However, in the actual experimental realizations involving lasers the initial states of the photon field are coherent states instead of number states, i.e.

$$\psi_i = \phi_i(x) \otimes \Phi. \tag{1.64}$$

The coherent states can be considered as a coherent superposition of number states of the form

$$\Phi = \sum_k c_k e^{ik\theta}, \qquad \text{with} \quad \sum_k |c_k|^2 = 1. \tag{1.65}$$

In the preceding sections we have taken the limit $\bar{n} \to \infty$ in which the coherent states become a $\delta_{1/2}(\theta - \theta_0)$ function. For the discussion of the exchanged photons we consider a large but finite $\bar{n}$, such that the coherent state is represented by a sharply peaked function that can be written as a superposition (1.65). Under this condition, the relations (1.62),(1.63) imply that the initial condition

$$\psi^{(i)} = \phi_i(x) \otimes \xi^{(i)}, \qquad \text{with} \quad \xi^{(i)} = \sum_k c_k e^{ik\theta}, \tag{1.66}$$

evolves at the end of the pulse to

$$\psi^{(f)} = \phi_f(x) \otimes \sum_k c_k e^{i(k-m)\theta} = \phi_f(x) \otimes e^{-im\theta}\xi^{(i)}(\theta). \tag{1.67}$$

Our aim here is to give a precise meaning to the statement that, also in this process involving coherent states, m photons have been absorbed: The probability to observe $\bar{n}+k$ photons at the initial time t_i is

$$P^{(i)}(\bar{n}+k) = |c_k|^2 \tag{1.68}$$

and at the end of the pulse

$$P^{(f)}(\bar{n}+k) = |c_{k+m}|^2 = P^{(i)}(\bar{n}+k+m), \tag{1.69}$$

which implies $P^{(f)}(\bar{n}+k-m) = P^{(i)}(\bar{n}+k)$, i.e. the probability to measure $\bar{n}+k-m$ photons at the end is equal to the probability to measure $\bar{n}+k$ at the beginning of the pulse.
In terms of averages and moments of photon numbers one can make the following statement: Eqs. (1.66)(1.67) imply that the photon expectation number changes by $-m$

$$\delta\langle N\rangle = \langle\psi^{(f)}| \ -i\frac{\partial}{\partial\theta}\ |\psi^{(f)}\rangle - \langle\psi^{(i)}| \ -i\frac{\partial}{\partial\theta}\ |\psi^{(i)}\rangle = -m \tag{1.70}$$

and the second moment of the relative number of photons at the end of the process is equal to the one at the beginning:

$$\langle\psi^{(f)}| \ \left(-i\frac{\partial}{\partial\theta}\right)^2 \ |\psi^{(f)}\rangle = \langle\psi^{(i)}| \ \left(-i\frac{\partial}{\partial\theta}\right)^2 \ |\psi^{(i)}\rangle. \tag{1.71}$$

1.5 Quasiperiodic Floquet representation

The treatment described in the preceding sections can be easily generalized to the case in which two (or several) lasers of frequencies $\omega_j, j = 1 \dots d$ act on the molecule, that leads to the so-called *quasiperiodic* Hamiltonian. We introduce the notation $\underline{\omega} = (\omega_1, \dots, \omega_d)$, and $\underline{\theta} = (\theta_1, \dots, \theta_d)$ which represents the phases at time $t = 0$ of the d lasers. The semiclassical Schrödinger equation reads

$$i\hbar \frac{\partial \phi}{\partial t} = H(x, \underline{\theta} + \underline{\omega} t)\phi \tag{1.72}$$

with, for example in a dipole coupling model with two lasers,

$$H(x, \underline{\theta} + \underline{\omega} t) = H_0(x) - \mu(x)\mathcal{E}_1 \cos(\theta_1 + \omega_1 t) - \mu(x)\mathcal{E}_2 \cos(\theta_2 + \omega_2 t), \tag{1.73}$$

where x symbolizes the degrees of freedom of the molecule, $\mu(x)$ is its dipole moment, $\mathcal{E}_1, \mathcal{E}_2$ the respective amplitudes of the two lasers and $H_0(x)$ the Hamiltonian of the free molecule. The corresponding Floquet Hamiltonian is defined as [18, 19, 20, 21, 6, 7]

$$\begin{aligned} K &= -i\hbar \underline{\omega} \cdot \frac{\partial}{\partial \underline{\theta}} + H(x, \underline{\theta}), & \text{(1.74a)} \\ &= -i\hbar \sum_{j=1}^{d} \omega_j \frac{\partial}{\partial \theta_j} - \mu(x)\mathcal{E}_1 \cos\theta_1 - \mu(x)\mathcal{E}_2 \cos\theta_2, & \text{(1.74b)} \end{aligned}$$

and acts on the enlarged Hilbert space

$$\mathcal{K} = \mathcal{H} \otimes \underbrace{\mathcal{L} \otimes \dots \otimes \mathcal{L}}_{d \text{ products}}, \tag{1.75}$$

where $\mathcal{L} := L_2(\mathbb{S}^1, d\theta_j/2\pi)$ denotes the space of square integrable functions on the circle $\mathbb{S}^1$ of length 2π. The tensor product $\mathcal{L} \otimes \dots \otimes \mathcal{L}$ is equivalent to $\mathcal{L}_2(\mathbf{T}^d, d\underline{\theta}/2\pi)$, i.e. the square integrable functions on the unit torus $\mathbf{T}^d$. The relations we have described for the single laser case extend in most practical cases to the d-laser case just by adapting the notation.

1.6 Unitary Floquet operator

1.6.1 Definition

We define the *unitary Floquet operator* U_F, restricted to the original Hilbert space $\mathcal{H}$, as the semiclassical propagator on a period $T = 2\pi/\omega$ [22]:

$$U_F := U(T, 0; \theta_0) \, : \, \mathcal{H} \to \mathcal{H}, \tag{1.76}$$

for a fixed phase θ_0 (e.g. $\theta_0 = 0$). The obvious property $U(nT, 0; \theta_0) = (U_F)^n$ shows that U_F gives the dynamics $\phi(t)$ at times that are integer multiples of the period T. We can interpret U_F as the quantum analog of the Poincaré section. The spectra of the operators U_F et K are linked by the following property (in a system of units such that $\hbar = 1$) :

i) If $\psi \in \mathcal{K}$ is an eigenstate of K : $K\psi = \lambda\psi$, then $\exists \Phi \in \mathcal{H}$ such that

$$\begin{aligned} \psi(\theta) &= e^{i\lambda\theta/\omega} U\left((\theta - \theta_0)/\omega, 0; \theta_0\right) \Phi & \text{(1.77a)} \\ &= e^{i\lambda\theta/\omega} U\left(0, -(\theta - \theta_0)/\omega; \theta\right) \Phi & \text{(1.77b)} \end{aligned}$$

and Φ is an eigenstate of U_F :

$$U_F\Phi = e^{-i\lambda T}\Phi \tag{1.78}$$

ii) Conversely, if $\Phi \in \mathcal{H}$ is eigenstate of U_F : $U_F\Phi = e^{-i\lambda T}\Phi$ then the state $\psi \in \mathcal{K}$ defined by Eq. (1.77) is eigenstate of K : $K\psi = \lambda\psi$.

In Eq. (1.77), we have used the property

$$U(t, s; \underline{\theta} + \underline{\omega}t) = U(t + a, s + a; \underline{\theta}). \tag{1.79}$$

1.6.2 Two-mode quasiperiodic unitary Floquet operator

One can generalize the unitary Floquet operator to the quasiperiodic case as follows [19]. We define the generalized unitary Floquet operator using the semiclassical propagator on the period $T_2 = 2\pi/\omega_2$ and the phase of the ω_2 field fixed to zero:

$$U_F(\theta_1) := \mathcal{T}^1_{-T_2} U(T_2, 0; \theta_1, 0) \; : \; \mathcal{H} \to \mathcal{H}, \tag{1.80}$$

where $U(t, t_0; \theta_1, \theta_2)$ is the propagator satisfying

$$\phi(t) = U(t, t_0; \theta_1, \theta_2)\phi(t_0), \tag{1.81}$$

associated to the quasiperiodic Hamiltonian $H(x, \theta_1, \theta_2)$. The one-phase translation operator is defined as

$$\mathcal{T}^1_{-T_2}\xi(\theta_1) = \xi(\theta_1 - \omega_1 T_2) \tag{1.82}$$

with $\xi \in \mathcal{L} \equiv L_2(\mathbb{S}^1, d\theta_1/2\pi)$. The generalized unitary Floquet operator, acting on $\mathcal{K}_1 \equiv \mathcal{H} \otimes \mathcal{L}$ has spectral properties equivalent to the ones of the quasienergy operator. One can generalize the preceding relations to this case:

i) If $\psi \in \mathcal{K}$ is an eigenstate of K : $K\psi = \lambda\psi$, then $\exists\Phi(\theta_1) \in \mathcal{K}_1$ such that

$$\psi(\theta_1, \theta_2) = e^{i\lambda\theta_2/\omega_2}\mathcal{T}^1_{-\theta_2/\omega_2} U\left(\theta_2/\omega_2, 0; \theta_1, 0\right)\Phi(\theta_1) \tag{1.83a}$$

$$= e^{i\lambda\theta_2/\omega_2} U\left(\theta_2/\omega_2, 0; \theta_1 - \theta_2\, \omega_1/\omega_2, 0\right)\Phi(\theta_1 - \theta_2\, \omega_1/\omega_2) \tag{1.83b}$$

$$= e^{i\lambda\theta_2/\omega_2} U\left(0, -\theta_2/\omega_2; \theta_1, \theta_2\right)\Phi(\theta_1 - \theta_2\, \omega_1/\omega_2) \tag{1.83c}$$

and Φ is an eigenstate of U_F :

$$U_F\Phi = e^{-i\lambda T_2}\Phi \tag{1.84}$$

ii) Conversely, if $\Phi(\theta_1) \in \mathcal{K}_1$ is eigenstate of U_F : $U_F\Phi = e^{-i\lambda T_2}\Phi$ then the state $\psi \in \mathcal{K}$ defined by Eq. (1.83) is eigenstate of K : $K\psi = \lambda\psi$.

1.6.3 Multi-mode quasiperiodic unitary Floquet operator

This can be generalized for the quasiperiodic case with m modes. We define the generalized unitary Floquet operator, using the semiclassical propagator on the period $T_m = 2\pi/\omega_m$ and the phase of the ω_m field fixed to zero

$$U_F(\theta_1, \cdots, \theta_{m-1}) := \mathcal{T}^{m-1}_{-T_m} U(T_m, 0; \theta_1, \cdots, \theta_{m-1}, 0) \; : \; \mathcal{H} \to \mathcal{H}, \tag{1.85}$$

where $U(t,t_0;\underline{\theta})$ is the propagator associated to the quasiperiodic Hamiltonian $H(x,\underline{\theta})$. The $(m-1)$-phase translation operator acts on the $m-1$ first phase as

$$\mathcal{T}_{-T_m}^{m-1}\xi(\theta_1,\cdots,\theta_{m-1}) = \xi(\theta_1-\omega_1 T_m,,\cdots,\theta_{m-1}-\omega_{m-1}T_m). \tag{1.86}$$

The generalized unitary Floquet operator, acting on $\mathcal{K}_{m-1} \equiv \mathcal{H}\otimes\underbrace{\mathcal{L}\otimes\ldots\otimes\mathcal{L}}_{m-1 \text{ products}}$ has spectral properties equivalent to the ones of the quasienergy operator:

i) If $\psi\in\mathcal{K}$ is an eigenstate of K : $K\psi=\lambda\psi$, then $\exists\Phi(\theta_1,\cdots,\theta_{m-1})\in\mathcal{K}_1$ such that

$$\psi(\underline{\theta}) = e^{i\lambda\theta_m/\omega_m}\mathcal{T}_{-\theta_m/\omega_m}^{m-1}U\left(\theta_m/\omega_m,0;\theta_1,\cdots,\theta_{m-1},0\right)\Phi(\theta_1,\cdots,\theta_{m-1}) \tag{1.87a}$$

$$= e^{i\lambda\theta_m/\omega_m}U\left(0,-\theta_m/\omega_m;\underline{\theta}\right)\Phi(\theta_1-\theta_m\,\omega_1/\omega_m,\cdots,\theta_{m-1}-\theta_m\,\omega_{m-1}/\omega_m) \tag{1.87b}$$

and Φ is an eigenstate of U_F :

$$U_F\Phi = e^{-i\lambda T_m}\Phi \tag{1.88}$$

ii) Conversely, if $\Phi(\theta_1)\in\mathcal{K}_1$ is eigenstate of U_F : $U_F\Phi = e^{-i\lambda T_m}\Phi$ then the state $\psi\in\mathcal{K}$ defined by Eq. (1.87) is eigenstate of K : $K\psi=\lambda\psi$.

1.6.4 Application to the numerical calculation of the Floquet spectrum

This formulation can be interesting from the practical point of view to determine the Floquet spectrum numerically. The alternative to the diagonalization of the full quasienergy Hamiltonian in a basis of $\mathcal{K}$ is as follows: We diagonalize the restricted Floquet matrix U_F constructed in the basis $\{\varphi_i, i=1..N\}$ in the original Hilbert space $\mathcal{H}$ associated to the free system H_0. The i^{th} column of U_F contains the solution $\phi(t=T)$ of the semiclassical time-dependent Schrödinger equation (that can be calculated by a numerical simulation in general) with the initial condition φ_i and calculated on one period T. This alternative requires thus a diagonalization in a smaller Hilbert space and N calculations of the semiclassical time-dependent Schrödinger equation on one period.

1.7 Extension to non-periodic time dependence

The notion of enlarged (or extended) Hilbert space constructed as the tensor product of the Hilbert space, in which the original Hamiltonian is defined, and the space of square integrable functions on the circle, first introduced by Sambe [3] in the periodic case, has been extended by Howland [4] for more general time-dependent Hamiltonians. It allows one to construct a time-independent *extended Hamiltonian*, which is the Floquet Hamiltonian in the periodic case.

We have used such a formalism to construct propagators for dynamics by ultrashort pulse, the so-called impulsive or sudden dynamics [23] (see also Chapter 7).

Moiseyev and collaborators have constructed computational algorithms that take advantage of this extended space to solve the time dependent Schrödinger equation by time-independent techniques, incorporating the complete time dependence in the extended space [named (t,t') technique] [24].

Chapter 2

Adiabatic Floquet theory

The models we have discussed so far correspond to continuous (CW) lasers with a fixed sharp frequency and constant intensity. They can be easily adapted to the case of pulsed lasers that have slowly varying envelopes [25, 26, 27, 28]. They can furthermore have a slowly rotating polarization and a chirped frequency, i.e. a frequency that changes slowly with time. The adiabatic chirped frequency within the Floquet formalism has been treated in [27, 28]. For periodic (or quasiperiodic) semiclassical Hamiltonians, the Floquet states are the stationary states of the problem. Processes controlled by chirped laser pulses include additional time dependent parameters (the pulse envelopes, swept frequencies and rotating polarizations), whose timescales are slow with respect to the optical frequencies. A first step is to relate the usual semiclassical time dependent Schrödinger equation to the time dependent Floquet Schrödinger equation, defined as the Schrödinger equation with the Floquet Hamiltonian. Since this equation does not have the fast optical time dependence we can treat it with adiabatic principles, by studying the properties of the spectrum of the Floquet Hamiltonian as a function of the slow parameters.

We first derive the time dependent Floquet Schrödinger equation relevant for processes induced by chirped laser pulses in the next section. The adiabatic principles to solve this equation and their consequences are next described, with an analysis of the occurrence of dynamical and geometric phases (Sections 2.2,2.3,2.4).

The use of adiabaticity in the Floquet dynamics will allow one to induce robust population transfers as will be described in the next chapter. One of the main aspect is to drive the system specifically through various *resonances*. The resonances can be classified as *zero-field* and *dynamical* resonances. The zero-field resonance is defined as an exact resonance identified when the coupling field is switched off. Such a resonance has an effect on the system even for a very small field amplitude. The dynamical resonance occurs beyond a threshold of field amplitude. They are defined and studied in Chapter 5.

For non-resonant processes, the Floquet states are *non-degenerate* at any time: The dynamics follows, up to a phase, the instantaneous Floquet state whose eigenenergy is continuously connected to the one associated to the initial Floquet state (Sections 2.2,2.3). This adiabatic transport can be generalized if more than one Floquet state is involved in the dynamics. Estimates from the deviation from a strict adiabatic dynamics are analyzed in Section 2.5 for non-resonant processes.

The adiabatic evolution for a zero-field resonant process depends on the way how the dynamics explores the resonance (Section 2.6). One can describe it on the example of a laser pulse of resonant (or quasi-resonant) carrying frequency leading to two degenerate (or quasi-degenerate) Floquet states at early times, such that the dynamics has to be described in the

subspace spanned by these two coupled states. The process can be described as follows: When the field rises, this degeneracy is *dynamically lifted*, which induces a sharing of the population between the two instantaneous Floquet branches whose eigenenergies are continuously connected to the initial degenerate ones. This process will be the origin of the creation of coherent superposition of states by adiabatic passage (see Section 3.4). We show that this lifting of degeneracy is instantaneous for one- and two-photon exact resonance processes. These two branches are next *followed adiabatically* by the dynamics if the pulse envelopes are slow enough, in the same way as in non-resonant processes. When the amplitude of pulse later decreases, the dynamics goes through the inverse process of *creation of degeneracy* which induces the interference of the two branches at the very end of the process. One can see in this example the necessity to consider an adiabatic transport along more than one Floquet state.

An alternative way to explore the zero-field resonance is to chirp a laser pulse which is switched on and off adiabatically sufficiently far from the resonance. The chirp is such that the frequency is swept through the resonance when the field is on. The resonance appears in a quasienergy diagram (as a function of time or as a function of the field parameters) as an *avoided crossing* (Section 2.7). This way leads to a qualitatively different description of the adiabatic evolution, since here a single Floquet state is involved in the dynamics as in non-resonant processes. An avoided crossing will mainly limit the application of the adiabatic theorem: if the dynamics is not slow enough, dynamical transitions, so-called non-adiabatic transitions, will be induced between the Floquet states forming the avoided crossing. A local Landau-Zener analysis can be invoked to determine this local non-adiabatic transition. Adiabatic passage along the avoided crossing induces in general a transition with respect to the bare states.

The dynamical resonances, which occur beyond a threshold of field amplitude, also usually appear as avoided crossings (see Section 5.2).

All these different types of resonances will be characterized geometrically in the next chapter.

2.1 The Floquet Schrödinger equation for chirped laser pulses of rotating polarization

We consider here for simplicity one chirped laser mode with an additional rotating polarization. Extension to multimode process is straightforward. The slow parameters of characteristic time τ are the laser pulse envelope $\Lambda(t)$, the frequency $\omega(t)$, and the dipole moment $\mu(t)$ (which includes the slowly rotating polarization for the dipole coupling of Eq. (1.1)). The time dependent phase can be written as

$$\theta + g(t), \quad \text{with} \quad g(t) = \omega(t)t \tag{2.1}$$

We consider a semiclassical Hamiltonian that depends on these slow parameters

$$\hat{H}^{[\Lambda(t),\mu(t),\omega(t)]}(t) = H^{[\Lambda(t),\mu(t)]}(\theta + g(t)). \tag{2.2}$$

For the dipole coupling with a pulse envelope

$$\mathcal{E}(t) = \Lambda(t)\,\mathcal{E}_{\max}, \tag{2.3}$$

chirped frequency $\omega(t)$, and rotating polarization $\mu(t)$ we take the semiclassical Hamiltonian

$$\hat{H}^{[\Lambda(t),\omega(t),\mu(t)]}(t) = H_0 - \mathcal{E}(t)\,\mu(t)\cos(\theta + \omega(t)\,t). \tag{2.4}$$

The parameter τ is here a measure of the total duration of the pulse. For instance we can take Gaussian pulses

$$\Lambda_{\text{Gaussian}}(t) = e^{-(t/\tau)^2} \tag{2.5}$$

of full width at half maximum $\tau_{\text{FWHM}} = \tau\sqrt{2\log_e 2}$ for the intensity. If we take a pulse of the form

$$\Lambda_{\text{trig}}(t) = \begin{cases} \sin^2\left(\pi\frac{t-t_i}{\tau}\right), & \text{if } t \in [t_i, t_i+\tau] \\ 0 & \text{elsewhere,} \end{cases} \tag{2.6}$$

usually called *trig pulse*, the parameter τ is the total length of the pulse. We use the square to ensure the continuity of the first derivative which avoids additional nonadiabatic losses as we will discuss.

Remark. For some arguments involving adiabatic evolution pulses that have a well-defined beginning and end present conceptual advantages, since they allow clear-cut statements. For other considerations (like the Dykhne-Davis-Pechukas analysis needed in Section 3.3) one needs real analytic pulse shapes, which excludes shapes that are identically zero on the complement of a finite interval.

We derive the Floquet Hamiltonian K associated to this semiclassical Hamiltonian by starting with the following definition of the corresponding propagator, which is the natural generalization of (1.13)

$$U^K(t, t_0; \theta) := \mathcal{T}_{-g(t)} U(t, t_0; \theta)\, \mathcal{T}_{g(t_0)}, \tag{2.7}$$

where $\mathcal{T}_{g(t)}$ is the translation operator which acts on $\mathcal{L}_2(S^1, d\theta)$ as $\mathcal{T}_{g(t)}\xi(\theta) = \xi(\theta + g(t))$.

The operator U is the propagator of the Schrödinger equation

$$i\hbar\frac{\partial}{\partial t} U(t, t_0; \theta) = H^{[\Lambda(t),\mu(t)]}(\theta + g(t))\, U(t, t_0; \theta) \tag{2.8}$$

if and only if U^K satisfies the Floquet Schrödinger equation

$$i\hbar\frac{\partial}{\partial t} U^K(t, t_0; \theta) = K^{[\Lambda(t),\mu(t),\omega_{\text{eff}}(t)]} U^K(t, t_0; \theta), \tag{2.9}$$

where

$$\omega_{\text{eff}}(t) = \frac{dg}{dt}(t) = \omega(t) + \dot{\omega}t \tag{2.10}$$

and

$$K^{[\Lambda(t),\mu(t),\omega_{\text{eff}}(t)]}(\theta) = H^{[\Lambda(t),\mu(t)]}(\theta) - i\hbar\omega_{\text{eff}}(t)\frac{\partial}{\partial\theta}. \tag{2.11}$$

In terms of states, Eq. (2.7) gives the correspondence between $\phi(t;\theta)$ the solution of Eq. (2.8) and $\psi(t,\theta)$ the solution of Eq. (2.9) [27]:

$$\phi(t;\theta) = \mathcal{T}_{g(t)}\psi(t,\theta) = \psi(t, \theta + g(t)). \tag{2.12}$$

The above result is proved in Appendix A. We point out the appearance of an *effective* instantaneous frequency in the Floquet Hamiltonian (2.11), which is the derivative of the phase of the field [27].

We remark that this correspondence between the semiclassical and Floquet dynamics with additional time dependent parameters is exact (i) without specific requirement on the number of oscillations of the classical field in the pulse, and (ii) even if these parameters do not have slow variations. Such slow variations will be convenient to yield robust processes as we will show below. The number of oscillations in the pulse will be relevant to apply resonant approximations as we will study.

2.2 Adiabatic evolution – Dynamical and geometric phases

The preceding analysis is well adapted when one considers slowly varying laser parameters. One can study the Floquet Schrödinger equation invoking adiabatic principles by analyzing the Floquet Hamiltonian as a function of the slow parameters.

It is convenient to consider explicitly the time-scale in the slow parameters: $\Lambda(t) =: \widetilde{\Lambda}(s)$ and $\omega_{\text{eff}}(t) =: \widetilde{\omega}_{\text{eff}}(s)$, where $s = t/\tau$ is a reduced time, τ a characteristic time for the slow parameters and t is the physical time. The slow parameters are gathered in a formal vector $\mathbf{r}(s) = \left[\widetilde{\Lambda}(s), \widetilde{\omega}_{\text{eff}}(s)\right]$. The Floquet Schrödinger equation reads

$$i\hbar \frac{d}{dt}|\psi(t)\rangle = K^{\mathbf{r}(t/\tau)}|\psi(t)\rangle \tag{2.13a}$$

or equivalently

$$i\frac{\hbar}{\tau}\frac{d}{ds}|\psi(\tau s)\rangle = K^{\mathbf{r}(s)}|\psi(\tau s)\rangle. \tag{2.13b}$$

We denote $P(t) = \sum_{m\in\mathcal{S}} \left|\psi_m^{\mathbf{r}(s)}\right\rangle \left\langle\psi_m^{\mathbf{r}(s)}\right|$ the projector at time t on $\mathcal{S}$, a subspace of $\mathcal{K}$, in which we want to apply the adiabatic evolution. The adiabatic theorem can be formulated as:

$$\lim_{\tau\to\infty} U^K(t, t_0; \theta)\, P(t_0) = \lim_{\tau\to\infty} P(t) U^K(t, t_0; \theta)\,, \tag{2.14}$$

if the instantaneous eigenenergies $\lambda_m^{\mathbf{r}(s)}, m \in \mathcal{S}$ are far enough from the other eigenenergies for all time $t \geq t_0$. Eq. (2.14) means that the dynamics is restricted inside the subspace $\mathcal{S}$ in the adiabatic limit $\tau \to \infty$.

In terms of eigenvectors, if one assumes a unique (nondegenerate) eigenvector $\left|\psi_m^{\mathbf{r}(s)}\right\rangle$ associated to the eigenenergy $\lambda_m^{\mathbf{r}(s)}$, one has $P(t) = \left|\psi_m^{\mathbf{r}(s)}\right\rangle \left\langle\psi_m^{\mathbf{r}(s)}\right|$ and the preceding formulation becomes :
If the system is at time $t_0 = \tau s_0$ in the Floquet instantaneous eigenstate $\psi(\theta, t_0) = \psi_m^{\mathbf{r}(s_0)}(\theta)$, then in the adiabatic limit $\tau \to \infty$ the state solution $\psi(\theta, t)$ of (2.13a) is up to a phase given by the instantaneous Floquet state whose eigenenergy is continuously connected to the initial one at t_0 :

$$\psi(\theta, t) \simeq \exp\left[i\delta_m^{\mathbf{r}(s)}(t)\right] \psi_m^{\mathbf{r}(s)}(\theta). \tag{2.15}$$

We remark that the formulation of the adiabatic theorem (2.14) in terms of projectors does not show any phase. It appears only when we consider the formulation in terms of states.

The phase consists of a sum of dynamical and geometric parts:

$$\delta_m^{\mathbf{r}(s)}(t) = -\frac{1}{\hbar}\int_{t_0}^{t} du\, \lambda_m^{\mathbf{r}(u/\tau)} + i\int_{\mathbf{r}(s_0)}^{\mathbf{r}(s)} d\mathbf{r}\cdot\langle\psi_m^{\mathbf{r}}|\,\nabla_{\mathbf{r}}\,|\psi_m^{\mathbf{r}}\rangle_{\mathcal{K}}\,. \tag{2.16}$$

This results from incorporating the form of the solution (2.15) in the Schrödinger equation (2.13a), which gives $d\delta_m^{\mathbf{r}(s)}/dt = -\lambda_m^{\mathbf{r}(s)}/\hbar + i(d\mathbf{r}/dt)\cdot\langle\psi_m^{\mathbf{r}}|\nabla_{\mathbf{r}}|\psi_m^{\mathbf{r}}\rangle_{\mathcal{K}}$, and hence Eq. (2.16).

The dynamical phase depends on the trajectory followed in the space parameter and on its speed. The geometric phase does not depend on its speed. Since the phase of the instantaneous Floquet states is not uniquely specified at each $\mathbf{r}$, on can always choose the geometric phase as zero, that is known as *parallel transport*:

$$\frac{d\mathbf{r}}{dt}\cdot\langle\psi_m^{\mathbf{r}}|\nabla_{\mathbf{r}}|\psi_m^{\mathbf{r}}\rangle_{\mathcal{K}} \equiv \langle\psi_m^{\mathbf{r}}|\frac{d}{dt}|\psi_m^{\mathbf{r}}\rangle_{\mathcal{K}} = 0. \tag{2.17}$$

This is equivalent to requiring $\langle\psi_m^{\mathbf{r}}\left|\psi_m^{\mathbf{r}+\mathbf{dr}}\right\rangle_{\mathcal{K}} = 1$ up to second order in $\mathbf{r}$ (or equivalently $\mathrm{Im}\,\langle\psi_m^{\mathbf{r}}|d\psi_m^{\mathbf{r}}\rangle_{\mathcal{K}} = 0$, using the fact that the bracket is purely imaginary), i.e. *to require the phase invariance of the eigenvectors after an infinitesimal change of the parameters*[1]. However, the preceding requirement is non-integrable: if one follows a closed loop $\mathcal{C}$ in the parameter space, the eigenvector at the end of the loop will differ in general from the initial one by a phase $\gamma(\mathcal{C})$:

$$\langle\psi_m^{\mathbf{r}_{\rm initial}}|\,\psi_m^{\mathbf{r}_{\rm final}}\rangle_{\mathcal{K}} = e^{i\gamma(\mathcal{C})}, \quad \gamma(\mathcal{C}) = i\oint_{\mathcal{C}} d\mathbf{r}\cdot\langle\psi_m^{\mathbf{r}}|\nabla_{\mathbf{r}}|\psi_m^{\mathbf{r}}\rangle_{\mathcal{K}} \tag{2.18}$$

This phase, which depends only on the geometry of the loop but not on the speed is the geometric Berry phase [29]. It is non zero when the eigenvalues have a degeneracy, and can be evaluated using the Stokes theorem as the flux through $\mathcal{C}$ of the magnetic field of a monopole located at the degeneracy [29]. If only one parameter is varied, this geometric phase is 0. If two parameters are varied, it can be π (if a degeneracy of the eigenvalues is enclosed by the loop in the parameter space) or 0 (if not) (see Section 2.4 for an explicit example). If more than two parameters are varied, it can take any value.

The adiabatic theorem is valid in two quite different situations:

(i) Well separated instantaneous eigenvalues (gap condition) [30, 31, 32] . In this case, if the initial condition is an instantaneous eigenstate, the evolution in the adiabatic limit follows the corresponding branch.

(ii) Exact crossing of eigenvalues. In this case the adiabatic evolution follows the initial branch across the intersection, as if the intersection did not exist [30, 31, 33, 34]. This situation of exact crossing occurs when the coupling between the states is exactly zero. Concerning the terminology, such crossing curves are often called *diabatic* curves. This can be misleading since in this case of exact crossing, the adiabatic dynamics follows diabatic curves. We remark that this terminology is more appropriate for the limit case of a thin avoided crossing (associated to a small coupling) with respect to a fast dynamics, allowing a jump from one (continuous) curve

[1]The expression "parallel transport" comes from geometry where angles take the role of quantum phases: A vector which is parallel-transported along a closed path may acquire an angle with respect to its initial direction. An intuitive classical example of such a situation [see B. Goss Levi, Phys. Today 46, 17 (1993)] is the parallel transport of a vector along a loop on a sphere. For instance, we define a path starting from the north pole, getting down to the equator, next going along the equator over a given distance, and finally getting back to the north pole. The vector stays tangential to the curved surface at all times and is initially oriented in the direction of the trajectory. It is next transported, remaining parallel to the direction it was pointing at before each infinitesimal displacement. After completing the loop, the vector goes back to the original point, but is rotated with respect to its initial direction. A smaller loop leads to a smaller rotation angle. For instance, when the loop surrounds one eighth of the sphere, the rotation angle amounts to 90°. The reason for this rotation is purely geometrical-topological since it is connected to the intrinsic curvature of the sphere. No such phenomenon would appear if vectors are parallel-transported along a flat manifold, such as a plane or a cylinder. The rotation angle is related to the integral of the curvature on the surface bounded by the loop.

to the other one. The topology of such a situation is however different since now the continuous curves, called *adiabatic* curves, surround the avoided crossing. This is locally described as a *diabatic dynamics. The adiabatic dynamics through exact crossing can be thus thought as the limit case of a diabatic dynamics through a thin avoided crossing.*

Thus, in both cases in the adiabatic limit the population is carried at all times by a single branch of instantaneous eigenstates. A quite general formulation of the adiabatic theorem which imposes only smoothness conditions on the instantaneous eigenprojections without a priori gap condition, and that contains both cases, has been presented recently by Avron and Elgart [35, 36].

In the applications to the control of molecular processes the property that is most often required is that the the population stays on a single branch. The case that is most detrimental is when two or several branches do not cross but come close to each other, e.g. in the form of narrowly avoided crossings. In this case, for a finite speed of the parameters there are *nonadiabatic transitions* between the branches, i.e. the population spreads among them. This behavior will be discussed in more detail below.

More than one Floquet state can be involved in the dynamics, for example if the initial condition is a linear combination of the instantaneous eigenvectors. These Floquet states span a subspace $\mathcal{S}$ and for the case of a subspace of *nondegenerate* eigenvectors, the adiabatic transport can be formulated in terms of eigenvectors:

$$\psi(\theta,t) \simeq \sum_{m\in\mathcal{S}} c_m \exp\left[i\delta_m^{\mathbf{r}(s)}(t)\right] \psi_m^{\mathbf{r}(s)}(\theta), \tag{2.19}$$

where the c_m are complex numbers determined by the initial condition

$$c_m = \left\langle \exp\left(i\delta_m^{\mathbf{r}(s_0)}(t_0)\right) \psi_m^{\mathbf{r}(s_0)}(\theta) \mid \psi(\theta,t_0)\right\rangle \tag{2.20}$$

A sketch of an argument that leads to the adiabatic theorem for the Floquet Hamiltonian of a $N-$level system is given below in section 2.3.

In the case of *globally degenerate eigenstates*, Wilczek and Zee have extended the scalar geometrical phases to a matrix representation, which is known in the literature as non-Abelian geometric phases [37].

The quantum geometric phase found by Berry [29] has been reformulated by Moore and Stedman [38] for *periodic* Hamiltonians in the Floquet formalism, extended by Aharanov and Anandan [39] for *arbitrary cyclic* evolution (see also [40]), and by Samuel and Bhandari [41] for a general *noncyclic and non-unitary* evolution.

2.3 The adiabatic theorem for Floquet Hamiltonians

We sketch here an argument that leads to the adiabatic theorem for an $N-$level system with a Floquet Hamiltonian denoted $K^{\mathbf{r}}$ which generates the Floquet Schrödinger equation [Eq. (2.13a)]

$$i\hbar\frac{\partial\psi(\theta,t)}{\partial t} = K^{\mathbf{r}(s)}\psi(\theta,t). \tag{2.21}$$

We have to show that in the adiabatic limit up to corrections of order $\mathcal{O}(1/\tau)$, the evolution is approximated by

$$\psi(\theta,t) \simeq \sum_{m\in\mathcal{S}} c_m \exp\left[i\delta_m^{\mathbf{r}(s)}(t)\right] \psi_m^{\mathbf{r}(s)}(\theta), \tag{2.22}$$

where the c_m are complex numbers determined by the initial condition

$$c_m = \left\langle \exp\left[i\delta_m^{\mathbf{r}(s_0)}(t_0)\right] \psi_m^{\mathbf{r}(s_0)}(\theta) \mid \psi(\theta, t_0)\right\rangle \tag{2.23}$$

Let $\{\psi_m^{\mathbf{r}(s)}\}$ be an orthonormal basis of instantaneous eigenvectors of $K^{\mathbf{r}(s)}$, which we assume to be sufficiently smooth as a function of s. We define the unitary operator $T^{\mathbf{r}(s)} := \sum_m |\psi_m^{\mathbf{r}(s)}\rangle\langle\psi_m^{\mathbf{r}(s_0)}|$, where s_0 is the initial time. This operator transforms the Floquet Hamiltonian by

$$D^{\mathbf{r}(s)} := \left(T^{\mathbf{r}(s)}\right)^\dagger K^{\mathbf{r}(s)} T^{\mathbf{r}(s)}, \tag{2.24}$$

into an operator $D^{\mathbf{r}(s)}$, which for all s is diagonal in the basis taken at s_0, $\{\psi_m^{\mathbf{r}(s_0)}\}$. Defining transformed states by

$$\widetilde{\psi}\,(\theta, s) = \left(T^{\mathbf{r}(s)}\right)^\dagger \psi\,(\theta, \tau s)\,. \tag{2.25}$$

the Schrödinger equation (2.21) can be rewritten as

$$\frac{i\hbar}{\tau}\frac{\partial\widetilde{\psi}(\theta, s)}{\partial s} = \left[D^{\mathbf{r}(s)} - \frac{i\hbar}{\tau}\left(T^{\mathbf{r}(s)}\right)^\dagger \frac{\partial T^{\mathbf{r}(s)}}{\partial s}\right]\widetilde{\psi}(\theta, s) \tag{2.26}$$

The last term of the right-hand side of Eq. (2.26) induces the *nonadiabatic couplings* between the instantaneous Floquet states (off-diagonal terms, of the form $\left|\psi_\ell^{\mathbf{r}(s_0)}\right\rangle\left\langle\psi_\ell^{\mathbf{r}(s)}\right|\dot{\mathbf{r}}\cdot\nabla_{\mathbf{r}}\left|\psi_m^{\mathbf{r}(s)}\right\rangle_{\mathcal{K}}\left\langle\psi_m^{\mathbf{r}(s_0)}\right|$, $\ell \neq m$) and the geometric phase (real diagonal terms). In the adiabatic limit $\tau \to \infty$, one can neglect the nonadiabatic couplings, i.e. the nondiagonal terms that are of order $\mathcal{O}(1/\tau)$:

$$\frac{i\hbar}{\tau}\frac{\partial\widetilde{\psi}(\theta, s)}{\partial s} \simeq \left[D^{\mathbf{r}(s)} - \frac{i\hbar}{\tau}\,\mathrm{diag}_{(s_0)}\left(\left(T^{\mathbf{r}(s)}\right)^\dagger \frac{\partial T^{\mathbf{r}(s)}}{\partial s}\right)\right]\widetilde{\psi}(\theta, s), \tag{2.27}$$

where $\mathrm{diag}_{(s_0)}$ denotes the diagonal part with respect to the initial time basis $\{\psi_m^{\mathbf{r}(s_0)}\}$. Developing $\psi(\theta, t)$ at an initial time $t_0 = \tau s_0$ in the eigenvector basis of $K^{\mathbf{r}(s_0)}$, spanning the subspace $\mathcal{S}$:

$$\psi(\theta, \tau s_0) = \sum_{m\in\mathcal{S}} c_m \psi_m^{\mathbf{r}(s_0)}(\theta), \tag{2.28}$$

one recovers Eq. (2.19). We remark that in many applications the initial time s_0 is taken before the rise of the laser pulse. In this case, since the interaction is off, the initial instantaneous basis coincides with the eigenvectors of the free molecule multiplied by those of the free field. The operator $D^{\mathbf{r}(s)}$ of Eq. (2.24) can then be written as

$$D^{\mathbf{r}(s)} = -i\hbar\omega\frac{\partial}{\partial\theta} + \mathsf{d}^{\mathbf{r}(s)} \tag{2.29}$$

where $\mathsf{d}^{\mathbf{r}(s)}$ is an operator in $\mathcal{H}$ that is diagonal in the basis of the eigenvectors of the free molecule.

2.4 A two-state example with a loop in a two-dimension parameter space: A two out-of-phase chirped pulse loop.

In this section, we consider the example of a circuit near a degeneracy of two states in the parameter space [29, 42] in the context of pulsed-driven two-state system (states $|-\rangle$ and $|+\rangle$)

$$H(s) = \frac{\hbar}{2}\begin{bmatrix} -\Delta(s) & \Omega(s)e^{-i\varphi} \\ \Omega(s)e^{i\varphi} & \Delta(s) \end{bmatrix}. \tag{2.30}$$

It characterizes a near-resonant process (in the rotating wave approximation) of Rabi frequency $\Omega(s)$ (assumed positive) associated to a field of phase φ at the origin and detuned by $\Delta(s)$ [43, 44]. (Such an Hamiltonian is used as an example all along this chapter, it is studied and constructed in the next part.) The state evolution $\phi(s)$ is given by the Schrödinger equation

$$i\hbar\frac{\partial\phi}{\partial s}(s) = \tau H(s)\phi(s), \quad \phi(s) = \begin{bmatrix} B_-(s) \\ B_+(s) \end{bmatrix} \in \mathbb{C}^2, \tag{2.31}$$

with $|B_-(s)|^2 + |B_+(s)|^2 = 1$, the scaled time $s = t/\tau$. We consider the coupling between the initial s_i and final s_f times with the initial condition: $B_-(s_i) = 1$, $B_+(s_i) = 0$.

The adiabatic states $\Phi_\pm(s)$ are defined as the eigenstates of $H(s)$, associated to the eigenvalues $\lambda_\pm(s)$:

$$H(s)\Phi_\pm(s) = \lambda_\pm(s)\Phi_\pm(s) \tag{2.32}$$

with here

$$\lambda_\pm(s) = \pm\frac{\hbar}{2}\delta(s) \tag{2.33}$$

and

$$\delta(s) = \sqrt{\Delta^2(s) + \Omega^2(s)}. \tag{2.34}$$

The Hamiltonian has two time-dependent parameters when the phase φ is kept fixed.

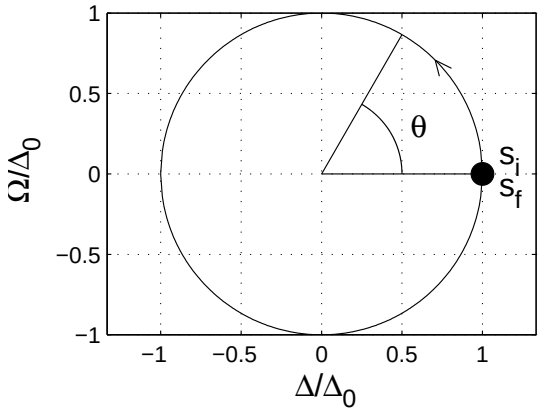

FIG. 2.1 - *Trajectory in the parameter space as a loop encircling the degeneracy (at $\Omega = \Delta = 0$) and parameterized by the radius Δ_0 and the angle θ.*

We consider the trajectory in the space parameter shown in Fig. 2.1. In practice, such a trajectory can be created by the pulse sequence of two identical chirped near-resonant pulses but with a decreasing (resp. increasing) chirp for the first (resp. second) pulse and an additional relative phase π between the two pulses. Both Rabi frequencies (considered without loss of generality as real) increases and decreases such that the distance $\hbar\delta = \hbar\Delta_0$ between the eigenvalues is kept fixed (i.e. the detuning is Δ_0 when the Rabi frequency is zero): The trajectory is a loop which encircles the degeneracy (at $\Omega = \Delta = 0$). We can rewrite the Hamiltonian with a single Rabi frequency $\widetilde{\Omega}(s) := \Omega e^{-i\varphi}$ considered first positive (i.e. with $\varphi = 0$) and next negative (i.e. with $\varphi = \pi$), and $\Delta = \Delta_0 \cos\theta$, $\widetilde{\Omega} = \Delta_0 \sin\theta$ with

$$\tan\theta = \widetilde{\Omega}/\Delta, \quad 0 \leq \theta < 2\pi, \tag{2.35}$$

The loop is described by θ varying from 0 to 2π with a constant radius $\hbar\Delta_0$.

In this case, gathering the adiabatic states in the columns of the unitary matrix $T(\theta) = [\Phi_-(\theta), \Phi_+(\theta)]$:

$$T(\theta(s)) = \begin{bmatrix} \cos(\theta(s)/2) & \sin(\theta(s)/2) \\ -\sin(\theta(s)/2) & \cos(\theta(s)/2) \end{bmatrix} \tag{2.36}$$

giving

$$T^\dagger(\theta(s))\tau H(s) T(\theta(s)) = \tau \begin{bmatrix} \lambda_- & 0 \\ 0 & \lambda_+ \end{bmatrix} \tag{2.37}$$

we can rewrite the Schrödinger equation as

$$i\hbar \frac{\partial}{\partial s}\phi_A(s) = H_A(s)\phi_A(s) \tag{2.38}$$

with

$$H_A(s) = \frac{\hbar}{2} \begin{bmatrix} -\tau\delta(s) & -i\gamma(s) \\ i\gamma(s) & \tau\delta(s) \end{bmatrix}, \tag{2.39}$$

the non-adiabatic coupling

$$\gamma(s) \equiv \frac{d\theta(s)}{ds} = \frac{\dot{\widetilde{\Omega}}(s)\Delta(s) - \widetilde{\Omega}(s)\dot{\Delta}(s)}{\Delta^2(s) + \Omega^2(s)}, \tag{2.40}$$

and

$$\phi_A(s) \equiv \begin{bmatrix} A_-(s) \\ A_+(s) \end{bmatrix} = T^\dagger(\theta(s))\phi(s) = T^\dagger(\theta(s)) \begin{bmatrix} B_-(s) \\ B_+(s) \end{bmatrix}. \tag{2.41}$$

Since $A_\pm(s) \equiv \langle \pm |\, \phi_A(s)\rangle = \langle \Phi_\pm(\theta(s))|\, \phi(s)\rangle$, one can interpret $|A_\pm(s)|^2$ as the population of the adiabatic states $|\Phi_\pm(\theta(s))\rangle$. In the adiabatic limit, mathematically defined as $\tau \to \infty$, the non-adiabatic coupling γ can be neglected and the dynamics follows the adiabatic states. By inspection of Eq. (2.39), the condition for adiabatic evolution reads more precisely $|\gamma(s)| \ll 2\tau\delta(s)$.

Note that the eigenvectors satisfy here the condition of *parallel transport* (2.17).

One has initially $\Omega(s_i) \to 0^+$ and $\Delta(s_i) > 0$, i.e. $\theta(s_i) \to 0$ and $\phi_A(s_i) = \phi(s_i)$, hence

$$A_-(s_i) = B_-(s_i) = 1, \quad A_+(s_i) = B_+(s_i) = 0. \tag{2.42}$$

In the adiabatic limit, one can directly calculate [without invoking Eq. (2.15)] the solution from Eq. (2.41) and obtains after the loop

$$\phi(s_f) = T(2\pi)\phi_A(s_f) = -e^{i\tau\Delta_0(s_f - s_i)/2} \begin{bmatrix} 1 \\ 0 \end{bmatrix}, \tag{2.43}$$

where the phase factor can be identified as the dynamical phase.

If we now apply the adiabatic theorem [i.e. using Eq. (2.15)], one obtains with the condition of parallel transport

$$\phi(s) = e^{i\tau\Delta_0(s-s_i)/2}\Phi_-(\theta(s)), \tag{2.44}$$

giving at the end of the process

$$\phi(s_f) = e^{i\tau\Delta_0(s_f-s_i)/2}e^{i\delta_g}\Phi_-(\theta=0) = e^{i\tau\Delta_0(s_f-s_i)/2}e^{i\delta_g}\begin{bmatrix}1\\0\end{bmatrix}, \tag{2.45}$$

where the geometric phase δ_g can be identified to be π, when we compare Eqs. (2.43) and (2.45). It corresponds exactly to the *phase discontinuity* of the eigenvectors between $\theta = 2\pi$ and $\theta = 0$:

$$\mathrm{Im}\log\left(\langle\Phi_-(\theta=2\pi)|\Phi_-(\theta=0)\rangle\right) = \pi, \tag{2.46}$$

as stated by Eq. (2.18).

Alternatively to the parallel transport, we can apply a gauge transform to the eigenvectors: $\widetilde{\Phi}_\pm(\theta) = e^{-i\theta/2}\Phi_\pm(\theta)$ to make them single-valued continuous for all θ. In this case, using $\widetilde{T}(\theta) = \left[\widetilde{\Phi}_-(\theta), \widetilde{\Phi}_+(\theta)\right]$, we obtain

$$i\hbar\frac{\partial}{\partial s}\widetilde{\phi}_A(s) = \widetilde{H}_A(s)\widetilde{\phi}_A(s) \tag{2.47}$$

with

$$\widetilde{H}_A(s) = \frac{\hbar}{2}\begin{bmatrix}-\tau\delta(s)-\dot{\theta} & -i\gamma(s)\\ i\gamma(s) & \tau\delta(s)-\dot{\theta}\end{bmatrix}. \tag{2.48}$$

The geometric phase appears here explicitly as $\int_{s_i}^{s_f} ds\,\dot{\theta}/2 = \int_0^{2\pi} d\theta/2 = \pi$, when we calculate directly the solution of Eq. (2.47) in the adiabatic limit.

If we had chosen a loop not encircling the degeneracy, we would have found 0 as the Berry geometrical phase.

The use of three variable parameters give in general a geometric phase of any value [29].

Such a construction has been generalized for a three-state system in [42].

2.5 Non-resonant deviations from adiabaticity: Perturbation theory, superadiabatic schemes and Dykhne-Davis-Pechukas formula

Deviations from strict adiabatic evolution given by the adiabatic theorem are of the order of $1/\tau$ (in amplitude) and can thus be estimated for short time by time-dependent perturbation theory in the adiabatic basis, which does not diverge for non-resonant processes, i.e. if there is no degeneracy nor quasi-degeneracy (appearing as avoided crossings) of the quasienergies. These deviations can be due (i) to the fact that τ is finite and (ii) to the possible non-smoothness of the parameters. These cases have been considered in [28] for nonsmooth pulse ends in a two-level model driven by a non-resonant field. It also shows that the first order correction, which involves the coupling of the Floquet zone considered with the other zones, captures well the small deviations, that appear as oscillations (see Section 3.1 of [28]).

It is however known that in fact the adiabatic passage is in general much more efficient when considered at the end of the process. This is well understood in two-level systems for which one has the following result: *for smooth analytic parameters and nondegenerate eigenvalues, the nonadiabatic corrections in the asymptotic adiabatic limit $\tau \to \infty$ are of order $e^{-|\text{const.}|\tau}$, exponential in τ, i.e. beyond all orders in $1/\tau$ at the end of the process.*

This result is due to Dykhne [45] and Davis and Pechukas [46] and has been extended to $N-$level systems [47]. The conditions of validity of the so-called Dykhne-Davis-Pechukas (DDP) formula has been established in [48, 49] (see Appendix D). This formula allows one to calculate in the adiabatic asymptotic limit the probability of the non-adiabatic transitions. This formula captures for example the result of the Landau-Zener formula, that we study below.

An alternative interpretation of this exponential nonadiabatic corrections has been given through *superadiabatic schemes*. The superadiabatic schemes allow one to transform the problem to more adapted new basis (the so-called superadiabatic basis), where transition amplitudes proportional to powers of $1/\tau$ are removed. The scheme can be either iterative or by expansion in power series of $1/\tau$. This series expansion has been introduced by Berry for parametrically time-dependent quantum systems [50]. The iterative scheme [51, 52, 53, 54] consists in constructing iteratively Schrödinger equations by successive appropriate unitary transformations of the effective dressed Hamiltonians. In the same spirit as we have done with the transformation (2.24) [or (2.36)], the first step corresponds to the instantaneous diagonalization (2.24) of the Hamiltonian giving the new exact Schrödinger equation (2.26), containing nonadiabatic couplings of first order in $1/\tau$. The next steps are diagonalizations of the new Hamiltonians which reduce the nonadiabatic couplings to higher orders. Neither the series nor the iterations converge in general. However Berry showed that, for this asymptotic series in two-level systems, an optimal order, corresponding to the minimization of the nonadiabatic couplings, gives an optimal superadiabatic basis with respect to which the transition amplitude acquires a universal error-function-like form. It is universal in the sense that it does not depend on the details of the Hamiltonian. This optimal superadiabatic basis coincides with the free basis (and also the adiabatic basis) at the beginning and at the end of the process when the fields are off. This means that if there are no degeneracies or quasi-degeneracies at the beginning and the end of the process, *the adiabatic passage is in fact supported by a superadiabatic transport between the beginning and the end of the process*. The nonadiabatic corrections are then given at the end of the process by the Berry's universal error function times an exponential in τ, in agreement with the DDP analysis [50, 54]. This approach has been successfully applied for a two-level atom strongly perturbed by a non-resonant field, in the full Floquet representation [28]. The resonant stimulated Raman adiabatic passage (STIRAP) process in a three-level system (that is studied below) is an example which has degeneracies of the eigenvalues at the beginning and the end of the process. It has been shown in [54] through an effective two-level model that in this case, the nonadiabatic correction at the end of the process is given, in addition to the DDP exponential term, by a *perturbative* term, whose dominant contribution is of first order in $1/\tau$.

Degeneracy and avoided crossing of the eigenvalues can be treated in a specific way, as shown below. Optimization of adiabatic evolution will be studied in section 3.3 with the use of geometric arguments.

Nonsmoothness of the parameters usually leads to nonadiabatic corrections in transition amplitude of order p if the nonsmoothness is characterized by a discontinuous $p-$th derivative. Nonsmooth pulse ends can be investigated [55] in the simplified model

$$H(t) = \frac{\hbar}{2} \begin{bmatrix} 0 & \Omega(t) \\ \Omega(t) & 2\Delta(t) \end{bmatrix}, \tag{2.49}$$

where we assume a real and positive Ω, which represents a two-level atom (with states $|1\rangle$ and $|2\rangle$) interacting with a one-photon quasi-resonant pulse in the rotating wave approximation [43, 44]. We consider a coupling characterized by a Rabi frequency $\Omega(t) = \Omega_0 \sin^2(\pi t/\tau)$, having discontinuous second derivatives at the beginning and at the end of the pulse. The frequency of the field is chirped in such a way that the distance between the two eigenenergies is kept constant: $\Delta(t) = \frac{|t|}{t}\sqrt{\Omega_0^2 - \Omega^2(t)}$ (this choice will appear clearer in Section 3.3). With this choice the nonadiabatic corrections are due uniquely to the nonsmoothness at the beginning and at the end. In the adiabatic limit the population mostly transferred from $|1\rangle$ to $|2\rangle$. For the nonadiabatic corrections in probability at the end of the pulse (i.e. the probability of the population to return to state $|1\rangle$), the first order nonadiabatic corrections in the adiabatic asymptotic limit $\tau \to \infty$, are given, after integrating twice by parts, by

$$P_1 \approx \frac{1}{4}\left(\frac{\pi}{\tau\Omega_0}\right)^4 \sin^2(\Omega_0\tau). \tag{2.50}$$

This gives, as expected, asymptotic non-adiabatic corrections in probability that scale as $(1/\tau)^4$, since the discontinuity is in the second derivatives.

2.6 Resonant laser fields – Lifting of degeneracy – Generalized π-pulse

Processes that are resonant at zero field (i.e. with a atomic Bohr frequency that is an integer multiple of the laser frequency) can be investigated through an effective Hamiltonian of the model constructed from a multi-level atom driven by a quasi-resonant pulsed and chirped radiation field (referred to as a pump field). If one considers a n-photon process between the considered atomic states $|1\rangle$ and $|2\rangle$ (of respective energy E_1 and E_2), one can construct an effective hamiltonian with the two dressed states $|1;0\rangle$ (dressed with 0 photon) and $|2;-n\rangle$ (dressed with $-n$ photons) coupled by the n-photon Rabi frequency $\Omega(t)$ (of order n with respect to the field amplitude) and a dynamical Stark (or light) shift of the energies. It reads in the two-photon RWA [see Section 6.2.2 and the Hamiltonian (6.61)], where we assume Ω real and positive for simplicity,

$$H(t) = \frac{\hbar}{2}\begin{bmatrix} 0 & \Omega(t) \\ \Omega(t) & 2\Delta(t) \end{bmatrix}, \tag{2.51}$$

with the effective detuning

$$\Delta(t) = \Delta_0(t) + S(t), \tag{2.52}$$

where $S(t)$ is the relative dynamical Stark shift (of second order) due to the contribution of the other states and $\Delta_0(t)$ the detuning associated to the multiphoton near-resonant process, which is time-dependent if a chirp is applied. The population resides initially in the atomic state $|1\rangle$.

Note that the Hamiltonian (2.51) is a good approximation for the one- and two-photon processes (as shown in Section 6.2.2 for the two-photon case), but that it is only a rough approximation for higher multiphoton processes, since the Stark shifts should contain additional terms of higher order to be consistent with the order of the effective Rabi frequency.

There is a resonance in this system if there exist times t for which $\Omega(t)$ is of the same order as $\Delta(t)$, as described more precisely in Subsection 6.2.2.

This is the situation we consider, i.e. $\max_t \Omega(t) > \Delta$ (assuming a constant detuning for simplicity). The question we address here is the early (or late) dynamics with a pulsed Rabi frequency, when $\Omega \sim \Delta$, to know if the subsequent dynamics, when $\Omega(t) > \Delta$, can be treated with adiabatic principles and if so how to determine the initial condition. As we will see, it is in general a superposition of the resonant states. Denoting τ as the characteristic time of the rising (or falling) of the pulse, we can identify three regimes, depending how fast one goes through the resonance. The slow dynamics defined by $\tau\Delta \ll 1$ allows the dynamics to follow at each time a *single* Floquet state (see Subsection 2.6.1). The fast dynamics defined by $\tau\Delta \ll 1$ induces a *lifting of degeneracy*, leading to a fast dynamical splitting of the dynamics between the two resonant Floquet states, as analyzed in Subsection 2.6.2. The intermediate regime $\tau\Delta \sim 1$ induces a non-trivial *lifting of quasidegeneracy* that should be treated specifically. In Subsection 2.6.3, we summarize the results that we obtained in Ref. [56].

2.6.1 Adiabatic evolution with a constant detuning

For this model (2.51) we can write the conditions for adiabatic behavior in detail using the procedure described above: One obtains the transformed Schrödinger equation (2.26):

$$i\frac{\partial}{\partial t}\widetilde{\psi}(t) = \frac{1}{2}\begin{bmatrix} -\delta(t) & -i\gamma(t) \\ i\gamma(t) & \delta(t) \end{bmatrix}\widetilde{\psi}(t), \tag{2.53}$$

with

$$\delta(t) = \sqrt{\Delta^2(t) + \Omega^2(t)} \tag{2.54}$$

and the nonadiabatic coupling

$$\gamma(t) = \frac{\Omega(t)\dot{\Delta}(t) - \dot{\Omega}(t)\Delta(t)}{\Delta^2(t) + \Omega^2(t)}. \tag{2.55}$$

The conditions for adiabatic evolution are satisfied if the nonadiabatic coupling is much smaller than the separation of the eigenvalues

$$|\gamma(t)| \ll 2\sqrt{\Omega^2(t) + \Delta^2(t)}. \tag{2.56}$$

If the detuning is constant, estimating $\dot{\Omega}(t) \sim \Omega_0/\tau$ with $\Omega_0 = \max_t \Omega(t)$ and taking $\Omega_0 \sim \Delta$, we obtain that *the dynamics is adiabatic if one assumes a large detuning with respect to* $1/\tau$, where τ characterizes the length of the pulse:

$$\tau\Delta \gg 1. \tag{2.57}$$

The dynamics is thus in this case at all times adiabatic in the sense that it mainly follows the *single* dressed eigenstate whose eigenvalue is continuously connected to the one associated to the initial dressed state. This adiabatic transport results at the end of the pulse in an (almost) complete return in the initially populated state. It is important to point out that the dynamics is affected by the resonance in the sense that the excited bare state $|2\rangle$ is highly populated during the pulse if Ω is of the same order as Δ or larger at the peak laser amplitude. For two-level systems, the nonadiabatic small corrections lost to the other eigenstate have been extensively studied (see for example [57] and references therein).

2.6.2 Lifting and creation of degeneracy – Instantaneous splitting and recombination of population

In the opposite case

$$\tau\Delta \ll 1, \tag{2.58}$$

a dynamical splitting of the dynamics between the resonant dressed states occurs. One can reinterpret the well-known $\pi-$pulse formula for a one-photon process and extend it for multiphoton processes [58, 59]. In the case of an exact $n-$photon resonance, defined by (2.58), the two relevant dressed states $|1;0\rangle$ and $|2;-n\rangle$ can be considered, before the rising of the pulse, as exactly degenerate with respect to the dynamics, associated to the dressed energy $E_1 = E_2 - n\hbar\omega$. The pulse rising induces a *dynamical splitting* of the population along two eigenstate branches. The splitting is *instantaneous* only in the cases of exact one-photon ($n = 1$) and two-photon ($n = 2$) resonances, since the non-adiabatic coupling is exactly zero. Thus we can calculate exactly the solution of the Schrödinger equation for the two-level effective Hamiltonian.

The one-photon resonance case induces an equal sharing of the dynamics along the two eigenstate branches, which allows one to recover the $\pi-$pulse formula

$$P_2 \equiv |\langle 2;-1|\,\psi\,(t_f)\rangle|^2 = \sin^2\frac{1}{2}\int_{t_i}^{t_f} dt\,|\Omega(t)|. \tag{2.59}$$

One can generalize it for the exact resonant case $n = 2$: one has (for α real)

$$\Delta(t) = S(t) = \alpha\mathcal{E}^2(t), \quad \Omega(t) = \beta\mathcal{E}^2(t),\ \beta = |\beta|e^{-i\varphi}, \tag{2.60}$$

and the effective Hamiltonian (2.51) written as

$$H(t) = \frac{\hbar}{2}\mathcal{E}^2(t)\begin{bmatrix} 0 & \beta \\ \beta^* & 2\alpha \end{bmatrix}. \tag{2.61}$$

At each time, the time independent unitary transformation (having on its column the dressed states $|\psi_+\rangle$ and $|\psi_-\rangle$)

$$T = \begin{bmatrix} \cos(\zeta/2) & -\sin(\zeta/2) \\ e^{i\varphi}\sin(\zeta/2) & e^{i\varphi}\cos(\zeta/2) \end{bmatrix}, \tag{2.62}$$

with

$$\tan\zeta = -\frac{|\beta|}{\alpha}, \quad 0 \le \zeta < \pi, \tag{2.63}$$

diagonalizes the Hamiltonian $H(s)$:

$$T^\dagger H(t) T = \begin{bmatrix} \lambda_+^{\mathcal{E}} & 0 \\ 0 & \lambda_-^{\mathcal{E}} \end{bmatrix} \equiv D(t), \tag{2.64}$$

with

$$\lambda_\pm^{\mathcal{E}} = \frac{\hbar}{2}\mathcal{E}^2\left(\alpha \pm \sqrt{\alpha^2 + |\beta|^2}\right). \tag{2.65}$$

This can be interpreted as the lifting of the degeneracy

$$|1;0\rangle = \cos(\zeta/2)\,|\psi_+\rangle - \sin(\zeta/2)\,|\psi_-\rangle\,, \tag{2.66a}$$

$$|2;-2\rangle = e^{-i\varphi}\left[\sin(\zeta/2)\,|\psi_+\rangle + \cos(\zeta/2)\,|\psi_-\rangle\right]. \tag{2.66b}$$

Since the population resides initially in the atomic state $|1\rangle$, one obtains a splitting of the dynamics along the two dressed states (with non equal weight in general):

$$|\psi(t)\rangle = \cos(\zeta/2)\exp\left[-\frac{i}{\hbar}\int_{t_i}^{t} du\,\lambda_+^{\mathcal{E}(u)}\right]|\psi_+\rangle - \sin(\zeta/2)\exp\left[-\frac{i}{\hbar}\int_{t_i}^{t} du\,\lambda_-^{\mathcal{E}(u)}\right]|\psi_-\rangle\,. \quad (2.67)$$

Note that Eq. (2.67) is exact, not an adiabatic approximation, since for the Hamiltonian (2.61) the nonadiabatic coupling is exactly zero. At the end of the pulse, the inverse mechanism of *instantaneous recombination of population* occurs at the *creation of degeneracy*

$$|\psi(t_f)\rangle = \left[\cos\gamma(t_f) + i\frac{\alpha}{\sqrt{\alpha^2+|\beta|^2}}\sin\gamma(t_f)\right]|1;0\rangle - i\frac{e^{i\varphi}|\beta|}{\sqrt{\alpha^2+|\beta|^2}}\sin\gamma(t_f)\,|2;-2\rangle\,, \quad (2.68)$$

with the phase

$$\gamma(t_f) = \frac{1}{2\hbar}\int_{t_i}^{t_f} du\,\left[\lambda_+^{\mathcal{E}(u)} - \lambda_-^{\mathcal{E}(u)}\right] = \frac{1}{2}\sqrt{\alpha^2+|\beta|^2}\int_{t_i}^{t_f} dt\,\mathcal{E}^2(t). \quad (2.69)$$

It can be interpreted as an interference of the two branches, with relative weight determined by $\gamma(t_f)$, which is equal to half the area between the two eigenvalues. One obtains the generalized two-photon $\pi-$pulse formula:

$$P_2 = \frac{|\beta|^2}{\alpha^2+|\beta|^2}\sin^2\left[\frac{1}{2}\sqrt{\alpha^2+|\beta|^2}\int_{t_i}^{t_f} dt\,\mathcal{E}^2(t)\right], \quad (2.70)$$

which means that if

$$\sqrt{\alpha^2+|\beta|^2}\int_{t_i}^{t_f} dt\,\mathcal{E}^2(t) = \pi, \quad (2.71)$$

one obtains the maximal population transfer to the state $|2;-2\rangle$. There is no complete transfer except in the limiting case $\alpha/|\beta| \to 0$. This can be interpreted by the fact that the dynamical Stark shift [the diagonal element of the Hamiltonian (2.61)] has moved away the states from the resonance. This process is not robust with respect to the pulse amplitude, since any deviation will in general change the area.

If one takes an area different from π, it leads to a final coherent superposition of states. For example, in the case of a one-photon process, one has [using formula (2.68) with $\alpha = 0$ and $\Omega = \beta\mathcal{E}$]

$$|\psi(t_f)\rangle = \cos\left(\int_{t_i}^{t_f} dt\,\frac{|\Omega(t)|}{2}\right)|1;0\rangle - ie^{i\varphi}\sin\left(\int_{t_i}^{t_f} dt\,\frac{|\Omega(t)|}{2}\right)|2;-1\rangle\,. \quad (2.72)$$

and the area $\int_{t_i}^{t_f} dt\,|\Omega(t)| = \pi/2$ leads to a superposition of states with equal sharing in probability

$$|\psi(t_f)\rangle = \frac{1}{\sqrt{2}}\left(|1;0\rangle - ie^{i\varphi}|2;-1\rangle\right). \quad (2.73)$$

Again, this creation of superposition of states is not robust with respect to the pulse amplitude. We will study in Section 3.4 a way to create a superposition of states whose coefficients are robust in probability (i.e. squared absolute value of the coefficients).

We have described the picture with the simplified effective two-level model (2.51). However, it is still valid in the more general case of a strong field resonant $n-$multiphoton ($n > 2$) process,

although the effective two-level model is rather inaccurate as already mentioned. In this case, one has to consider the full eigenenergies of the Floquet Hamiltonian that are relevant for the process (for example calculated numerically), denoted as $\lambda_+^{\mathcal{E}(t)}$ and $\lambda_-^{\mathcal{E}(t)}$, continuously connected to the degenerate energies $\lambda_+^{\mathcal{E}(t_i)} = \lambda_-^{\mathcal{E}(t_i)} = E_1 = E_2 - n\hbar\omega$. The associated Floquet states, which in general depend on the pulse amplitude, are denoted $\left|\psi_+^{\mathcal{E}(t)}\right\rangle$ and $\left|\psi_-^{\mathcal{E}(t)}\right\rangle$. The splitting of the dynamics along the two branches in this case is not instantaneous but in general dynamical. The splitting does not necessarily coincide with the lifting of the degeneracy. We assume here that it occurs however approximately *instantaneously* at a time $t_s > t_i$ (associated with the complex coefficients denoted a_+ and a_- such that $|a_+|^2 + |a_-|^2 = 1$), and that before this time, the solution is first shifted adiabatically into the Floquet state that is continuously connected to the initial one [58]:

$$|\psi(t_s)\rangle \simeq \exp\left(-\frac{i}{\hbar}\int_{t_i}^{t_s} du\, \lambda_-^{\mathcal{E}(u)}\right)\left|\psi_1^{\mathcal{E}(t_s)}\right\rangle \tag{2.74a}$$

$$\simeq \exp\left(-\frac{i}{\hbar}\int_{t_i}^{t_s} du\, \lambda_-^{\mathcal{E}(u)}\right)\left(a_+\left|\psi_+^{\mathcal{E}(t_s)}\right\rangle + a_-\left|\psi_-^{\mathcal{E}(t_s)}\right\rangle\right), \tag{2.74b}$$

where we have denoted before the splitting of the dynamics, for $t < t_s$, the Floquet states $\left|\psi_1^{\mathcal{E}(t)}\right\rangle$ and $\left|\psi_2^{\mathcal{E}(t)}\right\rangle$, continuously connected respectively to $|1;0\rangle$ and $|2;-n\rangle$, and assumed associated to the eigenenergies respectively $\lambda_-^{\mathcal{E}(t)}$ and $\lambda_+^{\mathcal{E}(t)}$. These two branches are next *followed adiabatically* if the pulse envelopes are slow enough, which gives (up to an irrelevant global phase):

$$|\psi(t)\rangle \simeq a_+ \exp\left(-\frac{i}{\hbar}\int_{t_s}^{t} du\, \lambda_+^{\mathcal{E}(u)}\right)\left|\psi_+^{\mathcal{E}(t)}\right\rangle + a_- \exp\left(-\frac{i}{\hbar}\int_{t_s}^{t} du\, \lambda_-^{\mathcal{E}(u)}\right)\left|\psi_-^{\mathcal{E}(t)}\right\rangle. \tag{2.75}$$

When the pulse later falls, the dynamics goes through the inverse process of recombination which occurs symmetrically at time $t'_s = t_f - t_s$ (if we assume a symmetric envelope) such that

$$\left|\psi_+^{\mathcal{E}(t'_s)}\right\rangle = a_+^*\left|\psi_1^{\mathcal{E}(t'_s)}\right\rangle - a_-\left|\psi_2^{\mathcal{E}(t'_s)}\right\rangle, \tag{2.76a}$$

$$\left|\psi_-^{\mathcal{E}(t'_s)}\right\rangle = a_-^*\left|\psi_1^{\mathcal{E}(t'_s)}\right\rangle + a_+\left|\psi_2^{\mathcal{E}(t'_s)}\right\rangle. \tag{2.76b}$$

The resulting final transfer can be written as [58, 60]

$$P_2 \simeq 4\,|a_+ a_-|^2 \sin^2\left[\frac{1}{2}\int_{t_s}^{t_f - t_s} du\, \left(\lambda_+^{\mathcal{E}(u)} - \lambda_-^{\mathcal{E}(u)}\right)\right]. \tag{2.77}$$

Since in general the relative distance $\lambda_+^{\mathcal{E}} - \lambda_-^{\mathcal{E}}$ between the eigenenergies is small at the beginning and at the end of the pulse (before the splitting of the population and after the recombination), the formula is well approximated by

$$P_2 \simeq 4\,|a_+ a_-|^2 \sin^2\left[\frac{1}{2}\int_{t_i}^{t_f} du\, \left(\lambda_+^{\mathcal{E}(u)} - \lambda_-^{\mathcal{E}(u)}\right)\right]. \tag{2.78}$$

Thus the transfer probability depends on (i) the way in which the population is split and recombined and (ii) the difference of the dynamical phases. In the context of complete transfer, the process has been named generalized or multiphoton π-pulse and has been tested numerically for

a five-photon resonance in a Morse potential [58]. This formula (2.78) also displays generalized Rabi oscillations.

We remark that this multiphoton process, like the one-photon process described by Eq. (2.59) and the two-photon process described by (2.70), are not robust with respect to the pulse area.

2.6.3 Intermediate quasi-resonant regimes – Dynamical splitting of population

Here we consider the intermediate quasi-resonant regime (for the one-photon quasi-resonant process), defined as

$$\tau\Delta \sim 1. \tag{2.79}$$

This leads to a lifting (or creation) of a quasi-degeneracy, and adiabaticity is not satisfied at early times, but only at asymptotic times. In this case, the unitary transformation T (2.62) is time dependent and as a consequence the splitting of population is not instantaneous and leads to a non trivial dynamics. It has been first studied numerically in, for example, [60, 61], and more systematically in [56].

Here we summarize the resultats obtained in this paper. We constructe formulas characterizing the dynamics at asymptotic times beyond the lifting of quasi-degeneracy, assuming adiabatic evolution along the two branches. Pulses with power-law, smooth exponential, and Gaussian rising are studied. We show that in the case of pulses with amplitude growing linearly in time, the problem of the lifting of quasi-degeneracy can be interpreted as a half Landau-Zener process [62].

Considering an early lifting of quasi-degeneracy, a late creation of quasi-degeneracy, and an adiabatic evolution in between, we have applied these results to obtain the approximate lineshape (i.e. the transition probability as a function of the detuning for a given pulse) of various pulsed resonant excitation with a very good approximation. We have recovered in particular with these tools the well-known lineshape for secant hyperbolic pulses (Demkov-Rosen-Zener formula) [63, 64] and determined quite precisely the lineshape for trigonometric pulses.

Note that the lineshape for Gaussian pulses has been recently calculated approximately using the Dykhne-Davis-Pechukas approach [65].

Here we follow the notation of Section 2.4 (but with a single pulse, not a loop, a constant detuning $\Delta(s) = \Delta_0 > 0$ and $\varphi = 0$). We assume that the time $t = T_0$ is *a characteristic time beyond which the evolution of the system is adiabatic*, i.e. without population transfer between adiabatic states. Our goal is to find the population transfer during the characteristic time *before* adiabaticity. We define the scaled time with respect to it: $s \equiv t/T_0$. We consider the following models of coupling between the initial s_i and a final time s_f:

(i) power law rising

$$\Omega(s) = \begin{cases} \Omega_0 s^n, \ \tau \geqslant s_i \\ 0, \ s < s_i, \end{cases} \tag{2.80}$$

with $s_i = 0$, $s_f \gtrsim 1$ for an integer $n \geq 1$,

(ii) smooth exponential rising

$$\Omega(s) = \Omega_0 e^s \tag{2.81}$$

with $s_i \to -\infty$, $s_f \gtrsim 0$, and

(iii) smooth Gaussian

$$\Omega(s) = \Omega_0 e^{-s^2} \tag{2.82}$$

with $s_i \to -\infty$ and $s_f \to +\infty$.

We assume $\Omega(s) \geq 0$. We moreover consider for the pulse rising the initial conditions at time s_i: $B_-(s_i) = 1$, $B_+(s_i) = 0$.

Adiabaticity beyond $s \sim 1$ requires

$$2T_0 \left[\Delta_0^2 + \Omega_0^2\right]^{1/2} \gg n. \tag{2.83}$$

for a power law coupling, and $\Delta_0 \ll \Omega_0$ with $T_0\Omega_0 \gg 1$ for exponential and Gaussian couplings.

Lifting of quasidegeneracy by linearly rising coupling

The initial condition $A_-(s_i) = B_-(s_i) = 1$, $A_+(s_i) = B_+(s_i) = 0$ leads to the amplitudes of the adiabatic states

$$A_\pm(s) \quad \rightsquigarrow \quad \frac{1}{\sqrt{2}} \left(a \mp b e^{\mp i\varphi}\right) e^{\mp i(\chi_0 + \eta_d(s))} \tag{2.84a}$$

$$\equiv \quad \sqrt{p_\pm}\; e^{\mp i(\chi_\pm + \eta_d(s))} \tag{2.84b}$$

with the transition probabilities

$$p_\pm = \frac{1}{2}\left|a \mp b e^{i\varphi}\right| = \frac{1}{2}\left(1 \mp \sqrt{1 - e^{-\pi\omega^2}}\cos\varphi\right), \tag{2.85}$$

$$\varphi = \arg\Gamma\left(1 - i\frac{\omega^2}{4}\right) - \arg\Gamma\left(\frac{1}{2} - i\frac{\omega^2}{4}\right) + \frac{\pi}{4}, \tag{2.86}$$

$$\omega = \frac{T_0\Delta_0}{\sqrt{2T_0\Omega_0}}, \tag{2.87}$$

$$a = \frac{1}{\sqrt{2}}\sqrt{1 + e^{-\pi\omega^2/2}},\; b = \frac{1}{\sqrt{2}}\sqrt{1 - e^{-\pi\omega^2/2}}, \tag{2.88}$$

(where Γ denotes the Gamma–function) and the phases

$$\chi_\pm = \chi_0 + \arg\left(a \mp b e^{i\varphi}\right), \tag{2.89}$$

$$\chi_0 = \arg\Gamma\left(\frac{1}{2} - i\frac{\omega^2}{4}\right) - \frac{\omega^2}{4}\left(1 - \ln\frac{\omega^2}{4}\right), \tag{2.90}$$

$$\eta_d(s) = \frac{T_0}{\hbar}\int_0^s ds\,\lambda_+(s) = \frac{T_0}{2}\int_0^s ds\,\sqrt{\Delta_0^2 + \Omega_0^2 s^2}. \tag{2.91}$$

This result is asymptotically exact. One can interpret $\sqrt{p_\pm}\exp\left(\pm i\chi_\pm\right)$ as the probability amplitudes of the adiabatic states from the initial bare state $|-\rangle$ resulting from the *lifting of degeneracy* and the *splitting of the population*. This splitting is accompanied by phase shifts $\pm\chi_\pm$. The additional phases $\pm\eta_d(\tau)$ given by the time integral of the adiabatic eigenvalues are thus the *dynamical phases* of the process.

At $s = 1$, we have observed already a precision of many digits both in population and phase.

One essential result is that the adiabatic populations $p_\pm$ and the phases $\chi_\pm$ *depend only on* ω [Eq. (2.87)]. The phases χ_+ and χ_- go asymptotically to $-\pi/2$ and 0 respectively for large ω. One can remark that χ_- is not very different from zero after the lifting of degeneracy for any detuning. This trend has been numerically checked to occur for any n.

Lifting of quasi-degeneracy by exponentially rising coupling

In the adiabaticity region where the population of the eigenstates is time independent, with the initial condition $A_-(s_i) = B_-(s_i) = 1$, $A_+(s_i) = B_+(s_i) = 0$ at $s_i \to -\infty$, we obtain the amplitudes of the adiabatic states

$$A_\pm(s) \rightsquigarrow \sqrt{p_\pm}\; e^{i(\xi \mp \zeta(s))} \tag{2.92}$$

with the transition probabilities

$$p_- = \frac{1}{1+e^{-\pi\varpi}}, \quad p_+ = \frac{e^{-\pi\varpi}}{1+e^{-\pi\varpi}}, \tag{2.93}$$

the instantaneous dimensionless pulse half-area (which is in fact an instantaneous Rabi frequency half-area)

$$\zeta(s) = \frac{T_0}{2}\int_{-\infty}^{s} ds'\,\Omega(s') = \frac{T_0}{2}\Omega_0 e^s, \tag{2.94}$$

the dimensionless detuning

$$\varpi = T_0\Delta_0 \tag{2.95}$$

and the phase

$$\xi = \arg\Gamma\left(\frac{1}{2} + i\frac{\varpi}{2}\right) + \varpi\ln 2 - \frac{\varpi}{2}\ln 2\zeta(s_i). \tag{2.96}$$

(In practice, s_i is to be taken as a finite large negative number.) The phase ξ of the amplitudes is a *common* phase for the resulting superposition of adiabatic states. There is no additional relative phase shift during the lifting of degeneracy.

It is remarkable that the transition probabilities *depend only on the detuning* $\Delta_0 T_0$ (and not on Ω_0). Moreover the preceding dynamical phase is here replaced by a pulse area.

Lifting of quasidegeneracy by power law rising coupling

Asymptotic analysis and perturbation theory allows us to obtain

$$A_{n,\pm}(s) \rightsquigarrow \sqrt{p_{n,\pm}}\; e^{\mp i(\chi_{n,\pm}+\eta_n(s))} \tag{2.97}$$

with the transition probabilities

$$p_{n,\pm} \equiv |A_{n,\pm}|^2 = \frac{1}{2}\left(1 \mp \sqrt{1-e^{-\pi\omega_n^2}}\cos\varphi_n\right), \tag{2.98}$$

$$\varphi_n = \arg\Gamma\left(1 - i\frac{\omega_n^2}{4}\right) - \arg\Gamma\left(\frac{1}{2} - i\frac{\omega_n^2}{4}\right) + \frac{\pi}{4}, \tag{2.99}$$

with

$$\omega_n \equiv T_0\Delta_0\left(\frac{1}{T_0\Omega_0}\right)^{\frac{1}{n+1}} \frac{\sqrt{2}}{[2(n+1)]^{n/(n+1)}} \frac{\Gamma\left(\frac{n+2}{2(n+1)}\right)}{\Gamma\left(\frac{2n+1}{2(n+1)}\right)}. \tag{2.100}$$

generalizing the ω of the linear rising, and the phases

$$\chi_{n,-} = \frac{\sin\left(\frac{\pi}{2}\frac{2n+1}{n+1}\right)}{\sin\left(\frac{\pi}{2}\frac{n+2}{n+1}\right)}\chi_{n,0} + \arg\left(a_n + b_n e^{i\varphi_n}\right), \tag{2.101}$$

$$\chi_{n,+} = \chi_{n,0} + n\arg\left(a_n - b_n e^{i\varphi_n}\right), \tag{2.102}$$

$$\chi_{n,0} = \arg\Gamma\left(\frac{1}{2} - i\frac{\omega_n^2}{4}\right) - \frac{\omega_n^2}{4}\left(1 - \ln\frac{\omega_n^2}{4}\right), \tag{2.103}$$

$$a_n = \frac{1}{\sqrt{2}}\sqrt{1 + e^{-\pi\omega_n^2/2}},\ b_n = \frac{1}{\sqrt{2}}\sqrt{1 - e^{-\pi\omega_n^2/2}}, \tag{2.104}$$

$$\eta_n(s) = \frac{T_0}{2}\int_0^s ds\,\sqrt{\Delta_0^2 + \Omega_0^2\tau^{2n}}. \tag{2.105}$$

It is remarkable that the amplitude depends essentially on ω_n (and also on the dynamical phase $\eta_n(s)$).

Lifting of quasidegeneracy in two-photon processes

The preceding analysis gives arguments to explain that for the two-photon process [i.e. with a time-dependent diagonal Shark shift in Eq. (2.51)], one expects to be able to compensate (at least partially) the Stark shift and to populate completely the excited state for a well chosen Δ_0 (time-independent). Such compensation has not yet been systematically studied.

2.7 Diabatic versus adiabatic dynamics around eigenenergy crossings and avoided crossings

As mentioned above, an avoided crossing can result from a chirping process or from a dynamical resonance induced by a field. An avoided crossing appears *locally* in the spectrum between two dressed states. One considers in general that the dynamics is *globally* adiabatic with respect to the other states in the subspace spanned by the dressed states forming the avoided crossing. The adiabatic approximation might fail *inside this subspace* when the dynamics encounters this avoided crossing.

If the coupling between the two dressed eigenvectors is zero, the eigenvalue crossing appears as a true crossing. This means that the branches ignore each other and the adiabatic approximation still holds through the true crossing.

If the coupling is different from zero, the dynamics can either *follow* the avoided crossing (*adiabatic* evolution), *cross* it (*diabatic* evolution) or partially cross it, depending on the speed of the dynamics with respect to the shape of the avoided crossing.

We assume that the model depends on one slow time-dependent parameter, denoted $r(t)$, and that the shape of the avoided crossing as a function of r is well described around the avoided crossing $r = r_c$ (occurring at time $t = t_c$) by its width h and its curvature C (see Fig. 2.2). We choose the parametrization such that $r_c = 0$. The eigenenergies read

$$\lambda_\pm^r = \pm h\sqrt{1 + \left(\frac{r}{\delta r}\right)^2}. \tag{2.106}$$

The curvature is defined by

$$C = \left|\frac{\partial^2\lambda_\pm}{\partial r^2}(r=0)\right| = \frac{h}{(\delta r)^2}. \tag{2.107}$$

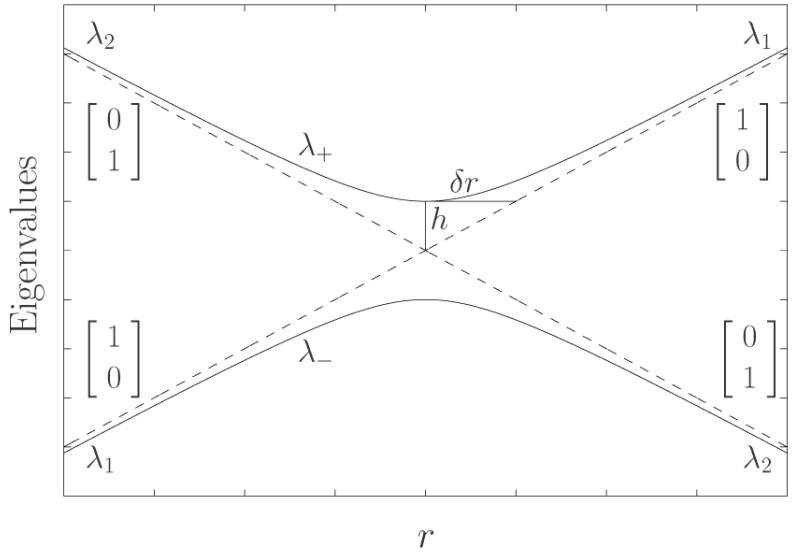

FIG. 2.2 - *Diagram of an avoided crossing of width* $2h$ *and of curvature* $C = h/(\delta r)^2$.

We label these two continuous branches by the instantaneous Floquet states $\psi_-^{r(t)}$ and $\psi_+^{r(t)}$. The two eigenvalues $\lambda_\pm^r$ can be deduced from an effective local dressed Hamiltonian

$$H_{\text{eff}} = h \begin{bmatrix} r/\delta r & 1 \\ 1 & -r/\delta r \end{bmatrix}, \tag{2.108}$$

in the basis

$$\psi_1 \equiv \psi_-^{r(t\to-\infty)} \equiv \begin{bmatrix} 1 \\ 0 \end{bmatrix}, \quad \psi_2 \equiv \psi_+^{r(t\to-\infty)} \equiv \begin{bmatrix} 0 \\ 1 \end{bmatrix}. \tag{2.109}$$

We can approximately characterize the dynamics by linearizing it in time around the avoided crossing: $r(t) = \dot{r}_c(t - t_c)$ and apply the Landau-Zener formula [66, 67] to calculate the probability to jump from the branch ψ_- to ψ_+ [26]:

$$P_{-\to+} = \exp\left(-\pi \frac{h \times \delta r}{\dot{r}_c}\right). \tag{2.110}$$

The asymptotic transition probability $P_{-\to+}$ is higher for (i) a thinner avoided crossing, (ii) a steeper curvature and (iii) a faster passage.
An avoided crossing gives rise to three qualitatively different regimes, that we can analyze considering the system starting in the initial state $\psi(t \to -\infty) = \psi_1$:

(a) If the speed is slow enough ($\dot{r}_c \ll h \times \delta r$), the dynamics is *adiabatic*, i.e. $P_{-\to+} \approx 0$ (meaning that the system goes into the state ψ_2 far after the avoided crossing);

(b) If the speed is fast enough ($\dot{r}_c \gg h \times \delta r$), the dynamics is *diabatic*, i.e. $P_{-\to+} \approx 1$ (meaning that the system stays in the state ψ_1 far after the avoided crossing);

(c) Any intermediate speed leads to a sharing of the dynamics into the two branches, which gives rise afterwards to two dynamical states which have their own adiabatic evolution.

Formula (2.110) defines thus the efficiency of the diabatic passage. We remark that the Landau-Zener formula gives the information for the whole range of gap distances, from the limit of exact crossings to widely separated ones.

If we apply this analysis locally in the Floquet spectrum, it provides the matching between the adiabatic evolution far from any avoided crossings and a local adiabatic or diabatic behavior around them.

We conclude that the only unfavorable situation (with respect to the robustness) is the intermediate regime in which the population is split among the branches. In systems encountered in applications there are often many levels that display exact and avoided crossings of different sizes. In order to have an adiabatic transfer concentrated on a single branch, it is required to choose the adiabatic speed in such a way that the population either goes completely across (in narrow avoided crossings) or completely stays in the same branch by going slowly enough at wide avoided crossings. *This gives a strategy for the design of adapted laser pulses.*
We remark that the preceding argument is based on the hypothesis that successive avoided crossings, involving the same or different branches, can be treated sequentially, independently of each other. There are cases where several avoided crossings interfere with each other, and the simple sequential Landau-Zener analysis does not apply (see for example [68]).

Chapter 3

Topology of the quasienergy surfaces - Elementary processes of population transfer

In order to achieve a given population transfer between the initial and target states by adiabatic passage, one has additionally to develop a global picture showing the possible paths that link these states, to design the appropriate field parameters as a function of time which will allow the desired adiabatic passage. We will describe how these connectivity properties of the Floquet states are determined by the topology of the quasienergy surfaces as a function of the time-dependent external field parameters [69, 70].

Adiabatic passage can result in a robust population transfer if one uses adiabatic variations of at least two *effective* parameters of the total laser fields. They can be the amplitude and the detuning of a single laser (chirping) or the amplitudes of two delayed pulses [stimulated Raman adiabatic passage (STIRAP), see [71] for a review]. The different eigenenergy surfaces are connected to each other by conical intersections, which are associated with resonances (which can be either zero field resonances or dynamical resonances appearing beyond a threshold of the the field intensities). The positions of these intersections determine the possible sets of paths that link an initial state and the different target states. The paths can be classified into topological equivalence classes. Two paths are topologically equivalent if one can be deformed into the other without cutting it nor leaving the surfaces. All paths linking the initial and target states that are in the same topology class are equivalent in the adiabatic limit. The topological aspect is the key of the robustness of the process in the sense that the final transfer does not depend on the precise shapes or areas of the laser pulses nor on precise tuning of laser frequencies.

The topology of the surfaces is essentially determined by the resonances, which produce avoided crossings of surfaces and conical intersections. When the surfaces do not interact (zero coupling), one can also observe one-dimension intersections. The main ingredients of adiabatic transport are a *global adiabatic passage* along *one* eigenstate combined with *local diabatic evolution* near conical intersections (or with local adiabatic evolution through the exact conical intersections). We will illustrate these properties using several simple examples.

We finally analyze the influence of a very few oscillations in a pulse. We show in a two-level system with the topological tools that the appearance of multiphoton resonances due to the broadening of the spectrum constitutes the limitation of the adiabatic Floquet theory.

3.1 Topology of adiabatic passage by a chirped pulse and SCRAP

The concept of the topology of adiabatic passage can be illustrated in the simple model of an effective two-level atom interacting with a one-photon or two-photon near-resonant pulse in the two-photon RWA [see Section 6.2.2 and the Hamiltonian (6.61)]

$$H(t) = \frac{\hbar}{2} \begin{bmatrix} 0 & \Omega(t) \\ \Omega(t) & 2\Delta(t) \end{bmatrix}, \tag{3.1}$$

where $\Omega(t)$ (assumed here a positive real) stands for a one- or two-photon Rabi frequency of a pump laser and $\Delta(t) = \Delta_0(t) + S(t)$ is the sum of $\Delta_0(t)$, the detuning from the one- or two-photon resonance, and $S(t)$ the dynamical Stark shift produced by the other states. One can consider two types of processes occurring in this effective two-level system:

(a) *Direct chirping*: the detuning from the resonance $\Delta_0(t)$ is time dependent due to an active sweeping of the laser frequency (see e.g. Ref. [72] for an effective two-photon chirping). If one considers moreover a one-photon chirp, the dynamical Stark shift $S(t)$ can be neglected.

(b) *Stark chirped rapid adiabatic passage (SCRAP)*: the quasi-resonant laser frequency (pump laser) is not chirped (the detuning Δ_0 is time independent). The effective chirping results from a total dynamical Stark shift $S(t) = S_S(t) + S_P(t)$, with $S_S(t)$ due to an auxiliary laser field (non resonant with any levels of the system), referred to as a Stark laser [73, 74] and $S_P(t)$ due to the pump laser itself. If one considers a one-photon quasi-resonance for the pump laser, the dynamical Stark shift $S_P(t)$ can be neglected.

The processes associated to this Hamiltonian (3.1) can be completely described in the diagram of the two eigensurfaces

$$\lambda_{\pm}(\Omega, \Delta) = \frac{\hbar}{2} \left(\Delta \pm \sqrt{\Omega^2 + \Delta^2} \right) \tag{3.2}$$

which represent the eigenenergies of (3.1) as functions of the instantaneous effective Rabi frequency Ω and the detuning Δ (see Fig. 3.1). All the quantities are normalized with respect to a characteristic detuning denoted $|\Delta_{\text{in}}|$. They display a conical intersection at $\Omega = 0, \Delta = 0$ induced by the crossing of the lines corresponding to the states $|1; 0\rangle$ and $|2; -1\rangle$ for $\Omega = 0$ and varying Δ. In the plane $\Omega = 0$, the states $|1; 0\rangle$ and $|2; -1\rangle$ do not interact. The crossing of these states in this plane $\Omega = 0$ can be seen consequently as a *mute (or passive) resonance*. Thus *adiabatic passage through the intersection or diabatic passage near the intersection leaves the system in the same state.* The way of passing around or through this conical intersection is the key of the successful transfer. Three generic curves representing all the possible passages with a negative initial detuning $-|\Delta_{\text{in}}|$ are shown in Fig. 3.1. Note that the three other equivalent curves with a positive initial detuning have not been drawn. The path (a) corresponds to a direct chirping of the laser frequency from the initial detuning $-|\Delta_{\text{in}}|$ to the final one $+|\Delta_{\text{in}}|$. The paths (b) and (c) correspond to SCRAP with $\Delta_0 = -|\Delta_{\text{in}}|$ for the case of a one-photon resonant pump. For the path (b), while the quasi-resonant pump pulse is off, another laser pulse (the Stark pulse, which is far from any resonance in the system) is switched on and induces positive Stark shifts $S(t) > 0$ (the Stark pulse frequency is chosen with this aim). The Stark pulse makes thus the eigenstates get closer and induces a resonance with the pump frequency . This resonance is mute since the pump pulse is still off, which results in the true crossing in the diagram. The pump pulse is switched on after the passage through

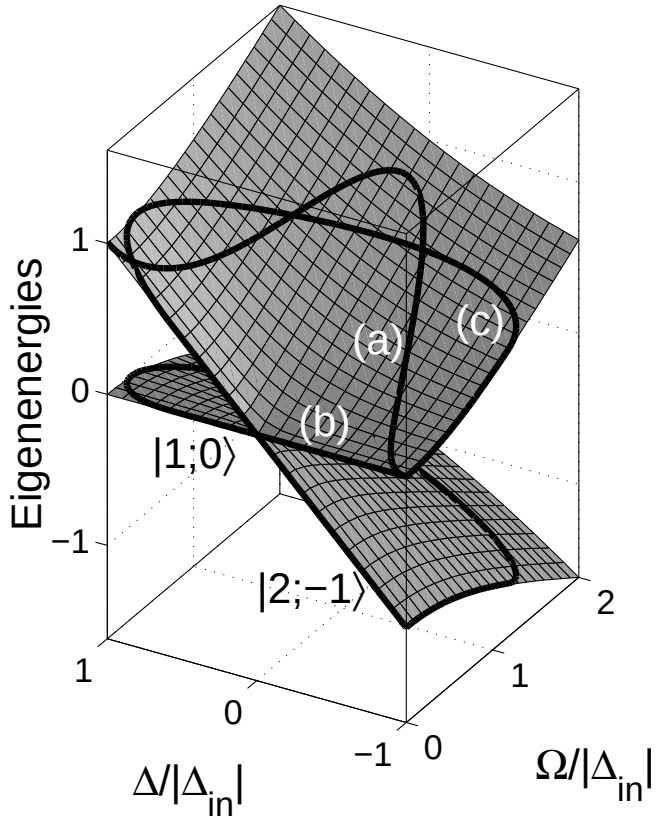

FIG. 3.1 - *Surfaces of eigenenergies (in units of $|\Delta_{in}|$) as functions of $\Omega/|\Delta_{in}|$ and $\Delta/|\Delta_{in}|$ (dimensionless). Three different paths (all starting from the state $|1;0\rangle$, $\Delta = -|\Delta_{in}|$ and $\Omega = 0$), denoted (a), (b) and (c) are depicted: (a) corresponds to a direct chirping, and (b) and (c) to SCRAP.*

the crossing while the Stark pulse decreases. This induces this time the passage through the non-mute resonance, generally characterized by an avoided crossing (which is located behind the true crossing in Fig. 3.1, see also Fig. 3.2b). Finally the pump pulse is switched off. As shown in the diagram, the adiabatic following of the path (b), combining the passage through the true crossing and through an avoided crossing, induces the complete population transfer from state $|1\rangle$ to state $|2\rangle$. The path (c) is similar to the path (b) but with the pulse sequence reversed: It leads exactly to the same effect. In this case, the pump pulse is indeed switched on first (making the eigenstates repel each other as shown in the diagram) before the Stark pulse $S(t) > 0$, which is then switched off after the pump pulse.

In summary, the three paths (a), (b) and (c) represent fully adiabatic passage from state $|1;0\rangle$ to state $|2;-1\rangle$; (a) passes around the conical intersection, (b) and (c) pass both once around the conical intersection and once through it.

We remark that the topology gives information on the dynamics for purely adiabatic passage. For real pulses of finite duration one has to complement these information with the analysis of the effects of non-adiabatic corrections.

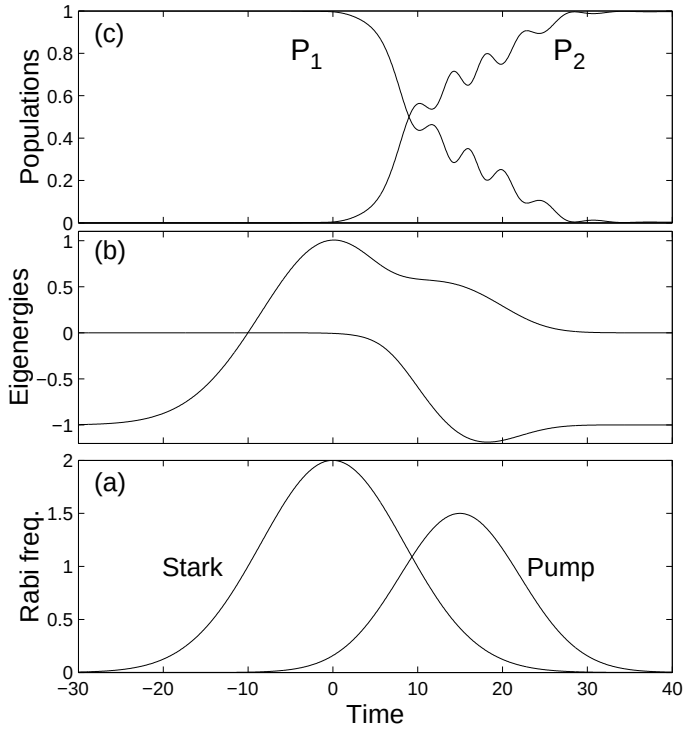

FIG. 3.2 - *Numerical calculation illustrating the SCRAP process with Gaussian pulses for the pulse peaks* $\Omega_0/|\Delta_{in}| = 1.5$, $S_0/|\Delta_{in}| = 2$, *the delay* $t_d|\Delta_{in}| = 15$, *and the pulse lengths* $\tau_p|\Delta_{in}| = 10$, $\tau_s|\Delta_{in}| = 12$ *(corresponding approximately to the path (b) of Fig. 3.1): (a) Population histories* $P_n(t) = |\langle n|\psi\rangle|^2$ *for* $n = 1, 2$ *as a function of time in units of* $1/|\Delta_{in}|$. *Population transfer* $P_2(\infty)$ *to the bare state* $|2\rangle$ *is nearly complete. (b) The associated eigenenergies* $\lambda_\pm/\hbar$ *(3.2) in units of* $|\Delta_{in}|$. *(c) The Rabi frequencies* $\Omega(t)$ *and* $S(t)$ *(in units of* $|\Delta_{in}|$*) respectively associated to pump and Stark pulses.*

3.2 Robustness of adiabatic passage as a consequence of the topological properties of the eigensurfaces

The process (a) is robust with respect to fluctuations of the two parameters since it is based on the passage of the dynamics around the conical intersection. Thus neither a precise path nor any phase condition are required. Adiabaticity conditions have additionally to be fulfilled for the success of a path. They are here given by (2.56). In the next subsection, we discuss optimized paths that minimize this nonadiabatic loss.

The processes (b) and (c) require an additional analysis around the crossing when the dynamics slightly misses it. One has to consider the neighborhood of the conical intersection as a thin avoided crossing. In this case, the dynamics meets locally a thin avoided crossing instead of an exact crossing. This avoided crossing has to be passed *diabatically* for the success of the process. The Landau-Zener analysis of Section 2.7 gives an estimation of the efficiency of the diabatic passage through Eq. (2.110) approximating the local dynamics around an avoided crossing with the linear time-dependent detuning $\Delta(t) = \dot{\Delta}(t_c)(t - t_c) \equiv \dot{\Delta}_c(t - t_c)$ and the coupling $\Omega(t) = \Omega(t_c) \equiv \Omega_c$, with t_c the time when the avoided crossing is passed. The condition

to achieve the diabatic passage locally can thus be formulated as

$$\dot{\Delta}_c \gg \pi\Omega_c^2/2. \tag{3.3}$$

Thus adiabatic passage in multi-level systems can be considered in general as *global adiabatic passage combined with local diabatic evolutions near conical intersections*. In multi-level systems, near a conical intersection, where one considers a local ideal diabatic evolution, it is essential that the evolution also be adiabatic with respect to the other states.

The peak amplitudes, the delay between the two fields and the pulse shapes are chosen such that the conditions (2.56) and (3.3) are met in the concerned regions. Detailed conditions to achieve diabatic and adiabatic passage can be found in [74, 75] for the example of delayed Gaussian pulses.

We remark that if condition (3.3) is not satisfied, which is the case if one misses the conical intersection in an intermediate regime ($\Omega_c^2 \approx \dot{\Delta}_c$), the Landau-Zener formula shows that the dynamics splits the population into the two surfaces near the intersection. This gives rise afterwards to two states which will have their own adiabatic evolution.

In Fig. 3.2, we have performed a numerical calculation of the dynamics corresponding to the path (b) and which confirms the preceding analysis. We have solved the time dependent Schrödinger equation: $i\partial\psi/\partial t = (H/\hbar)\psi$ in units of a characteristic detuning $|\Delta_{\rm in}|$, with Gaussian pulses for the pump and Stark lasers of respective characteristic length τ and τ_s: $\Omega(t) = \Omega_0 \exp[-(t-t_d)^2/\tau^2]$ $S(t) = S_0 \exp[-t^2/\tau_s^2]$. The pump is time-shifted by t_d. Fig. 3.2b clearly shows a crossing followed by the avoided crossing. Using Gaussian pulses (which are never zero) imply that we never have true crossings. However, the delay is chosen such that one has a diabatic passage through the thin avoided crossing which thus appears as a true crossing in Fig. 3.2b for the scale of the dynamics. We have used $\tau_p|\Delta_{\rm in}| = 10 \gg 1$ and $\tau_s|\Delta_{\rm in}| = 12 \gg 1$ to ensure the adiabatic passage condition (2.57) far after the crossing.

3.3 Optimization of adiabatic passage

Since in real experiments the pulses are of finite area, it is useful to analyze the conditions that will *optimize* the adiabatic passage, i.e. the conditions that will allow one *to minimize the nonadiabatic losses* for models with simple pulse and chirp shapes. Adiabatic passage can be optimized by inspection of the eigenenergy surfaces as functions of the time-dependent parameters of the coupling. A contour plot of the difference of the eigenenergy surfaces exhibits *level lines*. In Fig. 3.3, we have displayed level lines (as contours) corresponding to the eigenenergy surfaces of Fig. 3.1. For this example, they are half circles given by

$$\Omega^2 + \Delta^2 = \Delta_0^2, \tag{3.4}$$

with radius Δ_0 and center $\Omega = 0$, $\Delta = 0$. The radius Δ_0 corresponds to the chirp width for a one-photon chirping process in a two-level atom.

In [55], it was shown, for a class of two-level models (with analytic pulses), that *the passage along these level lines in the adiabatic regime minimizes the non-adiabatic correction*. The analysis is based on the Dykhne-Davis-Pechukas (DDP) formula [45, 46, 48, 49]. The nonadiabatic correction that is minimized is the dominant contribution given by the DDP formula [55] (see Appendix D). Note that if the pulses have some discontinuities, they dominate the nonadiabatic loss [see Eq. (2.50)], and the level lines do not have any more the preceding optimal property.

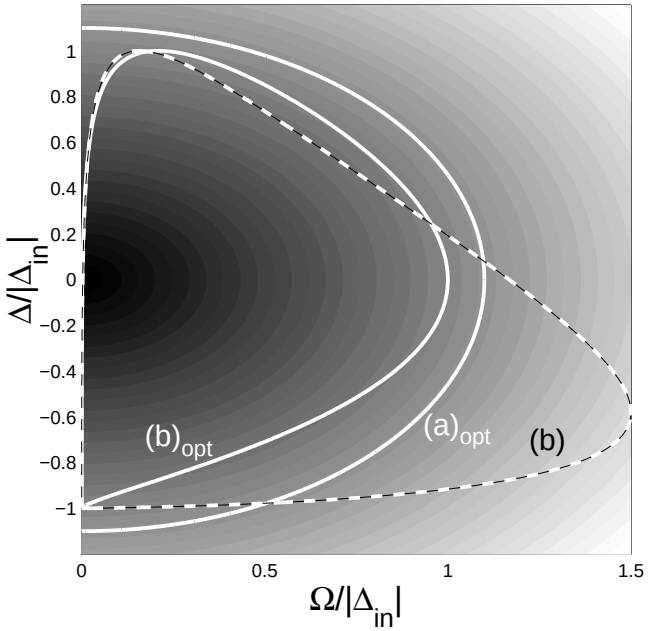

FIG. 3.3 - *Contour plot of the difference of the eigenenergies as a function of* $\Omega/|\Delta_{in}|$ *and* $\Delta/|\Delta_{in}|$. *Three different paths have be drawn: an optimal path* $(a)_{\rm opt}$ *(i.e. on a level line) corresponding to the topologically equivalent path (a) of Fig. 3.1 (with the final detuning* $\Delta_0 = 1.1|\Delta_{in}|$*), the path (b) corresponding to the numerical calculation of Fig. 3.2, and a path* $(b)_{\rm opt}$ *close to an optimal one corresponding to the numerical calculation of Fig. 3.5.*

This means that for a one-photon chirping process, if we choose the pulse shape $\Lambda(t)$, giving the Rabi frequency

$$\Omega(t) = \Omega_0 \Lambda(t), \tag{3.5}$$

the optimized detuning is then given by

$$\Delta(t) = \Delta_0 \frac{|\tau|}{\tau} \sqrt{1 - \Lambda^2(\tau)} \tag{3.6}$$

with

$$\Delta_0 = \Omega_0, \tag{3.7}$$

i.e. such that the distance between the quasienergies is kept constant and equal to $\hbar\Delta_0$ during the process.

The adiabatic criterion is thus reduced to the choice of a level line, which has to be far enough from the origin. For a one-photon chirping process, this corresponds to the choice of the chirp width Δ_0 such that

$$\Delta_0 \tau \gg 1, \tag{3.8}$$

with τ the length of the pulse, according to (2.57). In practice one observes that adiabaticity can be achieved for quite small pulse areas. For instance, for Gaussian pulses $\Lambda(t) = \mathrm{e}^{-t^2}$, the precise adiabaticity condition is $\Delta_0\tau \gg 1/\sqrt{2} \approx 0.7$. For the choice $\Delta_0\tau = 3.5 (= 5 \times 0.7)$, one observes a nonadiabatic loss in probability of only $P_1(+\infty) \approx 0.0015$ [55].

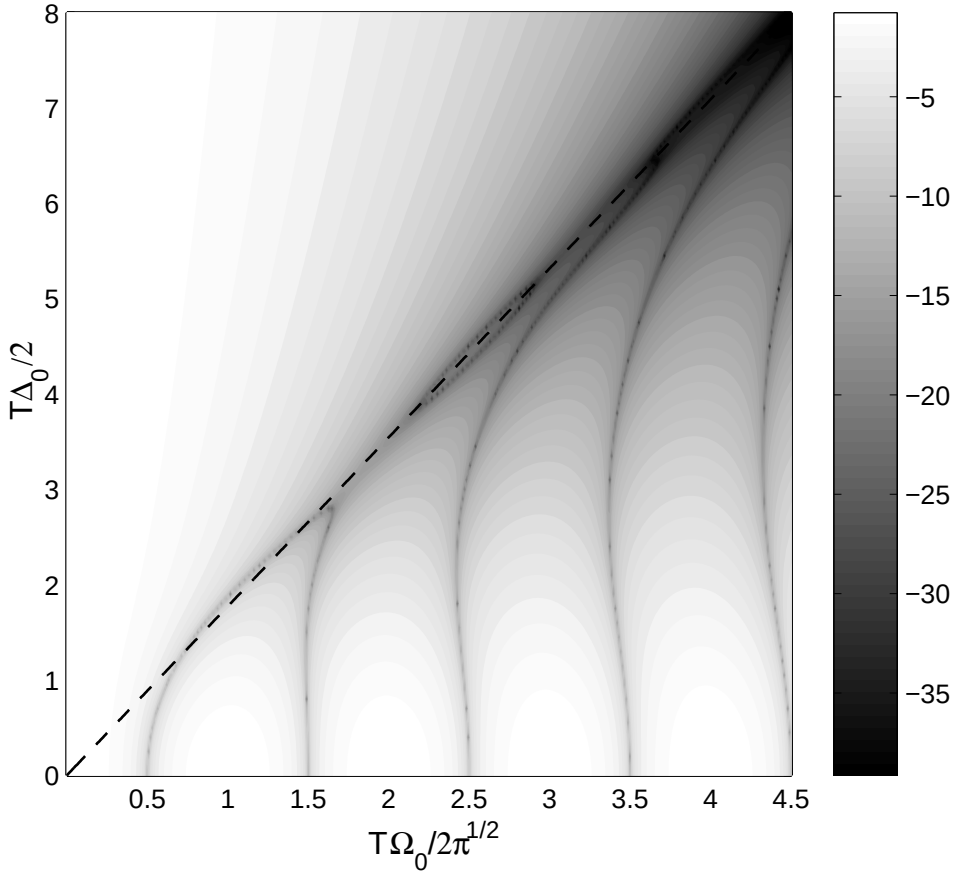

FIG. 3.4 - *For the gaussian pulse shape, contour map of natural logarithm of the non-adiabatic corrections at the end of the pulse* $\log[P_1(\infty)]$ *as a function of the normalized pulse area* $T\Omega_0/2\sqrt{\pi}$ *and the chirp widths* $T\Delta_0$ *(dimensionless). Darker points correspond to smaller* $P_1(\infty)$*. The dashed line correponds to the level lines* $\Delta_0 = \Omega_0$*.*

This is shown in Fig. 3.4 constructed for for various Rabi frequencies (3.5) and detunings (3.6). These trajectories in the space parameter correspond to half ellipses of minor and major axis of respective length $2\Delta_0$ and $2\Omega_0$, centered in $\Omega = 0$, $\Delta = 0$, and of respective equation

$$\left(\frac{\Omega}{\Omega_0}\right)^2 + \left(\frac{\Delta}{\Delta_0}\right)^2 = 1. \tag{3.9}$$

For $\Omega_0 = \Delta_0$, the trajectories are circles, i.e. on an optimal level line.

Although the choice of a one-parameter family of ellipses for comparison with the circular level lines is certainly not the most general one, it gives a simple and convenient way of illustrating the difference in transfer efficiency. Fig. 3.4 shows the contour plot of natural logarithm of the non-adiabatic corrections at the end of the pulse $\log[P_1(\infty)]$ as a function of $T\Delta_0$ and $T\Omega_0/\sqrt{\pi}$. We can observe for $\Delta_0 = 0$ (no chirp and zero detuning) oscillations of the population between 0 and 1, which correspond to the well known Rabi oscillations. In this model, the complete population transfer occurs exactly when Ω_0 satisfies

$$T\Omega_0 \int_{-\infty}^{+\infty} \Lambda(\tau) d\tau = T\Omega_0\sqrt{\pi} = (2k+1)\,\pi, \quad k \text{ integer}. \tag{3.10}$$

However this population transfer is not robust with respect to the pulse area as can be seen by the strong gradients of the population along $\Delta_0 = 0$ for the (dark) values of Ω_0 satisfying Eq. (3.10).

We remark that the contour lines emerging almost vertically from $\Delta_0 = 0$ can be interpreted as follows: for a given pulse area, the robustness is quite good with respect to Δ_0, close to $\Delta_0 = 0$, in this model.

The Rabi oscillations extend continuously for $\Delta_0 \neq 0$ with a larger width for larger $T\Delta_0$. For larger $T\Delta_0$, these oscillations become closer to zero in a large region: this corresponds to the robust almost complete population transfer of the adiabatic regime. As announced, the line of minimum $P_1(\tau_f)$ converges very fast to the level lines $\Omega_0 = \Delta_0$. We remark that the minimum pulse area leading to the (non-robust) transfer is obtained for $\Delta_0 = 0$ with $k = 0$ in Eq. (3.10).

It is important to note that *the level lines appear as a boundary between decreasing and oscillatory regimes for the non-adiabatic correction* $P_1(\tau_f)$.

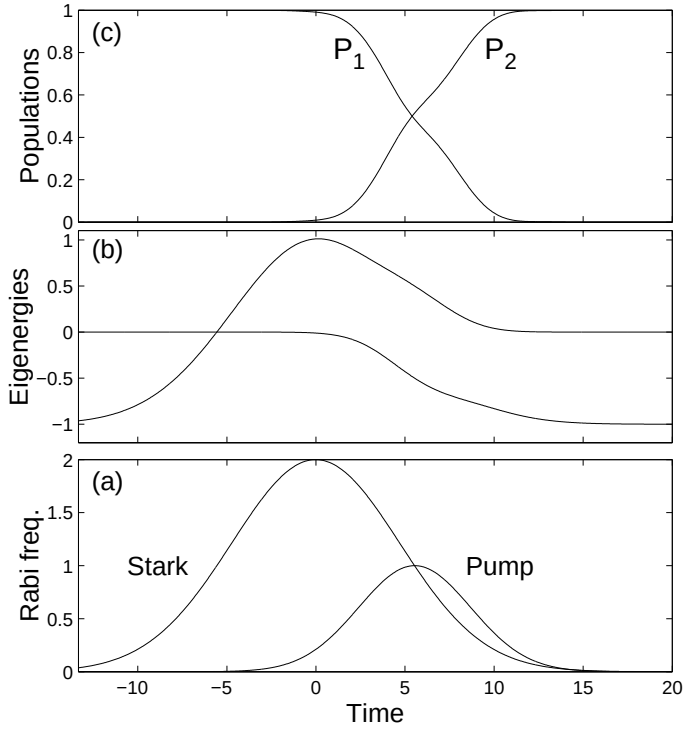

FIG. 3.5 - *As in Fig. 3.2 but for Gaussian pulses giving parameters close to optimal, corresponding to the path* $(b)_{\rm opt}$ *in Fig. 3.3: pulse peaks* $\Omega_0/|\Delta_{in}| = 1$, $S_0/|\Delta_{in}| = 2$, *the delay* $t_d|\Delta_{in}| = 8.3$, *and the (smaller) pulse lengths* $\tau_p|\Delta_{in}| = 6.7$ $\tau_s|\Delta_{in}| = 10$. *One can note the almost parallel eigenenergies after the crossing.*

This can be applied for the SCRAP process described above. We choose again Gaussian pulses, but with parameters such that the path is now close to the optimal one, i.e. a level line. The numerical calculation is shown in Fig. 3.5 and the associated path $(b)_{\rm opt}$ in Fig. 3.3. We can see that for smaller pulse areas compared to the ones used in Fig. 3.2, we obtain a better population transfer, which is moreover monotonic.

3.4 Resonant processes – Creation of coherent superposition of states – Half-SCRAP

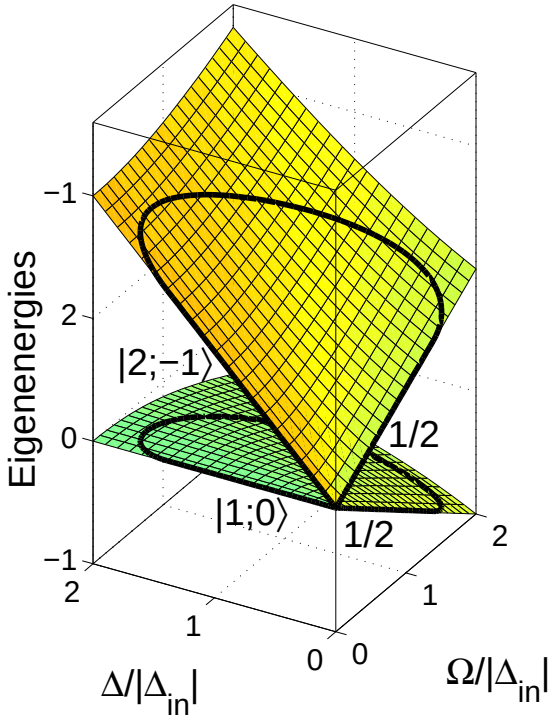

FIG. 3.6 - *Surfaces of eigenenergies (in units of $|\Delta_{in}|$) as functions of $\Omega/|\Delta_{in}|$ and $\Delta/|\Delta_{in}|$ for positive Δ. Two paths starting and ending at the conical intersection have been drawn. The coefficients $1/2$ refer to the equal sharing of the lifting of degeneracy in the $\Delta = 0-$plane. The dynamics, when starting in the $\Delta = 0-$plane, leads to this lifting of degeneracy involving the two paths, and ends with a superposition of states with equal sharing in absolute value and a relative dynamical phase. The dynamics, when starting in the $\Omega = 0-$plane, leads to a trivial lifting of degeneracy involving a single path [connected to the initial state, i.e. the lower (upper) path for the initial state $|1;0\rangle$ ($|2;-1\rangle$)], and ends with a superposition of states with equal sharing in absolute value and no relative dynamical phase.*

When the processes involve a zero-field resonance, one has to add the ingredient of lifting of degeneracy. This means that we have to consider the dynamics starting (or ending) near the conical intersection. This can be seen in Fig. 3.6 where the surfaces of Fig. 3.1 have been redrawn for positive detunings (case of a one-photon resonance). When the dynamics starts this way, it is characterized by two adiabatic paths, one on each surface. They will lead in general to coherent superpositions of states.

An essential point is that the result of the lifting (or creation) of degeneracy depends on the direction of the dynamics as already discussed in Section 2.6 for the case of one laser.

We study an exact resonant process ($\Delta_0 = 0$) starting (or ending) thus exactly at the conical intersection. We consider the cases that can be calculated analytically, with the Hamiltonian

$$H(t) = \frac{\hbar}{2} \begin{bmatrix} 0 & \Omega(t) \\ \Omega^*(t) & 2\Delta(t) \end{bmatrix} : \tag{3.11}$$

(i) a one-photon resonant pump (in this case, the Stark shift $S_P(t)$ can be neglected) giving the detuning $\Delta(t) = S_S(t)$ and the Rabi frequency $\Omega(t) = -\mu\mathcal{E}(t)/\hbar,\ \mu = |\mu|e^{-i\varphi}$;
(ii) a two-photon resonant pump giving $\Delta(t) = S_P(t)+S_S(t)$ with the effective two-photon Rabi frequency $\Omega(t) = \beta\mathcal{E}^2(t),\ \beta = |\beta|e^{-i\varphi}$ and its associated relative Stark shift $S_P(t) = \alpha\mathcal{E}^2(t)$.

We denote the eigenvalues

$$\lambda_\pm = \frac{\hbar}{2}\left(\Delta \pm \sqrt{\Delta^2 + |\Omega|^2}\right), \tag{3.12}$$

and the corresponding dressed eigenvectors $|\psi_\pm\rangle$. In the Δ (assumed positive) direction (i.e. for $\Omega = 0$), the lifting or creation of degeneracy occurs trivially along a unique surface:

$$|1;0\rangle = |\psi_-\rangle\,, \tag{3.13a}$$
$$|2;-n\rangle = |\psi_+\rangle\,. \tag{3.13b}$$

All the other directions lead to a lifting of degeneracy with a sharing of population into the two surfaces. The one-photon process gives in the Ω direction, or equivalently in the field-amplitude $\mathcal{E}$ direction:

$$|1;0\rangle = \frac{1}{\sqrt{2}}\left(|\psi_+\rangle - |\psi_-\rangle\right), \tag{3.14a}$$
$$|2;-1\rangle = \frac{e^{-i\varphi}}{\sqrt{2}}\left(|\psi_+\rangle + |\psi_-\rangle\right), \tag{3.14b}$$

which implies a lifting of the degeneracy occurring along the two surfaces with an equal weight. The lifting of degeneracy of the two-photon process in the field-amplitude $\mathcal{E}$ direction does not occur in the Ω direction due to the Stark shifts, as seen in Section 2.6:

$$|1;0\rangle = \cos(\zeta/2)\,|\psi_+\rangle - \sin(\zeta/2)\,|\psi_-\rangle\,, \tag{3.15a}$$
$$|2;-2\rangle = e^{-i\varphi}\left[\sin(\zeta/2)\,|\psi_+\rangle + \cos(\zeta/2)\,|\psi_-\rangle\right], \tag{3.15b}$$

with

$$\tan\zeta = -\frac{|\beta|}{\alpha}, \quad 0 \le \zeta < \pi. \tag{3.16}$$

The creation of degeneracy of the one-photon process is conversely given by

$$|\psi_+\rangle = \frac{1}{\sqrt{2}}\left(|1;0\rangle + e^{i\varphi}\,|2;-1\rangle\right), \tag{3.17a}$$
$$|\psi_-\rangle = \frac{1}{\sqrt{2}}\left(-\,|1;0\rangle + e^{i\varphi}\,|2;-1\rangle\right), \tag{3.17b}$$

and the one of the two-photon process by

$$|\psi_+\rangle = \cos(\zeta/2)\,|1;0\rangle + e^{i\varphi}\sin(\zeta/2)\,|2;-2\rangle\,, \tag{3.18a}$$
$$|\psi_-\rangle = -\sin(\zeta/2)\,|1;0\rangle + e^{i\varphi}\cos(\zeta/2)\,|2;-2\rangle\,, \tag{3.18b}$$

to which dynamical phases have to be added.

We analyze two kinds of paths which, starting in state $|1;0\rangle$, will lead to a coherent superposition of states:

(a) First, lifting of degeneracy in the Δ direction [according to (3.13a)] giving one dressed state involved in the dynamics, next adiabatic following on this dressed state along the lower surface with $\Omega \neq 0$ and finally creation of degeneracy for decreasing Ω [according to (3.17a) for the one-photon process and to (3.18a) for the two-photon process]. In Fig. 3.6, a particular path of the one-photon process has been drawn (i.e. creation of degeneracy for $\Delta = 0$), yielding a coherent superposition of states with equal weights in absolute value.

(b) First, lifting of degeneracy in a direction not parallel to the $\Omega = 0$ plane, which gives two dressed states involved in the dynamics [according to (3.14a) for the one-photon process and to (3.15a) for the two-photon process], next *independent* adiabatic following on these dressed states (along both the lower and upper surface) and finally creation of degeneracy in the Δ direction [according to (3.13)]. In Fig. 3.6, one can see the two path associated to this (one-photon) case, yielding also a coherent superposition of states with equal weights in absolute value.

These two cases are produced by two different sequences: respectively (a) first the Stark pulse and next the pump pulse (referred to as Stark-pump sequence), and (b) first the pump pulse and next the Stark pulse (referred to as pump-Stark sequence). The phases associated to the superposition of states resulting from these two different sequences are not identical. For the sequence Stark-pump, we start (at time t_i) with the lifting of degeneracy $|\psi(t_i)\rangle = |\psi_+\rangle$, which leads at the final time t_f to (up to an irrelevant global phase)

$$|\psi(t_f)\rangle = \cos(\zeta/2)\,|1;0\rangle + e^{i\varphi}\sin(\zeta/2)\,|2;-n\rangle\,. \tag{3.19}$$

For the sequence pump-Stark, we start with the lifting of degeneracy $|\psi(t_i)\rangle = \cos(\zeta/2)\,|\psi_+\rangle - \sin(\zeta/2)\,|\psi_-\rangle$. Using the adiabatic transport for each branch, the state solution reads at the end

$$|\psi(t_f)\rangle = \cos(\zeta/2)\,|2;-n\rangle - \mathrm{e}^{i\int_{t_i}^{t_f} ds\,(\lambda_+(s)-\lambda_-(s))}\sin(\zeta/2)\,|1;0\rangle\,. \tag{3.20}$$

Thus the two sequences lead to the same superposition in probabilities but with different phases. The sequence pump-Stark leads to an additional *non-robust* phase difference $\int_{t_i}^{t_f} ds\ [\lambda_+(s) - \lambda_-(s)]$ coinciding with the dynamical phase difference.

If one considers an initial coherent state for the photon field instead of a photon-number state, the superpositions of states have the additional optical phase, giving for (3.19)

$$|\phi(t_f)\rangle = \cos(\zeta/2)\,|1\rangle + e^{i\varphi}\sin(\zeta/2)\,\mathrm{e}^{-in\omega t}\,|2\rangle\,, \tag{3.21}$$

and for (3.20)

$$|\phi(t_f)\rangle = \cos(\zeta/2)\,\mathrm{e}^{-in\omega t}\,|2\rangle - \mathrm{e}^{i\int_{t_i}^{t_f} ds\,(\lambda_+(s)-\lambda_-(s))}\sin(\zeta/2)\,|1\rangle\,, \tag{3.22}$$

with $n = 2$ for the two-photon process.

This process leading to a coherent superposition of states has been suggested in [61] and named *half-scrap*, since it is very similar to the scrap process except it starts (or ends) in resonance.

The question of robustness with respect to the detuning for resonant processes has been studied in [56]. If one considers non exact one-photon resonance $\Delta \neq 0$, one obtains, by lifting of quasi-degeneracy, additional phases and amplitudes different from $1/\sqrt{2}$, that depend on the shape of the pulses. Referring to the notations of Subsection 2.6.3, one obtains that robustness with respect to the detuning is better for power law rising than for the exponential and Gaussian rising (better for small small and large Ω_0). Robustness with respect to the amplitude Ω_0 is

better for smoother rising (and better for the exponential rising, which is independent of Ω_0, than for the Gaussian rising, which is weakly dependent on Ω_0).

This half-Scrap could be generalized for a $n-$multiphoton process ($n > 2$) in a multi-level system, with the use of the full quasienergies and Floquet states (calculated numerically).

3.5 Topology of Stimulated Raman adiabatic passage (STIRAP) and STIRAP-like processes

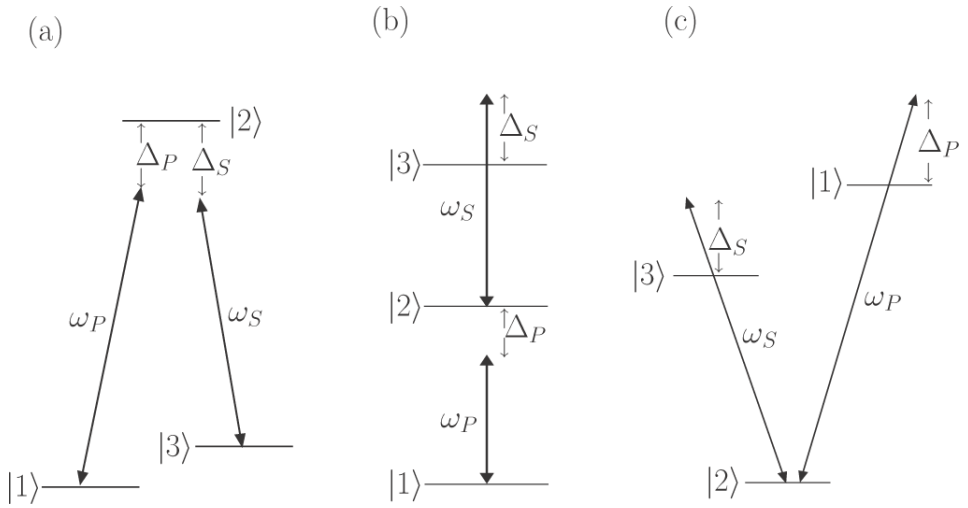

FIG. 3.7 - *Diagram of linkage patterns between three atomic states showing pump (P) and Stokes (S) transitions and the various detunings for (a) Λ, (b) ladder and (c) V systems.*

The adiabatic passage induced by two delayed laser pulses, the well known process of STIRAP [71], produces a population transfer in Λ systems (see Fig. 3.7a). The pump field couples the transition 1-2 and the Stokes field couples the transition 2-3. It is known that, with the initial population in state $|1\rangle$, a complete population transfer is achieved with delayed pulses, either (i) with a so-called counterintuitive temporal sequence (Stokes plulse before pump) for various detunings as identified in Refs [75, 76], or (ii) with two-photon resonant (or quasi-resonant) pulses but far from the one-photon resonance with the intermediate state $|2\rangle$, for any pulse sequence (demonstrated in the approximation of adiabatic elimination of the intermediate state [77]). Here we analyze the STIRAP process through the topology of the associated surfaces of eigenenergies as functions of the two field amplitudes. Our results are also valid for ladder and V systems. We consider the most general situation with a (small) two-photon detuning.

We also obtain the following results related to STIRAP: (i) We can explain the transfer of population to state $|3\rangle$ with intuitive (as well as with counterintuitive) specific quasi-resonant pulses *without invoking the approximation of adiabatic elimination.* (ii) With specific quasi-resonant pulses, we can *selectively* transfer the population to state $|2\rangle$ for an *intuitive* sequence or to state $|3\rangle$ for a *counterintuitive* sequence, and (iii) with an intuitive or counterintuitive sequence, we can *selectively* transfer the population to state $|2\rangle$ or to state $|3\rangle$ playing on the *detunings* and on the *ratio of the peak pulse amplitudes.*

We also analyze the counterpart of the preceding processes in V systems (see Fig. 3.7c): the initial population being in state $|2\rangle$, we show that with specific non-resonant pulses, (i) we

can *selectively* transfer the population to state $|1\rangle$ for an intuitive sequence or to state $|3\rangle$ for a counterintuitive sequence; (ii) we can *selectively* transfer the population to state $|1\rangle$ or to state $|3\rangle$ playing on the ratio of the peak pulse amplitudes.

The topology will allow us to classify all the possibilities of complete population transfer by adiabatic passage for a three-level system interacting with two delayed pulses, as it was done for the two-level system interacting with a chirped laser pulse.

The most general dressed Hamiltonian in the rotating wave approximation for these processes reads [71]

$$H(t) = \frac{\hbar}{2}\begin{bmatrix} 0 & \Omega_P(t) & 0 \\ \Omega_P(t) & 2\Delta_P & \Omega_S(t) \\ 0 & \Omega_S(t) & 2\left(\Delta_P - \Delta_S\right) \end{bmatrix}, \tag{3.23}$$

with $\Omega_j(t),\ j = P, S$ (assumed real and positive) the one photon Rabi frequencies associated respectively to the pump pulse (of carrier frequency ω_P) and the Stokes pulse (of carrier frequency ω_S). We have assumed that the states $|1\rangle$ and $|3\rangle$ have no dipole coupling and that spontaneous emission is negligibly small on the time scale of the pulse duration. The rotating wave approximation is valid if $\hbar\Omega_P(t) \ll |E_2 - E_1|$ and $\hbar\Omega_S(t) \ll |E_3 - E_2|$, where E_j, $j = 1, 2, 3$ are the energies associated to the bare states $|j\rangle$.

The detunings Δ_P and Δ_S are one-photon detunings with respect to the pump and Stokes frequencies respectively and

$$\delta = \Delta_P - \Delta_S \tag{3.24}$$

is the two-photon detuning.

For Λ, ladder and V systems (see respectively Fig. 3.7a, b and c), the one-photon detunings Δ_P, Δ_S are respectively defined as

$$\Lambda: \quad \hbar\Delta_P = E_2 - E_1 - \hbar\omega_P, \quad \hbar\Delta_S = E_2 - E_3 - \hbar\omega_S, \tag{3.25a}$$

$$\text{Ladder}: \quad \hbar\Delta_P = E_2 - E_1 - \hbar\omega_P, \quad \hbar\Delta_S = E_2 - E_3 + \hbar\omega_S, \tag{3.25b}$$

$$V: \quad \hbar\Delta_P = E_2 - E_1 + \hbar\omega_P, \quad \hbar\Delta_S = E_2 - E_3 + \hbar\omega_S, \tag{3.25c}$$

which determines the dressed basis in which the dressed Hamiltonian (3.23) has been written: respectively $\{|1;0,0\rangle, |2;-1,0\rangle, |3;-1,1\rangle\}$, $\{|1;0,0\rangle, |2;-1,0\rangle, |3;-1,-1\rangle\}$ and $\{|1;0,0\rangle, |2;1,0\rangle, |3;1,-1\rangle\}$. In the following, we consider the population of the atomic states.

In what follows we study the topology of the eigenenergy surfaces for various generic sets of the parameters. The topology depends on the detunings which determine the relative position of the energies at the origin. We study various *quasi-resonant* pulses in the sense that the detunings are smaller than or of the order of the associated peak Rabi frequencies, that is,

$$\Delta_P \lesssim \max_t(\Omega_P), \quad \Delta_S \lesssim \max_t(\Omega_S), \tag{3.26a}$$

$$\delta \lesssim \max_t(\Omega_P), \quad \delta \lesssim \max_t(\Omega_S). \tag{3.26b}$$

Such conditions ensure in particular the occurence of STIRAP processes, even without the strict two-photon resonance condition.

3.5.1 Transfer to a unique state

Allowing large enough amplitudes leads to three generic cases for $\delta > 0$ and three other cases for $\delta < 0$, which are equivalent by symmetry.

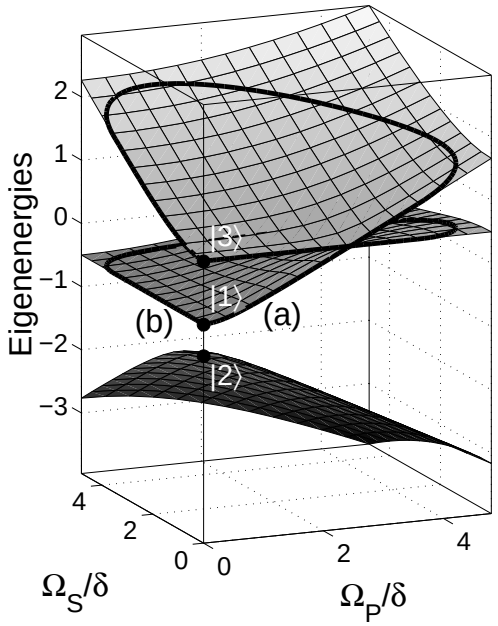

FIG. 3.8 - *Surfaces of eigenenergies (in units of δ) as functions of Ω_P/δ and Ω_S/δ when the dressed states (denoted λ_1, λ_2 and λ_3, respectively connected to E_1, E_2 and E_3 for fields off) are such that $\lambda_2 < \lambda_1 < \lambda_3$, with $\Delta_P = -\delta/2$ and $\Delta_S = -3\delta/2$, The paths (a) and (b) (constructed with delayed pulses of the same length and peak amplitude) correspond respectively to the intuitive and counterintuitive pulse sequences in Λ or ladder systems (for which the initial population resides in state $|1\rangle$).*

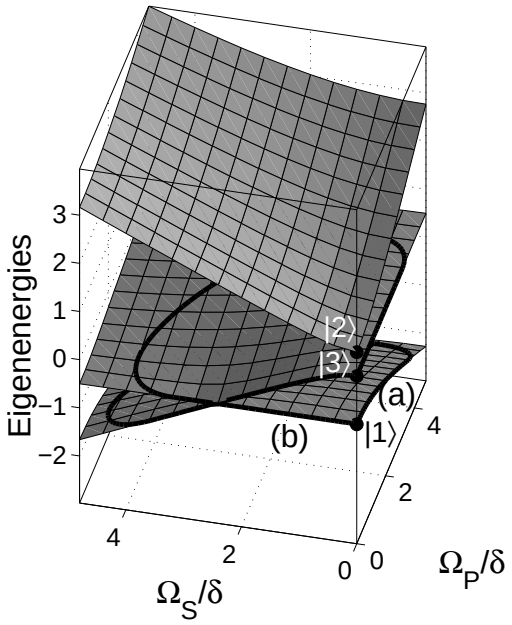

FIG. 3.9 - *Surfaces of eigenenergies (in units of δ) as functions of Ω_P/δ and Ω_S/δ for the case $\lambda_1 < \lambda_3 < \lambda_2$, with $\Delta_P = 3\delta/2$ and $\Delta_S = \delta/2$. The paths (a) and (b) (with pulses of the same length and peak amplitude) correspond respectively to the intuitive and counterintuitive pulse sequences in Λ or ladder systems.*

Two typical examples are displayed in Figs. 3.8 and 3.9. In both cases, the surface continuously connected to the state $|2\rangle$ is isolated from the two other surfaces which present a conical intersection for $\Omega_S = 0$ and for $\Omega_P = 0$, respectively. This crossing corresponds to a mute resonance as described above for chirping. (A resonance is called mute if the frequencies are in resonance but the corresponding coupling term is zero or small in the Hamiltonian).

The topologies shown on the respective figures 3.8 and 3.9 are generic for the condition

$$\Delta_P \Delta_S > 0, \tag{3.27}$$

with respectively

$$|\Delta_P| < |\Delta_S| \quad \text{and} \quad |\Delta_P| > |\Delta_S| \,. \tag{3.28}$$

In the following, we describe in detail the case of Fig. 3.8. For the process in Λ or ladder systems, where the initial population resides in state $|1\rangle$, two different adiabatic paths lead to the complete population transfer, depending on the pulse sequence. The path denoted (a) corresponds to an intuitive sequence for the rise of the pulses. The pump pulse is switched on first, making the levels connected to the states $|1\rangle$ and $|2\rangle$ repel each other (dynamical Stark shift) until the level connected to $|1\rangle$ crosses the level connected to $|3\rangle$. The Stokes pulse is switched on after the crossing. Next the two pulses can decrease in any order. The path (b) is associated to a counterintuitive sequence for the decrease of the pulses. The two pulses can be switched on in any order. The pump pulse has to decrease through the crossing when the Stokes pulse is already off. These two results are valid even without application of adiabatic elimination. The conditions of global adiabaticity are similar to the ones of the chirped frequency case (2.56). As discussed in Section 2.7, an analysis of the diabatic evolution near the conical intersections can be made locally with the Landau-Zener approximation (2.110).

The V systems are uninteresting in these cases since the final population comes back to the state $|2\rangle$ for any pulse sequence.

Another typical example is displayed in Fig. 3.10. The topology shown on this figure is generic for the condition

$$\Delta_P \Delta_S < 0. \tag{3.29}$$

In this configuration, two conical intersections involve the intermediate surface, one with the lower surface and the other one with the upper surface. This topology gives here more possibilities for transfer: *the combined choice of the pulse sequence and the ratio of the peak amplitudes allows the selective transfer into the two other states.*

Figure 3.10 shows that, for the process in Λ (or ladder) systems, two different adiabatic paths lead to different complete population transfers, depending on the pulse sequence. The path (a) corresponds to an intuitive pulse sequence (for the decrease of the pulses) and allows one to populate at the end the state $|2\rangle$. The Stokes and pump pulses can be switched on in any sequence and the pump pulse is switched off before the Stokes one. The path (b) corresponds to a counterintuitive pulse sequence (for the rise of the pulses) and allows one to populate at the end the state $|3\rangle$. The Stokes pulse is switched on before the pump and the Stokes pulse has to be switched off before the pump. We can thus selectively populate the states $|2\rangle$ or $|3\rangle$ provided the peak amplitudes are sufficiently strong to induce the adiabatic path to cross the intersection involved.

For the process in V systems, the paths (a) and (c) of Fig. 3.10 show the respective selective transfer into the states $|1\rangle$ or $|3\rangle$.

Figure 3.11 corresponds to the same topology of Fig. 3.10 but with a different path (a). Figure 3.11 shows that, for Λ (or ladder) systems, we can selectively populate the states $|2\rangle$

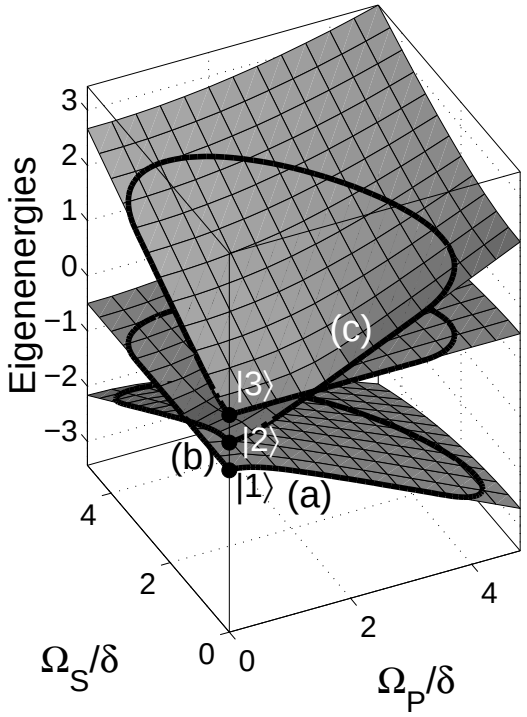

FIG. 3.10 - *Surfaces of eigenenergies (in units of δ) as functions of Ω_P/δ and Ω_S/δ for the case $\lambda_1 < \lambda_2 < \lambda_3$, with $\Delta_P = \delta/2$ and $\Delta_S = -\delta/2$. The paths (a) and (b) (with pulses of the same length and peak amplitude) correspond respectively to the intuitive (transfer to $|2\rangle$) and counterintuitive (transfer to $|3\rangle$) pulse sequences in Λ or ladder systems leading to the selective transfer. The paths (a) and (c) correspond to the selective transfer in V systems (for which the initial population resides in $|2\rangle$), respectively to $|1\rangle$ and $|3\rangle$.*

or $|3\rangle$ if the pulse sequences are designed differently in their order and their peak amplitude. Path (b) corresponds to path (b) of Fig. 3.10 and allows one to populate at the end the state $|3\rangle$. Path (a) corresponds to a longer pump pulse (still switched on after the Stokes pulse) of smaller peak amplitude which allows one to populate at the end the state $|2\rangle$. Note that we can obtain a similar path (a) with a counterintuitive pulse sequence and equal peak amplitudes if the detuning Δ_P is taken smaller so that the crossing for $\Omega_S = 0$ is pushed to a higher pump pulse amplitude Ω_P.

For V systems, Fig. 3.11 shows that this selectivity [paths (a) and (c)] also occurs (for any sequence of the pulses).

Figure 3.12 shows numerical calculations that illustrate some of the predictions of the above analysis. It displays the populations of the states $|2\rangle$ and $|3\rangle$ at the end of the pulses for intuitive and counterintuitive sequences with a large pulse area. The boundaries of the areas of efficient transfer (black areas) are predicted quite accurately by the topology analysis: They are determined by (i) the straight lines (thick full lines) $\Delta_P = 0$ and $\Delta_S = 0$ coming from the

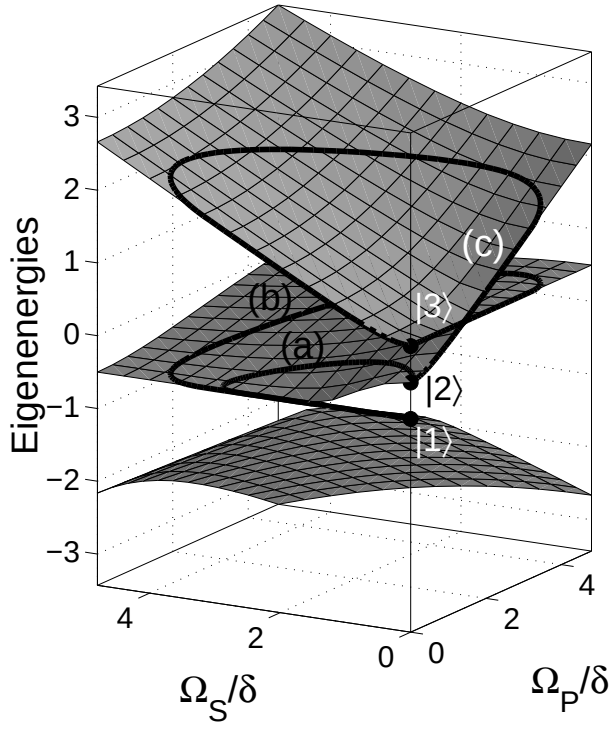

FIG. 3.11 - *Surfaces of eigenenergies (in units of δ) with the same parameters as Fig. 3.10 showing the selective transfer with pulses of different peak amplitudes and length. For counterintuitive sequences in Λ or ladder systems, the path (b) [corresponding to the path (b) of Fig. 3.10] shows the transfer to $|3\rangle$, and the path (a) (with pulses of different length and peak amplitude) characterizes the transfer to $|2\rangle$. The paths (a) and (c) correspond to the selective transfer in V systems.*

inequalities (3.27) and (3.29) and (ii) the branches of the hyperbolas (dashed lines)

$$\Delta_S = \Delta_P - \frac{(\Omega_{\max})^2}{4\Delta_P}, \tag{3.30a}$$

$$\Delta_P = \Delta_S - \frac{(\Omega_{\max})^2}{4\Delta_S}, \tag{3.30b}$$

which are determined from the positions of the conical intersections. Figure 3.12 shows that the efficiency of the robust population transfer to the states $|2\rangle$ or $|3\rangle$ is identical for the intuitive and counterintuitive sequences except in two regions: (i) areas bounded by $\Delta_P\Delta_S < 0$ and the branches of the hyperbolas, where the population is transferred in a robust way to state $|2\rangle$ for the intuitive sequence or to state $|3\rangle$ for the counterintuitive sequence and (ii) an area (smaller for longer pulse areas) near the origin where *non adiabatic effects* are strong for the intuitive sequence and where the population transfer depends precisely on the pulse areas of this intuitive sequence (see the comments below). *Non adiabatic effects*, which are smaller for larger pulse areas, also occur near the straight line boundary regions. *Non diabatic effects* arise as well near the hyperbolic boundaries.

For the concrete realization with finite pulses of moderate areas, we have to analyze the

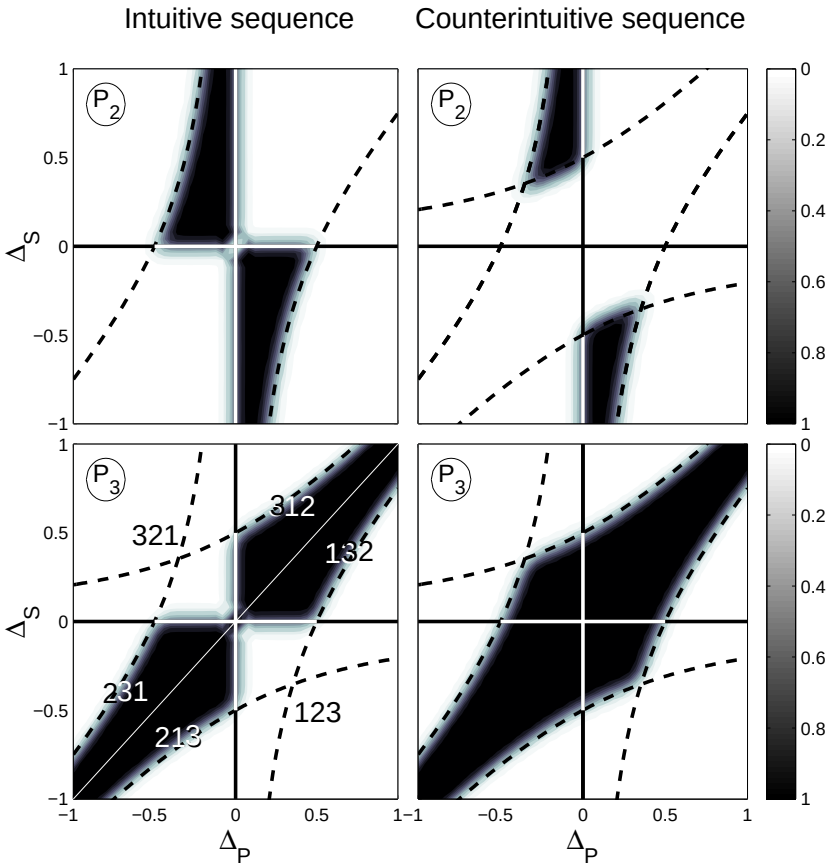

FIG. 3.12 - *Transfer efficiencies P_2 to $|2\rangle$ (upper row) and P_3 to $|3\rangle$ (lower row) as functions of the the detunings Δ_P and Δ_S (in units of $\Omega_{\max}$) at the end of the pulses for the intuitive (left column) and counterintuitive (right column) sequences of delayed sine-squared pulses with the same peak amplitude $\Omega_{\max}$ and a large temporal area $\Omega_{\max}\tau = 500$ (τ is the pulse length and the delay is $\tau/2$). The efficient population transfers are bounded by $\Delta_P = 0$ and $\Delta_S = 0$ (thick full lines) and the branches of hyperbolas (dashed lines). The areas bounded by the full lines are labelled by the cases 213, 132, 123, ... (These number sets are associated to the eigenenergies for zero field amplitudes from the smallest to the biggest, for example 213 means $\lambda_2 < \lambda_1 < \lambda_3$.) The three first ones correspond respectively to Figs 3.8, 3.9 and 3.10.*

precise influence of non adiabatic and non diabatic effects. We discuss here these non adiabatic effects referring to Fig. 3.8 supposing that the detunings are small enough with respect to the speed of the process to yield non adiabatic transitions:
In the intuitive case, at the beginning of the process, the states $|1\rangle$ and $|2\rangle$ are coupled by the pump pulse, and thus non adiabatic transitions can occur near the origin between the surfaces connected to $|1\rangle$ and $|2\rangle$. In the counterintuitive case, at the beginning of the process, state $|1\rangle$ is not coupled to the other levels and there are no non adiabatic transitions near the origin. At the end of the process, the adiabatic path ending in $|3\rangle$ is not coupled to the other levels, implying again absence of non adiabatic transitions near the origin. We thus recover the well known fact that resonant STIRAP (with very small detunings) is more favorable with a counterintuitive pulse sequence and leads to Rabi oscillations in the intuitive case.

3.5.2 Transfer to a coherent superposition of states

We study the various superposition of states that can be created by adiabatic passage in a robust way with respect to variations of the field amplitude, using the topological analysis with resonances of Section 3.4 (see also Section 2.6 for the case of one laser). This has been extensively studied in [78]. We assume that one starts (at time $t = t_i$) with a coherent state for the photon field and in the atomic state $|1\rangle$. We study here the $\Lambda-$system. Our results are easily extended to the other system (ladder and V), using the appropriate signs accompanying the field frequencies. We study the creation of a superposition of states at the final time $t = t_f$.

This can be analyzed with the help of Fig. 3.8, where we have taken $\Delta_P = 0$. The intuitive pump-Stokes sequence induces first a lifting of degeneracy with equal sharing between the dressed states $|\psi_+\rangle$ (the upper one, associated to the eigenenergy λ_+) and $|\psi_-\rangle$ (the lower one, associated to the eigenenergy λ_-) initially connected to $|1\rangle$ and $|2\rangle$. If we assume that the peak pump field amplitude is *beyond* the conical intersection, then the branches $|\psi_-\rangle$ and $|\psi_+\rangle$ respectively connect $-|2\rangle$ and $|3\rangle$ at the end. When $\Delta_S < 0$ (as in Fig 3.8), this leads at the end of the process to the coherent superposition with a dynamical phase (up to an irrelevant global phase)

$$|\psi(t_f)\rangle = \frac{1}{\sqrt{2}}\left[|3\rangle - \mathrm{e}^{i\int_{t_i}^{t_f} ds\,(\lambda_+(s)-\lambda_-(s))}\mathrm{e}^{-i\omega_S(t_i-t_f)}\,|2\rangle\right]. \tag{3.31}$$

When $\Delta_S > 0$, we obtain

$$|\psi(t_f)\rangle = \frac{1}{\sqrt{2}}\left[|3\rangle + \mathrm{e}^{-i\int_{t_i}^{t_f} ds\,(\lambda_+(s)-\lambda_-(s))}\mathrm{e}^{-i\omega_S(t_i-t_f)}\,|2\rangle\right]. \tag{3.32}$$

The counterintuitive Stokes-pump sequence leads to the transfer to the unique state $|3\rangle$.

If we assume that the peak pump field amplitude is *below* the conical intersection, then the branches $|\psi_-\rangle$ and $|\psi_+\rangle$ respectively connect $-|2\rangle$ and $|1\rangle$ at the end. This leads to coherent superpositions between the states $|1\rangle$ and $|2\rangle$.

If we have additionally $\Delta_S = 0$, the counterintuitive sequence gives the standard STIRAP (transfer to state $|3\rangle$) and the intuitive sequence induces interferences of the branches at the end of the processes, that do not lead to robust superposition of states.

We now analyze Fig. 3.9, where we assume $\Delta_S = 0$. When $\Delta_P > 0$ (as in Fig 3.9), this leads at the end of the process to the coherent superposition without dynamical phase (but still with the optical phase):

$$|\psi(t_f)\rangle = \frac{1}{\sqrt{2}}\left[|3\rangle - \mathrm{e}^{-i\omega_S(t_i-t_f)}\,|2\rangle\right]. \tag{3.33}$$

When $\Delta_S > 0$, we obtain

$$|\psi(t_f)\rangle = \frac{1}{\sqrt{2}}\left[|3\rangle + \mathrm{e}^{-i\omega_S(t_i-t_f)}|2\rangle\right]. \tag{3.34}$$

The topological analysis thus shows that *it is not possible with two quasi-resonant delayed lasers to end in a superposition of states between the lowest states* $|1\rangle$ *and* $|3\rangle$ *in a robust way.* We can remark that in [79], it has been shown that one can create by adiabatic passage such a superposition, however in a non-robust way in general (except when used in degenerate sub-magnetic Zeeman states with appropriate elliptic fields), by modifying the end of the STIRAP process (with the counterintuitive sequence), maintaining a fixed ratio of Stokes and pump pulse amplitudes.

The numerical calculations of Figure 3.12 show the predicted superpositions of states at $\Delta_P = 0$ and $\Delta_S = 0$. They also show that a final superposition between $|1\rangle$ and $|3\rangle$ is possible on some pieces of the hyperbolas (dashed lines). However they are not robust since the equation of these hyperbolas (3.30) depend on the peak field amplitudes.

3.5.3 Ground-state superpositions

The preceding analysis shows thus that a ground state superposition is topologically inaccessible. In [78], we have shown that using an additional Stark laser, we are able to modify the topology of the energy surfaces (creation or suppression of a conical intersection) in order to design such ground state superpositions.

In Subsections 8.2.2 and 8.2.3, we recall other existing strategies to generate ground-state superpositions, which additionally do not transiently populate the excited state.

3.6 Adiabatic Floquet theory for ultrashort pulses

We address here the influence of a small number of oscillations in the pulse so defined as an ultrashort pulse, and analyze the applicability of the adiabatic Floquet theory and the tools developed above. We show in the simple two-level model that these tools are still well adapted even for a very few cycles in the pulse. A particular care must be taken with the resonances since such an ultrashort pulse has a broad effective spectrum.

It is important to note that *the correspondence (2.7) is exact independently of the number of oscillations in the pulse.* We study below the consequences of this correspondence for an ultrashort pulse.

A small number of oscillations in the pulse signifies a broadening of the spectrum instantaneously available (i.e. not chirped) around the mean frequency. We study here the population transfer by adiabatic passage through the one-photon resonance. We define the number of oscillations in a pulse by the quantity

$$p := T\frac{\omega_{\text{eff}}}{2\pi} \tag{3.35}$$

with T the pulse length. Adiabatic passage requires in general as shown above $T\Omega_{\max} \gg 1$ giving $2\pi\Omega_{\max}/\omega_{\text{eff}} \gg 1/p$. If we take for instance $T\Omega_{\max} = 2\pi$, we have $\Omega_{\max}/\omega_{\text{eff}} = 1/p$. Thus the constraint of a few oscillations in the field implies that $\Omega_{\max}$ is of the same order as ω_{eff}. This condition $\Omega_{\max} \sim \omega_{\text{eff}}$ *prevents to apply the resonant approximation* and requires to take into account the full quasienergy operator.

We consider a two-level model, $|\pm\rangle$ of respective energy $\pm\omega_0/2$, driven by a pulsed and chirped field. The full Hamiltonian is in this case

$$H(\theta+g(t),t)=\frac{\hbar\omega_0}{2}\left[\begin{array}{cc}-1&0\\0&1\end{array}\right]+\hbar\Omega(t)\cos(\theta+g(t))\left[\begin{array}{cc}0&1\\1&0\end{array}\right], \tag{3.36}$$

with the atomic Bohr frequency $\omega_0>0$, the Rabi frequency $\Omega(t)=\mu\mathcal{E}(t)/\hbar$ (considered positive for simplicity), the dipole moment μ, the electric field envelope $\mathcal{E}(t)$ and its phase $\theta+g(t)$. The quasienergy operator reads:

$$K=-i\hbar\omega_{\rm eff}(t)\frac{\partial}{\partial\theta}+H(\theta,t),\quad \omega_{\rm eff}(t)=\dot{g}(t). \tag{3.37}$$

This operator when normalized by $\hbar\omega_0$ shows two independent parameters $\omega_{\rm eff}/\omega_0$ and Ω/ω_0. To make the connection with the resonant Hamiltonian, we apply a resonant transformation (see Chapter 5)

$$R=\left[\begin{array}{cc}1&0\\0&e^{-i\theta}\end{array}\right], \tag{3.38}$$

assuming that the mean frequency is one-photon quasi-resonant:

$$R^\dagger KR=-i\hbar\omega_{\rm eff}\frac{\partial}{\partial\theta}+\hbar\frac{\Delta-\omega_0}{2}\mathbb{1}_2+H_{\rm r}(t)+H_{\rm cr}(\theta,t) \tag{3.39}$$

with the dressed resonant Hamiltonian characterizing the one-photon resonance, the so-called rotating wave approximation Hamiltonian:

$$H_{\rm r}(t)=\frac{\hbar}{2}\left[\begin{array}{cc}-\Delta(t)&\Omega(t)\\\Omega(t)&\Delta(t)\end{array}\right], \tag{3.40}$$

the effective detuning

$$\Delta=\omega_0-\omega_{\rm eff} \tag{3.41}$$

and the "counter-rotating" (or anti-resonant) Hamiltonian

$$H_{\rm cr}(\theta,t)=\hbar\Omega(t)\left[\begin{array}{cc}0&e^{-2i\theta}\\e^{2i\theta}&0\end{array}\right]. \tag{3.42}$$

The associated semi-classical Hamiltonian is $H_{\rm r}(t)+\hat{H}_{\rm cr}(t)$ with

$$\hat{H}_{\rm cr}(t)=\frac{\hbar\Omega(t)}{2}\left[\begin{array}{cc}0&e^{-2i\left[\omega_0(t-t_i)-\int_{t_i}^t ds\,\Delta(s)\right]}\\e^{2i\left[\omega_0\tau(t-t_i)-\int_{t_i}^t ds\,\Delta(s)\right]}&0\end{array}\right]. \tag{3.43}$$

The dressed eigenelements in strong fields can be obtained from the numerical diagonalization of the Floquet Hamiltonian. Figure 3.13 shows two views of such numerical quasienergy surfaces (normalized with respect to ω_0) as a function of ω/ω_0 and Ω/ω_0. We denote here $\omega\equiv\omega_{\rm eff}$ for simplicity. The complete spectral information is contained in one Floquet zone composed of two surfaces inside a band of energy of width $\hbar\omega$. The other surfaces can be constructed using the periodicity of the spectrum: $\lambda_n=\lambda+n\omega$, for any (positive or negative) integer n, for a given surface λ. In Fig. 3.13 we display two surfaces composing one Floquet zone and an other shifted surface.

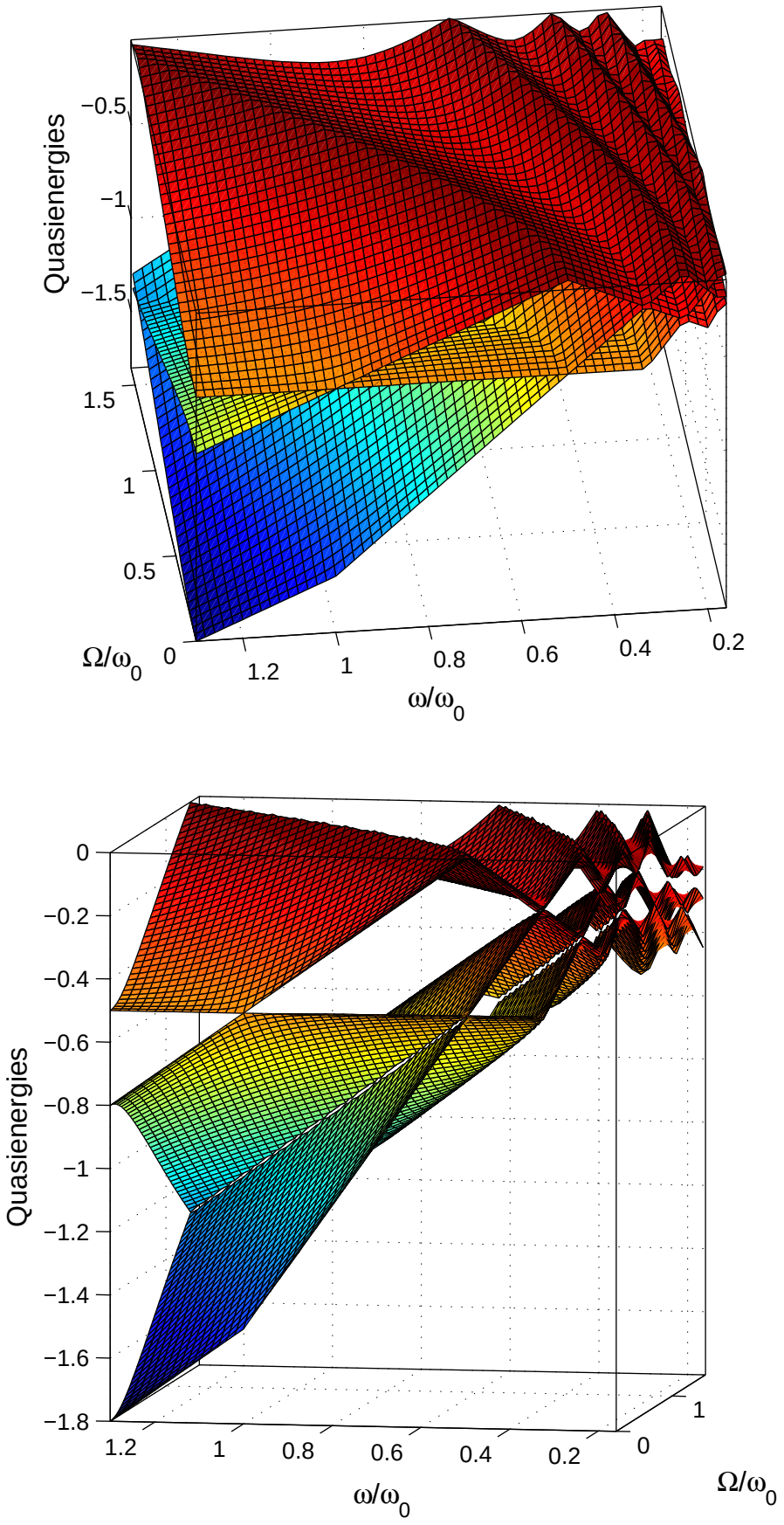

FIG. 3.13 - *Two views of the quasienergy surfaces (in units of ω_0) as functions of ω/ω_0 and Ω/ω_0 with the notation $\omega \equiv \omega_{\text{eff}}$.*

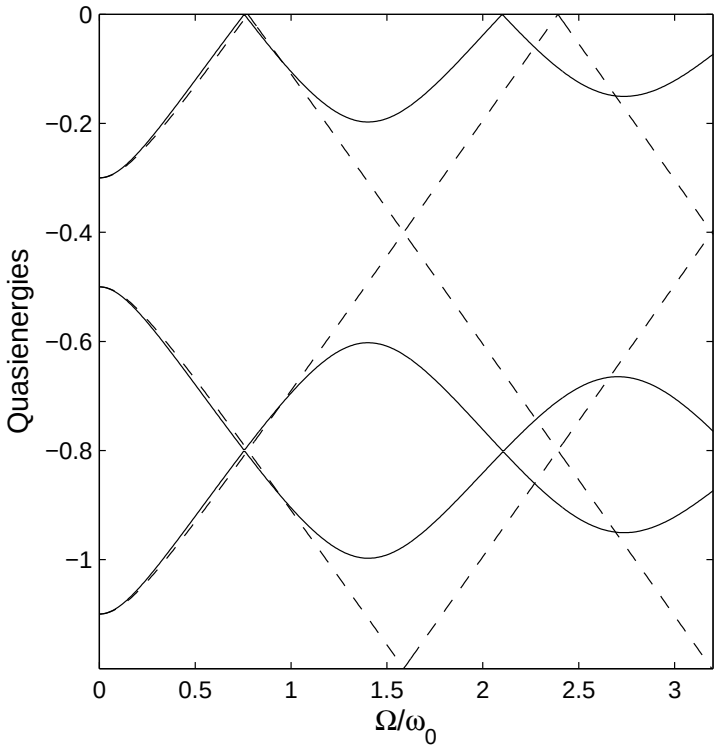

FIG. 3.14 - *Section (full lines) of the quasienergy surfaces of Fig. 3.13 as functions of* Ω/ω_0 *for* $\omega = 0.8\omega_0$ *(i.e.* $\Delta = 0.2\omega_0$*). The dashed lines are the quasienergies in the resonant approximation (here dressed with various numbers of photons). One can distinguish respectively the three-photon (five -photon) resonances as avoided crossings around* $\Omega = 1.4\omega_0$ *(*$\Omega = 2.7\omega_0$*).*

Around the one-photon resonance $\omega \approx \omega_0$ (for $\Omega \ll \omega_0$) one can recognize the surfaces of Fig. 3.1. For $\Omega = 0$, the horizontal line of energy $\lambda/(\hbar\omega_0) = -0.5$ corresponds to the lower state of the system. The crossing line corresponds to the upper state dressed with minus one photon.

One can distinguish in the plane $\Omega = 0$ resonances appearing as *crossings* at $\omega = \omega_0/(2k+1)$ with $k = 0, 1, 2\cdots$ For $\Omega \neq 0$, they become *avoided crossings*. For $\omega = \omega_0/(2k)$, we have exact crossings for any Ω, due to the particular symmetry of this model (one can see an example for $k = 1$). This means that only odd numbers of photons can be absorbed (or emitted) in such a system. The maxima of the upper surface correspond to crossings (for any Ω), and the valleys to avoided crossings (i.e. to resonances). One can observe that for increasing Ω, the position of the resonances are shifted in the direction of larger ω. This can be interpreted as a Stark shift of the states. This implies that moving along a straight line with $\omega \approx \omega_0$ for growing Ω allows one to cross dynamically the three-photon resonance. This is shown in Fig. 3.14. Larger Ω will allow one to cross next the five-photon resonance, and so on. The three-photon resonance represents thus a boundary that prevents the population transfer.

To achieve the population transfer, we suggest that one use level lines around the one photon resonance, while keeping a sufficient distance with the next three-photon resonance.

The labeling of the surfaces can be only local due to the multiple crossings. We denote around the one-photon resonance ($\omega \approx \omega_0$) respectively the upper (lower) surface as λ_+ (λ_-). Near the one-photon resonance, the surface λ_+ (λ_-) is connected to the state $|+, -1\rangle$ ($|-, 0\rangle$) (with the notation $|\pm, k\rangle$ for the state $|\pm\rangle$ dressed with k photon) for $\omega < \omega_0$ and to the state

$|-,0\rangle$ ($|+,-1\rangle$) for $\omega > \omega_0$.

The level lines around the one photon resonance correspond thus to the constant distances $|\lambda_+ - \lambda_-|$, as represented in Fig. 3.15 (left). The right part of Fig. 3.15 shows the level lines around the three-photon resonance.

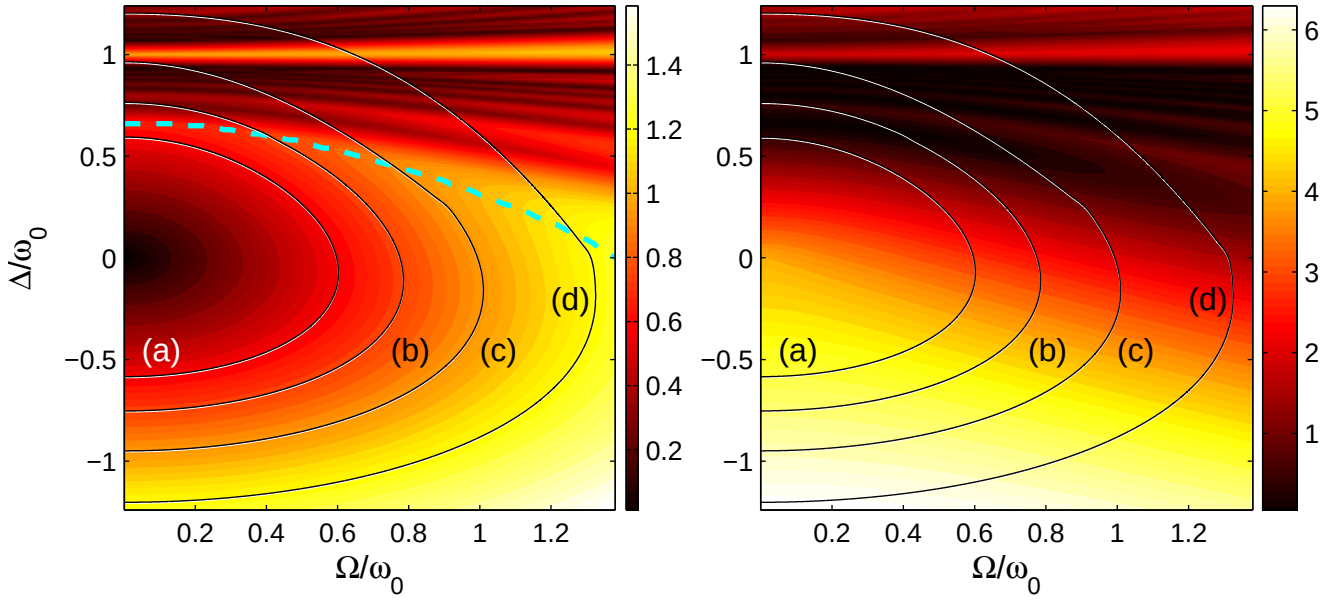

FIG. 3.15 - *Contour plot of $|\lambda_+ - \lambda_-|$ around the one-photon resonance (left), and around the three-photon resonance (right). Note the different scales between the two graphs. Four trajectories (a), (b), (c) and (d) are shown. The dashed line shows the position of the three-photon resonance.*

We use three different trajectories as shown in Fig. 3.15 around the one-photon resonance $\omega \approx \omega_0$, which gives for the dynamics $T\omega_0/2\pi \approx p$. We choose here roughly 5 oscillations in the pulse, i.e. $T\omega_0/2\pi \approx 5$ and Gaussian pulses

$$\Omega(t) = \Omega_{\max}\Lambda(t), \quad \Lambda(t) = e^{-(t/\tau)^2} \tag{3.44}$$

with the estimate $T \sim 2\pi\tau$ for the pulse duration giving $\tau\omega_0 \approx 5$.

The first trajectory (a) is a level line with $\Delta_0/\omega_0 = 0.6$, where $\Delta_0 \equiv |\Delta(\pm\infty)|$. The dynamics is such that $\tau\Delta_0 = 3$, which satisfies very roughly the adiabaticity condition [that we estimate from Section 3.3 as $\tau\Delta_0 \gg 0.7$, determined in the resonant approximation, see below Eq. (3.8)]. This trajectory slightly avoids the three-photon resonance. The dynamics is chosen to begin with $\Delta(-\infty) = \Delta_0$. (We have checked that we have the same final result if we start with $\Delta(-\infty) = -\Delta_0$.) It allows however a very efficient transfer as shown in Fig. 3.16.

The trajectories (b) and (c) follow in their lower parts a level line with $\Delta_0/\omega_0 = 0.76$ and $\Delta_0/\omega_0 = 0.96$ respectively and next cross the three-photon resonance. The trajectory (b) still allows an efficient transfer, but not (c) which is associated to a three-photon avoided crossing that is less narrow, as shown in Figs. 3.17 and 3.18. The loss can be analyzed in both cases in terms of Landau-Zener type non-adiabatic dynamics through the avoided crossing shown in both figures.

We have tested the limits of these tools using only approximately 2 oscillations in the pulse, i.e. $\tau\omega_0 = 2$. In this case, none of the level lines of Fig. 3.15 can satisfy the adiabatic condition

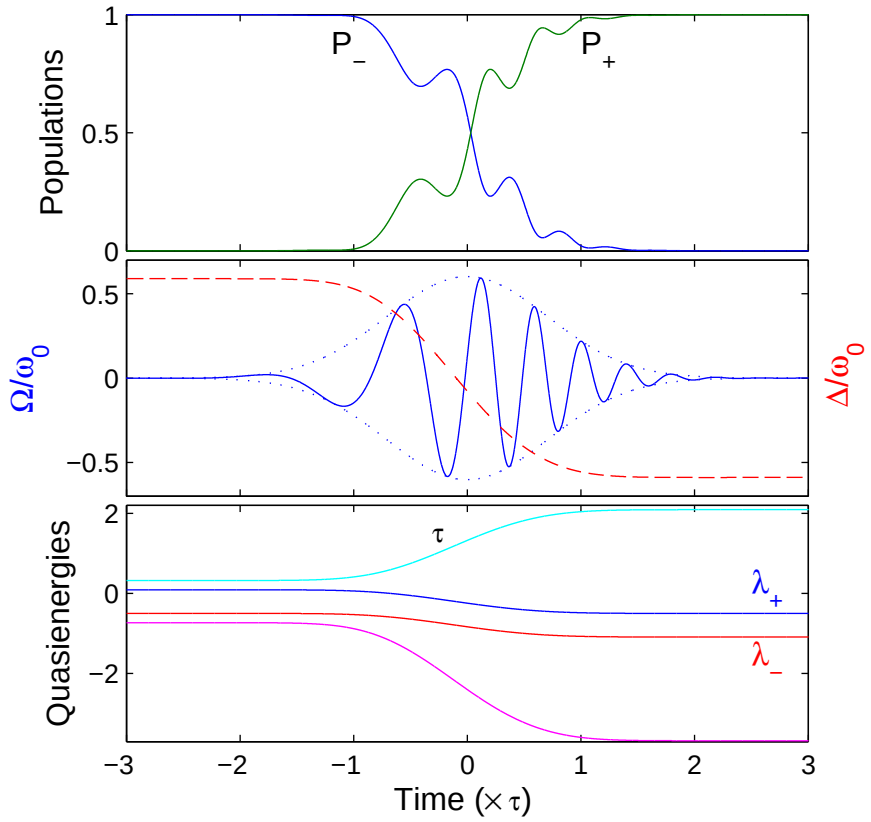

FIG. 3.16 - *Dynamics along the level line (a) of Fig. 3.15 with* $\Delta(t \to -\infty) = 0.6\omega_0$ *for a Gaussian pulse* $\Omega(t) = \Omega_{\max} e^{-(t/\tau)^2}$ *and the initial condition* $|\phi(t \to -\infty)\rangle = |-\rangle$. *Upper frame: Populations* $P_j := |\langle j|\phi(t)\rangle|^2$. *We obtain* $P_+ \approx 0.999$. *Middle frame: the normalized Rabi frequency (full line) with its envelope (dotted line) and the instantaneous normalized detuning (dashed line). Lower frame: the instantaneous quasienergies. The dynamics follows* λ_- *[connected to* $|-,0\rangle$ *(*$|+,-1\rangle$*) at early (late) times], slightly avoiding the three-photon resonance at early times, when the Rabi frequency is small, as shown by the two lowest curves. The lowest curve indeed is connected to* $|+,-3\rangle$ *(*$|-,-2\rangle$*) at early (late) times.*

$\tau\Delta_0 \gg 0.7$. We construct a trajectory (d) with the level line $\Delta_0/\omega_0 = 1.2$ in its lower part, which satisfies very roughly the adiabatic condition: $\tau\Delta_0 = 2.4$. As shown by Fig. 3.19, the population transfer is rather good. Here two avoided crossings are consecutively involved in the dynamics.

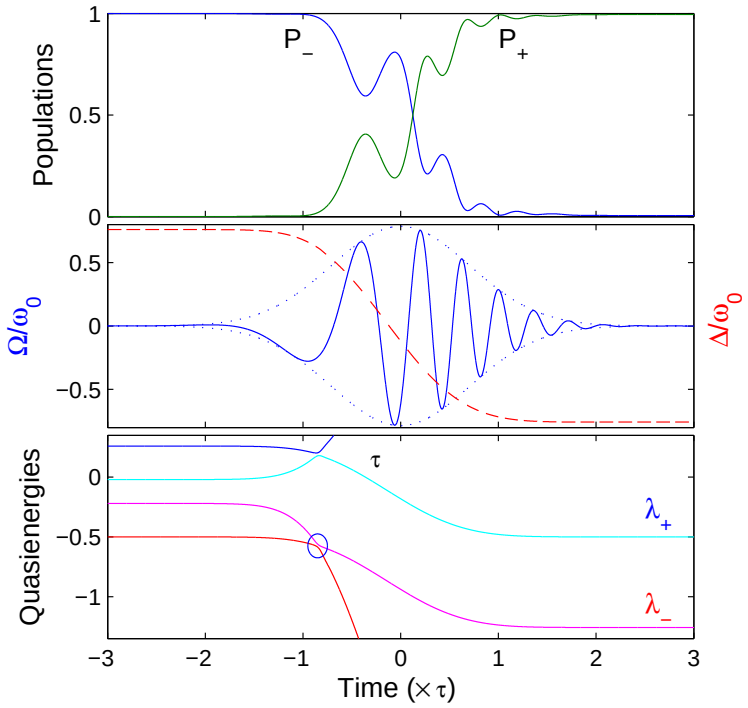

FIG. 3.17 - *Same as Fig. 3.16 but for a dynamics along the trajectory (b) of Fig. 3.15 with* $\Delta(t \to -\infty) = 0.76\omega_0$. *We obtain* $P_+ \approx 0.994$. *The lower frame shows a very thin avoided crossing (circled) around the three-photon resonances.*

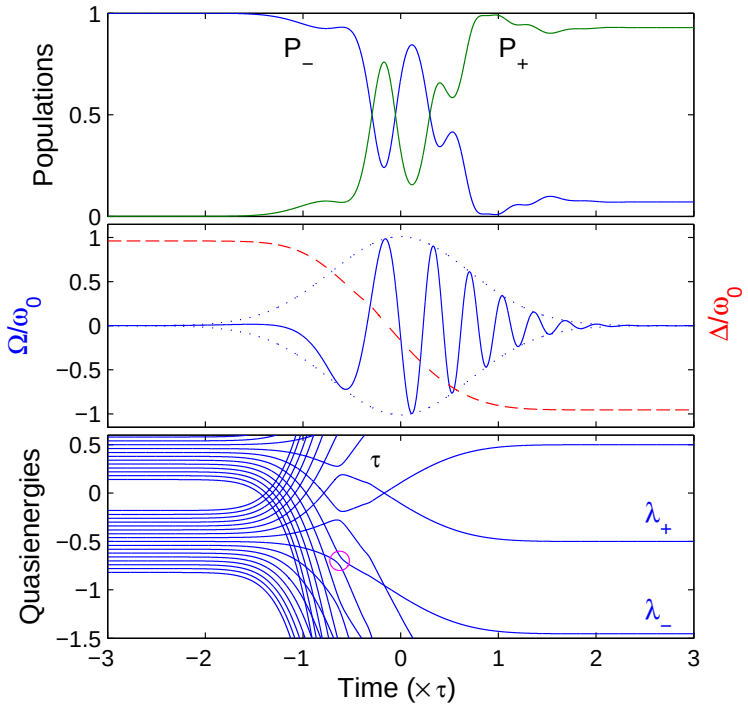

FIG. 3.18 - *Same as Fig. 3.16 but for a dynamics along the trajectory (c) of Fig. 3.15 with* $\Delta(t \to -\infty) = 0.96\omega_0$. *We obtain* $P_+ \approx 0.929$. *The lower frame shows a narrow avoided crossing (circled) around the three-photon resonances.*

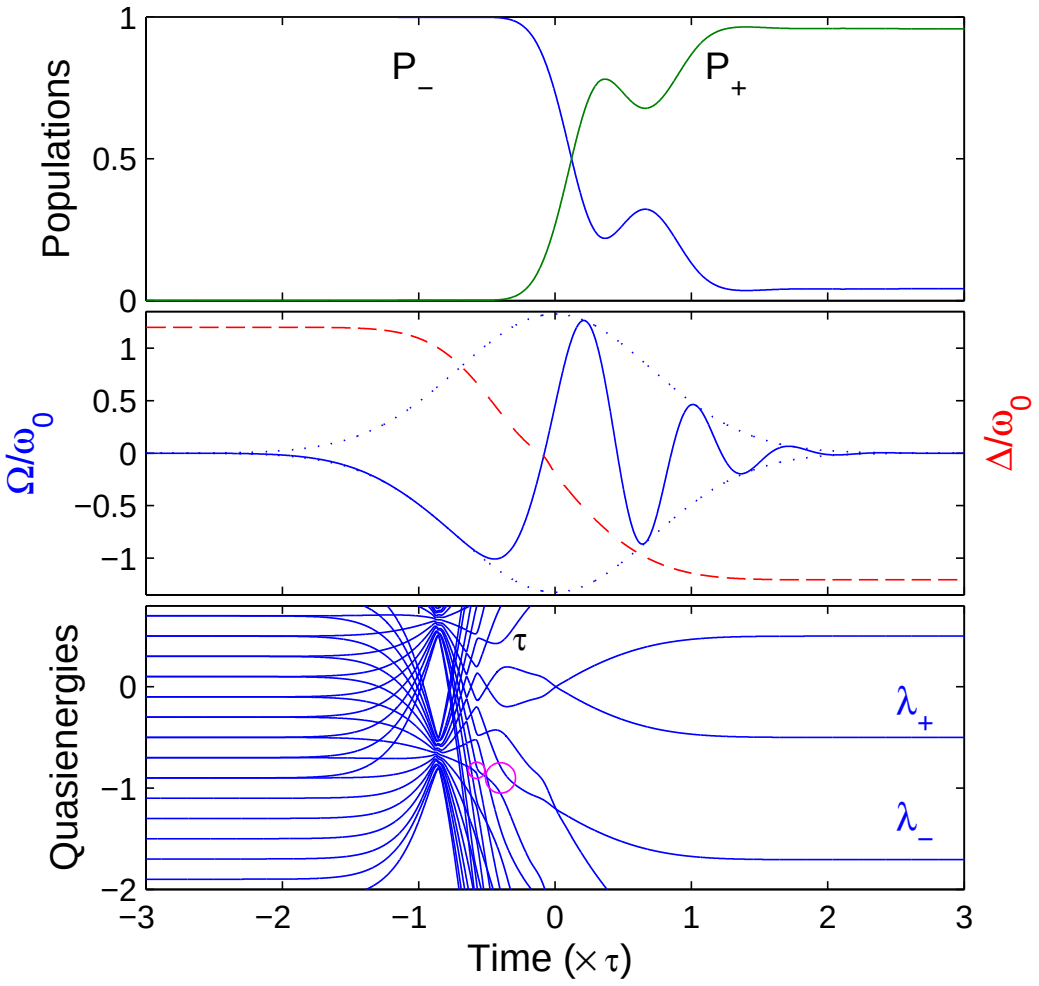

FIG. 3.19 - *Same as Fig. 3.16 but for a dynamics along the trajectory (d) of Fig. 3.15 with* $\Delta(t \to -\infty) = 1.2\omega_0$. *We obtain* $P_+ \approx 0.958$.

Appendix A

Relation between the semi-classical and the Floquet dynamics

We want to show the relation (1.13) of section 1.1 in a more general setting in which the semi-classical Hamiltonian can have other time dependent parameters, and in which the frequency can be chirped. This is the general setting needed for the treatment of adiabatic evolution with chirped pulses in Section 2.1, Eq. (2.7). We consider a semi-classical Hamiltonian of the form

$$H^{\mathbf{r}(t)}\left(\underline{\Theta}(t)\right), \tag{A.1}$$

where $\mathbf{r}(t)$ represents a set of parameters that can have an arbitrary time dependence (slow or not), and $\underline{\Theta}(t) = (\Theta_1(t) \dots \Theta_d(t))$ represents d phases corresponding to d lasers acting on the molecule.

Furthermore we consider a more general form of the time dependence of the phase

$$\underline{\Theta}(t) = \underline{\theta} + \underline{g}(t). \tag{A.2}$$

In the case of a chirped frequency we have e.g. $\underline{\Theta}(t) = \underline{\theta} + \underline{v}(t)\ t$. As mentioned in Section 2.1 the effective instantaneous frequency is defined as $\underline{\omega}_{\text{eff}}(t) = d\underline{\Theta}(t)/dt = d\underline{g}(t)/dt = \underline{v}(t) + \underline{\dot{v}}(t)\ t$. If we define the generalized translation operator

$$\left(\mathcal{T}_{\underline{g}(t)}\Psi\right)(\underline{\theta}) = \left(e^{\underline{g}(t)\frac{\partial}{\partial\underline{\theta}}}\Psi\right)(\underline{\theta}) = \Psi\left(\underline{\theta} + \underline{g}(t)\right), \tag{A.3}$$

the semiclassical Hamiltonian can be written as

$$H^{\mathbf{r}(t)}\left(\underline{\Theta}(t)\right) = \mathcal{T}_{\underline{g}(t)} H^{\mathbf{r}(t)}(\underline{\theta}) \mathcal{T}_{-\underline{g}(t)}. \tag{A.4}$$

Proposition. *The operator U is the propagator of the semi-classical Schrödinger equation (lifted to the enlarged space $\mathcal{K}$)*

$$i\hbar\frac{\partial}{\partial t}U\left(t, t_0; \underline{\theta}\right) = H^{\mathbf{r}(t)}\left(\underline{\Theta}(t)\right) U\left(t, t_0; \underline{\theta}\right), \quad U\left(t, t; \underline{\theta}\right) = \mathbb{1}_{\mathcal{H}}, \tag{A.5}$$

if and only if the operator U_K, defined by

$$U_K\left(t, t_0; \underline{\theta}\right) = \mathcal{T}_{-\underline{g}(t)} U\left(t, t_0; \underline{\theta}\right) \mathcal{T}_{\underline{g}(t_0)}, \tag{A.6}$$

satisfies

$$i\hbar\frac{\partial}{\partial t}U_K\left(t, t_0; \underline{\theta}\right) = K^{\mathbf{r}(t)} U_K\left(t, t_0; \underline{\theta}\right), \quad U_K\left(t, t; \underline{\theta}\right) = \mathbb{1}_{\mathcal{K}}, \tag{A.7}$$

with

$$K^{\mathbf{r}(t)} = -i\hbar\underline{\omega}_{\mathit{eff}}(t)\cdot\frac{\partial}{\partial\underline{\theta}} + H^{\mathbf{r}(t)}(\underline{\theta}), \tag{A.8}$$

where $\underline{\omega}_{\mathit{eff}}(t)$ *are the effective instantaneous frequencies*

$$\underline{\omega}_{\mathit{eff}}(t) = d\underline{\Theta}(t)/dt = d\underline{g}(t)/dt. \tag{A.9}$$

The Floquet Hamiltonian $K^{\mathbf{r}(t)}$ acts on the enlarged Hilbert space $\mathcal{K} = \mathcal{H}\otimes\mathcal{L}_2(\mathbf{T}^d, d\underline{\theta}/2\pi)$, where $\mathbf{T}^d$ is the d-dimensional unit torus.

Proof: We first remark that

$$\frac{\partial}{\partial t}\mathcal{T}_{\underline{g}(t)} \equiv \frac{\partial}{\partial t}e^{\underline{g}(t)\cdot\frac{\partial}{\partial\underline{\theta}}} = \frac{d\underline{g}(t)}{dt}\cdot\frac{\partial}{\partial\underline{\theta}}\mathcal{T}_{\underline{g}(t)} \equiv \mathcal{T}_{\underline{g}(t)\underline{\omega}_{\mathrm{eff}}}\cdot\frac{\partial}{\partial\underline{\theta}} \tag{A.10}$$

We start with (A.5) and invert eq. (A.6)

$$U\left(t,t_0;\underline{\theta}\right) = \mathcal{T}_{\underline{g}(t)}U_K\left(t,t_0;\underline{\theta}\right)\mathcal{T}_{-\underline{g}(t_0)}. \tag{A.11}$$

The time derivative of U can be expressed as

$$\frac{\partial}{\partial t}U = \frac{\partial}{\partial t}\mathcal{T}_{\underline{g}(t)}U_K\mathcal{T}_{-\underline{g}(t_0)} = \mathcal{T}_{\underline{g}(t)\underline{\omega}_{\mathrm{eff}}}\cdot\frac{\partial}{\partial\underline{\theta}}U_K\mathcal{T}_{-\underline{g}(t_0)} + \mathcal{T}_{\underline{g}(t)}\frac{\partial U_K}{\partial t}\mathcal{T}_{-\underline{g}(t_0)} \tag{A.12}$$

which after insertion into (A.5) and using (A.4) yields

$$i\hbar\mathcal{T}_{\underline{g}(t)}\left(\underline{\omega}_{\mathrm{eff}}\cdot\frac{\partial}{\partial\underline{\theta}}U_K + \frac{\partial U_K}{\partial t}\right)\mathcal{T}_{-\underline{g}(t_0)} = \mathcal{T}_{\underline{g}(t)}H^{\mathbf{r}(t)}(\underline{\theta})\mathcal{T}_{-\underline{g}(t)}\mathcal{T}_{\underline{g}(t)}U_K\mathcal{T}_{-\underline{g}(t_0)} \tag{A.13}$$

which by multiplication from the left by $\mathcal{T}_{-\underline{g}(t)}$ and from the right by $\mathcal{T}_{\underline{g}(t_0)}$ yields (A.7). The inverse implication follows from the same argument run backwards.

Appendix B

The structure of eigenvectors and eigenvalues of Floquet Hamiltonians. The concept of dressed Hamiltonian

In this section we show that the Floquet eigenvectors have the following general structure

$$\psi_{m,\underline{k}}(x,\underline{\theta}) = C(x,\underline{\theta})\left[\phi_m^B(x)\otimes e^{i\underline{k}\cdot\underline{\theta}}\right], \tag{B.1}$$

where $C(x,\underline{\theta})$ is a unitary operator in $\mathcal{K}$, and $\phi_m^B(x)\in\mathcal{H}$ are the eigenvectors of a time and $\underline{\theta}$ independent operator B acting on $\mathcal{H}$. The eigenvalues can be written in the form

$$\lambda_{m,\underline{k}} = \lambda_m^B + \hbar\underline{k}\cdot\underline{\omega}, \tag{B.2}$$

where λ_m^B are the eigenvalues of B. The eigenelements can thus be classified by two labels: m, related to the molecule, and $\underline{k}$, related to the photon field.

We remark that if λ is an eigenvalue of K with eigenvector ψ, then for any $\underline{k}\in\mathbb{Z}^d$, $\lambda+\hbar\underline{k}\cdot\underline{\omega}$ is also an eigenvalue with corresponding eigenvector $e^{i\underline{k}\cdot\underline{\theta}}\psi$. This is an immediate consequence of the form of $K=-i\hbar\underline{\omega}\cdot\frac{\partial}{\partial\underline{\theta}}+H(x,\underline{\theta})$. In the periodic case this leads to a periodic structure of the spectrum. For instance, if we take an N-level model for the molecule, the Floquet spectrum will consist of a group of N eigenvalues that are repeated at a distance $k\omega$ for all $k\in\mathbb{Z}$, i.e. an infinite number of times. This periodic structure can be called Floquet zones, or Brillouin zones in analogy to a similar property in crystals. Although the Floquet Hamiltonian has an infinite number of eigenvalues and eigenvectors, once N are known, all the others can be constructed trivially. As the examples in Chapter 9 show, the energies of two different Brillouin zones can overlap and even lead to resonances that strongly couple the zones, leading to non trivial physical effects.

In the quasiperiodic case of two or several incommensurate frequencies the Floquet eigenvalues cover the real line densely, and the overlap between Brillouin zones is much more intricate.

This structure of the eigenvectors and eigenvalues of Floquet Hamiltonians can be understood by considering an alternative interpretation of the Floquet eigenvalue problem:

We look for a unitary transformation $C(x,\underline{\theta}):\mathcal{H}\to\mathcal{H}$ (with $\underline{\theta}$ interpreted as a parameter) such that the semiclassical Schrödinger equation is transformed into an equation with a time-independent Hamiltonian B, i.e. such that

$$U^B(t,t_0;\underline{\theta}) = C(\underline{\Theta}(t))^{-1}U(t,t_0;\underline{\theta})C(\underline{\Theta}(t_0)) \tag{B.3}$$

satisfies

$$i\hbar\frac{\partial}{\partial t}U^B(t,t_0;\underline{\theta}) = BU^B(t,t_0;\underline{\theta}), \tag{B.4}$$

where $B = B(x)$ is a constant operator (i.e. independent of t and $\underline{\theta}$), acting on $\mathcal{H}$. If such a transformation exists, then

$$U(t,t_0;\underline{\theta}) = C(\underline{\Theta}(t))e^{-iB(t-t_0)/\hbar}C(\underline{\Theta}(t_0))^{-1} \tag{B.5}$$

and B can be expressed in terms of $C(\underline{\Theta}(t))$ and $H(\underline{\Theta}(t))$:

$$B = C(\underline{\Theta}(t))^{-1}H(\underline{\Theta}(t))C(\underline{\Theta}(t)) - i\hbar C(\underline{\Theta}(t))^{-1}\frac{\partial C(\underline{\Theta}(t))}{\partial\underline{\theta}}\cdot\frac{d\underline{\Theta}(t)}{dt}. \tag{B.6}$$

Acting with $\mathcal{T}_{-\underline{\omega}t}$ from the left on (B.5) and with $\mathcal{T}_{\underline{\omega}t_0}$ from the right, one obtains that C induces a unitary transformation of the Floquet Hamiltonian in the enlarged space $\mathcal{K}$

$$\begin{aligned}\mathcal{T}_{-\underline{\omega}t}U(t,t_0;\underline{\theta})\mathcal{T}_{\underline{\omega}t_0} &\equiv e^{-iK(t-t_0)/\hbar}\\ &= C(\underline{\theta})\mathcal{T}_{-\underline{\omega}t}e^{-iB(t-t_0)/\hbar}\mathcal{T}_{\underline{\omega}t_0}C(\underline{\theta})^{-1}\\ &= C(\underline{\theta})e^{-(i/\hbar)(t-t_0)(-i\hbar\underline{\omega}\cdot\partial/\partial\underline{\theta}+B)}C(\underline{\theta})^{-1},\end{aligned} \tag{B.7}$$

i.e.

$$K = C(\underline{\theta})(-i\hbar\underline{\omega}\cdot\frac{\partial}{\partial\underline{\theta}} + B)C(\underline{\theta})^{-1}. \tag{B.8}$$

Hence, the determination of the eigenelements of K in $\mathcal{K}$ is reduced to the determination of those of B in $\mathcal{H}$. When such a transformation $C(\underline{\theta})$ can be found, the operator B is called the *dressed Hamiltonian*. Although it acts only on the molecular Hilbert space $\mathcal{H}$, it contains the information on the photons, that "dress" the molecule. The transformation $C(\underline{\theta})$ can be interpreted as a change of representation. We remark that the transformation $C(x,\underline{\theta})$, and thus the dressed Hamiltonian B, is clearly not unique since $C(x,\underline{\theta})$ can be composed with any unitary transformation that acts inside $\mathcal{H}$.

We consider only the situation in which B has a purely discrete spectrum : $B\phi_m^B = \lambda_m^B\phi_m^B$. Since $-i\hbar\underline{\omega}\frac{\partial}{\partial\underline{\theta}}$ commutes with B, and its eigenelements are $\hbar\underline{k}\cdot\underline{\omega}$ and $e^{i\underline{k}\cdot\underline{\theta}}$, $\underline{k}\in\mathbb{Z}^M$, we can conclude that the eigenvalues and eigenvectors of K have the general structure given in Eqs. (B.2),(B.1). Since the sets of functions $\left\{\phi_m^B\right\}$ and $\left\{e^{i\underline{k}\cdot\underline{\theta}}\right\}$ are complete orthonormal bases of their respective spaces $\mathcal{H}$ and $\mathcal{L}_2(\mathbf{T}^d, d\underline{\theta}/2\pi)$, and since C is unitary, we conclude that $\{\psi_{m,\underline{k}}\}$ forms a complete basis of $\mathcal{K}$.

In order to arrive at the eigenvalue equation for K we remark that since B is hermitian in $\mathcal{H}$ there is a unitary transformation T that diagonalizes it in a reference base $\{|f_m\rangle\}$ of $\mathcal{H}$ (which e.g. in the case of a two-level model can be represented in coordinates by $\{(1,0)\ ,\ (0,1)\}$):

$$T^\dagger BT = D = \sum_m \lambda_m^B|f_m\rangle\langle f_m|. \tag{B.9}$$

T can be thought of as a matrix whose columns are the components of the eigenvectors of B expressed in the basis $\{f_m\}$:

$$T = \sum_m |\phi_m^B\rangle\langle f_m|, \tag{B.10}$$

which allows one to write

$$\psi_{m,\underline{k}}(x,\underline{\theta}) = C(x,\underline{\theta})(T\otimes\mathbb{1}_{\mathcal{L}})|f_m\otimes e^{i\underline{k}\cdot\underline{\theta}}\rangle. \tag{B.11}$$

Inserting (B.9) into (B.8) we obtain

$$K = C(\underline{\theta})T(-i\hbar\underline{\omega}\cdot\frac{\partial}{\partial\underline{\theta}} + D)T^{\dagger}C(\underline{\theta})^{-1} \tag{B.12}$$

or

$$KC(\underline{\theta})T = C(\underline{\theta})T(-i\hbar\underline{\omega}\cdot\frac{\partial}{\partial\underline{\theta}} + D). \tag{B.13}$$

Applying both sides of this operator relation to the elements of the basis $f_m \otimes e^{i\underline{k}\cdot\underline{\theta}}$ and using the fact that

$$(-i\hbar\underline{\omega}\cdot\frac{\partial}{\partial\underline{\theta}} + D)\ |f_m \otimes e^{i\underline{k}\cdot\underline{\theta}}\rangle = (\lambda_m^B + \hbar\underline{k}\cdot\underline{\omega})|f_m \otimes e^{i\underline{k}\cdot\underline{\theta}}\rangle, \tag{B.14}$$

we arrive at the eigenvalue equation for K:

$$K\psi_{m,\underline{k}}(x,\underline{\theta}) = \lambda_{m,\underline{k}}\psi_{m,\underline{k}}(x,\underline{\theta}). \tag{B.15}$$

Remark: Systems for which such a transformation $C(x,\underline{\theta})$ exists are called *reducible*. Due to the Floquet theorem this is always the case for time-periodic Hamiltonians (for finite or infinite dimensional $\mathcal{H}$). However, in the case of several incommensurate frequencies (quasiperiodic Hamiltonian) reducibility is not always satisfied, even for finite dimensional $\mathcal{H}$ [104, 105][106, 107] [20]. We remark that for finite dimensional $\mathcal{H}$ reducibility is equivalent to the property of K having no continuous spectrum[20].

Appendix C

Coherent states in the Floquet representation

In this Appendix we show that the coherent states are represented in Floquet theory by a generalized function $\Phi_{\theta_0}(\theta)$, which is real, and depends on $\theta-\theta_0$, where $\theta_0 \in \mathbb{S}^1$ is a fixed angle, and

$$\big(\Phi_{\theta_0}(\theta)\big)^2 = 2\pi\delta(\theta-\theta_0). \tag{C.1}$$

This can be obtained as follows. The photon field coherent states are eigenvectors of the annihilation operator

$$a\,|\,\alpha\,\rangle = \alpha\,|\,\alpha\,\rangle, \qquad \alpha = |\alpha|e^{-i\theta_0}. \tag{C.2}$$

In the usual Fock number state representation they are given, up to a phase factor, by

$$|\,\alpha\,\rangle = e^{-|\alpha|^2/2}\sum_{n=0}^{\infty}\frac{\alpha^n}{\sqrt{n!}}\,|\,n\,\rangle. \tag{C.3}$$

In the phase representation they can be written as

$$\begin{aligned}\Phi_{\theta_0}^{(\bar n)}(\theta) &= e^{i\zeta}e^{-|\alpha|^2/2}\sum_{n=0}^{\infty}\frac{\alpha^n}{\sqrt{n!}}\,e^{i(n-\bar n)\theta}\\ &= e^{-|\alpha|^2/2}\sum_{n=0}^{\infty}\frac{|\alpha|^n}{\sqrt{n!}}\,e^{i(n-\bar n)(\theta-\theta_0)}\end{aligned} \tag{C.4}$$

(where ζ is an arbitrary constant phase that we have chosen as $\zeta=\bar n\theta_0$). In order to obtain the representation of coherent states in Floquet theory we have to take $|\alpha|=\sqrt{\bar n}$, since the average photon number in a coherent state is given by $|\alpha|^2$, and then apply the limit $\bar n\to\infty$.

This can be rigorously done using directly the representation (C.4), as was shown in [10]. Here we discuss an alternative construction, that is formal but gives a useful intuition. We use an approximate expression of the coherent states for large $\bar n$, obtained in [9], by developing

$$a_{\bar n,\theta} = \sqrt{\bar n}\,e^{-i\theta}\sqrt{1-\frac{1}{\bar n}i\frac{\partial}{\partial\theta}} \quad \underset{\bar n\to\infty}{\rightharpoonup} \quad \sqrt{\bar n}\,e^{-i\theta}\left(1-\frac{1}{2\bar n}i\frac{\partial}{\partial\theta}\right), \tag{C.5}$$

This leads to the following asymptotic expression [9] for the normalized coherent state corresponding to $\alpha=\sqrt{\bar n}\,e^{-i\theta_0}$, obtained as solution of $e^{-i\theta}\big(1-i/(2\bar n)\partial/\partial\theta\big)\,\Phi_{\theta_0}^{(\bar n)} = e^{-i\theta_0}\Phi_{\theta_0}^{(\bar n)}$:

$$\Phi_{\theta_0}^{(\bar n)} \quad \underset{\bar n\to\infty}{\rightharpoonup} \quad \frac{1}{\nu}\exp\left\{-2\bar n\left[1-\cos\left(\theta-\theta_0\right)-i\left(\sin(\theta-\theta_0)-(\theta-\theta_0)\right)\right]\right\} \tag{C.6}$$

where the normalization constant is

$$\nu^2 = e^{-4\bar{n}} I_0(4\bar{n}) \tag{C.7}$$

with I_0 a Bessel function, which behaves asymptotically as

$$I_0(4\bar{n}) = \int_0^{2\pi} \frac{d\theta}{2\pi} \exp\left(4\bar{n}\cos\theta\right) \quad \underset{\bar{n}\to\infty}{\sim} \quad \frac{e^{4\bar{n}}}{(8\pi\bar{n})^{1/2}}. \tag{C.8}$$

Therefore

$$\left|\Phi_{\theta_0}^{(\bar{n})}(\theta)\right|^2 \quad \underset{\bar{n}\to\infty}{\sim} \quad (8\pi\bar{n})^{1/2} \exp\left\{-4\bar{n}\left[1-\cos(\theta-\theta_0)\right]\right\}, \tag{C.9}$$

noticing that the function $\exp\left\{-4\bar{n}\left[1-\cos(\theta-\theta_0)\right]\right\}$ behaves like $\exp\{-2\bar{n}(\theta-\theta_0)^2\}$ for $\bar{n}\to\infty$, we get

$$\left|\Phi_{\theta_0}^{(\bar{n})}(\theta)\right|^2 \quad \underset{\bar{n}\to\infty}{\sim} \quad 2\pi\delta(\theta-\theta_0), \tag{C.10}$$

where $\delta(\theta-\theta_0)$ is the usual Dirac delta function.
We remark that since the phase term in (C.4) (or in (C.6)) is odd in $\theta-\theta_0$, we obtain that $\Phi_{\theta_0}^{(\bar{n})}(\theta) \to \Phi_{\theta_0}(\theta)$ with $\Phi_{\theta_0}(\theta)$ real and

$$\left(\Phi_{\theta_0}^{(\bar{n})}(\theta)\right)^2 \underset{\bar{n}\to\infty}{\longrightarrow} 2\pi\delta(\theta-\theta_0). \tag{C.11}$$

Furthermore, using the well-known properties of the expectation values of N^m on coherent states, we obtain

$$\left\langle \Phi_{\theta_0}^{(\bar{n})}(\theta) \,\middle|\, -i\,\frac{\partial}{\partial\theta} \,\middle|\, \Phi_{\theta_0}^{(\bar{n})}(\theta) \right\rangle_{\mathcal{L}} = 0, \quad \text{for all } \bar{n}, \tag{C.12}$$

$$\left\langle \Phi_{\theta_0}^{(\bar{n})}(\theta) \,\middle|\, (-i)^m\,\frac{\partial^m}{\partial\theta^m} \,\middle|\, \Phi_{\theta_0}^{(\bar{n})}(\theta) \right\rangle_{\mathcal{L}} \underset{\bar{n}\to\infty}{\longrightarrow} \infty, \quad m \geq 2. \tag{C.13}$$

The subscripts in the scalar product symbols ($\langle \quad | \quad \rangle_{\mathcal{L}}$) indicate on which space they act. We conclude thus that in Floquet theory the photon coherent states are represented by the "square root of a δ-function", that we denote by $\Phi_{\theta_0}(\theta) = (2\pi)^{1/2}\delta_{1/2}(\theta-\theta_0)$. Since we will be interested in expectation values, only $|\Phi_{\theta_0}|^2$ will appear in our calculations. The formal calculus rules for $\delta_{1/2}(\theta-\theta_0)$ are given in Ref. [10].

Appendix D

Analytic solutions for two-level systems - Dykhne-Davis-Pechukas formula

We consider in this appendix the scaled Schrödinger equation (setting $\hbar = 1$)

$$i\frac{\partial\phi}{\partial s}(s) = \tau H(s)\phi(s), \quad \phi(s) = \begin{bmatrix} B_-(s) \\ B_+(s) \end{bmatrix} \in \mathbb{C}^2, \tag{D.1}$$

in the basis of the two states $\{|\pm\rangle\}$, with the scaled time $s = t/\tau$, the initial condition (at time $s_i = t_i/\tau \to -\infty$) $B_-(s_i) = 1$, $B_+(s_i) = 0$, and the Hamiltonian

$$H(s) = \frac{1}{2}\begin{bmatrix} -\Delta(s) & \Omega(s) \\ \Omega(s) & \Delta(s) \end{bmatrix}, \quad \Delta, \Omega \in \mathbb{R} \tag{D.2}$$

with a pulsed Rabi $\Omega(s) = \Omega_0\Lambda(s)$, $\Lambda(s \pm \infty) \to 0$. The natural question is the calculation of the transition probability $P_+ = |B_+(s_f)|^2$ at the end of the pulse, and its dependence on relevant parameters such as the pulse area $\tau\Omega_0 \int ds\, \Lambda(s)$, its shape $\Lambda(s)$, and the detuning (shape, initial and final values, slope, $\cdots$). Only few models are analytically solvable, the most popular ones are described in the following section. An alternative method consists in calculating the solution approximately. Perturbation theories usually give solutions for weak Rabi intensities. One can calculate solutions in the adiabatic limit $\tau \to \infty$ using an analysis due to Dykhne, Davis and Pechukas, as described below.

D.1 Analytic solutions

Most popular analytically solvable models include:

(a) The Rabi model [80]

$$\Omega = \text{const}, \quad \Delta = \text{const} \tag{D.3a}$$

$$P_+(t) = \frac{\Omega^2}{\Omega^2 + \Delta^2}\sin^2\left(\frac{1}{2}\sqrt{\Omega^2 + \Delta^2}\; t\right), \tag{D.3b}$$

or

$$\Delta = 0 \tag{D.4a}$$

$$P_+(t) = \sin^2\left(\frac{1}{2}\int_{t_i}^{t} dt\, \Omega(t)\right). \tag{D.4b}$$

(b) The Landau-Zener model [66, 67]

$$\Omega(s) = \Omega_0 = \text{const}, \quad \Delta = \beta^2 s \tag{D.5a}$$

$$P_+ = e^{-\frac{\pi}{2}\Omega_0^2/\beta^2}. \tag{D.5b}$$

Effects of finite coupling duration [62] and transition times [81] in this model have been investigated.

(c) The Demkov- Kunike model [82]

$$\Omega(s) = \Omega_0 \, \text{sech}(s) \equiv \Omega_0/\cosh(s), \quad \Delta(s) = \Delta_0 + B\tanh(s) \tag{D.6a}$$

$$P_+ = \frac{\cosh(\pi\tau B) - \cos(\pi\tau\sqrt{\Omega_0^2 - B^2})}{\cosh(\pi\tau B) + \cosh(\pi\tau\Delta_0)}, \tag{D.6b}$$

generalized in Refs. [83], and which includes as special cases the no-crossing Rosen-Zener model [63] with $B = 0$ (i.e. with $\Delta(s) = \Delta_0 = \text{const}$):

$$P_+ = \text{sech}^2\left(\frac{1}{2}\pi\tau\Delta_0\right)\sin^2\left(\frac{1}{2}\tau\int_{-\infty}^{+\infty} ds\,\Omega(s)\right) = \text{sech}^2\left(\frac{1}{2}\pi\tau\Delta_0\right)\sin^2\left(\frac{1}{2}\pi\tau\Omega_0\right), \tag{D.7}$$

the level-crossing Allen-Eberly model [44] (generalized by Hioe [84]) with $\Delta_0 = 0$ (i.e. with $\Delta(s) = B\tanh(s)$ crossing the resonance at $s = 0$):

$$P_+ = 1 - \frac{\cos^2\left(\frac{1}{2}\pi\tau\sqrt{\Omega_0^2 - B^2}\right)}{\cosh^2\left(\frac{1}{2}\pi\tau B\right)} \quad (\Omega_0 > B), \tag{D.8a}$$

$$P_+ = 1 - \frac{\cosh^2\left(\frac{1}{2}\pi\tau\sqrt{B^2 - \Omega_0^2}\right)}{\cosh^2\left(\frac{1}{2}\pi\tau B\right)} \quad (\Omega_0 < B), \tag{D.8b}$$

and the half crossing Bambini-Berman model [85] with $\Delta_0 = B$ (i.e. with $\Delta(s) = B[1+\tanh(s)]$ increasing monotonically from $\Delta(-\infty) = 0$ to $\Delta(+\infty) = 2B$). Ref. [85] includes other class of models, in particular with asymmetric pulses. We can also mention the Demkov model [64]

$$\Omega(s) = \Omega_0 e^{-|s|}, \qquad \Delta(s) = \Delta_0 = \text{const} \tag{D.9a}$$

$$P_+ = \text{sech}^2\left(\frac{1}{2}\pi\tau\Delta_0\right)\sin^2\left(\frac{1}{2}\tau\int_{-\infty}^{+\infty} ds\,\Omega(s)\right) = \text{sech}^2\left(\frac{1}{2}\pi\tau\Delta_0\right)\sin^2\left(\tau\Omega_0\right), \tag{D.9b}$$

closely related to the Rosen-Zener model since $\Omega(s)$ has the same asymptotic limits.

One can also mention the Nikitin model [86] used in the context of atomic and molecular collisions with crossings of electronic potential energy as a function of an internuclear distance as the adiabatic parameter [87].

Using the notion of lifting of quasidegeneracy by a quasiresonant rising pulse, which splits the population amongst two adiabatic branches, followed by an adiabatic transport along the two branches, and ended by the symmetrically inverse problem of the creation of degeneracy when the pulse fails, we have constructed approximate formulas of transition probability for truncated trigonometric pulses

$$\Omega(\tau) = \Omega_0 \sin^2\tau, \quad 0 \le \tau \le \pi \tag{D.10}$$

of power law endings (with respect to time) [56].

D.2 Dykhne-Davis-Pechukas formula

The Dykhne-Davis-Pechukas (DDP) formula [45, 46, 47] allows one to calculate in the adiabatic asymptotic limit $\tau \to \infty$ the probability of the non-adiabatic transitions $P_-(s_f) := |\langle -|\phi\rangle|^2$ at the final time $s_f = t_f/\tau \to +\infty$ as an exponential decay. It reads in the simplest case[1]

$$P_-(s_f) \rightsquigarrow \left|e^{i\tau\mathcal{D}(s_c)}\right|^2 = e^{-2\tau \mathrm{Im}\mathcal{D}(s_c)}, \tag{D.11}$$

where

$$\mathcal{D}\left(s_c\right) = \int_0^{s_c} ds\, \delta(s), \quad \delta(s) = \sqrt{\Delta^2(s) + \Omega^2(s)}, \tag{D.12}$$

is the integration of the analytic continuation of the difference of the eigenvalues up to s_c, the relevant complex *crossing point* of the eigenvalues defined by

$$\delta(s_c) = 0, \tag{D.13}$$

lying in the *upper* complex s-plane.

The criterion to choose this crossing point (which is not necessarily unique nor the closest one to the real axis, see below) has been established in [48] and for the cases where many crossing points are required, the formula (D.11) has been generalized in [49]. The analysis is based on the *Stokes lines* defined as the set of points s in the complex plane such that

$$\mathrm{Im}\mathcal{D}\left(s\right) = \mathrm{Im}\mathcal{D}\left(s_c\right) = \text{const.} \tag{D.14}$$

We remark that (i) such Stokes lines are not allowed to cross, (ii) the Stokes line leaves the crossing point in three different directions with an angle $2\pi/3$ between two consecutive ones. An algorithm to construct numerically the Stokes line, suggested by A. Joye, is described in [55]. The crossing points, denoted $s_c^{(n)}$, $n = 1, N$, that one has to take into account are the ones connected by *the Stokes line closest to the real axis*. If there are several crossing points on this Stokes line, it has been shown [49] that one has to replace the term $e^{i\tau\mathcal{D}(s_c)}$ of formula (D.11) by a coherent sum of exponentials, one for each crossing point connected by the lowest Stokes line:

$$P_-(s_f) \rightsquigarrow \left|\sum_{n=1}^{N} e^{i\tau\mathcal{D}(s_c^{(n)})}\right|^2. \tag{D.15}$$

The required hypothesis [48, 49] for the validity of the formulas (D.11) and (D.15) are *(i) $\delta(s)$ does not vanish for real s (e.g. no crossing at infinity) and (ii) $\delta(s)$ is analytic and single-valued throughout the region from the real axis to the relevant Stokes line.* We remark that for complex Hermitian Hamiltonians with three time dependent parameters, this formula has to be completed by geometrical prefactors [48, 50].

[1] The symbol $\rightsquigarrow$ means asymptotic limit.

Part II

Effective Hamiltonians

In atoms or molecules, the total Hilbert space available is much too large with respect to the dynamics typically considered in this work, in the sense that only a few states will be visited during the dynamics. Such states are usually termed as *essential states* or *active states* and they will be connected to the initial state (and possibly between each other) by *resonances*. The other states will participate in the dynamics in an effective way in the sense that they will only contribute in a non-resonant way to the coupling, as dynamical Stark shifts. We give here a systematic construction of the resulting effective Hamiltonians, constructed in the basis of the essential states and incorporating the perturbative effects of the other states.

This construction features two aspects. First a *partitioning* of the Hamiltonian by specific *perturbative* transformations. For a time-dependent Hamiltonian (with external fields), the partitioning should be considered taking into account two aspects of the driving field with respect to the field-free system: (i) the magnitude of the static coupling for each amplitude of the pulse, and (ii) the speed of the time variation of the coupling, since when it is large, it increases the available spectrum of the field. *We show that it is however sufficient to consider the magnitude of the static coupling under the conditions of monotonic rising and falling of the pulse.* This partitioning allows one to construct an effective quasienergy operator. Since in the Floquet representation the Hamiltonian K defined on the enlarged Hilbert space $\mathcal{K}$ is time independent, the perturbative treatment of step (i) can be done by stationary perturbation theory, instead of the usual time-dependent one. Here we present a general formulation of stationary perturbation theory based on the iteration of unitary transformations (called contact transformations or KAM transformations) constructed such that the form of the Hamiltonian gets simplified. More precisely it allows one to reduce the size ϵ of a perturbation with respect to a reference Hamiltonian from ϵ to ϵ^2 at each iteration. It is conceptually different from the Rayleigh-Schrödinger perturbation theory, which gives an expansion in powers of ϵ. In particular the KAM transformation has a superexponential speed of convergence. The results between the Rayleigh-Schrödinger and KAM perturbation theories are not very different at the lowest orders, but the latter formulation has the advantage to be formulated in terms of simple unitary transformations.

Next we determine within the subspace spanned by the essential states an effective *dressed* Hamiltonian, i.e. that does not depend on the field variable θ. This step requires as the main feature the identification and the treatment of the resonances of the system. It can be improved by additional perturbative transformations. The goal is to construct an effective Hamiltonian expressed with a closed formula.

The final step (which uses adiabatic principles and the topology of the eigenenergy surfaces) consists in diagonalizing the effective Hamiltonian. This step can be generally done with closed formulas only for a low dimensional matrix. However the topological analysis can be efficiently done even with a numerical calculation of the eigenenergy surfaces.

It is often of interest to use specific one-photon processes (thus of first order in field amplitude) to select the essential states, and to completely neglect the other states acting perturbatively with higher orders.

The concept of contact transformation and its application for partitioning is presented in Chapter 4. We show in particular the connection with the standard "adiabatic elimination", that allows us to make a partitioning at the level of the time-dependent Schrödinger equation.

This procedure by contact transformations allows us to detect in a simple way resonances. If resonances are present, the simple perturbative approach is not enough to capture the relevant effects. This necessitates to perform a different kind of unitary transformations, that are non-perturbative and are specifically adapted to the relevant resonances. This can be interpreted as

a generalization of rotating wave transformations to strong coupling regimes. This is studied in Chapter 5.

Chapter 6 is devoted to the construction of various effective dressed Hamiltonians for laser-driven atoms and molecules.

Another approach adapted for an interaction with an ultrashort pulse, where the instantaneous spectrum of the Hamiltonian has no particular meaning, consists in constructing directly the propagator for instance using a time-dependent perturbation theory. Since one can construct (at least formally) an extended Hilbert space and an associated Floquet-like time-independent operator for a general time dependence, we can apply the tools of contact transformation instead of using a time-dependent perturbation theory, as shown in Chapter 7.

Chapter 4

Contact transformations, partitioning, adiabatic elimination and high frequency perturbation theory

In this chapter, we first introduce the partitioning technique with the simple two-state system, showing the static and time-dependent aspects. We next formulate in a general setting the perturbation theory formulated as an iteration of unitary transformations, namely the contact transformation. We present its superconvergent formulation: the KAM technique (see Sections 4.2 and 4.3) and study some partial contact transformations (see Section 4.3). We show that the KAM technique allows us to partition at a desired order operators in orthogonal Hilbert subspaces in Section 4.4. This formulation is connected to the adiabatic elimination technique in Sections 4.5 and 4.6. We finally apply the contact transformation to the case of an interaction of high frequency with respect to the energy differences of the free system and show its connection with the standard Born Oppenheimer approximation.

4.1 Introduction to partitioning: static and time-dependent aspects

The two aspects of amplitude and speed of the coupling for partitioning can be analyzed in detail for the two-level system $|1\rangle$, $|2\rangle$ ($|1\rangle$ is the lower state) with the simple Hamiltonian:

$$H(t) = \frac{\hbar}{2} \begin{bmatrix} -\Delta & \Omega(t) \\ \Omega(t) & \Delta \end{bmatrix}. \tag{4.1}$$

The goal is here to give precise conditions to decouple the two states, i.e. to find a unitary time dependent transformation that transforms the Schrödinger equation into one with approximately diagonal Hamiltonian. We assume a constant (positive) detuning and a (real positive) pulsed Rabi frequency of the form

$$\Omega(t) = \Omega_{\max}\Lambda(t) \tag{4.2}$$

with $\Omega_{\max} \equiv \max_t \Omega(t)$, i.e. $0 \leq \Lambda(t) \leq 1$. The goal is to determine the conditions that will allow one to partition this Hamiltonian. Concerning the amplitudes of the coupling, it is clear that the partitioning is possible when

$$\varepsilon := \Omega_{\max}/\Delta \ll 1. \tag{4.3}$$

This partitioning can be formulated with a perturbative transformation T (i.e. not very different from the identity) yielding to

$$T^\dagger H T = D_p + \mathcal{O}(\varepsilon^3) \tag{4.4}$$

where the partitioned Hamiltonian D_p has to be diagonal, i.e. has to decouple the two states. If the initial condition is connected to state $|1\rangle$, we can considered that state $|2\rangle$ has been eliminated in the sense that its effect has been incorporated in D_p at a given order. We obtain here

$$D_p = \frac{\hbar}{2}\begin{bmatrix} -\delta(t) & 0 \\ 0 & \delta(t) \end{bmatrix} \tag{4.5}$$

with

$$\delta(t) = \Delta\left[1 + \frac{1}{2}\left(\frac{\Omega(t)}{\Delta}\right)^2\right] = \Delta[1 + \mathcal{O}(\varepsilon^2)]. \tag{4.6}$$

The additional diagonal terms are the dynamical Stark shifts of leading order ε^2. The transformation matrix T is exactly known in this two-state case; when developed with respect to ε, it reads

$$T = \mathbb{1} - \frac{1}{2}\begin{bmatrix} \frac{1}{4}\varepsilon^2\Lambda^2 & -|\varepsilon|\Lambda \\ |\varepsilon|\Lambda & \frac{1}{4}\varepsilon^2\Lambda^2 \end{bmatrix} + \mathcal{O}(\varepsilon^3). \tag{4.7}$$

Concerning the time-dependent aspect, we have to express the Schrödinger equation using the above transformation (as we did in the context of the adiabatic evolution). If we define the state evolution $\phi(t)$ given by the Schrödinger equation

$$i\hbar\frac{\partial\phi}{\partial t}(t) = H(t)\phi(t), \tag{4.8}$$

we obtain

$$i\hbar\frac{\partial}{\partial t}\widetilde{\phi}(t) = \widetilde{H}(t)\widetilde{\phi}(t) \tag{4.9}$$

with

$$\widetilde{H}(t) = \frac{\hbar}{2}\begin{bmatrix} -\delta(t) & -i\gamma(t) \\ i\gamma(t) & \delta(t) \end{bmatrix}, \tag{4.10}$$

the state in the new basis

$$\widetilde{\phi}(t) = T^\dagger\phi(t), \tag{4.11}$$

and the non-adiabatic coupling

$$\gamma(t) = \frac{\dot{\Omega}(t)\Delta}{\Delta^2 + \Omega^2(t)} = \dot{\Lambda}(t)\varepsilon[1 + \mathcal{O}(\varepsilon^2)], \tag{4.12}$$

To consider D_p as the correct effective Hamiltonian at each time for the problem, we thus need to be able to neglect the non-adiabatic coupling with respect to the distance between the diagonal elements:

$$\left|\frac{\gamma(t)}{\delta(t)}\right| \sim \frac{|\dot{\Lambda}(t)|}{\Delta}\varepsilon \ll 1. \tag{4.13}$$

One can determine precisely the effect of the non-adiabatic coupling by diagonalizing the new resulting Hamiltonian (4.10). This procedure is exactly the one that is applied for the adiabatic

principles (and the construction of a superadiabatic basis) with here ε as the small parameter instead of a slow time. One can here evaluate more simply, using the time dependent perturbation theory, the probability of *loss* in the excited state (whatever the speed is):

$$P_{\text{loss}} \sim |\varepsilon|^2 \ll 1, \tag{4.14}$$

considering a fast rising of the pulse up to its maximal value, and under the condition that the rising is *monotonic*. This excludes fast oscillations of the pulse. This shows that the loss induced by the non-adiabatic coupling is of the same order as the one induced by the static partitioning. Thus *the validity of the partitioning technique requires only the analysis with respect to the magnitude of the static coupling under the conditions of monotonic rising and falling of the pulse.*

In the limit defined by Eq. (4.13), one can take into account in the effective Hamiltonian the effect of the pulse speed, by applying again a perturbative transformation which will give

$$D_p = \frac{\hbar}{2}\begin{bmatrix} -\delta_c(t) & 0 \\ 0 & \delta_c(t) \end{bmatrix} \tag{4.15}$$

with a corrected diagonal term (that takes here into account only the first derivative of the pulse)

$$\delta_c(t) = \delta\left[1 + \frac{1}{2}\left(\frac{\gamma(t)}{\delta}\right)^2\right] = \Delta\left[1 + \frac{1}{2}\varepsilon^2\left(\Lambda^2(t) + \frac{\dot{\Lambda}^2(t)}{\Delta^2}\right) + \mathcal{O}(\varepsilon^4)\right]. \tag{4.16}$$

To use such an effective Hamiltonian, the further approximation $T \approx \mathbb{1}$ should be made. We have exactly $T = \mathbb{1}$ at the end of the pulse when the coupling vanishes, since the eigenvectors of the dressed Hamiltonian coincide then with those of the unperturbed one.

The goal of the next sections is to generalize the formulation of partitioning for many-state systems.

4.2 Perturbation theory formulated as an iteration of unitary transformations: KAM techniques, contact transformation and averaging.

We describe in this section an approach to perturbation theory that is based on applying unitary transformations that simplify the problem. The method is an iterative construction of unitary transformations that reduce the size of the coupling terms. The method of iterative unitary transformations can furthermore be adapted to the construction of effective models by partitioning of degrees of freedom. The idea is to simplify the problem by determining the most relevant subspace in Hilbert space and to construct a simplified Hamiltonian in which the coupling with the complement subspace is reduced by suitably chosen unitary transformations.

4.2.1 Iterative perturbation algorithm

We decompose the Hamiltonian with an unperturbed Hamiltonian H_0 and a perturbation εV_1:

$$H = H_0 + \varepsilon V_1. \tag{4.17}$$

The purpose of ε is only to keep track of the different orders, and at the end we can set $\varepsilon = 1$. The method is defined quite generally, independently of the particular form of H_0 and V_1. We assume that V_1 is a bounded operator. The idea is to construct a unitary transformation $e^{\varepsilon W_1}$, with $W_1^\dagger = -W_1$ such that

$$e^{-\varepsilon W_1} H e^{\varepsilon W_1} = H_0 + \varepsilon D_1 + \varepsilon^2 V_2 =: H_2, \tag{4.18}$$

where D_1 is a diagonal operator, i.e. satisfying $[H_0, D_1] = 0$. Thus the perturbation will be reduced from order ε to order ε^2. Once this is achieved, the approximation of order ε of the eigenvalues and the eigenvectors is obtained from $H_0 + \varepsilon D_1$, i.e. neglecting $\varepsilon^2 V_2$. The eigenvectors of $H_0 + \varepsilon D_1$ are the same as those of H_0, since the two operators commute. If the eigenvalues $\lambda_m^{(0)}$ of H_0 are nondegenerate, and we denote $D_1 = \mathrm{diag}\{d_m\}$, then the perturbed eigenvalues of first order (i.e. neglecting corrections of second order) are

$$\lambda_m^{(1)} = \lambda_m^{(0)} + \varepsilon d_m, \tag{4.19}$$

and the corresponding eigenvectors are

$$|\psi_m^{(1)}\rangle = e^{\varepsilon W_1} |\psi_m^{(0)}\rangle \tag{4.20}$$

with $|\psi_m^{(0)}\rangle = |e_m\rangle$, where $\{|e_m\rangle\}$ is the eigenbasis of H_0 in $\mathcal{H}$.

If some eigenvalues of H_0 are degenerate, the addition of D_1 can lift some degeneracies.

Since the transformed Hamiltonian H_2 is of the same general form a the one we started with (4.17), this procedure can be iterated. The order of the perturbation can thus be reduced successively from ε to ε^2, to ε^4, ... After N iterations the remaining perturbation is of order $\varepsilon^{2^N} = \varepsilon^{e^{N \ln 2}}$, i.e. we have a superexponential decrease. This type of iterative algorithms are therefore called superconvergent. We call this procedure a quantum KAM algorithm, since it is the quantum analogue of the Kolmogorov-Arnold-Moser (KAM) transformations developed in classical mechanics [88, 89, 90, 91, 92, 93, 94]. When this type of procedure is used to derive a non-superconvergent polynomial expansion of the eigenvalues, it is known as the van Vleck perturbation theory [95]. The transformations $e^{\varepsilon W_1}$ are called *contact transformations*, or *KAM transformations*. One step of the algorithm is roughly equivalent to first order perturbation theory. The idea is that instead of performing a perturbation calculation of high order, one can perform several times a calculation of first order. The acceleration of convergence can be explained by the fact that at each step of the iteration one develops around a different effective nonperturbed Hamiltonian, that contains already the corrections found in the previous iterations.

We remark that D_N, the diagonal part obtained after N iterations, is a function of ε that is not a polynomial, since as we will see below the construction involves rational functions and exponentials. However, if one expands D^N as a power series in ε up to a certain order (smaller than ε^{2^N}), the result must coincide with the Rayleigh-Schrödinger power series of that order, since the coefficients of this expansion are unique (even in the case when the series is only asymptotic, i.e. non convergent). In practice, performing one or two iterations gives already the main information of the processes we will study.

4.2.2 Construction of the contact transformations

We discuss now how one can construct the transformation for one step in the iterative algorithm. An equation to determine D_1 and W_1 can be obtained expanding eq. (4.18) in powers of ε and

requiring that the terms of order ε cancel out. This leads to the two equations

$$[H_0, W_1] + V_1 - D_1 = 0, \tag{4.21a}$$
$$[H_0, D_1] = 0. \tag{4.21b}$$

The solution of these equations can be given using the eigenvalues and eigenvectors of H_0 which we will denote by λ^0_ν and $|\nu, j\rangle$ [we represent the index m of (4.19) and (4.20) by an index ν that labels the different eigenvalues, and j distinguishes different basis vectors corresponding to a degenerate eigenvalue]. We define a projection operator Π_{H_0} that extracts from the perturbation V_1 the diagonal component with respect to the eigenbasis of H_0:

$$\Pi_{H_0} V_1 = \sum_{\nu,j,j'} |\nu, j\rangle\langle\nu, j|V_1|\nu, j'\rangle\langle\nu, j'|. \tag{4.22}$$

With this notation a solution of (4.21) can be written as

$$D_1 = \Pi_{H_0} V_1 = \text{diagonal part of } V_1, \tag{4.23a}$$
$$W_1 = -\sum_{\nu,j,j',\nu'\neq\nu} \frac{|\nu, j\rangle\langle\nu, j|V_1|\nu', j'\rangle\langle\nu', j'|}{\lambda^0_\nu - \lambda^0_{\nu'}}. \tag{4.23b}$$

The solution W_1 is not unique, since if A is any operator such that $[H_0, A] = 0$ then $W_1 + A$ is also a solution. The solution (4.23a) is singled out as the unique solution with zero diagonal blocks, $\Pi_{H_0} W_1 = 0$ [96].

There are two ways to proceed, depending on what we do with the diagonal part $\Pi_{H_0} V_1$ of the perturbation. It can be added to the unperturbed Hamiltonian either after or before the transformation.

(i) In the first case we take H_0 as the unperturbed Hamiltonian and the perturbation V_1 has a non-zero projection $\Pi_{H_0} V_1$, which leads to a term $D_1 = \Pi_{H_0} V_1$ in the solution (4.23a). In this case the second order perturbation that remains at the end of the transformation takes the form

$$\begin{aligned} \varepsilon^2 V_2 = {} & \frac{\varepsilon^2}{2}[V_1, W_1] + \frac{\varepsilon^3}{3}[[V_1, W_1], W_1] + \ldots + \varepsilon^M \frac{(M-1)}{M!} \underbrace{[\ldots[[V_1, W_1], W_1], \ldots]}_{M-1 \text{ commutators}} + \ldots \\ & + \frac{\varepsilon^2}{2!}[D_1, W_1] + \frac{\varepsilon^3}{3!}[[D_1, W_1], W_1] + \ldots + \frac{\varepsilon^M}{M!} \underbrace{[\ldots[D_1, W_1], W_1], \ldots]}_{M-1 \text{ commutators}} + \ldots \end{aligned} \tag{4.24}$$

We remark that defining an operator $L_{W_1} : V \mapsto L_{W_1}(V) := [V, W_1]$, the transformation (4.18) can be expressed as

$$e^{-\varepsilon W_1} H e^{\varepsilon W_1} = e^{L_{\varepsilon W_1}}(H) = \sum_{M=0}^{\infty} \varepsilon^M \frac{1}{M!} \left(L_{W_1}\right)^M (K) \tag{4.25}$$

and the above expression (4.24) can be written as

$$\varepsilon^2 V_2 = \sum_{M=2}^{\infty} \varepsilon^M \frac{(M-1)}{M!} \left(L_{W_1}\right)^{(M-1)} (V_1) + \sum_{M=2}^{\infty} \varepsilon^M \frac{1}{M!} \left(L_{W_1}\right)^{(M-1)} (D_1), \tag{4.26a}$$
$$= \sum_{M=2}^{\infty} \varepsilon^M \frac{1}{M!} \left(L_{W_1}\right)^{(M-1)} ((M-1)V_1 + D_1). \tag{4.26b}$$

(ii) The second possibility is to define a new unperturbed Hamiltonian $\tilde{H}_0^D$ in which the projection $\Pi_{H_0}V_1$ of the perturbation is already absorbed :

$$\tilde{H}_0^D = H_0 + \Pi_{H_0}V_1. \tag{4.27}$$

The remaining perturbation $V_1 - \Pi_{H_0}V_1$ has zero projection and thus there in no supplementary $\tilde{D}_1$ to be added. In this case the second order perturbation that remains at the end of the transformation takes the somewhat simpler form

$$\varepsilon^2 V_2 = \frac{\varepsilon^2}{2}[V_1, W_1] + \frac{\varepsilon^3}{3}[[V_1, W_1], W_1] + \ldots + \varepsilon^M \frac{(M-1)}{M!} \underbrace{[\ldots[[V_1, W_1], W_1], \ldots]}_{M-1 \text{ commutators}} + \ldots \tag{4.28}$$

Both alternatives can be useful; depending on the particular problem one of them can be more convenient than the other one. As we will see in Section 6, the second version is particularly adapted to the construction of effective Hamiltonians by the partitioning technique.

4.2.3 Interpretation as an averaging procedure

The perturbation theory outlined above can be interpreted as an averaging procedure [88, 89, 90, 91, 92, 96]: The projector can be expressed as

$$D_1 = \Pi_{H_0}V_1 = \lim_{\tau\to\infty} \frac{1}{\tau} \int_0^\tau ds\, e^{-iH_0 s} V_1 e^{iH_0 s} \tag{4.29}$$

and

$$W_1 = \lim_{\tau\to\infty} \frac{-i}{\tau} \int_0^\tau ds' \int_0^{s'} ds\, e^{-iH_0 s}(V_1 - \Pi_{H_0}V_1)e^{iH_0 s}. \tag{4.30}$$

The term $e^{-iH_0 s}V_1 e^{iH_0 s}$ in (4.29) is equal to the inverse time evolution that the operator V_1 would have in the Heisenberg picture for the dynamics generated by H_0. Thus, D_1, which is the term that is added to constitute the approximate effective Hamiltonian $H_{01} := H_0 + D_1$, can be interpreted as the average of the perturbation with respect to the dynamics generated by H_0.

Another equivalent expression is [97, 98]

$$D_1 = \Pi_{H_0}V_1 = \lim_{\beta\to 0^+} \beta \int_0^\infty ds\, e^{-\beta s} e^{-iH_0 s} V_1 e^{iH_0 s} \tag{4.31}$$

and

$$W_1 = -i \lim_{\beta\to 0^+} \beta \int_0^\infty ds'\, e^{-\beta s'} \int_0^{s'} ds\, e^{-iH_0 s}(V_1 - \Pi_{H_0}V_1)e^{iH_0 s}. \tag{4.32}$$

The relation between these two expression can be thought of as two equivalent realizations of the time average

$$\text{Average}(f) = \lim_{\beta\to 0^+} \beta \int_0^\infty ds'\, e^{-\beta s'} f(s') = \lim_{\tau\to\infty} \frac{1}{\tau} \int_0^\tau ds'\, f(s'). \tag{4.33}$$

A third alternative expression for W_1 is [97, 98]

$$W_1 = \lim_{\beta\to 0^+} -i \int_0^\infty ds\, e^{-\beta s} e^{-iH_0 s}(V_1 - \Pi_{H_0}V_1)e^{iH_0 s}. \tag{4.34}$$

4.3 Partial contact transformation

There are several ways to apply the contact transformation partially. For instance, one can ask to construct an effective Hamiltonian which is not fully diagonal, but instead block-diagonal. Within the Floquet theory, this is actually the usual goal: one wants to construct an effective dressed Hamiltonian (i) in a basis of essential states, and (ii) which does not depend on the θ variable. This means that we aim (i) to block-diagonalize in this basis of essential states and (ii) to diagonalize with respect to the θ variable. This construction is discussed in Chapter 6. The block-diagonalization is formulated in terms of partitioning in the next section.

We can also use another useful block-diagonalization of a Floquet Hamiltonian: the diagonalization with respect to the field-free system, and not with respect to θ. This is done in subsection 4.3.1. We also study in subsection 4.3.2 another partial contact transformation, which consists in treating only one part of the perturbation.

In both subsections, we start with a Floquet Hamiltonian

$$K = K_0 + \epsilon V_0 + \epsilon V_1 \tag{4.35}$$

with the perturbation of order ϵ

$$\epsilon V := \epsilon V_0 + \epsilon V_1 \tag{4.36}$$

4.3.1 Block-diagonalization with respect to bare system

Here we assume that $\epsilon V_0(\theta)$ is diagonal in the basis of H_0 but not in the one of $K_0 = -i\hbar\omega\frac{\partial}{\partial\theta} + H_0$:

$$[H_0, V_0] = 0, \qquad \left[-i\hbar\omega\frac{\partial}{\partial\theta}, V_0\right] \neq 0 \tag{4.37}$$

We assume that $V_1(\theta)$ has no diagonal element in the basis of the eigenstates of H_0: $\Pi_{H_0} V_1 = 0$.

We want here to *partially diagonalize* V_1 *with respect to* H_0. We thus construct the contact transformation $e^{\epsilon W_1}$:

$$W_1 = -\sum_{\nu,j,\nu'\neq\nu} \frac{|\nu, j\rangle\langle\nu, j|V_1|\nu', j'\rangle\langle\nu', j'|}{\lambda_\nu^{(0)} - \lambda_{\nu'}^{(0)}}, \qquad W_1^\dagger = -W_1, \tag{4.38}$$

that reduces the size of the perturbation ϵV_1 to the order ϵ^2:

$$e^{-\epsilon W_1} K e^{\epsilon W_1} = K_0 + \epsilon D_1(\theta) + \epsilon^2 V_2(\theta), \qquad [H_0, D_1] = 0, \tag{4.39}$$

This leads to the equation

$$[K_0, W_1] + V_0(\theta) + V_1(\theta) = D_1(\theta) \tag{4.40}$$

with the diagonal

$$D_1(\theta) = V_0(\theta). \tag{4.41}$$

At the second order, we obtain

$$e^{-\epsilon W_1} K e^{\epsilon W_1} = K_0 + \epsilon V_0 + \frac{\epsilon^2}{2}\mathrm{diag}_{H_0}[V_1, W_1] + \mathcal{O}(\epsilon^3), \tag{4.42}$$

with the diagonal part of a matrix A in a basis $|n\rangle$:

$$\mathrm{diag}_{H_0} A = \sum_n |n\rangle\langle n|A|n\rangle\langle n|. \tag{4.43}$$

4.3.2 Partial diagonalization of the perturbation

Here we assume that the perturbation V has no diagonal elements in the basis of the eigenvectors $\{|\nu, j\rangle\}$ of K_0, i.e.

$$\Pi_{K_0} V = 0. \tag{4.44}$$

We want *to extract the dominant contribution of* ϵV_1 *letting* ϵV_0 *unchanged* (for instance if V_0 is resonant). We thus construct the same transformation as above

$$e^{\epsilon W_1}, \qquad W_1^\dagger = -W_1, \tag{4.45}$$

that reduces the size of the perturbation ϵV_1 to the order ϵ^2, extracting a diagonal part independent of the dynamical variable θ :

$$e^{-\epsilon W_1} K e^{\epsilon W_1} = K_0 + \epsilon V_0 + \epsilon D_1 + \epsilon^2 V_2(\theta), \qquad [K_0, D_1] = 0, \tag{4.46}$$

and

$$D_1 = \Pi_{K_0} V_1 = 0. \tag{4.47}$$

Identifying the power expansion using (4.45), we obtain at the second order

$$e^{-\epsilon W_1} K e^{\epsilon W_1} = K_0 + \epsilon V_0 + \epsilon^2 [V_0, W_1] + \frac{\epsilon^2}{2} [V_1, W_1] + \mathcal{O}(\epsilon^3). \tag{4.48}$$

4.4 Partitioning: General formulation

We develop the standard partitioning technique (see for instance [99, 100, 101, 102]), but with the use of the iterative KAM perturbation algorithms. We derive an effective Hamiltonian of second order. The scheme we show can be easily extended to higher orders.

We consider the dynamics of a system defined on a Hilbert space $\mathcal{H}$ of dimension N, by a time-independent Hamiltonian H. We consider situations in which the Hilbert space can be split into two orthogonal subspaces $\mathcal{H} = \mathcal{H}^0 \oplus \mathcal{H}^1$, that are only weakly coupled by H. Introducing the projectors P^j into these subspaces, $\mathcal{H}^0 = P^0\mathcal{H}$ and $\mathcal{H}^1 = P^1\mathcal{H}$, the Hamiltonian can be separated into four parts:

$$H = H^{00} + H^{11} + H^{01} + H^{10} \qquad \text{with} \quad H^{ij} := P^i H P^j \ , \quad H^{01} = (H^{10})^\dagger. \tag{4.49}$$

We can represent this partition symbolically in matrix form as

$$H = \begin{pmatrix} H^{00} & H^{01} \\ H^{10} & H^{11} \end{pmatrix}. \tag{4.50}$$

The idea is that the coupling $H^{01} + H^{10}$ is small with respect to the other relevant energies of $|H^{11} - H^{00}|$. We think of it as being of order ε. We introduce the notation

$$\varepsilon V_1 := H^{01} + H^{10} = \varepsilon(\tilde{H}^{01} + \tilde{H}^{10}). \tag{4.51}$$

where ε is a formal parameter, that is useful to keep track of the orders of the different terms, and it is meant to reflect the fact that $H^{01}+H^{10}$ is small. Once the formulas for the perturbative procedure are obtained, ε can be set equal to 1. The whole construction can be made without introducing ε. Its role is exclusively as an intuitive aid to follow the construction. We will show

that the *effective Hamiltonian of second order* (connected with an initial condition in $\mathcal{H}^0$) reads as

$$H^{00}_{\text{eff}} = H^{00} + \frac{\varepsilon^2}{2} P^0 \left[\tilde{H}^{01} W_1^{10} + (\tilde{H}^{01} W_1^{10})^\dagger \right] P^0, \tag{4.52}$$

with W_1^{10} defined in Eq. (4.63c). In terms of the eigenvalues and eigenvectors of H^{00} restricted to the subspace $P^0\mathcal{H}$, which we denote by λ_n^{00} and $|n^{00}\rangle$, and those of H^{11} restricted to the subspace $P^1\mathcal{H}$ which we denote by λ_m^{11} and $|m^{11}\rangle$, it becomes

$$H^{00}_{\text{eff}} = H^{00} - \frac{1}{2} \sum_{n,\tilde{n}} |\tilde{n}^{00}\rangle \left[\sum_m \langle \tilde{n}^{00}|H^{01}|m^{11}\rangle\langle m^{11}|H^{10}|n^{00}\rangle \left(\frac{1}{\lambda_m^{11} - \lambda_n^{00}} + \frac{1}{\lambda_m^{11} - \lambda_{\tilde{n}}^{00}} \right) \right] \langle n^{00}|. \tag{4.53}$$

The goal is to find a unitary transformation S that transforms H into block-diagonal form, at least to some order of approximation:

$$S^\dagger H S = \begin{pmatrix} H^{00} + D_1^{00} & 0 \\ 0 & H^{11} + D_1^{11} \end{pmatrix}. \tag{4.54}$$

The idea is in general that instead of diagonalizing by perturbation methods the complete Hamiltonian, one first reduces it approximately to block-diagonal form, singling out a block $H^{00} + D_1^{00}$, of small dimension, that is the most relevant part for the dynamics of a particularly chosen initial condition. The Hamiltonian $H^{00} + D_1^{00}$ is called the *effective Hamiltonian* for the considered process. Since it is of small dimension it can often be analyzed in detail with non-perturbative methods (for example by exact diagonalization). The sub-block should contain all the states with which the initial state is mainly coupled by the dynamics. These states are called *essential states*. In other words, within each of the initial diagonal blocks the couplings can be strong, but the couplings between the blocks should be small. We assume in particular that the spectrum of H^{00} is well separated from the one of H^{11} by a minimal distance between eigenvalues denoted $\Delta\lambda_{min}$. We require that the norm of the coupling $H^{01} + H^{10}$ between the two blocks is small with respect to $\Delta\lambda_{min}$.

We thus construct a unitary transformation of the form $e^{\varepsilon W_1}$, with $W_1^\dagger = -W_1$ such that

$$e^{-\varepsilon W_1}(H^{00} + H^{11} + \varepsilon V_1)e^{\varepsilon W_1} = H^{00} + H^{11} + D_1 + \varepsilon^2 V_2, \tag{4.55}$$

where $D_1 = D_1^{00} + D_1^{11}$, with $D_1^{ii} = P^i D_1 P^i$, $i = 0, 1$, and V_2 is a remaining coupling term that is of order ε^2. We will use the notation $D_1 =: \varepsilon\tilde{D}_1$. Expansion of the exponentials and extractions of the non block-diagonal terms leads to the equations that D_1 and W_1 are required to fulfill:

$$\begin{aligned} [H^{00} + H^{11}, W_1] + V_1 - \tilde{D}_1 &= 0, & (4.56a) \\ \left[P^0, D_1^{00}\right] &= 0, & (4.56b) \\ \left[P^1, D_1^{11}\right] &= 0. & (4.56c) \end{aligned}$$

Defining

$$W_1^{ij} := P^i W_1 P^j, \tag{4.57}$$

and acting with the projectors P^0 and P^1 from the left and from the right in the four possible

combinations, equation (4.56a) can be decomposed in four independent equations:

$$\begin{aligned} H^{00}W_1^{01} - W_1^{01}H^{11} + \tilde{H}^{01} &= 0, && (4.58a)\\ H^{11}W_1^{10} - W_1^{10}H^{00} + \tilde{H}^{10} &= 0, && (4.58b)\\ D_1^{00} &= 0, && (4.58c)\\ D_1^{11} &= 0. && (4.58d) \end{aligned}$$

Equations (4.58c) (4.58d) are a direct consequence of the fact that $V_1 \equiv H^{01} + H^{10}$ have zero diagonal blocks and mean that $D_1 = 0$. We remark that equations (4.58a)-(4.58d) do not impose any condition on the components W_1^{00} and W_1^{11}, which can therefore be chosen arbitrarily. The choice that leads to the simplest expressions is $W_1^{00} = 0$ and $W_1^{11} = 0$. The two other components W_1^{10}, W_1^{01} are uniquely determined. In close analogy with the construction of Section 4.2.2, we define the projector Π by

$$\Pi V := P^0 V P^0 + P^1 V P^1. \tag{4.59}$$

A solution of equations (4.56a)(4.56b) is given by

$$\tilde{D}_1 = \Pi V_1 = 0 \tag{4.60}$$

and

$$\begin{aligned} W_1^{01} &= \lim_{\tau\to\infty} \frac{-i}{\tau} \int_0^\tau ds' \int_0^{s'} ds\, e^{-iH^{00}s} \tilde{H}^{01} e^{iH^{11}s}, && (4.61a)\\ &= \lim_{\beta\to 0^+} -i \int_0^\infty ds\, e^{-\beta s}\ e^{-iH^{00}s} \tilde{H}^{01} e^{iH^{11}s} && (4.61b) \end{aligned}$$

with

$$W_1^{10} = -\left(W_1^{01}\right)^\dagger. \tag{4.62}$$

This solution can be expressed in terms of the eigenvalues and eigenvectors of H^{00} and of H^{11} :

$$\begin{aligned} W_1 &= W_1^{01} + W_1^{10}, && (4.63a)\\ W_1^{01} &= -\sum_{n,m} \frac{|n^{00}\rangle\langle n^{00}|\tilde{H}^{01}|m^{11}\rangle\langle m^{11}|}{\lambda_n^{00} - \lambda_m^{11}}, && (4.63b)\\ W_1^{10} &= -\sum_{n,m} \frac{|m^{11}\rangle\langle m^{11}|\tilde{H}^{10}|n^{00}\rangle\langle n^{00}|}{\lambda_m^{11} - \lambda_n^{00}}. && (4.63c) \end{aligned}$$

Since $D_1 = 0$, we conclude that there is no contribution to the diagonal blocks in the first iteration, i.e. of first order in ε, and in analogy with Eq. (4.28), the remaining coupling term can be written as

$$\varepsilon^2 V_2 = \frac{\varepsilon^2}{2}[V_1, W_1] + \frac{\varepsilon^3}{3}[[V_1, W_1], W_1] + \ldots + \varepsilon^M \frac{(M-1)}{M!} \underbrace{[\ldots[[V_1, W_1], W_1], \ldots]}_{M-1 \text{ commutators}} + \ldots \tag{4.64}$$

We can obtain an effective Hamiltonian of second order with little supplementary effort: We first extract from the block-diagonal part of $\varepsilon^2 V_2$ the term

$$B_2 := \frac{\varepsilon^2}{2}[V_1, W_1], \tag{4.65}$$

which is the only one that carries the lowest power ε^2. Since $P^1[V_1, W_1]P^0 = 0$ and $P^0[V_1, W_1]P^1 = 0$, the term of power ε^2 has no off-block-diagonal part. Thus we can write

$$e^{-\varepsilon W_1}(H^{00} + H^{11} + \varepsilon V_1)e^{\varepsilon W_1} = H^{00} + H^{11} + \frac{\varepsilon^2}{2}[V_1, W_1] + \varepsilon^3 V_3 \tag{4.66}$$

with

$$\varepsilon^3 V_3 = \frac{\varepsilon^3}{3}[[V_1, W_1], W_1] + \ldots + \varepsilon^M \frac{(M-1)}{M!} \underbrace{[\ldots[[V_1, W_1], W_1], \ldots]}_{M-1 \text{ commutators}} + \ldots \tag{4.67}$$

or, symbolically, in matrix notation

$$\begin{aligned} H_2 &= e^{-\varepsilon W_1} \begin{pmatrix} H^{00} & H^{01} \\ H^{10} & H^{11} \end{pmatrix} e^{\varepsilon W_1} \\ &= \begin{pmatrix} H^{00} + \frac{\varepsilon^2}{2}\left(\tilde{H}^{01}W_1^{10} - W_1^{01}\tilde{H}^{10}\right) & 0 \\ 0 & H^{11} + \frac{\varepsilon^2}{2}\left(\tilde{H}^{10}W_1^{01} - W_1^{10}\tilde{H}^{01}\right) \end{pmatrix} + \varepsilon^3 V_3 \\ &= \begin{pmatrix} H^{00} + \frac{\varepsilon^2}{2}\left[\tilde{H}^{01}W_1^{10} + (\tilde{H}^{01}W_1^{10})^\dagger\right] & 0 \\ 0 & H^{11} - \frac{\varepsilon^2}{2}\left[(W_1^{10}\tilde{H}^{01})^\dagger + W_1^{10}\tilde{H}^{01}\right] \end{pmatrix} + \varepsilon^3 V_3. \end{aligned} \tag{4.68}$$

Thus we find the effective Hamiltonian (4.52) that gives the eigenvectors and eigenvalues of order ε^2 (and corrections of order ε^3).

Remark. In fact we can show that while the next order correction for the eigenvectors is indeed of order ε^3, the one for the eigenvalues is of order ε^4. The term of order ε^3 in (4.67) is $[[V_1, W_1], W_1]$ which has zero block-diagonal projection, since the product of two off-block-diagonal operators is block-diagonal, and the product of an off-block-diagonal operator with a block-diagonal operator is off-block-diagonal. Symbolically we can represent this by

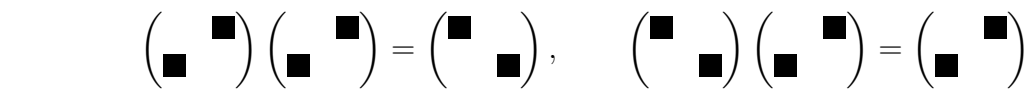

and shown for arbitrary operators A and B by

$$\left(P^0AP^1 + P^1AP^0\right)\left(P^0BP^1 + P^1BP^0\right) = P^0AP^1BP^0 + P^1AP^0BP^1 \tag{4.70}$$

and

$$\left(P^0AP^0 + P^1AP^1\right)\left(P^0BP^1 + P^1BP^0\right) = P^0AP^0BP^1 + P^1AP^1BP^0 \tag{4.71}$$

The fact that the term of order ε^3 in (4.67) is off-block-diagonal implies that, if we perform a second unitary transformation $e^{\varepsilon^3 W_3}$, there will be no term of order ε^3 in the diagonal block projection D_3, and thus the next order correction for the diagonal block, and therefore for eigenvalues, will be of order ε^4 (given by $\varepsilon^4[[[V_1, W_1], W_1], W_1]/8$).

4.5 Relation with adiabatic elimination

In the literature a different technique has been widely used to construct effective Hamiltonians, based on the partitioning technique combined with an approximation procedure known as

adiabatic elimination for the time-dependent Schrödinger equation (see Ref. [43], p. 1165). In this section we show that the effective Hamiltonian constructed by adiabatic elimination can be recovered from the above construction by choosing the reference of the energy appropriately. Our stationary formulation allows us moreover to estimate the order of the neglected terms, and to improve the approximation to higher orders in a systematic way.

The idea in the method of adiabatic elimination is that the time evolution of the components in $\mathcal{H}^1$ oscillates very rapidly with respect to the evolution of the components in $\mathcal{H}^0$. This justifies the substitution of the time dependent components in $\mathcal{H}^1$ by some average values. This leads then to an effective Hamiltonian in $\mathcal{H}^0$ that takes the form [see Ref. [43], p. 1166, Eq. (18.7-7), where there is a sign misprint]

$$H^{00}_{\text{eff,ae}} = H^{00} - H^{01}\left(H^{11}\right)^{-1} H^{10}. \tag{4.72}$$

This equation can be obtained from Eq. (4.52) as follows. Denoting by $\lambda^{00}_{\max}$ the largest eigenvalue of H^{00}, we can write the denominator of W^{10}_1 (4.63c) as

$$\lambda^{11}_m - \lambda^{00}_n = (\lambda^{11}_m - \lambda^{00}_{\max}) + (\lambda^{00}_{\max} - \lambda^{00}_n). \tag{4.73}$$

The condition that the time evolution of the components in $\mathcal{H}^1$ oscillate very rapidly with respect to the evolution of the components in $\mathcal{H}^0$ can be formulated by an inequality between the eigenvalues:

$$\lambda^{00}_{\max} - \lambda^{00}_n \ll \lambda^{11}_m - \lambda^{00}_{\max}. \tag{4.74}$$

Thus the expression (4.63c) can be approximated by

$$\begin{aligned} W^{10}_1 \approx -\sum_{n,m} \frac{|m^{11}\rangle\langle m^{11}|\tilde{H}^{10}|n^{00}\rangle\langle n^{00}|}{\lambda^{11}_m - \lambda^{00}_{\max}} &= -\sum_{n,m} |m^{11}\rangle\langle m^{11}| \left(H^{11} - \lambda^{00}_{\max}\mathbb{1}_{11}\right)^{-1} \tilde{H}^{10}|n^{00}\rangle\langle n^{00}| \\ &= -\left(H^{11} - \lambda^{00}_{\max}\mathbb{1}_{11}\right)^{-1} \tilde{H}^{10}, \end{aligned} \tag{4.75}$$

which gives for the effective Hamiltonian (4.52):

$$H^{00}_{\text{eff}} \approx H^{00} - H^{01}\left(H^{11} - \lambda^{00}_{\max}\mathbb{1}_{11}\right)^{-1} H^{10}. \tag{4.76}$$

Choosing the reference of energy $\lambda^{00}_{\max} = 0$ allows us to recover Eq. (4.72).

We remark that in the approach by adiabatic elimination a further approximation is implicitly made, since the eigenvectors (or the initial conditions) when it is applied to dynamics are not transformed with $e^{\varepsilon W_1}$. This amounts to the approximation $e^{\varepsilon W_1} = \mathbb{1} + \varepsilon W_1 + \ldots \approx \mathbb{1}$. This does not produce a big difference when adiabatic elimination is applied to adiabatic processes with laser pulses, since the initial and final eigenvectors of the perturbed Hamiltonian coincide with those of the unperturbed one.

4.6 High frequency partitioning

We here construct a *high frequency perturbation theory* adapted to the partitioning setup, which is another way to obtain the result of adiabatic elimination. We consider a partition represented symbolically in matrix form as

$$H = \begin{pmatrix} H^{00} - \lambda^{00}_{\max}\mathbb{1}_{00} & H^{01} \\ H^{10} & f\left(H^{11} - \lambda^{00}_{\max}\mathbb{1}_{11}\right) \end{pmatrix}, \tag{4.77}$$

in a regime where $f \to \infty$. Defining $\epsilon := 1/f$, we decompose accordingly as

$$\hat{H} := H/f = \begin{pmatrix} 0 & 0 \\ 0 & \hat{H}^{11} \end{pmatrix} + \epsilon \begin{pmatrix} \hat{H}^{00} & H^{01} \\ H^{10} & 0 \end{pmatrix} =: \hat{H}_0 + \epsilon \hat{V}_1, \tag{4.78}$$

where we have simplified the notation by defining $\hat{H}^{00} := H^{00} - \lambda^{00}_{\max} \mathbb{1}_{00}$ and $\hat{H}^{11} := H^{11} - \lambda^{00}_{\max} \mathbb{1}_{11}$. We construct a unitary transformation $\exp(\epsilon W_1)$ such that

$$e^{-\epsilon W_1}(\hat{H}_0 + \epsilon \hat{V}_1) e^{\epsilon W_1} = \hat{H}_0 + \epsilon D_1 + \epsilon^2 V_2 \tag{4.79}$$

with the condition

$$\left[P^1, D_1\right] = 0, \tag{4.80}$$

where P^1 is the projection into the subspace corresponding to the 11-block. We remark that defining the projector into the orthogonal complement, $P^0 := \mathbb{1} - P^1$, the condition (4.80) implies that also $[P^0, D_1] = 0$, which leads to

$$D_1 = P^1 D_1 P^1 + P^0 D_1 P^0. \tag{4.81}$$

As before, the generator W_1 can be chosen such that $P^1 W_1 P^1 = 0, \quad P^0 W_1 P^0 = 0$, and

$$D_1 = P^1 \hat{V}_1 P^1 + P^0 \hat{V}_1 P^0 = P^0 \hat{V}_1 P^0 = \begin{pmatrix} \hat{H}^{00} & 0 \\ 0 & 0 \end{pmatrix}. \tag{4.82}$$

The generator W_1 is determined by the equation

$$[\hat{H}_0, W_1] + \hat{V}_1 - D_1 = 0. \tag{4.83}$$

From the general procedure described in the preceding sections, $W_1 = W_1^{01} + W_1^{10}$ can be written e.g. as

$$W_1^{01} = \lim_{\beta \to 0^+} -i \int_0^\infty ds\, e^{-\beta s} H^{01} e^{i \hat{H}^{11} s}, \qquad W_1^{10} = -\left(W_1^{01}\right)^\dagger. \tag{4.84}$$

Alternatively we can write explicitly the equation (4.83), which in the present case becomes

$$\begin{aligned} 0 &= \left[\begin{pmatrix} 0 & 0 \\ 0 & \hat{H}^{11} \end{pmatrix}, \begin{pmatrix} 0 & W_1^{01} \\ W_1^{10} & 0 \end{pmatrix} \right] + \begin{pmatrix} 0 & H^{01} \\ H^{10} & 0 \end{pmatrix} \\ &= \begin{pmatrix} 0 & -W_1^{01} \hat{H}^{11} \\ \hat{H}^{11} W_1^{10} & 0 \end{pmatrix} + \begin{pmatrix} 0 & H^{01} \\ H^{10} & 0 \end{pmatrix} \end{aligned} \tag{4.85}$$

which leads to the solution

$$W_1^{01} = H^{01} \left(\hat{H}^{11}\right)^{-1}, \tag{4.86a}$$

$$W_1^{10} = -\left(W_1^{01}\right)^\dagger = -\left(\hat{H}^{11}\right)^{-1} H^{10}, \tag{4.86b}$$

and thus to the remaining corrections of order ϵ^2 of the form

$$\begin{aligned} H_2 &= e^{-\epsilon W_1} \begin{pmatrix} \hat{H}^{00} & H^{01} \\ H^{10} & f\hat{H}^{11} \end{pmatrix} e^{\epsilon W_1} \\ &= \begin{pmatrix} H^{00} + \frac{\epsilon^2}{2}\left(H^{01} W_1^{10} - W_1^{01} H^{10}\right) & \frac{\epsilon^2}{2} \hat{H}^{00} W_1^{01} \\ -\frac{\epsilon^2}{2} W_1^{10} \hat{H}^{00} & H^{11} + \frac{\epsilon^2}{2}\left(H^{10} W_1^{01} - W_1^{10} H^{01}\right) \end{pmatrix} + \epsilon^3 V_3. \end{aligned} \tag{4.87}$$

After a second transformation of the form $\exp(\epsilon^2 W_2)$ designed to eliminate the non-block-diagonal terms of order ϵ^2, one obtains an effective Hamiltonian of second order for the 00-block of the form

$$H^{00}_{\text{eff}} = H^{00} - \lambda^{00}_{\max}\mathbb{1}_{00} - H^{01}\left(H^{11} - \lambda^{00}_{\max}\mathbb{1}_{11}\right)^{-1} H^{10}. \tag{4.88}$$

We remark that, as opposed to Eqs. (4.68)- (4.52), in this construction two unitary transformations are needed to obtain the effective eigenvectors to second order (after the first transformation, where keeping only the diagonal blocks in (4.87) yields the eigenvalues to second order, but not the eigenvectors).

4.7 High frequency perturbation theory

A variation of the procedures described above can be applied to situations in which the frequency ω of the perturbation is high with respect to the internal frequencies of the considered system [103]. We start with a Floquet Hamiltonian of the form

$$K = -i\hbar\omega\frac{\partial}{\partial\theta} + H_0(x) + V_1(x,\theta) \tag{4.89}$$

where x symbolizes the degrees of freedom of the molecule. Since we are interested in the limit $\hbar\omega \to \infty$, we define a small parameter $\epsilon := 1/(\hbar\omega)$ and we rewrite

$$K = \hbar\omega\hat{K} \tag{4.90}$$

with

$$\hat{K} = -i\frac{\partial}{\partial\theta} + \epsilon\left(H_0 + V_1\right). \tag{4.91}$$

The eigenvectors of K are the same ones as those for $\hat{K}$, and the eigenvalues just have to be multiplied by $\hbar\omega$. The difference with the preceding discussion is that here H_0 and V are both of order ϵ. Thus we take as the unperturbed Floquet Hamiltonian just

$$\hat{K}_0 := -i\frac{\partial}{\partial\theta}. \tag{4.92}$$

If the frequency is large compared with the frequencies of the system, there will not be any resonances. We can thus proceed with the iterative perturbative KAM algorithm by first determining a unitary transformation $e^{\epsilon W_1(x,\theta)}$, with $W_1^\dagger = -W_1$ such that

$$e^{-\epsilon W_1}\hat{K}e^{\epsilon W_1} = \hat{K}_0 + \epsilon D_1 + \epsilon^2 V_2 =: K_2, \tag{4.93}$$

where D_1 is a θ-independent operator such that $[\hat{K}_0, D_1] = 0$. Thus the perturbation will be reduced from order ϵ to order ϵ^2. The generator W_1 of the contact transformation is determined by the equations

$$\begin{aligned} [K_0, W_1] + H_0 + V_1 - D_1 &= 0, & \text{(4.94a)}\\ [K_0, D_1] &= 0. & \text{(4.94b)} \end{aligned}$$

The equation (4.94a) can be written as

$$-i\frac{\partial W_1}{\partial\theta} + H_0 + V_1 - D_1 = 0, \tag{4.95}$$

whose general solution is given by

$$W_1 = -i \int^{\theta} d\theta \; (H_0 + V_1 - D_1) + C, \tag{4.96}$$

where C is an arbitrary θ-independent operator acting on $\mathcal{H}$, which one can choose as $C = 0$. Since $W_1(x, \theta)$ is a multiplication operator acting on functions of the angle θ, it must be necessarily 2π-periodic. This condition determines D_1 uniquely in terms of the average

$$\overline{V_1} := \int_0^{2\pi} \frac{d\theta}{2\pi} V_1(x, \theta) \tag{4.97}$$

as

$$D_1 = H_0 + \overline{V_1}. \tag{4.98}$$

Thus we obtain

$$W_1(x, \theta) = -i \int^{\theta} d\theta \; (V_1(x, \theta) - \overline{V_1}(x)). \tag{4.99}$$

We remark that the solution (4.98), (4.99) of Eqs. (4.94) can be obtained from the general equations (4.29), (4.30).

This contact transformation $e^{\epsilon W_1}$ can be interpreted, in the case where $[V_1(x, \theta), V_1(x, \theta')] = 0$, for all θ, θ', as the unitary transformation which allows one to diagonalize exactly the Hamiltonian $\hbar\omega \hat{K}_0 + V_1(x, \theta)$ with respect to θ, taking x as a parameter. We obtain $\lambda_k^{(0)} = \overline{V_1} + k\hbar\omega$ (k positive or negative integer) for the eigenvalues associated to the eigenvectors $\chi(\theta, x) = \exp(\epsilon W_1(x, \theta) + ik\theta)$. We remark that if $\overline{V_1} = 0$, the eigenvalues do not depend on the variable x.

Adapting the equation (4.26b) the remaining perturbation of order ϵ^2 can be written as

$$\epsilon^2 V_2 = \sum_{M=2}^{\infty} \varepsilon^M \frac{1}{M!} \left(L_{W_1}\right)^{(M-1)} \left((M-1)\left(H_0 + V_1\right) + D_1\right) = \frac{\epsilon^2}{2!}[V_1 + \overline{V_1} + 2H_0, W_1] + \epsilon^3 \ldots, \tag{4.100}$$

In the particular case where $[V_1(x, \theta), V_1(x, \theta')] = 0$ Eq. (4.100) reduces to $\epsilon^2 V_2 = \epsilon^2 [H_0, W_1] + \epsilon^3 \ldots$ We can apply a second contact transformation $e^{\epsilon^2 W_2}$ (with respect to $\hat{K}_0$),
$W_2 = -i \int^{\theta} d\theta \; (V_2 - \overline{V_2})$, which averages this rest (4.100) with respect to θ and leads to correction of order ϵ^3. In the basis of the eigenvectors $\chi(\theta, x)$ of $\hbar\omega \hat{K}_0 + V_1(x, \theta)$, the non-diagonal terms $V_2 - \overline{V_2}$ of this remaining term (4.100) can be seen as the couplings between the states corresponding to the eigenvalues $\lambda_k^{(0)}$ and the diagonal terms $\overline{V_2}$ will lead to geometrical phases for the dynamics (see Section 2.2). We thus obtain the effective high frequency Hamiltonian H^{HF} (independent of θ) of order ϵ^2

$$H^{\mathrm{HF}}(x) = H_0(x) + \overline{V_1}(x) + \overline{V_2}(x). \tag{4.101}$$

We remark that the standard Born-Oppenheimer approximation, allowing one to separate the fast electronic motion with respect to the slow vibrational motion of the nuclei of molecules, can be thought as a high frequency perturbation theory. For the Born-Oppenheimer, we identify formally K_0 with the kinetic energy of the electrons and ϵ with the mass of the electrons. As we stated above, the approximation consists in first applying a contact transformation which diagonalizes exactly with respect to the electronic coordinates, keeping the nuclei coordinates as parameters, and next in neglecting the non-diagonal coupling between the eigenvalues (which are associated to the electronic states).

Chapter 5

Nonperturbative treatment of resonances: Resonant transformations

Resonant effects that prevent convergence of the perturbation theory and that appear as small denominators has to be treated specifically. We present here such tools here and introduce the resonant transformations (RT).

The properties that we have stated in the preceding chapter allow us to analyze the situation in which there are resonances. The analysis of resonances involves two aspects: The first one is the determination of degenerate eigenvalues of an unperturbed Hamiltonian K_0, and the second one the detection of terms in the perturbation V_1 that couple these degenerate modes. We show that the projectors of type Π_{K_0} can be used to detect resonant terms in the coupling operators V_1. This is an alternative to another formulation that consists in writing down formally a Fourier series of the generator W_1 of the KAM transformation and detecting diverging terms, i.e. terms with zeros in the denominator and a finite numerator.

This leads to distinguish two types of resonances: the resonances induced by the field that occur beyond a threshold of the field, and resonances that occur for an arbitrary small value of the field. These are called respectively (i) the *dynamical resonances* (or equivalently *field induced resonances* or *nonlinear resonances*) and (ii) the *zero-field resonances*.

The zero-field resonances can be identified with respect to the system energy levels and the field frequency when the field is off. They are usually one- or two-photon resonances. The one-photon resonance is of first order with respect to the field amplitude in the sense that the degeneracy of the eigenvalues is lifted linearly with the field amplitude. The two-photon resonance is of second order since the degeneracy of the eigenvalues is lifted quadratically with the field amplitude. Multiphoton resonances (with more than two-photon) are more complicated since they are generally accompanied by dynamical shifts of second order before the actual occurrence of the resonance at a higher order. They are in general dynamical.

The dynamical resonance is due in general to dynamical Stark shifts. This is the case for instance for a (one-photon) resonant strong field driving a two-level system. A large field amplitude induces a Stark shift that allows multiphoton resonances (with an odd number of photons in atoms due to the selection rules). The first dynamical resonance encountered is a three-photon resonance. The dynamical Stark shift can be also due to an additional field, as in the process described in Chapter 9.

For very small field amplitudes, the multiphoton resonances can be treated by time-dependent perturbation theory combined with the rotating wave approximation (RWA) [11]. In strong field, all types of resonances can be treated by the concept of the rotating wave transformation, combined with an additional stationary perturbation theory (such as the KAM techniques ex-

plained above). It will allow one to construct an effective Hamiltonian in a subspace spanned by the resonant dressed states, degenerate at zero field.

To illustrate the effects of these two types of resonances, we consider the simplest concrete example of a two-level system driven by a strong field:

$$K = K_0 + V, \qquad K_0 = -i\hbar\omega\frac{\partial}{\partial\theta} + \frac{\beta}{2}\begin{pmatrix}1 & 0\\ 0 & -1\end{pmatrix}, \quad V = \varepsilon\cos\theta\begin{pmatrix}0 & 1\\ 1 & 0\end{pmatrix}, \tag{5.1}$$

with ε and β real and positive.

5.1 Zero-field resonances

We consider the one-photon resonant case $\beta = \omega$. There is a one photon resonance in K_0, since its eigenvalues are $\lambda^0_{m,k} = m\frac{\beta}{2} + k\omega; \quad m \in \{-1, +1\},\ k \in \mathbb{Z}$, and therefore $\lambda^0_{-1,k+1} = \lambda^0_{+1,k}$, i.e. all the eigenvalues are degenerate of order two. The degeneracy eigenspaces are spanned by the vectors

$$\psi^0_{-1,k+1} = e^{i(k+1)\theta} \otimes \begin{pmatrix}0\\1\end{pmatrix} \text{ and } \psi^0_{+1,k} = e^{ik\theta} \otimes \begin{pmatrix}1\\0\end{pmatrix}. \tag{5.2}$$

The projector Π_{K_0} applied on the coupling term yields

$$\Pi_{K_0} V \equiv V_{resonant} = \frac{\varepsilon}{2}\begin{pmatrix}0 & e^{-i\theta}\\ e^{i\theta} & 0\end{pmatrix}. \tag{5.3}$$

This resonant term cannot be eliminated by the KAM transformation. Instead we can treat it with a different type of transformation. We define a unitary transformation

$$R_1 = \begin{pmatrix}1 & 0\\ 0 & e^{i\theta}\end{pmatrix}, \tag{5.4}$$

that can be interpreted as a transformation that leaves unchanged the upper state, and dresses the lower state with +1 photon. Note that we could have used alternatively the transformation

$$R_1' = \begin{pmatrix} e^{-i\theta} & 0\\ 0 & 1\end{pmatrix} \tag{5.5}$$

that leaves unchanged the lower state, and dresses the upper state with -1 photon. As opposed to the KAM type transformation $e^{\varepsilon W}$, the transformation R_1 is not close to the identity. It is named *resonant transformation* (RT) (or equivalently *rotating wave transformation*) in contrast with the usual RWA for which only the resonant terms are kept, and the counter-rotating terms are neglected. It is defined in such a way that

$$R_1^\dagger V_{resonant} R_1 = \frac{\varepsilon}{2}\begin{pmatrix}0 & 1\\ 1 & 0\end{pmatrix}, \tag{5.6}$$

i.e. the resonant term becomes θ-independent. Thus

$$R_1^\dagger K R_1 = -i\omega\frac{\partial}{\partial\theta} + \frac{\varepsilon}{2}\begin{pmatrix}0 & 1\\ 1 & 0\end{pmatrix} + \frac{\varepsilon}{2}\begin{pmatrix}0 & e^{+i2\theta}\\ e^{-i2\theta} & 0\end{pmatrix} + \frac{\omega}{2}\mathbb{1}_{\mathcal{K}}. \tag{5.7}$$

This Floquet Hamiltonian can be further simplified by diagonalizing the constant matrix with $T_1 = \frac{1}{\sqrt{2}}\begin{pmatrix}1 & -1\\ 1 & 1\end{pmatrix}$:

$$K' = T_1^\dagger R_1^\dagger \; K \; R_1 T_1 = -i\omega\frac{\partial}{\partial\theta} + \frac{\varepsilon}{2}\begin{pmatrix}1 & 0\\ 0 & -1\end{pmatrix} + \frac{\varepsilon}{2}\begin{pmatrix}\cos(2\theta) & i\sin(2\theta)\\ -i\sin(2\theta) & -\cos(2\theta)\end{pmatrix} + \frac{\omega}{2}\mathbb{1}_{\mathcal{K}} \tag{5.8}$$

This transformed Floquet Hamiltonian can now be decomposed into a *renormalized* unperturbed part

$$K_0'(\varepsilon) = -i\omega\frac{\partial}{\partial\theta} + \frac{\varepsilon}{2}\begin{pmatrix}1 & 0\\ 0 & -1\end{pmatrix} + \frac{\omega}{2}\mathbb{1}_{\mathcal{K}} \tag{5.9}$$

(which is explicitly ε-dependent), and a perturbation

$$V' = \frac{\varepsilon}{2}\begin{pmatrix}\cos(2\theta) & i\sin(2\theta)\\ -i\sin(2\theta) & -\cos(2\theta)\end{pmatrix}. \tag{5.10}$$

In this form, the part of the perturbation that is left is not resonant anymore (for small ε), and we can apply KAM type transformations to eliminate it iteratively. This procedure is an adaptation of the technique developed by H. Eliasson to study the problem of localization in quasiperiodic potentials [104] and extended further to problems that are close to the one discussed here [105, 106, 107, 108, 109].

The RWA consists in neglecting V'. If we considers additionally a detuning $\Delta = \beta - \omega$, Eq. (5.7) becomes (before diagonalization)

$$R_1^\dagger K R_1 = -i\omega\frac{\partial}{\partial\theta} + \frac{1}{2}\begin{pmatrix}\Delta & \varepsilon\\ \varepsilon & -\Delta\end{pmatrix} + \frac{\varepsilon}{2}\begin{pmatrix}0 & e^{+i2\theta}\\ e^{-i2\theta} & 0\end{pmatrix} + \frac{\omega}{2}\mathbb{1}_{\mathcal{K}}. \tag{5.11}$$

and the effective RWA Hamiltonian reads (see e.g. [43, 44])

$$H_{\mathrm{RWA}} = \frac{1}{2}\begin{pmatrix}\Delta & \varepsilon\\ \varepsilon & -\Delta\end{pmatrix}. \tag{5.12}$$

This RWA Hamiltonian is a good approximation when the rest can be made negligible, i.e. far below the occurring of resonances by this rest. In this case, we can indeed average the Hamiltonian with respect to θ. This applies when $\varepsilon, \Delta \ll \beta$ (or ω).

5.2 Dynamical resonances

5.2.1 Floquet Hamiltonian

As we have stated, the Floquet Hamiltonian (5.8) has no terms that are resonant if we take small enough ε, and the iteration of the KAM procedure converges. However, if we take ε large enough, we encounter new resonances, that are not present at zero or small fields, i.e. there are not related to degeneracies of the unperturbed eigenvalues of K_0 that lead to the zero-field resonances we have discussed in the previous subsection. These new resonances are related to degeneracies of the new effective unperturbed operator $K_0'(\varepsilon)$, which appear at some specific finite values of ε. These are the dynamical resonances.

In the present case, the first nontrivial dynamical resonance (for $\omega > 0$) appears at $\varepsilon = 2\omega = 2\beta$, since the eigenvalues of $K_0'(\varepsilon)$ are of the form ${\lambda^{0'}}_{m,k}(\varepsilon) = m\varepsilon/2 + k\omega; \quad m \in \{-1, +1\},\ k \in \mathbb{Z},$

and thus ${\lambda^0}'_{-1,k+2}(\varepsilon = 2\omega) = {\lambda^0}'_{+1,k}(\varepsilon = 2\omega)$, i.e. all the eigenvalues are degenerate of order two at the resonant amplitude $\varepsilon = 2\omega$. This dynamical resonance can be interpreted as a two-photon resonance with respect to the effective Hamiltonian K_0', and a three-photon resonance with respect to the original Hamiltonian K_0. The degeneracy eigenspaces are spanned by the vectors

$$\psi^0_{-1,k+2} = e^{i(k+2)\theta} \otimes \begin{pmatrix} 0 \\ 1 \end{pmatrix} \text{ and } \psi^0_{+1,k} = e^{ik\theta} \otimes \begin{pmatrix} 1 \\ 0 \end{pmatrix}. \tag{5.13}$$

Again, we can detect the resonant terms of the perturbation V' by applying the projector $\Pi_{K_0'(\varepsilon=2\omega)}$:

$$\Pi_{K_0'(\varepsilon=2\omega)} V' \equiv V'_{resonant} = -\frac{\varepsilon}{4} \begin{pmatrix} 0 & e^{-i2\theta} \\ e^{i2\theta} & 0 \end{pmatrix}. \tag{5.14}$$

We notice that the eigenvalues of $K_0'(\varepsilon)$ are also degenerate at $\varepsilon = \omega$. But since there are no terms in V' with modes $e^{\pm i\theta}$, we have $\Pi_{K_0'(\varepsilon=\omega)} V' = 0$. This degeneracy does not give rise to an actual resonance. One can call it an inactive resonance. An equivalent way of stating this is that in the calculation of W for the perturbation analysis, the degeneracy of the eigenvalues leads to a zero in the denominator, but the corresponding numerator is identically zero.

As before, if we want to eliminate the perturbation by a KAM iteration for values of $\varepsilon \gtrsim 2\omega$, we first have to deal with the resonant term (5.14). This can be done as above by using a transformation, that is not close to the identity, of the form

$$R_2 = \begin{pmatrix} 1 & 0 \\ 0 & e^{i2\theta} \end{pmatrix}. \tag{5.15}$$

The transformed Floquet Hamiltonian becomes

$$R_2^\dagger K' R_2 = -i\omega \frac{\partial}{\partial\theta} + H_0'' + \frac{\varepsilon}{4} \begin{pmatrix} 2\cos(2\theta) & e^{i4\theta} \\ e^{-i4\theta} & -2\cos(2\theta) \end{pmatrix} + \frac{3}{2}\omega \mathbb{1}_{\mathcal{K}}, \tag{5.16}$$

with

$$H_0'' = \frac{\varepsilon}{2} \begin{pmatrix} (1 - 2\omega/\varepsilon) & -1/2 \\ -1/2 & -(1 - 2\omega/\varepsilon) \end{pmatrix}. \tag{5.17}$$

As before, the constant part H_0'' can be diagonalized by a transformation (which depends on ε, but not on θ):

$$T_2 = \frac{1}{d} \begin{pmatrix} \alpha_+ + \varepsilon/2 - \omega & \varepsilon/4 \\ -\varepsilon/4 & \alpha_+ + \varepsilon/2 - \omega \end{pmatrix}, \tag{5.18}$$

where $\alpha_\pm = \pm(\omega^2 + \varepsilon^2 5/16 - \varepsilon\omega)^{1/2}$ are the eigenvalues of H_0'' and $d = [(\alpha_+ + \varepsilon/2 - \omega)^2 + \varepsilon^2/16]^{1/2}$. The transformed Floquet Hamiltonian can thus be written as

$$\begin{aligned} K'' &= T_2^\dagger R_2^\dagger T_1^\dagger R_1^\dagger \; K \; R_1 T_1 R_2 T_2 \\ &= -i\omega \frac{\partial}{\partial\theta} + \left(\omega^2 + 5\varepsilon^2/16 - \varepsilon\omega\right)^{1/2} \begin{pmatrix} 1 & 0 \\ 0 & -1 \end{pmatrix} + \frac{\varepsilon}{4} V'' + \frac{3\omega}{2} \mathbb{1}_{\mathcal{K}}, \end{aligned} \tag{5.19}$$

where

$$V'' = T_2^\dagger \begin{pmatrix} 2\cos(2\theta) & e^{i4\theta} \\ e^{-i4\theta} & -2\cos(2\theta) \end{pmatrix} T_2. \tag{5.20}$$

This transformed Floquet Hamiltonian is non resonant for values of ε up to a certain amplitude $\varepsilon > 2\omega$, and the KAM iteration based on Eq. (5.19) can be expected to converge.

5.2.2 The cavity electrodynamics model

We apply the preceding formalism to the problem of a two-level atom interacting with a single mode of a quantized field beyond the resonant approximation (the resonant approximation in this model is known as the Jaynes-Cumming model [110]) [111].

JOURNAL OF MATHEMATICAL PHYSICS **46**, 042311 (2005)

Quantum averaging and resonances: Two-level atom in a one-mode quantized field

M. Amniat-Talab[a)]
Laboratoire de Physique, UMR CNRS 5027, Université de Bourgogne, B.P. 47870, F-21078 Dijon, France, and Physics Department, Faculty of Sciences, Urmia University, P.B. 165, Urmia, Iran

S. Guérin[b)] and H. R. Jauslin[c)]
Laboratoire de Physique, UMR CNRS 5027, Université de Bourgogne, B.P. 47870, F-21078 Dijon, France

(Received 13 July 2004; accepted 29 November 2004; published online 30 March 2005)

We construct a nonperturbative approach based on quantum averaging combined with resonant transformations to detect the resonances of a given Hamiltonian and to treat them. This approach, which generalizes the rotating-wave approximation, takes into account the resonances at low field and also at high field (nonlinear resonances). This allows us to derive effective Hamiltonians that contain the qualitative features of the spectrum, i.e., crossings and avoided crossings, as a function of the coupling constant. At a second stage the precision of the spectrum can be improved quantitatively by standard perturbative methods like contact transformations. We illustrate this method by determining the spectrum of a two-level atom interacting with a single-mode quantized field. © *2005 American Institute of Physics.* [DOI: 10.1063/1.1864252]

I. INTRODUCTION

Some important features of classical and quantum systems are determined by resonances of the system which cannot be treated by perturbative approaches. In the vicinity of resonances the perturbative formulas display small denominators that lead to the divergence of the perturbative expansions. A widely used model that incorporates a one-photon resonance is the Jaynes-Cummings Hamiltonian extracted from the full dressed Hamiltonian that describes a two-level system coupled with a single mode of a quantized field.[1] Its counterpart for an interaction with a semiclassical laser field is the RWA Hamiltonian (rotating-wave approximation).[2]

In this article we give a systematic method that allows us to construct effective Hamiltonians and determine their spectrum by treating the resonances with an adaptation of resonant transformations that were introduced in Ref. 3 in the context of laser-driven quantum systems in the Floquet representation. The semiclassical model with several incommensurate frequencies[4] has been treated by different methods in Refs. 5–8.

The goal is to obtain the spectrum for a whole interval of values of a parameter like the coupling constant. This is needed, e.g., in applications where the coupling changes adiabatically,[9] corresponding, e.g., to envelopes of laser pulses or to transversal spatial profiles of cavity fields. The method is based on the detection of resonances by a projector derived from quantum averaging. We illustrate it on the problem of a two-level atom interacting with a quantized field and show that a treatment of all the relevant resonances of the system in a given range of parameters allows us to reproduce with good accuracy the spectrum of this system. The treatment of the resonances yields the qualitative structure of the spectrum—the crossings and avoided

[a)]Electronic mail: amniyatm@u-bourgogne.fr
[b)]Electronic mail: sguerin@u-bourgogne.fr
[c)]Electronic mail: jauslin@u-bourgogne.fr

crossings—as a function of the coupling constant. Once this main structure is obtained, one can systematically improve the quantitative accuracy of the spectrum by applying perturbative methods. We use contact transformations with a Kolmogorov-Arnold-Moser (KAM) iteration,[3] which are particularly efficient due to its superconvergent properties.

The paper is structured as follows. In Sec. II, we describe the method of resonance analysis and the construction of effective Hamiltonians. Section III contains the presentation of the model and some preliminary considerations. In Sec. IV, taking into account the resonances of this model in the weak-coupling regime, we extract the effective Hamiltonians by quantum averaging techniques and resonant transformations. In the weak-coupling regime we have to iterate this procedure several times to derive the essential structure of the spectrum in larger ranges of the coupling constant. In Sec. V we extract the effective Hamiltonians in the strong-coupling regime where the qualitative properties of the spectrum can be globally obtained by some preliminary unitary transformations and one resonant transformation which treats the zero-field resonances. We obtain an accurate approximation valid for all values of the coupling constant that contains all the qualitative structures. Finally, in Sec. VI we give some conclusions.

II. PRINCIPLE OF THE METHOD

We consider a Hamiltonian $H=H_0+\epsilon V$, where H_0 is the reference (unperturbed) Hamiltonian, ϵV is the perturbation, and ϵ is an ordering parameter. The first analysis of this problem is in terms of perturbation theory: we look for a KAM-type unitary transformation $e^{\epsilon W}$ close to the identity that allows us to reduce the order of the perturbation from ϵ to ϵ^2:

$$e^{-\epsilon W}He^{\epsilon W}=H_0+\epsilon D+\epsilon^2V_2. \tag{1}$$

ϵD is a remaining term of order ϵ that satisfies $[H_0,D]=0$. The unknown W and D are solutions of the following equations:[3,10]

$$[H_0,W]+V=D, \tag{2a}$$

$$[H_0,D]=0. \tag{2b}$$

The remaining perturbation of order ϵ^2 is given by

$$\epsilon^2V_2=\sum_{m=2}^{\infty}\frac{\epsilon^m}{m!}((m-1)L_W^{m-1}V+L_W^{m-1}D), \tag{3}$$

where L_W is defined as

$$L_WB=[B,W]. \tag{4}$$

The solutions of Eqs. (2) can be written in terms of averaging:[3,11]

$$D=\overline{V}\equiv\Pi_{H_0}V:=\lim_{\tau\to\infty}\frac{1}{\tau}\int_0^{\tau}dse^{-iH_0s}Ve^{iH_0s}=\sum_{\nu,j,j'}|\nu,j\rangle\langle\nu,j|V|\nu,j'\rangle\langle\nu,j'|, \tag{5a}$$

$$W=\lim_{\tau\to\infty}\frac{-i}{\tau}\int_0^{\tau}ds\int_0^{s}ds'e^{-iH_0s'}(V-\Pi_{H_0}V)e^{iH_0s'}=-\sum_{\nu,j,j',\nu'\neq\nu}\frac{|\nu,j\rangle\langle\nu,j|V|\nu',j'\rangle\langle\nu',j'|}{E_\nu^{(0)}-E_{\nu'}^{(0)}}, \tag{5b}$$

where ν labels the different eigenvalues $E_\nu^{(0)}$ of H_0, and j is a degeneracy index which distinguishes different basis vectors $|\nu,j\rangle$ of the degeneracy eigenspace. The operator Π_{H_0} is the projector on the kernel of the application $A\mapsto[H_0,A]$. We remark that the integral representation of D,W in Eqs. (5) can be also well defined in cases where H_0 has a continuum spectrum. We can

iterate the KAM procedure taking $H_0+\epsilon D$ as the new reference Hamiltonian and $\epsilon^2 V_2$ as the new perturbation. The units are chosen such that $\hbar=1$. In the following discussion, we do not write explicitly the ordering parameter ϵ.

A *resonance* is defined as a degeneracy of an eigenvalue $E_\nu^{(0)}$ of H_0 and is said to be *active* if the perturbation V has nonzero matrix elements in the degeneracy subspace of $E_\nu^{(0)}$: $\langle \nu,j|V|\nu,j'\rangle \neq 0$ for some j,j'. Otherwise the resonance is called *passive* or *mute*. Equation (5b) shows that in the case of quasi-resonance (as opposed to exact resonance) where the denominator would be different from zero but very small with respect to the numerator, W can be very large, and thus the expansion cannot be expected to converge. The method we present here is a construction designed to avoid such divergences. We remark that the concept of resonance is defined intrinsically for H_0, while the distinction between active and passive depends on the relation between H_0 and V. The analysis of the resonances thus involves three aspects:

- Decomposition of the Hamiltonian into $H=H_0+V$. Different decompositions can be considered for different regimes of the parameters of H.
- Determination of degenerate eigenvalues of H_0.
- Detection of the *resonant terms* in the perturbation V that couple these degenerate eigenstates.

The resonant terms of V can be detected by projectors of type Π_{H_0} that extract a block-diagonal part of V relative to H_0, where the blocks are generated by the degeneracy subspaces. In the absence of active resonances, when all the eigenvalues of H_0 are nondegenerate or when the resonances are mute, the matrix representation of $\Pi_{H_0}V$ is in fact diagonal in the eigenbasis of H_0. In the presence of active resonances, the block-diagonal effective Hamiltonian that takes into account the considered resonance of the original Hamiltonian can be written as

$$H^{\text{eff}} = H_0 + \Pi_{H_0} V. \tag{6}$$

We will call the transformation that diagonalizes H^{eff} *resonant transformation* (RT). The Hamiltonian $H=H^{\text{eff}}+(V-\Pi_{H_0}V)$ is transformed under RT (denoted $\mathcal{R}$) as follows:

$$H_1 = \mathcal{R}^\dagger H \mathcal{R} = \mathcal{R}^\dagger H^{\text{eff}} \mathcal{R} + \mathcal{R}^\dagger (V - \Pi_{H_0} V)\mathcal{R} =: H_1^{(0)} + V_1, \tag{7}$$

where $H_1^{(0)}$ is defined as the new renormalized reference Hamiltonian and V_1 is the new perturbation. The effect of $\Pi_{H_0}V$ in (6) is to lift the degeneracy of H_0. This can happen in two ways: either the active resonance is transformed into a passive one (e.g., in the case of zero-field resonances) or the resonance disappears completely (when a crossing is transformed into an avoided crossing). The new Hamiltonian H_1 can, however, have other resonances at different values of the coupling parameter. If $H_1^{(0)}+V_1$ does not have any other active resonance in the considered range of the coupling constant, we can, at a second stage, improve the spectrum by a KAM-type perturbative expansion which is expected to converge. If there are other active resonances, we have to iterate the renormalization procedure by applying another RT. We remark that there are cases of multiphoton resonances where the active resonances appear only after applying one or several contact transformations.

III. DESCRIPTION OF THE MODEL AND PRELIMINARY CONSIDERATIONS

We consider as an illustration a two-level atom interacting with a single mode of a quantized field described by

$$H = \omega(a^\dagger a + 1/2) \otimes \mathbb{1}_2 + \frac{\omega_0}{2}\mathbb{1} \otimes \sigma_z + g(a + a^\dagger) \otimes \sigma_x, \tag{8}$$

where a, $a^\dagger$ are the annihilation and creation operators for the field mode with the commutation relation $[a,a^\dagger]=\mathbb{1}=\Sigma_{n=0}^{\infty}|n\rangle\langle n|$, σ_z,σ_x are Pauli matrices, and $\mathbb{1}_2$ is the 2×2 identity matrix. Here ω is the frequency of the field mode, ω_0 is the energy difference of the two atomic states, and g is the

dipole-coupling between the field mode and the atom. This Hamiltonian acts on the Hilbert space $\mathcal{K}=\mathcal{F}\otimes\mathcal{H}$ where $\mathcal{H}=\mathbb{C}^2$ is the Hilbert space of the atom generated by $|\pm\rangle$ (eigenvectors of σ_z) and $\mathcal{F}$ is the Fock space of the field mode generated by the orthonormal basis $\{|n\rangle; n=0,1,2,\ldots\}$, n being the photon number of the field.

For this system there is a parity operator

$$P = e^{i\pi a^\dagger a}\otimes\sigma_z = \sum_{n=0}^{\infty}(-1)^n|n\rangle\langle n|\otimes\sigma_z, \tag{9}$$

with the properties

$$[P,H]=0, \quad P=P^\dagger, \quad P^2=\mathbb{1}_{\mathcal{K}}\equiv\mathbb{1}\otimes\mathbb{1}_2. \tag{10}$$

As a consequence, the eigenstates of H can be separated into two symmetry classes, even or odd, under P:

$$P|\phi_{n,\pm}\rangle = \pm|\phi_{n,\pm}\rangle, \quad H|\phi_{n,\pm}\rangle = E_{n,\pm}|\phi_{n,\pm}\rangle. \tag{11}$$

The parity operator also commutes with any operator that depends only on $N=a^\dagger a$ and σ_z.

In spite of the simple form of (8), its exact solutions are not known. This can be related to the fact that the classical limit of this model is nonintegrable.[12] This model is of great interest as a physical model in quantum optics[13–16] and quantum chaos.[17,18] Some approximate solutions of this model have been studied among many others in Refs. 19 and 20 using different formalisms.

The conceptual framework for the solution of this system based on the construction of unitary transformations can be described as follows: First, we decompose the Hamiltonian in two terms as $H=H_0+V$. Depending on the considered ranges of the parameters of the system, different decompositions may be considered. H_0 is *a priori* an operator that is a regular function exclusively of the operators N and σ_z. The operators N and σ_z can be considered in the present model as quantum analogs of classical *global actions*,[21] and H_0 can be labeled *integrable*. The perturbation V contains functions that involve also the other operators $a, a^\dagger, \sigma_x, \sigma_y$. The goal is to determine a unitary transformation U, which should be expressed in terms of well-behaved regular functions of $a, a^\dagger, \sigma_x, \sigma_y, \sigma_z$, such that

$$U^\dagger(H_0(N,\sigma_z)+V(a,a^\dagger,\sigma_x,\sigma_y,\sigma_z))U = H'(N,\sigma_z), \tag{12}$$

where H' is a regular function f exclusively of the action operators N,σ_z: $H'(N,\sigma_z)=f(N,\sigma_z)$. With this transformation the eigenvectors of H can be expressed as $|\phi_{n,\pm}\rangle=U(|n\rangle\otimes|\pm\rangle)$ and the corresponding eigenvalues as $E_{n,\pm}=f(n,\pm1)$ where $N|n\rangle=n|n\rangle$ and $\sigma_z|\pm\rangle=\pm|\pm\rangle$.

We remark that in our context the important property for singling out the operators N,σ_z is that they commute with each other and their spectrum and eigenvectors are explicitly available. The question of whether for a given model there exists a regular unitary transformation U that accomplishes the above requirement is, to our knowledge, an open problem.

Most of the perturbative approaches can be interpreted as methods to find approximations of the transformation U. The presence of resonances is one of the central difficulties in the construction of U, as will be made precise below. In this paper we discuss an iterative approach that consists of constructing first some approximations of U that take into account the dominating effects of a certain number of resonances. The transformations involved in this stage are far from the identity and have a clearly nonperturbative character. Once we have a transformation that takes into account the main effect of a set of resonances that are relevant in a considered interval of the coupling constant g, a perturbative approach (like the KAM, Van Vleck, or other types of the contact transformation) can be applied to improve the approximation quantitatively. The transformations involved in this second stage can be considered as deformations of the identity, since they can be written in the form e^W. This stage cannot be implemented if the resonances are not taken care of beforehand. Indeed the perturbative formulations diverge close to resonances due to the appearance of *small denominators* as can be seen in Eq. (5b).

As in classical mechanics, the construction of the transformation U leading to a Hamiltonian that contains only action variables can often be considered in two steps: $U=U_1U_2$. In the first step, which is called *reduction*, the Hamiltonian is transformed by U_1 into a form that contains functions of $\sigma_z, \sigma_x, \sigma_y$ and N, but not of a and $a^\dagger$. The degree of freedom of the field is made trivial and the number of nontrivial degrees of freedom is thus reduced by one. When we apply this reduction to the effective Hamiltonian (6), we obtain a *reduced effective Hamiltonian*. We remark that in the literature, this "reduced effective Hamiltonian" is often called simply "effective Hamiltonian." In the second step, the reduced Hamiltonian is transformed under U_2 into a form that contains functions of only N and σ_z. For the model (8), the reduction step corresponds to diagonalization in the Fock space and the second step corresponds to diagonalization in the atomic Hilbert space which in this case is trivial. The construction of the RT is based on this reduction procedure.

IV. EFFECTIVE HAMILTONIANS IN THE WEAK-COUPLING REGIME

In this section we consider the Hamiltonian (8) at resonance $\omega_0=\omega$ in the weak coupling regime, so that H can be decomposed as follows:

$$H = H_0 + V,$$

$$H_0(N,\sigma_z) = \omega(N+1/2)\otimes \mathbb{1}_2 + \frac{\omega_0}{2}\mathbb{1}\otimes\sigma_z, \tag{13}$$

$$V(a,a^\dagger,\sigma_x,g) = g(a+a^\dagger)\otimes\sigma_x.$$

The eigenvalues and eigenvectors of H_0 are

$$E^{(0)}_{n,\pm} = \omega(n+1/2) \pm \frac{\omega_0}{2},$$

$$|\phi^{(0)}_{n,\pm}\rangle = |n,\pm\rangle = |n\rangle\otimes|\pm\rangle, \tag{14}$$

$$|n,+\rangle = \begin{pmatrix} |n\rangle \\ 0 \end{pmatrix}, \quad |n,-\rangle = \begin{pmatrix} 0 \\ |n\rangle \end{pmatrix}.$$

For $\omega_0=\omega$ there is a one photon resonance which corresponds to the degeneracies $E^{(0)}_{n,+}=E^{(0)}_{n+1,-}$. The degeneracy eigenspaces are spanned by the vectors $|\phi^{(0)}_{n,+}\rangle$ and $|\phi^{(0)}_{n+1,-}\rangle$. The resonant part of V is obtained by (5a):

$$V_{res} := \Pi_{H_0}V = \sum_{n=0}^{\infty}(|n,+\rangle\langle n,+|V|n+1,-\rangle\langle n+1,-| + |n+1,-\rangle\langle n+1,-|V|n,+\rangle\langle n,+|)$$
$$= g\begin{pmatrix} 0 & a \\ a^\dagger & 0 \end{pmatrix}, \tag{15}$$

where we have used the relations

$$a = \sum_{n=0}^{\infty}\sqrt{n+1}|n\rangle\langle n+1|, \quad a^\dagger = \sum_{n=0}^{\infty}\sqrt{n+1}|n+1\rangle\langle n|. \tag{16}$$

The effective Hamiltonian containing the one-photon resonance is the so-called Jaynes-Cummings Hamiltonian that can be written as

$$H_0^{\text{eff}} = H_{JC} = H_0 + \Pi_{H_0} V = \omega(N + 1/2) \otimes \mathbb{1}_2 + \frac{\omega}{2}\mathbb{1} \otimes \sigma_z + g\begin{pmatrix} 0 & a \\ a^\dagger & 0 \end{pmatrix}. \tag{17}$$

H_{JC} is a good approximation of (8) for low energies in the limit $g \ll \omega_0, |\omega - \omega_0| \ll \omega_0$. In this limit, the so-called counter-rotating terms $g\left(\begin{smallmatrix} 0 & a^\dagger \\ a & 0 \end{smallmatrix}\right)$ can be discarded (rotating-wave approximation). H can thus be written as $H = H_0^{\text{eff}}(N, a, a^\dagger, \sigma_x, \sigma_y; g) + (V - \Pi_{H_0} V)$. Next we transform H_0^{eff} by a resonant transformation $\mathcal{R}_1$ to a regular function of exclusively the action operators N, σ_z. Every resonant transformation is performed in two steps. To diagonalize H_0^{eff} in the Fock space (the reduction step of the RT denoted R_1) we define a transformation in such a way that the following condition is satisfied:

$$R_1^\dagger V_{res} R_1 = f(N) \otimes \sigma_x, \tag{18}$$

where f is a regular function of N which has to be determined. We require furthermore that $R_1^\dagger H_0 R_1$ stays a function of only N and σ_z. A suitable transformation satisfying these conditions is

$$R_1 := \begin{pmatrix} (aa^\dagger)^{-1/2} a & 0 \\ 0 & \mathbb{1} \end{pmatrix} \equiv \begin{pmatrix} \sum_{n=0}^{\infty} |n\rangle\langle n+1| & 0 \\ 0 & \mathbb{1} \end{pmatrix}. \tag{19}$$

This transformation is not unitary but *isometric*:[22]

$$R_1 R_1^\dagger = \mathbb{1}_{\mathcal{K}}, \quad R_1^\dagger R_1 = \mathbb{1}_{\mathcal{K}} - \begin{pmatrix} |0\rangle\langle 0| & 0 \\ 0 & 0 \end{pmatrix}, \tag{20}$$

where we have used the identity $a^\dagger (N+1)^{-1} a = \mathbb{1} - |0\rangle\langle 0|$. Applying this transformation on the resonant term gives

$$R_1^\dagger V_{res} R_1 = g a^\dagger (aa^\dagger)^{-1/2} a \otimes \sigma_x = g\sqrt{N} \otimes \sigma_x \tag{21}$$

and H is transformed under R_1 as

$$H_{R_1} = R_1^\dagger H R_1 = \omega N \otimes \mathbb{1}_2 + g\sqrt{N} \otimes \sigma_x + g\begin{pmatrix} 0 & A^\dagger \\ A & 0 \end{pmatrix}, \tag{22}$$

where

$$A = a(aa^\dagger)^{-1/2} a = \sum_{n=0}^{\infty} \sqrt{n+1} |n\rangle\langle n+2|, \tag{23}$$

with the properties

$$AA^\dagger = aa^\dagger, \quad A^\dagger A = a^\dagger a - \mathbb{1} + |0\rangle\langle 0|. \tag{24}$$

To each eigenvector $|\phi\rangle$ of H corresponds an eigenvector $R_1^\dagger|\phi\rangle$ of H_{R_1}, since

$$H_{R_1} R_1^\dagger |\phi\rangle = R_1^\dagger H R_1 R_1^\dagger |\phi\rangle = \lambda R_1^\dagger |\phi\rangle. \tag{25}$$

We remark that $R_1^\dagger|\phi\rangle \neq 0 \ \forall |\phi\rangle \in \mathcal{K}$. Every eigenvalue of the original Hamiltonian H is also an eigenvalue of the transformed Hamiltonian H_{R_1}. However, since $R_1|0,+\rangle = 0$, there is a difference in the spectrum between H and H_{R_1}: H_{R_1} has an extra zero eigenvalue with eigenvector $|0,+\rangle$. The spurious eigenvalue can be detected and eliminated after applying the transformation. Indeed, since $|0,+\rangle$ is not coupled to any vector in its orthogonal complement, one can eliminate it from the rest of the calculation by taking the projection of H_{R_1} into the orthogonal complement $H_{R_1,\perp(0,+)} = P_{\perp(0,+)} H_{R_1} P_{\perp(0,+)}$ with $P_{\perp(0,+)} = \mathbb{1}_{\mathcal{K}} - |0,+\rangle\langle 0,+|$. This difference between unitary and

isometric transformations was not taken into account in Ref. 23 in diagonalizing the Jaynes-Cummings Hamiltonian.

The second step of the RT is the diagonalization of $R_1^\dagger H_0^{\mathrm{eff}} R_1 = \omega N \otimes \mathbb{1}_2 + \sqrt{N} \otimes \sigma_x$ in the atomic Hilbert space. This can be performed by a $\pi/2$ rotation around the y-axis:

$$T = e^{-i(\pi/4)\sigma_y} = \frac{1}{\sqrt{2}} \begin{pmatrix} 1 & -1 \\ 1 & 1 \end{pmatrix}, \tag{26}$$

with the properties

$$T^\dagger \sigma_x T = \sigma_z, \quad T^\dagger \sigma_z T = -\sigma_x. \tag{27}$$

However, since the spurious eigenvector $|0,+\rangle$ can be separated and $|0,-\rangle$ is already an eigenvector of $R_1^\dagger H_0^{\mathrm{eff}} R_1$, the transformation T must be applied only on the subspace with $n \geqslant 1$ photons. The complete transformation (denoted T_1) reads thus

$$T_1 = P_0 \otimes \mathbb{1}_2 + P_{\perp 0} \otimes T, \tag{28}$$

where

$$P_0 = |0\rangle\langle 0|, \quad P_{\perp 0} = \sum_{n=1}^{\infty} |n\rangle\langle n|. \tag{29}$$

Applying T_1 gives

$$H_1 := T_1^\dagger R_1^\dagger H R_1 T_1 = H_1^{(0)}(N, \sigma_z; g) + V_1(a, a^\dagger, \sigma_z, \sigma_x, \sigma_y; g), \tag{30}$$

with

$$H_1^{(0)} = \omega N \otimes \mathbb{1}_2 + g\sqrt{N} \otimes \sigma_z,$$

$$V_1 = \frac{g}{2} \begin{pmatrix} A_{\perp 0} + A_{\perp 0}^\dagger & -A_{\perp 0} + A_{\perp 0}^\dagger \\ A_{\perp 0} - A_{\perp 0}^\dagger & -A_{\perp 0} - A_{\perp 0}^\dagger \end{pmatrix} + \frac{g}{\sqrt{2}} \begin{pmatrix} 0 & |2\rangle\langle 0| \\ |0\rangle\langle 2| & -|2\rangle\langle 0| - |0\rangle\langle 2| \end{pmatrix}, \tag{31}$$

where

$$A_{\perp 0} = P_{\perp 0} A P_{\perp 0} = \sum_{n=1}^{\infty} \sqrt{n+1} |n\rangle\langle n+2|, \tag{32}$$

and use has been made of the relations

$$A P_0 = P_0 A^\dagger = 0, \quad P_0 A P_{\perp 0} = |0\rangle\langle 2|. \tag{33}$$

The first RT is thus the combination of $R_1 T_1$. Since the transformation R_1 dresses the upper atomic state by (-1) photon,[15] $\mathcal{R}_1 = R_1 T_1$ can be called a one-photon RT.

$H_1^{(0)}$ is in fact the diagonalized Jaynes-Cummings Hamiltonian in the resonant case with the eigenvalues

$$E_{1,(n,\pm)}^{(0)}(g) = \omega n \pm g\sqrt{n}, \quad n = 0, 1, 2, \ldots . \tag{34}$$

The eigenvalues and therefore the degeneracies of $H_1^{(0)}$ depend on the coupling constant g. For small enough g and low energies, $H_1^{(0)}$ does not have other degeneracies besides the ones at $g = 0$ for which the new perturbation V_1 does not have resonant terms, and we can apply a finite number of KAM-type transformations to improve quantitatively the precision of the spectrum by iteration. We apply a finite number of KAM-type transformations with a cutoff in energy to improve iteratively the precision of the spectrum at small energies. This iteration cannot be

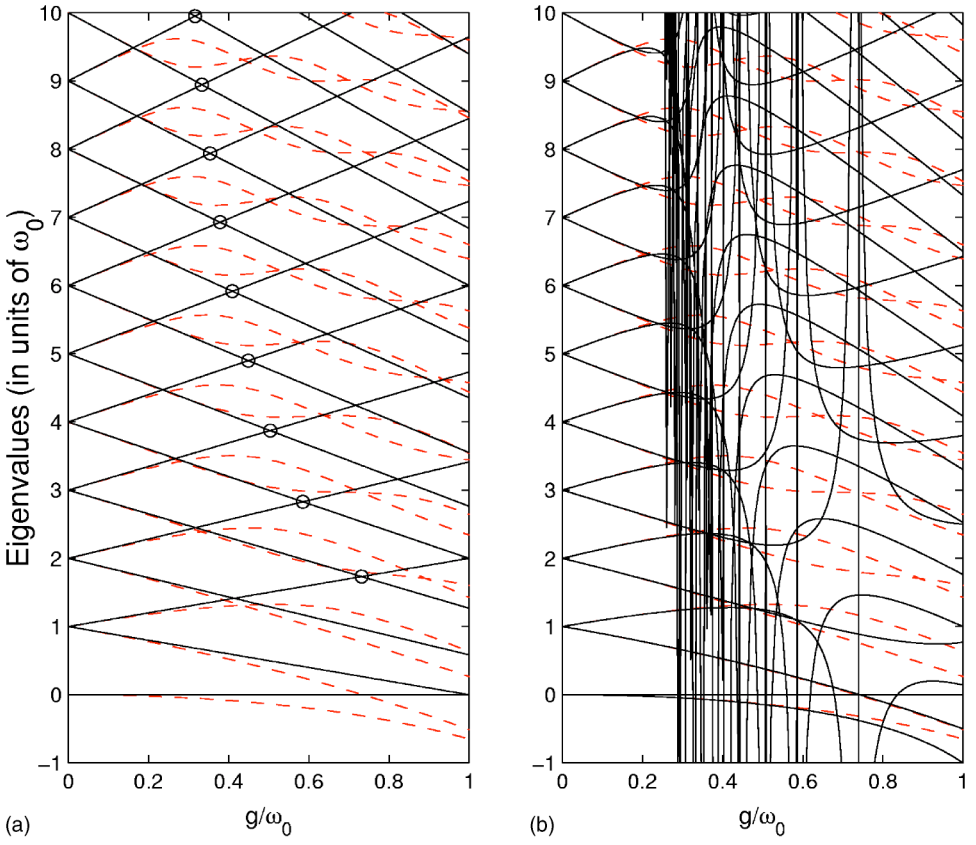

FIG. 1. Comparison of exact numerical eigenvalues (dashed lines) of (8) for one-photon resonance $\omega=\omega_0$ with the approximate ones (solid lines) obtained after (a) one one-photon RT given by (34) and (b) one one-photon RT plus one iteration of KAM-type perturbative expansion. The divergence observed around $g/\omega_0=0.3$ in panel (b) is due to the active nonlinear resonances of $H_1^{(0)}$ that occurred at the degeneracies marked by circles in panel (a). One can see clearly that the locations of these resonances depend on n according to Eq. (35).

expected to converge for all values of g in an interval $[0,g_0]$, because of the presence of a countable number of resonances at high energies at arbitrarily small values of g. A single KAM transformation (which is essentially equivalent to second-order perturbation theory) already gives quite good precision, as shown in Fig. 1(b) for $g/\omega_0<0.25$ for energies smaller than $10\omega_0$. If we take large enough g or larger energies, we encounter new resonances which appear at some specific finite values of g. These resonances are called *field-induced resonances* or *nonlinear resonances*. For larger values of the coupling $[g/\omega_0\approx 0.3$ for the shown energy interval in Fig. 1(b)], where we encounter nonlinear resonances, the KAM iteration diverges. The eigenvalues of $H_1^{(0)}$ are degenerate at $g_n=\omega/(\sqrt{n}+\sqrt{n+1})$ as $E^{(0)}_{1,(n,+)}(g_n)=E^{(0)}_{1,(n+1,-)}(g_n)$. But the corresponding resonant terms in V_1 are zero due to parity (mute resonances). The next degeneracies appear at

$$g_n=2\omega/(\sqrt{n}+\sqrt{n+2}), \tag{35}$$

as

$$E^{(0)}_{1,(n,+)}(g_n)=E^{(0)}_{1,(n+2,-)}(g_n), \tag{36}$$

which have been marked by circles in Fig. 1(a). All the other resonances are mute. There is an infinite family of nonlinear resonances located at different values of the coupling g_n. We observe from (35) that for higher energies the nonlinear resonances appear for arbitrary small coupling $(\lim_{n\to\infty} g_n=0)$. We can extract the resonant terms corresponding to the whole family in a single

step by working with the combined projector $\Sigma_n \Pi_{H_1^{(0)}(g_n)}$. The resonant terms in V_1 corresponding to the degeneracies (36) are

$$\sum_n \Pi_{H_1^{(0)}(g_n)} V_1 = -\frac{g}{2}\begin{pmatrix} 0 & A_{\perp 0} \\ A_{\perp 0}^\dagger & 0 \end{pmatrix} - \frac{g}{\sqrt{2}}\begin{pmatrix} 0 & 0 \\ 0 & |2\rangle\langle 0| + |0\rangle\langle 2| \end{pmatrix}, \tag{37}$$

and the new effective Hamiltonian is thus

$$H_1^{\text{eff}} = \omega N \otimes \mathbb{1}_2 + g\sqrt{N} \otimes \sigma_z + \sum_n \Pi_{H_1^{(0)}(g_n)} V_1. \tag{38}$$

To diagonalize H_1^{eff}, it can be decomposed according to three orthogonal subspaces:

$$H_1^{\text{eff}} = P_{(0,2,-)} H_1^{\text{eff}} P_{(0,2,-)} + P_{(0,+)} H_1^{\text{eff}} P_{(0,+)} + P_\perp H_1^{\text{eff}} P_\perp = H_1^{\text{eff}} P_{(0,2,-)} + H_1^{\text{eff}} P_{(0,+)} + H_1^{\text{eff}} P_\perp, \tag{39}$$

where the projectors, which commute with H_1^{eff}, are defined by

$$P_{(0,2,-)} = \begin{pmatrix} 0 & 0 \\ 0 & |0\rangle\langle 0| + |2\rangle\langle 2| \end{pmatrix}, \quad P_{(0,+)} = \begin{pmatrix} |0\rangle\langle 0| & 0 \\ 0 & 0 \end{pmatrix},$$

$$P_\perp = \mathbb{1}_{\mathcal{K}} - P_{(0,2,-)} - P_{(0,+)} = \begin{pmatrix} \sum_{n=1}^{\infty} |n\rangle\langle n| & 0 \\ 0 & \sum_{n=1,\neq 2}^{\infty} |n\rangle\langle n| \end{pmatrix}, \tag{40}$$

which leads to

$$H_1^{\text{eff}} P_{(0,+)} = 0, \quad H_1^{\text{eff}} P_{(0,2,-)} = \left[(2\omega - g\sqrt{2})|2\rangle\langle 2| - \frac{g}{\sqrt{2}}(|2\rangle\langle 0| + |0\rangle\langle 2|) \right] \begin{pmatrix} 0 & 0 \\ 0 & 1 \end{pmatrix},$$

$$H_1^{\text{eff}} P_\perp = \omega \begin{pmatrix} \sum_{n=1}^{\infty} n|n\rangle\langle n| & 0 \\ 0 & + \sum_{n=1,n\neq 2}^{\infty} n|n\rangle\langle n| \end{pmatrix} + g \begin{pmatrix} \sum_{n=1}^{\infty} \sqrt{n}|n\rangle\langle n| & 0 \\ 0 & \sum_{n=1,n\neq 2}^{\infty} \sqrt{n}|n\rangle\langle n| \end{pmatrix}$$
$$- \frac{g}{2}\begin{pmatrix} 0 & A_{\perp 0} \\ A_{\perp 0}^\dagger & 0 \end{pmatrix}. \tag{41}$$

$H_1^{\text{eff}} P_{(0,2,-)}$ can be directly diagonalized by

$$R_{(0,2,-)} = P_{(0,2,-)} \begin{pmatrix} 0 & 0 \\ 0 & \cos\theta(|2\rangle\langle 2| - |0\rangle\langle 0|) - \sin\theta(|2\rangle\langle 0| + |0\rangle\langle 2|) \end{pmatrix} P_{(0,2,-)}, \tag{42}$$

where the angle θ is defined by the relation

$$\tan 2\theta = \frac{g\sqrt{2}}{2\omega - g\sqrt{2}}, \quad 0 \leqslant \theta < \frac{\pi}{2}, \tag{43}$$

and the corresponding eigenvalues are

$$E^{\text{eff}}_{1,(0,+)} = 0, \quad E^{\text{eff}}_{1,(n=0,2,-)} = \omega - \frac{g}{\sqrt{2}} \pm \frac{1}{2}\sqrt{(2\omega - g\sqrt{2})^2 + 2g^2}. \tag{44}$$

The reduction step of the second RT to diagonalize $H_1^{\text{eff}} P_\perp$ in the Fock space can be defined as

$$R_{2,\perp} := P_\perp \begin{pmatrix} (A_{\perp 0} A_{\perp 0}^\dagger)^{-1/2} A_{\perp 0} & 0 \\ 0 & \mathbb{1} \end{pmatrix} P_\perp = \begin{pmatrix} \sum_{n=1}^{\infty} |n\rangle\langle n+2| & 0 \\ 0 & \sum_{n=1,\neq 2}^{\infty} |n\rangle\langle n| \end{pmatrix} \tag{45}$$

with the properties

$$R_{2,\perp} R_{2,\perp}^\dagger = P_\perp, \quad R_{2,\perp}^\dagger R_{2,\perp} = P_\perp - \begin{pmatrix} |1\rangle\langle 1| + |2\rangle\langle 2| & 0 \\ 0 & 0 \end{pmatrix}. \tag{46}$$

Equation (45) shows that $R_{2,\perp}$ dresses the upper atomic state by (-2) photons. Therefore $\mathcal{R}_{2,\perp}$ can be called a two-photon RT. Since $R_{2,\perp}|1,+\rangle = 0 = R_{2,\perp}|2,+\rangle$, the spectrum of $R_{2,\perp}^\dagger H_1^{\text{eff}} P_\perp R_{2,\perp}$ has two extra zero eigenvalues relative to the spectrum of $H_1^{\text{eff}} P_\perp$. Applying $R_{2,\perp}$ gives

$$R_{2,\perp}^\dagger H_1^{\text{eff}} P_\perp R_{2,\perp} = \omega \begin{pmatrix} \sum_{n=3}^{\infty} (n-2)|n\rangle\langle n| & 0 \\ 0 & \sum_{n=1,\neq 2}^{\infty} n|n\rangle\langle n| \end{pmatrix} + g \begin{pmatrix} \sum_{n=3}^{\infty} \sqrt{n-2}|n\rangle\langle n| & 0 \\ 0 & -\sum_{n=1,\neq 2}^{\infty} \sqrt{n}|n\rangle\langle n| \end{pmatrix}$$
$$- g/2 \sum_{n=3}^{\infty} \sqrt{n-1}|n\rangle\langle n| \otimes \sigma_x. \tag{47}$$

Combining the transformations on the different subspaces we can write the transformation that diagonalizes H_1^{eff} in the Fock space as

$$R_2 = R_{2,\perp} + R_{(0,2,-)} + P_{(0,+)}. \tag{48}$$

At the right-hand side of (47), the three matrices have entries that commute with each other so we can diagonalize the sum of them in the atomic Hilbert space (the second step of $\mathcal{R}_{2,\perp}$) as if they had scalar entries. The eigenvalues of $R_{2,\perp}^\dagger H_1^{\text{eff}} P_\perp R_{2,\perp}$ are thus

$$E^{\text{eff}}_{1,(n=1,-)} = \omega - g, \quad E^{\text{eff}}_{1,(n=1,+)} = 0, \quad E^{\text{eff}}_{1,(n=2,+)} = 0,$$

$$E^{\text{eff}}_{1,(n\geqslant 3,\pm)} = \omega(n-1) + \frac{g}{2}(\sqrt{n-2} - \sqrt{n}) \pm \frac{1}{2}[(-2\omega + g(\sqrt{n-2} + \sqrt{n}))^2 + g^2(n-1)]^{1/2}. \tag{49}$$

As it can be seen from (49), there are two extra zero eigenvalues which have been added by $R_{2,\perp}$ to the spectrum of H_1^{eff}.

Figures 2(a) and 2(b) compare respectively the exact spectrum of H calculated numerically with the spectrum of $H_0^{\text{eff}} = H_{JC}$ given by (34) and of H_1^{eff} given by (49) and (44). The crossings of the exact spectrum are all among the eigenvalues with different parities. It is found that the spectrum of H_0^{eff} coincides with the exact one only in the range of quite small coupling. The spectrum of H_1^{eff} has been modified with respect to the one of H_0^{eff} by transforming the encircled crossings between eigenvalues with the same parity into avoided crossings in the small g region. This procedure to treat resonances can be iterated to take into account other resonances appearing at larger values of g. Figures 2(a)–2(e) show how the combination of a one-photon RT and

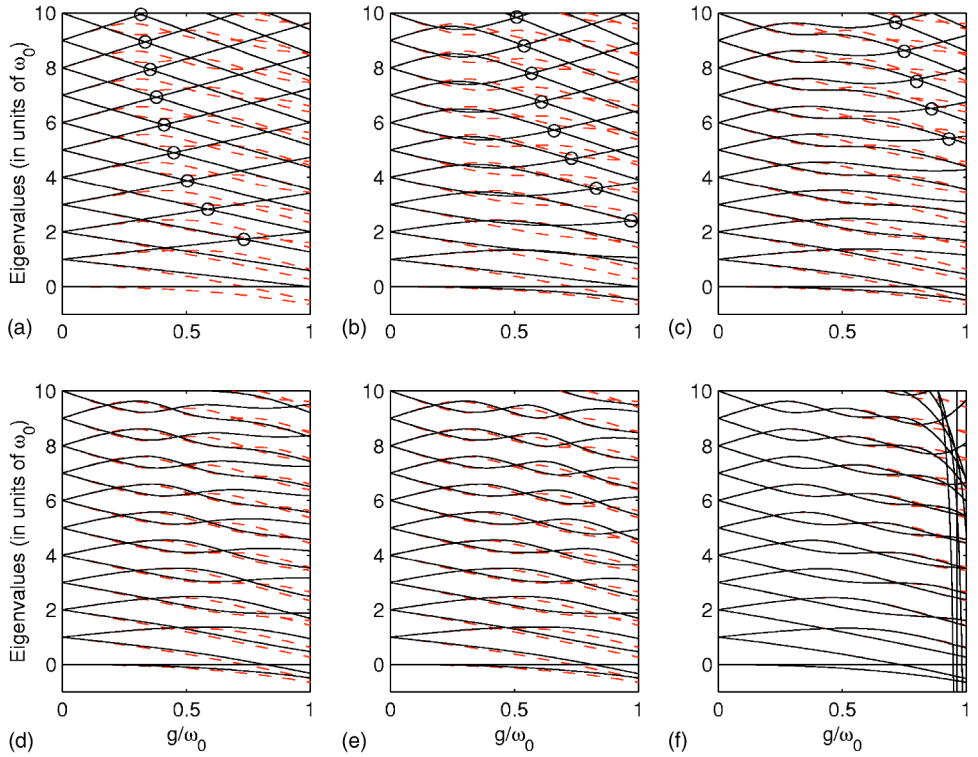

FIG. 2. Comparison of the exact numerical eigenvalues (dashed lines) of (8) for one-photon resonance $\omega=\omega_0$ with the approximate ones (solid lines) obtained respectively after (a) one one-photon RT given by (34), (b) one one-photon RT plus one two-photon RTs given by (49), (c) one one-photon RT plus two two-photon RTs, (d) one one-photon RT plus three two-photon RTs, (e) one one-photon RT plus four two-photon RTs, (f) one one-photon RT plus four two-photon RTs plus one iteration of KAM-type perturbative expansion. The divergence of the KAM transformation observed close to $g/\omega_0=1$ in panel (f) is due to the presence of active resonances at larger values of g.

consecutive two-photon RTs lift the artificial degeneracies (marked by circles) of the effective Hamiltonians. The successive steps, which we have implemented numerically, transform eigenvalue crossings into avoided crossings. We observe that these RTs also produce an improvement of the approximations of the spectrum. Figure 2(f) shows the effect of a KAM transformation after the fourth two-photon RT which improves quantitatively the result of Fig. 2(e). The divergence of the KAM transformation close to $g=1$ in Fig. 2(e) is due to the presence of active resonances at larger values of g.

V. EFFECTIVE HAMILTONIANS IN THE STRONG-COUPLING REGIME

In this section we use quantum averaging techniques and RT to obtain the effective Hamiltonians of (8) by starting the analysis from the strong-coupling regime. We derive a formula that reproduces the spectrum quite accurately in the whole range of g and for all energies. We consider an alternative decomposition of the Hamiltonian (8) in a way suggested by the strong coupling regime $g \gg \omega_0 > 0$,

$$H = H_0 + V,$$

$$H_0 = \omega(N + 1/2) \otimes \mathbb{1}_2 + g(a + a^\dagger) \otimes \sigma_x, \tag{50}$$

$$V = \frac{\omega_0}{2}\mathbb{1} \otimes \sigma_z$$

which can be interpreted as the system of a quantized field plus the coupling term perturbed by the two-level atom. We will use this decomposition as an alternative starting point. As it will be seen later, this approach will allow us to obtain the spectral data for the whole range of values of the coupling $g \in [0,\infty)$. We remark that in this decomposition, H_0 contains all the unbounded operators of the complete model and that the perturbation V is a bounded operator. In this case $H_0(N,a,a^\dagger,\sigma_z,\sigma_x;g)$ is integrable since we can explicitly transform it into a form involving a regular function exclusively of the action operators N,σ_z [given below in Eq. (55)]. To transform H_0 to a function of action operators, first we diagonalize the term $g(a+a^\dagger)\otimes\sigma_x$ in the atomic Hilbert space by the transformation (26):

$$T^\dagger H T = \omega(N + 1/2) \otimes \mathbb{1}_2 + g(a + a^\dagger) \otimes \sigma_z - \frac{\omega_0}{2}\mathbb{1} \otimes \sigma_x. \tag{51}$$

Next we apply a second unitary transformation,

$$U = \begin{pmatrix} e^{-(g/\omega)(a^\dagger - a)} & 0 \\ 0 & e^{(g/\omega)(a^\dagger - a)} \end{pmatrix}, \tag{52}$$

to transform $\omega(N+1/2)\otimes\mathbb{1}_2+g(a+a^\dagger)\otimes\sigma_z$ into a function of only N,σ_z (in this case only of N):

$$H_1 := U^\dagger T^\dagger H T U = \left[\omega(N + 1/2) - \frac{g^2}{\omega}\right] \otimes \mathbb{1}_2 - \frac{\omega_0}{2}\begin{pmatrix} 0 & e^{2(g/\omega)(a^\dagger - a)} \\ e^{-2(g/\omega)(a^\dagger - a)} & 0 \end{pmatrix}, \tag{53}$$

where use has been made of the commutation relations among a, $a^\dagger$, N, and the Hausdorff formula:

$$e^B C e^{-B} = C + [B,C] + \frac{1}{2!}[B,[B,C]] + \cdots. \tag{54}$$

We decompose H_1 as

$$H_1 = H_1^{(0)} + V_1,$$

$$H_1^{(0)} = U^\dagger T^\dagger H_0 T U = \left[\omega(N + 1/2) - \frac{g^2}{\omega}\right] \otimes \mathbb{1}_2, \tag{55}$$

$$V_1 = -\omega_0/2\begin{pmatrix} 0 & e^{2(g/\omega)(a^\dagger - a)} \\ e^{-2(g/\omega)(a^\dagger - a)} & 0 \end{pmatrix}.$$

The effective Hamiltonian of the system for strong-coupling regime can thus be written as

$$H_1^{\text{eff}} = H_1^{(0)} + \Pi_{H_1^{(0)}} V_1. \tag{56}$$

The eigenvalues of $H_1^{(0)}$ have a twofold degeneracy for every value of n as

$$E^{(0)}_{1,(n,\pm)} = \omega(n + 1/2) - \frac{g^2}{\omega}. \tag{57}$$

The average of V_1 relative to $H_1^{(0)}$ is thus

$$\begin{aligned}\Pi_{H_1^{(0)}} V_1 &= \sum_{n=0}^{\infty} \{|n,+\rangle\langle n,+|V_1|n,-\rangle\langle n,-| + |n,-\rangle\langle n,-|V_1|n,+\rangle\langle n,+|\} \\ &= -\frac{\omega_0}{2}\sum_{n=0}^{\infty} f_n |n\rangle\langle n| \otimes \sigma_x,\end{aligned} \tag{58}$$

with

$$\begin{aligned}f_n &= \langle n|e^{(-2g/\omega)(a^\dagger - a)}|n\rangle = \langle n|e^{(+2g/\omega)(a^\dagger - a)}|n\rangle = e^{-2g^2/\omega^2}\langle n|e^{(-2g/\omega)a^\dagger}e^{(+2g/\omega)a}|n\rangle \\ &= e^{-2g^2/\omega^2}\left(\sum_{j=0}^{n}\frac{(-2g/\omega)^j}{j!}\sqrt{\frac{n!}{(n-j)!}}\langle n-j|\right)\left(\sum_{i=0}^{n}\frac{(+2g/\omega)^i}{i!}\sqrt{\frac{n!}{(n-i)!}}|n-i\rangle\right) \\ &= e^{-2g^2/\omega^2}\sum_{j=0}^{n}\frac{(2g/\omega)^{2j}(-1)^j}{(j!)^2}\frac{n!}{(n-j)!} = e^{-2g^2/\omega^2}L_n\left(\frac{4g^2}{\omega^2}\right)\end{aligned} \tag{59}$$

where the L_n are the Laguerre polynomials. We remark that in the limit of a large photon number $(n\to\infty)$, f_n can be expressed as a zeroth-order Bessel function $J_0(4g\sqrt{n}/\omega)$.[15] H_1 can be reorganized as

$$H_1 = H_1^{\text{eff}} + (V_1 - \Pi_{H_1^{(0)}} V_1),$$

$$H_1^{\text{eff}} = \left(\omega(N + 1/2) - \frac{g^2}{\omega}\right)\otimes \mathbb{1}_2 - \frac{\omega_0}{2}F \otimes \sigma_x, \tag{60}$$

$$(V_1 - \Pi_{H_1^{(0)}} V_1) = -\frac{\omega_0}{2}\begin{pmatrix} 0 & G - F \\ G^\dagger - F & 0\end{pmatrix},$$

where

$$G = e^{(+2g/\omega)(a^\dagger - a)}, \quad F = \sum_{n=0}^{\infty} f_n |n\rangle\langle n|. \tag{61}$$

H_1^{eff} can easily be diagonalized by applying the transformation (26) that diagonalizes σ_x:

$$H_2 := T^\dagger H_1 T = H_2^{(0)} + V_2, \tag{62}$$

with

$$H_2^{(0)} = T^\dagger H_1^{\text{eff}} T = \left(\omega(N + 1/2) - \frac{g^2}{\omega}\right)\otimes \mathbb{1}_2 - \frac{\omega_0}{2}F \otimes \sigma_z, \tag{63}$$

and

$$V_2 = T^\dagger(V_1 - \Pi_{H_1^{(0)}} V_1)T = -\omega_0/4\begin{pmatrix} G + G^\dagger - 2F & G - G^\dagger \\ -G + G^\dagger & -G - G^\dagger + 2F\end{pmatrix}. \tag{64}$$

The eigenvalues of $H_2^{(0)}$ are therefore

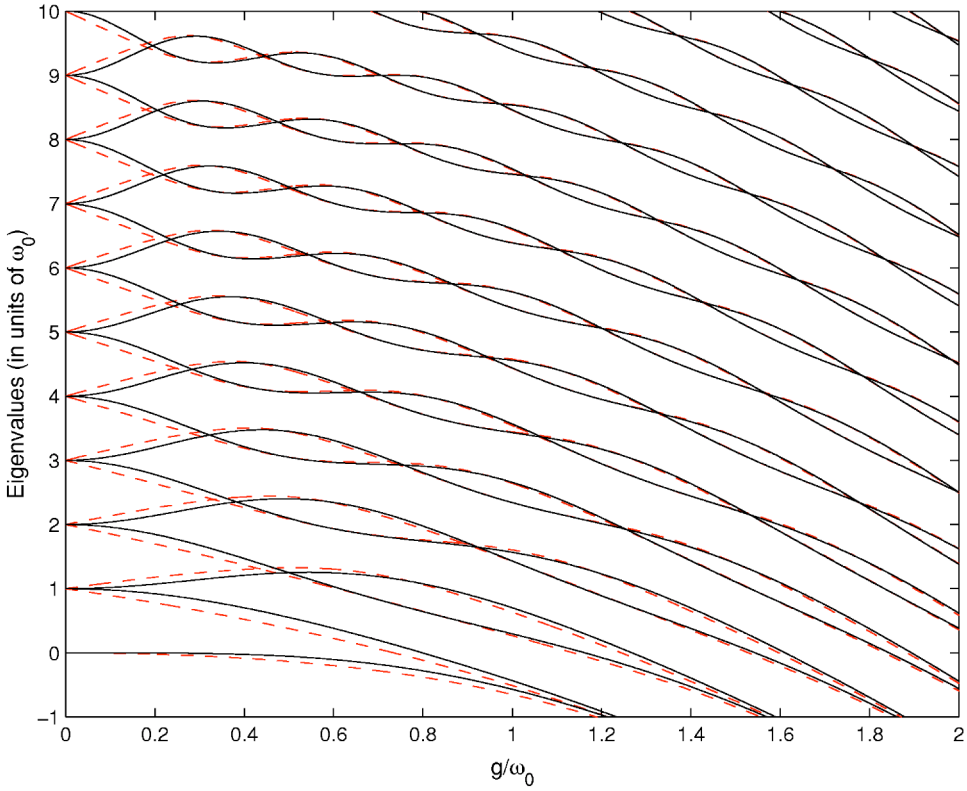

FIG. 3. Comparison of exact numerical eigenvalues (dashed lines) of (8) as a function of the coupling constant in the resonant case ($\omega=\omega_0$), with the approximate eigenvalues (solid lines) obtained from (65).

$$E^{(0)}_{2,(n,\pm)} = \omega(n+1/2) - \frac{g^2}{\omega} \mp \frac{\omega_0}{2} e^{-2g^2/\omega^2} L_n\left(\frac{4g^2}{\omega^2}\right), \tag{65}$$

which is the same result obtained in Refs. 17, 19, and 20 by other methods. Figure 3 compares the exact numerical spectrum of (8) with the approximation (65) for the resonant case $\omega=\omega_0$. One can see that for large enough g, the formula (65) reproduces the spectrum well. It is not very accurate for small values of g because of the presence of the one-photon zero-field resonances that we analyze as follows. In the limit $g\to 0$, we have

$$H_2^{(0),g\to 0} \rightsquigarrow \omega(N+1/2)\otimes \mathbb{1}_2 - \frac{\omega}{2}\mathbb{1}\otimes\sigma_z,$$

$$V_2^{g\to 0} \rightsquigarrow g\begin{pmatrix} 0 & a-a^\dagger \\ -(a-a^\dagger) & 0 \end{pmatrix}. \tag{66}$$

Thus degeneracies of $H_2^{(0),g\to 0}$ occur as

$$E^{(0),g\to 0}_{2,(n,+)} = E^{(0),g\to 0}_{2,(n-1,-)}. \tag{67}$$

They are made active by the resonant terms of $V_2^{g\to 0}$:

$$V_{2,res}^{g\to 0} = \Pi_{H_2^{(0)}}^{g\to 0} V_2^{g\to 0} = -g\begin{pmatrix} 0 & a^\dagger \\ a & 0 \end{pmatrix}. \tag{68}$$

The transformation (the reduction step of the RT) which transforms this resonant term to a regular function of N is

$$R_1 := \begin{pmatrix} \mathbb{1} & 0 \\ 0 & (aa^\dagger)^{-1/2}a \end{pmatrix} = \begin{pmatrix} \mathbb{1} & 0 \\ 0 & \sum_{n=0}^{\infty} |n\rangle\langle n+1| \end{pmatrix}, \tag{69}$$

with the properties

$$R_1 R_1^\dagger = \mathbb{1}_{\mathcal{K}}, \quad R_1^\dagger R_1 = \mathbb{1}_{\mathcal{K}} - \begin{pmatrix} 0 & 0 \\ 0 & |0\rangle\langle 0| \end{pmatrix}. \tag{70}$$

We remark that the definition of R_1 depends on the type of resonant terms. The reduction step of the RT presented here is different from (19). The Hamiltonian transformed under this RT has an extra zero eigenvalue corresponding to spurious eigenvector $|0, -\rangle$, while for the Hamiltonian transformed under (19), the extra zero eigenvalue corresponds to $|0, +\rangle$. Applying R_1 on H_2 gives

$$\begin{aligned} H_3 := R_1^\dagger H_2 R_1 &= \left(\omega N - \frac{g^2}{\omega}\right) \otimes \mathbb{1}_2 + R_1^\dagger V_2 R_1 \\ &+ \begin{pmatrix} \frac{\omega}{2}\left(1 - \sum_{n=0}^{\infty} f_n |n\rangle\langle n|\right) & 0 \\ 0 & -\frac{\omega}{2}\left(1 - \sum_{n=1}^{\infty} f_{n-1}|n\rangle\langle n|\right) - \left(\frac{\omega}{2} + \frac{g^2}{\omega}\right)|0\rangle\langle 0| \end{pmatrix}. \end{aligned} \tag{71}$$

Next, we take $H_3^{(0)} = \omega N \otimes \mathbb{1}_2$ and the rest of H_3 as V_3. Since $H_3^{(0)}$ has a twofold degeneracy as $E_{3,(n,+)}^{(0)} = E_{3,(n,-)}^{(0)}$, the average of V_3 relative to $H_3^{(0)}$ is thus

$$\Pi_{H_3^{(0)}} V_3 = \begin{pmatrix} \frac{\omega}{2} - \frac{g^2}{\omega} - \frac{\omega}{2}\sum_{n=0}^{\infty} f_n |n\rangle\langle n| & \sum_{n=1}^{\infty} -\frac{g}{\sqrt{n}} e^{-2g^2/\omega^2} L_{n-1}^{(1)}\left(\frac{4g^2}{\omega^2}\right)|n\rangle\langle n| \\ \sum_{n=1}^{\infty} -\frac{g}{\sqrt{n}} e^{-2g^2/\omega^2} L_{n-1}^{(1)}\left(\frac{4g^2}{\omega^2}\right)|n\rangle\langle n| & -\left(\frac{\omega}{2} + \frac{g^2}{\omega}\right)(1 - |0\rangle\langle 0|) + \frac{\omega}{2}\sum_{n=1}^{\infty} f_{n-1}|n\rangle\langle n| \end{pmatrix}, \tag{72}$$

where we have used the relation[16]

$$\langle m|e^{\pm(2g/\omega)(a^\dagger - a)}|n\rangle = \sqrt{\frac{n!}{m!}}\left(\frac{\pm 2g}{\omega}\right)^{m-n} e^{-(2g^2/\omega^2)} L_n^{(m-n)}\left(\frac{4g^2}{\omega^2}\right), \tag{73}$$

with $L_n^{(m-n)}(x)$ the associated Laguerre polynomials and $m \geqslant n$. The new effective Hamiltonian can thus be written as

$$H_3^{\text{eff}} = \omega N \otimes \mathbb{1}_2 + \Pi_{H_3^{(0)}} V_3. \tag{74}$$

Since all the entries of H_3^{eff} commute with N, it can be diagonalized in the atomic Hilbert space as if its entries were scalars. The eigenvalues of H_3^{eff} are thus

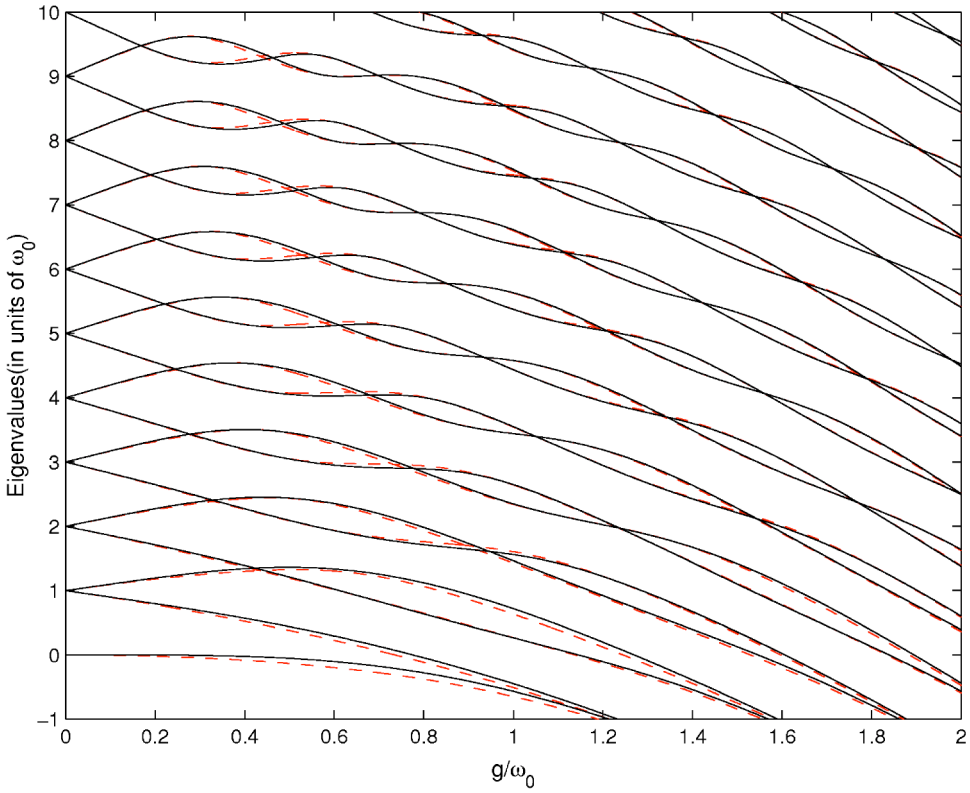

FIG. 4. Comparison of exact numerical spectrum of (8) (dashed lines) as a function of the coupling constant in the resonant case ($\omega=\omega_0$), with the quite accurate result (75) which has treated the zero-field resonances by a RT (solid lines).

$$E^{\text{eff}}_{3,(0,-)} = 0, \quad E^{\text{eff}}_{3,(0,+)} = \frac{\omega}{2} - \frac{g^2}{\omega} - \frac{\omega}{2} e^{-2g^2/\omega^2},$$

$$E^{\text{eff}}_{3,(n\geqslant 1,\pm)} = n\omega - \frac{g^2}{\omega} - \frac{\omega}{4} e^{-2g^2/\omega^2}\left(L_n\left(\frac{4g^2}{\omega^2}\right) - L_{n-1}\left(\frac{4g^2}{\omega^2}\right)\right)$$
$$\pm \frac{1}{2}\left[\left(\omega - \frac{\omega}{2} e^{-2g^2/\omega^2}\left(L_n\left(\frac{4g^2}{\omega^2}\right) + L_{n-1}\left(\frac{4g^2}{\omega^2}\right)\right)\right)^2 + \frac{4g^2}{n} e^{-4g^2/\omega^2}\left(L^{(1)}_{n-1}\left(\frac{4g^2}{\omega^2}\right)\right)^2\right]^{1/2}. \tag{75}$$

The zero eigenvalue is the extra spurious one that has been added by the RT to the spectrum. Figure 4 compares the exact numerical spectrum of (8) and the approximation (75) which has treated the zero-field resonances by a RT. The figure shows that treating all the active resonances of the system allows us to obtain all the qualitative features of the spectrum in the whole range of the coupling constant and for all energies. At a second stage, since we have treated all the active resonances, we can improve further this spectrum quantitatively by a KAM-type perturbative iteration.

VI. CONCLUSIONS

We have presented a nonperturbative method based on the quantum averaging technique to determine the spectral properties of systems containing resonances. It consists in the construction of unitary or isometric transformations that leads to an effective reduced Hamiltonian. These transformations are composed of two qualitatively distinct stages. The first one consists of non-

perturbative transformations (RTs) that are adapted to the structure of the resonances. Their role is to construct a first effective Hamiltonian that contains the main qualitative features of the spectrum—crossings and avoided crossings—in a given range of the coupling parameter. The diagonalized form of this effective Hamiltonian, which depends parametrically on the coupling constant, is then taken as a new reference Hamiltonian around which one can apply perturbative techniques to improve the quantitative accuracy of the spectrum. We formulate the perturbative approach in terms of a KAM-type iteration of contact transformations. Similar results can be obtained with other formulations of perturbation theory.

We have illustrated the method with a model of a two-level atom interacting with a single mode of a quantized field. The method can be applied to more general systems with several field modes. It can also be adapted to the treatment of semiclassical models in which the field is described as a time-dependent function.

We have analyzed the resonances in two regimes of weak and strong coupling. The results we obtained in the weak-coupling regime can be expected to be applicable to quite general models. The analysis of the strong-coupling regime of this model leads to results that are valid for all values of the coupling and for all energies. The possibility to obtain such a global result is due to a particular property of the model, and one cannot expect to obtain it for general models. The particular property is that the part we selected as the reference Hamiltonian H_0 in the strong-coupling regime contains all the unbounded operators of the complete model and is explicitly solvable. The term that was left to be treated by RT and perturbation theory is a bounded operator.

ACKNOWLEDGMENTS

M.A-T. wishes to acknowledge the financial support of the French Society SFERE and the MSRT of Iran. We acknowledge support for this work from the Conseil Régional de Bourgogne.

[1] E. Jaynes and F. Cummings, Proc. IEEE **51**, 89 (1963).
[2] J. Shirley, Phys. Rev. **138**, 979 (1965).
[3] H. R. Jauslin, S. Guérin, and S. Thomas, Physica A **279**, 432 (2000).
[4] P. M. Blekher, H. R. Jauslin, and J. L. Lebowitz, J. Stat. Phys. **68**, 271 (1992).
[5] G. Gentile, J. Stat. Phys. **115**, 1605 (2004).
[6] G. Gentile, Commun. Math. Phys. **242**, 221 (2003).
[7] W. F. Wreszinski and S. Casmeridis, J. Stat. Phys. **90**, 1601 (1998).
[8] J. C. Barata, Rev. Math. Phys. **12**, 25 (2000).
[9] S. Guérin and H. R. Jauslin, Adv. Chem. Phys. **125**, 147 (2003).
[10] J. Bellissard, in *Trends and Developments in the Eighties*, edited by S. Albeverio and P. Blanchard (World Scientific, Singapore, 1985).
[11] H. Primas, Rev. Mod. Phys. **35**, 710 (1963).
[12] P. W. Milonni, J. R. Ackerhalt, and H. W. Galbraith, Phys. Rev. Lett. **50**, 966 (1983).
[13] L. Allen and J. H. Eberly, *Optical Resonance and Two-Level Atoms* (Wiley, New York, 1975).
[14] P. Lais and T. Steimle, Opt. Commun. **78**, 346 (1990).
[15] C. Cohen-Tannoudji, J. Dupont-Roc, and G. Grynberg, *Atom-Photon Interactions* (Wiley, New York, 1992), Chap. 6, pp. 408 and 485.
[16] M. Frasca, Phys. Rev. A **66**, 023810 (2002).
[17] R. Graham and M. Höhnerbach, Z. Phys. B: Condens. Matter **57**, 233 (1984).
[18] R. Graham and M. Höhnerbach, Phys. Lett. **101A**, 61 (1984).
[19] I. Franchuk, L. Komarov, and A. Ulyanenkov, J. Phys. A **29**, 4035 (1996).
[20] E. Tur, Opt. Spectrosc. **89**, 574 (2000).
[21] S. Weigert and G. Müller, Chaos, Solitons Fractals **5**, 1419 (1995).
[22] M. Reed and B. Simon, *Methods of Modern Mathematical Physics: Functional Analysis* (Academic, London, 1980), Vol. 1.
[23] Y. Bérubé-Lauzière, V. Hussin, and L. Nieto, Phys. Rev. A **50**, 1725 (1994).

Chapter 6

Effective dressed Hamiltonians for laser-driven atoms and molecules

We combine here the general ideas of the iterative perturbation algorithms by unitary transformations and of the resonant transformation, to construct effective models within the Floquet theory.

When considering the stationary Floquet Hamiltonian $K = -i\hbar\omega\frac{\partial}{\partial\theta} + H(\theta)$, $H(\theta) = H_0 + \varepsilon V(\theta)$, describing the dynamics of a quantum (atomic or molecular) system H_0, illuminated by a strong photon field (of one frequency), we have to extend the preceding partitioning to the enlarged space $\mathcal{K} = \mathcal{H} \otimes \mathcal{L}$. This is in practice done in two steps:

(i) First we identify a set of atomic (or molecular) essential states, connected with the initial condition, whose population will be appreciable during the dynamics. This means that these states are in multiphoton resonance (or quasi-resonance). This allows one to split the Hilbert space into two orthogonal subspaces $\mathcal{H} = \mathcal{H}^0 \oplus \mathcal{H}^1$, and thus the enlarged Hilbert space also into two orthogonal subspaces

$$\mathcal{K} = (\mathcal{H}^0 \otimes \mathcal{L}) \oplus (\mathcal{H}^1 \otimes \mathcal{L}) = \mathcal{K}^0 \oplus \mathcal{K}^1. \tag{6.1}$$

We next partition the Floquet Hamiltonian with respect to these atomic blocks. We obtain effective Floquet Hamiltonians inside each block.

(ii) The second step is the construction of an effective dressed Hamiltonian, independent of the $\theta-$variable, inside the block connected to the initial condition. This can be done by the KAM iterations combined by the resonant transformation techniques to treat the resonances. The second step depends on the specific problem that is treated.

This is calculated for single-mode and two-mode fields.

We review the one- and two-photon processes occurring in atoms (Section 6.2) and treat some of these in diatomic molecules (Section 6.3). In atoms, we recover known effective Hamiltonians (see for instance [43]), but using the fully time independent formulation. This is systematically extended for molecules where we determine original effective Hamiltonians that will be used for the control related to the alignment of molecules in Chapter 10.

6.1 Partitioning Floquet Hamiltonians

We formulate in a general way the first step for partitioning the Floquet Hamiltonian up to the second order. The free Hamiltonian is defined on a Hilbert space $\mathcal{H}$ of dimension N. We

assume that the Hamiltonian $H(\theta)$ features two distinct weakly coupled sets of states, such that it can be separated into four parts, represented symbolically in matrix form as

$$K = \begin{pmatrix} K_0^{00} + \varepsilon V^{00}(\theta) & \varepsilon V^{01}(\theta) \\ \varepsilon V^{10}(\theta) & K_0^{11} + \varepsilon V^{11}(\theta) \end{pmatrix}, \tag{6.2}$$

with

$$\begin{aligned} K_0^{ii} &= -i\hbar\omega \frac{\partial}{\partial\theta} \otimes \mathbb{1}_{\mathcal{H}^i} + H_0^{ii}, && \text{(6.3a)} \\ V &= V^{00} + V^{11} + V^{01} + V^{10}, && \text{(6.3b)} \\ H_0 &= H_0^{00} + H_0^{11}. && \text{(6.3c)} \end{aligned}$$

In the enlarged space, the splitting can be interpreted as two weakly coupled subspaces $\mathcal{K}^0$ and $\mathcal{K}^1$.

We construct a unitary transformation of the form $e^{\varepsilon W_1}$, with $W_1^\dagger = -W_1$ such that

$$e^{-\varepsilon W_1}(K_0^{00} + K_0^{11} + \varepsilon V)e^{\varepsilon W_1} = K_0^{00} + K_0^{11} + \varepsilon D_1(\theta) + \varepsilon^2 V_2(\theta), \tag{6.4}$$

where $D_1 = D_1^{00} + D_1^{11}$, with $D_1^{ii} = P^i D_1 P^i$, $i = 0, 1$, and giving the remaining coupling

$$\begin{aligned} \varepsilon^2 V_2 &= \frac{\varepsilon^2}{2}[V, W_1] + \frac{\varepsilon^3}{3}[[V, W_1], W_1] + \ldots + \varepsilon^M \frac{(M-1)}{M!} \underbrace{[\ldots[[V, W_1], W_1], \ldots]}_{M-1 \text{ commutators}} + \ldots \\ &\quad + \frac{\varepsilon^2}{2!}[D_1, W_1] + \frac{\varepsilon^3}{3!}[[D_1, W_1], W_1] + \ldots + \frac{\varepsilon^M}{M!} \underbrace{[\ldots[D_1, W_1], W_1], \ldots]}_{M-1 \text{ commutators}} + \ldots \end{aligned} \tag{6.5}$$

Since we have here a block-diagonal perturbation, we can choose

$$D_1 = V^{00} + V^{11}, \tag{6.6}$$

which in this case is not necessarily zero, as opposed to Eqs (4.58). This leads to $W^{00} = 0 = W^{11}$. We obtain a Floquet Hamiltonian of second order, in matrix notation

$$\begin{aligned} K_2 &= e^{-\varepsilon W_1}(K_0^{00} + K_0^{11} + \varepsilon V)e^{\varepsilon W_1} \\ &= \begin{pmatrix} K^{00} + \varepsilon V^{00} + \frac{\varepsilon^2}{2}\left[V^{01}W_1^{10} + (V^{01}W_1^{10})^\dagger\right] & \frac{\varepsilon^2}{2}\left(V^{00}W_1^{01} - W_1^{01}V^{11}\right) \\ \frac{\varepsilon^2}{2}\left(V^{11}W_1^{10} - W_1^{10}V^{00}\right) & K^{11} + \varepsilon V^{11} - \frac{\varepsilon^2}{2}\left[(W_1^{10}V^{01})^\dagger + W_1^{10}V^{01}\right] \end{pmatrix} \\ &\quad + \mathcal{O}(\varepsilon^3). \end{aligned} \tag{6.7}$$

We obtain the effective Floquet Hamiltonian (assuming that the initial condition is connected to the block $\mathcal{K}_0$) of second order:

$$K_{\text{eff}}^{00} = -i\hbar\omega \frac{\partial}{\partial\theta} \otimes \mathbb{1}_{\mathcal{H}^0} + H_0^{00} + \varepsilon V^{00} + \frac{\varepsilon^2}{2}\left[V^{01}W_1^{10} + (V^{01}W_1^{10})^\dagger\right]. \tag{6.8}$$

The next corrections of order ε^3 are given by $\frac{\varepsilon^3}{3}[[V_1, W_1], W_1] + \frac{\varepsilon^3}{3!}[[D_1, W_1], W_1]$. The particular case

$$V^{00} + V^{11} = 0, \tag{6.9}$$

leads to $D_1 = 0$, and to corrections for the eigenvalues of order ε^4, given by $\varepsilon^4[[[V, W_1], W_1], W_1]/8$.

It is convenient to calculate the term of order ε^2 of the effective Floquet Hamiltonian by expansion of V^{01} and W_1^{10} in Fourier series. The perturbation can be indeed written as

$$V(\theta) = \sum_\ell \widetilde{V}_\ell \; e^{i\ell\theta}. \tag{6.10}$$

Writing W_1 in the basis of eigenvectors $|n,k\rangle$ of K_0, denoting the corresponding eigenvalues $\lambda^0_{n,k} = E_n + k\hbar\omega$ with E_n the eigenvalues of H_0 :

$$W_1 = \sum_{n,m,k,k',(m,k')\neq(n,k)} \frac{|n,k\rangle\langle n,k|V(\theta)|m,k'\rangle\langle m,k'|}{\lambda^0_{m,k'} - \lambda^0_{n,k}}, \tag{6.11}$$

gives

$$W_1 \;=\; \sum_{n,m,k,k',\ell} \frac{|n\rangle\langle n|\widetilde{V}_\ell|m\rangle\langle m| \otimes [|k\rangle\langle k|e^{i\ell\theta}|k'\rangle\langle k'|]}{E_m + k'\hbar\omega - (E_n + k\hbar\omega)} = \sum_{n,m,\ell} \frac{|n\rangle\langle n|\widetilde{V}_\ell|m\rangle\langle m|}{E_m - E_n - \ell\hbar\omega} \otimes e^{i\ell\theta}, \tag{6.12}$$

since

$$\sum_k |k\rangle\langle k-\ell| = e^{+i\ell\theta}. \tag{6.13}$$

We can thus expand W_1 in the Fourier modes

$$W_1 = \sum_\ell \widetilde{W}_{1,\ell} \; e^{i\ell\theta}, \quad \widetilde{W}_{1,\ell} = \sum_{n,m} \frac{|n\rangle\langle n|\widetilde{V}_\ell|m\rangle\langle m|}{E_m - E_n - \ell\hbar\omega}. \tag{6.14}$$

Defining $W_1^{ij} := P^i W_1 P^j$, and choosing $W_1^{00} = 0$ and $W_1^{11} = 0$, we obtain as before, in terms of the eigenvalues and eigenvectors (in the enlarged space) of K^{00} and of K^{11}:

$$W_1 \;=\; W_1^{01} + W_1^{10}, \tag{6.15a}$$

$$W_1^{01} \;=\; \sum_\ell \widetilde{W}^{01}_{1,\ell} \; e^{i\ell\theta}, \quad \widetilde{W}^{01}_{1,\ell} = \sum_{n,m} \frac{|n^{00}\rangle\langle n^{00}|\widetilde{V}^{01}_\ell|m^{11}\rangle\langle m^{11}|}{E^{11}_m - E^{00}_n - \ell\hbar\omega}, \tag{6.15b}$$

$$W_1^{10} \;=\; \sum_\ell \widetilde{W}^{10}_{1,\ell} \; e^{i\ell\theta}, \quad \widetilde{W}^{10}_{1,\ell} = \sum_{n,m} \frac{|m^{11}\rangle\langle m^{11}|\widetilde{V}^{10}_\ell|n^{00}\rangle\langle n^{00}|}{E^{00}_n - E^{11}_m - \ell\hbar\omega} \tag{6.15c}$$

with

$$\widetilde{V}^{10}_\ell = \left(\widetilde{V}^{01}_{-\ell}\right)^\dagger \;, \quad \widetilde{W}^{10}_{1,\ell} = -\left(\widetilde{W}^{01}_{1,-\ell}\right)^\dagger. \tag{6.16}$$

We remark that the denominators of W_1 allow us to detect resonant states of the subspace $\mathcal{H}^1$ that should be thus included in the subspace $\mathcal{H}^0$ in the partitioning.

We obtain for the second order effective Floquet Hamiltonian

$$\begin{aligned} K^{00}_{\text{eff}} \;=\; & -i\hbar\omega\frac{\partial}{\partial\theta} \otimes \mathbb{1}_{\mathcal{H}^0} + H^{00}_0 + \varepsilon V^{00} \\ & -\frac{\varepsilon^2}{2} \sum_{n,\widetilde{n},\ell,\ell',m} \left(\frac{e^{i(\ell+\ell')\theta}}{E^{11}_m - E^{00}_n + \ell\hbar\omega} + \frac{e^{i(\ell+\ell')\theta}}{E^{11}_m - E^{00}_{\widetilde{n}} - \ell'\hbar\omega} \right) \\ & \qquad \times |\widetilde{n}^{00}\rangle\langle\widetilde{n}^{00}|\widetilde{V}^{01}_{\ell'}|m^{11}\rangle\langle m^{11}|\widetilde{V}^{10}_\ell|n^{00}\rangle\langle n^{00}|. \end{aligned} \tag{6.17}$$

We can easily extend this formula to the multifrequency case by adapting the notations: $\omega \to \underline{\omega}$, $\theta \to \underline{\theta}$, $\ell \to \underline{\ell}$, and $\ell' \to \underline{\ell}'$ (see also Section 1.5):

$$\begin{aligned} K_{\rm eff}^{00} &= -i\hbar\underline{\omega}\cdot\frac{\partial}{\partial\underline{\theta}}\otimes\mathbb{1}_{\mathcal{H}^0} + H_0^{00} + \varepsilon V^{00} \\ &\quad -\frac{\varepsilon^2}{2}\sum_{n,\widetilde{n},\underline{\ell},\underline{\ell}',m}\left(\frac{e^{i(\underline{\ell}+\underline{\ell}')\cdot\underline{\theta}}}{E_m^{11}-E_n^{00}+\underline{\ell}\cdot\hbar\underline{\omega}}+\frac{e^{i(\underline{\ell}+\underline{\ell}')\cdot\underline{\theta}}}{E_m^{11}-E_{\widetilde{n}}^{00}-\underline{\ell}'\cdot\hbar\underline{\omega}}\right) \\ &\qquad\qquad \times|\widetilde{n}^{00}\rangle\langle\widetilde{n}^{00}|\widetilde{V}_{\underline{\ell}'}^{01}|m^{11}\rangle\langle m^{11}|\widetilde{V}_{\underline{\ell}}^{10}|n^{00}\rangle\langle n^{00}|. \end{aligned} \tag{6.18}$$

6.2 Effective Hamiltonian in atoms for one- and two-photon processes

We consider an atom, of Hamiltonian H_0, illuminated by a laser, such that two atomic states $|a\rangle$ and $|b\rangle$ (of respective energies $E_a = \hbar\omega_a$ and $E_b = \hbar\omega_b$ giving $H_0^{00} = \mathrm{diag}[E_a, E_b]$ in the basis $\{|a\rangle, |b\rangle\}$) are in (one- or two-photon) quasi-resonance. The coupling is made through the electric dipole moment $\overrightarrow{\mu} = -e\sum_i \overrightarrow{r}_i$, with $\overrightarrow{r}_i$ the position of each electron i and $-e$ the elementary electric charge (with the origin of the axis taken in the nucleus):

$$K = -i\hbar\omega\frac{\partial}{\partial\theta} + H_0 - \overrightarrow{\mu}\cdot\overrightarrow{E}. \tag{6.19}$$

Since we consider a general linearly or elliptically polarized field, we have to consider two manifolds of degenerate states for a given J, labeled $\{|a(J_a, m_a)\rangle\}$ and $\{|b(J_b, m_b)\rangle\}$. We omit below the mention of the angular and magnetic quantum numbers when unnecessary.

In practice, one very often considers a transition of a single electron (of position denoted $\overrightarrow{r}$), which should be then taken into account as the unique contribution in the summation $\overrightarrow{\mu} = -e\overrightarrow{r}$. As a consequence, we have $\langle n|\overrightarrow{\mu}|n\rangle = \overrightarrow{0}$, $n = a, b$, since the atomic states have a well-defined symmetry, and the components of the moment dipole are odd functions.

We first recall the results for one-photon resonant processes, for linearly and elliptically polarized fields (see for instance [43] and more recently [112]).

6.2.1 RWA for a linearly or elliptically polarized one-photon resonant field

We assume a near-resonant laser field of frequency ω:

$$\omega_a + \omega + \Delta = \omega_b, \tag{6.20}$$

linearly polarized along the z axis, or elliptically polarized in the plane $x-y$ (see Appendix A):

$$\text{linear}: \quad \overrightarrow{E} = \mathcal{E}\cos\omega t\,\overrightarrow{e}_z \tag{6.21a}$$

$$\text{elliptic}: \quad \overrightarrow{E} = \frac{\mathcal{E}}{\sqrt{2}}\sin\alpha\begin{pmatrix}\cos(\omega t+\eta/2)\\ \sin(\omega t+\eta/2)\\ 0\end{pmatrix} + \frac{\mathcal{E}}{\sqrt{2}}\cos\alpha\begin{pmatrix}\cos(\omega t-\eta/2)\\ -\sin(\omega t-\eta/2)\\ 0\end{pmatrix} \tag{6.21b}$$

with the angles $-\frac{\pi}{4} \le \alpha < \frac{3\pi}{4}$ ($\alpha = \pi/2$ for the left circularly polarized field, and $\alpha = 0$ for the right circularly polarized field) and the relative phase $0 \le \eta < 2\pi$ between the two circular fields.

In this resonant case, as shown below the leading order is of first order in field amplitude and can be obtained directly by the RWA. We can neglect higher orders that would be obtained by the preceding partitioning method.

Selection rules

We recall the selection rules, using the spectroscopic notation $n\,{}^{2S+1}X_J$, where n is the principal quantum number of the considered electron, $X = S, P, D, \cdots$ for respectively the total orbital quantum number $L = 0, 1, 2, \cdots$, S is the total spin quantum number, $2S+1$ is the multiplicity of the state, and $|L-S| \leq J \leq L+S$:

$$\Delta S = 0 \tag{6.22a}$$
$$\Delta L = 0, \pm 1 \tag{6.22b}$$
$$\Delta J = 0, \pm 1 \qquad (\text{but} \quad J = 0 \to J = 0 \quad \text{forbidden}) \tag{6.22c}$$
$$\text{parity change of} \quad \sum_i \ell_i \tag{6.22d}$$

where ℓ_i is the orbital quantum number of the electron i. The two first rules concerning S and L are approximate (better for light elements); they presume that the angular momenta $\vec{L}$ and $\vec{S}$ are well defined, i.e. that the coupling between each other is weak. The two last rules are exact. The last rule is known as the Laporte rule, which is due to the fact that the eigenfunctions of the total orbital angular momentum are either odd or even with an electronic inversion (i.e. replacement of all $\vec{r}_i$ by $-\vec{r}_i$) and that the dipole moment is odd. Since, as mentioned above, we consider a single active electron (i.e. a coupling between the $\vec{l}_i$ not too strong) of orbital quantum number denoted ℓ (and the other one in the ground state $1s$), we have $\sum_i \ell_i = \ell$, and the combination of the second and fourth selection rules becomes

$$\Delta L = \Delta \ell = \pm 1. \tag{6.23}$$

Concerning the magnetic quantum number m_J of the considered electron, such that $|m_J| \leq J$, and which gives the degeneracy of the state, we have

$$\Delta m_J = 0, \pm 1, \quad \text{and for } \Delta J = 0, \;\; \Delta m_J = \pm 1, \tag{6.24}$$

as detailed below.

Quasienergy operator

For the linear polarization along the z axis (usually denoted π, or with the symbol (0) when we refer to the associated standard components of the dipole moment, see below), the Floquet Hamiltonian reads

$$K^{(0)} = -i\hbar\omega \frac{\partial}{\partial\theta} + H_0 - \mu_z \mathcal{E}(t) \cos\theta. \tag{6.25}$$

In the case of elliptic polarization, it reads

$$K^{(\text{ell})} = -i\hbar\omega \frac{\partial}{\partial\theta} + H_0 + \frac{\mathcal{E}(t)}{2} \left[\mu_{+1} \sin\alpha \; e^{-i(\theta+\eta/2)} - \mu_{-1} \cos\alpha \; e^{-i(\theta-\eta/2)} + c.c. \right], \tag{6.26}$$

where *c.c.* denotes the complex conjugate (and the transpose for the operators), with the so-called *standard (or spherical)* components μ_q, $q = \pm 1, 0$ of the dipole moment:

$$\mu_{\pm 1} = \mp \frac{\mu_x \pm i\mu_y}{\sqrt{2}} \quad (\mu_{+1}^\dagger = -\mu_{-1}), \quad \mu_0 = \mu_z. \tag{6.27}$$

The use of such a decomposition of an elliptic field into two circular fields and the standard components are well adapted to treat one-photon resonant cases. Particular circular polarizations are for $\alpha = \pi/2$, denoted σ_+:

$$K^{(+)} = -i\hbar\omega \frac{\partial}{\partial\theta} + H_0 - \frac{\mathcal{E}(t)}{2}(\mu_{-1} e^{i(\theta+\eta/2)} - \mu_{+1} e^{-i(\theta+\eta/2)}) \tag{6.28}$$

and for $\alpha = 0$, denoted σ_-:

$$K^{(-)} = -i\hbar\omega \frac{\partial}{\partial\theta} + H_0 - \frac{\mathcal{E}(t)}{2}(\mu_{-1} e^{-i(\theta-\eta/2)} - \mu_{+1} e^{i(\theta-\eta/2)}). \tag{6.29}$$

In the resonant approximation (see below), the Hamiltonian $K^{(+)}$ will allow an absorption of a σ_+ photon and an emission of a σ_- photon; the Hamiltonian $K^{(-)}$ will allow an absorption of a σ_- photon and an emission of a σ_+ photon.

Wigner-Eckart theorem

The angular part of the matrix elements of the dipole moment can be calculated by the Wigner-Eckart theorem:

$$\begin{aligned}
\langle J_b, m_b|\mu_q|J_a, m_a\rangle &= \langle J_a 1 m_a q|J_b m_b\rangle \langle J_b||\mu||J_a\rangle = \langle J_a 1 m_a q|J_b m_b\rangle \frac{(J_b||\mu||J_a)}{\sqrt{2J_b+1}} && \text{(6.30a)}\\
&= (-1)^{J_a-1+m_b} \begin{pmatrix} J_b & J_a & 1 \\ -m_b & m_a & q \end{pmatrix} (J_b||\mu||J_a) && \text{(6.30b)}\\
&= (-1)^{J_b-m_b} \begin{pmatrix} J_b & 1 & J_a \\ -m_b & q & m_a \end{pmatrix} (J_b||\mu||J_a) && \text{(6.30c)}
\end{aligned}$$

$$\text{selection rule :} \quad m_b = m_a + q, \tag{6.31}$$

with the two standard definitions of the reduced matrix elements (independent of the m numbers) $\langle J_b||\mu||J_a\rangle$ and $(J_b||\mu||J_a)$ connected each other by $\langle J_b||\mu||J_a\rangle = (J_b||\mu||J_a)/\sqrt{2J_b+1}$, and connected to the transition strength $S(J_a, J_b) = S(J_b, J_a)$ by $S(J_a, J_b) = |(J_b||\mu||J_a)|^2/(ea_0)^2$, $\langle J_a 1 m_a q|J_b m_b\rangle$ the Clebsch-Gordan coefficients, and the three-j symbols $\begin{pmatrix} j_1 & j_2 & j \\ m_1 & m_2 & m \end{pmatrix}$ (whose values are unchanged after an even permutation, and multiplied by $(-1)^{j_1+j_2+j}$ after an odd permutation or after multiplying the lower row by -1). Other quantum numbers needed for the complete definition of the states have been omitted here for simplicity. This allows one to determine the selection rules between the m values and to calculate the ratio between these couplings.

Linear polarization

For a linear polarization, we thus have $m_a = m_b$ and the effective RWA Hamiltonian writes in the basis $\{|J_a\rangle, |J_b\rangle\}$

$$H_{\text{eff}}^{(0)} = \frac{\hbar}{2} \begin{pmatrix} 0 & \Omega_{ba}(t) \\ \Omega_{ba}(t) & 2\Delta \end{pmatrix} \tag{6.32}$$

with the one-photon Rabi frequency (assumed real)

$$\Omega_{ba}(t) = -\mathcal{E}(t)\langle b(J_b, m_b = m_a)|\mu_z|a(J_a, m_a)\rangle/\hbar. \tag{6.33}$$

This approximation holds when

$$\text{partitioning :} \qquad |\Omega_{ba}| \ll |\Delta_m|, |2\omega + \Delta_m| \tag{6.34a}$$

$$\text{resonant approximation :} \qquad |\Omega_{ba}|, |\Delta| \ll \omega \tag{6.34b}$$

with the *single resonant one-photon detunings* with respect to the other states than a and b (i.e. $m \neq a, b$) defined as

$$\Delta_m = \omega_m - \omega_a - \omega, \tag{6.35}$$

the anti-resonant detunings $2\omega + \Delta_m$. Such conditions have to persist for the resonant elliptical polarization processes studied below.

Elliptic polarization

For an elliptic polarization, $m_b = m_a \pm 1$ states are a priori involved in the resonance for a given m_a leading to a multi-state linkage. We assume in what follows that $\omega_a < \omega_b$. In this case, the circular σ_+ (resp. σ_-) term proportional to $\sin\alpha$ (resp. $\cos\alpha$) in (6.26) is resonant allowing an absorption of one-photon from $|a\rangle$ to $|b\rangle$ with $m_b = m_a + 1$ (resp. $m_b = m_a - 1$).

These circular and linear resonant processes are symbolized in Fig. (6.1).

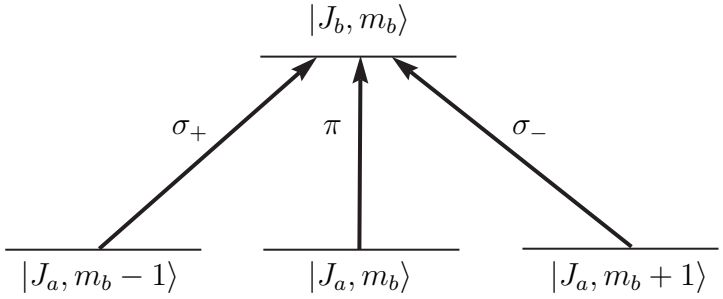

FIG. 6.1 - *Schematic representation of resonant processes by linear π and circular $\sigma_\pm$ pulses with $J_b = J_a, J_a \pm 1$.*

Example 1. Λ system: STIRAP by adiabatic rotation of polarization We consider the Λ-system: $J_a = 1$, $J_b = 0$, for instance the states $2\,^3S_1$ - $2\,^3P_0$ in metastable helium (see Fig. 6.2). The elliptic polarization allows one to connect $|J_a = 1, m_a = -1\rangle$ and $|J_a = 1, m_a = +1\rangle$ to $|J_b = 0\rangle$ with the couplings

$$\langle 0,0|\mu_{+1}|1,-1\rangle = \langle 0,0|\mu_{-1}|1,1\rangle = (J_b||\mu||J_a)/\sqrt{3} = -\langle 0,0|\mu_z|1,0\rangle, \tag{6.36}$$

using $\begin{pmatrix} j & j & 0 \\ m & -m & 0 \end{pmatrix} = \frac{(-1)^{j-m}}{\sqrt{2j+1}}$. This gives the effective RWA Hamiltonian in the basis $\{|J_a = 1, m_a = -1\rangle, |J_b = 0\rangle, |J_a = 1, m_a = +1\rangle\}$

$$H_{\text{eff}} = \frac{\hbar}{2}\begin{pmatrix} 0 & \Omega_{ba}^*(t)\sin\alpha\ e^{i\eta/2} & 0 \\ \Omega_{ba}(t)\sin\alpha\ e^{-i\eta/2} & 2\Delta & -\Omega_{ba}(t)\cos\alpha\ e^{i\eta/2} \\ 0 & -\Omega_{ba}^*(t)\cos\alpha\ e^{-i\eta/2} & 0 \end{pmatrix} \tag{6.37}$$

with the Rabi frequency that can be evaluated here for the linear polarization:

$$\Omega_{ba}(t) = -\mathcal{E}(t)\langle b(J_b = 0)|\mu_z|a(J_a = 1, m_a = 0)\rangle/\hbar. \tag{6.38}$$

Such Hamiltonian shows that one can generate STIRAP processes (see Section 8.2), i.e. transfer population from state $|1, -1\rangle$ to state $|1, +1\rangle$ by using (i) two different delayed (but overlapping) σ_- (first) and σ_+ (next) fields of fixed polarization or (ii) an elliptic pulse of rotating angle α from $\alpha = 0$ to $\alpha = \pi/2$.

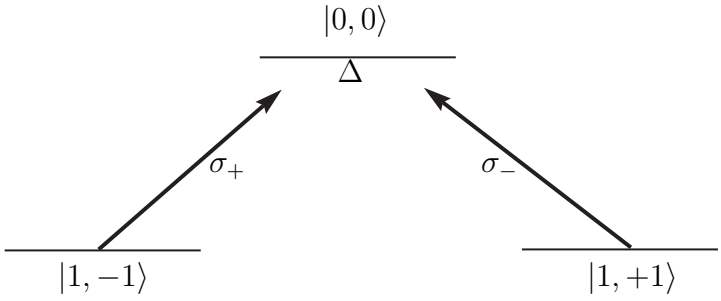

FIG. 6.2 - *Linkage of the Λ system (example 1).*

Example 2. *V* **system** We consider $J_a = 0$, and $J_b = 1$ (with $\omega_a < \omega_b$), for instance respectively the states $2\ ^1S_0$ - $2\ ^1P_1$ (or $2\ ^3P_0$ - $2\ ^3S_1$) in metastable helium (see Fig. 6.3). The elliptic polarization allows one to connect $|J_a = 0\rangle$ to $|J_b = 1, m_b = -1\rangle$ and $|J_b = 1, m_b = +1\rangle$ with the respective couplings

$$\langle 1, -1|\mu_{-1}|0, 0\rangle = \langle 1, 1|\mu_{+1}|0, 0\rangle = (J_b||\mu||J_a)/\sqrt{3} = \langle 1, 0|\mu_z|0, 0\rangle. \tag{6.39}$$

This leads to the following effective RWA Hamiltonian in the basis $\{|J_b = 1, m_b = -1\rangle, |J_a = 0\rangle, |J_b = 1, m_b = +1\rangle\}$

$$H_{\text{eff}} = \frac{\hbar}{2}\begin{pmatrix} 2\Delta & -\Omega_{ba}(t)\cos\alpha\ e^{i\eta/2} & 0 \\ -\Omega^*_{ba}(t)\cos\alpha\ e^{-i\eta/2} & 0 & \Omega^*_{ba}(t)\sin\alpha\ e^{i\eta/2} \\ 0 & \Omega_{ba}(t)\sin\alpha\ e^{-i\eta/2} & 2\Delta \end{pmatrix} \tag{6.40}$$

with the Rabi frequency that can be evaluated here for the linear polarization $m_a = m_b = 0$:

$$\Omega_{ba}(t) = -\mathcal{E}(t)\langle b(J_b = 1, m_b = 0)|\mu_z|a(J_a = 0)\rangle/\hbar. \tag{6.41}$$

We remark that a circular polarization is state-selective and allows a two-level approximation in such a system.

6.2.2 Two-photon single-mode processes

We here consider a two-photon transition between the states of energy $E_a = \hbar\omega_a$ and $E_b = \hbar\omega_b > E_a$:

$$\omega_a + 2\omega + \delta = \omega_b \tag{6.42}$$

with no intermediate single-photon resonances.

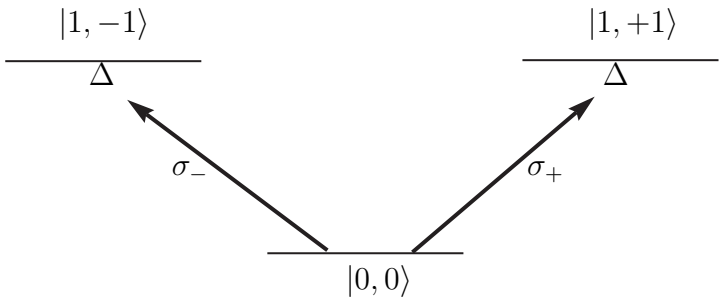

FIG. 6.3 - *Linkage of the V-system (example 2).*

We distinguish below processes that couple one initial state to a *single* state [when the polarization linear or circular (σ_- or σ_+)], with the ones that couple the initial state to a *subspace* of states (when the polarization is elliptic, and not linear nor circular).

We first partition the Floquet Hamiltonian such that the states $|a\rangle$ and $|b\rangle$ span the Hilbert subspace $\mathcal{H}^0$ and the other atomic states $\{|1\rangle, \cdots |N\rangle\}$ the Hilbert subspace $\mathcal{H}^1$.

The interaction can be written in general with the use of cartesian components:

$$\overrightarrow{\mu} = \sum_{i=1}^{3} \mu_i \overrightarrow{e}_i, \qquad \overrightarrow{E} = \sum_{i=1}^{3} \mathcal{E}_i \cos(\omega t + \phi_i) \overrightarrow{e}_i. \tag{6.43}$$

From Eq. (6.17), we obtain for the diagonal elements ($n = a, b$):

$$\begin{aligned} \langle n|K^{00}_{\text{eff}}|n\rangle &= -i\hbar\omega\frac{\partial}{\partial\theta} + \langle n|H^{00}_0|n\rangle - \frac{1}{2}\overrightarrow{E}(t,\theta)\cdot\langle n|\overrightarrow{\overrightarrow{\alpha}}(\omega)|n\rangle\cdot\overrightarrow{E}(t,\theta) \\ &\quad -\frac{i}{4}\sum_{i\neq j}\mathcal{E}_i\mathcal{E}_j\sin(\phi_i-\phi_j)\langle n|\alpha_{ij}|n\rangle \end{aligned} \tag{6.44}$$

with the effective *induced dipole moment* in the $\mathcal{H}_0$ subspace

$$\overrightarrow{\mu}^0_{\text{eff}}(\omega) = \frac{1}{2}\sum_{n,n'=a,b}|n'\rangle\langle n'|\overrightarrow{\overrightarrow{\alpha}}(\omega)|n\rangle\langle n|\overrightarrow{E}(t,\theta), \tag{6.45}$$

and the components of the *dynamical* (i.e. frequency dependent) *electronic polarizability tensor* $\overrightarrow{\overrightarrow{\alpha}}$ in the $\mathcal{H}_0$ subspace

$$\langle n'|\alpha_{ij}(\omega)|n\rangle = \sum_{m\neq a,b}\left[\frac{\langle n'|\mu_i|m\rangle\langle m|\mu_j|n\rangle}{\hbar(\omega_m-\omega_n-\omega)} + \frac{\langle n'|\mu_j|m\rangle\langle m|\mu_i|n\rangle}{\hbar(\omega_m-\omega_{n'}+\omega)}\right]. \tag{6.46}$$

Note that the indices ij are interchanged in the second summation. These matrix elements have the properties

$$\langle n'|\alpha_{ij}(\omega)|n\rangle = \langle n|\alpha_{ji}(\omega)|n'\rangle^* = \langle n'|\alpha_{ji}(-\omega)|n\rangle. \tag{6.47}$$

For atoms, the electronic polarizability tensor that connects the same electronic states is diagonal:

$$\langle n|\alpha_{ij}|n\rangle = \alpha_i\delta_{ij}, \tag{6.48}$$

with $\alpha_i = \alpha$ for all i in a spherical s-state. This finally leads to the simple form

$$\langle n|K_{\rm eff}^{00}|n\rangle = -i\hbar\omega\frac{\partial}{\partial\theta} + \langle n|H_0^{00}|n\rangle - \frac{1}{2}\overrightarrow{E}(t,\theta)\cdot\langle n|\,\overrightarrow{\overrightarrow{\alpha}}\,(\omega)|n\rangle\cdot\overrightarrow{E}(t,\theta). \tag{6.49}$$

We remark that the result (6.49) is valid for any field polarization and quantum axis.

Selection rules

The selection rules for this two-photon process are thus

$$\Delta S = 0 \tag{6.50a}$$
$$\Delta L = \Delta l = 0, \pm 2 \tag{6.50b}$$
$$\Delta J = 0, \pm 2 \tag{6.50c}$$
$$\Delta m_J = 0, \pm 2 \tag{6.50d}$$

As mentioned above, we have $\mu_{aa} = \mu_{bb} = 0$. The selection rules entail furthermore $\mu_{ba} = 0$ for a two-photon transition. A linear polarized field (along the z) direction will give $\Delta m_J = 0$. A circular σ_+ (resp. σ_-) in the $x-y$ plane will give $\Delta m = +2$ (resp. $\Delta m = -2$).

Effective Hamiltonian with a linear or circular field: The two-photon RWA

We consider here two-photon processes by a linear or circular pulse, as shown in Fig. 6.4. The quantum axis is chosen as the z-axis. The standard components for the dipole moment are here appropriate for the circular fields, as shown below.

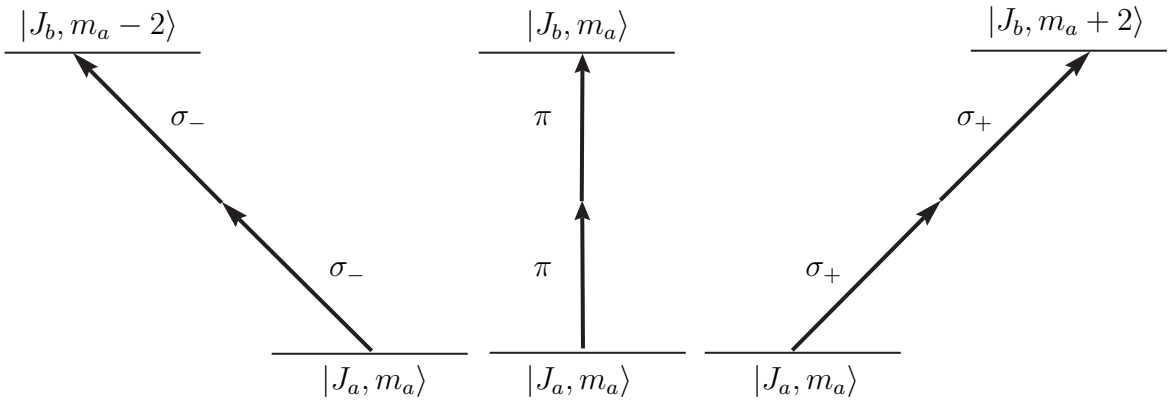

FIG. 6.4 - *The three linkage patterns for a two-photon process with a linear or circular field with* $J_b = J_a, J_a \pm 2$.

Construction of the effective dressed Hamiltonian. Denoting the matrix elements $\mu_{nn'}^{(q)}$ with $q = 0, +, -$ respectively for the linear π, circular σ_+, and circular σ_- polarizations, and applying Eq. (6.17), we obtain for the second order effective Floquet Hamiltonian

$$K_{\rm eff}^{(q)} = -i\hbar\omega\frac{\partial}{\partial\theta} + H_0^{00} + \mathcal{E}^2 V_2^{(q)}(\theta) \tag{6.51}$$

with

$$V_2^{(q)}(\theta) = \begin{pmatrix} V_{2,aa}^{(q)}(\theta) & V_{2,ba}^{(q)\,*}(\theta) \\ V_{2,ba}^{(q)}(\theta) & V_{2,bb}^{(q)}(\theta) \end{pmatrix}, \tag{6.52}$$

the diagonal elements from Eq. (6.49)

$$\mathcal{E}^2 V_{2,nn}^{(q)} = -\frac{1}{2}\langle n|\overrightarrow{E}(t,\theta)\cdot\overrightarrow{\overrightarrow{\alpha}}(\omega)\cdot\overrightarrow{E}(t,\theta)|n\rangle, \tag{6.53a}$$

and the coupling which reads for the linear polarization

$$V_{2,ba}^{(0)} = -\frac{1}{8\hbar}\sum_{m\neq a,b}\mu_{bm}^{(0)}\mu_{ma}^{(0)}\sum_{\ell,\ell'\in\{-1,1\}}\left(\frac{e^{i(\ell+\ell')(\theta+\phi_0)}}{\omega_m-\omega_a+\ell\omega}+\frac{e^{i(\ell+\ell')(\theta+\phi_0)}}{\omega_m-\omega_b-\ell'\omega}\right). \tag{6.53b}$$

ϕ_q is the phase of the field of polarization $q=-,0,+$, defined for the circular fields as

$$\phi_\pm = \pm\eta/2. \tag{6.54}$$

This gives for the diagonal elements for the linear polarization

$$V_{2,nn}^{(0)} = -\frac{1}{4}\langle n|\alpha_{zz}(\omega)|n\rangle\cos^2(\theta+\phi_0), \tag{6.55a}$$

and for the elliptic polarization

$$V_{2,nn}^{(q)} = -\frac{1}{4}\langle n|\big[\alpha_{xx}(\omega)\cos^2(\theta+\phi_q)+\alpha_{yy}(\omega)\sin^2(\theta+\phi_q)\big]|n\rangle. \tag{6.55b}$$

The non-diagonal perturbation term $V_{2,ba}^{(q)}$ can be calculated for $q=\pm1$ using the definition of the circular perturbations in Eqs. (6.28) and (6.29). Although we do not explicitly indicate this, the sums should also include a principal-value integral over continuum states. To determine an effective dressed Hamiltonian (i.e. independent of θ) from the second order perturbation term (6.52), we next apply a contact transformation consisting in averaging the Hamiltonian (6.51) with respect to $K_0 := -i\hbar\omega\partial/\partial\theta + H_0^{00}$, i.e. in diagonalizing it with respect to θ and to the basis $\{|a\rangle,|b\rangle\}$. Since $V_2^{(q)}(\theta)=\sum_{\ell\in\{-2,\cdots,2\}}\widetilde{V}_{2,\ell}^{(q)}\,e^{i\ell\theta}$, this could be done using $W_2^{(q)}(\theta)=\sum_\ell\widetilde{W}_{2,\ell}^{(q)}\,e^{i\ell\theta}$ satisfying (6.14), with, for example, the b,a component of the mode $\ell=-2$

$$\mathcal{E}^2\langle b|\widetilde{W}_{2,-2}^{(q)}|a\rangle = \frac{-\Omega_{ba}^{(q)}e^{-2i\phi_q}}{\omega_a-\omega_b+2\omega}, \tag{6.56}$$

where we denote the effective two-photon Rabi frequency

$$\Omega_{ba}^{(q)} = -\frac{\mathcal{E}^2}{4\hbar^2}\sum_{m\neq a,b}\left(\frac{\mu_{bm}^{(q)}\mu_{ma}^{(q)}}{\omega_m-\omega_a-\omega}+\frac{\mu_{bm}^{(q)}\mu_{ma}^{(q)}}{\omega_m-\omega_b+\omega}\right). \tag{6.57}$$

It reads for the linear polarization

$$\Omega_{ba}^{(0)} = -\frac{\mathcal{E}^2}{4\hbar}\langle b|\alpha_{zz}(\omega)|a\rangle \tag{6.58}$$

and for the elliptical polarization (here written with cartesian components, see below for the standard components)

$$\Omega_{ba}^{(\pm)} = -\frac{\mathcal{E}^2}{8\hbar}\left[\langle b|\alpha_{xx}(\omega)|a\rangle-\langle b|\alpha_{yy}(\omega)|a\rangle\pm i(\langle b|\alpha_{xy}(\omega)|a\rangle+\langle b|\alpha_{yx}(\omega)|a\rangle)\right]. \tag{6.59}$$

We emphasize that the electronic polarizability tensor that connects different electronic states (generally of different symmetry) is not diagonal in general.
This leads to a *quasi-divergence* of the W which occurs *when the numerator is equal or larger than the denominator in absolute value*. It is due to the quasiresonance $\omega_b - \omega_a - 2\omega = \delta$ and occurs thus when $|\Omega_{ba}| \gtrsim |\delta|$. We thus apply instead the two-photon RT

$$R_2 = \mathrm{diag}[1, \exp(-2i\theta)], \tag{6.60}$$

giving the effective Hamiltonian as the part of $R_2^\dagger K_{\mathrm{eff}} R_2$ independent of θ, by averaging with respect to θ [this corresponds to applying the contact transformation $\exp(\mathcal{E}W_\theta^{(q)})$ with $W_\theta^{(q)} = -i\int^\theta \left(R_2^\dagger V_2^{(q)}(\theta) R_2 - \overline{R_2^\dagger V_2^{(q)}(\theta) R_2}\right)$ and $\overline{f(\theta)} = (\frac{1}{2\pi})\int_0^{2\pi} d\theta\ f(\theta)$], retaining terms up to $\mathcal{E}^2$. With this procedure, *the diagonal elements of the effective Hamiltonian are thus simply given by the averaging with respect to θ of the diagonal elements (6.44) of the Hamiltonian (6.17).*

The effective dressed Hamiltonian (independent of θ) finally reads (with the energy reference $E_a = 0$)

$$H_{\mathrm{eff}} = \frac{\hbar}{2}\begin{pmatrix} 2S_a^{(q)} & \Omega_{ba}^{(q)^*} e^{2i\phi_q} \\ \Omega_{ba}^{(q)} e^{-2i\phi_q} & 2(S_b^{(q)} + \delta) \end{pmatrix} \tag{6.61}$$

with the effective two-photon Rabi frequency (6.57) and the *Stark (or light) shift* of the state n reading for the linear polarization

$$S_n^{(0)} = -\frac{\mathcal{E}^2}{4\hbar}\langle n|\alpha_{zz}(\omega)|n\rangle = -\frac{\mathcal{E}^2}{2\hbar^2}\sum_{m\neq a,b} |\mu_{nm}^{(0)}|^2 \frac{\omega_m - \omega_n}{(\omega_m - \omega_n)^2 - \omega^2} \tag{6.62}$$

and for the elliptical polarization

$$S_n^{(\pm)} = -\frac{\mathcal{E}^2}{8\hbar}\left[\langle n|\alpha_{xx}(\omega)|n\rangle + \langle n|\alpha_{yy}(\omega)|n\rangle\right]. \tag{6.63}$$

This approximation holds when

$$\text{partitioning :} \qquad |\Omega_{ba}^{(q)}| \ll |\Delta_m|, |2\omega + \Delta_m| \tag{6.64a}$$

$$\text{resonant approximation :} \qquad |\Omega_{ba}^{(q)}|, |\delta| \ll 2\omega \tag{6.64b}$$

with the resonant one-photon detunings ($m \neq a, b$)

$$\Delta_m = \omega_m - \omega_a - \omega, \tag{6.65}$$

and the anti-resonant detunings $2\omega + \Delta_m$.

We can furthermore approximate the effective two-photon Rabi frequency as

$$\Omega_{ba}^{(q)} \approx -\frac{\mathcal{E}^2}{2\hbar^2}\sum_{m\neq a,b} \frac{\mu_{bm}^{(q)}\mu_{ma}^{(q)}}{\omega_m - \omega_a - \omega}, \tag{6.66}$$

neglecting the correction of the order $\delta/(\omega_m - \omega_a - \omega)$, when

$$|\delta| \ll |\Delta_m|, \tag{6.67}$$

i.e. when the two-photon detuning is much smaller than any one-photon detuning with the intermediate states (in absolute value). This approximation is implicitly present in the conditions (6.64) to get the effective Hamiltonian (6.61), if we take into account that a non-negligible population transfer occurs when $\Omega_{ba}^{(q)} \gtrsim \delta$.

This effective Hamiltonian (6.61) constructed by the combination of a partitioning of the Floquet Hamiltonian, of a two-photon RT, and of a final $\theta-$averaging can be seen as a *two-photon RWA*, which extends the usual (one-photon) RWA [43, 44]. We have thus rederived a well-known result, using stationary techniques that allows us to estimate easily the order of the neglected terms. This method allows us also to calculate higher order corrections.

One important point is that the extension to the two-photon RWA leads to a Stark shift that is of the same order of the Rabi frequency in field amplitude, and that cannot be consequently neglected. This Stark shift can be seen as an effect that moves away from the resonance, and that thus should be compensated by the detuning to preserve the resonance (see for instance [76, 113]).

Connection with the standard components of the polarizabilities. One can relate the two-photon Rabi frequency and the Stark shifts to the standard components of the tensor electronic polarizability operator, extending the definition of the polarizability components α_{ij} (6.46) to the standard components $\alpha_{qq'}$:

$$\Omega_{ba}^{(q)} = -\frac{\mathcal{E}^2}{4\hbar}\langle b|\alpha_{qq}(\omega)|a\rangle, \tag{6.68a}$$

$$S_n^{(q)} = (-1)^{q+1}\frac{\mathcal{E}^2}{4\hbar}\langle n|\alpha_{-qq}(\omega)|n\rangle, \tag{6.68b}$$

using the correspondence

$$\alpha_{++} + \alpha_{--} = \alpha_{xx} - \alpha_{yy}, \tag{6.69a}$$

$$\alpha_{++} - \alpha_{--} = i(\alpha_{xy} + \alpha_{yx}), \tag{6.69b}$$

$$\alpha_{+-} + \alpha_{-+} = -(\alpha_{xx} + \alpha_{yy}), \tag{6.69c}$$

$$\alpha_{+-} - \alpha_{-+} = i(\alpha_{xy} - \alpha_{yx}). \tag{6.69d}$$

Increasing the coupling and related approximations. We can remark that in order to have a large two-photon Rabi frequency, one can *approach* the frequency to a single photon resonance:

$$\omega_a + \omega + \Delta_{a0} = \omega_0 \tag{6.70}$$

with the effective Hamiltonian (6.61) still valid as long as $\Omega_{ba} \ll \Delta_{a0}$. If one assumes additionally that the contribution of the other states are negligible:

$$\Delta_{a0} \ll \Delta_{am}, \Delta_{am} + \delta, \tag{6.71}$$

where $\{\Delta_{am}, m \in \mathcal{H}_1, m \neq 0\}$ are all the other single-photon detunings, we obtain (if $\delta \ll \Delta_{a,0}$)

$$\Omega_{ba}^{(q)} \approx -\frac{\mathcal{E}^2}{2\hbar^2}\frac{\mu_{b0}^{(q)}\mu_{0a}^{(q)}}{\Delta_{a0}}, \qquad S_n^{(q)} \approx -\frac{\mathcal{E}^2}{4\hbar^2}\frac{|\mu_{n0}^{(q)}|^2}{\Delta_{a0}}, \tag{6.72}$$

and the effective Hamiltonian

$$H_{\text{eff}}^{(q)} \approx \frac{\hbar}{2}\begin{pmatrix} -\frac{\mathcal{E}^2}{2\hbar^2\Delta_{a0}}|\mu_{a0}^{(q)}|^2 & -\frac{\mathcal{E}^2}{2\hbar^2\Delta_{a0}}\left(\mu_{b0}^{(q)}\mu_{0a}^{(q)}\right)^* e^{2i\phi_q} \\ -\frac{\mathcal{E}^2}{2\hbar^2\Delta_{a0}}\mu_{b0}^{(q)}\mu_{0a}^{(q)}e^{-2i\phi_q} & -\frac{\mathcal{E}^2}{2\hbar^2\Delta_{a0}}|\mu_{b0}^{(q)}|^2 + 2\delta \end{pmatrix}. \tag{6.73}$$

If we have $\mu_{a0}^{(q)} = \mu_{b0}^{(-q)}$, then the Stark shift is the same for both states, and has consequently no relative effect (but would give a global phase for the dynamics).

Effective Hamiltonian for an elliptic field

From an initial state $|a(J_a, m_a)\rangle$, a two-photon process by an elliptic field of the form

$$\overrightarrow{E} = \frac{\mathcal{E}}{\sqrt{2}} \sin\alpha \begin{pmatrix} \cos(\omega t + \eta/2) \\ \sin(\omega t + \eta/2) \\ 0 \end{pmatrix} + \frac{\mathcal{E}}{\sqrt{2}} \cos\alpha \begin{pmatrix} \cos(\omega t - \eta/2) \\ -\sin(\omega t - \eta/2) \\ 0 \end{pmatrix} \tag{6.74}$$

can induce transitions in a chainwise-connected multistate system $\cdots \leftrightarrow |a(J_a, m_a - 4)\rangle \leftrightarrow |a(J_a, m_a - 2)\rangle \leftrightarrow |a(J_a, m_a)\rangle \leftrightarrow |a(J_a, m_a + 2) \leftrightarrow |a(J_a, m_a + 4)\rangle \leftrightarrow \cdots$ by Raman-type processes, and also in the excited state $\{\cdots, |b(J_b, m_a{-}4)\rangle, |b(J_b, m_a{-}2)\rangle, |b(J_b, m_a)\rangle, |b(J_b, m_a{+}2), |b(J_b, m_a + 4)\rangle, \cdots\}$ (see Fig. 6.5).

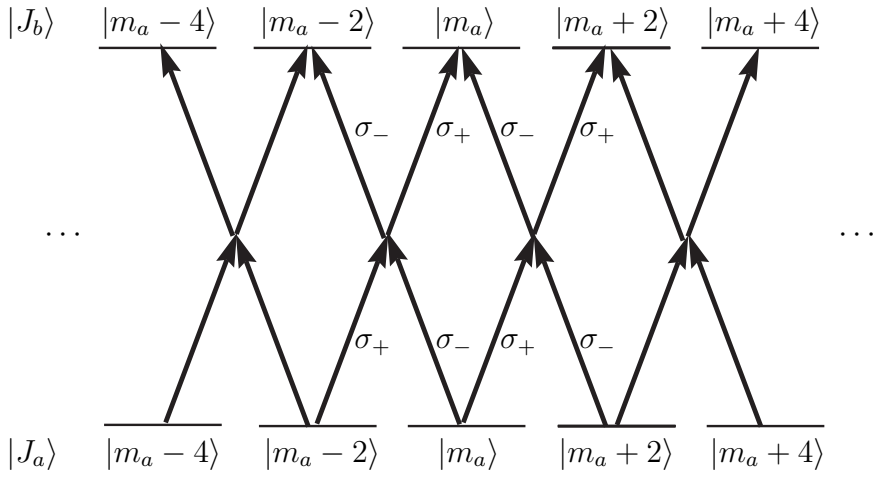

FIG. 6.5 - *Chainwise-linked multistate system with $J_b = J_a, J_a \pm 2$ for an elliptically polarized field interaction.*

To construct the effective dressed Hamiltonian, we follow the procedure described above: The off-block-diagonal coupling term of the ba component is given by the mode $\ell = -2$ of the effective Floquet Hamiltonian (6.17), and the block-diagonal term ($n = a, b$) by the θ-averaged diagonal term of (6.17):

$$\begin{aligned} \langle b|H_{\text{eff}}^{(\text{ell})}|a\rangle &= -\frac{\mathcal{E}_1}{8\hbar}\langle b|\big[2(\alpha_{++}(\omega)e^{-i\eta}\sin^2\alpha + \alpha_{--}(\omega)e^{i\eta}\cos^2\alpha) \\ &\quad -(\alpha_{-+}(\omega) + \alpha_{+-}(\omega))\sin 2\alpha\big]|a\rangle, \qquad (6.75a) \\ \langle n|H_{\text{eff}}^{(\text{ell})}|n\rangle &= E_n - \frac{\mathcal{E}^2}{8\hbar}\langle n|\big[(\alpha_{++}(\omega)e^{-i\eta} + \alpha_{--}(\omega)e^{i\eta})\sin 2\alpha \\ &\quad -2(\alpha_{-+}(\omega)\sin^2\alpha + \alpha_{+-}(\omega)\cos^2\alpha)\big]|n\rangle \qquad (6.75b) \\ &= E_n - \frac{\mathcal{E}^2}{4\hbar}\langle n|\big[\alpha_{++}(\omega)\cos\eta\sin 2\alpha - \alpha_{+-}(\omega)\big]|n\rangle \qquad (6.75c) \end{aligned}$$

where $-2\hbar\omega$ should be added for $\langle b|H_{\text{eff}}^{(\text{ell})}|b\rangle$.

The block-diagonal terms of Eq. (6.75c) proportional to $\mathcal{E}^2$ can be here interpreted as *Stark shifts* of the respective subspaces $|a(J_a)\rangle$ and $|b(J_b)\rangle$, and also as *Raman couplings* between the states of the respective degenerate-level manifolds that span the two subspaces. Such block-diagonal terms are thus referred below to as Raman-Stark terms. Within each diagonal block, the term proportional to $\sin 2\alpha$ is the off-diagonal coupling, characterizing an absorption of a photon σ_+ (σ_-) and an emission of a photon σ_- (σ_+). The next term is the Stark shift. This leads to the tridiagonal effective block-Hamiltonian in the $\{\cdots, |n(J_n, m_a - 2)\rangle, |n(J_n, m_a)\rangle, |n(J_n, m_a + 2)\rangle, \cdots\}$ basis (here written for $n = a$):

$$\langle a|H_{\rm eff}^{\rm (ell)}|a\rangle = \frac{\hbar}{2}\begin{pmatrix} \ddots & \ddots & \ddots & \ddots & \ddots \\ \ddots & 2S_{m_a-2} & \Omega^*_{m_a-2\to m_a} e^{i\eta}\sin 2\alpha & 0 & \ddots \\ \ddots & \Omega_{m_a-2\to m_a} e^{-i\eta}\sin 2\alpha & 2S_{m_a} & \Omega^*_{m_a\to m_a+2} e^{i\eta}\sin 2\alpha & \ddots \\ \ddots & 0 & \Omega_{m_a\to m_a+2} e^{-i\eta}\sin 2\alpha & 2S_{m_a+2} & \ddots \\ \ddots & \ddots & \ddots & \ddots & \ddots \end{pmatrix} \tag{6.76}$$

with

$$\Omega_{m\to m+2} = -\frac{\mathcal{E}^2}{4\hbar}\langle a(J_a, m+2)|\alpha_{++}(\omega)|a(J_a, m)\rangle, \tag{6.77a}$$

$$S_m = \frac{\mathcal{E}^2}{4\hbar}\langle a(J_a, m)|\alpha_{+-}(\omega)|a(J_a, m)\rangle. \tag{6.77b}$$

For $\eta = 0$ (giving an ellipse of semiaxes a and b, see Appendix A), the Hamiltonian becomes

$$\langle a|H_{\rm eff}^{(\rm ell,\eta=0)}|a\rangle = E_a - \frac{\mathcal{E}^2}{4\hbar}\langle a|\big[\alpha_{xx}(\omega)a^2 + \alpha_{yy}(\omega)b^2\big]|a\rangle. \tag{6.78}$$

Alternative expression for the Raman-Stark terms [114]

One can determine a simple form for the Raman-Stark terms, of the most general expression (6.75b), decomposing the electric field in terms $\overrightarrow{E}^{(\pm)}$ associated respectively to the positive frequency and to the negative frequency as

$$\overrightarrow{E}^{(+)} := \overrightarrow{E}e^{-i\omega t}, \qquad \overrightarrow{E}^{(-)} := \overrightarrow{E}e^{+i\omega t} = \left(\overrightarrow{E}^{(+)}\right)^\star. \tag{6.79}$$

Following the convention of Born and Wolf [115], we define

$$\overrightarrow{e}_\pm = \mp\frac{1}{\sqrt{2}}\left(\overrightarrow{e}_x \pm i\overrightarrow{e}_y\right) \tag{6.80}$$

and obtain for the circularly polarized fields

$$\overrightarrow{E}^{(+)}_\pm = \mp\overrightarrow{e}_\pm\frac{\mathcal{E}}{2}e^{-i(\omega t\pm\eta/2)}. \tag{6.81}$$

One obtains for any field polarization [114, 43]

$$\langle n|H_{\rm eff}|n\rangle = E_n - \overrightarrow{E}^{(-)}\cdot\overrightarrow{\overrightarrow{\alpha}}\cdot\overrightarrow{E}^{(+)}. \tag{6.82}$$

Note that in this expression, the scalar product is done without additional complex conjugation.

This expression is still valid when the polarizability is non-diagonal, as considered in Eq. (6.75b).

6.2.3 Two-mode processes

We now consider various two-photon transitions with two different photons ω_1 and ω_2 between the states $E_a = \hbar\omega_a$ and $E_b = \hbar\omega_b$:

$$\text{ladder :} \qquad \omega_a + \omega_1 + \omega_2 + \delta = \omega_b, \tag{6.83a}$$

$$\text{Raman :} \qquad \omega_a + \omega_1 - \omega_2 + \delta = \omega_b \tag{6.83b}$$

with no intermediate single-photon resonances. In the general case of elliptically polarized pulses, the diagonal elements of the interaction cannot take the simple form (6.49).

We distinguish here again processes that couple one initial state to a *single* state (when a single polarization or two different circular polarizations for the two photons are considered), with the ones that couple the initial state to a *subspace*.

Two-mode processes with a single polarization

The field contains two modes of a single polarization

$$\text{linear } (q = 0 \text{ or } z) \quad \overrightarrow{E}(t, \omega_1 t, \omega_2 t) = \sum_{j=1,2} \mathcal{E}_j(t) \cos(\omega_j t + \phi_j) \overrightarrow{e}_z, \tag{6.84a}$$

$$\text{circular } \sigma_+ \ (q = +) \quad \overrightarrow{E}(t, \omega_1 t, \omega_2 t) = \sum_{j=1,2} \frac{\mathcal{E}_j(t)}{\sqrt{2}} \left[\cos(\omega_j t + \phi_j) \overrightarrow{e}_x + \sin(\omega_j t + \phi_j) \overrightarrow{e}_y\right], \tag{6.84b}$$

$$\text{circular } \sigma_- \ (q = -) \quad \overrightarrow{E}(t, \omega_1 t, \omega_2 t) = \sum_{j=1,2} \frac{\mathcal{E}_j(t)}{\sqrt{2}} \left[\cos(\omega_j t + \phi_j) \overrightarrow{e}_x - \sin(\omega_j t + \phi_j) \overrightarrow{e}_y\right]. \tag{6.84c}$$

The considered two-photon processes are here (i) *ladder* processes similar to the ones shown in Fig. 6.4, but with different frequencies for the two photons, and (ii) a *Raman* process with π-polarized pulses. The selection rules are as for the two-photon RWA. We obtain (ϵ is here to keep track of the different order; it corresponds to $\mathcal{E}_1$ or $\mathcal{E}_2$, and the second order ϵ^2 to quadratic terms in $\mathcal{E}_j$, $j = 1, 2$)

$$K_{\text{eff}}^{(q)} = -i\hbar\omega_1 \frac{\partial}{\partial\theta_1} - i\hbar\omega_2 \frac{\partial}{\partial\theta_2} + H_0^{00} + \epsilon^2 V_2^{(q)}(\theta_1, \theta_2) \tag{6.85}$$

with for the linear field

$$\begin{aligned} \epsilon^2 V_{2,nn}^{(0)} &= -\frac{1}{2\hbar} \sum_{j=1,2} \mathcal{E}_j \cos^2(\theta_j + \phi_j) \sum_{m\neq a,b} \left(\frac{|\mu_{nm}^{(0)}|^2}{\omega_m - \omega_n - \omega_j} + \frac{|\mu_{nm}^{(0)}|^2}{\omega_m - \omega_n + \omega_j} \right) \\ &\quad -\frac{1}{\hbar} \mathcal{E}_1 \mathcal{E}_2 \cos(\theta_1 + \phi_1) \cos(\theta_2 + \phi_2) \sum_{m\neq a,b} \left(\frac{|\mu_{nm}^{(0)}|^2}{\omega_m - \omega_n - \omega_2} + \frac{|\mu_{nm}^{(0)}|^2}{\omega_m - \omega_n + \omega_1} \right) \end{aligned} \tag{6.86a}$$

$$\epsilon^2 V_{2,ba}^{(0)} = -\frac{1}{8\hbar} \sum_{m\neq a,b} \mu_{bm}^{(0)} \mu_{ma}^{(0)} \sum_{\underline{\ell},\underline{\ell}'} \mathcal{E}_{\underline{\ell}}^{(0)} \mathcal{E}_{\underline{\ell}'}^{(0)} \left(\frac{e^{i(\underline{\ell}+\underline{\ell}')\cdot\underline{\theta}}}{\omega_m - \omega_a + \underline{\ell}\cdot\underline{\omega}} + \frac{e^{i(\underline{\ell}+\underline{\ell}')\cdot\underline{\theta}}}{\omega_m - \omega_b - \underline{\ell}'\cdot\underline{\omega}} \right) \tag{6.86b}$$

with $\underline{\ell}, \underline{\ell}' \in \{(-1,0), (1,0), (0,-1)(0,1)\}$, and

$$\mathcal{E}_{\underline{\ell}}^{(0)} \equiv \begin{cases} \mathcal{E}_1 & \text{for} \quad \underline{\ell} = (\pm 1, 0) \\ \mathcal{E}_2 & \text{for} \quad \underline{\ell} = (0, \pm 1) \end{cases} \tag{6.87}$$

Static polarizabilities. We remark that only if we consider static polarizabilities (i.e. $\omega \to 0$), we recover a simple form of the effective interaction $-\frac{1}{2}\overrightarrow{E}(t,\theta_1,\theta_2)\cdot\overrightarrow{\overrightarrow{\alpha}}(0)\cdot\overrightarrow{E}(t,\theta_1,\theta_2))$ with an induced dipole by the two fields:

$$\epsilon^2 V^{(0)}_{2,nn} = -\frac{1}{2\hbar}\left[\mathcal{E}_1\cos(\theta_1+\phi_1)+\mathcal{E}_2\cos(\theta_2+\phi_2)\right]^2\langle n|\alpha_{00}(0)|n\rangle \tag{6.88a}$$

$$\epsilon^2 V^{(0)}_{2,ba} = -\frac{1}{2\hbar}\left[\mathcal{E}_1\cos(\theta_1+\phi_1)+\mathcal{E}_2\cos(\theta_2+\phi_2)\right]^2\langle b|\alpha_{00}(0)|a\rangle. \tag{6.88b}$$

Such a consideration with static polarizabilities can be relevant only for Raman processes.

Resonant approximation. The resonant approximation leads to the effective Hamiltonian

$$H_{\rm eff} = \frac{\hbar}{2}\begin{pmatrix} 2S^{(q)}_a & \Omega^{(q)*}_{ba}e^{i(\phi_1\pm\phi_2)} \\ \Omega^{(q)}_{ba}e^{-i(\phi_1\pm\phi_2)} & 2S^{(q)}_b+\delta \end{pmatrix}, \tag{6.89}$$

where the symbol $\pm$ corresponds to $+$ $(-)$ for the ladder (Raman) process, with the effective two-photon Rabi frequency [where the condition $|\delta| \ll |\Delta_{j,m}|$ extending (6.67), and here again implicitly present in the approximations, has been taken into account]

$$\text{ladder}: \qquad \Omega^{(q)}_{ba} = -\frac{\mathcal{E}_1\mathcal{E}_2}{4\hbar}\langle b|\alpha_{qq}(\omega_1)|a\rangle, \tag{6.90a}$$

$$\text{Raman}: \qquad \Omega^{(z)}_{ba} = -\frac{\mathcal{E}_1\mathcal{E}_2}{4\hbar}\langle b|\alpha_{zz}(\omega_1)|a\rangle, \tag{6.90b}$$

and the Stark shift of the state n due to both fields

$$S^{(q)}_n = (-1)^{(q+1)}\sum_{j=1,2}\frac{\mathcal{E}_j^2}{4\hbar}\langle n|\alpha_{-qq}(\omega_j)|n\rangle. \tag{6.91}$$

This approximation holds when

$$\text{partitioning}: \qquad \Omega^{(q)}_{ba}| \ll |\Delta_{j,m}|, |\omega_1+\omega_2+\Delta_{j,m}| \tag{6.92a}$$

$$\text{resonant approximation}: \qquad |\Omega^{(q)}_{ba}|, |\delta| \ll \omega_1 \pm \omega_2 \tag{6.92b}$$

where the symbol $\pm$ corresponds to $+$ $(-)$ for the ladder (Raman) process, with the single resonant one-photon detunings ($m \in \mathcal{H}_1$, $j = 1, 2$)

$$\Delta_{j,m} = \omega_m - \omega_a - \omega_j. \tag{6.93}$$

Two-mode processes with two circular polarizations

The field contains two modes of different circular polarizations:

$$\begin{aligned}\overrightarrow{E}(t) = {} & \frac{\mathcal{E}_1(t)}{\sqrt{2}}\left[\cos(\omega_1 t+\eta_1/2)\overrightarrow{e}_x+\sin(\omega_1 t+\eta_1/2)\overrightarrow{e}_y\right] \\ & +\frac{\mathcal{E}_2(t)}{\sqrt{2}}\left[\cos(\omega_2 t-\eta_2/2)\overrightarrow{e}_x-\sin(\omega_2 t-\eta_2/2)\overrightarrow{e}_y\right].\end{aligned} \tag{6.94}$$

This allows one to consider the schemes shown in Fig. 6.6.

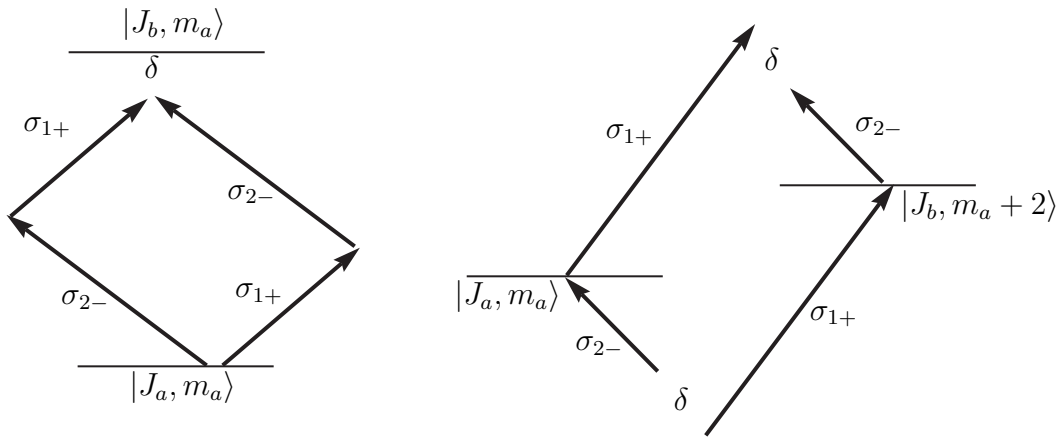

FIG. 6.6 - *The ladder (left) and Raman (right) linkage patterns for two-mode processes with two circular polarizations with* $J_b = J_a, J_a \pm 2$.

We obtain

$$H_{\text{eff}} = \frac{\hbar}{2} \begin{pmatrix} 2S_a & \Omega_{ba}^* e^{i(\eta_1 \mp \eta_2)/2} \\ \Omega_{ba} e^{-i(\eta_1 \mp \eta_2)/2} & 2S_b + \delta \end{pmatrix} \tag{6.95}$$

with the Rabi frequency

$$\text{ladder :} \qquad \Omega_{ba} = \frac{\mathcal{E}_1 \mathcal{E}_2}{4\hbar} \langle b|\alpha_{-+}(\omega_1)|a\rangle, \tag{6.96a}$$

$$\text{Raman :} \qquad \Omega_{ba} = -\frac{\mathcal{E}_1 \mathcal{E}_2}{4\hbar} \langle b|\alpha_{++}(\omega_1)|a\rangle, \tag{6.96b}$$

and the Stark shift of the state n due to both fields

$$S_n = \frac{\mathcal{E}_1^2}{4\hbar} \langle n|\alpha_{-+}(\omega_1)|n\rangle + \frac{\mathcal{E}_2^2}{4\hbar} \langle n|\alpha_{+-}(\omega_2)|n\rangle. \tag{6.97}$$

The symbol $\mp$ corresponds to $-$ $(+)$ for the ladder (Raman) process. These systems, when considered with intermediate one-photon quasi-resonant states and with two independent paths of controllable *relative phase*, lead to interesting interference effects [116, 117].

Two-mode processes with two elliptic polarizations

With two elliptic fields of the form, $j = 1, 2$:

$$\overrightarrow{E}_j = \frac{\mathcal{E}_j}{\sqrt{2}} \sin\alpha_j \begin{pmatrix} \cos(\omega_j t + \eta_j/2) \\ \sin(\omega_j t + \eta_j/2) \\ 0 \end{pmatrix} + \frac{\mathcal{E}_j}{\sqrt{2}} \cos\alpha_j \begin{pmatrix} \cos(\omega_j t - \eta_j/2) \\ -\sin(\omega_j t - \eta_j/2) \\ 0 \end{pmatrix}, \tag{6.98}$$

the process can be of ladder-type, similar to the one shown in Fig. 6.5 but with two different colors. The coupling from J_a to J_b is made by all the possible combinations with the two colors: $\sigma_{+,1} - \sigma_{+,2}$, $\sigma_{-,1} - \sigma_{-,2}$, $\sigma_{+,1} - \sigma_{-,2}$, and $\sigma_{-,1} - \sigma_{+,2}$; the Raman-Stark term of each subspace J_n, $n = a, b$, by a single color: $\sigma_{+,1} - \sigma_{-,1}$ and $\sigma_{+,2} - \sigma_{-,2}$. The process of Raman-type leads to the same combinations for the Raman-Stark term and coupling from J_a to J_b.

The off-block-diagonal coupling term of the ba component is given by the mode $\ell_1 = -1, \ell_2 = -1$ of the effective Floquet Hamiltonian (6.18) for the ladder process, and by the mode $\ell_1 = -1, \ell_2 = +1$ for the Raman process:

$$\begin{aligned}
\text{ladder: } \langle b|H_{\rm eff}^{\rm (ell)}|a\rangle &= -\frac{\mathcal{E}_1\mathcal{E}_2}{4\hbar}\langle b|\big[\alpha_{++}e^{-i(\eta_1+\eta_2)/2}\sin\alpha_1\sin\alpha_2 + \alpha_{--}e^{i(\eta_1+\eta_2)/2}\cos\alpha_1\cos\alpha_2 \\
&\quad -\alpha_{-+}\sin\alpha_1\cos\alpha_2 e^{-i(\eta_1-\eta_2)/2} - \alpha_{+-}\cos\alpha_1\sin\alpha_2 e^{i(\eta_1-\eta_2)/2}\big]|a\rangle, \quad (6.99a) \\
\text{Raman: } \langle b|H_{\rm eff}^{\rm (ell)}|a\rangle &= -\frac{\mathcal{E}_1\mathcal{E}_2}{4\hbar}\langle b|\big[\alpha_{++}e^{-i(\eta_1+\eta_2)/2}\sin\alpha_1\cos\alpha_2 + \alpha_{--}e^{i(\eta_1+\eta_2)/2}\cos\alpha_1\sin\alpha_2 \\
&\quad -\alpha_{-+}\sin\alpha_1\sin\alpha_2 e^{-i(\eta_1-\eta_2)/2} - \alpha_{+-}\cos\alpha_1\cos\alpha_2 e^{i(\eta_1-\eta_2)/2}\big]|a\rangle, \quad (6.99b)
\end{aligned}$$

where we have shortened the notation $\alpha_{ij} \equiv \alpha_{ij}(\omega_1)$. We have used the approximation

$$\begin{aligned}
\text{ladder :} \qquad & \omega_a + \omega_1 \approx \omega_b - \omega_2, & (6.100a) \\
\text{Raman :} \qquad & \omega_a + \omega_1 \approx \omega_b + \omega_2 & (6.100b)
\end{aligned}$$

to involve the polarizability with the single frequency dependence ω_1.

The block-diagonal term ($n = a, b$) is determined by the θ-averaged diagonal term of (6.18), which extends Eq. (6.75b) for two fields:

$$\langle n|H_{\rm eff}^{\rm (ell)}|n\rangle = E_n - \sum_{j=1,2}\Big\{\frac{\mathcal{E}_j^2}{4\hbar}\langle n|\big[\alpha_{++}(\omega_j)\cos\eta_j\sin 2\alpha_j - \alpha_{+-}(\omega_j)\big]|n\rangle\Big\}, \quad (6.101)$$

where $-\hbar(\omega_1+\omega_2)$ [resp. $\hbar(\omega_2-\omega_1)$] should be added for $\langle b|H_{\rm eff}^{\rm (ell)}|b\rangle$ in the ladder (resp. Raman) process.

Alternative expression for the effective Raman Hamiltonian

One can extend the simple form of the Raman-Stark terms (6.82) to the two-mode process in the resonant approximation as follows [43]:

$$\begin{aligned}
\langle b|H_{\rm eff}|a\rangle &= -\overrightarrow{E}_2^{(-)}\cdot\langle b|\,\overrightarrow{\overrightarrow{\alpha}}\,(\omega_1)|a\rangle\cdot\overrightarrow{E}_1^{(+)}e^{i(\omega_1-\omega_2)t}, & (6.102a) \\
\langle n|H_{\rm eff}|n\rangle &= E_n - \sum_{j=1,2}\overrightarrow{E}_j^{(-)}\cdot\langle n|\,\overrightarrow{\overrightarrow{\alpha}}\,(\omega_j)|n\rangle\cdot\overrightarrow{E}_j^{(+)}. & (6.102b)
\end{aligned}$$

Beyond the resonant approximation. If we have $|E_b - E_a| \ll |E_m - E_{a,b} \pm \hbar\omega_{1,2}|$ (relevant for the Raman process), which can be interpreted as a quasi-degenerate subspace $\{|a\rangle, |b\rangle\}$ with respect to the electronic states involved in the polarizability, and if the coupling $\langle b|H_{\rm eff}|a\rangle$ (6.102a) calculated above (i.e. with the resonant approximation) is larger or the same order than $|E_b - E_a|$, the Hamiltonian cannot be treated with the resonant approximation, and the coupling becomes

$$\langle b|H_{\rm eff}|a\rangle = -\overrightarrow{E}^{(-)}\cdot\langle b|\,\overrightarrow{\overrightarrow{\alpha}}\,(\omega_1)|a\rangle\cdot\overrightarrow{E}^{(+)}. \quad (6.103)$$

6.3 Effective Hamiltonian in diatomic molecules

To determine an effective dressed Hamiltonian characterizing a molecule excited by strong laser fields, we have to apply the standard construction of the free effective Hamiltonian (such as the Born-Oppenheimer approximations) [118, 119], taking into account the interaction with the field non-perturbatively (if resonances occur). This leads to four different time-scales in general: (i) for the motion of the electrons, (ii) for the vibrations of the nuclei, (iii) for the rotation of the nuclei, and (iv) for the frequency of the interacting field. It is well known that it is a good strategy to take into account the time scales from the fastest to the slowest one.

6.3.1 The Born-Oppenheimer free Hamiltonian

In molecules, the Born-Oppenheimer approximation allows one to decouple first the electronic motion from the nuclear vibrational and rotational motions, and next the nuclear vibrational motion from the rotational motion.

Solving the Schrödinger equation $H_0\Psi = E\Psi$ with respect to the electron coordinates $\mathbf{r} = \{\overrightarrow{r_1}, \overrightarrow{r_2} \cdots\}$ with $\overrightarrow{r}_i$ the position of each electron i gives rise to the electronic states $\Psi_n(\mathbf{r}, \mathbf{R}) = \langle \mathbf{r} \,|n(\mathbf{R})\rangle$, $n = 0, \cdots, N_e$, where the electronic scalar product is defined as $\langle n(\mathbf{R}) \,|n'(\mathbf{R})\rangle_{\mathbf{r}} = \int d\mathbf{r}\ \Psi_n^*(\mathbf{r}, \mathbf{R})\Psi_{n'}(\mathbf{r}, \mathbf{R})$. The electronic states have respective energies $\{E_n^{(\mathrm{e})}(R)\}$ as functions of the nuclear coordinates, characterized by $\mathbf{R} \equiv (R, \Theta, \varphi)$ with R the internuclear distance and Θ, φ the spherical coordinates of the molecular axis (with the origin taken at its center of mass). We assume a finite number of N_e+1 bound electronic states. This gives in the electronic state basis

$$H_0 = T^{(\mathrm{n})} + \mathrm{diag}\left[E_0^{(\mathrm{e})}(R), E_1^{(\mathrm{e})}(R), \cdots, E_{N_e}^{(\mathrm{e})}(R)\right] \tag{6.104}$$

where

$$T^{(\mathrm{n})} = T_{\mathrm{vib}}^{(\mathrm{n})}(\partial/\partial R) + T_{\mathrm{rot}}^{(\mathrm{n})}(R, \partial/\partial\Theta, \partial/\partial\varphi) \tag{6.105}$$

is the kinetic energy of the nuclei with

$$T_{\mathrm{vib}}^{(\mathrm{n})} = -\frac{\hbar^2}{2m}\frac{\partial^2}{\partial R^2} \tag{6.106a}$$

$$T_{\mathrm{rot}}^{(\mathrm{n})} = B(R)\hat{J}^2 = \frac{\hbar^2}{2mR^2}\left[-\frac{1}{\sin\Theta}\frac{\partial}{\partial\Theta}\left(\sin\Theta\frac{\partial}{\partial\Theta}\right) - \frac{1}{\sin^2\Theta}\frac{\partial^2}{\partial\varphi^2}\right] \tag{6.106b}$$

$$=: \frac{\hbar^2}{2mR^2}(T_\Theta + T_\varphi), \tag{6.106c}$$

$B(R) = \hbar^2/2I(R)$ the rotational "constant" defined through the principal moment of inertia $I(R) = mR^2$, $\hat{J}^2$ the angular momentum operator and $m = m_1m_2/(m_1+m_2)$ the reduced mass of the two atoms of respective masses m_1 and m_2.

The Born-Oppenheimer approximation consists precisely in neglecting the nucleus kinetic energies that are nondiagonal with respect to this electronic basis of eigenvectors. This approximation is well justified thanks to the ratio of electronic and nucleus masses. The ground state electronic surface is usually well approximated by a Morse potential:

$$E_0^{(\mathrm{e})}(R) = D[1 - e^{-\beta(R-R_e)}]^2, \tag{6.107}$$

with R_e the equilibrium distance between the nuclei (for which the energy is chosen as zero) and D the dissociation energy (see below in Subsection 6.3.4 for details of the Morse potential spectrum).

Taking Θ and φ as parameters, we next diagonalize $T^{(\mathrm{n})}_{\mathrm{vib}} + E^{(\mathrm{e})}_n(R)$ and denote the eigenvalues by $E^{(\mathrm{v})}_{n,0}, \ldots, E^{(\mathrm{v})}_{n,N_v}$ and the basis of eigenvectors by $\{|n, v=0\rangle, |n, v=1\rangle, \cdots |n, v=N_{n,v}\rangle\}$ where we assume $N_{n,v}+1$ bound vibrational states for a given n electronic state. The Born-Oppenheimer approximation consists here in neglecting the terms of $T^{(\mathrm{n})}_{\mathrm{rot}}$ that are nondiagonal with respect to this vibrational basis of eigenvectors (*rigid rotor* approximation). This approximation is well justified, at least for the lowest vibrational states, since there the vibrational motion is of small amplitude and much faster than the rotational motion. The first (diagonal) correction leading to a non-rigid rotor can be obtained by a contact transformation from the small nondiagonal terms and leads to a centrifugal force term of the form $-D_{n,v}\hat{J}^4$, $D_{n,v} > 0$.

We can finally diagonalize with respect to the rotational coordinates. We obtain the $2J+1$ degenerate eigenvalues and the associated eigenvectors

$$E^{(\mathrm{r})}_{n,v,J} = E^{(\mathrm{v})}_{n,v} + B_{n,v}J(J+1) - D_{n,v}[J(J+1)]^2 \tag{6.108a}$$

$$\langle \varphi, \Theta | n, v, J, M\rangle = |n, v\rangle\ \Xi^M_J(\Theta)\ e^{iM\varphi} \tag{6.108b}$$

with the mean rotational constants in the n electronic state and the v vibrational state:

$$B_{n,v} = \langle n, v|B|n, v\rangle \approx B_{n,e} - \alpha_{n,e}\Big(v+\frac{1}{2}\Big), \qquad \alpha_{n,e} \ll B_{n,e} \tag{6.109a}$$

$$D_{n,v} \approx D_{n,e} + \beta_{n,e}\Big(v+\frac{1}{2}\Big), \qquad \beta_{n,e} \ll D_{n,e} \tag{6.109b}$$

$J = 0, 1, \cdots$, $|M| \leq J$ and the normalized associated Legendre polynomial $\Xi^M_J(\Theta)$. The constant $D_{n,e}$ (which is $D_{0,e} = 4B^3_e/\omega^2_e$ in the ground electronic state) is very small compared to $B_{n,e}$ and can often be neglected. The constant $B_{n,e}$ is the rotational constant at the equilibrium in the n electronic state; it is large compared to the constant $\alpha_{n,e}$ when we consider the lowest vibrational states, since in this case the change in internuclear distance by the vibration is small compared to the internuclear distance itself. In the ground electronic state, the constant $\alpha_{0,e}/B_{0,e}$ has been empirically found to be slightly larger than $\omega_e x_e/\omega_e$.

Electronic angular momentum and spin effects. We have so far considered only the rotation of the nuclei for which the moment of inertia about the internuclear axis is necessarily 0. This leads to a *simple rotator*, i.e. with a single moment of inertia perpendicular to the internuclear axis, of spectrum

$$E_{\mathrm{s.r.}} = B(R)J(J+1). \tag{6.110}$$

However the electronic cloud yields an additional moment of inertia, very small with respect to the nuclear one, owing to the smallness of the mass of the electrons. But since the electrons rotate much more rapidly, the associated angular momentum is of the same order than the angular momentum associated to the nuclei. Thus a more correct model would require considering additionally this electronic moment of inertia leading to a *symmetric top rotor*, i.e. a rotor with two different moments of inertia $I^{(\mathrm{n})}$ (about the axis orthogonal to the internuclear axis, essentially due to the nuclei alone, i.e. $I^{(\mathrm{n})} \approx I$ to a very good approximation) and $I^{(\mathrm{e})}$ (about the internuclear axis, only due to the electrons), and to a total angular momentum $\vec{J} = \vec{R} + \vec{L}$ with $\vec{R}$ the nuclear rotational angular momentum and $\vec{L}$ the electronic orbital angular momentum (if the electronic spin is neglected). The total angular part should thus read in a given electronic state n:

$$T^{(\mathrm{n})}_{\mathrm{rot}} + T^{(\mathrm{e})}_n = B(R)(J^2_x + J^2_y) + B^{(\mathrm{e})}_n J^2_z \tag{6.111}$$

with the z axis defined along the internuclear axis and the rotational constant $B^{(\mathrm{e})}$ (independent of R) associated to the moment of inertia $I^{(\mathrm{e})}$. The spectrum of this symmetric top rotor is [120]

$$E_{\mathrm{s.t.r.}} = B(R)J(J+1) + (B_n^{(\mathrm{e})} - B(R))\Lambda_n^2 \approx B(R)J(J+1) + B_n^{(\mathrm{e})}\Lambda_n^2, \tag{6.112}$$

with Λ_n ($|\Lambda_n| \leq J$ integer) the projection of $\vec{L}$ (i.e. of $\vec{J}$) on the internuclear axis in the electronic state n and $B_n^{(\mathrm{e})} \gg B(R)$. The electronic states are labeled following the values of Λ: $\Lambda = 0, 1, 2, 3, \cdots$ respectively corresponds to the state $\Sigma, \Pi, \Delta, \Phi \cdots$. The rotational spectrum is at the lowest order of approximation doubly degenerate for $\Lambda_n \neq 0$, owning to the two possible signs of Λ_n(the degeneracy is in fact lifted by considering further coupling, such as the Σ-Π coupling, called Λ-doubling). At the lowest order of approximation, this shows a *shift* in a given electronic state with respect to the simple rotor, which is *global* for the rovibrational structure.

We have to consider as well the electronic spin, which leads to a fine structure due to the spin-orbit coupling. If we consider the ground electronic state, which is very often (but not always, see below) a $^1\Sigma$ state (as is studied in the next sections), i.e. a singlet state ($S = 0$) associated to $\Lambda_0 = 0$ (the case for molecules with closed shells), the simple rotor is exact [Eq. (6.106b)]. The Σ states are generally associated to the so-called Hund's case (b), corresponding to a weak spin-orbit coupling. Furthermore, in the Born-Oppenheimer approximation, we assume that the electronic orbital angular momentum is strongly coupled to the internuclear axis. This is assumed in the Hund's cases (a) and (b). Only in highly excited rotational states, for fast moving nuclei, we expect a breakdown of this approximation.

When there is one (or more) electron outside the closed shell, one has to consider its spin $\vec{S}$ (of projection Σ on the internuclear axis) and electronic orbital angular momentum, leading to the total angular momentum $\vec{J} = \vec{R}+\vec{L}+\vec{S}$, of projection on the internuclear axis $\Omega = \Lambda+\Sigma$. For alkakine-earth mono-halogenides with a $^2\Sigma_{1/2}$ ground state corresponding to a single electron outside a closed shell (such as CaF), we have $J = S = 1/2$ (i.e. $\Lambda = 0$). In this case, the total angular part reads (the ground vibrational state is considered)

$$\langle n = 0, v = 0|T_{\mathrm{rot}}^{(\mathrm{n})} + T_n^{(\mathrm{e})}|n = 0, v = 0\rangle = B\hat{N}^2 + \gamma_{sr}\hat{S}\hat{N} \tag{6.113}$$

with $\hat{N} = \hat{J} - \hat{S}$ (see for instance [121]). Since $\gamma_{sr} \ll B$ (weak coupling between the spin and the internuclear axis), the rotational spectrum consists of a simple rotor (described by the quantum number N) with a doublet spin rotation splitting ($\rho-$doubling) for rotationally excited states: $J = 1/2, 3/2$ for $N = 1$, $J = 3/2, 5/2$ for $N = 2$, $\cdots$

Other standard examples of rotational structures more complicated than simple rotators are [122]: (i) the O_2 molecule (with two unpaired electrons outside a closed shell), of ground state $^3\Sigma$, i.e. with $\Lambda = 0, S = 1$, giving a triplet splitting $J = N - 1, N, N + 1$ for $N > 0$ (which is small since the spin is weakly coupled to the internuclear axis) to the simple rotor structure (described by the quantum number N); (ii) the NO molecule (with a single unpaired electron outside a closed shell: $S = 1/2$), of ground state consisting of two non degenerate states $^2\Pi_{1/2}$,$^2\Pi_{3/2}$, i.e. with $L = 1$ and $\Lambda = \pm 1$. This is close to Hund's case (a), associated to a strong coupling with the molecular axis of both the electronic orbital angular momentum and the electronic spin.

The nuclear spin, symmetry and statistics The spins of the nuclei generates an additional angular momentum denoted $\vec{I}$, giving the total angular momentum $\vec{F} = \vec{J} + \vec{I}$,

$|J - I| \leq F \leq J + I$. The resultant value I_i of the angular momentum of the atom i follows the rules: (i) half-integer for nuclei with an odd mass number, (ii) integral for nuclei with an even mass number but an odd charge number, (iii) zero for nuclei with an even mass number and an even charge number. The associated hyperfine interaction leads to an additional splitting. This splitting is not explicitly considered in this work. We remark that it can be used to define qubits in quantum information (see for instance [121]).

For homonuclear molecules ($I_1 = I_2$), the nuclear spin adds a symmetry to the molecule by an exchange of the nuclei. The consideration of the total symmetry of the molecular state allows one to determine statistics weights that have to multiply the thermal weights for the rotational states.

We classify the rotational levels of the molecule according the behavior of the total eigenfunction, considered in the Born-Oppenheimer approximation as a product of an electronic, a vibrational, a rotational and a nuclear spin contribution. The following particular symmetries are considered: (i) *parity*, given by the electronic inversion (i.e. replacement of all electronic coordinates by their opposite); (ii) *symmetry by electronic reflection*, given by the reflection of the electrons at a plane through the internuclear axis (σ_v reflection); (iii) *symmetry of permutation of nuclear spin states*; (iv) *symmetry of nucleus exchange*, given by the exchange of the labels of the two nuclei. The inversion (i) allows one to classify the electronic states as g (unchanged function by the inversion) or u (opposite function by the inversion). The reflection (ii) allows one to classify the Σ electronic states as $+$ (unchanged function by the reflection) or $-$ (opposite function by the reflection): $\sigma_v|\Sigma^\pm\rangle = \pm|\Sigma^\pm\rangle$. The vibrational contribution is not involved in the symmetries (i) and (ii). The vibrational ground state is not involved in the symmetries (iii) and (iv), but the excited ones are. The symmetry of the permutation (iii) is given by the multiplet states due to the total nuclear spin $\vec{I} = \vec{I_1} + \vec{I_2}$ of the two atoms: $0 \leq I \leq 2I_1$.

The symmetry of nucleus exchange (iv) is equivalent to the sequence [123]: (0) rotation of the molecule by π about a perpendicular axis (C_2 rotation), (i) electronic inversion, (ii) σ_v reflection, and (iii) permutation of nuclear spin states.

The relevant rule to be used here is the Pauli principle for the nuclei: The state is totally anti-symmetric (resp. symmetric) with the exchange of the nucleus labels (iv) when they are fermions (resp. bosons). This defines a spin degeneracy factor g_J for each J.

Following the above sequence, we obtain (denoting $+1$ for symmetric and -1 for antisymmetric): (0) $(-1)^J$ for the simple rigid rotor ($\Lambda = 0$ is considered) and $(-1)^v$ for the vibration, (i) ± 1 according to whether the electronic state is g or u, (ii) ± 1 according to whether the electronic state is $\Sigma^\pm$.

For $I_1 = I_2 = 0$ nuclear spins (bosons), the total function has to be symmetric. In the case of a Σ_g^+ electronic ground state, such as CO_2 molecules (not diatomic, but linear and symmetric about the C atom, i.e. having a similar behavior with the homonuclear diatomic molecules apart the multimode vibrations), only the even J exist and are thermally populated in the $v = 0$ state. In the case of a Σ_g^- electronic ground state, such as O_2 molecules, only the odd J are thermally populated in the $v = 0$ state.

If the nuclear spins are different from 0, we have to determine the symmetry of the multiplet states. For instance, the H_2 molecule (Σ_g^+ electronic ground state) is composed of fermions since $I_1 = I_2 = 1/2$: It has to be associated to an antisymmetric function. The permutation of the spins leads to three symmetric states, thus associated to the odd (antisymmetric) J, and to a single state antisymmetric, thus associated to the even (symmetric) J. Hence, we have $g_{J=2p} = 1$ and $g_{J=2p+1} = 3$ with an integer $p \geq 0$ in the $v = 0$ state. The N_2 molecule (Σ_g^+

electronic ground state) is composed of bosons since $I_1 = I_2 = 1$: It has to be associated to a symmetric function. It leads to six symmetric states and three antisymmetric states with the permutation of the spins. Hence, we have $g_{J=2p} = 6$ and $g_{J=2p+1} = 3$ with an integer $p \geq 0$ in the $v = 0$ state. More generally, one can show that the ratio of the symmetric over the antisymmetric states with the permutation of the spins is

$$\frac{N_+}{N_-} = \frac{I_1 + 1}{I_1}. \tag{6.114}$$

Thermal distribution of the states. We will consider that only the rotational states of the ground vibrational state is thermally populated (i.e. in thermal equilibrium), which is true at a very good approximation for light diatomic molecules up to room temperature (293° K). Examples of the ratio of the number of molecule in the first to that the zeroth vibrational level are at T=300° K: 3×10^{-5} for CO, 0.07 for Cl_2, 0.36 for I_2.

For a given temperature T, we have thus to consider a statistical ensemble of molecules with J_0, M_0 distributed according to the Boltzmann weights (independent of M_0 and normalized $\sum_{J_0=0}^{\infty} \sum_{M_0=-J_0}^{J_0} \rho_{J_0} = 1$):

$$\rho_{J_0} = \frac{g_{J_0} e^{-\widetilde{B} J_0(J_0+1)}}{\sum_{J=0}^{\infty} g_J (2J+1) e^{-\widetilde{B} J(J+1)}} \tag{6.115}$$

with g_{J_0} the spin degeneracy factor as defined above, the Boltzmann constant $k = 1.38 \times 10^{-23}$ J/K, and the normalized (dimensionless) rotational constant

$$\widetilde{B}_0 = \frac{B_0}{kT}. \tag{6.116}$$

We will consider below dynamical processes (during or after an interaction with a laser field) occurring on a timescale so short that the thermal equilibrium will not be recovered. This will allow us to use the time-dependent Schrödinger equation to describe such a dynamics with a statistical averaging with the Boltzmann weights ρ_{J_0} for each dynamics $|\psi_{J_0,M_0}(t)\rangle$ generated from the initial condition $|J_0, M_0\rangle$.

6.3.2 The selection rules

One can consider one- or multi-photon resonances between electronic states, as we did in atoms, with selection rules depending on the symmetry of the electronic states. Taking into account the rovibrational structure, we have to evaluate the components of the total dipole moment $\overrightarrow{\mu} = -e \sum_i \overrightarrow{r}_i + e \sum_s Z_s \overrightarrow{R}_s$ with $\overrightarrow{R}_s$ denoting the location of the nucleus of charge $Z_s e$, using the eigenvectors determined in the Born-Oppenheimer approximation:

$$\overrightarrow{\mu} = \sum_{n,n'} |n(\mathbf{R})\rangle \, \overrightarrow{\mu}_{nn'}(\mathbf{R}) \, \langle n'(\mathbf{R})| \;, \quad \overrightarrow{\mu}_{nn'}(\mathbf{R}) = \langle n(\mathbf{R})| \, \overrightarrow{\mu} \, |n'(\mathbf{R})\rangle_{\mathbf{r}} \,. \tag{6.117}$$

$\overrightarrow{\mu}_{00}(\mathbf{R})$ is the permanent dipole moment of the ground electronic state, also denoted as $\overrightarrow{\mu}_{00}(\mathbf{R}) \equiv \overrightarrow{\mu}_0(\mathbf{R})$. If the molecule is homopolar, $\overrightarrow{\mu}_0(\mathbf{R}) = \overrightarrow{0}$. The couplings from the ground vibronic state $|n = 0, v = 0\rangle$ to an excited one $|n', v'\rangle$ involves as a first approximation the Franck-Condon factors $S^{(n')}(v') := |\langle n', v'|0, 0\rangle|^2$ corresponding to the overlap integral between the two vibrational states in their respective electronic states (times the electric dipole moment for the electronic transition taken independent of the location of the nuclei $\mu_{n'0}$ in this

approximation), thus associated to the rotational selection rule [the same applies on N instead of J for the Hund's case (b)]:

$$\Delta J = 0, \pm 1 \text{ (but not } J = 0 \to J = 0) \quad \text{and for } \Omega = 0 \to \Omega = 0, \;\; \Delta J = \pm 1. \tag{6.118}$$

The P-, Q- and R-branches are respectively defined for $\Delta J = -1$, $\Delta J = 0$ and $\Delta J = +1$. The Q-branch is allowed only if at least one of the two electronic states considered is such that $\Lambda \neq 0$ (where Λ is the projection of the electronic orbital angular momentum on the internuclear axis).

Other relevant selection rules read [118, 119]:

$$g \to u, \quad \Sigma^+ \to \Sigma^+, \; \Sigma^- \to \Sigma^-, \tag{6.119a}$$
$$\Delta\Lambda = 0, \pm 1 \;\text{ and }\; \Delta S = 0 \;\text{ [Hund's cases (a) and (b)]}, \tag{6.119b}$$
$$\Delta\Omega = 0, \pm 1 \;\text{ [Hund's case (c)]} \tag{6.119c}$$
$$\Delta\Sigma = 0 \;\text{ [Hund's case (a)]} \tag{6.119d}$$

We remark that the selection rule on Λ corresponds exactly to the selection rule for M_L for atoms, standing for a very strong field able to break the spin-orbit coupling or for $S = 0$. For diatomic molecules, the transitions $\Delta\Lambda = 0$ holds for a transition moment lying in the direction of the internuclear axis, so-called *parallel transition*. The transitions $\Delta\Lambda = \pm 1$ holds for a transition moment perpendicular to the internuclear axis, so-called *perpendicular transition*. Two-photon transitions has been studied for instance in [124].

Within a single electronic state, the selection rules of the vibration-rotation transitions (where the rotational constant weakly changes between closest vibrational states) due (i) to the permanent dipole moment (infrared one-photon transition) of a polar molecule are

$$\text{one photon}: \quad \Delta v = \pm 1, \quad \Delta J = (0), \pm 1, \quad (\text{but not } J = 0 \to J = 0) \tag{6.120}$$

and (ii) to the (anisotropic) polarizability (Raman transition)

$$\text{Raman}: \quad \Delta v = \pm 1, \quad \Delta J = 0, (\pm 1), \pm 2, \quad (\text{but not } J = 0 \to J = \pm 1) \tag{6.121}$$

The transitions in parenthesis refer to as transitions for the symmetric top rotor, i.e. when $\Lambda \neq 0$ (see below). The vibrational selection rule $\Delta v = \pm 1$ is in both cases approximate: the transition moment associated to $\Delta v = \pm 1$ is much larger than the one associated to $\Delta v = \pm 2$, itself much larger than the one associated to $\Delta v = \pm 3$, and so on. For infrared one-photon transition, the Q-branch ($\Delta J = 0$) is allowed only when the molecule possesses angular momentum parallel to the internuclear axis, i.e. only if $\Lambda \neq 0$ (diatomic molecule as a symmetric top). For Raman transition, the P- and R-branches are allowed only if $\Lambda \neq 0$.

The selection rules of the pure rotational transition within a single vibronic state (allowed for the one-photon process only when the molecule is heteronuclear, i.e. possesses a permanent dipole moment) are

$$\text{one photon}: \qquad \Delta J = (0), \pm 1, \quad \Delta M = 0, \pm 1, \tag{6.122}$$
$$\text{Raman}: \qquad \Delta J = 0, (\pm 1), \pm 2, \quad \Delta M = 0, \pm 1. \tag{6.123}$$

The transitions in parenthesis refer to as transitions for the symmetric top rotor, i.e. when $\Lambda \neq 0$ (see above). We have added the rules on M, valid for all the case above. These rules are analyzed in details below.

We study below molecule in its ground electronic state only as $^1\Sigma$ state (molecules with closed shells), i.e. $\Lambda = 0, S = 0$ [corresponding to an exact Hund's case (b) with $J \equiv N$]. The symmetric top will not thus be taken into account: we will model the diatomic molecule as a simple rotor [Eq. (6.106b)].

We consider below a field of low frequency with respect to the electronic excitation such that the excited electronic states will be taken into account through polarizability-type coupling.

We will study vibrational excitations by one-photon and two-photon (with a two-mode field) processes.

A high field frequency with respect to the vibrations and consequently also with respect to the rotations will lead to Raman rotational excitations in the ground vibrational state of the ground electronic state (i.e. the ground vibronic state).

6.3.3 The Floquet Hamiltonian

The Floquet Hamiltonian of the molecule driven by a field $\overrightarrow{E}(t, \omega t)$ (of frequency ω), in the dipole coupling approximation, can be written as

$$K = -i\hbar\omega \frac{\partial}{\partial\theta} + H_0 - \overrightarrow{\mu} \cdot \overrightarrow{E}(t, \theta) \tag{6.124}$$

For a process with a multimode laser, the Floquet Hamiltonian is (see Section 1.5)

$$K = -i\hbar\underline{\omega} \cdot \frac{\partial}{\partial\underline{\theta}} + H_0 - \overrightarrow{\mu} \cdot \overrightarrow{E}(t, \underline{\theta}). \tag{6.125}$$

6.3.4 Resonant single-photon excitations: Rotationless model

We can use infrared linearly polarized laser pulses (of amplitude $\mathcal{E}$) adapted to climb the vibrational ladder with a selection of a specific target vibrational state, since $T_{\text{vib}} \sim 10$ fs is the timescale of the vibrational motion. However picosecond timescale chirped fields will not be in general selective with respect to the rotation with $T_{\text{rot}} \sim 1 - 10$ ps as timescale of the motion ($T_{\text{rot}} \approx 1$ ps for very light molecules as H_2). Applying the preceding tools, we consider thus below the construction of a rotationless model (i.e. for $\Theta = 0$) in the ground electronic state driven by a linearly polarized field.

The Floquet Hamiltonian reads in this case

$$K = -i\hbar\omega \frac{\partial}{\partial\theta} + H_0^{(\text{vib})} - \mu_0 \mathcal{E} \cos\theta \tag{6.126}$$

For simplicity, one considers the $N + 1$ lowest bound states $\{|0\rangle, |1\rangle, \cdots, |N\rangle\}$, associated to the energies $E_0 < E_1 < \cdots < E_N$ of a Morse potential coupled by a field whose effective frequency is one-photon near-resonant: $\hbar\omega_{\text{eff}} \approx E_1 - E_0 \approx E_2 - E_1 \approx \cdots \approx E_N - E_{N-1}$. The effective Hamiltonian in the resonant approximation, that takes into account the one-photon near resonances of one Floquet zone reads as a tridiagonal matrix:

$$H_{\text{eff}} = \frac{\hbar}{2} \begin{bmatrix} 0 & \Omega_{0,1} & 0 & \cdots & 0 \\ \Omega_{0,1} & 2\Delta_1 & \Omega_{1,2} & \ddots & \vdots \\ 0 & \Omega_{1,2} & 2\Delta_2 & \ddots & 0 \\ \vdots & \ddots & \ddots & \ddots & \Omega_{N-1,N} \\ 0 & \cdots & 0 & \Omega_{N-1,N} & 2\Delta_N \end{bmatrix} \tag{6.127}$$

with

$$\Delta_v := \frac{E_v - E_0}{\hbar} - v\omega_{\text{eff}} = v\left[\omega_e + (v+1)\,a - \omega_{\text{eff}}\right], \tag{6.128}$$

the Rabi frequency (assumed real and positive without loss of generality)

$$\Omega_{i,j} = -\mathcal{E}(t)\,\langle i|\,\mu_0\,|j\rangle\,/\hbar, \tag{6.129}$$

the (constant) anharmonicity $a \equiv -\omega_e x_e$:

$$a := \left[(\omega_{v+1} - \omega_v) - (\omega_v - \omega_{v-1})\right]/2 = -\hbar\omega_e^2/4D \tag{6.130}$$

with D the dissociation energy, and the frequency ω_e related to the energy of the Morse potential (6.107):

$$E_n = \hbar\omega_e\Big(v+\frac{1}{2}\Big) + \hbar a\Big(v+\frac{1}{2}\Big)^2, \qquad v = 0, \cdots,\ \text{Int}\Big(\frac{\sqrt{2mD}}{\beta\hbar} - \frac{1}{2}\Big) \tag{6.131}$$

with $\omega_e = \beta\sqrt{2D/m}$, and Int$(\cdot)$ corresponding to the integer part function. This effective Hamiltonian is valid for moderate field intensities $\Omega_{i,j} \ll \omega_e$ (in practice not larger than 10^{13} W/cm^2 to avoid ionization), for small detunings and anharmonicity $|\Delta_v|, |a| \ll \omega_e$ and for N significantly smaller than the total number of bound states.

We will se that the alignment of the molecule by a non-resonant field will allow us to transfer the rovibrational population selectively.

6.3.5 Raman processes in the ground vibronic state by a single linear or elliptic laser: Rotational excitations

We assume that the frequency of the laser is such that no excited electronic state is coupled by a one- or two-photon resonance with the ground electronic state.

Effective Hamiltonian in the ground electronic state

The partitioning is in this case as follows: the electronic state $|n=0\rangle$ spans the Hilbert subspace $\mathcal{H}_e^0$ and the other electronic states $\{|1\rangle, \cdots |N_e\rangle\}$ the Hilbert subspace $\mathcal{H}_e^1$. The dipole moment can be decomposed into diagonal and non-diagonal parts: respectively $\overrightarrow{\mu}_{nn}$ and $\overrightarrow{\mu}_{nn'}, n \neq n'$. Denoting $\overrightarrow{\mu}_{nn'} = [\mu_{1,nn'}, \mu_{2,nn'}, \mu_{3,nn'}]$ in a cartesian coordinate system (of unit vectors $\overrightarrow{e}_1, \overrightarrow{e}_2, \overrightarrow{e}_3$) to be defined, and applying Eq. (6.44), we obtain for the second order effective Floquet Hamiltonian connected to the ground electronic state

$$K_{\text{eff}}^{(\text{e})} = -i\hbar\omega\frac{\partial}{\partial\theta} + T^{(\text{n})} + E_0^{(\text{e})} - \overrightarrow{\mu}_0 \cdot \overrightarrow{E}(t,\theta) - \frac{1}{2}\overrightarrow{E}(t,\theta)\cdot\overrightarrow{\overrightarrow{\alpha}}_0\cdot\overrightarrow{E}(t,\theta) - \frac{i}{4}\sum_{i\neq j}\mathcal{E}_i\mathcal{E}_j\sin(\phi_i-\phi_j)\alpha_{0,ij} \tag{6.132a}$$

or equivalently [from Eq. (6.82)]

$$K_{\text{eff}}^{(\text{e})} = -i\hbar\omega\frac{\partial}{\partial\theta} + T^{(\text{n})} + E_0^{(\text{e})} - \overrightarrow{\mu}_0 \cdot \overrightarrow{E}(t,\theta) - \overrightarrow{E}^{(-)}\cdot\overrightarrow{\overrightarrow{\alpha}}_0\cdot\overrightarrow{E}^{(+)} \tag{6.132b}$$

with the dynamical electronic polarizability tensor $\overrightarrow{\overrightarrow{\alpha}}_0(\omega)$ (here denoted $\overrightarrow{\overrightarrow{\alpha}}_0$ for simplicity) in the ground electronic state, already encountered for atoms, of components

$$\alpha_{0,ij} = \sum_{m\neq 0}\left(\frac{\mu_{i,0m}\mu_{j,m0}}{E_m^{(\text{e})} - E_0^{(\text{e})} + \hbar\omega} + \frac{\mu_{j,0m}\mu_{i,m0}}{E_m^{(\text{e})} - E_0^{(\text{e})} - \hbar\omega}\right) \tag{6.133}$$

and a linearly or elliptically polarized field (see Appendix A) in general written as

$$\overrightarrow{E}(t,\omega t)=\sum_{i=1}^{3}\mathcal{E}_i\cos(\omega t+\phi_i)\overrightarrow{e}_i. \tag{6.134}$$

This allows us to define an effective dipole moment $\overrightarrow{\mu}_{\rm eff}$ as the sum of the permanent and induced dipole moments in the ground electronic state:

$$\overrightarrow{\mu}_{\rm eff}=\overrightarrow{\mu_0}+\frac{1}{2}\overrightarrow{\overrightarrow{\alpha}}_0\cdot\overrightarrow{E}(t,\omega t), \tag{6.135}$$

such that the effective Floquet Hamiltonian can be written as

$$K^{(\rm e)}_{\rm eff}=-i\hbar\omega\frac{\partial}{\partial\theta}+T^{(\rm n)}+E^{(\rm e)}_0-\overrightarrow{\mu}_{\rm eff}\cdot\overrightarrow{E}(t,\theta)-\frac{i}{4}\sum_{i\neq j}\mathcal{E}_i\mathcal{E}_j\sin(\phi_i-\phi_j)\alpha_{0,ij}. \tag{6.136}$$

Unlike in atoms, the polarizability tensor that couples the ground state with itself is not diagonal (except if we consider the molecular frame), leading to the additional sum term. However, as shown below in Eq. (6.139), the polarizability tensor is real symmetric in the laboratory frame. This entails that the sum term of Eqs. (6.132a) and (6.136) is zero for a field linearly polarized along the z-axis of the laboratory frame or for a field elliptically polarized in the $x-y$ plane. For these two cases of interest, the effective Floquet Hamiltonian reads

$$K^{(\rm e)}_{\rm eff}=-i\hbar\omega\frac{\partial}{\partial\theta}+T^{(\rm n)}+E^{(\rm e)}_0-\overrightarrow{\mu}_{\rm eff}\cdot\overrightarrow{E}(t,\theta). \tag{6.137}$$

For a linear molecule, when the system of coordinates is chosen such that the third axis is along the molecular axis, the electronic polarizability tensor (in the molecular frame) is diagonal (but anisotropic as opposed to atoms):

$$\overrightarrow{\overrightarrow{\alpha}}_M(R)=\mathrm{diag}\left[\alpha_\perp(R),\alpha_\perp(R),\alpha_\parallel(R)\right]. \tag{6.138}$$

Transforming the polarizability into the laboratory frame:

$$\overrightarrow{\overrightarrow{\alpha}}_L=\begin{pmatrix}\bar\alpha+\Delta\alpha(\sin^2\Theta\cos^2\varphi-1/3) & \Delta\alpha\sin^2\Theta\cos\varphi\sin\varphi & -\Delta\alpha\sin\Theta\cos\Theta\cos\varphi\\ \Delta\alpha\sin^2\Theta\cos\varphi\sin\varphi & \bar\alpha+\Delta\alpha(\sin^2\Theta\sin^2\varphi-1/3) & -\Delta\alpha\sin\Theta\cos\Theta\sin\varphi\\ -\Delta\alpha\sin\Theta\cos\Theta\cos\varphi & -\Delta\alpha\sin\Theta\cos\Theta\sin\varphi & \bar\alpha+\Delta\alpha(\cos^2\Theta-1/3)\end{pmatrix} \tag{6.139}$$

with the average polarizability $\bar\alpha\equiv\bar\alpha(R)=(2\alpha_\perp(R)+\alpha_\parallel(R))/3$ and the anisotropic polarizability

$$\Delta\alpha\equiv\Delta\alpha(R)=\alpha_\parallel(R)-\alpha_\perp(R)>0, \tag{6.140}$$

we obtain the effective Floquet Hamiltonian in the ground electronic state of the linear molecule

(i) for a linearly polarized laser $\overrightarrow{E}(t,\omega t)=\mathcal{E}(t)\cos(\omega t+\phi)\overrightarrow{e}_z$:

$$\begin{aligned}K^{(\rm e)}_{\rm eff} &= -i\hbar\omega\frac{\partial}{\partial\theta}+T^{(\rm n)}+E^{(\rm e)}_0(R)-\mu_0(R)\mathcal{E}(t)\cos\Theta\cos(\theta+\phi)\\ &\quad -\frac{1}{2}\left(\alpha_\perp(R)+\Delta\alpha(R)\cos^2\Theta\right)\mathcal{E}^2(t)\cos^2(\theta+\phi),\end{aligned} \tag{6.141}$$

(ii) for an elliptically polarized field of general form (with $A^2 + B^2 = 1$)

$$\begin{aligned} \overrightarrow{E}(t,\omega t) &= \mathcal{E}(t)[A\cos(\omega t+\phi_x)\overrightarrow{e}_x + B\cos(\omega t+\phi_y)\overrightarrow{e}_y], && \text{(6.142a)} \\ &\equiv E_x(t,\omega t)\overrightarrow{e}_x + E_y(t,\omega t)\overrightarrow{e}_y, && \text{(6.142b)} \end{aligned}$$

$$\begin{aligned} K_{\text{eff}}^{(\text{e})} &= -i\hbar\omega\frac{\partial}{\partial\theta} + T^{(\text{n})} + E_0^{(\text{e})}(R) - \mu_0(R)\sin\Theta(E_x(t,\theta)\cos\varphi + E_y(t,\theta)\sin\varphi) \\ &\quad -\frac{1}{2}\left[\alpha_\perp(R)(E_x^2(t,\theta)+E_y^2(t,\theta)) + \Delta\alpha(R)\sin^2\Theta\,(E_x(t,\theta)\cos\varphi + E_y(t,\theta)\sin\varphi)^2\right] \end{aligned} \tag{6.143}$$

with $\Delta\alpha(R) = \alpha_\perp(R) - \alpha_\parallel(R)$, where $\Theta \in [0,\pi]$, $\varphi \in [0,2\pi[$ are the angles of the usual spherical coordinates of origin at the center of mass of the molecule, and we recall that R is the internuclear distance.

It is usually a good approximation to consider the *static electronic polarizability* [i.e. Eq. (6.133) with $\omega = 0$] instead of the dynamical one when we are in the limit of a low frequency with respect to the electronic states:

$$E_n^{(\text{e})} - E_0^{(\text{e})} \gg \hbar\omega. \tag{6.144}$$

Effective Hamiltonian in the ground vibrational state

Using the Born-Oppenheimer approximation (or equivalently the high frequency approximation, see Section 4.7) to effectively eliminate the fast vibrational motion with respect to the slow rotational one, we can obtain the Hamiltonian for the rotation of the free molecule in the ground electronic state by diagonalizing with respect to the vibrations of the nuclei (described here by the internuclear distance R), taking the angles Θ and φ as parameters.

We assume that the laser frequency is far from any resonance between the ground vibrational state and the excited ones, such that the partitioning is very similar to the one made with the electronic states: the vibrational state $|v=0\rangle$ spans the Hilbert subspace $\mathcal{H}_v^0$ and the other vibrational states $\{|1\rangle, \cdots |N_v\rangle\}$ the Hilbert subspace $\mathcal{H}_v^1$. We obtain for the second order effective Floquet Hamiltonian connected to the ground vibrational state of the ground electronic state for the linear field:

$$\begin{aligned} K_{\text{eff}}^{(v)} &= -i\hbar\omega\frac{\partial}{\partial\theta} + T_{\text{rot},00}^{(\text{n})} + E_{0,0}^{(v)} - \mu_{0,00}\mathcal{E}\cos\Theta\cos(\theta+\phi) \\ &\quad -\frac{1}{2}\left[\alpha_{\perp,00} + (\Delta\alpha_{00} + \alpha_0^{(v)})\cos^2\Theta\right]\mathcal{E}^2\cos^2(\theta+\phi) \end{aligned} \tag{6.145}$$

with $E_{0,0}^{(v)} = \langle v=0|E_0^{(\text{e})}|v=0\rangle_R$ and $\alpha_0^{(v)}$ the effective polarizability in the ground vibrational state induced by the other vibrational states, given by

$$\alpha_0^{(v)} = \sum_{v\neq 0}\left(\frac{|\mu_{0,0v}|^2}{E_v^{(v)} - E_0^{(v)} + \hbar\omega} + \frac{|\mu_{0,0v}|^2}{E_v^{(v)} - E_0^{(v)} - \hbar\omega}\right), \tag{6.146}$$

where we have denoted $T_{\text{rot},vv'}^{(\text{n})} := \langle v|T_{\text{rot}}^{(\text{n})}|v'\rangle_R$, $\mu_{0,vv'} = \langle v|\,\mu_0(R)\,|v'\rangle_R$, $\alpha_{\parallel,vv'} = \langle v|\,\alpha_\parallel(R)\,|v'\rangle_R$, $\alpha_{\perp,vv'} = \langle v|\,\alpha_\perp(R)\,|v'\rangle_R$ and $\Delta\alpha_{vv'} = \alpha_{\parallel,vv'} - \alpha_{\perp,vv'}$. We have $\mu_{0,00} = \mu_0(R_e)$. It is usually a good approximation to take only the contribution of the first excited vibrational state $E_1^{(v)}$ in the summation of $\alpha_0^{(v)}$ since the higher couplings are much smaller: $\mu_{0,01} \gg \mu_{0,02} \gg \mu_{0,03}\cdots$

Moreover, for usual laser of wavelength far from one-photon vibrational resonances, we have $\Delta\alpha_{00} \gg \alpha_0^{(v)}$.

For an elliptically polarized field, we obtain a similar result with $\alpha_0^{(v)}$ adding to $\Delta\alpha_{00}$ (see below for the final result).

Effective Hamiltonian for Raman rotational excitations

We now consider the rotational coordinates for the free Hamiltonian in the ground vibrational state of the ground electronic state and suppose that the field is able to populate a priori many rotational states, which we treat thus as essential states.

Neglecting $T^{(\mathrm{n})}_{\mathrm{rot},vv'}$ for $v \neq v'$ according to the Born-Oppenheimer approximation, we approximate the ground vibronic state as a rigid rotor with the vibrational energies independent of the rotational coordinates (higher corrections corresponding for example to centrifugal distortion can be obtained from the non-diagonal terms $T^{(\mathrm{n})}_{\mathrm{rot},vv'}$ for $v \neq v'$):

$$T^{(\mathrm{n})}_{\mathrm{rot},00} := B_0 \hat{J}^2, \quad B_0 = \langle v=0|B|v=0\rangle_R. \tag{6.147}$$

Choosing $E^{(v)}_{0,0} = 0$, we obtain the effective Floquet Hamiltonian

$$K^{(v)}_{\mathrm{eff}} = -i\hbar\omega \frac{\partial}{\partial\theta} + B_0 \hat{J}^2 + V^{(v)}_{\mathrm{eff}}(\theta, \Theta). \tag{6.148}$$

Below we determine for different cases of field polarization in the ground vibrational state the dressed Hamiltonian $H^{(v)}_{\mathrm{d}}$, that is decoupled from the photon field variable θ, i.e. satisfying

$$\widetilde{K}^{(v)}_{\mathrm{eff}} \equiv S^\dagger K^{(v)}_{\mathrm{eff}} S = -i\hbar\omega \frac{\partial}{\partial\theta} + H^{(v)}_{\mathrm{eff}} \tag{6.149}$$

with a perturbative transformation S to be defined. The dressed Hamiltonian is written as

$$H^{(v)}_{\mathrm{eff}} = B_0 \hat{J}^2 + V(\Theta, \varphi) \tag{6.150}$$

with the (dressed) potential $V(\Theta, \varphi)$ [see Eqs. (6.159), (6.161), (6.162), (6.165), and (6.166)].

Linear polarization. For the case of linear field (and not considering anymore ϕ since it will not have any effect), we obtain

$$V^{(v)}_{\mathrm{eff}}(\theta, \Theta) = -\mu_{0,00}\mathcal{E}\cos\Theta\cos\theta - \frac{1}{2}\left[\alpha_{\perp,00} + (\Delta\alpha_{00} + \alpha_0^{(v)})\cos^2\Theta\right]\mathcal{E}^2\cos^2\theta. \tag{6.151}$$

We consider the *high frequency limit* with respect to the rotation

$$\hbar\omega \gg B_0, \tag{6.152}$$

and apply the results of Section 4.7 with the Hamiltonian written as

$$K^{(v)}_{\mathrm{eff}}/\hbar\omega = -i\frac{\partial}{\partial\theta} + \epsilon\left[B_0\hat{J}^2 + V^{(v)}_{\mathrm{eff}}(\theta, \Theta)\right], \tag{6.153}$$

with the small parameter $\epsilon := 1/(\hbar\omega)$ and identifying the quantities of Section 4.7: $x \equiv \Theta$, $H_0 \equiv B_0\hat{J}^2$, $V_1 \equiv V^{(v)}_{\mathrm{eff}}$. We first apply the contact transformation $S_1 = \exp(\epsilon W_1)$ with $W_1(\Theta, \theta) =$

$-i\int^{\theta}(V_{\rm eff}^{(v)}-\overline{V}_{\rm eff}^{(v)})d\theta$ and the average with respect to θ: $\overline{V}_{\rm eff}^{(v)}(\Theta)=\frac{1}{2\pi}\int_0^{2\pi}d\theta\ V_{\rm eff}^{(v)}(\theta,\Theta)$. Splitting $\hat{J}^2:=T_\Theta+T_\varphi$, we obtain the exact result (i.e. the terms of order ϵ^n, $n>3$, are exactly zero):

$$S_1^\dagger\frac{K_{\rm eff}^{(v)}}{\hbar\omega}S_1=-i\frac{\partial}{\partial\theta}+\epsilon\left(B_0\hat{J}^2+\overline{V}_{\rm eff}^{(v)}\right)+\epsilon^2B_0\left[T_\Theta,W_1\right]+\frac{\epsilon^3}{2}B_0\left[\left[T_\Theta,W_1\right],W_1\right]. \tag{6.154}$$

We apply again a contact transformation $S_2=\exp(\epsilon^2W_2)$ with $W_2(\Theta,\theta)=-i\int^\theta\left(V_2-\overline{V}_2\right)d\theta$, and

$$V_2=B_0\left[T_\Theta,W_1\right]+\frac{\epsilon}{2}B_0\left[\left[T_\Theta,W_1\right],W_1\right], \tag{6.155}$$

which averages with respect to θ and gives, to second order in $1/\hbar\omega$,

$$S_2^\dagger S_1^\dagger\frac{K_{\rm eff}^{(v)}}{\hbar\omega}S_1S_2=-i\frac{\partial}{\partial\theta}+\epsilon\left(B_0\hat{J}^2+\overline{V}_{\rm eff}^{(v)}\right)+\epsilon^2B_0\overline{[T_\Theta,W_1]}+\epsilon^3\left(\frac{B_0}{2}\overline{\left[\left[T_\Theta,W_1\right],W_1\right]}+B_0[T_\Theta,W_2]\right). \tag{6.156}$$

A final contact transformation S_3 of the same type allows one to obtain

$$\begin{aligned}S_3^\dagger S_2^\dagger S_1^\dagger\frac{K_{\rm eff}^{(v)}}{\hbar\omega}S_1S_2S_3=&-i\frac{\partial}{\partial\theta}+\epsilon\left(B_0\hat{J}^2+\overline{V}_{\rm eff}^{(v)}\right)+\epsilon^2B_0\overline{[T_\Theta,W_1]}\\&+\epsilon^3\left(\frac{B_0}{2}\overline{\left[\left[T_\Theta,W_1\right],W_1\right]}+B_0\overline{[T_\Theta,W_2]}\right).\end{aligned} \tag{6.157}$$

We calculate

$$\overline{V}_{\rm eff}^{(v)} = -\frac{\mathcal{E}^2}{4}\left[\alpha_{\perp,00}+(\Delta\alpha_{00}+\alpha_0^{(v)})\cos^2\Theta\right],\quad \overline{[T_\Theta,W_1]}=0, \tag{6.158a}$$

$$W_1 = \frac{i\mathcal{E}^2}{8}\left[\alpha_{\perp,00}+(\Delta\alpha_{00}+\alpha_0^{(v)})\cos^2\Theta\right]\sin2\theta+i\mathcal{E}\mu_{0,00}\cos\Theta\sin\theta, \tag{6.158b}$$

$$\overline{\left[\left[T_\Theta,W_1\right],W_1\right]} = -2\overline{\left(\frac{\partial W_1}{\partial\Theta}\right)^2}, \tag{6.158c}$$

$$= \frac{\mathcal{E}^4}{64}\left(\Delta\alpha_{00}+\alpha_0^{(v)}\right)^2\sin^2 2\Theta+\mu_{0,00}^2\mathcal{E}^2\sin^2\Theta \tag{6.158d}$$

and obtain the dressed potential of second order in $1/\hbar\omega$ and of second order in field amplitude $\mathcal{E}$ [103]

$$V(\Theta,\varphi)=-\frac{\mathcal{E}^2}{2}\left[\frac{\alpha_{\parallel,00}+\alpha_0^{(v)}}{2}-\left(\frac{\Delta\alpha_{00}+\alpha_0^{(v)}}{2}+\frac{B_0\mu_{0,00}^2}{(\hbar\omega)^2}\right)\sin^2\Theta\right]. \tag{6.159}$$

Since we consider a linear polarization, the coupling does not depend on the angle φ and we can thus consider this Hamiltonian (6.159) acting on a state of the form $\psi(\theta,\varphi;t)=\phi(\theta;t)e^{iM\varphi}/\sqrt{2\pi}$, with M the preserved projection of the angular momentum $\hat{J}$ on the field polarization axis, which leads to

$$\widetilde{K}_{{\rm eff},M}^{(v)}=-i\hbar\omega\frac{\partial}{\partial\theta}+B_0T_\Theta+V_M(\Theta,\varphi) \tag{6.160}$$

with

$$V_M(\Theta,\varphi)=\frac{M^2}{\sin^2\Theta}-\frac{\mathcal{E}^2}{2}\left[\frac{\alpha_{\parallel,00}+\alpha_0^{(v)}}{2}-\left(\frac{\Delta\alpha_{00}+\alpha_0^{(v)}}{2}+\frac{B_0\mu_{0,00}^2}{(\hbar\omega)^2}\right)\sin^2\Theta\right]. \tag{6.161}$$

The effective potential (6.159) has been used to show the adiabatic alignment of molecules by a laser field (see for example [125, 103]).

Elliptic polarization. For an elliptically polarized laser (6.142), a similar calculation gives

$$\begin{aligned} V(\Theta,\varphi) &= -\frac{\mathcal{E}^2}{4}\left[\alpha_{\perp,00}+(\Delta\alpha_{00}+\alpha_0^{(v)})\sin^2\Theta\left(A^2\cos^2\varphi+B^2\sin^2\varphi+AB\sin 2\varphi\cos\phi\right)\right] \\ &+ \frac{\mathcal{E}^2}{2}\frac{B_0\mu_{0,00}^2}{(\hbar\omega)^2}\left[\cos^2\Theta(A^2\cos^2\varphi+B^2\sin^2\varphi)+\sin^2\Theta(A^2\sin^2\varphi+B^2\cos^2\varphi)\right] \quad (6.162a) \\ &= -\frac{\mathcal{E}^2}{4}\left[\alpha_{\perp,00}+(\Delta\alpha_{00}+\alpha_0^{(v)})\left(A^2\cos^2\Theta_x+B^2\cos\Theta_y+AB\sin^2\Theta\sin 2\varphi\cos\phi\right)\right] \\ &+ \frac{\mathcal{E}^2}{2}\frac{B_0\mu_{0,00}^2}{(\hbar\omega)^2}\left[\cos^2\Theta(A^2\cos^2\varphi+B^2\sin^2\varphi)+\sin^2\Theta(A^2\sin^2\varphi+B^2\cos^2\varphi)\right] \quad (6.162b) \end{aligned}$$

with $\phi=\phi_y-\phi_x$, and where we have introduced the (squared) direction cosines with respect to the three axis

$$\cos^2\Theta_x \equiv \sin^2\Theta\cos^2\varphi, \quad (6.163a)$$
$$\cos^2\Theta_y \equiv \sin^2\Theta\sin^2\varphi, \quad (6.163b)$$
$$\cos^2\Theta_z \equiv \cos^2\Theta, \quad (6.163c)$$

of property

$$\cos^2\Theta_x+\cos^2\Theta_y+\cos^2\Theta_z=1. \quad (6.164)$$

Such Hamiltonian has been used to show the dynamical alternation of alignment (with $\phi=\pi/2$, which gives $\eta=0$ for the ellipse, i.e. $A\equiv a$ and $B\equiv b$, see Appendix A) [126] (see also Section 10.3).

Circular polarization. The particular case of a circular field ($\phi=\pi/2, A^2=B^2=1/2$) gives

$$V(\Theta,\varphi) = -\frac{\mathcal{E}^2}{8}\left[\alpha_{\parallel,00}+\alpha_0^{(v)}-(\Delta\alpha_{00}+\alpha_0^{(v)})\cos^2\Theta\right]+\frac{\mathcal{E}^2}{4}\frac{B_0\mu_{0,00}^2}{(\hbar\omega)^2}, \quad (6.165)$$

which shows a potential independent of φ, very similar to the linear one [Eq. (6.161) with the selection rule $\Delta M=0$], except the factor 1/2, the sine become a cosine, and the term proportional to $\mu_{0,00}^2$ which appears now as a constant not multiplying $\cos^2\Theta$. As a consequence, this term will not be involved in alignment processes by circularly polarized fields. More importantly, the maxima and the minima are reversed with respect to the linear polarization.

Variable linear polarization. We consider the particular case of a linear field with a variable polarization in the plane (x,y) (given by $\phi=0$):

$$\begin{aligned} V(\Theta,\varphi) &= -\frac{\mathcal{E}^2}{4}\left[\alpha_{\perp,00}+(\Delta\alpha_{00}+\alpha_0^{(v)})\sin^2\Theta\left(A\cos\varphi+B\sin\varphi\right)^2\right] \\ &+\frac{\mathcal{E}^2}{2}\frac{B_0\mu_{0,00}^2}{(\hbar\omega)^2}\left[\cos^2\Theta(A^2\cos^2\varphi+B^2\sin^2\varphi)+\sin^2\Theta(A^2\sin^2\varphi+B^2\cos^2\varphi)\right]. \end{aligned} \quad (6.166)$$

One can notice the difference between the effective Hamiltonians for an elliptic field (with for instance $\phi=\pi/2$) and a variable linear polarization only due to the crossed term $AB\sin 2\varphi$.

Such potential has been used to induce an optical centrifuge that can rotationally accelerate diatomic molecules from low angular momentum states to the rotational dissociation [127, 128, 129, 130]. This aim is obtained when the linear polarization is adiabatically rotated (for instance with a linear chirp $\phi(t) = \beta t^2/2$). Such a field can be generated by a combination of two counter-rotating circularly polarized beams of opposite relative frequency chirp:

$$\begin{aligned}
\overrightarrow{E}(t,\omega t) &= \mathcal{E}(t)\cos\omega t[A(t)\overrightarrow{e}_x + B(t)\overrightarrow{e}_y], \quad A(t) \equiv \cos(\phi(t)) && \text{(6.167a)}\\
&= \frac{\mathcal{E}(t)}{2}\left[\cos(\omega t+\phi(t))\overrightarrow{e}_x + \sin(\omega t+\phi(t))\overrightarrow{e}_y\right] \\
&\quad + \frac{\mathcal{E}(t)}{2}\left[\cos(\omega t-\phi(t))\overrightarrow{e}_x - \sin(\omega t-\phi(t))\overrightarrow{e}_y\right]. && \text{(6.167b)}
\end{aligned}$$

Chapter 7

Construction of propagators for short-pulse-driven quantum dynamics

In this chapter, we present the time-dependent contact transformations adapted to the treatment of intense and short pulsed interactions. This allows one in particular to go beyond the impulsive regime, where the time dependence of the interaction is considered as a δ-function, and to take into account the duration of the pulse. We have first formulated it using an extended space where the Hamiltonian is time independent [23]. Instead of using an extended space, we formulate in this paper [131] the derivation in a simpler way, by stating the perturbation iterations directly at the level of the evolution operator in the original Hilbert space. We show in particular that there is a freedom in choosing secular terms and we use it to optimize the accuracy of the approximation. We apply this formulation to the unitary KAM superconvergent technique and improve the accuracy by several orders of magnitude with respect to the Magnus expansion. This work has been developed in Ref. [132]. It has been applied for the orientation of molecules by a strong short pulse of area different from zero [133].

RAPID COMMUNICATIONS

PHYSICAL REVIEW A **68**, 051402(R) (2003)

Optimized time-dependent perturbation theory for pulse-driven quantum dynamics in atomic or molecular systems

D. Daems*
Center for Nonlinear Phenomena and Complex Systems, Université Libre de Bruxelles, Code Postal 231, 1050 Brussels, Belgium

S. Guérin and H. R. Jauslin
Laboratoire de Physique de l'Université de Bourgogne, UMR CNRS 5027, Boîte Postale 47870, 21078 Dijon, France

A. Keller and O. Atabek
Laboratoire de Photophysique Moléculaire du CNRS, Université Paris-Sud, Bâtiment 210, Campus d'Orsay, 91405 Orsay Cedex, France
(Received 11 July 2003; published 24 November 2003; publisher error corrected 4 December 2003)

We present a time-dependent perturbative approach adapted to the treatment of intense pulsed interactions. We show there is a freedom in choosing secular terms and use it to optimize the accuracy of the approximation. We apply this formulation to a unitary superconvergent technique and improve the accuracy by several orders of magnitude with respect to the Magnus expansion.

DOI: 10.1103/PhysRevA.68.051402 PACS number(s): 42.50.Hz, 31.15.Md, 03.65.−w, 02.30.Mv

Perturbation theory when combined with a specific treatment for resonances is quite well understood in classical and quantum mechanics for time-independent systems. This includes also time-periodic driven systems for which the periodicity can be treated by Floquet theory in a way that yields a time-independent formulation [1,2]. One knows that resonances yield divergent terms that appear as small denominators, which have to be specifically removed. The counterpart of the concept of resonance for time-dependent systems is generally associated to secular terms whose size grows with time (see Ref. [3] and references therein).

With the advent of short ($\simeq 10$ fs) and intense (10^{13}–10^{15} W/cm^2) laser pulses, atomic or molecular systems can be strongly perturbed in a timescale shorter than characteristic times corresponding to the free evolution of the system and adiabatic theories are not applicable (see, e.g., Ref. [4]). The goal of this paper is to formulate a time-dependent perturbation theory well adapted for perturbations localized in time.

The conceptual framework of perturbation theory can be described as follows: The Hamiltonian of the considered system can be decomposed as the sum of two terms $H_1=H_0+\epsilon V_1$. The first term H_0 is assumed to have a structure simple enough to lead to explicitly known solutions for its associated propagator $U_{H_0}(t,t_0)$. The term ϵV_1 is supposed to be small with respect to H_0, in a sense specified below. Time-independent perturbation theories can be equivalently formulated at the level of eigenvectors or operators [5]. A large class of these approaches amounts to construct a unitary transformation T such that

$$T^\dagger H_1 T = H^e + \epsilon' V', \tag{1}$$

where H^e is still of simple structure [i.e., its propagator $U_{H^e}(t,t_0)$ can be explicitly computed] and $\epsilon' V'$ is a perturbation whose size is smaller than the original one. To compute the transformation T explicitly, one represents it in general either (i) in terms of some power series

$$T=e^{-iW}, \quad W=\sum_k \epsilon^k W_k, \tag{2}$$

or (ii) by an iterative construction as a composition of transformations

$$T=\prod_k e^{-i\epsilon_k W_k}. \tag{3}$$

These procedures generally differ. The former one is referred to as the time-independent Poincaré—Von Zeipel technique, which has been shown to be equivalent to the usual Rayleigh-Schrödinger perturbation theory [6]. The latter procedure includes the Van Vleck technique (for which $\epsilon_k=\epsilon^k$) and the superconvergent Kolmogorov-Arnold-Moser (KAM) expansion (where $\epsilon_k=\epsilon^{2^{k-1}}$ and W_k is ϵ_k dependent) [7]. The perturbative procedure converges if the remaining perturbation $\epsilon' V'$ can be made to go to zero, as the number of terms in the power series (2) or as the number of compositions in Eq. (3) goes to infinity.

In this description one has to state precisely what class of Hamiltonians H^e can be considered simple. For the first order or the first iteration, one considers $H^e=H_0+\epsilon D_1$ with the condition that D_1 should be *compatible* with H_0 in the sense that if the propagator of H_0 is known, that of $H_0+\epsilon D_1$ can also be obtained explicitly. In the case of time-independent Hamiltonians the condition of compatibility is

$$[H_0,D_1]=0. \tag{4}$$

For the case of time-dependent Hamiltonians, we show that the condition of compatibility can be generalized to

$$[H_0(t),D_1(t)]=i\frac{\partial D_1}{\partial t}. \tag{5}$$

*Email address: ddaems@ulb.ac.be

The construction of transformations of the type of Eqs. (2) or (3) involves finding the generator $-i\epsilon W_1(t)$ of the transformation $T_1(t)$, that is the solution to

$$i[W_1(t),H_0(t)]+V_1(t)-D_1(t)=\frac{\partial W_1}{\partial t}. \tag{6}$$

This equation, together with the constraint (5), are usually called *cohomology equations* in the time-independent case [8] and are here generalized to the time-dependent case. These cohomology equations are exactly of the same form for higher orders or successive iterations.

Here we formulate the time-dependent perturbation theory by transforming directly the evolution operator instead of considering the perturbed Hamiltonian as is usually done in time-independent theory. We obtain perturbative corrections to the full propagator in the form of a product of propagators which exhibit free parameters appearing through the general solutions of related differential equations. We recover in particular the Magnus expansion [9] as a special case of the time-dependent Poincaré—Von Zeipel theory. This extension also gives the precise correspondence between time-independent resonances and time-dependent secular terms. In the context of pulsed perturbations with a finite duration, the secular terms need not be eliminated. We show the remarkable result that they can be used to improve the convergence of the method at a given order. This optimization is achieved without any *a priori* knowledge of the solution by locating the minimum of a given eigenvalue as a function of the relevant free parameters that are identified. The efficiency of the method is illustrated on a two-level system driven by a short intense pulse.

Perturbation theory, resonances and secular terms. We consider the Hamiltonian $H_1(t)=H_0(t)+\epsilon V_1(t)$, where $H_0(t)$ is associated to a known propagator $U_{H_0}(t,t_0)$. The formulation is presented here for the superconvergent KAM method, consisting in iterations of transformations which are exactly of the same form at each step. The first iteration involves a unitary operator $T_1(t)$ which transforms the propagator $U_{H_1}(t,t_0)$ according to

$$T_1^\dagger(t)U_{H_1}(t,t_0)T_1(t_0)=U_{H_2}(t,t_0), \tag{7}$$

into a propagator $U_{H_2}(t,t_0)$ associated with the sum $H_2(t)$ of an effective Hamiltonian $H_1^e(t)\equiv H_0(t)+\epsilon D_1(t)$ which contains contributions up to order ϵ and a remainder $\epsilon^2 V_2(t)$. This new propagator, generated by a sum of two Hamiltonians, can be written as the product

$$U_{H_2}(t,t_0)=U_{H_1^e}(t,t_0)R_2(t,t_0), \tag{8}$$

where $R_2(t,t_0)$ is the unitary operator associated with the Hamiltonian $\epsilon^2 U_{H_1^e}(t_0,t)V_2(t)U_{H_1^e}(t,t_0)$. Similarly we can factorize $U_{H_1^e}(t,t_0)=U_{H_0}(t,t_0)S_1(t,t_0)$, where $S_1(t,t_0)$ is a unitary operator related to $\epsilon D_1(t)$

$$i\frac{\partial}{\partial t}S_1(t,t_0)=\epsilon U_{H_0}(t_0,t)D_1(t)U_{H_0}(t,t_0)S_1(t,t_0). \tag{9}$$

The full propagator reads

$$U_{H_1}(t,t_0)=T_1(t)U_{H_0}(t,t_0)S_1(t,t_0)R_2(t,t_0)T_1^\dagger(t_0), \tag{10}$$

which yields the first-order KAM approximation for $R_2(t,t_0)$ replaced by the identity. In this construction the only restriction on the Hamiltonian $\epsilon D_1(t)$ is that it be of order ϵ. Hence we have the freedom to choose the Hamiltonian in Eq. (9) as t-independent, giving

$$D_1(t)=U_{H_0}(t,t_0)D_1(t_0)U_{H_0}(t_0,t) \tag{11}$$

with $D_1(t_0)$ arbitrary, which is the general solution of Eq. (5). This allows one to obtain the solution of Eq. (9) as

$$S_1(t,t_0)=\exp[-i(t-t_0)\epsilon D_1(t_0)]. \tag{12}$$

Differentiating Eq. (10) and substituting $T_1(t)=\exp[-i\epsilon W_1(t)]$ leads to Eq. (6). The rest involves a series of k nested commutators that reads

$$\epsilon^2 V_2(t)=\sum_{k=1}^{\infty}\frac{1}{(k+1)!}i^k\epsilon^{k+1}\times[W_1(t),\cdots[W_1(t),kV_1(t)+D_1(t)]\cdots].$$

It has exactly the same structure at each iteration which is useful for applications, particularly when high-order computations are needed.

Iterating the time-dependent KAM algorithm reduces the size of the remaining perturbation in a superconvergent way from order $\epsilon^{2^{n-1}}$ to ϵ^{2^n} at step n. The time-dependent Van Vleck technique would allow one to reduce the size of the remaining perturbation from order ϵ^n to ϵ^{n+1}. These methods, in the formulation presented here, are unitary upon truncation. The superconvergent character of the KAM algorithm has been shown numerically by applying the method to a two-level system perturbed by a short time-dependent interaction [10].

The *time-independent problem*, i.e., the problem of finding a transformation T_1 that enables one to simplify the time independent Hamiltonian H_1 according to $T_1^\dagger H T_1=H_0+\epsilon D_1+\epsilon^2 V_2$, is recovered when one conveniently chooses the transformation T_1 as time independent. In this case all the operators, and in particular D_1 and W_1, are time independent and the standard cohomology equations are recovered: $[H_0,D_1]=0$ and $V_1-D_1+i[W_1,H_0]=0$. Their solutions can be determined using the following key property [8]: W_1 exists if and only if $\Pi_{H_0}(D_1-V_1)=0$, where Π_{H_0} is the projector in the kernel of the application $A\mapsto[A,H_0]$ (for an operator A acting on the same Hilbert space as H_0). The projector Π_{H_0} applied on an operator A captures thus all the part B of A which commutes with H_0: $[B,H_0]=0$. The unique solution D_1 allowing W_1 to exist and satisfying Eq. (4) is thus

RAPID COMMUNICATIONS

$$D_1 = \Pi_{H_0} V_1 \equiv \lim_{T\to\infty} \frac{1}{T} \int_0^T e^{-itH_0} V_1 e^{itH_0}. \quad (13)$$

The *resonances* are associated with terms of V_1 which commute with H_0. Application of Eq. (13) can be interpreted as an *averaging* of V_1 with respect to H_0 which allows one to extract resonances.

For the *time-dependent problem*, the general solution of Eq. (6) reads [up to a term $U_{H_0}(t,t_0)B_1 U_{H_0}(t_0,t)$ with B_1 any constant self-adjoint operator that we set to 0 for simplicity]:

$$W_1(t) = \int_{t_1'}^{t} ds U_{H_0}(t,s)[V_1(s) - D_1(s)]U_{H_0}(s,t), \quad (14)$$

with t_1' any real number. Defining the average

$$\Pi_- V_1 \equiv \lim_{\tau\to\infty} \frac{1}{\tau} \int_{t-\tau}^{t} ds U_{H_0}(t,s) V_1(s) U_{H_0}(s,t), \quad (15)$$

one can show the following property: if $W_1(t)$ is bounded for negative infinite times, then $\Pi_-(V_1 - D_1) = 0$. This is satisfied by $D_1 = \Pi_- V_1$, the only solution compatible with Eqs. (5) and (15). This means that the averaging $D_1 = \Pi_- V_1$ allows one to remove secular terms at negative infinite times. We remark that this definition of the average (15) can be in fact recovered from the formal calculation of the KAM average $\Pi_{K_0} V_1$ (13) with respect to $K_0 = -i(\partial/\partial t) + H_0$ in an extended space, which includes time as a coordinate [10,11]. This gives the precise correspondence between the resonances of stationary problems and the secular terms of time-independent problems.

We now consider a class of perturbations $V_1(t)$ that are arbitrary for $t_i < t < t_f$, and constant otherwise where one has $[U_{H_0}(t,t'), V_1(t)] = 0$ for $t,t' \leqslant t_i$ and $t,t' \geqslant t_f$. This includes many physical situations such as a pulsed perturbation switched on at t_i and off at t_f. For this class of systems, Eq. (15) becomes $\Pi_- V_1 = U_{H_0}(t,t_i) V(t_i) U_{H_0}(t_i,t)$, which is a particular solution of Eq. (5) corresponding to the choice $D_1(t_0) \equiv U_{H_0}(t_0,t_i) V(t_i) U_{H_0}(t_i,t_0)$ in Eq. (11). An alternate definition of the average: $\Pi_+ V_1 = \lim_{\tau\to\infty} (1/\tau) \int_t^{t+\tau} ds U_{H_0}(t,s) V_1(s) U_{H_0}(s,t)$ would give a different averaging $\Pi_+ V_1 = U_{H_0}(t,t_f) V(t_f) U_{H_0}(t_f,t)$ and would allow one to remove secular terms at positive infinite times. Generally one cannot remove simultaneously the secular terms at negative and positive large times. This shows a conceptual difference between stationary resonances and secular terms associated with perturbations localized in time. Furthermore, it suggests that the averaging such as Eq. (15) is not appropriate, but that a definition which combines the two definitions gives a new secular term that could improve the convergence of the algorithm. This suggests to work with the general solution (11) of Eq. (5), written with the perturbation evaluated at a free time t_1 as the arbitrary operator

$$D_1(t) = U_{H_0}(t,t_1) V_1(t_1) U_{H_0}(t_1,t). \quad (16)$$

The free t_1 can then be chosen to minimize the rest after the first iteration, as described below.

One has n such free parameters t_k, $k = 1, n$ for n iterations of the KAM algorithm. There is only one such free parameter for the time-dependent Poincaré-Von Zeipel and Van Vleck methods that are order by order techniques. An interesting result is that we recover the Magnus expansion from the time-dependent Poincaré—Von Zeipel in the particular case of $D_k = 0$ and $t_k' = t_0$ with $k = 1,n$.

Optimization of the perturbation theory. After one iteration, the rest $R_2(t,t_0)$ defined in Eq. (8) is associated with a second-order operator through $R_2(t,t_0) \equiv e^{-i\epsilon^2 G_2(t)}$ with $G_2(t_0) = 0$. The closer $R_2(t,t_0)$ is to the identity, the smaller the correction terms are, i.e., the more accurate the approximation is. We evaluate the lowest-order contribution to $\epsilon^2 G_2(t)$ as

$$\epsilon^2 G_2^{(2)}(t) = \epsilon^2 \int_{t_0}^{t} du U_{H_1^e}(t_0,u) V_2(u) U_{H_1^e}(u,t_0). \quad (17)$$

It is this operator that has to remain small for the algorithm to converge. The size of an operator A can be characterized by the norm $||A|| = \sup_{||\psi||=1} ||A\psi||$ with ψ in the appropriate Hilbert space. For an Hermitian matrix this norm reduces to the largest of the absolute values of its eigenvalues.

In order to improve the accuracy we thus seek to minimize $\lambda_2(t)$, the largest of the absolute values of the eigenvalues of $\epsilon^2 G_2^{(2)}(t)$, with respect to the free parameters. To optimize the KAM algorithm, we have at our disposal two free parameters t_k and t_k' at each iteration. We expect that the parameters t_k will significantly affect the convergence of the algorithm, as they are related to secular terms.

Perturbation theory for short intense pulses. We consider a system described by the Hamiltonian $\hat{H}$ (autonomous or not) and perturbed by a time-dependent Hamiltonian $\hat{V}(s)$ whose characteristic duration is τ. The perturbation is assumed to satisfy $[\hat{V}(s), \hat{V}(s_0)] = 0$, $\forall s, s_0$ which is realized in many situations of interest. We define a *sudden parameter* ϵ as follows. A dimensionless time t and dimensionless operators H and $V(t)$ are defined through $s \equiv \tau t$, $\hat{H} \equiv \hbar\omega H$, and $\hat{V}(s) \equiv (\hbar/\tau) V(t)$, leading to the dimensionless Schrödinger equation $i(\partial/\partial t) U(t,t_0) = \{V(t) + \epsilon H\} U(t,t_0)$, where the sudden parameter is defined as $\epsilon \equiv \omega\tau$. To apply the perturbation theory described above we can then identify $H_0(t) \equiv V(t)$ and $V_1 \equiv H$. This formulation is suited to treat intense short pulses.

Illustration on a pulsed-driven two-level system. We consider the case where $H_0(t) = \Omega(t)\sigma_1$ and $V_1 = \sigma_3$ with $\Omega(t)$ a pulse that is switched on at t_i and off at t_f, and σ_k the Pauli matrices. Notice that, as discussed above, the role of the perturbation and reference Hamiltonian is interchanged. The pulse area $A \equiv \int_{t_i}^{t_f} \Omega(u) du$ is a dimensionless parameter that can be fixed independently of the sudden parameter ϵ. The error between the numerical solution of the Schrödinger equation at the end of the pulse and the result of n iterations

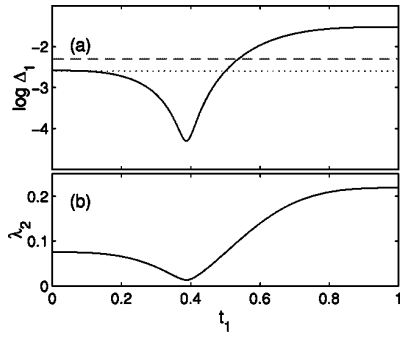

FIG. 1. (a) Natural logarithm of the error Δ_1 for the first-order Dyson expansion (dashed line), the first-order Magnus expansion (dotted line), and the first KAM iteration (solid line); and (b) largest eigenvalue of $\epsilon^2 G_2^{(2)}(t_f)$ as a function of t_1, for $A=1$, $\epsilon=0.5$ and $t_1'=t_0$.

is defined as $\Delta_n \equiv ||U_{H_1}(t_f,t_i) - U_{H_1}^{(n)}(t_f,t_i)||$. We use the pulse shape $\Omega(t)=2A\sin^2(\pi t)$ for $0 \leqslant t \leqslant 1$, and 0 elsewhere.

Figure 1 shows a comparison of the first-order Dyson, first-order Magnus, and one-iteration KAM methods as a function of t_1 for a nonperturbative area chosen to produce comparable errors Δ_1 for the Magnus and nonoptimized ($t_1 = t_0$) KAM techniques. The lower panel displays λ_2 the largest of the absolute values of the eigenvalues of $\epsilon^2 G_2^{(2)}(t_f)$ defined in Eq. (17). We clearly see that the error of the first KAM iteration is correctly estimated by this eigenvalue λ_2 and, in particular, minimized when λ_2 is minimized, i.e., for the value $t_1^\star$. It is worth noting that modifying t_1 covers almost three orders of magnitude in the error, a situation that is not restricted to this particular value of A. The optimized solution provides an improvement of the accuracy of almost two orders of magnitude with respect to the Magnus calculation.

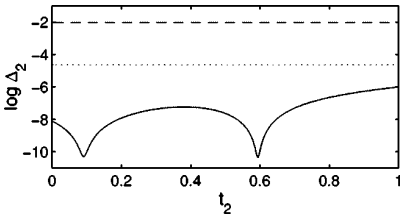

FIG. 2. Natural logarithm of the error Δ_2 for the second-order Dyson expansion (dashed line), the second-order Magnus expansion (dotted line), and the second KAM iteration (solid line) with the same parameters as Fig. 1 and $t_1=t_1^\star \approx 0.39$.

Figure 2 displays a comparison of the second-order Dyson, second-order Magnus, and two-iteration KAM methods as a function of t_2 for $t_1=t_1^\star$. It is seen that the Dyson approach is not applicable in this context of strong field as the second order performs worse than the first one. Figure 2 also shows that the second KAM iteration can be enhanced by at least four orders of magnitude with an appropriate choice of t_1 and t_2. This optimized second KAM iteration provides an improvement of more that five orders of magnitude with respect to the second-order Magnus technique. Higher iterations of the KAM technique can also be optimized and produce still better improvement owing to its superconvergent character.

In conclusion, we have presented an optimized perturbation theory for pulse-driven systems, which applies to a wide class of processes controlled by intense femtosecond laser pulses. The optimization reduces to the evaluation of eigenvalues and is therefore easy to implement. We anticipate that this approach will be usefull in the context of the laser control of atomic and molecular processes, such as phase space localisation of Rydberg electron [12], or alignment and orientation of molecules [4].

This research was supported in part by FNRS, ACI *Photonique*, and *Conseil Régional de Bourgogne*.

[1] J.C.A. Barata and W.F. Wreszinski, Phys. Rev. Lett. **84**, 2112 (2000).
[2] S. Guérin and H.R. Jauslin, Adv. Chem. Phys. **125**, 147 (2003).
[3] P.W. Langhoff, S.T. Epstein, and M. Karplus, Rev. Mod. Phys. **44**, 602 (1972).
[4] H. Stapelfeldt and T. Seideman, Rev. Mod. Phys. **75**, 543 (2003).
[5] H. Primas, Rev. Mod. Phys. **35**, 710 (1963).
[6] W. Scherer, J. Phys. A **27**, 8231 (1994).
[7] W. Scherer, Phys. Rev. Lett. **74**, 1495 (1995).
[8] H.R. Jauslin, S. Guérin, and S. Thomas, Physica A **279**, 432 (2000).
[9] P. Pechukas and J.C. Light, J. Chem. Phys. **44**, 3897 (1966).
[10] D. Daems, A. Keller, S. Guérin, H.R. Jauslin, and O. Atabek, Phys. Rev. A **67**, 052505 (2003).
[11] W. Scherer, Phys. Lett. A **233**, 1 (1997).
[12] D.G. Arbó, C.O. Reinhold, J. Burgdörfer, A.K. Pattanayak, C.L. Stokely, W. Zhao, J.C. Lancaster, and F.B. Dunning, Phys. Rev. A **67**, 063401 (2003).

Appendix A

Elliptic polarization

We study in this appendix a field

$$\overrightarrow{E} = E_x \overrightarrow{e}_x + E_y \overrightarrow{e}_y \tag{A.1}$$

of general elliptic polarization (in the plane $x - y$). It can be constructed from the ellipse of equation

$$\left(\frac{E_X}{a}\right)^2 + \left(\frac{E_Y}{b}\right)^2 = \mathcal{E}^2 \tag{A.2}$$

(i.e. with

$$\overrightarrow{E} = E_X \overrightarrow{e}_X + E_Y \overrightarrow{e}_Y, \qquad \{E_X = \mathcal{E} a \cos\omega t, E_Y = \pm \mathcal{E} b \sin\omega t\}, \tag{A.3}$$

the normalized semiaxes $a, b \in [0,1]$, $a^2 + b^2 = 1$, and the two signs distinguishing the two possible senses in which the end point of the electric vector may describe the ellipse) in a frame $(0X, 0Y)$, rotated of an angle $\eta/2$ ($0 \leq \eta < 2\pi$) about the z-axis from the axis $(0x, 0y)$ (see Fig. A.1):

$$\overrightarrow{E} = \mathcal{E} \begin{pmatrix} \cos(\eta/2) & -\sin(\eta/2) & 0 \\ \sin(\eta/2) & \cos(\eta/2) & 0 \\ 0 & 0 & 1 \end{pmatrix} \begin{pmatrix} a\cos\omega t \\ \pm b \sin\omega t \\ 0 \end{pmatrix}. \tag{A.4}$$

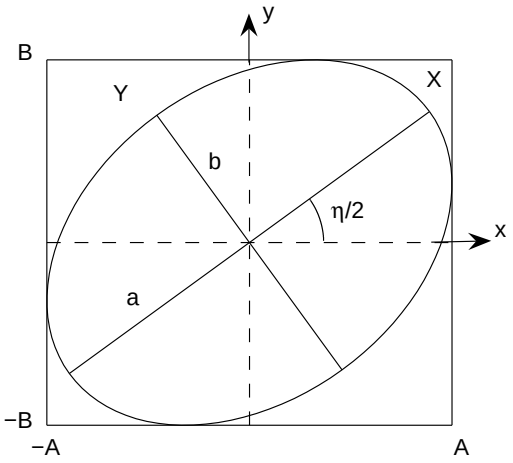

FIG. A.1 - *Ellipse described by an elliptically polarized field.*

We can also write it as

$$\overrightarrow{E} = \mathcal{E} \begin{pmatrix} A\cos(\omega t + \phi_x) \\ B\cos(\omega t + \phi_y) \\ 0 \end{pmatrix} \tag{A.5}$$

with (see for instance [115]) $a^2 + b^2 = A^2 + B^2 = 1$,

$$A^2 = a^2\cos^2(\eta/2) + b^2\sin^2(\eta/2), \tag{A.6a}$$
$$B^2 = b^2\cos^2(\eta/2) + a^2\sin^2(\eta/2), \tag{A.6b}$$
$$\tan\delta = \frac{B}{A}, \quad 0 \leq \delta \leq \pi/2, \tag{A.6c}$$
$$\tan\eta = \tan 2\delta\cos(\phi_y - \phi_x) = \frac{2AB}{A^2 - B^2}\cos(\phi_y - \phi_x), \tag{A.6d}$$
$$\tan\chi = \mp\frac{b}{a}, \quad -\pi/4 < \chi \leq \pi/4 \text{ for } a > b, \tag{A.6e}$$
$$\sin 2\chi = \sin 2\delta\ \sin(\phi_y - \phi_x), \quad \text{i.e. } \mp ab = AB\sin(\phi_y - \phi_x). \tag{A.6f}$$

We have the same energy density for the linear and elliptic fields for a given $\mathcal{E}$.

It can be also decomposed as the sum of left (rotating anti-clockwise[1], proportional to $a \pm b$, denoted σ_+) and right (rotating clockwise, proportional to $a \mp b$, denoted σ_-) circularly polarized fields, with the relative phase η:

$$\overrightarrow{E} = \mathcal{E}\frac{a \pm b}{2}\begin{pmatrix} \cos(\omega t + \eta/2) \\ \sin(\omega t + \eta/2) \\ 0 \end{pmatrix} + \mathcal{E}\frac{a \mp b}{2}\begin{pmatrix} \cos(\omega t - \eta/2) \\ -\sin(\omega t - \eta/2) \\ 0 \end{pmatrix} \tag{A.7}$$

It is convenient in this case to use an angle α for the parametrization of the ellipticity:

$$\sin\alpha = \frac{a \pm b}{\sqrt{2}} \qquad \cos\alpha = \frac{a \mp b}{\sqrt{2}} \qquad -\frac{\pi}{4} \leq \alpha < \frac{3\pi}{4}, \tag{A.8}$$

such that

$$\overrightarrow{E} = \frac{\mathcal{E}}{\sqrt{2}}\sin\alpha\begin{pmatrix} \cos(\omega t + \eta/2) \\ \sin(\omega t + \eta/2) \\ 0 \end{pmatrix} + \frac{\mathcal{E}}{\sqrt{2}}\cos\alpha\begin{pmatrix} \cos(\omega t - \eta/2) \\ -\sin(\omega t - \eta/2) \\ 0 \end{pmatrix}. \tag{A.9}$$

One recovers for instance the linear polarization along the $x-$axis ($y-$axis) for $\alpha = \pi/4$ ($\alpha = -\pi/4$) and $\eta = 0$. The left and right circularly polarized fields are respectively for $\alpha = \pi/2$ and $\alpha = 0$:

$$\overrightarrow{E}_+ \equiv \overrightarrow{E}(\alpha = \pi/2), \qquad \overrightarrow{E}_- \equiv \overrightarrow{E}(\alpha = 0). \tag{A.10}$$

Thus apart a global phase (which comes to change the origin of time), one can express any elliptic field by Eq. (A.9) defining the angles $-\frac{\pi}{4} \leq \alpha < \frac{3\pi}{4}$ and $0 \leq \eta < 2\pi$. The angle α allows one to characterize the ellipticity, and is related to the axial ratio by

$$\frac{b}{a} = \frac{|1 - \tan\alpha|}{1 + \tan\alpha}. \tag{A.11}$$

We also have

$$AB\cos(\phi_y - \phi_x) = \frac{1}{2}\sin 2\alpha\sin\eta, \qquad AB\sin(\phi_y - \phi_x) = \frac{1}{2}\cos 2\alpha. \tag{A.12}$$

[1] We adopt here the common convention in optics, opposite to the one used in elementary particle physics

Part III

Control processes in atoms and molecules by laser fields

Chapter 8

Elementary processes of population transfer with constraints

As an alternative to the non-robust π-pulse (or generalized π-pulse) techniques, the development of efficient and robust schemes based on adiabatic passage for selective population transfer have opened new opportunities for coherent control of atomic and molecular processes. Atoms and molecules prepared in well-defined quantum states or in a coherent superposition of states, are essential in various fields of contemporary quantum physics. Applications can be found in control of chemical reactions [134], design of atom mirrors, beam splitters, and atomic interferometers in atomic optics [135, 136], manipulation of atomic wave packets in laser cooling experiments [137], creation of photon-number Fock states in cavity QED [228], conversion of an atomic condensate to a molecular one in Bose-Einstein Condensation (BEC) through photoassociation [139], construction of quantum gates, quantum teleportation, and quantum cryptography [140], control of localization and suppression of tunneling [141, 142, 143].

We however remark that in general adiabatic passage is time and energy consuming since it requires a large pulse area, and that can be detrimental for some applications. For instance in quantum computation, we need very precise and fast gates. The accuracy requires to implement a method of reduced sensitivity to the relaxation of the atoms and the cavity photons. In this case, it can be of interest to use fast methods i.e. based on π-pulses, if the pulses can be well controlled, with respect to the slow adiabatic passage. We notice that the question of sensitivity to the relaxation can be solved in adiabatic passage by using *dark states* immune to relaxation, as shown in Section 8.2.

More generally speaking, one can thus require additional *constraints* for processes of population transfer. Here we study the constraints of (i) minimization of the total pulse area, or (ii) the absence of transient population in intermediate lossy states.

Such requirements can be studied using *optimal control techniques* (see e.g. [144, 145]). It has been in particular shown that STIRAP emerges from an optimal control theory algorithm with the use of a penalty function on the population of the intermediate state [146]. Using the approach of geometric control theory [147], Boscain et al. have shown that the π pulse strategy emerges naturally as the strategy which minimizes the pulse area [148].

In this chapter we describe processes for population transfer with such constraints, in particular (i) π-pulse type transfers that minimize the pulse area, and (ii) adiabatic passage techniques that allow one to transfer the population without transient population in lossy intermediate states, i.e. STIRAP [71], fractional STIRAP [79], and tripod STIRAP [149, 150].

We remark that these techniques can be used in the context of cavity QED by replacing one or two laser fields by cavity-mode fields.

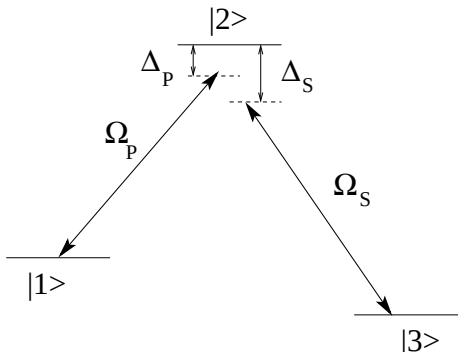

FIG. 8.1 - *Linkage pattern scheme of the STIRAP technique.*

8.1 Elementary population transfers minimizing the pulse area

With the use of an approach of geometric control theory [147], it has been shown that the π pulse strategy emerges naturally as the strategy which minimizes the pulse area. field [148]. This shows in particular that an additional controllable time-dependent frequency (chirping) does not improve the minimization. The π-pulse strategy is also the one which minimizes the *fluence* (i.e. the integral of the squared pulse) for a given transfer time, or equivalently the one which minimizes the transfer time with a given constraint on the field amplitude. It has been found in this Ref. [148] the *counterpart of the "π-pulse transfer" in three-level systems* driven by two resonant fields, i.e. the pulse parametrization which minimizes the total pulse area ℓ (defined as the integral of the squared root of the sum of the squared field amplitudes). It has been found $\ell = \sqrt{3}\pi/2$ as the minimum.

8.2 Adiabatic transfer without transient population of excited states - Dark states

8.2.1 STIRAP

We recall that the technique of stimulated Raman adiabatic passage (STIRAP) uses the coherence of two pulsed laser fields to achieve a complete population transfer from an initially populated state $|1\rangle$ to a target state $|3\rangle$ via an intermediate state $|2\rangle$ (see Fig. 8.1). In this configuration one assumes that the states $|1\rangle$ and $|3\rangle$ (which are usually ground states) are metastable, i.e., with negligible spontaneous emission in the considered time scale. The excited state $|2\rangle$ has a relatively short lifetime, due to spontaneous emission. Instead of applying the pulses in the intuitive sequence, where the pump pulse (linking the states $|1\rangle$ and $|2\rangle$) precedes the Stokes pulse (linking the states $|2\rangle$ and $|3\rangle$), the Stokes pulse precedes the pump pulse (as the so called counterintuitive pulse ordering). If the condition of two-photon resonance is satisfied, if there is sufficient overlap of the two pulses, and if the pulses are sufficiently strong such that the time evolution is adiabatic, then the complete population transfer occurs between the states $|1\rangle$ and $|3\rangle$, without populating the state $|2\rangle$.

Construction of the effective Hamiltonian

We write the Hamiltonian of a three-level atom with Λ-configuration coupled with the pump and Stark pulses in the resonant (or rotating wave) approximation, i.e. discarding the anti-resonant (or counter-rotating) terms, as (in units such that $\hbar = 1$)

$$H = \begin{pmatrix} \omega_1 & \frac{1}{2}\Omega_P(t)e^{+i(\omega_P t+\theta_P)} & 0 \\ \frac{1}{2}\Omega_P(t)e^{-i(\omega_P t+\theta_P)} & \omega_2 & \frac{1}{2}\Omega_S(t)e^{-i(\omega_S t+\theta_S)} \\ 0 & \frac{1}{2}\Omega_S(t)e^{+i(\omega_S t+\theta_S)} & \omega_3 \end{pmatrix}, \tag{8.1}$$

where $\omega_i, i = 1,2,3$ are the energies of the atomic bare states, $\Omega_i(t) = -\mu\mathcal{E}_i(t), i = P,S$ are the Rabi frequencies of the laser pulses, and $\omega_i, \theta_i,\ i = P,S$ are respectively the carrier frequency and the phase of the laser pulses. We have used here a simplified notation omitting the factor 1/2 for the Rabi frequencies (or equivalently defining them with this factor 1/2). The effective Hamiltonian of the system can be obtained by applying the following rotating wave transformation on H (written here in the time representation),

$$R(t) = \begin{pmatrix} 1 & 0 & 0 \\ 0 & e^{-i\omega_P t} & 0 \\ 0 & 0 & e^{-i(\omega_P-\omega_S)t} \end{pmatrix}, \tag{8.2}$$

which leads to the effective Hamiltonian:

$$H^{\text{eff}}(t) = R^\dagger H R - iR^\dagger\frac{\partial R}{\partial t} = \begin{pmatrix} 0 & \frac{1}{2}\Omega_P(t)e^{+i\theta_P} & 0 \\ \frac{1}{2}\Omega_P(t)e^{-i\theta_P} & \Delta_P & \frac{1}{2}\Omega_S(t)e^{-i\theta_S} \\ 0 & \frac{1}{2}\Omega_S(t)e^{+i\theta_S} & \Delta_P - \Delta_S \end{pmatrix}, \tag{8.3}$$

where we have shifted the origin of the energy by ω_1, and used the detunings

$$\Delta_P = \omega_2 - \omega_1 - \omega_P, \qquad \Delta_S = \omega_2 - \omega_3 - \omega_S. \tag{8.4}$$

The relation between the state vector $|\Psi(t)\rangle$ corresponding to $H(t)$, and the state vector $|\Phi(t)\rangle$ corresponding to $H^{\text{eff}}(t)$ can be established by $|\Psi(t)\rangle = R(t)|\Phi(t)\rangle$.

An essential condition for the STIRAP process is the two-photon resonance between the states $|1\rangle$ and $|3\rangle$ which means $\Delta_P = \Delta_S = \Delta$. Then the three instantaneous eigenstates of H^{eff} (the adiabatic states) are given by

$$\begin{aligned} &\lambda_\pm(t) = \frac{1}{2}\left(\Delta \pm \sqrt{\Delta^2 + \Omega_P^2(t) + \Omega_S^2(t)}\right), \qquad \lambda_0(t) = 0 \\ &|\phi_-(t)\rangle = \begin{pmatrix} \sin\vartheta\cos\varphi e^{i\theta_P} \\ -\sin\varphi \\ \cos\vartheta\cos\varphi e^{i\theta_S} \end{pmatrix} \ |\phi_0(t)\rangle = \begin{pmatrix} \cos\vartheta e^{i\theta_P} \\ 0 \\ -\sin\vartheta e^{i\theta_S} \end{pmatrix} \ |\phi_+(t)\rangle = \begin{pmatrix} \sin\vartheta\sin\varphi e^{i\theta_P} \\ \cos\varphi \\ \cos\vartheta\sin\varphi e^{i\theta_S} \end{pmatrix} \end{aligned} \tag{8.5}$$

where the mixing angles $\vartheta(t)$ and $\varphi(t)$ are defined by

$$\tan\vartheta(t) = \frac{\Omega_P(t)}{\Omega_S(t)}, \qquad \vartheta(t) \in [0,\pi], \tag{8.6a}$$

$$\tan 2\varphi(t) = \frac{\sqrt{\Omega_P^2 + \Omega_S^2}}{\Delta}, \qquad \varphi(t) \in [0,\pi/2]. \tag{8.6b}$$

The STIRAP technique is based on the use of the zero-eigenvalue adiabatic state $|\phi_0(t)\rangle$, which is a superposition of the initial state $|1\rangle$ and the final state $|3\rangle$. This adiabatic state has no component of the excited state $|2\rangle$, and hence it has no possibility of spontaneous emission during the adiabatic evolution (dark state). For the counterintuitive Stokes-pump pulse sequence, we have:

$$\lim_{t\to t_i}\frac{\Omega_P}{\Omega_S}=0, \qquad \lim_{t\to t_f}\frac{\Omega_P}{\Omega_S}=\infty. \tag{8.7}$$

This leads to $\vartheta(t_i)=0$ and $\vartheta(t_f)=\pi/2$, and

$$|1\rangle \xleftarrow{t_i\leftarrow t} |\phi_0(t)\rangle \xrightarrow{t\to t_f} |3\rangle. \tag{8.8}$$

Thus, the state $|\phi_0(t)\rangle$ connects adiabatically the initial state $|1\rangle$ to the target state $|3\rangle$ at the end of the interaction.

Condition of global adiabaticity

In order to achieve a complete population transfer from $|1\rangle$ to $|3\rangle$, we have to force the system to stay in the dark state during the whole process, without nonadiabatic transitions to other adiabatic states. This adiabatic condition requires that the coupling between each pair of adiabatic states is negligible compared to the difference between the energies of these states. With respect to the dark state $|\phi_0(t)\rangle$, the adiabatic condition reads

$$|\lambda_0-\lambda_\pm| \gg \left|\left\langle \frac{d\phi_0}{dt}\middle|\phi_\pm\right\rangle\right|. \tag{8.9}$$

In the case of one-photon resonance ($\Delta=0,\ \varphi(t)=\pi/4$), the adiabaticity condition simplifies and becomes

$$\sqrt{\Omega_P^2+\Omega_S^2} \gg \left|\frac{d\vartheta}{dt}\right| \sim \frac{1}{T}, \tag{8.10}$$

where T is the pulse duration. Assuming that the pump and Stokes pulses have the same peak Rabi frequency Ω_0, this condition can be roughly written as

$$\Omega_0 T \gg 1. \tag{8.11}$$

Hence, adiabaticity requires a large pulse area. Therefore, the conditions for STIRAP process are:
(i) Two-photon resonance between the initial state and the target state,
(ii) Counterintuitive pulse sequence of Stark-pump,
(iii) Large pulse area.

Implementation of one-qubit phase gate

There is an interesting application of the STIRAP technique in an implementation of one-qubit phase gates [151]. Figure 8.2 represents the corresponding linkage pattern where the qubits are stored in the atomic bare states $|0\rangle$ and $|1\rangle$. The state $|0\rangle$ is decoupled from the others, and thus is a stationary state during the gate operation ($|0\rangle \to |0\rangle$). The operation of a one-qubit phase gate of phase γ,

$$U_P=\begin{pmatrix} 1 & 0 \\ 0 & e^{i\gamma} \end{pmatrix}, \tag{8.12}$$

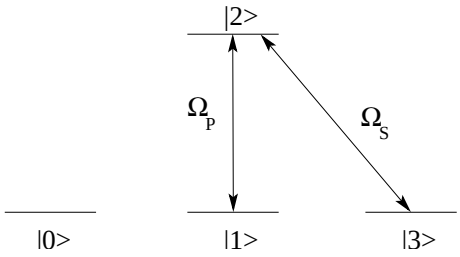

FIG. 8.2 - *Linkage pattern scheme for construction of a quantum phase gate. The qubits are stored in the states* $|0\rangle$ *and* $|1\rangle$.

is expressed using the initial state $|\psi_i\rangle = \alpha|0\rangle + \beta|1\rangle$ as follows:

$$|\psi_i\rangle \to |\psi_f\rangle = U_P|\psi_i\rangle = \alpha|0\rangle + e^{i\gamma}\beta|1\rangle. \tag{8.13}$$

The effective Hamiltonian of this system is given by (8.3), where detunings are zero $\Delta_P = \Delta_S = 0$. The dark state $|\phi_0\rangle$ can be written as

$$|\phi_0(t)\rangle = \frac{1}{\sqrt{\Omega_P^2 + \Omega_S^2}}(\Omega_S e^{i\theta_S}|1\rangle - \Omega_P e^{i\theta_P}|3\rangle). \tag{8.14}$$

The quantum phase gate is implemented in two stages by an STIRAP and then by a reverse STIRAP with different Stokes pulses $\Omega_S^{(1)}$ and $\Omega_S^{(2)}$ (see Fig. 8.3). The dark state (8.14) indicates

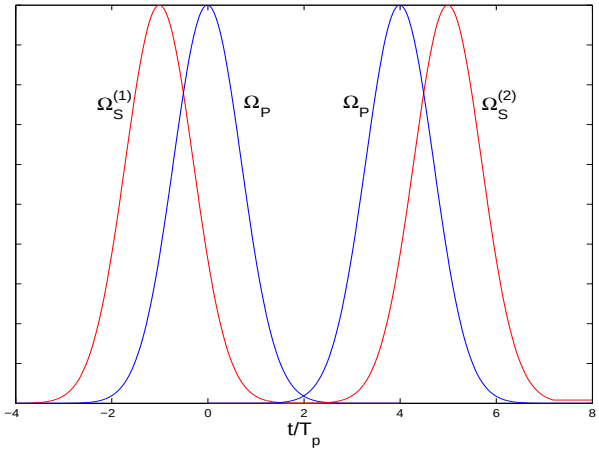

FIG. 8.3 - *Pulse sequences (dimensionless) for two STIRAP Processes required for implementing a one-qubit phase gate.*

that the result of the first STIRAP is to transfer the population from the state $|1\rangle$ into $|3\rangle$ as

$$|1\rangle \to |\phi_0(t)\rangle \to -e^{-i(\omega_P-\omega_S)(t_f-t_i)}e^{i(\theta_P-\theta_S^{(1)})}|3\rangle, \tag{8.15}$$

where t_i, t_f are the starting and ending times of the first STIRAP, and we have included the effect of the transformation (8.2). The result of the second STIRAP (with Ω_P arriving before $\Omega_S^{(2)}$) is

$$-|3\rangle \to |\phi_0(t)\rangle \to e^{i(\theta_S^{(2)}-\theta_P)}|1\rangle. \tag{8.16}$$

Hence, the overall effect of the two STIRAP processes on the initial state of the system is:

$$\alpha|0\rangle + \beta|1\rangle \to \alpha|0\rangle + e^{i\gamma}\beta|1\rangle, \tag{8.17}$$

with

$$\gamma = \theta_S^{(2)} - \theta_S^{(1)} + (\omega_S - \omega_P)(t_f - t_i). \tag{8.18}$$

We emphasize the presence of an optical phase $(\omega_S - \omega_P)(t_f - t_i)$ in γ. The control of this phase is in practice very difficult. This phase can be eliminated by taking $\omega_S = \omega_P$, which implies that the ground states $|1\rangle, |3\rangle$ must be degenerate . For instance, the linkage pattern can be formed by the sublevels in the $J = 1 \leftrightarrow J' = 0$ transition by using a linearly polarized pump pulse and a circularly σ^- polarized Stokes pulse. The states $|0\rangle, |1\rangle, |3\rangle$ correspond respectively to Zeeman sublevels $|J = 1,\ m = -1, 0, 1\rangle$, and the state $|2\rangle$ to $|J' = 0,\ m = 0\rangle$.

This has been generalized in [151] to generate any one-qubit gate as a general propagator of $SU(2)$ symmetry.

The concrete realization of this process is discussed in Section 15.1.

8.2.2 Fractional STIRAP

Fractional STIRAP (f-STIRAP) is a variation of STIRAP, which allows one the creation of any preselected coherent superposition of two states. As in STIRAP, the Stokes pulse linking the initially unpopulated states $|2\rangle, |3\rangle$ arrives before the pump pulse linking the initially populated state $|1\rangle$ to the excited state $|2\rangle$, but unlike STIRAP where the Stokes pulse vanishes first, here the two pulses vanish simultaneously while maintaining a constant finite ratio of amplitudes. As a result, a coherent superposition of states $|1\rangle, |3\rangle$ is created, in which the ratio of the probability amplitudes of these states is proportional to the turn-off ratio between the pump and Stokes pulses. The f-STIRAP has been shown to increase the coherence between the lower states of Λ-systems in nonlinear optics experiments [152].

The system is assumed to be initially in the state $|1\rangle$,

$$|\Psi(t_i)\rangle = |1\rangle, \tag{8.19}$$

and we wish to transform it at the end of the interaction into the coherent superposition

$$|\Psi(t_f)\rangle = \cos\alpha|1\rangle - \sin\alpha\ e^{i\varphi}|3\rangle. \tag{8.20}$$

The possibility of creation of this coherent superposition arises from the following behavior of the dark state (8.14) for the counterintuitive Stokes-pump pulse sequence:

$$\lim_{t\to t_i} \frac{\Omega_P}{\Omega_S} = 0, \qquad \lim_{t\to t_f} \frac{\Omega_P}{\Omega_S} = \tan\alpha. \tag{8.21}$$

This leads to the initial and the final mixing angles $\vartheta(t_i) = 0$ and $\vartheta(t_f) = \alpha$, and

$$|1\rangle \xleftarrow{t_i \leftarrow t} |\phi_0(t)\rangle \xrightarrow{t\to t_f} \cos\alpha\ e^{i\theta_P}|1\rangle - \sin\alpha\ e^{i\theta_S}|3\rangle. \tag{8.22}$$

Thus, the state $|\phi_0(t)\rangle$ connects adiabatically the initial state $|1\rangle$ to the target superposition state $\cos\alpha|1\rangle - \sin\alpha\ e^{i\varphi}|3\rangle$ at the end of interaction, with

$$\varphi = \theta_S - \theta_P. \tag{8.23}$$

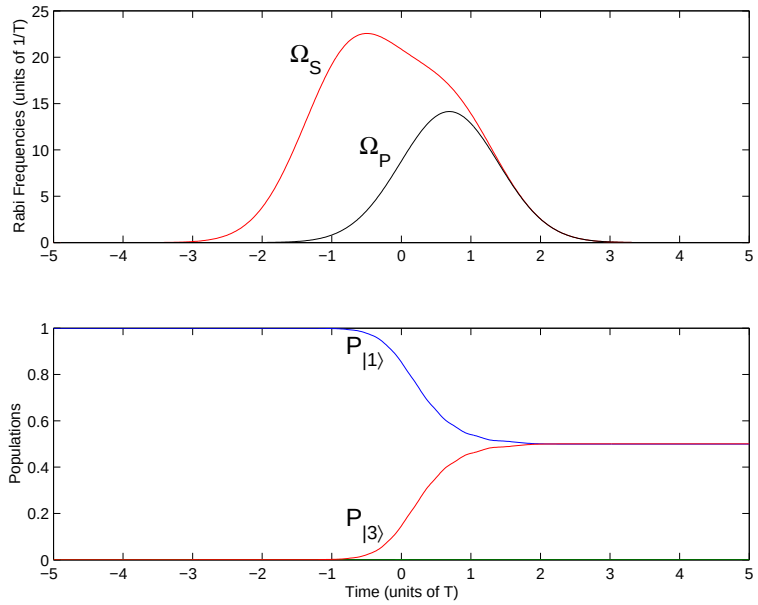

FIG. 8.4 - *Stokes-pump Pulse sequence and populations as function of the time for the half-STIRAP process with Rabi frequencies given by Eq. (8.24).*

The special case of $\varphi = \pi$ and $\alpha = \pi/4$, known as half-STIRAP, leads to $|1\rangle \rightarrow \frac{1}{\sqrt{2}}(|1\rangle + |3\rangle)$ and $|3\rangle \rightarrow \alpha|1\rangle + \beta|2\rangle + \gamma|3\rangle$. The two-photon resonance between the states $|1\rangle, |3\rangle$ is necessary for f-STIRAP as for STIRAP. The optical phase factor $e^{-i(\omega_S - \omega_P)t}$ is eliminated in a degenerate linkage pattern $\omega_1 = \omega_3$.

The f-STIRAP scheme proposed Vitanov *et al* [79] is made robust by realizing the condition (8.21) in Zeeman sublevels for the states 1 and 3: $|1\rangle \equiv |m = -1\rangle$, $|3\rangle \equiv |m = +1\rangle$, with the excited state $|2\rangle \equiv |m = 0\rangle$ and by using polarized pulses: one is of σ^- polarization associated to the Rabi frequency $\Omega_0 e^{-(t+\tau)^2/T^2}$, and another one with the time-dependence $\Omega_0 e^{-(t-\tau)^2/T^2}$ of elliptic polarization $\cos\alpha\ \sigma^- + \sin\alpha\ \sigma^+$. This scheme is as robust as STIRAP, and leads to the Rabi frequencies of the pump (with σ^+ polarization) and Stokes (with σ^- polarization) pulses as

$$\begin{aligned} \Omega_P(t) &= \Omega_0 \sin\alpha\ e^{-(t-\tau)^2/T^2}, \\ \Omega_S(t) &= \Omega_0 e^{-(t+\tau)^2/T^2} + \Omega_0 \cos\alpha\ e^{-(t-\tau)^2/T^2}. \end{aligned} \tag{8.24}$$

Figure 8.4 (lower panel) shows the time evolution of the populations in the f-STIRAP process. The pulse shapes (upper panel) are defined by Eq. (8.24) with $\alpha = \pi/4$, $\tau = 0.7T$, and $\Omega_0 = 20/T$. The population evolves smoothly from initially populated state $|1\rangle$ to the coherent superposition $\frac{1}{\sqrt{2}}(|1\rangle - |3\rangle)$ at the end of process.

8.2.3 Tripod STIRAP

The tripod STIRAP technique, first proposed by Unanyan *et al* [149], is an extension of STIRAP in which a third laser pulse (the Control) couples the excited state $|2\rangle$ to a fourth ground state $|4\rangle$ (see Fig. 8.5). Such a four-level system with three control parameters features an additional non trivial geometric phase. In this section we show, following Ref. [149], that for a

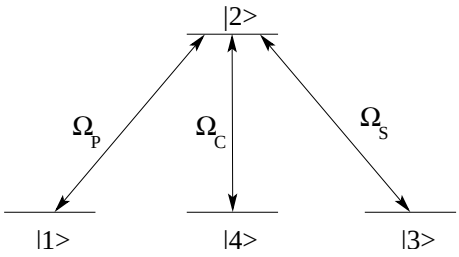

FIG. 8.5 - *Linkage pattern scheme of the tripod STIRAP technique.*

proper sequence of pump, Stokes, and control pulses, tripod STIRAP allows one to create not only a coherent superposition of states $|1\rangle$ and $|3\rangle$, but also to construct coherently one-qubit rotation and phase gates in the subspace of $|1\rangle$ and $|3\rangle$.

Construction of the effective Hamiltonian

The Hamiltonian of the tripod system in the resonant approximation can be written as

$$H(t) = \frac{1}{2}\begin{pmatrix} 0 & \Omega_P(t)e^{i(\omega_P t+\theta_P)} & 0 & 0 \\ \Omega_P(t)e^{-i(\omega_P t+\theta_P)} & 2\omega_2 & \Omega_S(t)e^{-i(\omega_S t+\theta_S)} & \Omega_C(t)e^{-i(\omega_C t+\theta_C)} \\ 0 & \Omega_S(t)e^{+i(\omega_S t+\theta_S)} & 0 & 0 \\ 0 & \Omega_C(t)e^{+i(\omega_C t+\theta_C)} & 0 & 0 \end{pmatrix}, \tag{8.25}$$

where the energy of the ground states $|1\rangle, |4\rangle, |3\rangle$ is taken as zero. In the resonant case: $\omega_2 = \omega_P = \omega_S = \omega_C = \omega$, the effective Hamiltonian of the system is obtained by applying the rotating wave transformation

$$R(t) = \begin{pmatrix} 1 & 0 & 0 & 0 \\ 0 & e^{-i(\omega t+\theta_P)} & 0 & 0 \\ 0 & 0 & e^{-i(\theta_P-\theta_S)} & 0 \\ 0 & 0 & 0 & e^{-i(\theta_P-\theta_C)} \end{pmatrix}, \tag{8.26}$$

as

$$\begin{aligned} H^{\text{eff}}(t) &= R^\dagger H R - iR^\dagger \frac{\partial R}{\partial t} \\ &= \frac{1}{2}\begin{pmatrix} 0 & \Omega_P(t) & 0 & 0 \\ \Omega_P(t) & 0 & \Omega_S(t) & \Omega_C(t) \\ 0 & \Omega_S(t) & 0 & 0 \\ 0 & \Omega_C(t) & 0 & 0 \end{pmatrix}. \end{aligned} \tag{8.27}$$

The relation between the state vector $|\Psi(t)\rangle$ corresponding to $H(t)$, and the state vector $|\Phi(t)\rangle$ corresponding to $H^{\text{eff}}(t)$ can be established as $|\Psi(t)\rangle = R(t)|\Phi(t)\rangle$. In the subspace of $|1\rangle$ and $|3\rangle$, the transformation R is reduced to a one-qubit phase gate

$$R \to U_P = \begin{pmatrix} 1 & 0 \\ 0 & e^{i\gamma} \end{pmatrix}, \qquad \gamma = \theta_S - \theta_P. \tag{8.28}$$

Construction of the adiabatic Hamiltonian

The next step of the analysis is to find the degenerate dark states (with null eigenvalues and zero component along the excited state $|2\rangle$) of the effective Hamiltonian. Since in the adiabatic evolution of this system its dynamics follows simultaneously two dark states, we prefer to calculate the corresponding propagator in the adiabatic approximation. The dark states are

$$|\phi_1(t)\rangle = \begin{pmatrix} \cos\vartheta(t) \\ 0 \\ -\sin\vartheta(t) \\ 0 \end{pmatrix}, \qquad |\phi_2(t)\rangle = \begin{pmatrix} \sin\vartheta(t)\sin\varphi(t) \\ 0 \\ \cos\vartheta(t)\sin\varphi(t) \\ -\cos\varphi(t) \end{pmatrix}, \tag{8.29}$$

and the other instantaneous eigenvectors are

$$|\phi_3(t)\rangle = \frac{1}{\sqrt{2}} \begin{pmatrix} \sin\vartheta(t)\cos\varphi(t) \\ 1 \\ \cos\vartheta(t)\cos\varphi(t) \\ \sin\varphi(t) \end{pmatrix}, \qquad |\phi_4(t)\rangle = \frac{1}{\sqrt{2}} \begin{pmatrix} \sin\vartheta(t)\cos\varphi(t) \\ -1 \\ \cos\vartheta(t)\cos\varphi(t) \\ \sin\varphi(t) \end{pmatrix}, \tag{8.30}$$

where the mixing angles are given by

$$\tan\vartheta(t) = \frac{\Omega_P(t)}{\Omega_S(t)}, \qquad \tan\varphi(t) = \frac{\Omega_C(t)}{\sqrt{\Omega_P^2(t)+\Omega_S^2(t)}}. \tag{8.31}$$

The angle $\vartheta(t)$ is the mixing angle used in standard STIRAP, and $\varphi(t)$ is an additional mixing angle related to the control pulse.

The unitary transformation between the atomic bare states and the adiabatic states is

$$T(t) = \begin{pmatrix} \cos\vartheta(t) & \sin\vartheta(t)\sin\varphi(t) & \frac{1}{\sqrt{2}}\sin\vartheta(t)\cos\varphi(t) & \frac{1}{\sqrt{2}}\sin\vartheta(t)\cos\varphi(t) \\ 0 & 0 & \frac{1}{\sqrt{2}} & -\frac{1}{\sqrt{2}} \\ -\sin\vartheta(t) & \sin\varphi(t)\cos\vartheta(t) & \frac{1}{\sqrt{2}}\cos\vartheta(t)\cos\varphi(t) & \frac{1}{\sqrt{2}}\cos\vartheta(t)\cos\varphi(t) \\ 0 & -\cos\varphi(t) & \frac{1}{\sqrt{2}}\sin\varphi(t) & \frac{1}{\sqrt{2}}\sin\varphi(t) \end{pmatrix} \tag{8.32}$$

Hence, the Hamiltonian in the basis of adiabatic states can be written as

$$T^\dagger H^{\text{eff}} T - iT^\dagger \frac{\partial T}{\partial t} = \begin{pmatrix} 0 & -i\dot\vartheta\sin\varphi(t) & \frac{-i}{\sqrt{2}}\dot\vartheta\cos\varphi(t) & \frac{-i}{\sqrt{2}}\dot\vartheta\cos\varphi(t) \\ i\dot\vartheta\sin\varphi(t) & 0 & \frac{i}{\sqrt{2}}\dot\varphi & \frac{i}{\sqrt{2}}\dot\varphi \\ \frac{+i}{\sqrt{2}}\dot\vartheta\cos\varphi(t) & \frac{-i}{\sqrt{2}}\dot\varphi & \frac{1}{2}\Omega(t) & 0 \\ \frac{+i}{\sqrt{2}}\dot\vartheta\cos\varphi(t) & \frac{-i}{\sqrt{2}}\dot\varphi & 0 & -\frac{1}{2}\Omega(t) \end{pmatrix}, \tag{8.33}$$

where

$$\Omega(t) = \sqrt{\Omega_P^2(t)+\Omega_S^2(t)+\Omega_C^2(t)}. \tag{8.34}$$

The dynamics corresponding to this Hamiltonian is given by $i\frac{\partial}{\partial t}|\Upsilon(t)\rangle = \left(T^\dagger H^{\text{eff}} T - iT^\dagger\frac{\partial T}{\partial t}\right)|\Upsilon(t)\rangle$. The relation between $|\Phi(t)\rangle$, the state vector corresponding to $H^{\text{eff}}(t)$, and $|\Upsilon(t)\rangle$ is established by the unitary transformation $T(t)$ as

$$|\Phi(t)\rangle = T(t)|\Upsilon(t)\rangle. \tag{8.35}$$

In the adiabatic limit, which we assume to be applicable, the time derivative of the mixing angles $\vartheta(t)$ and $\varphi(t)$ is small compared to the splitting of eigenvalues given by $\Omega(t)$. Under

this condition there is negligible nonadiabatic coupling of the adiabatic states $|\phi_1(t)\rangle$ or $|\phi_2(t)\rangle$ to the states $|\phi_3(t)\rangle$ and $|\phi_4(t)\rangle$. Therefore, in the adiabatic limit we must take into account only transitions between degenerate adiabatic states. This leads to the adiabatic dynamics $i\frac{\partial}{\partial t}|\Upsilon(t)\rangle = H^{\rm ad}(t)|\Upsilon(t)\rangle$ with

$$H^{\rm ad}(t) = \begin{pmatrix} 0 & -i\dot{\vartheta}\sin\varphi(t) & 0 & 0 \\ +i\dot{\vartheta}\sin\varphi(t) & 0 & 0 & 0 \\ 0 & 0 & \frac{1}{2}\Omega(t) & 0 \\ 0 & 0 & 0 & -\frac{1}{2}\Omega(t) \end{pmatrix}. \tag{8.36}$$

This Hamiltonian commutes with itself at different times, since it can be diagonalized by a time independent transformation. The corresponding propagator thus reads

$$\begin{aligned} U^{\rm ad}(t,t_i) &= e^{-i\int_{t_i}^{t} ds\, H^{\rm ad}(s)} \\ &= \begin{pmatrix} \cos\Theta(t) & -\sin\Theta(t) & 0 & 0 \\ \sin\Theta(t) & \cos\Theta(t) & 0 & 0 \\ 0 & 0 & e^{-i\delta(t)} & 0 \\ 0 & 0 & 0 & e^{+i\delta(t)} \end{pmatrix}, \end{aligned} \tag{8.37}$$

where $\delta(t) = \frac{1}{2}\int_{t_i}^{t} ds\,\Omega(s)$ is the dynamical phase, and $\Theta(t)$ is the geometrical phase:

$$\Theta(t) = \int_{t_i}^{t} ds\,\dot{\vartheta}(s)\sin\varphi(s). \tag{8.38}$$

Using $|\Upsilon(t)\rangle = U^{\rm ad}(t,t_i)|\Upsilon(t_i)\rangle$, Equation (8.35) leads to

$$|\Phi(t)\rangle = T(t)U^{\rm ad}(t,t_i)T^{\dagger}(t_i)|\Phi(t_i)\rangle = U^{\rm eff}(t,t_i)|\Phi(t_i)\rangle, \tag{8.39}$$

where we have defined the effective propagator of the system as

$$U^{\rm eff}(t,t_i) := T(t)U^{\rm ad}(t,t_i)T^{\dagger}(t_i). \tag{8.40}$$

At the final step, we have to consider the transformation $R(t)$ to obtain the propagator corresponding to $H(t)$ as

$$|\Psi(t)\rangle = R(t)U^{\rm eff}(t,t_i)R^{\dagger}(t_i)|\Psi(t_i)\rangle. \tag{8.41}$$

Implementation of one-qubit quantum gates by geometric phase

In this subsection we show that an adapted sequence of pump, Stokes, and control pulses in tripod STIRAP, results an implementation of one-qubit phase and rotation gates in a relatively robust (in a sense specified below) and coherent way [150].

Taking the pulse sequence such that

$$\vartheta(t_i) = \vartheta(t_f) = 0, \quad \varphi(t_i) = \varphi(t_f) = \frac{\pi}{2}, \tag{8.42}$$

leads to the effective propagator

$$U^{\rm eff}(t_f,t_i) = \begin{pmatrix} \cos\Theta(t_f) & 0 & -\sin\Theta(t_f) & 0 \\ 0 & \cos\delta(t_f) & 0 & -i\sin\delta(t_f) \\ \sin\Theta(t_f) & 0 & \cos\Theta(t_f) & 0 \\ 0 & -i\sin\delta(t_f) & 0 & \cos\delta(t_f) \end{pmatrix}. \tag{8.43}$$

The matrix representation of $U^{\text{eff}}(t_f, t_i)$ in the subspace of the bare states $|1\rangle, |3\rangle$ is decoupled from the other states $|2\rangle, |4\rangle$. Therefore, if the initial state of the system is $|\Psi(t_i)\rangle = |1\rangle$, the state vector of the system at the end of the evolution is

$$|\Psi(t_f)\rangle = R(t_f)U^{\text{eff}}(t_f, t_i)|1\rangle = U_f|1\rangle, \tag{8.44}$$

where U_f is the propagator of the system in the subspace spanned by $|1\rangle, |3\rangle$ defined as

$$U_f = \begin{pmatrix} \cos\Theta(t_f) & -\sin\Theta(t_f) \\ \sin\Theta(t_f) & \cos\Theta(t_f)\, e^{i(\theta_S - \theta_P)} \end{pmatrix}. \tag{8.45}$$

The propagator U_f is a one-qubit phase gate for $\Theta(t_f) = 0$, and a one-qubit rotation gate for $\theta_S = \theta_P$. Starting from the initial state $|3\rangle$, the final state of the system is a coherent superposition

$$|\Psi(t_f)\rangle = -\sin\Theta(t_f)|1\rangle + e^{i(\theta_S - \theta_P)}\cos\Theta(t_f)|3\rangle. \tag{8.46}$$

The geometrical phase $\Theta(t_f)$ can be expressed as

$$\begin{aligned} \Theta(t_f) &= \int_{t_i}^{t_f} ds\, \dot{\vartheta}(s)\sin\varphi(s) \\ &= \oint_{\mathcal{C}} \sin\varphi\; d\vartheta \\ &= \oint_{\mathcal{C}} \frac{\Omega_C(\Omega_S d\Omega_P - \Omega_P d\Omega_S)}{(\Omega_P^2 + \Omega_S^2)\sqrt{\Omega_P^2 + \Omega_S^2 + \Omega_C^2}}, \end{aligned} \tag{8.47}$$

where $\mathcal{C}$ is a closed path in a three dimensional space of the three time-dependent parameters $\Omega_P, \Omega_S, \Omega_C$. The corresponding path of the system in this space, starts from the point $\Omega_P = \Omega_S = \Omega_C = 0$, and ends at the same point. For a quantitative analysis of the geometrical phase $\Theta(t_f)$, we assume a Gaussian time-dependence of the Rabi frequencies which satisfies the condition (8.42),

$$\begin{aligned} \Omega_P(t) &= P_0 e^{-(t/T)^2}, \\ \Omega_S(t) &= S_0 e^{-[t/(2T)]^2}, \\ \Omega_C(t) &= C_0 e^{-[(t-\tau)/(4T)]^2}. \end{aligned} \tag{8.48}$$

In general, $\Theta(t_f)$ depends on three parameters: the ratio of peak Rabi frequencies P_0/S_0, C_0/S_0, and the time delay τ between the control pulse and the two other pulses. Figure 8.6 shows that for $\tau = 0$, the final population of the system remains in the initially populated state $|1\rangle$, i.e. $\Theta(t_f) = 0$. In order to transfer the population into a superposition of the states $|1\rangle$ and $|3\rangle$ [non-zero $\Theta(t_f)$] at the end of tripod-STIRAP process, having a *non-zero time delay* is essential (see Fig. 8.7). Although this technique is robust against variations of pulse areas, of detunings from resonances, and of pulse shapes, the control of pulses to obtain a predetermined value of $\Theta(t_f)$ is expected in practice to be difficult.

Implementation of one-qubit quantum gates using static phases

An alternative process on the same system, but with a different pulse sequence, to generate one-qubit quantum gate in a robust way (comparable to STIRAP robustness) has been proposed [151]. It uses the static phases of the laser instead of geometric phases (see chapter 15).

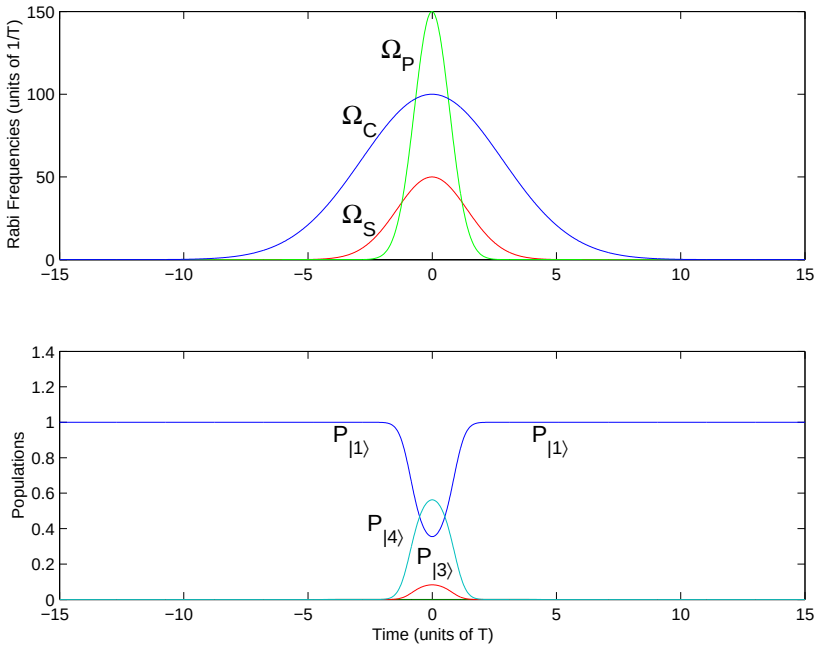

FIG. 8.6 - *The sequence of the pump, Stokes, and control Gaussian-shaped pulses (8.48),* without time-delay *between them, for tripod-STIRAP process which satisfies the conditions (8.42), and the corresponding populations as function of time. We observe at the end of process that the system is in the state* $|1\rangle$*, which means* $\Theta(t_f) = 0$.

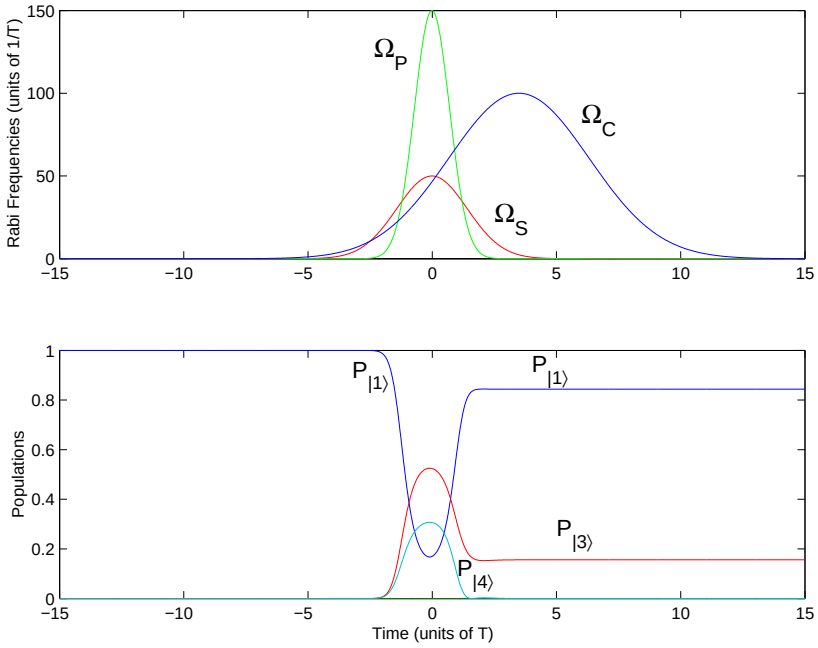

FIG. 8.7 - *As in Fig. 8.6, but with a time delay between the control pulse and pump-Stokes pulses. This time delay is necessary to transfer the population into a superposition of the states* $|1\rangle$ *and* $|3\rangle$ *[non-zero* $\Theta(t_f)$*] at the end of tripod-STIRAP process.*

Chapter 9

Bichromatic adiabatic passage beyond the resonant approximation

In this chapter, we analyze the population transfer induced by a *bichromatic* adiabatic passage. In a two-level system, this means that we use two fields of different frequencies that are both near resonant with the transition. Technically we cannot apply a simple resonant approximation since we have to construct it with a single frequency. In three-state systems, both fields are near resonant with both transitions [153].

Such bichromatic fields induce in the system remarkable properties of multiphoton transfer. For a sufficiently high field amplitude, the system can indeed absorb some photons of one mode and emit these photons to the other mode when the two fields partially overlap. Adiabatic passage allows the control of such multiphoton transfers [69]. The adiabatic Floquet theory is thus here relevant to study these effects.

The technique to generate experimentally the two near resonant frequency with a controllable relative phase through a controlled Doppler shift has been proposed in [154]. The experimental implementation has been realized for the first step, i.e. the complete transfer population (absorption of one photon) [155].

Bichromatic effects with CW lasers in population trapping have been also investigated in [156].

We here first construct the effective bichromatic quasienergy operator in Section 9.1.

We show in Section 9.2 the application of this effect to the deflexion of a two-state atomic beam, which is controlled through the topological quantization of the absorption and emission of the photons. The atomic beam encountering two counterpropagating fields, when absorbing from one field to emitting to the other field, will be indeed deflected by the conservation of the global momentum of the system atom+fields.

Bichromatic STIRAP is studied in Section 9.3.

9.1 The effective quasienergy operator

We study processes with two fields of different carrier frequencies ω_1 and ω_2 which act in resonance (or in quasi-resonance) on the same atomic transition, which are referred to as *bichromatic processes*. They induce dynamical resonances in the system due to the beat frequency

$$\delta = \omega_1 - \omega_2. \tag{9.1}$$

We consider Hamiltonians of the form

$$H(\underline{\omega}t+\underline{\theta}) = H_0 - \mathbf{d}\cdot\left[\sum_{j=1}^{2}\mathbf{e}_j\mathcal{E}_j(t)\cos(\omega_j t+\theta_j)\right] \tag{9.2}$$

where H_0 is the Hamiltonian of the free atomic system of energies E_ℓ, $\ell = 1,\cdots,N$ associated to the states $\{|\ell\rangle\}$ spanning the Hilbert space $\mathcal{H} = \mathbb{C}^N$ on which H_0 and the dipole moment operator $\mathbf{d}$ act. The total electric field, containing two carrier frequencies $\underline{\omega} = (\omega_1,\omega_2)$, is characterized by unit polarization vectors $\mathbf{e}_j$, smooth pulse-shaped envelope functions of time $\underline{\mathcal{E}}(t) = [\mathcal{E}_1(t),\mathcal{E}_2(t)]$ and the initial phases $\underline{\theta} = (\theta_1,\theta_2)$. The interaction is thus characterized by the time-dependent Rabi frequencies $\Omega_j^{(m\ell)}(t) = -\langle m|\mathbf{d}\cdot\mathbf{e}_j|\ell\rangle\,\mathcal{E}_j(t)/\hbar$, $j=1,2$ when the frequency ω_j is quasi-resonant between the states $|m\rangle$ and $|\ell\rangle$. One additionally assumes that the fields are weak enough such that $|\hbar\Omega_j^{(m\ell)}(t)| \ll |E_\ell - E_m|$ for all times, meaning that the nonresonant terms can be neglected. The fields are however sufficiently strong such that, for some $|m\rangle$ and $|\ell\rangle$, the peak Rabi frequency is comparable to the beat frequency: $\max_t\left|\Omega_j^{(m\ell)}(t)\right| \sim |\delta|$. The resonant terms with respect to the frequency difference δ will be kept, since they will produce dynamical resonances.

In the Floquet representation

$$K = -i\hbar\underline{\omega}\cdot\frac{\partial}{\partial\underline{\theta}} + H(\underline{\theta}), \tag{9.3}$$

the effective Hamiltonian will be derived with the following change of variables

$$\begin{cases} \theta = \theta_1 - \theta_2 \\ \theta_a = \theta_2 \end{cases}, \tag{9.4}$$

giving

$$\begin{cases} \partial/\partial\theta_1 = \partial/\partial\theta \\ \partial/\partial\theta_2 = \partial/\partial\theta_a - \partial/\partial\theta \end{cases}$$

and

$$K = -i\hbar\omega_2\frac{\partial}{\partial\theta_a} - i\hbar\delta\frac{\partial}{\partial\theta} + H(\underline{\theta}). \tag{9.5}$$

We will apply specific rotating wave transformations R that will allow us to identify resonant terms and to eliminate the nonresonant ones. We obtain an effective one-mode Floquet Hamiltonian of the form

$$K_{\text{eff}} = -i\hbar\delta\frac{\partial}{\partial\theta} + H_{\text{eff}}(\theta) \simeq R^\dagger K R, \tag{9.6}$$

that will take into account non trivial resonant bichromatic effects with respect to the frequency δ. Although the field intensities are moderate, the system exhibits dynamical resonances that in the case of a single laser are usually encountered only in a strong-field regime.

The dynamics of the atom+field system is determined by the effective one-mode time dependent Schrödinger equation

$$i\hbar\frac{\partial}{\partial t}\psi(\theta,t) = K_{\text{eff}}(t)\psi(\theta,t), \tag{9.7}$$

where $\psi(\theta,t)$ is a N-element column vector. The exact solution will thus be approximated by $R\psi(\theta,t)$.

These bichromatic resonances and their consequences will be studied in two- and three-level systems.

9.2 Two-level systems – Topological quantization of atomic beam deflection

9.2.1 The effective Hamiltonian

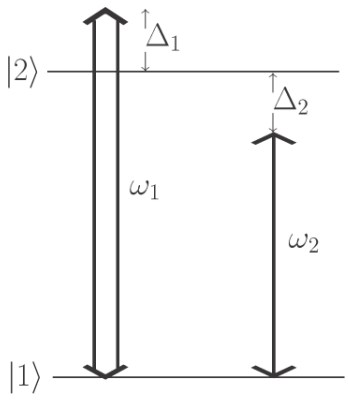

FIG. 9.1 - *Diagram of linkage patterns between two atomic states.*

We consider a two-level system ($E_2 > E_1$) [69] driven by two quasi-resonant fields of detunings $\Delta_j \equiv (E_2 - E_1)/\hbar - \omega_j,\ j = 1, 2$, as depicted in Fig. 9.1. We assume that the dipole moment couples only the two levels: $\langle 1 \left| \mathbf{d} \cdot \mathbf{e}_j \right| 1 \rangle = \langle 2 \left| \mathbf{d} \cdot \mathbf{e}_j \right| 2 \rangle = 0$. The two characteristic Rabi frequencies denoted $\Omega_j(t) = -\langle 1 \left| \mathbf{d} \cdot \mathbf{e}_j \right| 2 \rangle \mathcal{E}_j(t)/\hbar,\ j = 1, 2$ involve the same transition $1 - 2$. In the basis $\{|1\rangle, |2\rangle\}$, the Hamiltonian reads

$$H(\underline{\theta}) = \begin{bmatrix} E_1 & 0 \\ 0 & E_2 \end{bmatrix} + \hbar \left(\Omega_1(t) \cos\theta_1 + \Omega_2(t) \cos\theta_2 \right) \begin{bmatrix} 0 & 1 \\ 1 & 0 \end{bmatrix}. \tag{9.8}$$

The beat frequency is here $\delta \equiv \omega_1 - \omega_2 = \Delta_2 - \Delta_1$. We study the non-perturbative regime $|\delta| \lesssim \max_t |\Omega_j(t)| \ll (E_2 - E_1)/\hbar, \quad j = 1, 2$.

We use the rotating wave transformation dressing the state $|2\rangle$ with minus one ω_1- photon:

$$R = \begin{bmatrix} 1 & 0 \\ 0 & \mathrm{e}^{-i\theta_1} \end{bmatrix}. \tag{9.9}$$

Applying this transformation to the Floquet Hamiltonian (9.3) gives

$$\begin{aligned} R^\dagger K R \ = \ & -i\hbar \underline{\omega} \cdot \frac{\partial}{\partial \underline{\theta}} + \frac{\hbar}{2} \begin{bmatrix} 0 & \Omega_1 \\ \Omega_1 & 2\Delta_1 \end{bmatrix} + \frac{\hbar\Omega_2}{2} \begin{bmatrix} 0 & \mathrm{e}^{-i(\theta_1 - \theta_2)} \\ \mathrm{e}^{i(\theta_1 - \theta_2)} & 0 \end{bmatrix} \\ & + \frac{\hbar\Omega_1}{2} \begin{bmatrix} 0 & \mathrm{e}^{-2i\theta_1} \\ \mathrm{e}^{2i\theta_1} & 0 \end{bmatrix} + \frac{\hbar\Omega_2}{2} \begin{bmatrix} 0 & \mathrm{e}^{-i(\theta_1 + \theta_2)} \\ \mathrm{e}^{i(\theta_1 + \theta_2)} & 0 \end{bmatrix}, \end{aligned} \tag{9.10}$$

which can be approximated, after the transformation (9.4), by the effective Floquet Hamiltonian [157]

$$K_{\text{eff}} = -i\hbar\delta \frac{\partial}{\partial \theta} + \frac{\hbar}{2} \begin{bmatrix} 0 & \Omega_1 \\ \Omega_1 & 2\Delta_1 \end{bmatrix} + \frac{\hbar\Omega_2}{2} \begin{bmatrix} 0 & \mathrm{e}^{-i\theta} \\ \mathrm{e}^{i\theta} & 0 \end{bmatrix}. \tag{9.11}$$

Since $-i\hbar\omega_2 \partial/\partial\theta_a$ is decoupled from the rest of the Floquet Hamiltonian, it acts trivially and can be omitted. This effective model is valid only if two different frequencies are assumed.

The derivative term represents the relative number of photon pairs, one ω_1-photon minus one ω_2-photon. Thus the absorption of one "effective photon" of frequency δ in the effective model (9.11) corresponds in the complete model (9.3) to the absorption of one photon of frequency ω_1 and the emission of one photon of frequency ω_2. If the two laser fields are counterpropagating, perpendicularly to the atomic beam, this double photon exchange results in a net transfer of momentum to the atom of $\hbar(\omega_1+\omega_2)/c$ which manifests as a deflection of the beam.

The second term of the effective Hamiltonian (9.11) is the usual RWA Hamiltonian (associated to the ω_1 field), with eigenvalues $2\lambda^0_\pm = \hbar\Delta_1 \pm \hbar\sqrt{(\Delta_1)^2+(\Omega_1)^2}$. The third term can be viewed as a perturbation of this RWA Hamiltonian.

The analysis of the dynamics consists of (i) the calculation of the quasienergy surfaces of the effective quasienergy operator as a function of the two Rabi frequencies Ω_1 and Ω_2, (ii) the analysis of their topology, and (iii) the application of adiabatic principles to determine the dynamics of processes in view of the topology of the surfaces.

9.2.2 Eigenenergy surface topology

In the following, we will consider for simplicity the case $\Delta_1 = -\Delta_2$ so that $\delta = -2\Delta_1$. For frozen values of the two fields Ω_1 and Ω_2, we calculate Floquet states and quasienergies by diagonalizing K_{eff}. The eigenelements can be labelled with two indices: one, denoted n, refers to the levels of the atom, and another one denoted k, refers to the relative photon numbers. The index k stands for the number of the ω_1-photons absorbed and the number of ω_2-photons emitted. The eigenvalues and eigenvectors have the following property of periodicity:

$$\lambda_{n;k,-k} = \lambda_{n;0,0} + k\hbar\delta, \quad |n;k,-k\rangle_{\text{eff}} = |n;0,0\rangle_{\text{eff}} \exp(ik\theta) .$$

The eigenelements appear as two families, each of which consists of an infinite set of eigenvalues with equal spacing $\hbar\delta$. The eigenstates of K_{eff}, $|1;k,-k\rangle_{\text{eff}}$ and $|2;k,-k\rangle_{\text{eff}}$, can thus be labelled by $|1;k,-k\rangle$ and $|2;-1+k,-k\rangle$, $k\in\mathbb{Z}$ in the original basis of (9.3). If one starts with the initial state $|n_i;0,0\rangle$, the state $|n_f;k_1,k_2\rangle$ at the end of the process will characterize the atom in the state $|n_f\rangle$ with emission of k_i photons of frequency ω_i if $k_i>0$ or absorption of k_i photons if $k_i<0$, $i=1,2$.

On Fig. 9.2, we display eigenenergy surfaces, calculated numerically, as functions of the scaled Rabi frequencies Ω_1/δ and Ω_2/δ, assumed positive without loss of generality. Together with the adiabatic analysis, the topology of these surfaces gives insight into the various atomic population and photon transfers that can be produced by choosing appropriately the temporal evolution of the pulses. The process starts in the state $|1;0,0\rangle$, i.e. the lowest atomic state with zero ω_1 and ω_2 photons. Its energy is shown as the starting point of various paths. We define the *transfer state* as the Floquet eigenvector which is adiabatically followed, i.e. on which the population resides during the dynamics. There are two infinite families of quasienergy surfaces, that are constructed by the translations by $\hbar\delta k$, $k\in\mathbb{Z}$ of two surfaces. Any two neighboring surfaces have points of contact that are conical intersections. In the present model all the points of intersection are located either at the line $\Omega_1=0$ or at the line $\Omega_2=0$, corresponding to the situations where only one of the laser fields is interacting with the atom. Besides these true crossings, the quasienergy surfaces display avoided crossings. These true crossing and avoided crossings are associated with dynamical resonances as we will show below.

Three kinds of adiabatic paths can occur in this topology, as shown in Fig. 9.2 which displays three examples of adiabatic paths leading to three different final atomic population and photon transfers. They are labelled as (a), (b) and (c).

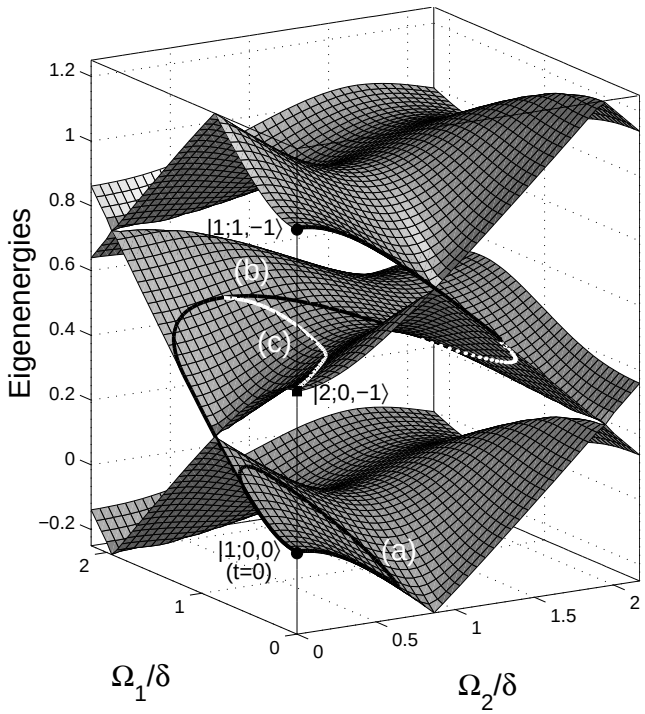

FIG. 9.2 - *Quasienergy surfaces (in units of δ) as functions of Ω_1 and Ω_2 for $\delta = -2\Delta_1 = 2\Delta_2$. Three different paths (denoted a, b and c) depending on the temporal evolution of the pulses are depicted.*

For the curve (a), the shifts of the eigenvalues are smaller than the energy of the first intersections. As a consequence, the path stays on a single surface, and at the end the system returns to the initial state, without any final transfer of photons nor of the atomic population.

The curve (b) corresponds to shifts that are larger than the first intersections. The crossing of the first intersection as Ω_1 increases with $\Omega_2 = 0$ brings the population into the first upper quasienergy surface. Turning on and increasing the amplitude Ω_2 (while Ω_1 decreases) moves the path across this surface. When the second field Ω_2 decreases, the curve crosses an intersection (with $\Omega_1 = 0$) that brings the system to the third level surface, on which the curve stays until the end of the pulse Ω_2. The transfer state is finally connected to state $|1; 1, -1\rangle$: there is no transfer of atomic population, but one ω_2-photon has been absorbed and one ω_1-photon has been emitted at the end of the process. This path is produced with two delayed pulses of approximately the same peak amplitudes. Two dynamical resonances occur in this system. Each is crossed twice, appearing as one true crossing and one avoided crossing. This appears clearer in the temporal representation of the quasienergies shown in Fig. 9.4b (see below for details of the dynamics). They can be described as follows: the field 1 dynamically shifts the eigenvalues which become resonant with the field 2. This resonance is mute when the field 2 is off (left true crossing) and becomes effective when the field 2 is on (left avoided crossing). The second dynamical resonance occurs symmetrically from dynamical Stark shift due to field 2 which makes the eigenvalues resonant with the field 1. The topology shows the connection of the adiabatic paths related to the preceding dynamical resonances.

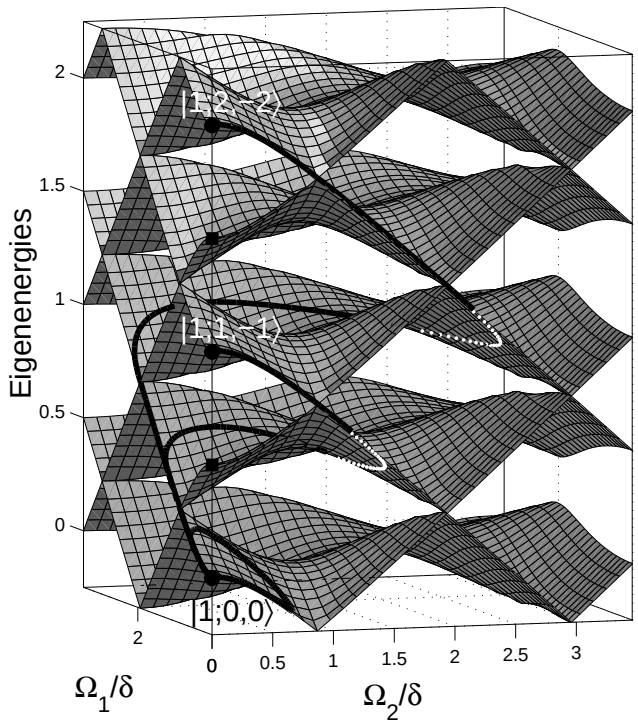

FIG. 9.3 - *Same figure as 9.2, but for stronger field amplitudes*

If the field amplitudes are taken even larger, such that two dynamical resonances are crossed (corresponding to the true crossings when Ω_1 rises with $\Omega_2 = 0$ and when Ω_2 decreases with $\Omega_1 = 0$), the final state is $|1; 2, -2\rangle$, i.e. there is no atomic population transfer but an absorption of two ω_2-photons and an emission of two ω_1-photons. This path is shown in Fig. 9.3. This kind of process can be generalized to paths yielding the connectivity of the transfer state to $|1; k, -k\rangle$, i.e. the emission of k ω_1-photons and the absorption of k ω_2-photons (k positive for pulse 1 before pulse 2 and negative for pulse 2 before pulse 1), with no atomic population transfer.

The path (c) in Fig. 9.2 involves a crossing of one conical intersection of the two described above. The first resonance is crossed by the rising pulse 1 (with $\Omega_2 = 0$). The second pulse is chosen with a smaller peak amplitude in order to avoid the passage through the resonance that would lead the system to the third level surface. This leads to an atomic population transfer, accompanied with absorption of one ω_2 -photon, since the path ends at $|2; 0, -1\rangle$. This can be generalized for upper and lower paths: the connectivity leads to $|2; -1+k, -k\rangle$, with k positive (pulse 1 before smaller pulse-2 amplitude) or negative or zero integer (pulse 2 before smaller pulse-1 amplitude).

The topology of the quasienergy surfaces thus shows which appropriate delays and peak amplitudes induce desired atomic population and photon transfers. In the adiabatic regime, these loops can be classified into topologically inequivalent classes. If the evolution is adiabatic, all paths of a given class lead to the same end effect. This property underlies the robustness of the process.

9.2.3 Analytical construction of the quasienergies

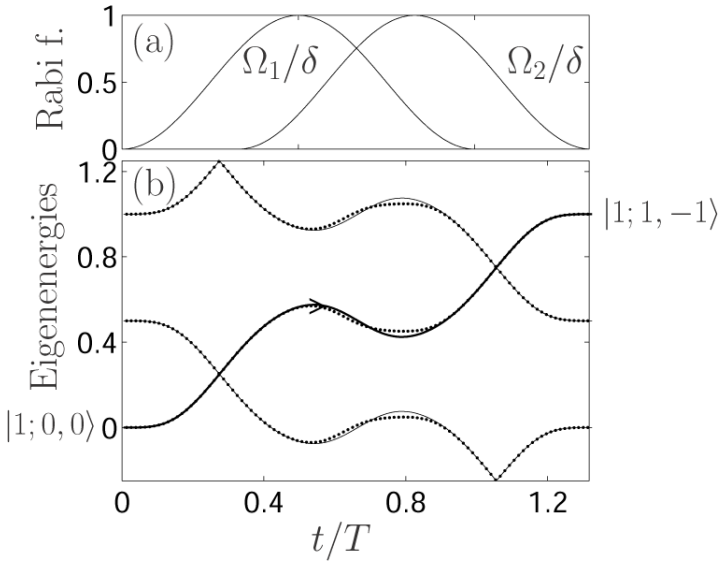

FIG. 9.4 - *(a) Rabi frequencies (in units of δ) from squared trig function envelopes. (b) Quasienergy curves (in units of δ), corresponding to the path b of Fig. 9.2 ($\Omega_{\max} = 1.5\delta$) from formula (9.12) (dotted lines) and exact numerical result (full line). The arrow indicates the adiabatic path (thick line).*

With the technique combining the rotating wave transformations and contact transformations developed in Section 5, one can treat accurately the dynamical resonances and construct approximately the quasienergies. If we take into account the first two dynamical resonances by appropriate RWT's [associated with the path (b)], one obtains the following explicit expression for the quasienergy surfaces

$$\frac{\lambda_{\pm,k}}{\hbar} = \frac{\Delta_1}{2} + k\delta \mp \left[\frac{1}{4}\left(\sqrt{A} - \delta\right)^2 + \frac{\left(\varepsilon^2 \Omega_1 \lambda_-^0\right)^2}{\hbar^2 A}\right]^{\frac{1}{2}} \tag{9.12}$$

with $A = \left\{\left[\left(\Delta_1\right)^2 + \left(\Omega_1\right)^2\right]^{1/2} - \delta\right\}^2 + 4\left(\varepsilon\lambda_-^0/\hbar\right)^2$ and $2\varepsilon = -\Omega_2/\sqrt{\left(\Delta_1\right)^2 + \left(\Omega_1\right)^2}$. Figure 9.4b displays these eigenvalues as functions of time for the dynamics described below. They are in close agreement with the exact eigenvalues calculated numerically from the Hamiltonian (9.11). The explicit consideration of the small perturbative corrections from the full model (9.3) by contact transformations does not change the topology of the surfaces in the sense that the conical intersections are not removed but only slightly shifted.

This systematic method can also be applied to treat the next dynamical resonances occurring for higher field amplitudes.

9.2.4 Dynamics and topological quantization of the number of exchanged photons

The path described above can be constructed by two smooth pulses, associated to the Rabi frequencies $\Omega_1(t)$ and $\Omega_2(t)$, with a time delay τ. To a sequence of such pulses corresponds

a closed loop in the parameter plane Ω_1 and Ω_2. Each of the two black curves (labelled a and b) correspond to a sequence of two smooth pulses of equal length T and equal peak Rabi frequencies $\Omega_{\max} \equiv \max_t [\Omega_1(t)] = \max_t [\Omega_2(t)]$, separated by a delay such that the pulse 1 is switched on before the pulse 2. This path has been redrawn as a function of time on Fig. 9.4b, using $\sin^2$ envelopes of length $T = 100/\delta$ and a delay of $\tau = T/3$, shown on Fig. 9.4a. Details of this dynamics of bichromatic processes, in particular in relation with the initial condition for the photon field, are given and discussed in the next subsection. The path (c) needs two pulses with different peak amplitudes.

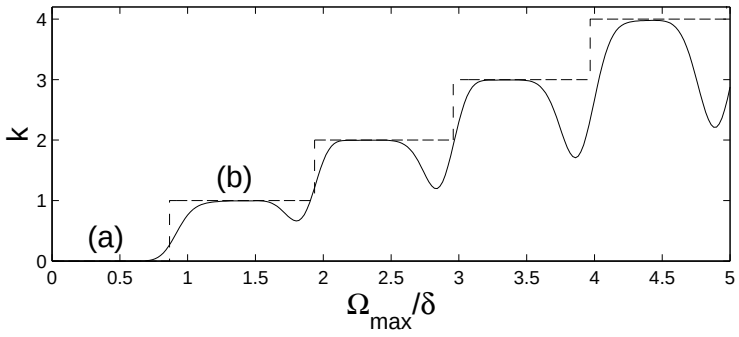

FIG. 9.5 - *Comparison of the number k of effective photons emitted at the end of the process [Eq. 9.13] (dashed line) with the average number of effective photons from the exact numerical result (full line) . The plateaux labelled (a) and (b) refer to the two paths of Fig. 9.2 for pulse length $T = 100/\delta$ and delay $\tau = T/3$.*

For equal peak amplitudes, we display in Fig. 9.5 the final average effective number k of exchanged photons as a function of the peak Rabi frequencies, calculated numerically by solving the Floquet time-dependent Schrödinger equation. This shows the consequence of the topology described above. Since the connectivity of the transfer state to $|1; k, -k\rangle$ is based on the crossings, we can determine analytically the final number of effective photons k as a function of the peak Rabi frequencies $\Omega_{\max}/\delta$ (taken equal) in the purely adiabatic regime:

$$k = \text{Integer part of } \sqrt{(\Omega_{\max}/\delta)^2 + (\Delta_1/\delta)^2}. \tag{9.13}$$

It predicts the adiabatic plateaux of Fig. 9.5, that can be interpreted as a topological quantization of the number of exchanged photons. The dips are due to nonadiabatic Landau-Zener transitions when the pulse overlap is in the neighborhood of the intersections. With a configuration of counterpropagating laser fields, perpendicular to an atomic beam, this translates into the possibility of deflection of the beam by the quantized transfer of a momentum $k\hbar(\omega_1+\omega_2)/c$.

9.3 Three-level systems: Bichromatic STIRAP

The full semi-classical Hamiltonian (9.2) contains

$$H_0 = \begin{bmatrix} E_1 & 0 & 0 \\ 0 & E_2 & 0 \\ 0 & 0 & E_3 \end{bmatrix}, \qquad \mathbf{d} = \begin{bmatrix} 0 & \mathbf{d}_{12} & 0 \\ \mathbf{d}_{21} & 0 & \mathbf{d}_{23} \\ 0 & \mathbf{d}_{32} & 0 \end{bmatrix}, \tag{9.14}$$

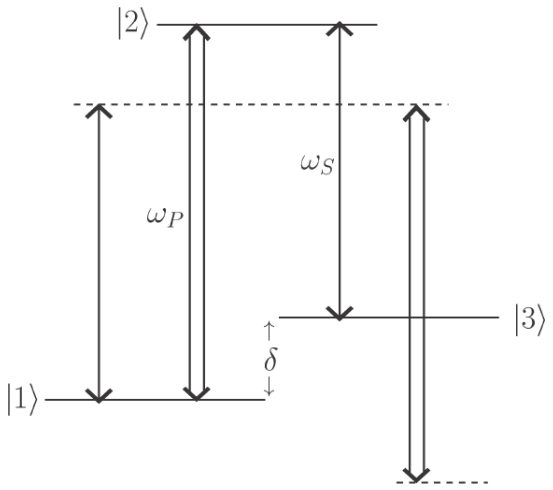

FIG. 9.6 - *Diagram of linkage patterns between three atomic states (full horizontal lines), showing pump (P or 1) and Stokes (S or 2) laser frequencies.*

which are respectively the Hamiltonian of the free three-level system, acting on the Hilbert space $\mathcal{H} = \mathbb{C}^3$ spanned by the vector set $\{|1\rangle, |2\rangle, |3\rangle\}$, and the dipole moment operator (coupling transitions 1-2 and 2-3, but not 1-3). We take for simplicity equal coupling for the transitions 1-2 and 2-3. The system is characterized by the time-dependent Rabi frequencies $\hbar\Omega_1(t) = -\langle 1|\mathbf{d}\cdot\mathbf{e}_1|2\rangle\mathcal{E}_1(t) = -\langle 2|\mathbf{d}\cdot\mathbf{e}_1|3\rangle\mathcal{E}_1(t)$ and $\hbar\Omega_2(t) = -\langle 1|\mathbf{d}\cdot\mathbf{e}_2|2\rangle\mathcal{E}_2(t) = -\langle 2|\mathbf{d}\cdot\mathbf{e}_2|3\rangle\mathcal{E}_2(t)$. We consider the situation where the frequency ω_1 is one-photon quasi-resonant with the 1-2 transition, and the frequency ω_2 is one-photon quasi-resonant with the 2-3 transition. We study the intermediate field intensities regime

$$|\delta| \lesssim \max_t \left[|\Omega_1(t)|, |\Omega_2(t)|\right] \ll (E_2 - E_1)/\hbar, (E_3 - E_2)/\hbar. \tag{9.15}$$

In particular we consider $\Lambda-$systems, depicted in Fig. 9.6, where the lasers 1 and 2 are respectively called *pump* and *Stokes* lasers. We use here resonant frequencies $\hbar\omega_1 = E_2 - E_1$, $\hbar\omega_2 = E_2 - E_3$ so that the two-field combination maintains the two-photon resonance between the states $|1\rangle$ and $|3\rangle$, as for the usual STIRAP process [71]. We have thus here $\delta \equiv \omega_1 - \omega_2 = (E_3 - E_1)/\hbar$. The main results of this part can be found in [153, 158, 109].

9.3.1 The effective Hamiltonian

To obtain the effective Floquet Hamiltonian, we apply the rotating wave transformation (RWT)

$$R(\underline{\theta}) = \begin{bmatrix} 1 & 0 & 0 \\ 0 & \mathrm{e}^{-i\theta_1} & 0 \\ 0 & 0 & \mathrm{e}^{i(\theta_2-\theta_1)} \end{bmatrix}, \tag{9.16}$$

to obtain (setting $E_1 = 0$ as the reference of the energies)

$$R^\dagger K R = -i\hbar\underline{\omega}\cdot\frac{\partial}{\partial\underline{\theta}} + \frac{\hbar}{2}\begin{bmatrix} 0 & \Omega_1 & 0 \\ \Omega_1 & 0 & \Omega_2 \\ 0 & \Omega_2 & 0 \end{bmatrix} + V_1(\underline{\theta}) \tag{9.17}$$

with

$$V_1(\underline{\theta}) = \frac{\hbar}{2}\begin{bmatrix} 0 & \Omega_1 e^{-2i\theta_1} & 0 \\ \Omega_1 e^{2i\theta_1} & 0 & \Omega_2 e^{2i\theta_2} \\ 0 & \Omega_2 e^{-2i\theta_2} & 0 \end{bmatrix} + \frac{\hbar}{2}\begin{bmatrix} 0 & \Omega_2 e^{-i(\theta_1+\theta_2)} & 0 \\ \Omega_2 e^{i(\theta_1+\theta_2)} & 0 & \Omega_1 e^{i(\theta_1+\theta_2)} \\ 0 & \Omega_1 e^{-i(\theta_1+\theta_2)} & 0 \end{bmatrix} + \frac{\hbar}{2}\begin{bmatrix} 0 & \Omega_2 e^{-i(\theta_1-\theta_2)} & 0 \\ \Omega_2 e^{i(\theta_1-\theta_2)} & 0 & \Omega_1 e^{-i(\theta_1-\theta_2)} \\ 0 & \Omega_1 e^{i(\theta_1-\theta_2)} & 0 \end{bmatrix}. \quad (9.18)$$

The usual RWA consists in neglecting the $\underline{\theta}$-dependent operator V_1. The first term of V_1 (9.18) contains the counter-rotating terms of the pump laser on the 1-2 transition and of the Stokes laser on the 2-3 transition. The next two terms correspond to the interactions of the pump laser on the 2-3 transition and of the Stokes laser on the 1-2 transition. Following the hypothesis (9.15), we neglect the first two terms and keep the last term which becomes large (see [109] for details) when $\max_t [|\Omega_1(t)|, |\Omega_2(t)|]$ approaches or overcomes $|\delta|$. The (approximate) effective one-mode Floquet Hamiltonian is thus

$$K_{\text{eff}} = -i\hbar\delta\frac{\partial}{\partial\theta} + \frac{\hbar}{2}\begin{bmatrix} 0 & \Omega_1 & 0 \\ \Omega_1 & 0 & \Omega_2 \\ 0 & \Omega_2 & 0 \end{bmatrix} + \frac{\hbar}{2}\begin{bmatrix} 0 & \Omega_2 e^{-i\theta} & 0 \\ \Omega_2 e^{i\theta} & 0 & \Omega_1 e^{-i\theta} \\ 0 & \Omega_1 e^{i\theta} & 0 \end{bmatrix}. \quad (9.19)$$

The derivation term is the relative number operator for pairs of photons, one pump-field photon minus one Stokes-field photon. The second term is the well-known RWA Hamiltonian (dressed Hamiltonian used in the usual STIRAP) and the third one can be viewed as a perturbation of this RWA Hamiltonian.

We choose to have zero pump and Stokes photon at the beginning of the process. The initial condition is thus $|1;0,0\rangle$, which corresponds here to $|\psi(t=t_i)\rangle = |1;0\rangle$ for the effective one-mode Schrödinger equation (9.7). At each value of Ω_1 and Ω_2, the eigenvalues of K_{eff} can be decomposed as $\lambda_{n;-k,k} = \lambda_{n;0,0} - k\delta = \lambda_{n;0,0} - k\omega_1 + k\omega_2$ and their respective eigenvectors as $|n;-k,k\rangle_{\text{eff}} = |n;0,0\rangle_{\text{eff}} \exp[-ik\theta]$. The eigenstates of K_{eff} $|1;-k,k\rangle_{\text{eff}}$, $|2;-k,k\rangle_{\text{eff}}$ and $|3;-k,k\rangle_{\text{eff}}$ can thus be respectively labelled by $|1;-k,k\rangle$, $|2;-1-k,k\rangle$ and $|3;-1-k,k+1\rangle$ $k \in \mathbb{Z}$ in the original basis of (9.3). If one starts with the initial state $|n_i;0,0\rangle$, the state $|n_f;k_1,k_2\rangle$ at the end of the process will characterize the atom in the state $|n_f\rangle$ with emission of k_i photons of frequency ω_i if $k_i > 0$ or absorption of k_i photons if $k_i < 0$, $i = 1,2$. The eigenvalues appear as three families with periodic replicas (with period $2\pi/\delta$) and yield one-mode Floquet zones which can interact each other.

9.3.2 Eigenenergy surface topology

In Fig. 9.7, we display quasienergy surfaces, calculated numerically, as functions of the scaled Rabi frequencies Ω_1/δ and Ω_2/δ (assumed positive without loss of generality). The process starts in the state $|1;0,0\rangle$, i.e. the lowest atomic state with zero ω_1 and ω_2 photons. Its energy (which is zero in Fig. 9.7) is shown as the starting point of various paths. There are three infinite families of quasienergy surfaces, constructed by the translations by $\hbar\delta k$, $k \in \mathbb{Z}$ of three surfaces. The surfaces exhibit conical intersections between two neighbours. In the present model all the points of intersection are located either at the line $\Omega_1 = 0$ or at the line $\Omega_2 = 0$, corresponding to the situations where only one of the laser fields is interacting with the atom. Besides these true crossings, the quasienergy surfaces display avoided crossings. These crossings

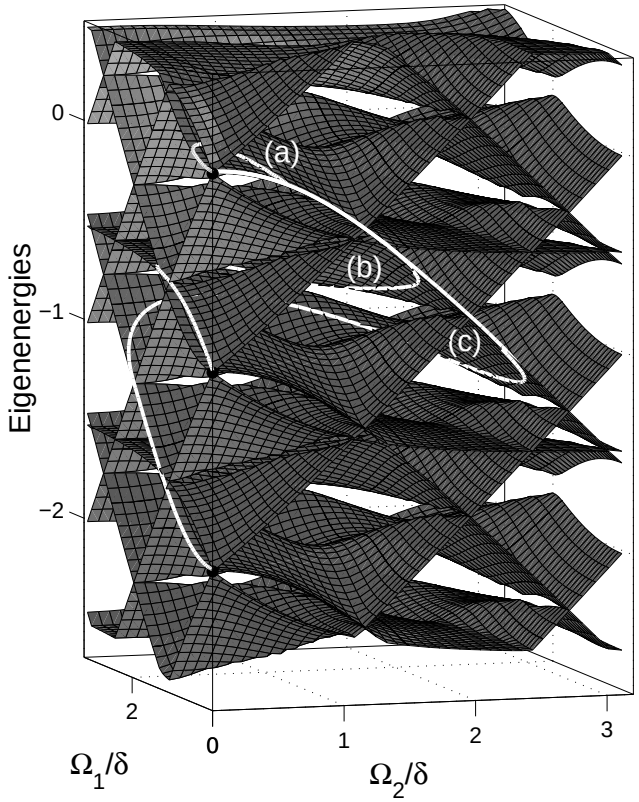

FIG. 9.7 - *Quasienergy surfaces (in units of δ) as functions of Ω_1/δ and Ω_2/δ. Three characteristic paths are shown, all starting at the same state of energy zero, and with a sequence of pulses Ω_1 - Ω_2 of different peak amplitudes: path (a) corresponding to a STIRAP-like process, whose dynamics is shown in Figs 9.8 and 9.9, is of relatively small amplitude and makes a small loop in a single eigenenergy surface; path (b) giving a superposition of states $(|1;-1,1\rangle+|2;-2,1\rangle)/\sqrt{2}$ (of energy $-\delta$); and path (c) giving a STIRAP-like process accompanied with three ω_1- photons absorbed and three ω_2- photons emitted, whose dynamics is shown in Figs 9.10 and 9.11.*

and avoided crossings are also associated with dynamical resonances of the same type as the ones shown above in the two-level system.

The lifting of the degeneracy in the Ω_1 or Ω_2 directions is the same as in the case of the usual STIRAP, since this lifting of degeneracy occurs for very small field intensities: The lifting of degeneracy is such that the state solution is adiabatically connected to $|1;0,0\rangle$ in the Ω_2 direction. We study below the conditions yielding complete population transfer from $|1\rangle$ to $|3\rangle$, for pulses in counterintuitive orders, i.e. for delayed Ω_1 (pump pulse) switching on *after* Ω_2 (Stokes pulse).

Figure 9.7 shows that for $\max_t \Omega_1(t) \sim \max_t \Omega_2(t) < \delta$, we recover a STIRAP-type path (denoted as path a), i.e. connecting $|1;0,0\rangle$ to $|3;-1,1\rangle$. The creation of degeneracy is indeed such that the middle state (connected to the energy zero) is adiabatically connected to $|3;-1,1\rangle$ in the Ω_1 direction. The upper and lower states (connected to the energy zero) are respectively connected to the superpositions of states: $\left(|1;0,0\rangle + |2;-1,0\rangle\right)/\sqrt{2}$ and $\left(|1;0,0\rangle - |2;-1,0\rangle\right)/\sqrt{2}$, in the Ω_1 direction. In the case of path a, the last term of the Hamiltonian (9.19) can be seen as a small perturbation of the RWA Hamiltonian of the standard resonant STIRAP. This has been studied in details in [109]. The effect of this perturbation is a distortion of the path (see Fig. 9.9b for a time evolution of this path). The dynamics associated to this path is studied below.

Increasing the intensity of Ω_2, we obtain a path (path b in Fig. 9.7) connecting $|1;0,0\rangle$ to the superposition of states $\left(|1;-1,1\rangle + |2;-2,1\rangle\right)/\sqrt{2}$ (of energy $-\delta$). Increasing again the intensity of Ω_2, we obtain a path (path c) connecting $|1;0,0\rangle$ to $|3;-3,3\rangle$ (of energy -2δ). This is similar to the usual STIRAP in the sense that this path allows one to transfer the atomic population from $|1\rangle$ to $|3\rangle$, however with the nontrivial effect of an absorption of three ω_1-photons and an emission of three ω_2-photons. For higher intensities of Ω_2 we can generalize the preceding connections. In summary, the topology shows two kinds of adiabatic connections: (i) from $|1;0,0\rangle$ to $\left(|1;-(2k+1),2k+1\rangle + |2;-(2k+2),2k+1\rangle\right)/\sqrt{2}$ and (ii) from $|1;0,0\rangle$ to $|3;-(2k+1),2k+1\rangle$, $k \geq 0$.

9.3.3 Dynamics

We study the dynamics for the complete transfer to state $|3\rangle$. The dynamics is considered either with the semiclassical Schrödinger equation

$$i\hbar\frac{\partial}{\partial t}\phi(t) = H_{\text{eff}}(t)\phi(t), \tag{9.20}$$

with the effective time dependent Hamiltonian, constructed with K_{eff} (9.19)

$$H_{\text{eff}} = \frac{\hbar}{2}\begin{bmatrix} 0 & \Omega_1 + \Omega_2 e^{-i\delta t} & 0 \\ \Omega_1 + \Omega_2 e^{i\delta t} & 0 & \Omega_2 + \Omega_1 e^{-i\delta t} \\ 0 & \Omega_2 + \Omega_1 e^{i\delta t} & 0 \end{bmatrix} \tag{9.21}$$

or with the Floquet Schrödinger equation (9.7) with the effective time dependent quasienergy Hamiltonian (9.19). We recall that the semiclassical Schrödinger equation (9.20) is equivalent to the Floquet Schrödinger equation (9.7) with a coherent state as the initial condition for the photon field. Studying the Floquet Schrödinger equation (9.7) with a number state as the initial condition for the photon field allows one to characterize the dynamics by each path considered above. It is important to note that in these examples *the information on the number of photons*

exchanged with the system, obtained from the calculation with the number state as the initial condition, is still valid at the end of the pulse for a coherent state as an initial condition.

We consider two specific conditions, one for which the semiclassical and the Floquet approaches are equivalent (which is the case for the STIRAP configuration) with respect to the number of photons exchanged at the end of the process, and another one for which the Floquet theory brings the additional information of multiphoton processes.

To ensure that the interactions have a finite duration, we consider truncated $\sin^2$ envelopes. Time and frequency are scaled with respect to δ. The scaled pulse length is set to $T = 100/\Omega_0$ and the delay $\tau = 0.33T$. The pulses have to be applied in the so-called counterintuitive order: the ω_2- Stokes pulse precedes the ω_1- pump pulse with the delay τ. To fulfill the standard adiabatic condition, the relevant Rabi frequencies Ω have to be sufficiently large $\Omega T \gg 1$.

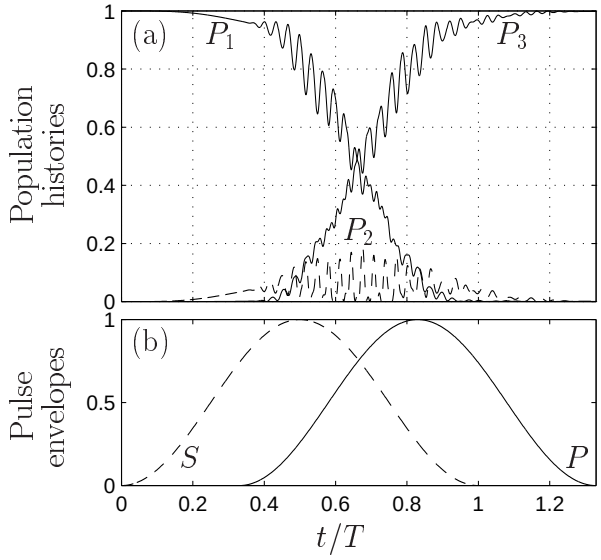

FIG. 9.8 - *From the semiclassical Schrödinger equation, (a) population histories $P_n(t)$ for $n = 1, 2, 3$ with $\delta = 2\Omega_0$ and $\Omega_{\max} = \Omega_0$ (top frame) and excitation by trig function pulse envelopes (of length $T = 100/\Omega_0$ and delay $0.33T$) with pump (full line) before Stokes (dashed line) shown in bottom frame (b). Population transfer $P_3(\infty)$ to bare state $|3\rangle$ is nearly complete.*

For the parameters $\delta = 2\Omega_0$ and $\Omega_{\max} = \Omega_0$, corresponding to the path (a) on the surfaces in Fig. 9.7, we show in Fig. 9.8 the solution of the semiclassical Schrödinger equation (9.20). It features a STIRAP-like process inducing a complete population transfer for this choice of the delays. Two zones of the quasienergy spectrum associated to the surfaces of Fig. 9.7 are pictured as a function of time in Fig. 9.9b. We notice that the state $|1; 0, 0\rangle$ is adiabatically connected to the final target state $|3; -1, 1\rangle$. This implies a complete population transfer from the bare state $|1\rangle$ to the bare state $|3\rangle$ with absorption of one pump photon and emission of one Stokes photon at the end of the process.

This is confirmed by the numerical solution of the Floquet Schrödinger equation (9.7) with a number state as the initial condition for the photon field $|1; 0, 0\rangle$: It shows that the solution statevector $\psi(t)$ (the transfer state, which in the bare basis is given by $R\psi(\theta, t)$) mainly projects on the transfer eigenvector during the process. Additional informations of the Floquet solution during time are shown on Fig. 9.9a and 9.9c. Figure 9.9a displays the probabilities of being in

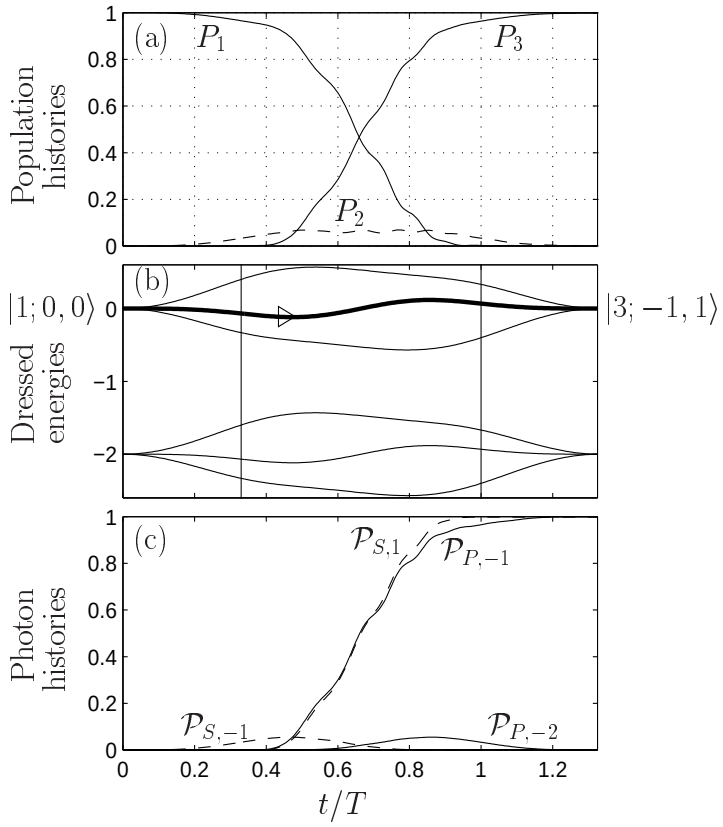

FIG. 9.9 - *From the Floquet Schrödinger equation, with the same parameters as in Fig. 9.8, (a) population histories $P_n(t)$ for $n = 1, 2, 3$ (top frame), (c) photon histories (bottom frame), associated to the quasienergy spectrum in middle frame (b). The arrow characterizes the transfer eigenvector. Vertical lines indicate where the pump pulse starts and the Stokes pulse ends.*

the bare states 1, 2 and 3:

$$P_n = \sum_{k_P,k_S} |\langle n; k_P, k_S|R|\psi(t)\rangle_{\mathcal{K}}|^2, \quad n = 1,2,3 \tag{9.22a}$$

$$= \frac{1}{(2\pi)^2}\int_0^{2\pi} d\theta_1 \int_0^{2\pi} d\theta_2 \; |\langle n|R\psi(t)\rangle_{\mathcal{H}}|^2. \tag{9.22b}$$

Figure 9.9c shows the respective probabilities of one and two ω_1- pump photon absorption $\mathcal{P}_{P,-1}$, $\mathcal{P}_{P,-2}$, and of one ω_2- Stokes photon emission and absorption $\mathcal{P}_{S,1}$, $\mathcal{P}_{S,-1}$, defined with the respective formulas of the probabilities of ℓ ω_1- photons emissions and of ℓ ω_2- photons emissions

$$\mathcal{P}_{P,\ell} = \sum_{n,k_2} |\langle n; \ell, k_2|R|\psi(t)\rangle_{\mathcal{K}}|^2, \tag{9.23a}$$

$$\mathcal{P}_{S,\ell} = \sum_{n,k_1} |\langle n; k_1, \ell|R|\psi(t)\rangle_{\mathcal{K}}|^2. \tag{9.23b}$$

The other probabilities of photon emissions or absorptions are negligible. During the process, we remark that small transient ω_1- and ω_2- photon absorption probabilities arise. An early

ω_2- photon absorption is observed, coinciding exactly with the (negative) shift of the transfer eigenvector. The first effects of the ω_2- pulse are indeed (i) to split the unpopulated Floquet states connected to $|2\rangle$ and $|3\rangle$, and (ii) to produce a Stark shift of the Floquet state connected to $|1\rangle$ (the early part of the transfer state), which is equivalent to a partial absorption of a ω_2- photon. Symmetrically, a late ω_1- photon absorption occurs. It is due to a (positive) Stark shift of the Floquet state connected to $|3\rangle$ (the late part of the transfer state). Arising near the end of the process, for which one ω_1- photon has already been absorbed, it leads to a partial absorption of a second ω_1- photon. At the end of the process the complete population transfer from state $|1\rangle$ to state $|3\rangle$ is accompanied by the loss of a ω_1- photon and the gain of a ω_2- photon. Thus the final result is not different from the semiclassical result.

Comparing Figs. 9.8a and 9.9a, we notice that, as expected, the solution of the Floquet Schrödinger equation, with a number state as initial condition for the photon field, *averages* the solution of the semiclassical Schrödinger equation, with respect to the formula (9.22b).

We now study the situation when the detuning from the transition frequencies satisfies $\delta < \Omega_{\max}$ so that different Floquet zones cross.

To that effect, we choose the parameters $\delta = 2\Omega_0$ and $\Omega_{\max} = 4.4\Omega_0$, corresponding to the path c on the surfaces in Fig. 9.7. As shown on Fig. 9.10, the solution of the semiclassical Schrödinger equation (9.20) leads to nearly complete population transfer from state $|1\rangle$ to state $|3\rangle$. The analysis of the surfaces shows that the state $|1;0,0\rangle$ connects $|3;-3,3\rangle$. Thus the complete population transfer from the bare state $|1\rangle$ to the bare state $|3\rangle$ must be accompanied with absorption of three pump photons and emission of three Stokes photons at the end of the process. This is confirmed by the numerical solution of the Floquet Schrödinger equation (9.7) with the initial state as a number state for the photon field $|1;0,0\rangle$, shown in Fig. 9.11a: the statevector $\psi(t)$ approximately projects on the transfer eigenvectors during the process. It shows the probabilities of being in the bare states 1, 2 and 3. Figure 9.11c shows the respective probabilities of one, two, three and four ω_1- photon absorptions, of one ω_2- photon absorption, and of one, two and three ω_2- photon emissions, calculated with the formulas (9.23). The other probabilities of photon emissions or absorptions are negligible. As in the preceding case, we observe an early Stokes photon absorption and a late pump photon absorption characterizing Stark shifts of the Floquet state connected to $|1\rangle$ and the one connected to $|3\rangle$ respectively. Moreover in this case the field is so strong that it induces absorption (respectively emission) of one, two and then three pump (respectively Stokes) photons. The complete population transfer from state $|1\rangle$ to state $|3\rangle$ is now accompanied by the loss of three ω_1- photons and the gain of three ω_2- photons at the end of the process.

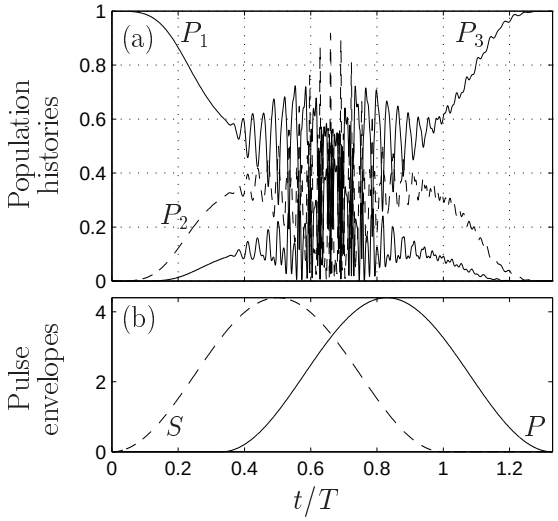

FIG. 9.10 - *From the semiclassical Schrödinger equation, (a) population histories $P_n(t)$ for $n = 1, 2, 3$ with $\delta = 2\Omega_0$ and $\Omega_{\max} = 4.4\Omega_0$ and (b) pulse excitation. Population transfer $P_3(\infty)$ to bare state $|3\rangle$ is nearly complete.*

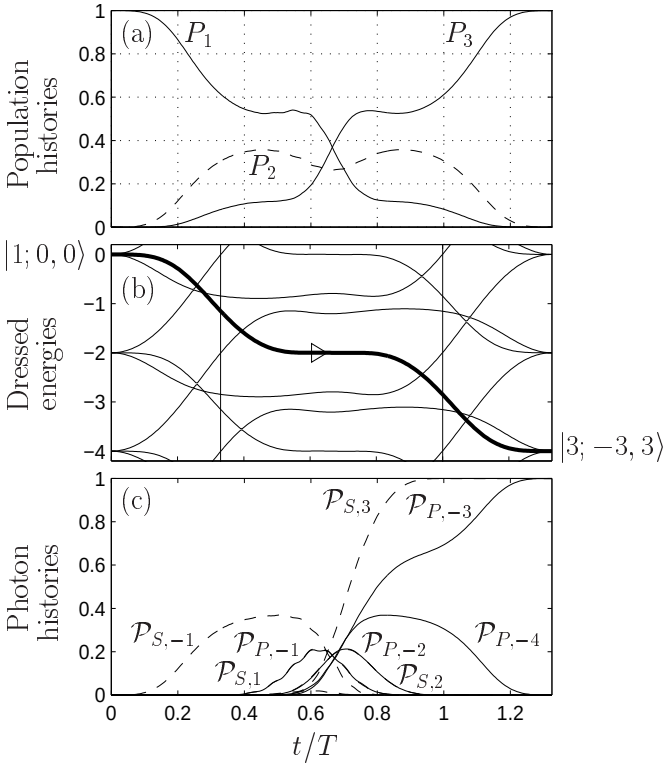

FIG. 9.11 - *From the Floquet Schrödinger equation, with the same parameters as in Fig. 9.10, (a) population histories $P_n(t)$ for $n = 1, 2, 3$ (top frame) and (c) photon histories (with $\mathcal{P}_{P,-1} \approx \mathcal{P}_{S,1}$ and $\mathcal{P}_{P,-2} \approx \mathcal{P}_{S,2}$), associated to the Floquet spectrum in middle frame (b).*

Chapter 10

Control of alignment and orientation of molecules

The control of the external degrees of freedom[1] of a quantum object necessitates the manipulation of its internal states by an external field. One important aspect is the control of the rotation of the molecule, i.e. of the alignment with respect to a given axis, or the orientation when the two directions of the alignment for a polar molecule are considered [159].

In this chapter, we analyze and construct various processes to align and orient molecules, *during* an appropriate field or *after* the field (named postpulse or field-free alignment). The strategy is in two steps. First we identify specific quantum states as aligned (or oriented) states, that we name *target states*, next we construct appropriate external fields to reach such states. Important aspects are the robustness of the process with respect to the thermal averaging.

In particular, it is known that a non-resonant short pulse allows one to align quite efficiently. Here we analyze in detail such an alignment and study this efficiency with an approximate solvable model in terms of target state. We show that its counterpart for orientation by a short pulsed electric field is not so efficient. We present alternative processes that allow us to orient efficiently during or after the pulse. A short elliptic pulse is also shown to alternate the direction of alignment dynamically.

The degree of alignment with respect to a reference axis is measured through the quantum average of the observable constructed with the direction cosine $\langle\cos^2\Theta\rangle$, where Θ is the angle between the reference axis and the molecular axis. When the molecule is aligned $\langle\cos^2\Theta\rangle \to 1$.

Two basic strategies can be developed to align and orient molecules by rotational excitations through Raman processes using vibrationally non-resonant pulses. The effective dressed Hamiltonian for this process is of the form:

$$H = B_0\hat{J}^2 + V(\Theta,\varphi) \tag{10.1}$$

with the potential $V(\Theta,\varphi)$, a function of the field amplitude squared, such as the ones constructed in Subsection 6.3.5 [see Eqs. (6.159), (6.162), (6.165), and (6.166)]. We consider here for simplicity a cold molecule, i.e. in the rotational state $|J=0\rangle$ before switching the field.

Adiabatic pulses, turned on slowly compared with the rotational periods, i.e. of characteristic duration τ satisfying

$$\tau \gg \hbar/B_0, \tag{10.2}$$

[1]Such a nomenclature refers to the classical mechanics. Internal degree in freedom refers to the motion of the molecule with respect to its frame (i.e. vibration), and external degree in freedom with respect to a laboratory frame (i.e. translation and global rotation).

allow the dynamics to follow the eigenstate of H connected to the initial one [125, 160]. This eigenstate is the state of *minimum potential energy* V, when we consider initially $|J=0\rangle$. The eigenvectors of the dressed Hamiltonian are called *pendular states* and are labeled with $\tilde{J}$. Their associated energies as a function of the field amplitude form of curves that are continuously connected to the bare states $|J\rangle$.

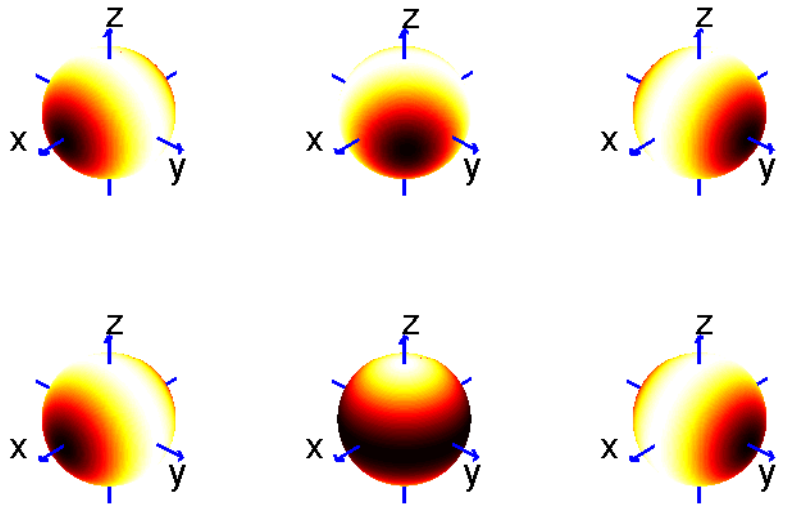

FIG. 10.1 - *Contour plot (darker areas correspond to smaller values of V) of the potential (6.162) (where the term or order $1/(\hbar\omega)^2$ has been neglected for simplicity) on the sphere for (i) the upper row: $\phi = 0$ (linear field) and $a = 1$ (left), $a = 1/\sqrt{2}$ (middle), $a = 0$ (right); (ii) the lower row: $\phi = \pi/2$ and $a = 1$ (left, linear), $a = 1/\sqrt{2}$ (middle, circular), $a = 0$ (right, linear).*

A qualitative picture can be thus made by the analysis of the minima of $V(\Theta, \varphi)$. Fig. 10.1 shows a contour plot of the potential (6.162) as functions of Θ and φ on the sphere for various parameters of a and ϕ . This shows that, when the field is adiabatically switched on, the alignment *during* the interaction with the field is closely related to the polarization of the field . In particular, the molecule aligns along the axis of polarization of a linear field since the effective potential is in this case a double-well potential whose minima are in the directions of the field polarization. The wells are deeper and thinner for a stronger field, and less deep and larger for a higher M [125, 160]. This has been demonstrated experimentally in [161]. In the case of a subsequently adiabatic rotation of polarization, the alignment follows the polarization axis. On the other hand, the molecule delocalizes in the plane of the ellipse of an elliptic field, following its shape when it is deformed adiabatically. For instance a linear field of polarization rotating from x to y allows the molecule to rotate from x to y while the field is on. On the other hand, an elliptic field of variable half axis for instance from $a = 1, b = 0$ to $a = 0, b = 1$ allows also the molecule to rotate form x to y, but passing through a completely delocalized state in the $x - y$ plane when the field is circular ($a = b = 1/\sqrt{2}$).

An alternative strategy consists in using an *ultrashort* pulse, i.e. satisfying

$$\tau \ll \hbar/B_0, \tag{10.3}$$

which creates a large superposition of rotational states. This results in a field-free postpulse transient alignment occurring periodically in time due to revivals of rotational wavepackets, as

long as the coherence of the process is preserved [162, 160, 163]. This has been experimentally demonstrated in [164, 165, 166].

The dynamics induced by an ultrashort pulse can be interpreted as follows. An intense and short linearly polarized pulse allows one to populate high J states, with constant M_0 for a given initial $|J_0, M_0\rangle$ state (belonging to the set of states that are thermally populated at a given temperature) [see Eq. (6.159)]. The final state $|\varphi^{(J_0,M_0)}\rangle$ can be thus decomposed in the $|J\rangle$ basis: $|\varphi^{(J_0,M_0)}\rangle = \sum_J c_J|J\rangle$ with non-negligible coefficients c_J such that $J \gg M_0$. This entails that $\vec{J}$ is approximately included and *delocalized* in a plane orthogonal to the field axis (say z axis). After the pulse, $\vec{J}$ is a constant of motion since we have $i\frac{d\langle\vec{J}\rangle}{dt} = \langle[H_0, \vec{J}]\rangle = 0$. If one considers the classical limit of a molecule orthogonal to $\vec{J}$ and rotating about $\vec{J}$, the molecule is, in the two extreme cases, *aligned* for some time along the z axis, and *delocalized* for some time in the $x-y$ plane. A simplified model developed below shows that the final states $|\varphi^{(J_0,M_0)}(t)\rangle$ for most J_0 and M_0 have approximately the same phases when they represent aligned or delocalized molecules. These rephasing times occurs thus for the *extrema* of the potential V.

In summary, a strong and short pulse allows the molecule to visit dynamically the extrema of the potential after the pulse, while an adiabatic pulse allows the visit only of the minimum of the potential during the pulse.

Classically, a field linearly polarized along z gives a torque to the molecule, which rotates subsequently in a plane orthogonal to $\vec{J}$, which is in the $x-y$ plane in the limit of a strong field (its precise direction depends on the initial condition of the rotor). The classical average $\cos^2\Theta$ on a period of rotation is thus: $\frac{1}{T}\int_0^T dt\, \cos^2\Theta(t) = 1/2$. In quantum mechanics we expect the same value for the average of $\cos^2\Theta$ but interpreted as the double average: $\frac{1}{T}\int_0^T dt\, \langle\cos^2\Theta\rangle(t) = 1/2$.

To obtain oriented molecules (when the direction of the alignment is considered), the molecule has to interact with the field through its permanent dipole moment. The degree of orientation can be quantified by $\langle\cos\Theta\rangle$. Such a coupling by a permanent dipole moment can be obtained with a constant static field switched on adiabatically [167, 168]. However such static fields cannot be intense and do not allow an efficient orientation. When such static fields are combined with an intense non-resonant laser pulse, a significant orientation can be reached as shown theoretically [169] and experimentally [170], however still during the static field on. It has been proposed to use a short *Half-cycle pulse* (HCP) [171, 172] to obtain significant orientation in field-free conditions. Such an asymmetric pulse is made of fast rising and decreasing ramps of large area, followed by a long and weak field of area of same absolute value but of opposite sign, such that the total area made by the electric field is zero (as required to propagate in the free space). The latter part of the HCP can be generally neglected since it is weak. Such an HCP can be experimentally produced with quite high amplitudes [173, 174, 175].

We have shown [176] that a higher efficiency can been obtained by adiabatic passage, i.e. during the field (see Section 10.4) using a 2+1 process originally suggested in this context in Ref. [177, 178].

The problem of *efficiency* of alignment and orientation in particular in field-free conditions is intensively studied. We can give a precise formulation in terms of the concept of optimal *target* states, which are states in a finite dimensional subspace, identified as corresponding to well aligned (or oriented) molecules. Once identified, the goal is to reach these states by an appropriate process [179, 180]. In the case of alignment through the anisotropic polarizability, the optimal target states are defined as the states which give the largest value of $\langle\cos^2\Theta\rangle$ projected in an Hilbert subspace $\mathcal{H}_N \in \mathcal{H}$ of dimension N spanned by the lowest even rotational

states $|J\rangle$, $J = 0, 2, \cdots, 2(N-1)$ (for $|J=0\rangle$ as initial condition) . The target state gives thus the most efficient aligned state in a given Hilbert subspace $\mathcal{H}_N$ of dimension N. *For a given N, the target state can be simply expressed as the eigenstate of* $\cos^2_N\Theta \equiv \Pi_N \cos^2\Theta\Pi_N$ *with the largest eigenvalue*, where $\Pi_N = \sum_{J=0}^{N-1} |J\rangle\langle J|$ the projector on $\mathcal{H}_N$. We remark that considering a finite subspace yields an operator with discrete spectrum.

On the other hand a higher intensity can populate higher J levels during the interaction with the field. This leads to a choice of the subspace $\mathcal{H}_N$ that depends on the field intensity. The *duration* of the alignment, which is another aspect of interest, is expected to be larger if the dynamics stays within a space $\mathcal{H}_N$ of smaller dimension.

All these aspects of the target states can be rephrased for molecular orientation with the use of the observable $\cos\Theta$ and the Hilbert subspace $\mathcal{H}_N \in \mathcal{H}$ of dimension N spanned by the lowest rotational states $|J\rangle$, $J = 0, 1, \cdots, N-1$.

Thus a good strategy of alignment (or orientation) can be formulated as (i) *generating a subspace* $\mathcal{H}_N$ by an appropriate field intensity for a chosen duration of alignment, and (ii) *manipulating the state* within $\mathcal{H}_N$ such that it becomes at a certain time the optimal target state. In practice, these two requirements are not independent. One expects that one cannot choose N too small if one wants to obtain a large degree of alignment.

One cannot expect that a short single laser field allows one to reach exactly the target state: Indeed it does not, but only allows one to approach it (see the section below). It is also known that a single HCP (resp. impulsive non-resonant excitation) leads to an *intrinsic saturation* of the orientation (resp. alignment) in a rigid rotor model as a function of the field amplitude [172] (resp. [181]).

On the other hand, *the adiabatic switching of a field allows one in principle to reach a target state* since the dynamics is described by the lowest eigenvector of

$$H = B_0\hat{J}^2 + V(\Theta,\varphi) \to V(\Theta,\varphi) \sim -I\cos^2\Theta \tag{10.4}$$

in the limit of high field intensities I, which corresponds thus to the highest eigenvector of $\cos^2\Theta$ (i.e associated to its highest eigenvalue).

Two strategies have been proposed to overcome the saturation. Since alignment by adiabatic passage does not show a saturation in principle, one can use an asymmetric field adiabatically switched on, that will align efficiently, combined with a sudden switch off, that will leave the molecule aligned recurrently preserving the efficiency obtained by the adiabatic process [163, 182]. This has been named the *switched wave packet* strategy.

On the other hand a sequence of multiple impulsive non-resonant laser pulses (HCPs) have been shown to enhance the alignment [181] (orientation [179, 180, 183]), since they allow one to approach much better the target state as demonstrated in the context of orientation [179, 180].

We have presented another strategy consisting of a combination of a HCP and a non-resonant laser pulse [184], named *hybrid pulse*. Another strategy could be the use of an asymmetric 2+1 field adiabatically switched on [176] combined to a sudden switch off.

Another important point consists in *enhancing* the coupling (through the polarizability or the permanent dipole moment) by the use of a near-resonant process. Near-resonant alignment has been studied in the impulsive regime [163] and in the context of electronic resonances [185]. Since the detunings in the impulsive regime are negligible in a first approximation, this alignment has been shown to be similar (however with a more favorable scaling due to the one-photon coupling by the dipole moment) to the nonresonant alignment. In particular the saturation as a function of the field intensity is still present in the impulsive regime. We study

below the use of a vibrational near resonant process to enhance the alignment by a single laser field, and the orientation by a (2+1) process.

This chapter is organized as follows: We first characterize the alignment and orientation using a solvable model in Section 10.1. The concept of target state is defined, and the saturation of the postpulse alignment induced by short pulses is shown. We next briefly summarize various methods to measure the alignment in Section 10.2. The dynamical field-free two-direction alignment alternation of linear molecules by elliptic laser pulses is presented in Section 10.3. Adiabatic orientation by a 2+1 process is studied in Section 10.4. We next show in Section 10.5 that the adiabatic alignment and orientation can be enhanced by the use of vibrational resonances. We finally show in Section 10.8 an efficient postpulse orientation by an hybrid pulse.

10.1 Characterization or alignment and orientation - Solvable model, target state and saturation

10.1.1 Characterization of alignment

We consider an initial condition at $t = t_i$ as a pure state eigenvector of $H_0 : |\psi_{J_0,M_0}\rangle(t = t_i) = |J_0, M_0\rangle$ and an interaction between times t_i and t_f through the polarizability, that preserves the quantum number M_0. The state vector of the free molecule evolves as

$$\psi_{J_0,M_0}(t > t_f) = \exp\left[-iH_0(t - t_f)/\hbar\right] \psi_{J_0,M_0}(t_f) \tag{10.5}$$

with $\psi_{J_0,M_0}(\Theta, \varphi, t) = \phi_{J_0,M_0}(\Theta, t) \exp(iM_0\varphi)$. After the field interaction, one can expand the state solution as

$$|\psi_{J_0,M_0}(t)\rangle = \sum_J c_J^{J_0,M_0} \; e^{i\left[D(J(J+1))^2 - BJ(J+1)\right]t/\hbar} \, |J, M_0\rangle \tag{10.6}$$

with

$$c_J^{J_0,M_0} = \left|c_J^{J_0,M_0}\right| e^{i\theta_J^{J_0,M_0}}, \quad \sum_J |c_J|^2 = 1. \tag{10.7}$$

If the interaction is made only through the polarizability (and $\cos^2\Theta$), the J *are all either odd or even* since only the matrix elements $\langle J, M_0| \cos^2\Theta \, |J, M_0\rangle$ and $\langle J+2, M_0| \cos^2\Theta \, |J, M_0\rangle$ are different from zero. One can calculate the quantity characterizing the alignment (neglecting the centrifugal distortion for simplicity):

$$\left\langle \cos^2\Theta \right\rangle_{J_0,M_0}(t) = \sum_J \alpha_{J,M_0} \left|c_J^{J_0,M_0}\right|^2 + 2\sum_J \beta_{J,M_0} \mathcal{R}\left[\overline{c}_{J+2}^{J_0,M_0} c_J^{J_0,M_0} e^{i\omega_J t}\right] \tag{10.8a}$$

$$= \sum_J \alpha_{J,M_0} \left|c_J^{J_0,M_0}\right|^2 + 2\sum_J \beta_{J,M_0} \left|c_J^{J_0,M_0} c_{J+2}^{J_0,M_0}\right| \cos\left[\omega_J t + \theta_J^{J_0,M_0} - \theta_{J+2}^{J_0,M_0}\right] \tag{10.8b}$$

where $\mathcal{R}(\cdot)$ denotes the real part and $\overline{c}$ is the complex conjugate of c, with

$$\omega_J = 2B(2J + 3)/\hbar, \tag{10.9}$$

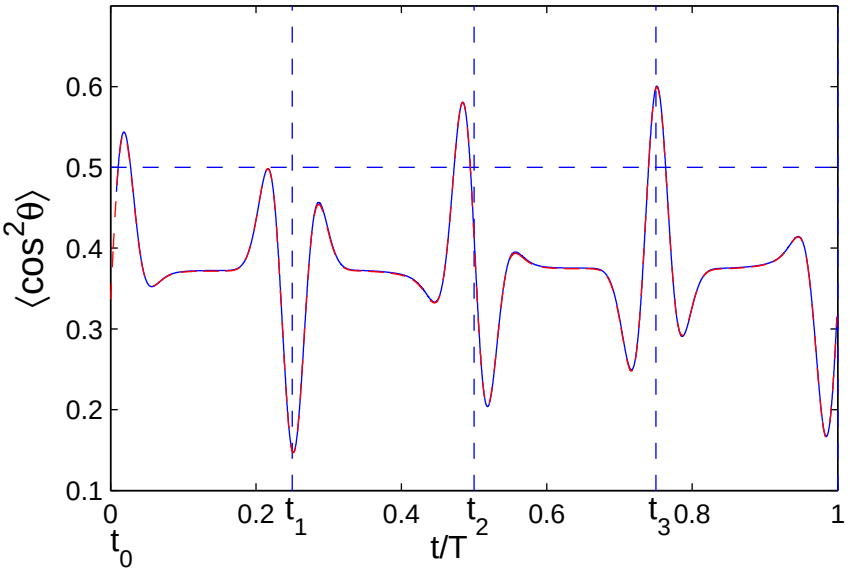

FIG. 10.2 - $\langle \cos^2 \Theta \rangle$ *as a function of* t/T *for* CO_2 *molecule* ($B \approx 0.39\ cm^{-1}$) *for* $T = 11$ *K (corresponding to* $\widetilde{B} \approx 0.051$, *giving initially non negligible thermally populated states up to* $J_0 = 12$*), the peak field intensity* $I = 12\ TW/cm^2$ *and the full width at half maximum* $T_{\text{FWHM}} = 100$ *fs. The full numerical calculation (full line) and the sudden approximation [see Eq. (10.25b)] (dashed line) are almost undistinguishable.* t_p, $p = 0, \cdots, 3$ *are referred to as the revival times.*

α_{J,M_0} the Stark shift of the $|J, M_0\rangle$ state and β_{J,M_0} the coupling $|J, M_0\rangle \rightleftharpoons |J+2, M_0\rangle$ defined as

$$\alpha_{J,M_0} = \langle J, M_0 | \cos^2 \Theta | J, M_0 \rangle \tag{10.10a}$$

$$= \frac{1}{3} + \frac{2}{3} \frac{J(J+1) - 3M_0^2}{(2J+3)(2J-1)}, \tag{10.10b}$$

$$\beta_{J,M_0} = \langle J+2, M_0 | \cos^2 \Theta | J, M_0 \rangle \tag{10.10c}$$

$$= \frac{1}{2J+3} \sqrt{\frac{(J+1-M_0)(J+2-M_0)}{(2J+1)(2J+5)}} \sqrt{(J+1+M_0)(J+2+M_0)}. \tag{10.10d}$$

Eqns. (10.8) show that each J-component of $\langle \cos^2 \Theta \rangle_{J_0,M_0}(t)$ oscillates periodically with the period $\pi\hbar/[B(2J+3)]$, and thus that $\langle \cos^2 \Theta \rangle_{J_0,M_0}(t)$ oscillates periodically with the common period $T = \pi\hbar/B$. The average $\langle \cos^2 \Theta \rangle_{J_0,M_0}(t)$ oscillates around the quantity $\sum_J \alpha_{J,M_0} |c_J|^2$ which corresponds to the *permanent* or mean alignment. This quantity is expected to go to $1/2$ when the alignment is efficient (see the comment above about the classical dynamics of the rigid rotor). Through this general expression (10.8b), one can define the *alignment* (*planar delocalization*) which occurs when the second summation is larger (smaller) than 0, such that $\langle \cos^2 \Theta \rangle_{J_0,M_0}(t)$ is larger (smaller) than $\sum_J \alpha_{J,M_0} |c_J|^2$.

Equation (10.8b) shows that the rephasing of the signal and thus a transient significant alignment or planar delocalization occurs for a given initial condition $J_0\ M_0$ if the phase $\theta_J^{J_0,M_0} - \theta_{J+2}^{J_0,M_0}$ is independent of J:

$$\theta_J^{J_0,M_0} - \theta_{J+2}^{J_0,M_0} = \Delta^{J_0,M_0} \tag{10.11}$$

with $-\pi \leq \Delta^{J_0,M_0} < \pi$ (independent of J). Since all the J are either even or odd, the summation for $\langle \cos^2 \Theta \rangle$ accumulates indeed for all J only around four specific times $t_p = pT/4$ in one period, leading to *four main transient peaks of alignment and planar delocalization*, called *revivals* [162].

The accumulation in the summation of Eq. (10.8b) gives more precisely extremal values when the cosine can be ± 1 for specific times and for all J, i.e. when $\Delta^{J_0,M_0} = k\pi/2$, k positive or negative integer. For example, when $\Delta^{J_0,M_0} = -\pi/2$, one obtains for $\langle \cos^2 \Theta \rangle_{J_0,M_0}$ (i) a value of $\sum_J \alpha_{J,M_0} \left| c_J^{J_0,M_0} \right|^2$ at $t = t_0 = 0$ and $t = t_2 = T/2$, with a maximum right before $t = t_0 = 0$ and right after $t = t_2 = T/2$ and a minimum right after $t = t_0 = 0$ and right before $t = t_2 = T/2$, (ii) a local maximum (resp. minimum) at $t = t_3 = 3T/4$ for even (resp. odd) J, and a local minimum (resp. maximum) at $t = t_1 = T/4$ for even (resp. odd) J. This example will be shown below to be approximately the case when a short nonresonant pulse interaction is used (see Fig. 10.2).

We remark that, if we take into account even *and* odd J, only two revivals appear around $pT/2$.

All the revivals described above are preserved at any temperature if the phases $\theta_J^{J_0,M_0} - \theta_{J+2}^{J_0,M_0}$ are additionally independent of the initial condition characterized by J_0, M_0:

$$\theta_J^{J_0,M_0} - \theta_{J+2}^{J_0,M_0} = \Delta. \tag{10.12}$$

We recall that taking into account the temperature T, we have to consider a statistical ensemble of molecules with different initial conditions J_0, M_0 distributed according to the Boltzmann weights (independent of M_0 and normalized $\sum_{J_0=0}^{\infty} \sum_{M_0=-J_0}^{J_0} \rho_{J_0} = 1$):

$$\rho_{J_0} = \frac{g_{J_0} e^{-\widetilde{B} J_0 (J_0+1)}}{\sum_{J=0}^{\infty} g_J (2J+1) e^{-\widetilde{B} J(J+1)}} \tag{10.13}$$

with g_{J_0} the nuclear spin degeneracy factor, the Boltzmann constant $k = 1.38 \times 10^{-23}$ J/K, and the normalized (dimensionless) rotational constant

$$\widetilde{B} = \frac{B}{kT}. \tag{10.14}$$

The alignment is characterized by

$$\left\langle \cos^2 \Theta \right\rangle (t) \equiv \sum_{J_0=0}^{\infty} \rho_{J_0} \sum_{M_0=-J_0}^{J_0} \left\langle \cos^2 \Theta \right\rangle_{J_0,M_0} (t), \tag{10.15a}$$

$$= \sum_J \left(\sum_{J_0=0}^{\infty} \rho_{J_0} \sum_{M_0=-J_0}^{J_0} \alpha_{J,M_0} \left| c_J^{J_0,M_0} \right|^2 \right)$$

$$+ 2 \sum_J \left(\sum_{J_0=0}^{\infty} \rho_{J_0} \sum_{M_0=-J_0}^{J_0} \beta_{J,M_0} \left| c_J^{J_0,M_0} c_{J+2}^{J_0,M_0} \right| \right) \cos \left[\omega_J t + \Delta \right]. \tag{10.15b}$$

Depending on the value of the spin degeneracy factor, one expects the cancelation of some revivals. For instance, if the g_{J_0} can only be even, as in CO_2 molecules (or only odd), the four revivals appear. If the g_{J_0} can be even and odd with the same value: $g_{2k+1} = g_{2k}$, as in CO molecules, the revivals at times t_1 and t_3 vanish. If the g_{J_0} can be even and odd with different values, as in NO molecules (for which $g_{2k} = 2g_{2k+1}$), the revivals at times t_1 and t_3 partially vanish.

10.1.2 Characterization of orientation

We can reformulate the preceding arguments for the orientation problem, with an interaction (that preserves the quantum number M_0) through the permanent dipole moment and $\cos\Theta$. We obtain

$$\langle\cos\Theta\rangle_{J_0,M_0}(t) = 2\sum_J \gamma_{J,M_0}\left|c_J^{J_0,M_0}c_{J+1}^{J_0,M_0}\right|\cos\left[2B(J+1)t/\hbar + \theta_J^{J_0,M_0} - \theta_{J+1}^{J_0,M_0}\right] \tag{10.16}$$

with

$$\gamma_{J,M_0} = \langle J+1, M_0|\cos\Theta|J, M_0\rangle, \tag{10.17a}$$

$$= \sqrt{\frac{(J+1)^2 - M_0^2}{4(J+1)^2 - 1}}. \tag{10.17b}$$

The J-components of $\langle\cos\Theta\rangle_{J_0,M_0}(t)$ oscillate periodically with the period $\pi/([2B(J+1)]$, and thus $\langle\cos\Theta\rangle_{J_0,M_0}(t)$ oscillates periodically with the common period $T = \pi/B$ around 0. The orientation is defined when $\langle\cos\Theta\rangle_{J_0,M_0}(t)$ is different from 0, and its sign gives the direction of orientation.

The orientation is significant when the phase $\theta_J^{J_0,M_0} - \theta_{J+1}^{J_0,M_0} = \Delta^{J_0,M_0}$ is independent of J:

$$\theta_J^{J_0,M_0} - \theta_{J+1}^{J_0,M_0} = \Delta^{J_0,M_0}. \tag{10.18}$$

The summation for $\langle\cos\Theta\rangle$ accumulates for all J (which are here any positive or zero integer) only around $t = pT$, with p an integer:

$$\langle\cos\Theta\rangle^{J_0,M_0}(pT) = 2\sum_J \gamma_{J,M_0}\left|c_J^{J_0,M_0}c_{J+1}^{J_0,M_0}\right|\cos\left[2(J+1)p\pi + \Delta^{J_0,M_0}\right]. \tag{10.19}$$

On one period T, this gives one maximum and one minimum located around $t = 0$ for $\Delta^{J_0,M_0} \neq 0, \pi$. For $\Delta^{J_0,M_0} = 0$ (π), we have one maximum (minimum) with an optimum accumulation. Here again, the orientation is robust with respect to the temperature when $\theta_J^{J_0,M_0} - \theta_{J+1}^{J_0,M_0}$ are additionally independent of the initial condition characterized by J_0, M_0:

$$\theta_J^{J_0,M_0} - \theta_{J+1}^{J_0,M_0} = \Delta. \tag{10.20}$$

An interaction with a short half cycle pulse (HCP) gives, as shown below, the phase $\Delta \approx -\pi/2$ (for a positive field amplitude) and yields $\langle\cos\Theta\rangle$ of the form presented in Fig. 10.3 with a symmetric orientation along two directions at different times roughly around $t = 0$ (and $t = T$) for a strong field.

10.1.3 Target state: Definitions

We assume that the dynamics is mainly in a subspace $\mathcal{H}_N$ of dimension N spanned by the states $\{|J_{\min}\rangle, |J_{\min}+2\rangle, \cdots, |J_{\max}-2\rangle, |J_{\max}\rangle\}$ with $N = (J_{\max} - J_{\min})/2 + 1$ for interaction through the polarizability. The maximal value of $\langle\cos^2\Theta\rangle_{J_0,M_0}(t_p)$ is reached when the values $c_J^{J_0,M_0}$ are such that

$$\sum_{J=J_{\min}}^{J_{\max}-2} \beta_{J,M_0}\left|c_J^{J_0,M_0}c_{J+2}^{J_0,M_0}\right| \tag{10.21}$$

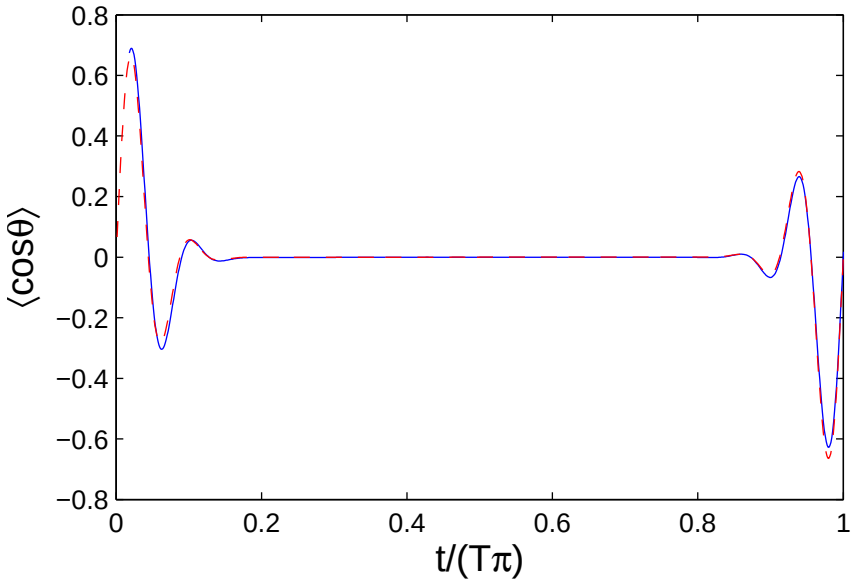

FIG. 10.3 - $\langle \cos\Theta \rangle$ *as a function of* t/T *for KCl molecule* ($B \approx 0.13\ cm^{-1}$) *for* $T = 3.5\ K$ *(corresponding to* $\widetilde{B} \approx 0.053$*), the peak amplitude* $\mathcal{E}_0 = 4 \times 10^7\ V/m$ *of the HCP and the full width at half maximum* $T_{\rm FWHM} = 450\ fs$*. Numerics (full line), sudden approximation [see Eq. (10.36)] (dashed line).*

is maximal. This is equivalent to requiring that the state solution $|\psi_{J_0,M_0}(t)\rangle$ is at a certain time the *largest eigenvector* of the operator $\langle \cos^2\Theta \rangle$, i.e. associated to its largest eigenvalue. This state is identified as the *optimal* aligned state in the subspace $\mathcal{H}_N$.

When we consider the interaction through the dipole moment, we assume that the dynamics is mainly in a subspace $\mathcal{H}_N$ of dimension N spanned by the states $\{|J_{\rm min}\rangle, |J_{\rm min}+1\rangle, \cdots, |J_{\rm max}-1\rangle, |J_{\rm max}\rangle\}$ with $N = J_{\rm max} - J_{\rm min} + 1$, and the maximal value of $\left|\langle \cos\Theta \rangle^{J_0,M_0}(t_p)\right|$ is reached when the values $c_J^{J_0,M_0}$ are such that

$$\sum_{J=J_{\rm min}}^{J_{\rm max}-1} \gamma_{J,M_0} \left| c_J^{J_0,M_0} c_{J+1}^{J_0,M_0} \right| \tag{10.22}$$

is maximal. This is equivalent to requiring that the state solution $|\psi_{J_0,M_0}(t)\rangle$ is at a certain time the *largest or smallest eigenvector* of the operator $\langle \cos\Theta \rangle$, i.e. associated to its respectively largest or smallest eigenvalue. This state is identified as the *optimal* oriented state in the subspace $\mathcal{H}_N$.

This notion of target state has been extended for a thermal ensemble in [186].

10.1.4 Alignment dynamics by an ultrashort non-resonant laser pulse

We consider a nonresonant short pump pulse

$$\overrightarrow{E}_p(t) = \overrightarrow{e}\,\mathcal{E}_0 \sqrt{\Lambda(t)}\cos\omega t \tag{10.23}$$

of frequency ω, pulse intensity envelope $0 \leq \Lambda(t) \leq 1$ centered at $t = 0$ and of duration T_p, peak amplitude $\mathcal{E}_0$ and fixed polarization vector $\overrightarrow{e}$ in the sudden (or impulsive) regime $T_p \ll B/\hbar$.

For simplicity we consider $M = 0$ and use the interaction (6.161), at the lowest order in $1/(\hbar\omega)$, neglecting $\alpha_0^{(v)}$: $\alpha_0^{(v)} \ll \alpha_\parallel, \Delta\alpha_{00}$, and simplify the notation by omitting the indices 0:

$$V(\Theta,\varphi) = -\frac{\mathcal{E}^2(t)}{4}\left(\alpha_\perp + \Delta\alpha\cos^2\Theta\right) \tag{10.24}$$

with $\mathcal{E} = \mathcal{E}_0\sqrt{\Lambda(t)}$.

The sudden approximation

The propagator can be approximately written as [187]

$$U(t,t_i) = U_0(t,t_c)U_V U_0(tc,t_i) \tag{10.25a}$$

$$= e^{i\gamma_\perp \mathcal{A}B(t-t_i)/\hbar} e^{-iB\hat{J}^2(t-t_c)/\hbar} e^{i2\zeta\cos^2\Theta} e^{iBJ^2(t_i-t_c)/\hbar} \tag{10.25b}$$

with U_0 the free propagator, U_V the propagator during the interaction considered as a $\delta(t)$-distribution (allowing one to neglect $B\hat{J}^2$ during the interaction), t_c the center of the pulse (here $t_c = 0$),

$$\gamma_\perp = \frac{\mathcal{E}_0^2}{4B}\alpha_\perp, \quad \Delta\gamma = \frac{\mathcal{E}_0^2}{4B}\Delta\alpha, \tag{10.26a}$$

$$\zeta = \mathcal{A}\frac{\Delta\gamma}{2} = \frac{\mathcal{E}_0^2\Delta\alpha}{8\hbar}\int_{t_i}^{t_f} dt\,\Lambda(t), \tag{10.26b}$$

$$\mathcal{A} = \frac{B}{\hbar}\int_{t_i}^{t_f} dt\,\Lambda(t). \tag{10.26c}$$

The last term characterizes the normalized area of the pump intensity envelope. The additional phase $e^{i\gamma_\perp \mathcal{A}B(t-t_i)/\hbar}$ independent of J will not affect the quantity $\langle\cos^2\Theta\rangle_{J_0,M_0}(t)$. We obtain for non-polar linear molecules and for Gaussian pulses of full width at half maximum $T_{\rm FWHM}$ (in intensity)

$$\zeta \approx \Delta\alpha[\text{Å}^3] \times I[\text{TW/cm}^2] \times T_{\rm FWHM}[\text{ps}] \tag{10.27}$$

with I the peak intensity. For the CO_2 molecule ($B \approx 0.39$ cm^{-1}), this leads to $\zeta_{CO_2} \approx 2.22 \times I[\text{TW/cm}^2] \times T_{\rm FWHM}[\text{ps}]$.

Numerics

Numerics shows the following additional features:

(i) At low temperature, the highest peak of $\langle\cos^2\Theta\rangle$ as a function of time occurs around t_2 (for a sufficiently high intensity pulse area), it is the highest for $J_0 = 0$.

(ii) At higher temperature, the highest peak of $\langle\cos^2\Theta\rangle$ as a function of time occurs at t_3 (resp. t_1) if even (resp. odd) J_0 are considered (for a sufficiently high intensity pulse area).

(iii) The maximum alignment $\max_t \langle\cos^2\Theta\rangle_{J_0,M_0}$ shows an asymptotic plateau as a function of the intensity pulse area.

(iv) for a given initial $J_0 > 0$, the peaks are of larger duration when $|M_0|$ is smaller.

The last point can be understood if we remark that for large $J_0, |M_0|$ with $J_0 \sim |M_0|$ one has

$$\beta_{J_0,M_0} \to \frac{1}{\sqrt{2}J_0}. \tag{10.28}$$

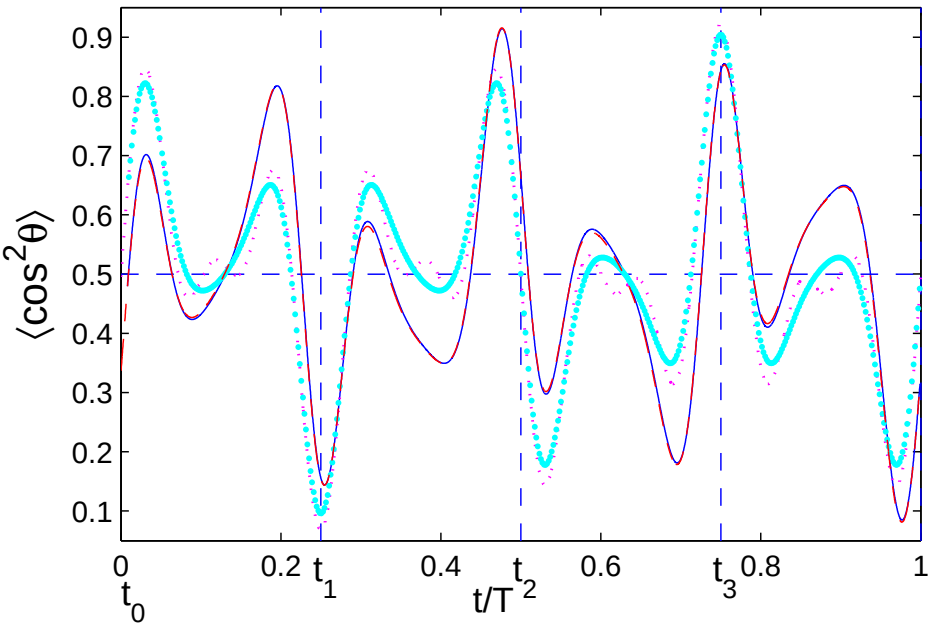

FIG. 10.4 - $\langle \cos^2 \Theta \rangle$ *as a function of* t/T *for* CO_2 *molecule for* $T = 0$ *K, the peak field intensity* $I = 12$ *TW/cm*^{2} *and the full width at half maximum* $T_{\rm FWHM} = 100$ *fs: numerics (full line), impulsive approximation (dashed line), with the solvable model (large dotted line), and the optimal solution for* $N = 4$ *with the optimal state determined with the solvable model of subsection 10.1.6 (thin dotted line). The sudden approximation is almost undistinguishable from the full numerics.*

This means that the coupling $\langle J_0 + 2, M_0 | \cos^2 \Theta | J_0, M_0 \rangle$ decreases as J_0 grows from 0 to $|M_0|$. This suggests that one analyze the limit of large J defined as $J \gg |M_0|$ for the populated states, which will allow us to construct an analytic solvable model that was proposed by T. Seideman [188, 163] (see below). This model is expected to be more appropriate for strong fields when population transfer in large J is expected. This model will allow us to explain the saturation.

Adding the small centrifugal diagonal term in Eq. (10.8) will slightly change the frequency of the oscillations, which will shift the revivals more significantly for larger times.

Figure 10.2 corresponds to $\zeta \approx 2.66$ and $T = 11$ K. Figure 10.4 shows a situation corresponding to the same ζ and $T = 0$ K, which is the case that gives approximately the maximum alignment by this process $\max_t \langle \cos^2 \Theta \rangle (t) \approx 0.915$. It is well approximated by

$$\begin{aligned} \left\langle \cos^2 \Theta \right\rangle (t) \approx 0.5 + 0.5[&0.19 \sin (6Bt/\hbar - 0.42\pi) + 0.4 \sin (14Bt/\hbar - 0.07\pi) \\ &+ 0.19 \sin (22Bt/\hbar - 0.03\pi) + 0.037 \sin (30Bt/\hbar - 0.02\pi)], \end{aligned} \tag{10.29}$$

which except for $J = 0$ shows that $\Delta \approx -\pi/2$.

This short non-resonant pulse is quite efficient. Starting with a cold molecule, one obtains here $\max_t \langle \cos^2 \Theta \rangle (t) \approx 0.91$, which corresponds to an angle $\Theta \approx 17^\circ$.

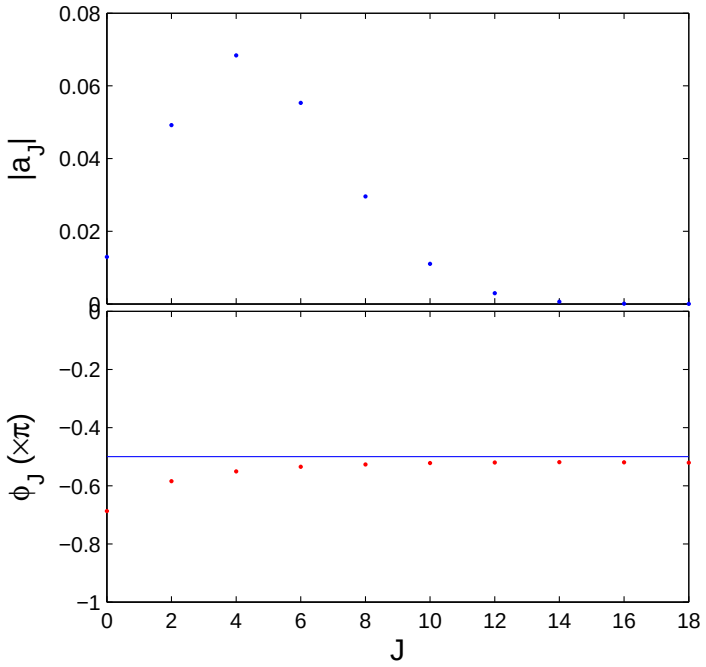

FIG. 10.5 - *Amplitudes $|a_J|$ (upper graph) and phases ϕ_J (lower graph) of the Fourier components of $\langle\cos^2\Theta\rangle(t)$ defined in Eq. (10.30), in the conditions of Fig. 10.2.*

Fourier decomposition

To determine the phases Δ^{J_0,M_0} associated to the dynamics shown in Fig. 10.2, we have calculated the Fourier components $|a_J|$ and ϕ_J of $\langle\cos^2\Theta\rangle(t)$ defined as

$$\langle\cos^2\Theta\rangle(t) =: C_0 + \sum_J |a_J|\cos(\omega_J t + \phi_J). \tag{10.30}$$

The phase shown in Fig. 10.5 are close to $\pi/2$, except for the first one.

Angular distribution

The angular distributions are shown in Fig. 10.6. The molecule is well aligned for $\langle\cos^2\Theta\rangle$ larger than the permanent alignment, and delocalized in the $x-y$ plane when $\langle\cos^2\Theta\rangle$ is smaller than the permanent alignment. We notice the remarkable feature that the molecule shows a superposition of the alignment and the planar delocalization at a time when $\langle\cos^2\Theta\rangle$ is equal to the superposition: $|S\rangle = \frac{1}{\sqrt{2}}(|A\rangle + |D\rangle)$ where $|A\rangle$, $|D\rangle$, and $|S\rangle$ denote respectively the aligned, delocalized, superposed states.

Alignment features as a function of the intensity area

The alignment generated by a short pulse has to be characterized by ζ, i.e. by the pulse intensity for a given pulse area. This degree of alignment is better for high intensity up to a *saturation*, as can be seen in Fig. 10.7, which shows the permanent alignment C (from which $1/3$ has been subtracted) and $\max_t\langle\cos^2\Theta\rangle(t) - 1/3 - C$ as a function of the peak intensity (see also the subsection 10.1.6 for more details).

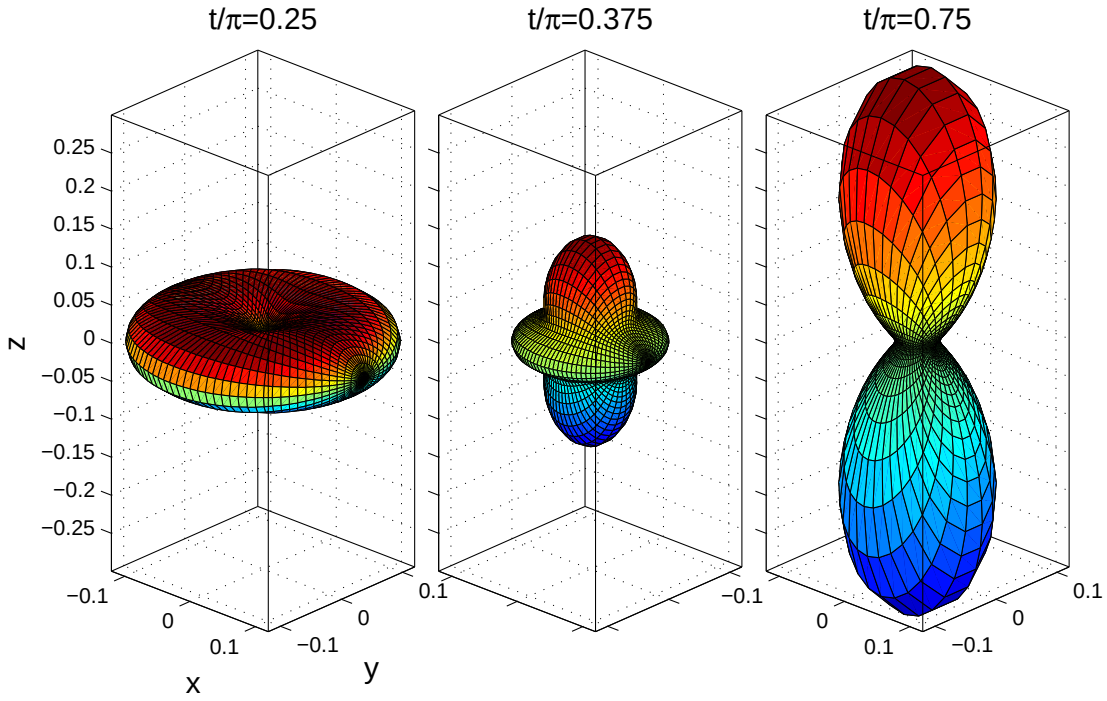

FIG. 10.6 - *Angular distribution of the state solution in the conditions of Fig. 10.2 for* $t/\pi = 1/4$ *(left)* $t/\pi = 3/8$ *(middle),* $t/\pi = 3/4$ *(right).*

It allows us to conclude that for low intensities

$$\langle \cos^2 \Theta \rangle(t) - 1/3 \approx \beta\zeta^2 + \kappa\zeta f(t) \approx \kappa\zeta f(t), \tag{10.31}$$

where, for given molecule and temperature, κ and β are constant and $f(t)$ is a specific function independent of ζ. We can notice that the regime of low intensities extends the result of the perturbative regime, even if it is not itself a perturbative regime (usually defined as a small population transfer), since it can show a non negligible alignment ($\max\langle \cos^2 \Theta \rangle(t) \approx 0.45$ for $I = 30$ TW/cm^2). We also have $\beta\zeta^2 \ll \kappa\zeta$, which shows that the permanent alignment is negligible for low intensities. For moderate intensity, Fig. 10.7 shows that the permanent alignment is linear with the peak field intensity, which leads to

$$\langle \cos^2 \Theta \rangle(t) - 1/3 \approx [\delta + \kappa f(t)]\zeta. \tag{10.32}$$

We can thus conclude that at low and moderate intensities (i.e. below the saturation of alignment), $\langle \cos^2 \Theta \rangle(t) - 1/3$ is approximately proportional to ζ.

10.1.5 Orientation dynamics by a half cycle pulse

We study the interaction with a half-cycle pulse (HCP) in the ground electronic state, in the sudden regime, considering only the high amplitude part:

$$\mathcal{E}(t) = \mathcal{E}_0 \Lambda(t) \tag{10.33}$$

of shape $0 \leq \Lambda(t) \leq 1$, centered at $t = 0$, of duration T_p, and of peak amplitude $\mathcal{E}_0$. The effective Hamiltonian reads in this case

$$H_{\text{eff}} = B\hat{J}^2 - \mu_{0,00}\mathcal{E}_0\Lambda(t)\cos\Theta, \tag{10.34}$$

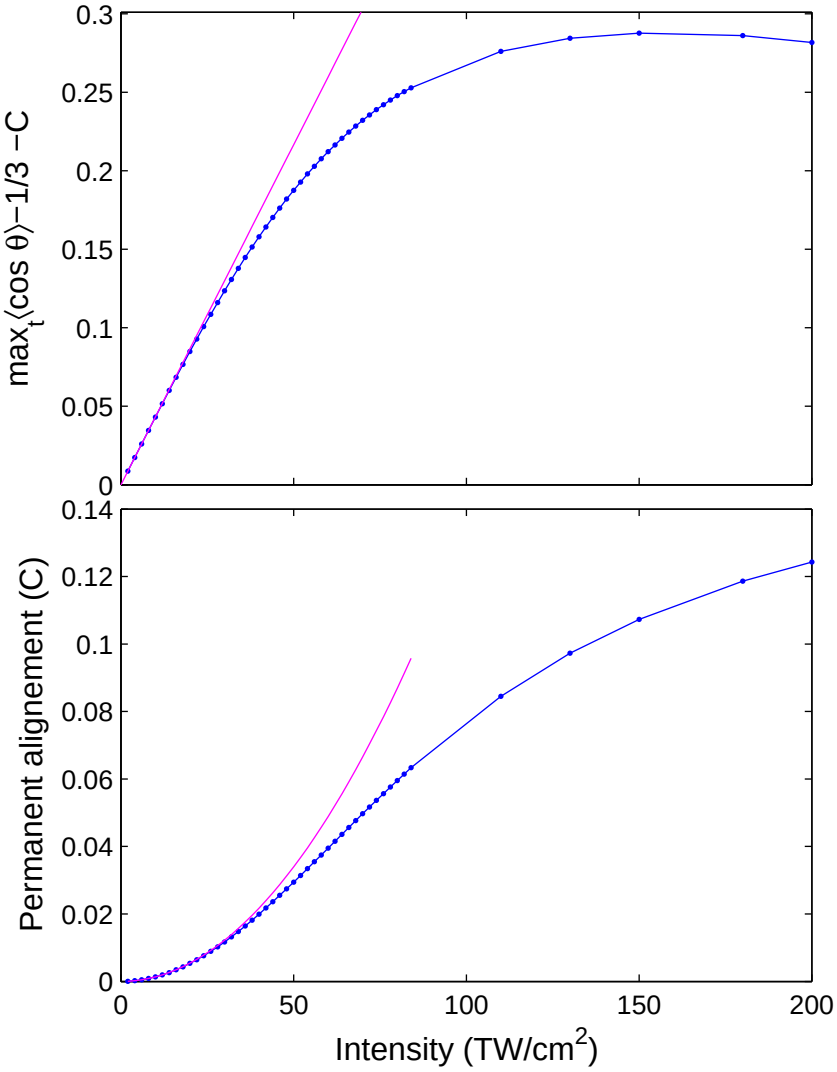

FIG. 10.7 - *Permanent alignment* $C \equiv \sum_J \left(\sum_{J_0=0}^{\infty} \rho_{J_0} \sum_{M_0=-J_0}^{J_0} \alpha_{J,M_0} \left| c_J^{J_0,M_0} \right|^2 \right) - 1/3$ *and* $\max\langle\cos^2\Theta\rangle(t) - 1/3 - C$ *as a function of the peak pump Gaussian intensity of* $\tau_{FWHM} = 0.1$ *ps in* CO_2 *at* $T = 293$ *K (dotted lines). The former varies as the squared intensity (full fitting line) approximately up to* $I = 30$ TW/cm^2 *and is linear for higher intensities. The latter is linear (full fitting line) for moderate intensities. Similar dependencies can be found for other linear molecules and temperatures.*

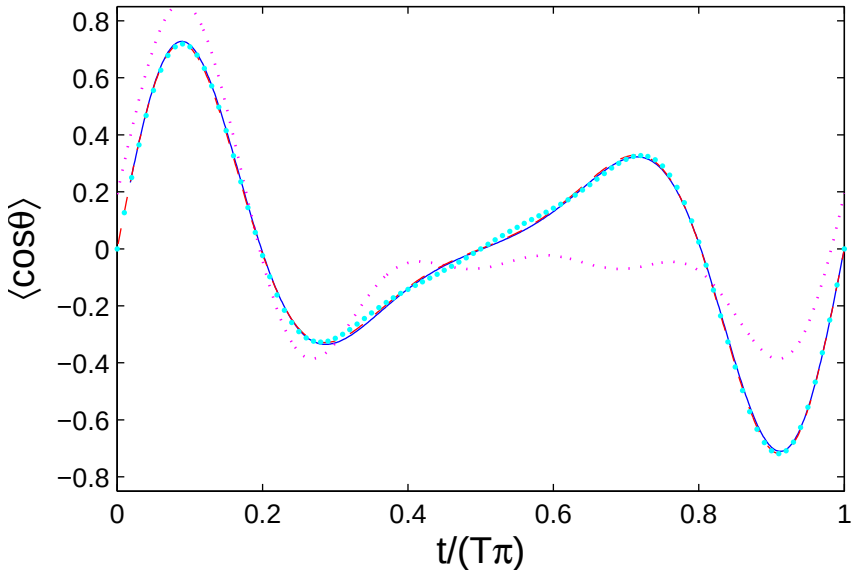

FIG. 10.8 - $\langle \cos\Theta \rangle$ *as a function of* t/T *for KCl molecule for* $T = 0$ *K, the peak amplitude* $\mathcal{E}_0 = 10^7$ *V/m and the full width at half maximum* $T_{\mathrm{FWHM}} = 450$ *fs. Numerics (full line), impulsive approximation (dashed line), approximative model (see Subsection 10.1.6, large dotted line). These calculations are very close. The optimal solution is shown for* $N = 5$ *with the optimal state determined with the solvable model of subsection 10.1.6 (thin dotted line).*

if we assume that

$$|\mu_{01}\mathcal{E}_0| \ll E_1^{(e)} - E_0^{(e)}, \qquad |\mu_{0,01}\mathcal{E}_0| \ll E_1^{(v)} - E_0^{(v)} \tag{10.35}$$

i.e. that the electric field cannot respectively populate the first excited electronic state $E_1^{(e)}$ through the electric dipole moment μ_{01} (that can be estimated at the equilibrium of the nuclei in the Franck-Condon principle) and the first excited vibrational state $E_1^{(v)}$. The propagator is in this case in the sudden approximation

$$U(t, t_i) = e^{-iBJ^2 t/\hbar} e^{i\xi \cos\Theta} \tag{10.36}$$

with

$$\xi = \frac{\mu_{0,00}\mathcal{E}_0}{\hbar} \int_{t_i}^{t_f} dt\, \Lambda(t). \tag{10.37}$$

We obtain for Gaussian pulses of full width at half maximum T_{FWHM} (in amplitude)

$$\xi \approx 6.73 \times 10^{-8} \mu_{0,00}[\mathrm{D}] \times \mathcal{E}_0[\mathrm{V/m}] \times T_{\mathrm{FWHM}}[\mathrm{ps}]. \tag{10.38}$$

Typical values of the dipole moment in the ground vibronic state go from for CO molecule: $\mu_{0,00} \approx 0.11$ D ($B \approx 1.92$ cm$^{-1} \approx 8.76 \times 10^{-6}$ u.a.) to for KCl: $\mu_{0,00} \approx 10.3$ D ($B \approx 0.13$ cm^{-1}).

Numerics

Starting with a cold molecule in $J = 0$, Fig. 10.8 shows $\langle \cos\Theta \rangle$ obtained by numerical simulation for $\xi \approx 3.12$ and $\tau B/\hbar \approx 0.011$ [which corresponds to a half-cycle of amplitude 10^7 V/m (experimentally reachable) for the KCl molecule]. With such a field one obtains $\max_t \langle \cos\Theta \rangle (t) \approx 0.65$, which corresponds to an angle $\Theta \approx 50°$ showing an oriented molecule.

Adding the thermal averaging is not favorable since the initial condition $J = 1$ mainly orients in the other direction with respect to the initial condition $J = 0$. The thermal averaging shifts thus the peaks towards $t = 0, \pi$.

We conclude that orientation by the strategy by one half-cycle leads to a noticeable orientation, but of a limited efficiency, essentially due to thermal averaging.

Orientation features as a function of the HCP amplitude

One observes that $\max_t |\langle \cos\Theta \rangle|$ increases linearly with the field amplitude from low to intermediate field amplitudes. Next it saturates approximately at $\max_t |\langle \cos\Theta \rangle| \approx 0.75$ for a molecule initially cold (see Fig. 2 in section 10.8).

10.1.6 A solvable model in the limit of large J

Definition

We evaluate below the target state for alignment and orientation in an approximate solvable model. Within this model, we calculate $\langle \cos^2\Theta \rangle_{J_0,M_0}(t)$ induced by a short non-resonant pulse interaction, and $\langle \cos\Theta \rangle_{J_0,M_0}(t)$ by a HCP in the limit of large J, i.e.

$$J \gg |M_0| \tag{10.39}$$

for the populated states. This leads to

$$\alpha_{J,M_0} \to 1/2, \quad \beta_{J,M_0} \to 1/4, \quad \gamma_{J,M_0} \to 1/2, \tag{10.40}$$

i.e. to the same Stark shifts for all the J levels [188, 163]. (We will simplify the notation denoting $|J\rangle \equiv |J, M_0\rangle$.) This model is expected to be more appropriate for strong fields when population transfer to large J is expected. When $M_0 = 0$, this is a good approximation for β_{J,M_0} and γ_{J,M_0} already when $J = 1$: $\beta_{0,0} \approx 0.298$, $\beta_{1,0} \approx 0.262$, $\beta_{2,0} \approx 0.256$, ... $\gamma_{0,0} \approx 0.577$, $\gamma_{1,0} \approx 0.516$, $\gamma_{2,0} \approx 0.507$, ... and for $\alpha_{J,M_0}$when $J = 2$: $\alpha_{0,0} = 1/3$, $\alpha_{1,0} = 0.6$, $\alpha_{2,0} \approx 0.524$, $\alpha_{3,0} \approx 0.511...$ In this limit, one obtains

$$\left\langle \cos^2\Theta \right\rangle_{J_0,M_0}(t) = \frac{1}{2} + \frac{1}{2}\sum_J \left| c_J^{J_0,M_0} c_{J+2}^{J_0,M_0} \right| \cos\left[\omega_J t + \theta_J^{J_0,M_0} - \theta_{J+2}^{J_0,M_0} \right], \tag{10.41}$$

$$\left\langle \cos\Theta \right\rangle_{J_0,M_0}(t) = \sum_J \left| c_J^{J_0,M_0} c_{J+1}^{J_0,M_0} \right| \cos\left[\omega'_J t + \theta_J^{J_0,M_0} - \theta_{J+1}^{J_0,M_0} \right], \tag{10.42}$$

with $\omega_J = 2B(2J+3)/\hbar$, $\omega'_J = 2B(J+1)/\hbar$, which shows that the mean (permanent) alignment goes to 1/2 in this limit. This approximation is not very accurate for the transitions $|J = 0\rangle \rightleftharpoons |J = 2\rangle$, $|J = 0\rangle \rightleftharpoons |J = 1\rangle$, but allows one to determine quite precisely the target state, and to reproduce the main features of $\langle \cos^2\Theta \rangle$ generated a short non-resonant pulse interaction, and $\langle \cos\Theta \rangle$ generated by an HCP, even if the initial condition is a cold molecule $|J_0 = 0\rangle$. This calculation generalizes the one made in Refs [188, 163] for the initial condition $|\phi(t_i = 0)\rangle = |J_0 = 0\rangle$.

We first consider even J. We define the operator (with even positive or zero integer J)

$$C = C_0 + V/2, \tag{10.43}$$

with

$$C_0 = \frac{1}{2} \sum_{J \text{ even}} |J\rangle \langle J| , \tag{10.44a}$$

$$V = \frac{1}{2} \sum_{J \text{ even}} \left(|J-2\rangle \langle J| + |J+2\rangle \langle J| \right) , \quad |-2\rangle = 0. \tag{10.44b}$$

Since this gives in the basis $\{|0\rangle , |2\rangle , |4\rangle , \cdots\}$

$$C = \frac{1}{4} \begin{bmatrix} 2 & 1 & 0 & \cdots \\ 1 & 2 & 1 & \ddots \\ 0 & 1 & \ddots & \ddots \\ \vdots & \ddots & \ddots & \ddots \end{bmatrix} , \tag{10.45}$$

using the limit (10.40), we can substitute $\cos^2 \Theta$ by the operator C.

For an interaction with the permanent dipole moment, we define the operator

$$B = \frac{1}{2} \sum_{J} \left(|J-1\rangle \langle J| + |J+1\rangle \langle J| \right) , \quad |-1\rangle = 0. \tag{10.46}$$

Since this gives in the basis $\{|0\rangle , |1\rangle , |2\rangle , \cdots\}$

$$B = \frac{1}{2} \begin{bmatrix} 0 & 1 & 0 & \cdots \\ 1 & 0 & 1 & \ddots \\ 0 & 1 & \ddots & \ddots \\ \vdots & \ddots & \ddots & \ddots \end{bmatrix} , \tag{10.47}$$

using the limit (10.40), we can substitute $\cos \Theta$ by the operator B.

The target state

With this model, we can determine exactly the target state for the orientation problem

$$|\chi_{N,\pm}\rangle = \sqrt{\frac{2}{N+1}} \sum_{J=J_{\min}}^{J_{\max}} (\pm 1)^{J-J_{\min}+1} \sin \left[\pi \frac{J - J_{\min} + 1}{N+1} \right] |J\rangle, \tag{10.48}$$

and for the alignment problem (i.e. with only even or odd J)

$$|\chi_{N}\rangle = \sqrt{\frac{2}{N+1}} \sum_{J=J_{\min}}^{J_{\max}} \sin \left[\pi \frac{(J - J_{\min})/2 + 1}{N+1} \right] |J\rangle, \tag{10.49}$$

whose coefficients form a half-period-sine shape, peaked around the average value between $J_{\min}$ and $J_{\max}$. This leads to

$$\langle \chi_{N,\pm}| \cos_N \Theta |\chi_{N,\pm}\rangle = \pm \cos \left(\frac{\pi}{N+1} \right) , \tag{10.50a}$$

$$\sum_{J=J_{\min}}^{J_{\max}-1} \left| c_J^{J_0,M_0} c_{J+1}^{J_0,M_0} \right| = \cos \left(\frac{\pi}{N+1} \right) , \tag{10.50b}$$

and

$$\langle\chi_N|\cos_N^2\Theta|\chi_N\rangle = \frac{1}{2}\left[1+\cos\left(\frac{\pi}{N+1}\right)\right], \tag{10.51a}$$

$$\sum_{J=J_{\min}}^{J_{\max}-2}\left|c_J^{J_0,M_0}c_{J+2}^{J_0,M_0}\right| = \cos\left(\frac{\pi}{N+1}\right), \tag{10.51b}$$

giving the maximum as a function of N for the orientation:

$$\max_t|\langle\cos\Theta\rangle_{J_0,M_0}(t)| = \cos\left(\frac{\pi}{N+1}\right), \tag{10.52}$$

and for the alignment:

$$\max_t\langle\cos^2\Theta\rangle_{J_0,M_0}(t) = \frac{1}{2}\left[1+\cos\left(\frac{\pi}{N+1}\right)\right]. \tag{10.53}$$

We have checked that, for any value of N, the target state associated to the maximum eigenvalue (in absolute value) of $\cos_N^2\Theta$ (resp. $\cos_N\Theta$) for the alignment (orientation) problem, obtained with this solvable model is very close to the exact (numerical) eigenstate.

This implies that the value of the angle corresponding to the alignment is always smaller than the one corresponding to the orientation for a given N, since $\sqrt{\frac{1}{2}\left[1+\cos\left(\frac{\pi}{N+1}\right)\right]} > \cos\left(\frac{\pi}{N+1}\right)$, i.e. *the alignment given by the target state is more efficient than the orientation for a given N.*

We have reported in Fig. 10.9 the theoretical maximum (10.52) for different N with $J_{\min} = 0$, comparing it with the equal weight solution (all the $c_J^{J_0,M_0}$ equal to $1/\sqrt{N}$) and random coefficient solution averaged (the $|c_J^{J_0,M_0}|^2$ are uniformly randomly distributed). Figure 10.9 shows that, as expected, $\max_t|\langle\cos\Theta\rangle_{J_0,M_0}(t)|$ eventually reaches one for sufficiently many populated states whatever are the coefficient $c_J^{J_0,M_0}$. However for more and more populated states, this maximum become more and more narrow. It is thus of interest to maximize $\max_t|\langle\cos\Theta\rangle_{J_0,M_0}(t)|$ with a number of populated states as small as possible to have a broader maximum.

Dynamics by an impulsive non-resonant laser pulse

The propagator can be decomposed as

$$e^{i2\zeta C} = e^{i\zeta}e^{i\zeta V}, \tag{10.54}$$

where we have exactly

$$e^{i\zeta V} = \sum_{J,J'\text{ even}} u_J^{J'}(\zeta)\,|J\rangle\langle J'|, \tag{10.55}$$

with for $\zeta > 0$, defining $u_J^{-2} = 0$,

$$u_J^{J'}(\zeta) = e^{i\frac{\pi}{4}(J-J')}\frac{J-J'+2}{\zeta}\mathcal{J}_{J/2-J'/2+1}(\zeta) + u_{J+2}^{J'-2}(\zeta), \tag{10.56a}$$

$$= e^{i\frac{\pi}{4}(J-J')}\frac{2}{\zeta}\sum_{n=0}^{J'/2}(-1)^n\,a_n\mathcal{J}_{a_n}(\zeta), \tag{10.56b}$$

$$a_n = J/2 - J'/2 + 1 + 2n, \tag{10.56c}$$

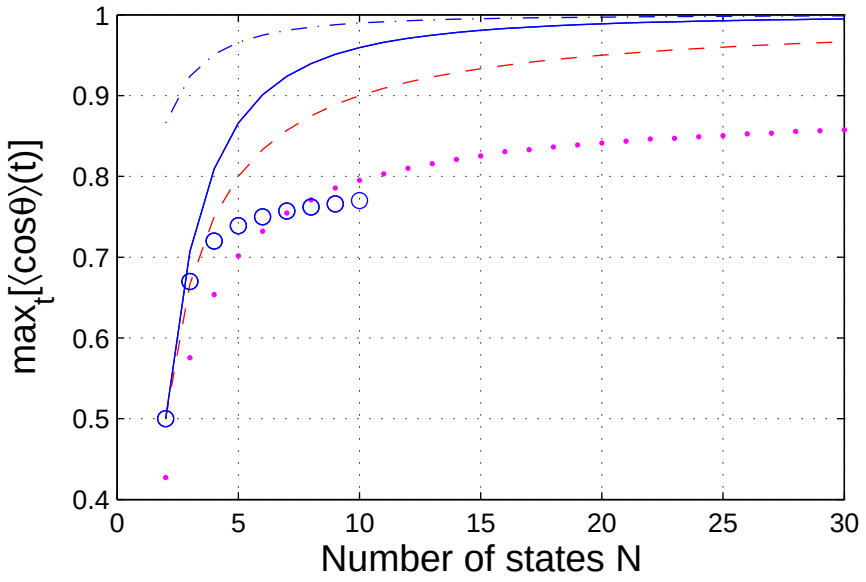

FIG. 10.9 - *Theoretical maximum* $\max_t[\langle\cos\Theta\rangle(t)]$ *as a function of the size* N *of the subspace* $\mathcal{H}_N$ *spanned by the* N *lowest rotational states: optimum given by Eq. (10.52) (full line), square root of the optimum given by Eq. (10.53)* $\sqrt{\frac{1}{2}\left[1+\cos\left(\frac{\pi}{N+1}\right)\right]}$ *(dotted dashed line), equal weight solution (dashed line), random coefficients (dotted line), and the numerical simulation obtained for a half-cycle interaction at* $T=0$ *(circles).*

and $\mathcal{J}_J(\cdot)$ the bessel functions of integer (positive or negative) order. The diagonal operator $e^{i2\zeta}$ gives only an additional phase independent of J, which does not contribute in the calculation of $\langle\cos^2\Theta\rangle(t)$.

If the initial condition is $|\phi(t_i=0)\rangle = |J_0\rangle$, the solution reads

$$|\phi(t)\rangle = e^{i(\mathcal{A}B\gamma_\perp t/\hbar+\zeta)} \sum_{J \text{ even}} u_J^{J_0}(\zeta)\, e^{-iBJ(J+1)t/\hbar}\,|J\rangle \tag{10.57a}$$

with

$$u_J^{J_0}(\zeta) = e^{i\frac{\pi}{4}(J-J_0)}\frac{2}{\zeta}\sum_{n=0}^{J_0/2}(-1)^n\, a_n \mathcal{J}_{a_n}(\zeta) = e^{i\frac{\pi}{4}(J-J_0)}[\mathcal{J}_{(J-J_0)/2}(\zeta)+\mathcal{J}_{(J+J_0)/2+2}(\zeta)], \tag{10.58a}$$

$$a_n = J/2 - J_0/2 + 1 + 2n. \tag{10.58b}$$

The diagonal operator $e^{i(\mathcal{A}B\gamma_\perp t/\hbar+\zeta)}$ gives only an additional phase independent of J, which does not contribute in the calculation of $\langle\cos^2\Theta\rangle$ and can be thus ignored in the calculation.

If a cold molecule is considered ($J_0=0$), one obtains [162]

$$u_J^0(\zeta) = e^{i\frac{\pi}{4}J}\frac{J+2}{\zeta}\mathcal{J}_{J/2+1}(\zeta) = e^{i\frac{\pi}{4}J}[\mathcal{J}_{J/2}(\zeta)+\mathcal{J}_{J/2+2}(\zeta)]. \tag{10.59}$$

If we now consider odd J, the preceding results can be trivially extended as follows

$$u_J^{J'}(\zeta) = e^{i\frac{\pi}{4}(J-J')}\frac{2}{\zeta}\sum_{n=0}^{(J'-1)/2}(-1)^n\, a_n \mathcal{J}_{a_n}(\zeta). \tag{10.60}$$

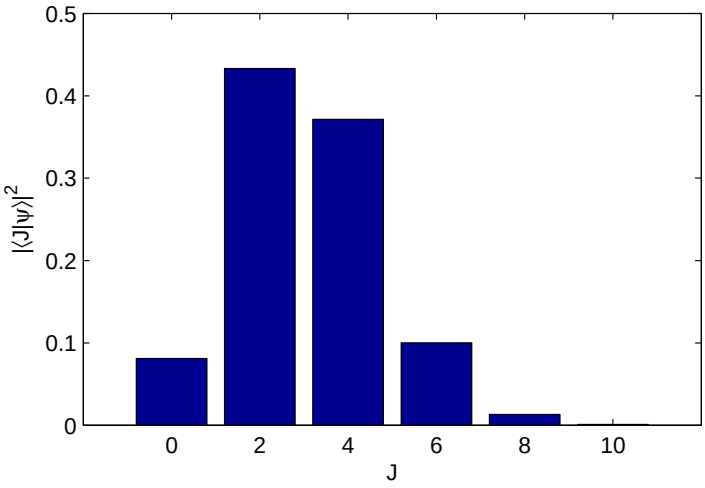

FIG. 10.10 - *Postpulse distribution of the dynamics in J in the conditions of Fig. 10.4.*

If a cold molecule is considered, Eq. (10.59) leads to

$$\left\langle \cos^2\Theta \right\rangle_{0,0}(t) = \frac{1}{2} + \frac{2}{\zeta^2} \sum_{J \text{ even}} (J/2+1)\, \mathcal{J}_{J/2+1}(\zeta)\, (J/2+2)\, \mathcal{J}_{J/2+2}(\zeta) \sin(\omega_J t)\,. \tag{10.61}$$

We thus obtain in (10.8b) the following phases

$$\theta_J^{0,0} - \theta_{J+2}^{0,0} = \frac{\pi}{2}(\mathrm{sgn}\left[\mathcal{J}_{J/2+1}(\zeta)\right] - \mathrm{sgn}\left[\mathcal{J}_{J/2+2}(\zeta)\right] - 1) \tag{10.62a}$$

$$= \pm\pi/2 \tag{10.62b}$$

with the sign function $\mathrm{sgn}(x) = +1$ if $x \geq 0$ and -1 otherwise. Detailled analysis of this expression shows that since the Bessel functions $\mathcal{J}_{J/2+1}(\zeta)$ have the same sign for all even J for $\zeta \lesssim 3.83$, we have in this case $\theta_J^{0,0} - \theta_{J+2}^{0,0} = -\pi/2$ for all even J. In this case, the components of the sines have all the same signs (positive) and will thus accumulate for all J only around $t = t_p \equiv pT/4 = p\pi/4B$, with p an integer: one obtains for $\langle\cos^2\Theta\rangle_{0,0}$ a value of 0.5 at $t = t_0 = 0$ and $t = t_2 = T/2$, the main maximum at $t = t_3 = 3T/4$ [$\sin(\omega_J t) = 1$], the main minimum at $t = t_1 = T/4$ [$\sin(\omega_J t) = -1$]. Around $t = T/2$, one obtains a local maximum (for $t < T/2$) and a local minimum (for $t > T/2$) that can be evaluated by expanding $\sin(\omega_J t)$.

The comparison between the full numerical calculation and the use of this solvable model is made in Fig. 10.4 for a strong field, which transfers efficiently the population from $J = 0$. (This postpulse distribution in J is shown in Fig. 10.10.) One observes only a global qualitative similarity in Fig. 10.4. The duration of the alignment revivals are well predicted. The main point is that *the maximum alignment is quantitatively well predicted but not on the right peak.* This feature is observed for strong fields near the saturation of alignment, as shown below. This is preserved for other temperature. We conclude that this solvable model is quite well adapted to analyze the maximum of alignment and its duration for strong field.

Saturation of alignment

Since we have the approximate asymptotic value

$$S_0 := \frac{2}{\zeta^2} \sum_{k=1}^{\infty} k \mathcal{J}_k(\zeta)\, (k+1)\, \mathcal{J}_{k+1}(\zeta) \underset{\zeta\to\infty}{\to} 0.424413, \tag{10.63}$$

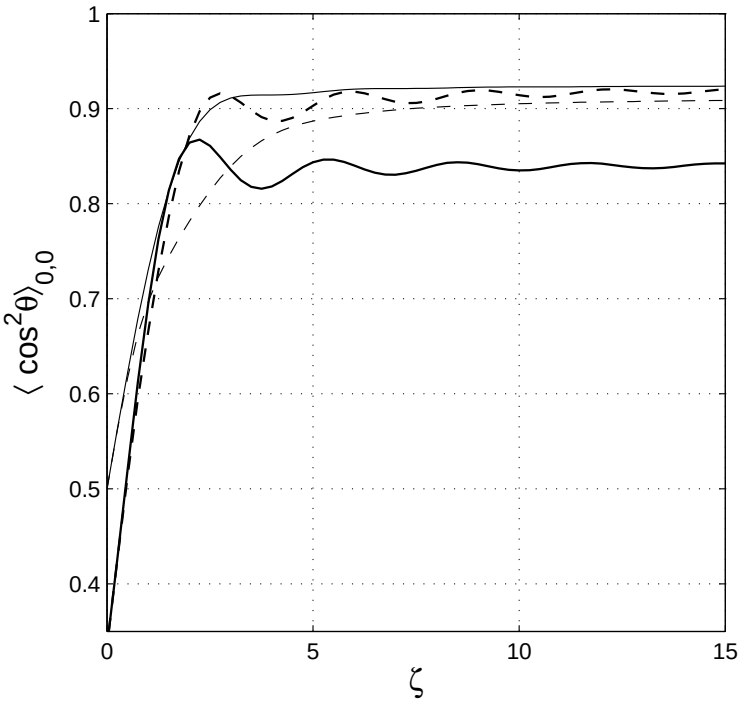

FIG. 10.11 - $\max_t \langle \cos^2\Theta \rangle_{0,0}$ *as a function of* ζ *for the second peak (near* t_2*) (dashed lines) and for the third peak (at* t_3*) (full lines) obtained with the full model (10.24) with no centrifugal distortion (thick lines) and the approximate model [where* $\cos^2\Theta$ *is substituted by* C *(10.45)] (thin lines).*

this model shows a *saturation* of the maximum alignment as a function of ζ induced by a short non-resonant pulse:

$$\left\langle \cos^2\Theta \right\rangle_{0,0}(t_3) \simeq 0.924413. \tag{10.64}$$

Figure 10.11 displays the maximum of the third peak $\langle \cos^2\Theta \rangle_{0,0}(t_3)$ and the maximum of the second peak around t_2 : $\max_{t\sim t_2} \langle \cos^2\Theta \rangle_{0,0}$ as a function of ζ. This shows that the model is accurate for the second peak and quantitatively a bit inaccurate for the third peak, but however shows its saturation. This confirms the preceding conclusion, that the maximum alignment is quantitatively well predicted within this model but not on the right peak.

This saturation value is already approximately obtained for modest (however still in the strong field regime) values of ζ: we obtain $\langle \cos^2\Theta \rangle_{0,0}(t_3) \simeq 0.911$ for $\zeta = 3$, corresponding to $I = 13.5$ TW/cm^2 in the CO_2 molecule for $T_{FWHM} = 0.1$ ps. The alignment saturation is thus already reached in this case for values of $\zeta \lesssim 3.83$ satisfying $\theta_J^{0,0} - \theta_{J+2}^{0,0} = -\pi/2$. This explains the remarkable efficiency of the alignment for cold molecules.

For a thermal ensemble, we have to consider a set of initial conditions. The solution (10.56) shows that the phase in (10.8b) is $\theta_J^{J_0,M_0} - \theta_{J+2}^{J_0,M_0} = \pm\pi/2$ for any J_0, M_0 and consequently that the alignment is expected to be efficient for any initial condition at the third (resp. first) peak at t_3 (resp. t_1) where $\sin[2B(2J+3)t/\hbar] = 1$ (resp. $\sin[2B(2J+3)t/\hbar] = -1$) if we consider even (resp. odd) J_0, and robust with respect to the thermal averaging, if the sine contributions do not cancel. Indeed, for an initial condition J_0, we obtain in the limit of strong field the

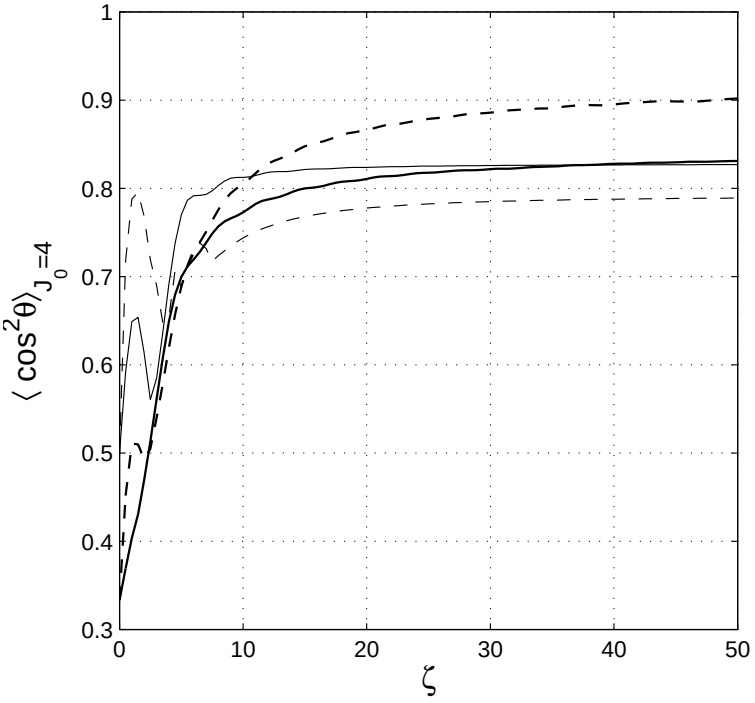

FIG. 10.12 - $\max_t \sum_{M_0=-J_0}^{+J_0} \langle \cos^2\Theta \rangle_{J_0,M_0} - 1/3$ *for* $J_0 = 4$ *as a function of* ζ *for the second peak (near* t_2*) (dashed lines) and for the third peak (at* t_3*) (full lines) obtained with the full model (10.24) with no centrifugal distortion (thick lines) and the approximate model [where* $\cos^2\Theta$ *is substituted by* C *(10.45)] (thin lines).*

following minimum and maximum

$$\left\langle \cos^2\Theta \right\rangle_{J_0,M_0}(t_1) \rightsquigarrow \begin{cases} \frac{1}{2} - \sum_{n=0}^{J_0/2} (-1)^n S_n, \text{ for even } J_0 \\ \frac{1}{2} + \sum_{n=0}^{(J_0-1)/2} (-1)^n S_n, \text{ for odd } J_0 \end{cases} \tag{10.65a}$$

$$\left\langle \cos^2\Theta \right\rangle_{J_0,M_0}(t_3) \rightsquigarrow \begin{cases} \frac{1}{2} + \sum_{n=0}^{J_0/2} (-1)^n S_n, \text{ for even } J_0 \\ \frac{1}{2} - \sum_{n=0}^{(J_0-1)/2} (-1)^n S_n, \text{ for odd } J_0 \end{cases} \tag{10.65b}$$

with

$$S_n = \frac{2}{\zeta^2} \sum_{k=1}^{\infty} k \mathcal{J}_k(\zeta) \left(k + 2n + 1\right) \mathcal{J}_{k+2n+1}(\zeta). \tag{10.66}$$

The main contributions are associated to the phase $\theta_J^{J_0,M_0} - \theta_{J+2}^{J_0,M_0} = -\pi/2$. We obtain a saturation of the S_n in the limit of strong ζ with the approximate values: $S_0 \to 0.42$, $S_1 \to 0.086$, $S_2 \to -0.013$, $S_3 \to 0.006$, $\cdots$, $\lim_{n\to\infty} S_n = 0$. The expressions (10.65) show thus a saturation for any J_0: For $J_0 = 2$: $\langle \cos^2\Theta \rangle_{J_0,M_0}(t_3) \to 0.84$, for $J_0 = 4$: $\langle \cos^2\Theta \rangle_{J_0,M_0}(t_3) \to 0.825$, for $J_0 = 6$: $\langle \cos^2\Theta \rangle_{J_0,M_0}(t_3) \to 0.82$. This peak thus quickly saturates as a function of J_0, at $\langle \cos^2\Theta \rangle_{J_0,M_0}(t_3) \simeq 0.82$, *meaning that the alignment saturation is expected to occur below and close to* 0.82 *for moderately cold to hot molecules.*

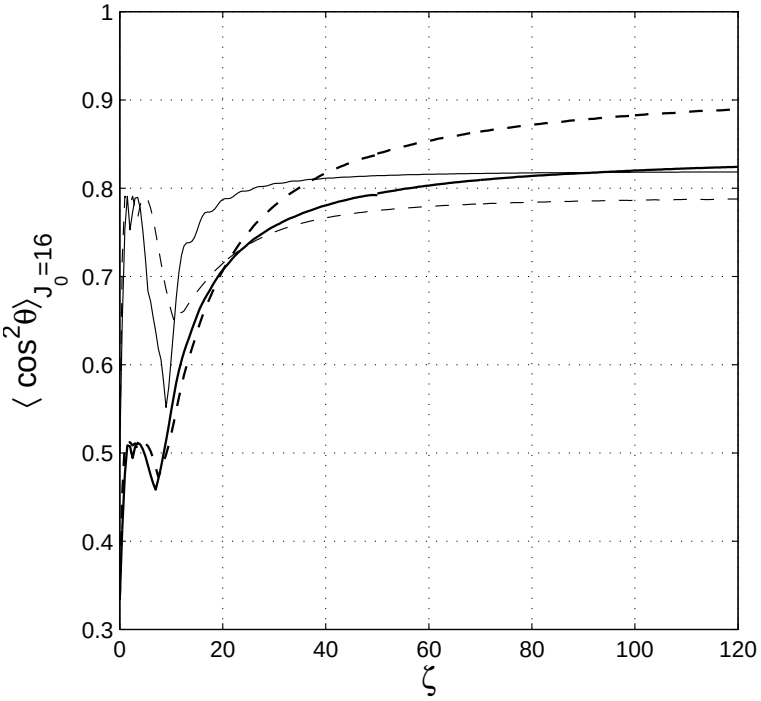

FIG. 10.13 - *Same as in Fig. 10.12 for* $J_0 = 16$.

Figs. 10.12 and 10.13, in the case of even J_0, display the maximum of the third peak $\langle \cos^2\Theta \rangle_{J_0}(t_3) := \sum_{M_0=-J_0}^{+J_0} \langle \cos^2\Theta \rangle_{J_0,M_0}(t_3)$ and the maximum of the second peak around t_2 : $\max_{\sim t_2} \langle \cos^2\Theta \rangle_{J_0}$ as a function of ζ respectively for $J_0 = 4$ (corresponding to the most initially populated states at $T = 20$ K for the CO_2 molecule) and $J_0 = 16$ (corresponding to $T = 296$ K). This shows that the saturation of the third peak is very well predicted by the model and that this saturation occurs at a stronger fields for higher temperatures. The model is quantitatively quite inaccurate for the second peak, but however shows its saturation.

Comparison of the dynamics with the target state

We show the comparison of the dynamics by a sudden laser pulse with the optimal solution calculated in the preceding solvable model in Fig. 10.4. The solvable model and the target state are remarkably close for the subspace dimension $N = 4$. We calculate indeed using the approximate dynamics (with the solvable model) $|\langle \chi_4 | \psi_{\text{approx}}(t_3) \rangle|^2 \approx 0.88$ at the third peak. We calculate, using the exact (numerical) dynamics: $|\langle \chi_4 | \psi(t_{\text{exact}} \approx t_2) \rangle|^2 \approx 0.83$ at the maximum of $\langle \cos^2\Theta \rangle(t)$.

Dynamics by an HCP

The propagator can be written as

$$e^{i\xi B} = \sum_{J,J'} u_J^{J'}(\xi) \, |J\rangle \langle J'| \,, \tag{10.67}$$

with for $\xi > 0$ and $u_{J,-1} = 0$

$$u_J^{J'}(\xi) = 2e^{i\frac{\pi}{2}(J-J')}\frac{J-J'+1}{\xi}\mathcal{J}_{J-J'+1}(\xi) + u_{J+1,J'-1}(\xi), \tag{10.68a}$$

$$= e^{i\frac{\pi}{2}(J-J')}\frac{2}{\xi}\sum_{n=0}^{J'}(-1)^n\, a_n \mathcal{J}_{a_n}(\xi), \tag{10.68b}$$

$$a_n = J - J' + 1 + 2n, \tag{10.68c}$$

For $\xi < 0$, since

$$\mathcal{J}_J(\xi) = \mathcal{J}_J(|\xi|)e^{-i\pi J}, \tag{10.69}$$

we have

$$u_J^{J'}(\xi) = 2e^{-i\frac{\pi}{2}(J-J')}\frac{J-J'+1}{|\xi|}\mathcal{J}_{J-J'+1}(|\xi|) + u_{J+1,J'-1}(\xi), \tag{10.70a}$$

$$= e^{-i\frac{\pi}{2}(J-J')}\frac{2}{|\xi|}\sum_{n=0}^{J'}(-1)^n\, a_n \mathcal{J}_{a_n}(|\xi|), \tag{10.70b}$$

$$a_n = J - J' + 1 + 2n. \tag{10.70c}$$

This can be summarized for all ξ by

$$u_J^{J'}(\pm|\xi|) = e^{\pm i\frac{\pi}{2}(J-J')}\frac{2}{|\xi|}\sum_{n=0}^{J'}(-1)^n\, a_n \mathcal{J}_{a_n}(|\xi|). \tag{10.71}$$

If the initial condition is $|\phi(t_i = 0)\rangle = |J_i\rangle$, the solution reads right after the pulse

$$|\phi(t_f)\rangle \equiv e^{i\xi B}\,|\phi(t_i)\rangle\,, \tag{10.72a}$$

$$= \sum_J u_J^{J_i}(\xi)\,|J\rangle\,. \tag{10.72b}$$

If additionally $J_i = 0$, one obtains

$$|\phi(t_f)\rangle = \sum_J u_J^0(\xi)\,|J\rangle\,, \tag{10.73a}$$

$$u_J^0(\pm\,|\xi|) = 2e^{\pm i\frac{\pi}{2}J}\frac{J+1}{|\xi|}\mathcal{J}_{J+1}(|\xi|). \tag{10.73b}$$

This approximation gives $\Delta^{J_0,M_0} = -\pi/2$ for positive area ξ, $\Delta^{J_0,M_0} = +\pi/2$ for negative area ξ, and

$$\langle\cos\Theta\rangle_{J_0,M_0}(t) \simeq 4\ \mathrm{sgn}(\xi)\sum_J (J+1)\frac{\mathcal{J}_{J+1}(\xi)}{\xi}(J+2)\frac{\mathcal{J}_{J+2}(\xi)}{\xi}\sin\left[2B\,(J+1)\,t/\hbar\right]. \tag{10.74}$$

The comparison between the full numerical calculation and the use of this solvable model is made in Fig. 10.8. One observes a very good agreement, better than for alignment by a short non-resonant pulse. We conclude that this solvable model is very well adapted to analyze the orientation in strong field.

Comparison of the dynamics with the target state

We show the comparison of the dynamics by a sudden laser pulse with the optimal solution calculated in the preceding solvable model in Fig. 10.8. The solvable model and the target state are quite close for the subspace dimension $N = 5$, but not so than for the alignment by the sudden non-resonant pulse. We calculate indeed using the approximate dynamics (with the solvable model) $|\langle\chi_5|\psi_{\text{approx}}(t)\rangle|^2 \approx 0.79$ at the peak of orientation. We calculate, using the exact (numerical) dynamics: $|\langle\chi_5|\psi(t_{\text{exact}} \approx t_2)\rangle|^2 \approx 0.80$ at the maximum of $\langle\cos^2\Theta\rangle(t)$.

Saturation of orientation

Using the same arguments as for alignment, we conclude that the orientation is expected to saturate in a very similar way. Since the phases are not favorable (i.e. $\Delta \approx \pi/2$), the value of the saturation will be lower than the theoretical one. In particular, for a cold molecule, using (10.63), we expect the saturation at

$$\max_t |\langle\cos\Theta\rangle_{J_0,M_0}(t)| < 0.848. \tag{10.75}$$

We obtain numerically $\max_t |\langle\cos\Theta\rangle_{J_0,M_0}(t)| \approx 0.75$.

10.1.7 Perturbation theory from low to moderate intensities

One can calculate beyond the standard time-dependent perturbation theory, expanding the sudden approximation propagator (10.25b) in Bessel functions:

$$e^{i2\zeta\cos^2\Theta} = e^{i\zeta}\left[\mathcal{J}_0(\zeta) + 2\sum_{n=1}^{\infty} i^n \mathcal{J}_n(\zeta)\cos(2n\Theta)\right] \tag{10.76}$$

using the iterative formula to express $\cos(2n\Theta)$ as a function of $\cos^2(\Theta)$ of known matrix elements:

$$\text{even } n: \quad \cos(2n\Theta) = 2^{n-1}(2\cos^2\Theta - 1)^n - \frac{1}{2}C^n_{n/2} - \sum_{\ell=1}^{n/2-1} C^n_{n/2-\ell}\cos(4\ell\Theta), \tag{10.77a}$$

$$\text{odd } n: \quad \cos(2n\Theta) = 2^{n-1}(2\cos^2\Theta - 1)^n - \sum_{\ell=1}^{(n-1)/2} C^n_{(n-1)/2+\ell}\cos(2(2\ell-1)\Theta). \tag{10.77b}$$

We obtain at the lowest order (appropriate for low intensities, but which allows non-negligible population transfers as opposed to the standard time-dependent perturbation theory)

$$\begin{aligned} e^{i2\zeta\cos^2\Theta}e^{-i\zeta}|J_0, M_0\rangle = &[\mathcal{J}_0(\zeta) + 2i\mathcal{J}_1(\zeta)(2\alpha_{J_0,M_0} - 1)]\,|J_0\rangle \\ &+ 4i\mathcal{J}_1(\zeta)\left(\beta_{J_0,M_0}|J_0+2\rangle + \beta_{J_0-2,M_0}|J_0-2\rangle\right), \end{aligned} \tag{10.78}$$

i.e. apart the irrelevant global phase

$$c^{J_0,M_0}_{J_0} \approx \mathcal{J}_0(\zeta) + 2i\mathcal{J}_1(\zeta)(2\alpha_{J_0,M_0} - 1), \tag{10.79a}$$

$$c^{J_0,M_0}_{J_0+2} \approx 4i\mathcal{J}_1(\zeta)\beta_{J_0,M_0}, \quad c^{J_0,M_0}_{J_0-2} \approx 4i\mathcal{J}_1(\zeta)\beta_{J_0-2,M_0}. \tag{10.79b}$$

Developing the Bessel functions as functions of ζ:

$$\mathcal{J}_0(\zeta) \approx 1 - \frac{\zeta^2}{4} + \mathcal{O}(\zeta^4), \tag{10.80a}$$

$$\mathcal{J}_1(\zeta) \approx \frac{\zeta}{2} + \mathcal{O}(\zeta^3), \tag{10.80b}$$

one recovers at the relevant lowest order the squared form of the permanent alignment, and the linear form of the peak alignment as a function of the field intensity at the lowest order as numerically shown in Fig. 10.7.

For moderate intensities, a good approximation consists in (i) keeping the first Bessel functions, for instance the first three: $\mathcal{J}_0(\zeta)$, $\mathcal{J}_1(\zeta)$, and $\mathcal{J}_2(\zeta)$, that allows a precise calculation of the probability amplitudes on the states $|J_0, M_0\rangle$, $|J_0 \pm 2, M_0\rangle$, and $|J_0 \pm 4, M_0\rangle$, and in (ii) calculating the largest contribution of the other probability amplitudes assuming that $\mathcal{J}_2(\zeta) \ll \mathcal{J}_3(\zeta) \ll \mathcal{J}_4(\zeta) \ll \cdots$ The latter calculation is conducted by noticing that, using the expansion (10.76), the largest probability amplitude on the state $|J_0 + 2n, M_0\rangle$ is given by the operator $\cos^{2n}\Theta$, i.e.

$$\langle J_0 \pm 2n| \left[2 \sum_{m=3}^{\infty} i^m \mathcal{J}_m(\zeta) \cos(2m\Theta) \right] |J_0\rangle \approx 2^{2n} i^n \mathcal{J}_n(\zeta) \langle J_0 \pm 2n| \cos^{2n}\Theta |J_0\rangle. \tag{10.81}$$

We finally obtain (omitting the irrelevant global phase)

$$c_{J_0}^{J_0,M_0} \approx \mathcal{J}_0(\zeta) + 2i\mathcal{J}_1(\zeta)(2\alpha_{J_0,M_0} - 1) + 2\mathcal{J}_2(\zeta)(8\alpha_{J_0,M_0} - 8\alpha_{J_0,M_0}^2 - 8\beta_{J_0,M_0}^2 - 8\beta_{J_0-2,M_0}^2 - 1), \tag{10.82a}$$

$$= \frac{2}{\zeta}\mathcal{J}_1(\zeta) + 2i\mathcal{J}_1(\zeta)(2\alpha_{J_0,M_0} - 1) + 16\mathcal{J}_2(\zeta)(\alpha_{J_0,M_0} - \alpha_{J_0,M_0}^2 - \beta_{J_0,M_0}^2 - \beta_{J_0-2,M_0}^2 - 3/16) \tag{10.82b}$$

$$c_{J_0+2}^{J_0,M_0} \approx 4i\mathcal{J}_1(\zeta)\beta_{J_0,M_0} + 16\mathcal{J}_2(\zeta)\beta_{J_0,M_0}(1 - \alpha_{J_0,M_0} - \alpha_{J_0+2,M_0}) \tag{10.82c}$$

$$c_{J_0-2}^{J_0,M_0} \approx 4i\mathcal{J}_1(\zeta)\beta_{J_0-2,M_0} + 16\mathcal{J}_2(\zeta)\beta_{J_0-2,M_0}(1 - \alpha_{J_0,M_0} - \alpha_{J_0-2,M_0}) \tag{10.82d}$$

$$c_{J_0+2n}^{J_0,M_0} \approx 2^{2n} i^n \mathcal{J}_n(\zeta)\beta_{J_0,M_0}\beta_{J_0+2,M_0}\cdots\beta_{J_0+2(n-1),M_0}, \quad n > 1, \tag{10.82e}$$

$$c_{J_0-2n}^{J_0,M_0} \approx 2^{2n} i^n \mathcal{J}_n(\zeta)\beta_{J_0-2,M_0}\beta_{J_0-4,M_0}\cdots\beta_{J_0-2n,M_0}, \quad n > 1. \tag{10.82f}$$

If we assume $\alpha_{J_0,M_0} \approx 1/2$, and $\beta_{J_0\pm 2n,M_0} \approx 1/4$ for all $n \geq 0$ (which implicitly means that $J_0 \to \infty$, such that the bottom of the rotational spectrum is ignored), we simply obtain

$$c_{J_0\pm 2n}^{J_0,M_0} \approx i^n \mathcal{J}_n(\zeta), \quad n \geq 0. \tag{10.83}$$

We remark that in the limits $J_0 \to \infty$, $\alpha_{J_0,M_0} = 1/2$, and $\beta_{J_0\pm 2n,M_0} = 1/4$, this latter solution is in fact exact after the full summation of the expansion (10.76).

10.1.8 A model for moderately cold to hot molecules

When the temperature is sufficiently high such that the maximum initial population $(2J_0+1)\rho_{J_0}$ is located at $J_0 \gg 0$ (i.e. from moderately cold to hot molecules), from the preceding analysis,

we can calculate the solution, ignoring the bottom of the rotational spectrum (omitting the irrelevant global phase):

$$|\psi_{J_0,M_0}(t)\rangle \approx \sum_{\Delta J \geq |M_0|-J_0} i^{|\Delta J|/2} \mathcal{J}_{|\Delta J|/2}(\zeta) e^{-iB(J_0+\Delta J)(J_0+\Delta J+1)t/\hbar} |J_0+\Delta J, M_0\rangle \,. \quad (10.84)$$

We obtain in that case

$$\left\langle \cos^2\Theta \right\rangle_{J_0,M_0}(t) = \frac{1}{2} + \frac{1}{2} \sum_{n\in\mathbb{Z}} \mathcal{J}_{|n|}(\zeta)\mathcal{J}_{|n+1|}(\zeta) \sin\left(\omega_{J_0+2n} t\right). \quad (10.85)$$

Such an approximation has been used for the control of alignment by shaped laser pulses in [189]. This approximation allows us to show in particular that for an intermediate regime of field intensities ($\sim 10^{13} - 10^{14}$ W/cm^2), the resulting alignment signal after two short pulses is obtained by superposing the two signals that would be obtained if the molecule experienced the two pulses independently.

This approximation leads for the saturation

$$\max_t |\left\langle \cos^2\Theta \right\rangle_{J_0,M_0}(t)| = \frac{1}{2} + \sum_{n\geq 0} \mathcal{J}_{|n|}(\zeta)\mathcal{J}_{|n+1|}(\zeta) \approx 0.82, \quad (10.86)$$

consistent with what obtained earlier.

10.2 Measuring alignment

Most of the quantitative measurement of alignment have been realized by breaking the molecule through multi-electron dissociative ionization (MEDI) (see for instance [164, 190]). In the alignment experiment of Ref. [161], the probe was implemented by low laser intensity through a resonant dissociation followed by the ionization of the fragments. In these works, the quantitative characterization of the alignment, i.e. the evaluation of $\langle\cos^2\Theta\rangle$, is deduced from the angular distribution of the ionized fragments. Such breaking of the molecule induces an additional alignment which is difficult to separate from the alignment due to the pump field.

An alternative method suggested in [165, 166] consists in measuring a signal proportional to the difference between $\langle\cos^2\Theta\rangle$ and its isotropic value 1/3 (or its square), and thus to access *directly* the measure of the alignment, without breaking the molecule. This has been referred to as *non-intrusive* measurement techniques. The first method of this type, that was proposed in [165], is based on a weak field polarization spectroscopy technique [191]. This technique has been related to a measurement by a weak probe of the birefringence induced by the alignment of the molecular sample [166].

Another non-intrusive method that was recently developed in [192] is a technique based on the *cross defocusing* of a time-delayed probe pulse produced by the spatial distribution of aligned molecules. Field-free alignment leads indeed to a spatial gradient of the time dependent refractive index as a result of the rotational response. The effect can be seen as the creation in the medium of a time-dependent nonlinear lens. Next, a weak probe pulse crosses the pump pulse at the focus and experiences refractive-index gradient, from which one can extract the degree of alignment.

10.3 Field-free two-direction alignment alternation by elliptic laser pulses

In this article [126], we show that a linear molecule subjected to a short specific elliptically polarized laser field yields postpulse revivals exhibiting alignment alternatively located along the orthogonal axis and the major axis of the ellipse. The effect is experimentally demonstrated by measuring the optical Kerr effect along two different axes using the defocusing technique. The conditions ensuring an optimal field-free alternation of high alignments along both directions are derived.

PRL 95, 063005 (2005) PHYSICAL REVIEW LETTERS week ending 5 AUGUST 2005

Field-Free Two-Direction Alignment Alternation of Linear Molecules by Elliptic Laser Pulses

D. Daems,[1,2,*] S. Guérin,[1,†] E. Hertz,[1] H. R. Jauslin,[1] B. Lavorel,[1] and O. Faucher[1]

[1]*Laboratoire de Physique de l'Université de Bourgogne, UMR CNRS 5027, BP 47870, 21078 Dijon, France*

[2]*Center for Nonlinear Phenomena and Complex Systems, Université Libre de Bruxelles, 1050 Brussels, Belgium*

(Received 31 January 2005; published 5 August 2005)

We show that a linear molecule subjected to a short specific elliptically polarized laser field yields postpulse revivals exhibiting alignment alternatively located along the orthogonal axis and the major axis of the ellipse. The effect is experimentally demonstrated by measuring the optical Kerr effect along two different axes. The conditions ensuring an optimal field-free alternation of high alignments along both directions are derived.

DOI: 10.1103/PhysRevLett.95.063005 PACS numbers: 33.80.−b, 32.80.Lg, 42.50.Hz

Preparing controlled alignment of molecules is of considerable importance for a large variety of processes (see [1] for a review). It is well established theoretically and experimentally that the alignment of a linear molecule along the axis of a linearly polarized field can be of two types: adiabatic alignment during the interaction with the field, or transient alignment revivals after a short pulse. The latter is in general preferred for further manipulations since it offers field-free aligned molecules. The adiabatic alignment has been extended to three dimensional alignment of an asymmetric top molecule [2].

A natural subsequent question was to generate an alignment of a linear molecule with dynamically varying directions. This question has been studied using a field of slowly spinning polarization axes which allows one to spin the axis of alignment and thus the molecule itself [3]. This effect, demonstrated experimentally [4], has been analyzed using classical and quantum models [5], and in terms of adiabatic passage through level avoided crossings [6]. The analysis shows that the molecule can exhibit a classical rotational motion *while the field is on*. In this Letter we show a fundamentally different process in which a linear molecule can dynamically alternate from one direction to another under field-free conditions. This purely quantum effect is induced by a suitable short elliptically polarized pulse. The two directions of the alternation are the major axis and the direction orthogonal to the plane of the ellipse. The result can be explained using the following qualitative analysis. It is known that a linear rigid molecule in its ground vibronic state (of rotational constant B) driven by a nonresonant linearly polarized field (of amplitude $\mathcal{E}$) leads to the Hamiltonian $H = H_0 + V_{\text{int}}$ with $H_0 = BJ^2$, $V_{\text{int}} = -\mathcal{E}^2\Delta\alpha\cos^2\theta/4$ (up to a θ-independent constant), the polarizability anisotropy $\Delta\alpha > 0$, and θ the polar angle between the field polarization axis and the molecule's axis. This leads to periodic field-free sequences of revivals that mainly correspond to alternate alignment along the field axis and planar delocalization *orthogonal* to the field axis [1]. We emphasize that unlike the alignment along an axis, the planar delocalization is a specific quantum effect resulting from the fact that the linear polarization does not break the planar symmetry orthogonal to the field axis. The effects of alignment and planar delocalization persist after thermal averaging since, for each molecule, the wave packet produced with different initial conditions allowed by the thermal Boltzmann distribution keeps the same periodicity. This has been established theoretically and experimentally [7,8]. The use of a circular polarization leads to a similar Hamiltonian: $V_{\text{int}} = \mathcal{E}^2\Delta\alpha\cos^2\theta'/8$ (up to a θ-independent constant) with here θ' the polar angle between the axis orthogonal to the field polarization and the molecule axis: the revivals show an alternation between planar delocalization (in the plane of the field polarization) and alignment along its *orthogonal* direction [1]. Hence, we deduce that in contrast to the adiabatic case, where the alignment is in the direction of the minimum of the induced potential ($\theta = 0, \pi$ and $\theta' = \pi/2$ for, respectively, linear and circular polarization), a short pulse induces transient alignment (or planar delocalization) in the directions of the *extrema* of the induced potential. This suggests that an elliptical polarization can provide an alignment along its major axis (as a linear polarization would do) and an alignment orthogonal to the ellipse's plane (as a circular polarization would do.) We establish the validity of this scheme by first calculating explicitly the effective Hamiltonian. We then identify the optimal parameters of the elliptical polarization that allow for the alternation of highest alignments between the two directions.

We consider a linear (nonpolar) molecule subjected to an elliptically polarized laser field

$$\vec{\mathcal{E}}(t) = \mathcal{E}(t)(\vec{e}_x a\cos\omega t + \vec{e}_y b\sin\omega t) \tag{1}$$

of amplitude $\mathcal{E}(t)$, optical frequency ω, and where a represents the half-axis of the ellipse along the x axis (whereas b corresponds to the y axis) with $a^2 + b^2 = 1$. When no excited electronic states and vibrational states are resonantly coupled, the Hamiltonian is given by [9]

PRL 95, 063005 (2005) PHYSICAL REVIEW LETTERS week ending 5 AUGUST 2005

$$H = H_0 - \frac{1}{2}\vec{\mathcal{E}}(t)\cdot\vec{\vec{\alpha}}\,\vec{\mathcal{E}}(t), \quad (2)$$

with $\vec{\vec{\alpha}}$ the dynamical polarizability tensor which includes the contribution of the excited electronic states. If we consider frequencies that are low with respect to the excited electronic states, the dynamical polarizabilities are well approximated by the static ones. In the limit of high frequency with respect to the rotation and far from vibrational resonances [10], we obtain the effective Hamiltonian $H_{\rm eff}(t) = H_0 + V_{\rm int}$ with

$$V_{\rm int} = -\frac{\Delta\alpha}{4}\mathcal{E}^2(t)\sin^2\theta_z\left[(a^2-b^2)\cos^2\phi_z + b^2\right], \quad (3)$$

with ϕ_z the azimuthal angle and θ_z the polar angle, with the choice of the quantum axis along the z axis orthogonal to the ellipse plane (x, y). Noting that the normalized associated Legendre functions $\Theta_j^m(\theta)$, i.e., the θ-dependent part of the spherical harmonics $|j, m\rangle$, are not necessarily orthogonal to each other when the sets of indices (j, m) are different, we obtain

$$\begin{aligned}\langle j', m'|\cos^2\phi_z\sin^2\theta_z|j, m\rangle = {} & \delta_{m',m}\{A_m^j\delta_{j',j} + B_m^{j'}\delta_{j',j+2} + B_m^j\delta_{j',j-2}\} + \delta_{m',m+2}\{C_m^j\delta_{j',j} + D_m^j\delta_{j',j+2} + D_{-m'}^{j'}\delta_{j',j-2}\} \\ & + \delta_{m',m-2}\{C_{m'}^j\delta_{j',j} + D_{-m}^j\delta_{j',j+2} + D_{m'}^{j'}\delta_{j',j-2}\}. \quad (4)\end{aligned}$$

The coefficients $A_m^j \equiv [1-(c_m^j)^2-(c_m^{j+1})^2]/2$ and $B_m^j \equiv -c_m^{j-1}c_m^j/2$ are related to θ_z only, featuring the standard quantity $c_m^j \equiv [(j-m)(j+m)/(2j-1)(2j+1)]^{1/2}$, in contrast to the following coefficients due to both angles: $C_m^j \equiv -[(j-m)(j-m-1)(j+m+2)(j+m+1)]^{1/2}/2(2j-1)(2j+3)$ and $D_m^j \equiv [(j+m+4)!/\{(2j+1)\times(2j+5)(j+m)!\}]^{1/2}/4(2j+3)$. We use a laser pulse of short duration that can be treated in the sudden approximation, where the intensity of the field is characterized by the dimensionless parameter [11,12] $\xi = \frac{\Delta\alpha}{4\hbar}\int dt\mathcal{E}^2(t)$.

To analyze the alignments along the two axes, in addition to $\langle\cos^2\theta_z\rangle(t) \equiv \langle\psi(\theta_z,\phi_z;t)|\cos^2\theta_z|\psi(\theta_z,\phi_z;t)\rangle$ one can consider the observable $\langle\cos^2\phi_z\rangle(t) \equiv \langle\psi(\theta_z,\phi_z;t)\times|\cos^2\phi_z|\psi(\theta_z,\phi_z;t)\rangle$, where $|\psi(\theta_z,\phi_z;t)\rangle$ is the state of the molecule given by the Schrödinger equation. However, it is more appropriate to introduce the observables $\langle\cos^2\theta_x\rangle(t) \equiv \langle\cos^2\phi_z\sin^2\theta_z\rangle(t)$ and $\langle\cos^2\theta_y\rangle(t) \equiv \langle\sin^2\phi_z\sin^2\theta_z\rangle(t)$, θ_x (θ_y) corresponding to the polar angle with respect to the x axis (y axis). This is motivated by the fact that these observables are closely related to the experimental measurements and the fact that they will allow us to identify the ellipticity leading to quantitatively equivalent alignments along both the major axis (x or y) of the polarization ellipse and the z axis orthogonal to the ellipse. Because of the relation $\Sigma_{i=x,y,z}\langle\cos^2\theta_i\rangle(t) = 1$, the alignment alternation can be measured with any pair of observables among $\{\langle\cos^2\theta_i\rangle(t), i = x, y, z\}$. Figure 1 displays the temporal behavior of these thermally averaged quantities for an elliptically polarized field interacting with a molecule at the dimensionless temperature $\tilde{T} := kT/B = 20$ (an initial statistical ensemble of even values of j is considered). This amounts to having $T = 11$ K for a CO_2 molecule. Here $a^2 = 1/3$ and $\xi = 11.1$ (corresponding approximately to a pulse of peak intensity $I = 25\times10^{12}$ W/cm^2 and of duration $\tau_{\rm FWHM} = 100$ fs for CO_2). During each rotational period $\tau_{\rm rot}$ we can identify four revivals for both $\langle\cos^2\theta_y\rangle(t)$ and $\langle\cos^2\theta_z\rangle(t)$. The revivals occur around the times $t_n = n\tau_{\rm rot}/4$ for both expectation values, as is the case for a linear polarization. The localization properties of the rotational wave packet are however fundamentally different. Near the highest peaks of $\langle\cos^2\theta_z\rangle(t)$ (at the times t_1, slightly after t_2 and also slightly before t_4), the molecule is predominantly aligned along the z direction (small θ_z), i.e., orthogonally to the polarization ellipse. This state is represented in spherical coordinates at time $t = t_1 \equiv \tau_{\rm rot}/4$ in Fig. 2 (left panel). At the highest peaks of $\langle\cos^2\theta_y\rangle(t)$ (slightly before t_2, at the time t_3 and also slightly after t_4), coinciding with the minima of $\langle\cos^2\theta_z\rangle(t)$, the molecule is aligned along the major axis (small θ_y and θ_z close to $\pi/2$). A representation of the molecular state is displayed at time $t = t_3 \equiv 3\tau_{\rm rot}/4$ in Fig. 2 (right panel).

As will be discussed below, the alignments revivals are quantitatively similar in both the y and z directions for the particular value $a^2 = 1/3$. The quantities $\langle\cos^2\theta_z\rangle(t)$ and $\langle\cos^2\theta_y\rangle(t)$ displayed in Fig. 1 are symmetric with respect to the approximate value 0.36, implying that $\langle\cos^2\theta_x\rangle(t)$ is close to 1/3 for all times. The angular distributions shown in Fig. 2 for $t = \tau_{\rm rot}/4$ and $t = 3\tau_{\rm rot}/4$ are superposable upon rotation.

Between the revivals, when the averaged observables are approximately flat as a function of time, locally near the times $t = (2p+1)\tau_{\rm rot}/8$ (with integer p), it is remarkable

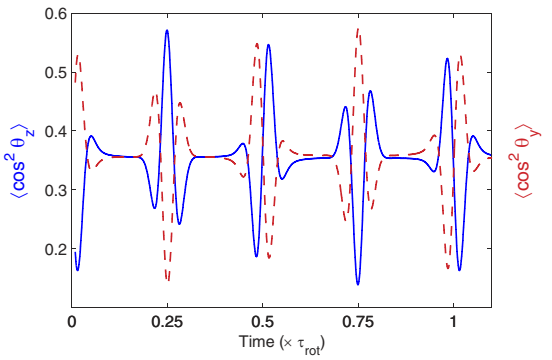

FIG. 1 (color online). Expectation values of the observables $\cos^2\theta_z$ (full line) and $\cos^2\theta_y$ (dashed line) for $a^2 = 1/3$, $\xi = 11.1$, and $\tilde{T} = 20$, as a function of normalized time.

PRL 95, 063005 (2005) PHYSICAL REVIEW LETTERS week ending 5 AUGUST 2005

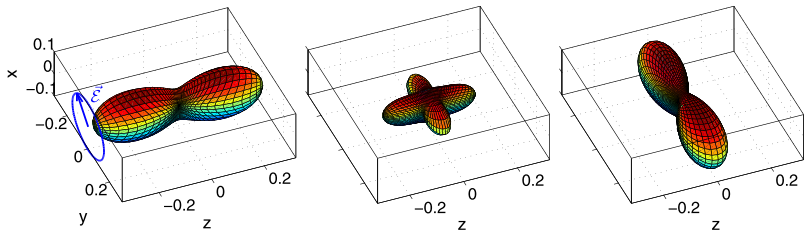

FIG. 2 (color online). Representation of the molecular state in spherical coordinates $\{r \equiv |\psi(\theta_z, \phi_z; t)|^2, \theta_z, \phi_z\}$ for $a^2 = 1/3$, $\xi = 11.1$, $\tilde{T} = 20$, at times $t = \tau_{\rm rot}/4$ (left panel), $t \approx 3\tau_{\rm rot}/8$ (middle panel), and $t = 3\tau_{\rm rot}/4$ (right panel). The polarization ellipse of the field $\vec{\mathcal{E}}$ is sketched in the (x, y) plane.

that the state of the molecule is approximately an equal weight superposition of the two aligned states, as illustrated in Fig. 2 (middle panel). This can be interpreted as an extension of a recent proposal made in the linearly polarized case [13], where fractional revivals at odd multiples of $\tau_{\rm rot}/8$ are shown to combine aligned (along the linear polarization axis) and antialigned (delocalized in the plane orthogonal to the axis) components with equal weights. In the current elliptic case, both components correspond to aligned states.

So far we have considered $a^2 = 1/3$. We now turn to the question of determining the value of this parameter giving an optimal two-direction alignment alternation, in the sense that both alignments correspond to similar (i.e., superposable upon rotation) delocalized angular distribution. Choosing $a = a_{\rm lin} \equiv 0$ ($a = 1$) gives a linear polarization along the y axis (x axis).

The circular polarization is obtained with $a^2 = b^2 = a^2_{\rm circ} \equiv 1/2$. The optimal value is obtained when the maxima (over time) of both expectation values $\langle\cos^2\theta_z\rangle$ and $\langle\cos^2\theta_y\rangle$ for $a^2 < 1/2$ ($\langle\cos^2\theta_x\rangle$ for $a^2 > 1/2$) are equal. In Fig. 3 we plot these maxima as a function of a^2. The intersection points are near $a^2 = 1/3$ (corresponding to the ellipticity chosen for Figs. 1 and 2) and $a^2 = 2/3$. This can be understood by rewriting the interaction term (3) in terms of the observable $\cos^2\theta_y$ rather than $\cos^2\phi_z$:

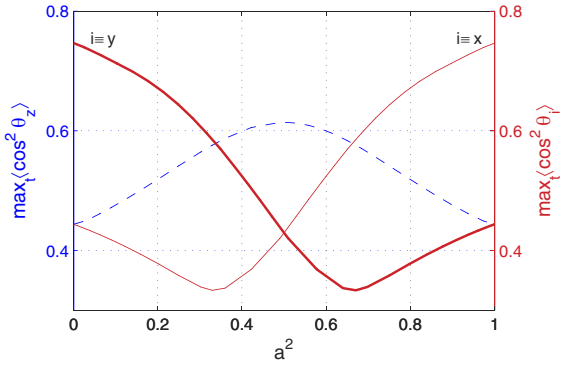

FIG. 3 (color online). Maximum over time of $\langle\cos^2\theta_z\rangle$ (dashed line), $\langle\cos^2\theta_y\rangle$ (full thick line), and $\langle\cos^2\theta_x\rangle$ (full thin line) with $\xi = 11.1$ and $\tilde{T} = 20$, as a function of a^2.

$$V_{\rm int} = -\frac{\Delta\alpha}{4}\mathcal{E}^2(t)[(1-2a^2)\cos^2\theta_y + a^2\sin^2\theta_z]. \quad (5)$$

When the ellipticity is chosen such that $1 - 2a^2 = a^2$, i.e., $a^2 = 1/3$, the directions θ_y and θ_z play a symmetric role. Notice from (5) that the minima in one direction correspond to the maxima in the other direction. In the sudden regime, both types of extrema are visited equivalently in contrast to the adiabatic case. The ellipticity $a^2 = 1/3$ can be interpreted as the best compromise between linear and circular polarizations with the remarkable feature that the angular distribution associated with the highest revivals are similar in both directions (see Fig. 2). It is worth noting that this value is not the arithmetic average of $a^2_{\rm circ}$ and $a^2_{\rm lin}$. The case $a^2 = 2/3$ involves the direction θ_x instead of θ_y. In Fig. 3 we also recognize the case of a circular polarization for $a^2 = 1/2$ where the alignment along z is large whereas the maxima of $\langle\cos^2\theta_x\rangle$ and $\langle\cos^2\theta_y\rangle$ are equal, reflecting the fact that the rotational wave packet is delocalized for all times in the (x, y) plane.

We have demonstrated the effect experimentally in CO_2 molecules at room temperature by measuring the optical Kerr effect along the two orthogonal directions, x and y respectively (both orthogonal to the z direction of propagation of the beam). The measurements have been performed with a Ti:sapphire chirped-pulse amplifier producing 100-fs pulses at 1 kHz. Recently it has been shown [14] that measuring the defocusing of a time-delayed weak probe pulse produced by a spatial distribution of aligned linear molecules yields a signal proportional to $[\langle\cos^2\theta\rangle(t) - 1/3]^2$, with θ the angle between the molecular axis and the direction of the probe field. Choosing the polarization of the probe either in the y or x direction, we can thus obtain $[\langle\cos^2\theta_i\rangle(t) - 1/3]^2$ [shown in Figs. 4(a) and 4(c)], where θ_i is the angle between the molecular axis and the i axis ($i = x, y$). From these we can deduce $\langle\cos^2\theta_y\rangle$ and $\langle\cos^2\theta_x\rangle$ which characterize the alignment along the major and minor axes of the ellipse, respectively, [Figs. 4(b) and 4(d)]. The shape and amplitude of the recorded signal are in good agreement with the theoretical predictions. The quasi-isotropic feature of the alignment along the x axis mentioned above for this specific ellipticity is confirmed by this experiment, where a

PRL 95, 063005 (2005) PHYSICAL REVIEW LETTERS week ending 5 AUGUST 2005

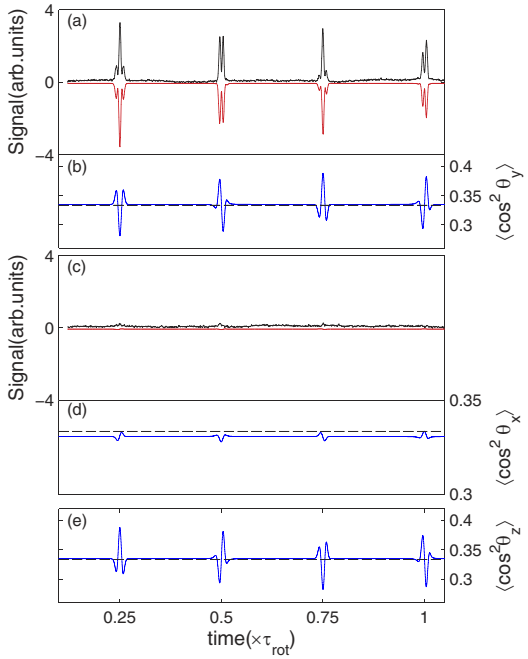

FIG. 4 (color online). Field-free alignment of an ensemble of CO_2 molecules ($T = 296$ K, $P = 4 \times 10^4$ Pa) produced by an elliptically polarized pump field [$a^2 \approx 1/3$, see Eq. (1)] of peak intensity 25 TW/cm^2 and pulse duration $\tau_{\mathrm{FWHM}} = 100$ fs. Cross defocusing signal recorded as a function of delay with the probe field linearly polarized along (a) the y axis (major field axis) and (c) the x axis (minor field axis). In (a) and (c), the theoretical results (thick lines) are shown as mirror images of the experimental ones. Corresponding observables (b) $\langle\cos^2\theta_y\rangle$ and (d) $\langle\cos^2\theta_x\rangle$. (e) $\langle\cos^2\theta_z\rangle$ along the propagation z axis deduced from (b) and (d). The isotropic values $1/3$ are indicated with dashed lines.

signal close to zero is observed in Fig. 4(c). The alignment along the z axis, characterized by $\langle\cos^2\theta_z\rangle(t)$ [Fig. 4(e)], can be deduced from the other two observables through the relation $\Sigma_{i=x,y,z}\langle\cos^2\theta_i\rangle(t) = 1$. The results of Figs. 4(b) and 4(e) show clearly the experimental alternation of the alignment predicted theoretically and represented in Fig. 1. It should be noted that the experimental signal related to the measurement of $[\langle\cos^2\theta_x\rangle(t) - 1/3]^2$ is found to be minimum for the ellipticity $a^2 = 1/3$, as predicted by the model. As discussed above, the fact that $\langle\cos^2\theta_x\rangle(t) \approx 1/3$ (in a strong field) is a clear-cut signature of optimal alignments in the two other directions. An exhaustive experimental investigation with other ellipticities has been performed and shows strong modifications of both shape and amplitude of the recorded signals, in agreement with numerical simulations.

In conclusion, we have shown, both theoretically and experimentally, that a linear molecule subjected to a short specific elliptically polarized laser field can be aligned, alternatively, at specific times along the orthogonal axis and the major axis of the ellipse. Contrary to the adiabatic case where only the minima of the induced potential are populated, for short pulses all the extrema of the potential are dynamically visited and appear as revivals. The control of this field-free two-direction alignment alternation is a challenging perspective that could find applications in nanotechnology; for instance to generate a 3D molecular switch [1]. In the context of quantum information, the advantage of an elliptic polarization over a linearly polarized field employed in a recent proposal [15], is to have a superposition of alignments along two axes, instead of a superposition of an alignment and a planar delocalization.

This research was supported by the Conseil Régional de Bourgogne, the Action Concertée Incitative Photonique from the French Ministry of Research, and a Marie Curie European Reintegration Grant within the 6th European Community RTD Framework Programme.

*Electronic address: ddaems@ulb.ac.be
†Electronic address: sguerin@u-bourgogne.fr

[1] H. Stapelfeldt and T. Seideman, Rev. Mod. Phys. **75**, 543 (2003).
[2] J. J. Larsen, K. Hald, N. Bjerre, H. Stapelfeldt, and T. Seideman, Phys. Rev. Lett. **85**, 2470 (2000).
[3] J. Karczmarek, J. Wright, P. B. Corkum, and M. Ivanov, Phys. Rev. Lett. **82**, 3420 (1999).
[4] D. M. Villeneuve, S. A. Aseyev, P. Dietrich, M. Spanner, M. Y. Ivanov, and P. B. Corkum, Phys. Rev. Lett. **85**, 542 (2000).
[5] M. Spanner, K. M. Davitt, and M. Y. Ivanov, J. Chem. Phys. **115**, 8403 (2001).
[6] N. V. Vitanov and B. Girard, Phys. Rev. A **69**, 033409 (2004).
[7] F. Rosca-Pruna and M. J. J. Vrakking, Phys. Rev. Lett. **87**, 153902 (2001); F. Rosca-Pruna and M. J. J. Vrakking, J. Chem. Phys. **116**, 6567 (2002); F. Rosca-Pruna and M. J. J. Vrakking, J. Chem. Phys. **116**, 6579 (2002).
[8] V. Renard, M. Renard, S. Guérin, Y. T. Pashayan, B. Lavorel, O. Faucher, and H. R. Jauslin, Phys. Rev. Lett. **90**, 153601 (2003); V. Renard, M. Renard, A. Rouzée, S. Guérin, H. R. Jauslin, B. Lavorel, and O. Faucher, Phys. Rev. A **70**, 033420 (2004).
[9] B. Friedrich and D. Herschbach, Phys. Rev. Lett. **74**, 4623 (1995).
[10] A. Keller, C. M. Dion, and O. Atabek, Phys. Rev. A **61**, 023409 (2000).
[11] N. E. Henriksen, Chem. Phys. Lett. **312**, 196 (1999).
[12] D. Daems, S. Guérin, H. R. Jauslin, A. Keller, and O. Atabek, Phys. Rev. A **69**, 033411 (2004).
[13] M. Spanner, E. A. Shapiro, and M. Ivanov, Phys. Rev. Lett. **92**, 093001 (2004).
[14] V. Renard, O. Faucher, and B. Lavorel, Opt. Lett. **30**, 70 (2005).
[15] K. F. Lee, D. M. Villeneuve, P. B. Corkum, and E. A. Shapiro, Phys. Rev. Lett. **93**, 233601 (2004).

10.4 Adiabatic orientation 2+1 [176]

We show that two overlapping linearly polarized laser pulses of frequencies ω and its second harmonic 2ω can strongly orient linear polar molecules, by adiabatic passage along dressed states. The resulting robust orientation can be interpreted as a laser-induced localization in the effective double well potential created by the fields, which induces a preliminary molecular alignment. The direction of the orientation can be selected by the relative phase of the fields. We use an excited vibrational state to generate a controllable and enhanced hyperpolarizability (of third order in field amplitude) in the ground vibronic state (see also the next section for more details).

VOLUME 88, NUMBER 23 PHYSICAL REVIEW LETTERS 10 JUNE 2002

Orientation of Polar Molecules by Laser Induced Adiabatic Passage

S. Guérin,* L. P. Yatsenko,† H. R. Jauslin, O. Faucher, and B. Lavorel

Laboratoire de Physique de l'Université de Bourgogne, UMR CNRS 5027, BP 47870, 21078 Dijon, France

(Received 13 November 2001; published 28 May 2002)

We show that two overlapping linearly polarized laser pulses of frequencies ω and its second harmonic 2ω can strongly orient linear polar molecules, by adiabatic passage along dressed states. The resulting robust orientation can be interpreted as a laser-induced localization in the effective double well potential created by the fields, which induces a preliminary molecular alignment. The direction of the orientation can be selected by the relative phase of the fields.

DOI: 10.1103/PhysRevLett.88.233601 PACS numbers: 42.50.Hz, 32.80.Lg, 33.80.–b

Introduction.— Intense laser fields offer a rich variety of control processes, allowing us to manipulate the internal and external degrees of freedom of molecules (see, for example, the recent works [1–4]).

In particular a strong nonresonant linearly polarized laser field allows one to align small molecules along the electric field axis through their anisotropic polarizability [5,6]. One approach is to use an ultrashort pulse which creates a superposition of rotational states. This results in a field-free transient alignment occurring periodically in time due to revivals of rotational wave packets, as long as the coherence of the process is preserved [7–9].

On the other hand, nanosecond pulses have been shown theoretically [8] and experimentally [10] to yield alignment during the pulse (adiabatic alignment). The laser field has to be turned on slowly compared with the rotational periods in order to induce an adiabatic transport along a dressed state. This process has been interpreted as a rigid rotor dressed by an effective double-well potential whose minima are in the directions of the field polarization. The wells are deeper and thinner for a stronger field [5,8]. One considers the initial state to be $J = 0, M = 0$ and linear polarized fields. The projection M of the rotational angular momentum along the field axis is a constant of motion. The eigenvectors of the dressed Hamiltonian are called *pendular states* and are labeled with $\tilde{J}$. Their associated eigenenergies as a function of the field amplitude form curves that are continuously connected to the bare states $|J\rangle$. The lowest ones are well localized in the wells and correspond thus to the molecular alignment. The molecular population initially in the rotational state $|J = 0\rangle$ is *adiabatically* carried along the pendular state $|\tilde{J} = 0\rangle$ whose eigenenergy is continuously connected to the state $|J = 0\rangle$. This process can be interpreted as Stark shifts that align the molecules.

Strong electrostatic fields have been shown to yield molecular orientation for molecules through their permanent dipole moment [11,12]. Its combination with a coherent laser field has been proved theoretically to enhance significantly this orientation [4,13]. The additional electrostatic field indeed allows one to break the double-well symmetry induced by the laser field favoring one well with respect to the other one. Another technique using extremely short electrical pulses has been shown also to give orientation [14]. Lasers resonant with the first excited vibrational state can induce a modest transient orientation [15].

The purpose of this article is to show that an off-resonant pulse of frequency ω when accompanied by its second harmonic 2ω, can transform the adiabatic alignment of molecules into orientation during the pulse. These two pulses induce a hyper-Raman type process. More precisely, the orientation is successful if the alignment can be obtained by each laser pulse taken separately and if the hyper-Raman three-photon coupling between the pendular states $|\tilde{J} = 0\rangle$ and $|\tilde{J} = 1\rangle$ (whose eigenenergy is continuously connected to the state $|J = 1\rangle$) allows adiabatic passage along the dressed states. The relative phase between the two pulses allows us to choose the direction of the orientation. This new mechanism we propose is robust with respect to all the pulse parameters, including the relative phase. The orientation is more efficient if the hyper-Raman coupling is assisted by a near resonant vibrational state (see Fig. 1). This mechanism can be interpreted as a natural *dynamical laser-induced localization* in the double-well alignment potential as follows.

The first step consists in identifying *oriented states*: Since the fields create a symmetric effective double well potential, the two lowest pendular states $|\tilde{J} = 0\rangle$ and $|\tilde{J} = 1\rangle$ are quasidegenerate and are, respectively, symmetric and antisymmetric. The two lowest states come closer to degeneracy for stronger fields. Thus the states $(|\tilde{J} = 0\rangle + |\tilde{J} = 1\rangle)/\sqrt{2}$ and $(|\tilde{J} = 0\rangle - |\tilde{J} = 1\rangle)/\sqrt{2}$ are well

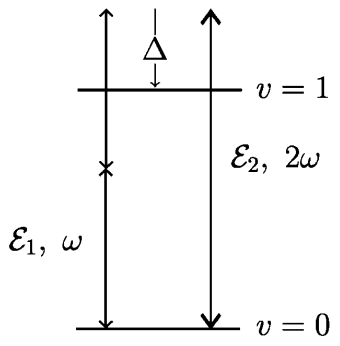

FIG. 1. Coupling scheme.

 0031-9007/02/88(23)/233601(4)$20.00

VOLUME 88, NUMBER 23 PHYSICAL REVIEW LETTERS 10 JUNE 2002

localized in one of the wells and can thus be identified as "*oriented pendular states*" if the field is strong enough.

The second step consists in finding the pulse parameters which will carry in a robust way the dynamics into one of these oriented states from the initial state $|J = 0\rangle$. For increasing fields, the induced pendular states $|\tilde{J} = 0\rangle$ and $|\tilde{J} = 1\rangle$ come closer to the degeneracy and the hyper-Raman process $(2\omega, \omega)$, initially off resonant, comes closer to the three-photon resonance. This gives rise to a dynamical resonance which is characterized, as a function of the field amplitudes, by an avoided crossing. Far after this avoided crossing, we will show that the two dressed branches will be identified with a very good approximation as the previously defined oriented states if the relative phase ϕ between the two fields is *not close* to $\pi/2(\mathrm{mod}\pi)$. Thus under this condition, the adiabatic passage along this avoided crossing will yield molecular orientation. Choosing ϕ around either 0 or π will allow control of the direction of the orientation in a robust way.

We will develop more precisely the strategy for orientation described above and will show numerically the efficiency of this strategy on the example of HCN molecules.

The strategy for orienting.—We consider a linear polar molecule, modeled as a rigid rotor, in its ground electronic and vibrational state, subject to a laser field. The molecule interacts with the field through its permanent dipole moment $\mu_0(R)$, coupling the vibrations (of coordinate R) with one-photon processes, and, if one considers its frequency sufficiently far from any resonances with the excited electronic states, through its polarizability, coupling the vibrations by Raman processes. The dynamical polarizability includes the components $\alpha_\parallel(R)$ and $\alpha_\perp(R)$, respectively, parallel and perpendicular to the molecular axis. The Hamiltonian between vibrational blocks $H_{v',v} = \langle v'|H|v\rangle$, of energy E_v and of rotational constant B_v, reads in this case [6]

$$H_{v'v} = (E_v + B_v J^2)\delta_{v',v} - \mu_{0,v'v}\mathcal{E}(t)\cos\theta - \frac{1}{2}\mathcal{E}^2(t)[(\alpha_{\perp,v'v} - \alpha_{\parallel,v'v})\sin^2\theta + \alpha_{\parallel,v'v}], \quad (1)$$

with $\mu_{0,v'v} = \langle v'|\mu_0|v\rangle$, $\alpha_{\perp,v'v} = \langle v'|\alpha_\perp|v\rangle$, $\alpha_{\parallel,v'v} = \langle v'|\alpha_\parallel|v\rangle$, J the angular momentum. θ is the polar angle between the molecular axis and the direction of the field $\mathcal{E}(t) = \mathcal{E}_0\sqrt{\Lambda(t)}\cos\omega t$, with ω the carrier frequency, $\mathcal{E}_0$ the peak amplitude, and $\Lambda(t)$ the envelope of the field intensity. It is a good approximation to choose $\alpha_\parallel$ and $\alpha_\perp$ as the static polarizabilities when the laser frequencies are far red detuned from the excited electronic states (i.e., low frequencies with respect to the electronic surfaces). If additionally the field is off resonant between the ground and the excited vibrational states, the dressed Hamiltonian in the ground vibrational state can be approximated in the high frequency limit (with respect to the rotational constant B_0) [16] as

$$H_{00}^{\mathrm{eff}} = E_0 + B_0 J^2 + \mathcal{E}_0^2\Lambda(t)a_{00}(\omega), \quad (2)$$

with

$$a_{vv}(\omega) = \alpha_{vv}^{\mathrm{eff}}(\omega)\sin^2\theta - \alpha_{\parallel,vv}/4 \quad (3)$$

and

$$\alpha_{vv}^{\mathrm{eff}}(\omega) = \frac{B_0|\mu_{0,vv}|^2}{2(\hbar\omega)^2} + \frac{\alpha_{\parallel,vv} - \alpha_{\perp,vv}}{4}. \quad (4)$$

For linear molecules ($\alpha_\parallel > \alpha_\perp$), the rigid rotor B_0J^2 is thus effectively subject to a double-well potential, with minima at $\theta = 0$ and $\theta = \pi$ for $M = 0$ [5]. This potential is deeper and thinner for stronger fields. The condition for adiabatic transport has been identified as

$$\tau \gg \hbar/B_0 \quad (5)$$

by Ortigoso *et al.* [8], with τ characterizing the pulse duration. In practice, if we consider smooth pulses, such as Gaussian pulses of shape $\Lambda(t) = \exp[-(t/\tau)^2]$, the adiabatic regime is already well attained for $B_0\tau = 5\hbar$. For a given pulse amplitude $\mathcal{E}_0$, the dimensionless quantity which characterizes the alignment regime is [8]

$$\gamma = \mathcal{E}_0^2\alpha_{00}^{\mathrm{eff}}(\omega)/B_0. \quad (6)$$

Already for $\gamma = 30$, one obtains in the adiabatic regime $\langle\cos^2\theta\rangle \approx 0.8$.

In the dressed state representation as a function of the field intensity, stronger fields induce pendular states $|\tilde{J} = 0\rangle$ and $|\tilde{J} = 1\rangle$, of respective dressed energies λ_0 and λ_1 becoming closer to degenerate as shown as dashed lines in Fig. 2, meaning a more efficient alignment. We have found numerically that, under the condition $\gamma \leq 30$, this degeneracy can be quite well represented by

$$\lambda_1 - \lambda_0 = 2B_0\exp(-0.17\gamma). \quad (7)$$

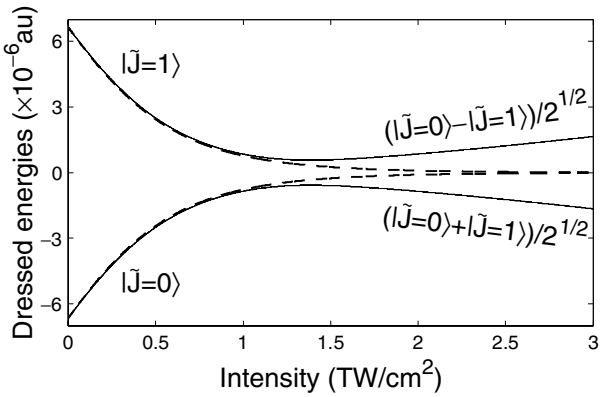

FIG. 2. The dressed energies as a function of the field intensity I_1 for the example of HCN (see text for details) characterizing (i) the process of alignment with one field (dashed lines) and (ii) the process of orientation with the two fields (full lines). The two energies have been represented relative to their average [i.e., $\lambda_j - (\lambda_1 + \lambda_2)/2$]. They can be approximately labeled before the avoided crossing by the pendular states, and after by the oriented states.

The exponential law can be obtained from a semiclassical treatment of the tunnel splitting. Note that for $\gamma > 30$, the degeneracy follows the law $\lambda_1 - \lambda_0 \sim \exp(-a\sqrt{\gamma})$ [17].

As already noticed in the introduction, the oriented states are well identified: they are characterized by the linear combinations $(|\tilde{J} = 0\rangle \pm |\tilde{J} = 1\rangle)/\sqrt{2}$. The goal is now to reach this state by adiabatic passage. We use the hyper-Raman coupling with the combination of the two lasers $(\omega, 2\omega)$ giving the total electric field $\mathcal{E}(t) = \mathcal{E}_1(t) \times \cos\omega t + \mathcal{E}_2(t)\cos(2\omega t + \phi)$, with $\mathcal{E}_1(t) = \mathcal{E}_{01}\Lambda(t)$, $\mathcal{E}_2(t) = \mathcal{E}_{02}\Lambda(t)$, and ϕ the relative phase. The frequencies are detuned by $\Delta = E_1 - E_0 - 2\hbar\omega$ from the first excited vibrational state (see Fig. 1). The detuning Δ is chosen as small as possible and negative to prevent any detrimental multiphoton vibrational resonance (with other low vibrational states). Since we have in general $\mu_{0,00} \approx \mu_{0,11}$ and $(\alpha_{\parallel,\perp})_{00} \approx (\alpha_{\parallel,\perp})_{11}$, the Hamiltonian (1) becomes in the high frequency limit and in the quasi-resonant approximation (rotating wave approximation) [18] (where the constant energy E_0 has been omitted)

$$H_{00}^{\text{eff}} = B_0 J^2 + \mathcal{E}_1^2 a_{00}(\omega) + \mathcal{E}_2^2 a_{00}(2\omega), \tag{8a}$$

$$H_{11}^{\text{eff}} = B_1 J^2 + \mathcal{E}_1^2 a_{11}(\omega) + \mathcal{E}_2^2 a_{11}(2\omega) + \Delta, \tag{8b}$$

$$H_{01}^{\text{eff}} = (H_{10}^{\text{eff}})^* = -\frac{\mu_{0,01}}{2}\mathcal{E}_2 e^{i\phi}\cos\theta - \mathcal{E}_1^2\left(\frac{\alpha_{\perp,01} - \alpha_{\parallel,01}}{8}\sin^2\theta + \frac{\alpha_{\parallel,01}}{8}\right). \tag{8c}$$

The pendular states are defined as the eigenvectors of the Hamiltonian (8a) when the coupling (8c) is zero. This coupling between the two pendular states $|\tilde{J} = 0\rangle$ and $|\tilde{J} = 1\rangle$ gives initially and for sufficiently low field a three-photon off-resonant process. For stronger fields, the Stark shifts in H_{00}^{eff} make $|\tilde{J} = 0\rangle$ and $|\tilde{J} = 1\rangle$ become closer to degeneracy (alignment process) until the three-photon hyper-Raman coupling has a non-negligible effect. This leads to a dynamical resonance characterized by an avoided crossing of the eigenvalues $\tilde{\lambda}_\pm$ of the Hamiltonian (8) (full lines in Fig. 2).

After a standard adiabatic elimination, the effective two-level avoided crossing between $|\tilde{J} = 0\rangle$ and $|\tilde{J} = 1\rangle$ can take the following approximate form, in the basis of the pendular states $\{|\tilde{J} = 0\rangle, |\tilde{J} = 1\rangle\}$:

$$\tilde{H}^{01} = \begin{bmatrix} \lambda_0 + s_0 & \kappa\mathcal{E}_1^2\mathcal{E}_2\cos\phi \\ \kappa\mathcal{E}_1^2\mathcal{E}_2\cos\phi & \lambda_1 + s_1 \end{bmatrix}, \tag{9}$$

with $\lambda_1 - \lambda_0$ as in Eq. (7) with $\gamma = [\mathcal{E}_1^2\alpha_{00}^{\text{eff}}(\omega) + \mathcal{E}_2^2\alpha_{00}^{\text{eff}}(2\omega)]/B_0$, κ the three-photon coupling strength, and $s_j, j = 0, 1$ the additional dynamical Stark shifts of the pendular state $|j\rangle$ induced by the three-photon process, and which depend on the field amplitudes and on the frequency ω. The Hamiltonian (9) shows that, when the relative laser phase is $\phi = \pi/2(\text{mod}\pi)$, the coupling vanishes and the two levels become decoupled. In this case, we recover the process of alignment (represented in the dressed energy diagram of Fig. 2 by the dashed lines) without any orientation. This can be interpreted as destructive interferences of the two fields with respect to the orientation. The strongest coupling is obtained when ϕ is 0 or π.

If we consider a strong field, we have $\lambda_1 \rightarrow \lambda_0$ (aligned molecule). Furthermore, we consider additionally $|\Delta| \gg B_0, B_1$, so that one has $s_0 \approx s_1$. This means that the three-photon coupled $|\tilde{J} = 0\rangle$ and $|\tilde{J} = 1\rangle$ states experience the same Stark shifts because the fields act very similarly on these states. Under these considerations, beyond the avoided crossing, the dressed states read

$$|\tilde{J}_\pm\rangle = \frac{1}{\sqrt{2}}[|\tilde{J} = 0\rangle \pm \text{sgn}(\cos\phi)|\tilde{J} = 1\rangle], \tag{10}$$

where $\text{sgn}(\cos\phi)$ is 1 (respectively -1) for positive (respectively negative) $\cos\phi$ and where $|\tilde{J}_+\rangle$ (respectively $|\tilde{J}_-\rangle$) connects the field-free state $|J = 1\rangle$ (respectively $|J = 0\rangle$). The two dressed states, beyond the avoided crossing, are thus the oriented states previously identified. Thus passing *adiabatically* along the avoided crossing will lead to an oriented molecule. Any nonidentical Stark shifts between the pendular states in the Hamiltonian (9) would give different linear combinations and would be detrimental for the orientation by adiabatic passage. On the opposite situation, passing very fast (*diabatic* passage), meaning that the coupling is ignored, would lead to $|\tilde{J} = 0\rangle$, the aligned state without orientation, meaning that the oriented states $|\tilde{J}_+\rangle$ and $|\tilde{J}_-\rangle$ would be equally populated beyond the avoided crossing. We thus remark that this avoided crossing has different properties from the Landau-Zener avoided crossing, especially concerning the diabatic passage.

In summary the guideline to achieve the orientation in the ground vibrational state is as follows: One has to apply sufficiently strong fields such that $\gamma \gg 1$ to ensure alignment. These fields have to be adiabatically switched on such that the avoided crossing is passed adiabatically. The laser frequencies have to be chosen with a negative detuning Δ with an absolute value as small as possible such that the excited vibrational state assists the three-photon transition. On the other hand, the detuning Δ has to be large enough, such that $|\Delta| \gg B_0, B_1$, to ensure parallel Stark shifts.

Illustration on HCN.—We illustrate the strategy for the orientation of the bond C—H ($B_0 \approx 1.46\ \text{cm}^{-1}$) of the molecule H—C≡N. As in [15], we neglect the stretching motion CN and the bending motion. Accurate couplings calculated by *ab initio* methods can be found in [18]. We make the calculation with the laser fundamental frequency $\omega = 1706\ \text{cm}^{-1}$ leading to $\Delta = -200\ \text{cm}^{-1}$. We have checked that it is a good approximation to consider as the effective Hamiltonian the first two vibrational states. The overlapping pulses are Gaussian of duration $\tau = 800$ ps. They have peak intensities $I_1 = 3 \times 10^{12}\ \text{W/cm}^2$ for the field of frequency ω and $I_2 = 10^{12}\ \text{W/cm}^2$ for the second harmonic field. The relative phase $\phi = \pi$ is chosen. Here $\tau B_0/\hbar \gtrsim 220$ has been required at this intensity to satisfy adiabatic passage. Note that this is a more restrictive

VOLUME 88, NUMBER 23 PHYSICAL REVIEW LETTERS 10 JUNE 2002

condition than for the simple alignment where $\tau B_0/\hbar \gtrsim 5$ is enough.

The results are collected in Fig. 3, where $\langle\cos^2\theta\rangle(t)$ and $\langle\cos\theta\rangle(t)$, the usual measures of alignment and orientation, respectively, have been plotted as a function of time. One can observe a preliminary alignment which becomes for higher field an orientation ($\langle\cos\theta\rangle(t) \approx 0.9$) during approximately 1 ns. This orientation occurs efficiently beyond the field *threshold* $I_1^{\text{th}} \approx 1.4 \times 10^{12}$ W/cm^2 given by the position of the avoided crossing of Fig. 2, i.e., after the dynamics has passed the avoided crossing. This can be seen in the bottom of Fig. 3 where the projections $|\langle\tilde{J}|\Psi(t)\rangle|^2$ on the pendular states $|\tilde{J}=0\rangle$ and $|\tilde{J}=1\rangle$ of the state solution $|\Psi(t)\rangle$ have been plotted. The alignment becomes orientation when these projections are approximately $1/2$.

The orientation that is obtained is robust with respect to the pulse parameters (phases, amplitudes, delay, and frequencies). Changing the relative phase ϕ from π to 0 flips the orientation of the molecule, whose efficiency at the peak intensities is well approximated by

$$\langle\cos\theta\rangle \approx 0.9[-1 + 2\Theta(\phi - \pi/2)], \qquad (11)$$

where $\Theta(\phi)$ is the Heaviside step function (1 if $\phi > 0$, $1/2$ for $\phi = 0$, and 0 otherwise). The orientation is lost only when ϕ comes very close to $\pi/2$.

Conclusion.—In summary, we have shown that two overlapping laser pulses of frequency ω and 2ω allow us to orient very efficiently a polar molecule by adiabatic passage. This result is general in the sense that it can be applied for many different linear polar molecules. The main differences of the technique we propose with respect to other schemes is that it avoids the use of a static field and that it is induced by nanosecond pulses, in the vibrational infrared domain. One achieves orientation while the laser is in interaction. We have considered the example of the molecule HCN to illustrate the mechanism. Other molecules such as CO could be candidates to validate experimentally the mechanism we propose.

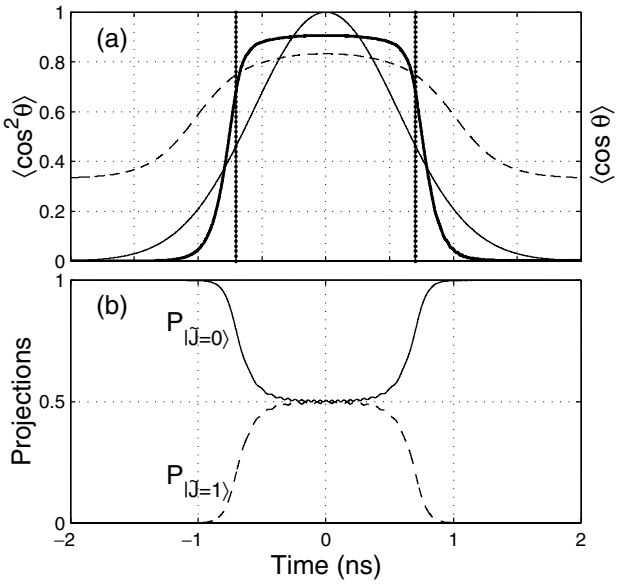

FIG. 3. (a) $\langle\cos^2\theta\rangle(t)$ (dashed line), $\langle\cos\theta\rangle(t)$ (thick full line) and the Gaussian amplitude $\Lambda(t)$ (thin full line) as a function of time. The position of the avoided crossing of Fig. 2 is represented by the vertical dotted lines. (b) The projection of the dynamics in the pendular states $|\tilde{J}=0\rangle$ (full line) and $|\tilde{J}=1\rangle$ (dashed line).

S. G. and H. R. J. thank Claude Dion and Arne Keller for stimulating discussions. We acknowledge the financial supports by the *Action Concertée Incitative Photonique* from the French Ministry of Research, by INTAS 99-00019, and by the Conseil Régional de Bourgogne. S. G. thanks the Institute of Physics of the National Academy of Sciences of Ukraine in Kiev for kind hospitality.

*Email address: sguerin@u-bourgogne.fr
†Permanent address: Institute of Physics, National Academy of Sciences of Ukraine, prospekt Nauky, 46, Kiev-22, Ukraine.

[1] T. Seideman, J. Chem. Phys. **111**, 4397 (1999).
[2] J. Karczmarek, J. Wright, P. Corkum, and M. Ivanov, Phys. Rev. Lett. **82**, 3420 (1999).
[3] M. Shapiro and P. Brumer, Adv. At. Molec. Phys. **42**, 287 (2000).
[4] L. Cai, J. Marango, and B. Friedrich, Phys. Rev. Lett. **86**, 775 (2001).
[5] B. Friedrich and D. Herschbach, Phys. Rev. Lett. **74**, 4623 (1995).
[6] C. M. Dion, A. Keller, O. Atabek, and A. D. Bandrauk, Phys. Rev. A **59**, 1382 (1999).
[7] T. Seideman, Phys. Rev. Lett. **83**, 4971 (1999).
[8] J. Ortigoso, M. Rodriguez, M. Gupta, and B. Friedrich, J. Chem. Phys. **110**, 3870 (1999).
[9] T. Seideman, J. Chem. Phys. **115**, 5965 (2001).
[10] J. J. Larsen, H. Sakai, C. P. Safvan, I. Wendt-Larsen, and H. Stapelfeldt, J. Chem. Phys. **111**, 7774 (1999).
[11] H. J. Loesch, Annu. Rev. Phys. Chem. **46**, 555 (1995).
[12] T. D. Hain, R. M. Moision, and T. J. Curtiss, J. Chem. Phys. **111**, 6797 (1999).
[13] B. Friedrich and D. Herschbach, J. Chem. Phys. **111**, 6157 (1999).
[14] T. Seideman, J. Chem. Phys. **103**, 7887 (1995); C. M. Dion, A. Keller, and O. Atabek, Eur. Phys. J. D **14**, 249 (2001); M. Machholm and N. E. Henriksen, Phys. Rev. Lett. **87**, 193 001 (2001); I. Sh. Averbukh and R. Arvieu, Phys. Rev. Lett. **87**, 163 601 (2001).
[15] C. M. Dion, A. D. Bandrauk, O. Atabek, A. Keller, H. Umeda, and Y. Fujimura, Chem. Phys. Lett. **302**, 215 (1999).
[16] A. Keller, C. M. Dion, and O. Atabek, Phys. Rev. A **61**, 023409 (2000).
[17] B. Friedrich and D. Herschbach, J. Phys. Chem. **103**, 10 280 (1999).
[18] C. Dion, PhD. thesis, Université de Paris-Sud and Université de Sherbrooke, 1999.

10.5 Enhanced alignment and orientation by resonance

Here we study the adiabatic alignment of a polar molecule by a field that is vibrationally quasi-resonant. In the adiabatic regime, the detunings play in general a crucial role and are expected to qualitatively change the mechanism of alignment. We show in particular that in this regime the resonant field much enhances the efficiency of the alignment and (2+1) orientation with respect to a nonresonant field by analytical and numerical analysis. We show that the quasi-resonant field leads to a dressed state as a *vibrational pendular state*, made of a specific combination of rovibrational states.

For intermediate intensities, the quasi-resonant process dominates for the alignment through the permanent dipole moment. Larger intensities allow the polarizability to come into play, and to efficiently align with the use of the dipole moment and the polarizability.

10.5.1 Alignment

The model and analysis

We consider the vibrational states $\{|v\rangle, v = 0, 1, \cdots\}$ of one vibrational mode of a linear polar molecule in its ground electronic state. Each vibrational state is modeled as a rigid rotor. The molecule is subject to a linearly polarized laser field of low frequency with respect to the excited electronic states, i.e. far red-detuned from any resonances with them. We thus consider the interaction through its permanent dipole moment $\mu_0(x)$, coupling the vibrations (of coordinate x) with one-photon processes, and through its polarizability, coupling the vibrations by Raman processes.The dynamical polarizability includes the components $\alpha_\parallel(x)$ and $\alpha_\perp(x)$, respectively parallel and perpendicular to the molecular axis. The polarizability in the Born-Oppenheimer approximation corresponds to a Raman coupling through excited electronic states in the ground electronic state. It is a good approximation to choose $\alpha_\parallel$ and $\alpha_\perp$ as the static polarizabilities when the laser frequencies are far red-detuned from the excited electronic states. The Hamiltonian $H_{v',v} = \langle v'|H|v\rangle$, of energy E_v and of rotational constant B_v, reads in this case

$$\begin{aligned} H_{v'v} = &\left(E_v + B_v J^2\right)\delta_{v',v} - \mu_{0,v'v}\mathcal{E}(t)\cos(\omega t+\phi)\cos\theta \\ &+ \mathcal{E}^2(t)\cos^2(\omega t+\phi)\left(\Delta\alpha_{v'v}\sin^2\theta - \alpha_{\parallel,v'v}\right)/2. \end{aligned} \tag{10.87}$$

with $\mu_{0,v'v} = \langle v'|\mu_0|v\rangle$, $\alpha_{\perp,v'v} = \langle v'|\alpha_\perp|v\rangle$, $\alpha_{\parallel,v'v} = \langle v'|\alpha_\parallel|v\rangle$, $\Delta\alpha_{v'v} = \alpha_{\parallel,v'v} - \alpha_{\perp,v'v}$, and J the angular momentum. θ is the angle between the molecular axis and the direction of the aligning field of amplitude $\mathcal{E}(t) = \mathcal{E}_0\sqrt{\Lambda(t)}$, carrier frequency ω and initial phase ϕ, with $\mathcal{E}_0$ the peak amplitude and $0 \leq \Lambda(t) \leq 1$ the envelope of the field intensity.

Nonresonant field. If the field frequency is far blue-detuned from the (lower) excited vibrational states, the effective (dressed) Hamiltonian in the ground vibrational state (of energy E_0) can be approximated in the high frequency limit (with respect to the rotational constant B_0) as

$$H_{00}^{\mathrm{HF}} = E_0 + B_0 J^2 + V_0 \tag{10.88}$$

with

$$V_0 = \frac{1}{4}\mathcal{E}^2(t)\left(\Delta\alpha_{00}^{\mathrm{eff}}(\omega)\sin^2\theta - \alpha_{\parallel,00}\right) \tag{10.89}$$

and

$$\Delta\alpha_{vv}^{\text{eff}}(\omega) = \Delta\alpha_{vv} + \frac{2B_v \left|\mu_{0,vv}\right|^2}{(\hbar\omega)^2}. \tag{10.90}$$

For linear molecules ($\alpha_\parallel > \alpha_\perp$), the rigid rotor $B_0 J^2$ is thus effectively subject to a double-well potential of the form $\sin^2\theta$, with minima at $\theta = 0$ and $\theta = \pi$ for the magnetic quantum number $M = 0$ [125] (see an example in Fig. 10.14). This potential becomes deeper and more narrow for stronger fields. The condition for adiabatic transport is estimated with respect to the smaller detuning $6B_0$ of the two-photon process between the rotational states [160]:

$$\tau \gg \hbar/6B_0, \tag{10.91}$$

with τ characterizing the pulse duration. In practice, one can consider that adiabatic passage is achieved when the observable $\langle\cos^2\theta\rangle$ that is a quantitative measure of the degree of alignment is back at the end of the pulse to its isotropic value 1/3 without oscillating. This condition is very restrictive in the sense that even a small loss ϵ of population to the upper state $|J = 2\rangle$ induces final oscillations of $\langle\cos^2\theta\rangle$ of amplitude of the order of $\sqrt{\epsilon}$. If we consider smooth pulses, such as gaussian pulses with intensity of the shape $\Lambda(t) = e^{-4\log 2(t/\tau)^2}$ (where τ is here the full width at half maximum), the adiabatic regime is well attained for $\tau B_0 \gtrsim 3\hbar$ (i.e. when the final oscillations of $\langle\cos^2\theta\rangle$ are of amplitude less than approximately 0.01). For a given pulse amplitude $\mathcal{E}$, the dimensionless quantity characterizing the alignment regime is

$$\gamma = \mathcal{E}^2 \Delta\alpha_{00}^{\text{eff}}(\omega)/4B_0, \tag{10.92}$$

through the approximative formula [125]

$$\langle\cos^2\theta\rangle \to 1 - 1/\sqrt{\gamma} \tag{10.93}$$

in the limit of low temperature T, such that $kT/B_0 \ll 1$, and high field regime: $\gamma \gg 1$. Already for $\gamma = 30$, one obtains in the adiabatic regime $\langle\cos^2\theta\rangle \approx 0.82$.

Resonant field. We now study a field quasi-resonant between the ground state and the first excited vibrational state, with a detuning $\hbar\Delta = E_1 - E_0 - \hbar\omega$. Since the polarizability in the Born-Oppenheimer approximation corresponds to a Raman coupling through excited electronic states, considering a resonant process through vibrational states in the ground electronic state does not drastically change its value. We thus still use the static polarizability. We first consider for simplicity a model including only those two vibrational states. In Section B, we will present numerical simulations including the effects of all vibrational states. The Hamiltonian (10.87) becomes in the high frequency limit and in the resonant approximation:

$$H = \begin{bmatrix} B_0 J^2 + \frac{1}{4}\mathcal{E}^2(t)\left(\Delta\alpha_{00}^{\text{eff}}\sin^2\theta - \alpha_{\parallel,00}\right) & -\frac{1}{2}\mathcal{E}(t)\mu_{0,01}e^{i\phi}\cos\theta \\ -\frac{1}{2}\mathcal{E}(t)\mu_{0,01}e^{-i\phi}\cos\theta & B_1 J^2 + \frac{1}{4}\mathcal{E}^2(t)\left(\Delta\alpha_{11}^{\text{eff}}\sin^2\theta - \alpha_{\parallel,11}\right) + \hbar\Delta \end{bmatrix}. \tag{10.94}$$

To obtain the counterpart of the effective double-well potential V_0 (10.89) driving the alignment in this resonant case, we use the fact that $B_0 \approx B_1$, $\alpha_{\parallel,00} \approx \alpha_{\parallel,11}$, and $\alpha_{\perp,00} \approx \alpha_{\perp,11}$. For the CO molecule, the relative differences between B_0 and B_1, $\alpha_{\parallel,00}$ and $\alpha_{\parallel,11}$, $\alpha_{\perp,00}$ and $\alpha_{\perp,11}$ are of the order of 1%.

We first consider the simplest case of exact vibrational resonance $\Delta = 0$, which will be shown below to give the most efficient alignment. We block-diagonalize the effective Hamiltonian (10.94):

$$\widetilde{H} := S_1^\dagger H S_1 = B_0 J^2 + \begin{bmatrix} V_{1,+} & 0 \\ 0 & V_{1,-} \end{bmatrix} \tag{10.95}$$

with the transformation from the bare to the adiabatic (with respect to the vibration) basis

$$S_1 = \frac{1}{\sqrt{2}} \begin{bmatrix} e^{i\phi} & e^{i\phi} \\ -1 & 1 \end{bmatrix} \tag{10.96}$$

and the dressed potentials

$$V_{1,\pm} = \frac{1}{4}\mathcal{E}^2(t)\left(\Delta\alpha_{00}^{\text{eff}}\sin^2\theta - \alpha_{\parallel,00}\right) \pm \frac{1}{2}\mathcal{E}(t)\mu_{0,01}\cos\theta. \tag{10.97}$$

Each potential $V_{1,+}$ ($V_{1,-}$) allows the molecule to orient towards $\theta = \pi$ ($\theta = 0$). The connection of the initial state with the adiabatic state is made through the transformation S_1: $\widetilde{\psi} = S_1^\dagger\psi$, where ψ and $\widetilde{\psi}$ are respectively the state of the system in the bare and in the adiabatic basis. It shows that, if the molecule is initially in the ground state $|v = 0, J = 0\rangle$, half of the population is trapped in the potential $V_{1,-}$ and half in $V_{1,+}$. The global alignment is given by

$$\langle\cos^2\theta\rangle = \frac{1}{2}\left(\langle\cos^2\theta\rangle_{1,-} + \langle\cos^2\theta\rangle_{1,+}\right), \tag{10.98}$$

where $\langle\cos^2\theta\rangle_{1,i}$, $i = \pm$ corresponds to the adiabatic alignment that would be effectively obtained in the potential $V_{1,i}$ (with a single vibrational state). Since we have $\langle\cos^2\theta\rangle_{1,-} = \langle\cos^2\theta\rangle_{1,+}$, we finally obtain:

$$\langle\cos^2\theta\rangle = \langle\cos^2\theta\rangle_{1,\pm}. \tag{10.99}$$

We can estimate the condition for adiabatic transport using the smallest detuning of the one-photon process between the rovibrational states (i.e. to avoid Rabi oscillations):

$$\tau \gg \hbar/\left|2B_0 + \hbar\Delta\right|. \tag{10.100}$$

We remark that this condition cannot be satisfied for $\hbar\Delta \sim -2B_0$, i.e. when the field is *exactly* resonant between the rovibrational states $|v = 0, J = 0\rangle$ and $|v = 1, J = 1\rangle$.

In summary, if the molecule is initially in the ground state $|v = 0, J = 0\rangle$, the resonant adiabatic transport splits first instantaneously the state with equal weights in the two vibrational states $\frac{1}{\sqrt{2}}(e^{i\phi}|v = 0\rangle + |v = 1\rangle)$ and $\frac{1}{\sqrt{2}}(e^{i\phi}|v = 0\rangle - |v = 1\rangle)$, each next subject to the potential $V_{1,-}$ and $V_{1,+}$ respectively, and the global alignment is half of the sum of the alignment obtained in each potential. For any phase ϕ, this alignment is the same as the one obtained in a single effective vibrational state with the potential (10.97) (taking the plus or minus contribution). This leads to a more favorable scaling than the non resonant potential V_0 (10.89) (linear in the amplitude $\mathcal{E}$ instead of the intensity $\mathcal{E}^2$, see Fig. 10.14).

We can remark that in the limit of high alignment efficiency (in practice for $\langle\cos^2\theta\rangle \gtrsim 0.7$), the alignment dynamics can be approximately characterized by a single dressed potential

$$V_1 = \frac{1}{4}\mathcal{E}^2(t)\left(\Delta\alpha_{00}^{\text{eff}}\sin^2\theta - \alpha_{\parallel,00}\right) - \frac{1}{2}|\mathcal{E}(t)\mu_{0,01}\cos\theta|. \tag{10.101}$$

Figure 10.14 displays this potential for the CO molecule.

During this adiabatic alignment, the wavepacket is thus a vibrational pendular state, which is made of a specific combination of rotational states of both rotors. If we align a cold molecule initially in the state $v = 0, J = 0$ by an adiabatic rising, and if the field is next switched off (i) adiabatically, the molecule returns to the state $v = 0, J = 0$, or (ii) suddenly, the molecule will show periodic revivals, as described in Ref. [163] for a prior non-resonant adiabatic rising.

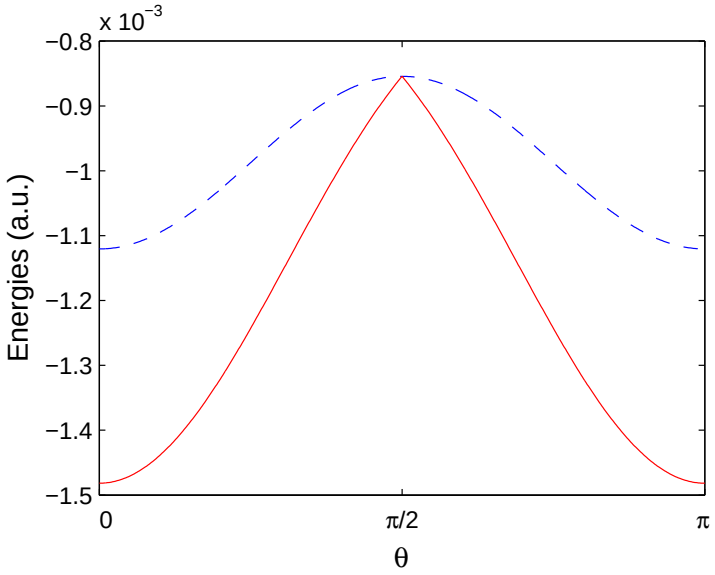

FIG. 10.14 - *Non-resonant (10.89) (dashed line) and approximate resonant (10.101) (full line) dressed potentials for the CO molecule with $I = 10$ TW/cm^2. The resonant potential is much deeper and leads thus to more aligned molecules.*

We remark that if the molecule is initially prepared in the state $\frac{1}{\sqrt{2}}(e^{i\phi}|v=0,J=0\rangle + |v=1,J=0\rangle)$ [resp. $\frac{1}{\sqrt{2}}(e^{i\phi}|v=0,J=0\rangle - |v=1,J=0\rangle)$], it is subject to the potential $V_{1,-}$ (resp. $V_{1,+}$) by the resonant process. In this case the molecule is oriented towards $\theta = 0$ (resp. $\theta = \pi$).

When the process is near-resonant (with a detuning Δ), one can make a similar analysis with the potentials

$$V_{1,\pm} = \frac{1}{4}\mathcal{E}^2(t)\left(\Delta\alpha_{00}^{\rm eff}\sin^2\theta - \alpha_{\parallel,00}\right) + \frac{1}{2}\left[\hbar\Delta \pm \sqrt{(\hbar\Delta)^2 + (\mathcal{E}(t)\mu_{0,01}\cos\theta)^2}\right] . \quad (10.102)$$

In this case the transformation is however time-dependent and the adiabatic analysis is not so straightforward (see Section 2.6).

If we now suppose that $N+1$ vibrational states are near-resonant, we have to consider a more general effective Hamiltonian [see appendix 10.6, Eq. (10.114)]. The preceding analysis can be directly extended in the exact resonant case with the following additional approximations: (i) the Ω_{vv+1} are taken equal for all v: $\Omega_{N-1N} \approx \cdots \approx \Omega_{01} =: \Omega_0$, (ii) the limit of a small detuning Δ and a small anharmonicity a: $\Omega_0 \gg N(\Delta + (N-1)a)$, and (iii) $B_0 \approx B_1 \approx \cdots \approx B_N$. In this case, we can block-diagonalize the effective Hamiltonian and determine the associated transformation. The resulting potentials have also a part that scales as the field amplitude leading in general to a more efficient alignment than the non-resonant case.

Numerics

We show the relevance of the preceding qualitative analysis by numerical simulations using the effective Hamiltonian (10.94) with the parameters of the CO molecule using the ab initio calculations of Ref. [193].

Figure 10.15 shows dynamical simulations of $\langle\cos^2\theta\rangle = \langle\psi(t)|\cos^2\theta|\psi(t)\rangle$ with $|\psi(t)\rangle$ solution of the time dependent Schrödinger equation, for a rising $\gamma(t)$ and as a function of the

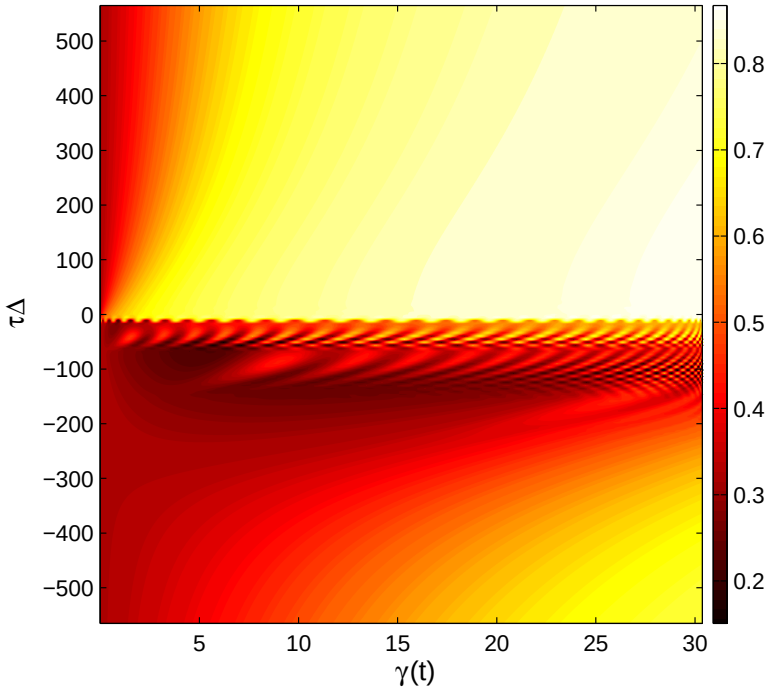

FIG. 10.15 - *Dynamical contour plot of* $\langle \cos^2\theta \rangle$ *for an increasing field of intensity envelope* $\Lambda(t) = e^{-4\log 2(t/\tau)^2}$ *with the full width half maximum* $\tau = 25$ *ps [giving here* $\tau B_0 \approx 9$ *and satisfying thus the adiabatic condition (10.100) for* $\Delta \gtrsim 0$*], and of peak intensity* $I = 10$ TW/cm^2*, as a function of the laser intensity parameterized by* γ *(10.92) (*$\gamma = 30$ *corresponds to the approximative field intensity* 10 TW/cm^2 *for the CO molecule) and* Δ*. Only the two lowest vibrational states have been taken into account.*

initial detuning Δ. The alignment efficiency is better (i.e. larger $\langle \cos^2\theta \rangle$) for a lighter plot. In Fig. 10.15, only the two lowest vibrational states are considered. The figure features *three regimes* of different alignment efficiency. The higher part $\Delta \geq 0$ (corresponding to a laser frequency *below* the vibrational resonance) shows an efficient alignment, which becomes better for a larger field amplitude and for a process closer to the vibrational resonance (i.e. for Δ closer to approximately 0), as expected from the above analysis. This result is obtained provided that the adiabaticity condition (10.100) is still satisfied by taking sufficiently long pulses. This condition excludes an exact resonance between any rovibrational states. For the part $\Delta < 0$ (corresponding to a laser frequency *above* the vibrational resonance), one can see a much weaker alignment. For approximately $0 < \Delta\tau \lesssim -200$, the contour plot shows a complicated pattern due to Rabi oscillations between rovibrational states. For such a small negative detuning, some rotational states associated to $v = 0$ become indeed resonant with the ones associated to $v = 1$. For approximately $\Delta\tau > -200$, the detuning is large enough (in absolute value) to prevent the resonances and Rabi oscillations between rovibrational states. Such a regime can be well approximated by neglecting the resonant part of the effective Hamiltonian, i.e. taking into account only the non-resonant polarizability. This approximation is obviously better for higher $|\Delta|$. We recover in this case the well-known non-resonant alignment, with better efficiency for higher field amplitude.

However, in general, one cannot ignore the higher excited vibrational states, and since the vibrational anharmonicity is negative, one expects additional detrimental resonances from the rotational structure of these states. Fig. 10.16 shows dynamical simulations of $\langle \cos^2\theta \rangle$ when

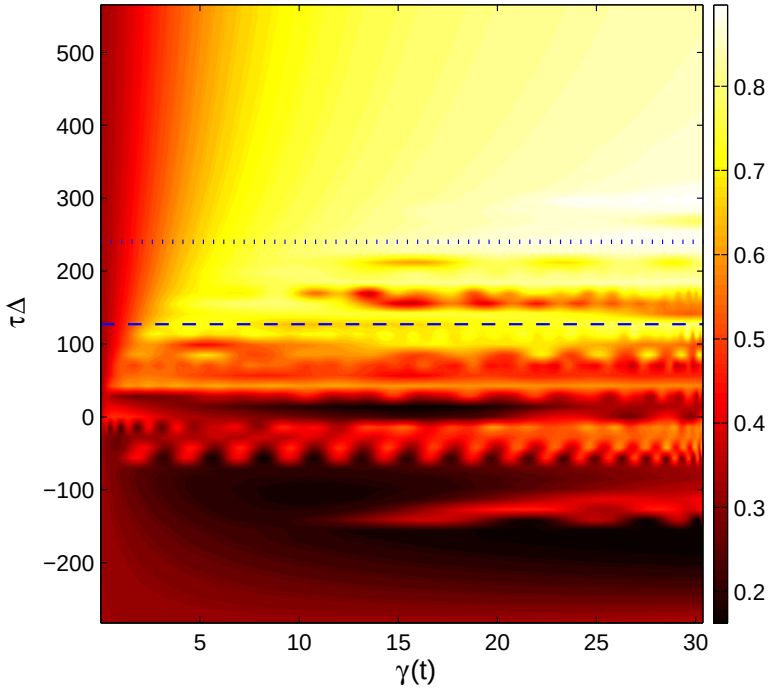

FIG. 10.16 - *Same as Fig. 10.15, but for a full account of the vibrational structure. The straight (dashed and dotted) lines correspond to the plots of Fig. 10.17*

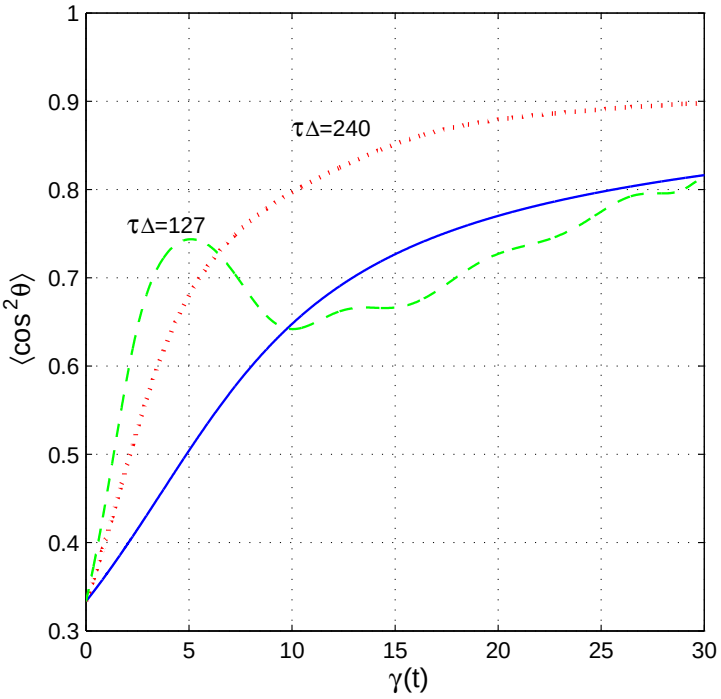

FIG. 10.17 - *Dynamical plot of* $\langle \cos^2 \theta \rangle$ *for an increasing field intensity (same as in Fig. 10.16) as a function of* γ *(10.92) for* $\tau\Delta = 127$ *(dashed line),* $\tau\Delta = 240$ *(dotted line), and the far from resonance case (full line). The dashed and dotted lines correspond to the lines of Fig. 10.16*

.

the complete vibrational structure is taken into account (the ten lowest vibrational states of the CO molecule have been used here; addition of higher vibrational states do not change the result). When we compare Figs. 10.15 and 10.16, one can see that the consideration of the full vibrational structure *shifts* the efficiency region to higher values of Δ. The well-known non-resonant alignment (not shown in Fig. 10.16) is recovered for a large negative Δ. Two strategies can be considered from a detailed inspection of Fig. 10.17: (i) If a modest alignment is desired, one can use a quite low value of Δ (see one example in Fig. 10.17, dashed line), which requires a modest field intensity with respect to the non-resonant case (full line); (ii) A stronger alignment can be obtained for a larger Δ and a larger field amplitude (dotted line), still more efficiently than for the non-resonant case.

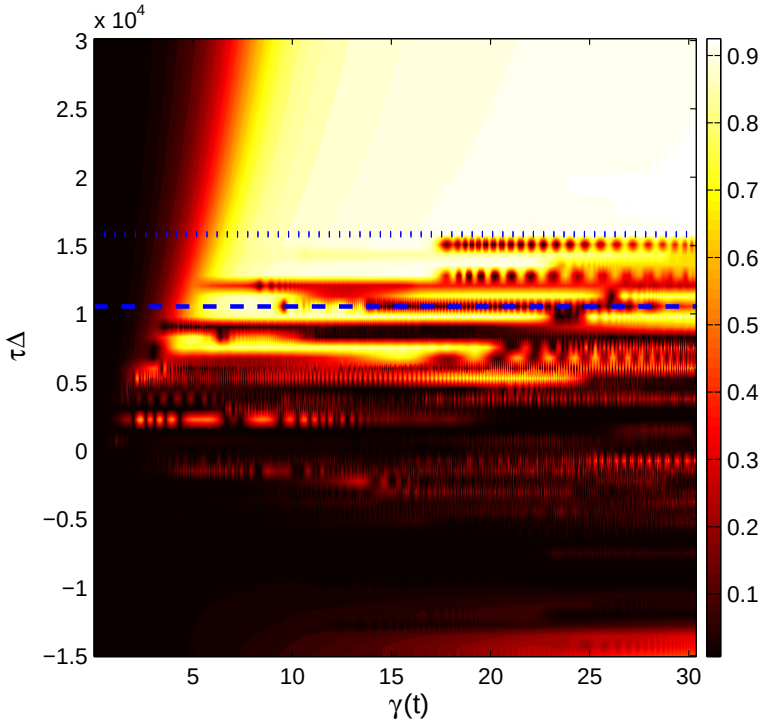

FIG. 10.18 - *Dynamical contour plot of* $|\langle\cos\theta\rangle|$ *for increasing fields with the full width half maximum* $\tau = 1.33$ *ns of peak intensities* $I_1 = 10$ *TW/cm*^{2}, $I_2 = 2$ *TW/cm*^{2} *(giving here* $\tau B_0 \approx 480$*), and* $\phi = \pi$*, as a function of* γ *(determined for* I_1*) and* Δ*, with a full account of the vibrational states. The straight (dashed and dotted) lines refer to the plots of Fig. 10.19.*

10.5.2 2+1 Orientation

We consider a 2+1 hyper-Raman coupling with the combination of the two lasers $(\omega, 2\omega)$ giving the total electric field $\mathcal{E}(t) = \mathcal{E}_1(t)\cos\omega t + \mathcal{E}_2(t)\cos(2\omega t + \phi)$, with $\mathcal{E}_1(t) = \mathcal{E}_{01}\Lambda(t)$, $\mathcal{E}_2(t) = \mathcal{E}_{02}\Lambda(t)$, and ϕ the relative phase

We recall [176] that the orientation is obtained by adiabatic passage along the dressed (pendular) state $|\tilde{J} = 0\rangle$ connected to the initial state $|J = 0\rangle$, when the dynamics goes beyond the three-photon avoided crossing generated by the 2+1 hyper-Raman coupling, leading to one of the oriented states $(|\tilde{J} = 0\rangle \pm |\tilde{J} = 1\rangle)/\sqrt{2}$. The relative phase ϕ allows to choose the direction of orientation of the molecule. Detailed calculations giving the effective Hamiltonian that is used in our calculations, can be found in Appendix 10.7.

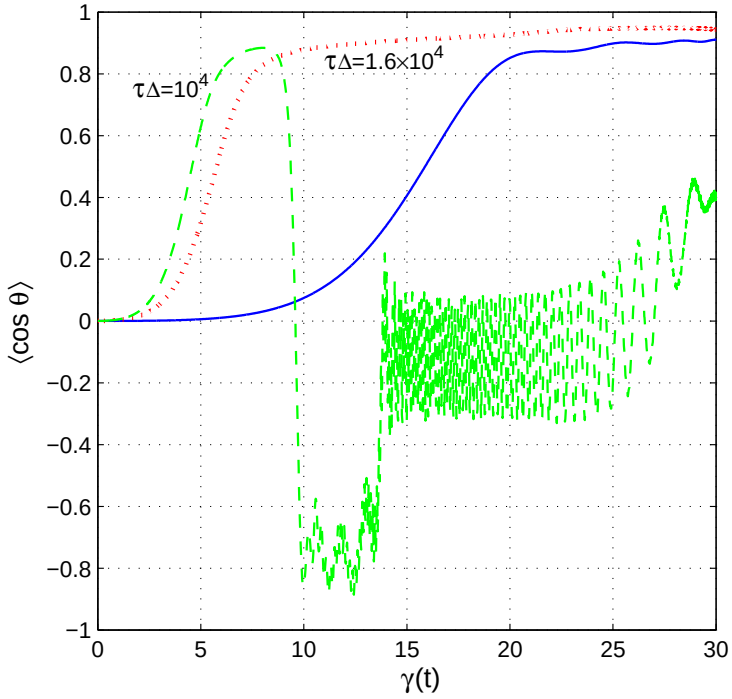

FIG. 10.19 - *Dynamical plot of* $\langle \cos\theta \rangle$ *for an increasing field intensity (same as in Fig. 10.18) as a function of* γ *for* $\tau\Delta = 10^4$ *(dashed line),* $\tau\Delta = 1.6 \times 10^4$ *(dotted line), and the non-resonance case (full line). The dashed and dotted lines correspond to the lines of Fig. 10.18.*

Figures 10.18 and 10.19, the counterpart of Figs. 10.15 and 10.16 for orientation, show that the orientation efficiency by adiabatic passage is improved, when the 2+1 coupling is such that the one photon coupling is near resonant with the vibrational ladder. This extends to orientation processes the improvement of alignment shown in the preceding section.

As it was the case for alignment, one can use specific detunings that give (i) a quite efficient orientation for a modest field amplitudes (dashed line of Fig. 10.19) or (ii) a more efficient orientation but for higher field amplitudes (dotted line of Fig. 10.19).

10.5.3 Conclusion

We have shown that vibrationally resonant fields strongly improve the alignment and the 2+1 orientation by adiabatic passage, when only one dressed rovibrational state is populated during the dynamics. The resulting aligned and oriented states are specific vibrational pendular states. We have numerically shown this improvement using the parameters of the CO molecule. We expect similar results with weaker field amplitudes for other diatomic molecules of larger dipole moment.

10.6 Appendix A: Effective Hamiltonians for vibrationally resonant alignment

We extend the calculation of the non-resonant Raman effective Hamiltonian in Subsection 6.3.5 to the case where N vibrational states are quasi-resonant. When two vibrational states

are consider, the Floquet Hamiltonian is of the form

$$K/\hbar\omega = -i\frac{\partial}{\partial\theta_L} + \epsilon \begin{bmatrix} H_{00} & H_{01} \\ H_{10} & H_{11} \end{bmatrix}. \tag{10.103}$$

We define the transformations

$$T_n \equiv \begin{bmatrix} T_{n,0} & 0 \\ 0 & T_{n,1} \end{bmatrix}, \quad T_{n,v} \equiv e^{\epsilon^n W_{n,v}}. \tag{10.104}$$

The three iterations described above give here

$$T_3^\dagger T_2^\dagger T_1^\dagger \left(K/\hbar\omega\right) T_1 T_2 T_3 = \begin{bmatrix} K_{4,0} & V_{4,01} \\ V_{4,01}^\dagger & K_{4,1} \end{bmatrix} \tag{10.105}$$

with

$$\begin{aligned} K_{4,v} &:= T_{3,v}^\dagger T_{2,v}^\dagger T_{1,v}^\dagger \left(K_{0+}\epsilon H_{v,v}\right) T_{1,v} T_{2,v} T_{3,v} \\ &= K_0 + \epsilon\overline{H_{vv}} + \epsilon^2\overline{V_{2,v}} + \mathcal{O}(\epsilon^4), && \text{(10.106a)} \\ V_{2,v} &= B_0[J^2, W_{1,v}] - \epsilon\left(\frac{\partial W_{1,v}}{\partial\theta}\right)^2, && \text{(10.106b)} \\ V_{4,01} &= \epsilon e^{-\epsilon^3 W_{3,0}} e^{-\epsilon^2 W_{2,0}} H_{01} e^{\epsilon(W_{1,1}-W_{1,0})} e^{\epsilon^2 W_{2,1}} e^{\epsilon^3 W_{3,0}}, && \text{(10.106c)} \end{aligned}$$

and

$$\begin{aligned} W_{1,v}(\theta_L) &= -i\int^{\theta_L} d\theta'_L \ (H_{vv}(\theta'_L) - \overline{H_{vv}}), && \text{(10.107a)} \\ W_{2,v}(\theta_L) &= -i\int^{\theta_L} d\theta'_L \ (V_{2,v}(\theta'_L) - \overline{V_{2,v}}). && \text{(10.107b)} \end{aligned}$$

Resonant approximation. In the case of two near resonant vibrational states with the aligning laser (associated with the detuning $\hbar\Delta = E_1 - E_0 - \hbar\omega$), the non-diagonal element can be expanded as a function of ϵ and $\mathcal{E}$ from which we can extract the resonant term . The other non-resonant terms are discarded (resonant approximation), which leads to:

$$\begin{aligned} &T_3^\dagger T_2^\dagger T_1^\dagger K T_1 T_2 T_3 \\ &\simeq \begin{bmatrix} \hbar\omega K_{4,0} & -\frac{1}{2}\mu_{0,v'v}\mathcal{E}e^{i\phi}\cos\theta \\ -\frac{1}{2}\mu_{0,v'v}\mathcal{E}e^{-i\phi}\cos\theta & \hbar\omega K_{4,1} - \hbar\omega \end{bmatrix}, \end{aligned} \tag{10.108}$$

where

$$K_{4,v} = -i\frac{\partial}{\partial\theta_L} + \epsilon\left(E_v + H_v^{\mathrm{HF}}\right) + \mathcal{O}(\epsilon^4, \mathcal{E}^3) \tag{10.109}$$

with

$$H_v^{\mathrm{HF}} = B_v J^2 + \frac{1}{4}\mathcal{E}^2\left(\Delta\alpha_{vv}^{\mathrm{eff}}\sin^2\theta - \alpha_{\parallel,vv}\right). \tag{10.110}$$

and

$$\Delta\alpha_{vv}^{\mathrm{eff}} = \Delta\alpha_{vv} + 2B_v\left|\mu_{0,vv}\right|^2/\left(\hbar\omega\right)^2. \tag{10.111}$$

This gives the effective Hamiltonian for the two vibrational quasi-resonant states (where the constant energy E_0 has been omitted):

$$H = \begin{bmatrix} H_0^{\rm HF} & -\frac{\hbar}{2}\Omega_{01}e^{i\phi} \\ -\frac{\hbar}{2}\Omega_{01}e^{-i\phi} & H_1^{\rm HF}+\hbar\Delta \end{bmatrix} \tag{10.112}$$

with the Rabi frequency

$$\Omega_{vv+1} = \mu_{0,vv+1}\mathcal{E}\cos\theta/\hbar. \tag{10.113}$$

This result can be extended to $N+1$ vibrational states in a direct way:

$$H = \begin{bmatrix} H_0^{\rm HF} & -\frac{\hbar}{2}\Omega_{01}e^{i\phi} & 0 & \cdots & 0 \\ -\frac{\hbar}{2}\Omega_{01}e^{-i\phi} & H_1^{\rm HF}+\hbar\Delta & -\frac{\hbar}{2}\Omega_{12}e^{i\phi} & \ddots & \vdots \\ 0 & -\frac{\hbar}{2}\Omega_{12}e^{-i\phi} & H_2^{\rm HF}+2\hbar(\Delta+a) & \ddots & 0 \\ \vdots & \ddots & \ddots & \ddots & -\frac{\hbar}{2}\Omega_{N-1N}e^{i\phi} \\ 0 & \cdots & 0 & -\frac{\hbar}{2}\Omega_{N-1N}e^{-i\phi} & H_N^{\rm HF}+N\hbar(\Delta+(N-1)a) \end{bmatrix}, \tag{10.114}$$

if one considers the vibrational states as eigenstates of a Morse potential associated to the anharmonicity

$$a := \left[(E_{v+1}-E_v)-(E_v-E_{v-1})\right]/2\hbar = -\hbar\omega_e^2/4D \tag{10.115}$$

with D the dissociation energy, and the frequency ω_e related to the eigenenergies of the Morse potential: $E_v = \hbar\omega_e\left(v+1/2\right)+\hbar a\left(v+1/2\right)^2$, and $B_v = B_e-\alpha_e(v+1/2)$, $v=0,\cdots,N$.

Block-diagonalization. We can block-diagonalize with respect to the vibration the preceding effective Hamiltonian considering that the Ω_{vv+1} are approximately equal for all v: $\Omega_{N-1N}\approx\cdots\approx\Omega_{01} =: \Omega_0$, in the limit of a small detuning Δ and a small anharmonicity a: $\Omega_0 \gg N(\Delta+(N-1)a)$, and for $B_0\approx B_1\approx\cdots\approx B_N$. We obtain with these approximations:

$$S_N^\dagger H S_N \approx B_0 J^2 + {\rm diag}\left[V_{N,0}V_{N,1}\cdots V_{N,N}\right] \tag{10.116}$$

with the adiabatic potentials ($n=0,\cdots,N$)

$$V_{N,n} = \frac{1}{4}\mathcal{E}^2(t)\left(\Delta\alpha_{00}\sin^2\theta-\alpha_{\parallel,00}\right)+\cos\left[\frac{n+1}{N+2}\pi\right]\mathcal{E}(t)\mu_{0,01}\cos\theta \tag{10.117}$$

and the transformation $S_N = \left[S_N^{(m,n)}\right]_{m=0,N;n=0,N}$ from the bare to the adiabatic basis with the matrix elements

$$S_N^{(m,n)} = \sqrt{\frac{2}{N+2}}e^{i[(N-m)\phi+m\pi]}\sin\left[\frac{(n+1)(m+1)}{N+2}\pi\right]. \tag{10.118}$$

The global alignment is given by

$$\langle\cos^2\theta\rangle = \sum_{n=0}^{N}\left|S_N^{(n,0)}\right|^2\langle\cos^2\theta\rangle_{N,n}, \tag{10.119}$$

where $\langle\cos^2\theta\rangle_{N,n}$ corresponds to the adiabatic alignment that would be effectively obtained in the potential $V_{N,n}$ (with a single vibrational state).

10.7 Appendix B: Effective Hamiltonians for 2+1 Orientation

We construct the effective Hamiltonian for the orientation with a 2+1 hyper-Raman coupling given by the combination of the two lasers ($\omega_1 \equiv \omega, \omega_2 \equiv 2\omega$) giving the total electric field $\mathcal{E}(t) = \mathcal{E}_1(t)\cos\omega t + \mathcal{E}_2(t)\cos(2\omega t + \phi)$, with $\mathcal{E}_1(t) = \mathcal{E}_{01}\Lambda(t)$, $\mathcal{E}_2(t) = \mathcal{E}_{02}\Lambda(t)$, and ϕ the relative phase. In the basis of the vibrational states $|v\rangle$, the Floquet operator reads:

$$\langle v'|\, K\, |v\rangle = \delta_{v'v}\left(-i\hbar\omega_1\frac{\partial}{\partial\theta_1} - i\hbar\omega_2\frac{\partial}{\partial\theta_2}\right) + H_{v'v}(\theta_1,\theta_2) \tag{10.120}$$

with

$$H_{v'v}(\theta_1,\theta_2) = \left(E_v + B_v J^2\right)\delta_{v'v} - \mu_{0,v'v}\left(\sum_{j=1,2}\mathcal{E}_j\cos\theta_j\right)\cos\theta + \frac{1}{2}\left(\sum_{j=1,2}\mathcal{E}_j\cos\theta_j\right)^2\left(\Delta\alpha_{v'v}\sin^2\theta - \alpha_{\parallel,v'v}\right). \tag{10.121}$$

Here we extend the preceding analysis to the (2+1) process: we determine the effective Hamiltonian with the two approximations: (i) the two field high frequency approximation with respect to the rotational states ($\hbar\omega \gg B_v$), and (ii) the resonant approximation (rotating wave approximation) simultaneously for the two fields: the 2ω field (ω field) is one-photon (two-photon) near-resonant between the two vibrational states.

We remark that we describe below the formulation for two fields of arbitrary high frequencies ω_1 and ω_2. Since here these frequencies are commensurable, we could have used instead a formulation with a single frequency.

Single vibrational state

We study first a single vibrational state, i.e. the Floquet operator $\langle 0|\, K\, |0\rangle$. We define the small parameter $\epsilon := 1/(\hbar\omega_1)$ and consider

$$K/\hbar\omega_1 = K_0 + \epsilon H_{00}(\theta_1,\theta_2) \tag{10.122}$$

with the unperturbed Floquet Hamiltonian

$$K_0 := -i\frac{\partial}{\partial\theta_1} - i\frac{\omega_2}{\omega_1}\frac{\partial}{\partial\theta_2}. \tag{10.123}$$

We can apply the iterative perturbative KAM algorithm ($T_1 = e^{\epsilon W_1}$):

$$T_1^\dagger(K/\hbar\omega_1)T_1 = K_0 + \epsilon D_1 + \epsilon^2 V_2 := K_2 \tag{10.124}$$

with $[K_0, D_1] = 0$ and

$$-i\frac{\partial W_1}{\partial\theta_1} - i\frac{\omega_2}{\omega_1}\frac{\partial W_2}{\partial\theta_2} + H_{00}(\theta_1,\theta_2) - D_1 = 0. \tag{10.125}$$

This two-frequency problem has to be treated by a two-mode Fourier series:

$$W_j = \sum_{n_1,n_2} W_j^{(n_1,n_2)} e^{i(n_1\theta_1+n_2\theta_2)}, \quad j = 1,2. \tag{10.126}$$

The averaging formulates thus as

$$D_1 = \overline{H_{00}} := \left(\frac{1}{2\pi}\right)^2 \int_0^{2\pi} d\theta_1 \int_0^{2\pi} d\theta_2 \; H_{00}(\theta_1,\theta_2) \tag{10.127a}$$

$$= E_0 + B_0 J^2 + \frac{1}{4}\left(\sum_{j=1,2} \mathcal{E}_j^2\right)\left(\Delta\alpha_{00}\sin^2\theta - \alpha_{\parallel,00}\right). \tag{10.127b}$$

We finally obtain for the effective high frequency Hamiltonian H_0^{HF} of order ϵ^2 and $\mathcal{E}^2$

$$H_0^{\mathrm{HF}} = B_0 J^2 + \frac{1}{4}\sum_{j=1,2} \mathcal{E}_j^2 \left(\Delta\alpha_{00,j}^{\mathrm{eff}}\sin^2\theta - \alpha_{\parallel,00}\right) \tag{10.128}$$

with

$$\Delta\alpha_{00,j}^{\mathrm{eff}} = \Delta\alpha_{00} + 2B_0\left|\mu_{0,00}\right|^2/\left(\hbar\omega_j\right)^2. \tag{10.129}$$

Two near-resonant vibrational states

We extend the preceding calculation using the resonant approximation for both fields and obtain the effective Hamiltonian

$$H = \begin{bmatrix} H_0^{\mathrm{HF}} & H_{01} \\ H_{01}^* & H_1^{\mathrm{HF}} + \hbar\Delta \end{bmatrix} \tag{10.130}$$

with

$$H_v^{\mathrm{HF}} = B_v J^2 + \frac{1}{4}\sum_{j=1,2} \mathcal{E}_j^2 \left(\Delta\alpha_{vv,j}^{\mathrm{eff}}\sin^2\theta - \alpha_{\parallel,vv}\right), \tag{10.131a}$$

$$H_{01} = -\frac{\mu_{0,01}}{2}\mathcal{E}_2 \mathrm{e}^{i\phi}\cos\theta + \frac{1}{8}\mathcal{E}_1^2\left(\Delta\alpha_{01}\sin^2\theta - \alpha_{\parallel,01}\right), \tag{10.131b}$$

and

$$\Delta\alpha_{vv,j}^{\mathrm{eff}} = \Delta\alpha_{vv} + 2B_v\left|\mu_{0,vv}\right|^2/\left(\hbar\omega_j\right)^2. \tag{10.132}$$

This result can be extended to more than two vibrational states in a quite direct way: We obtain the Hamiltonian of the form (10.114), with the terms (10.131a) on the diagonal, and the off-diagonal terms

$$H_{vv+1} = H_{v+1v}^* = -\frac{\mu_{0,vv+1}}{2}\mathcal{E}_2 \mathrm{e}^{i\phi}\cos\theta + \frac{1}{8}\mathcal{E}_1^2\left(\Delta\alpha_{vv+1}\sin^2\theta - \alpha_{\parallel,vv+1}\right). \tag{10.133}$$

10.8 Postpulse orientation by hybrid pulse [184]

We show that a combination of a half-cycle pulse and a short nonresonant laser pulse produces a strongly enhanced postpulse orientation. Robust transients that display both efficient and long-lived orientation are obtained. The mechanism is analyzed in terms of optimal oriented target states in finite Hilbert subspaces and shows that hybrid pulses can prove useful for other control issues.

PRL 94, 153003 (2005) PHYSICAL REVIEW LETTERS week ending 22 APRIL 2005

Efficient and Long-Lived Field-Free Orientation of Molecules by a Single Hybrid Short Pulse

D. Daems,[1,2,*] S. Guérin,[1,†] D. Sugny,[1] and H. R. Jauslin[1]

[1]*Laboratoire de Physique de l'Université de Bourgogne, UMR CNRS 5027, BP 47870, 21078 Dijon, France*

[2]*Center for Nonlinear Phenomena and Complex Systems, Université Libre de Bruxelles, 1050 Brussels, Belgium*

(Received 23 November 2004; published 20 April 2005)

We show that a combination of a half-cycle pulse and a short nonresonant laser pulse produces a strongly enhanced postpulse orientation. Robust transients that display both efficient and long-lived orientation are obtained. The mechanism is analyzed in terms of optimal oriented target states in finite Hilbert subspaces and shows that hybrid pulses can prove useful for other control issues.

DOI: 10.1103/PhysRevLett.94.153003 PACS numbers: 33.80.−b, 32.80.Lg, 42.50.Hz

Laser controlled processes such as molecular alignment and orientation are challenging issues that have received considerable attention both theoretically and experimentally [1]. Whereas strong nonresonant adiabatic pulses can exhibit efficient alignment and orientation only when the pulse is on [2–4], linear polar molecules can be oriented under field-free conditions after the extinction of a short half-cycle pulse (HCP) [5,6]. Its highly asymmetrical temporal shape imparts a sudden momentum kick through the permanent dipole moment of the molecule, which orients it. This extends the use of a permanent static field (combined with pulsed nonresonant laser fields) [7,8]. Similar to the alignment process by a nonresonant short pulse [9] (measured by $\langle\cos^2\theta\rangle$, with θ the angle between the axis of the molecule and the polarization direction of the laser field), the orientation by a HCP (measured by $\langle\cos\theta\rangle$) increases as a function of the field amplitude until it reaches a saturation at $\langle\cos\theta\rangle \approx 0.75$, which corresponds to an angle $\cos^{-1}\langle\cos\theta\rangle \approx 41°$. Overcoming this saturation has been theoretically proved with the use of trains of laser pulses (HCP kicks) in the case of alignment [9] (orientation [10]). For applications, it is of importance to reach an efficient orientation. Another crucial point that has received less attention so far [10,11] is the duration during which the orientation is above a given threshold, which one would like to keep as long as possible. An important step made in [10] was to establish *a priori* the two oriented target states (of opposite direction) in a given finite subspace generated by the lowest rotational states. These target states are optimal in the sense that they lead, respectively, to the maximum and minimum values of $\langle\cos\theta\rangle$ in this given subspace. The choice of a suitable small dimension of the subspace allows one to generate an oriented target state of relatively long duration. The identification of such an optimal target state opens, in particular, the possibility to use standard optimization procedures (see, e.g., [12]).

One of the main challenges consists now in reaching such an optimal target state in a subspace of low dimension, characterizing a long-lived and efficient orientation, by a simple external field in a robust way and to ensure the persistence of this effect with respect to thermal averaging of finite temperature. We propose in this Letter a process that possesses such properties. By superimposing a pump laser field to a half-cycle pulse, we show that the maximal orientation reached after the pulse is significantly beyond the one induced by a HCP, and furthermore that it displays a larger duration. We obtain, in particular, the saturation $\langle\cos\theta\rangle \approx 0.89$, which corresponds to the angle $\cos^{-1}\langle\cos\theta\rangle \approx 27°$. This efficient and long-lived orientation is obtained by adjusting only two parameters: the amplitudes of the laser and the HCP fields. We obtain robust regions of the parameters generating this orientation.

We show that this process allows one to approach an optimal target state in one step. Under the action of a single hybrid pulse, the number of rotational states that are significantly populated remains finite and controllable. This generates a finite dimensional subspace in which an optimal target state can be constructed. When the dimension of this subspace increases, the associated optimal state yields a higher orientation efficiency while its duration decreases. By choosing appropriate intensities of the pump laser field and of the half-cycle pulse, we can both select and reach the target state with the desired efficiency and duration.

We consider a linear molecule in its ground vibronic state described in the 3D rigid rotor approximation. The effective Hamiltonian including its interaction with a HCP simultaneously combined with a pump laser field of respective amplitudes $\mathcal{E}_{\mathrm{HCP}}(t)$ and $\mathcal{E}_{\mathrm{L}}(t)$ is given by

$$H_{\mathrm{eff}}(t) = BJ^2 - a_{\mathrm{HCP}}(t)\cos\theta - a_{\mathrm{L}}(t)\cos^2\theta, \qquad (1)$$

where B is the rotational constant, $a_{\mathrm{HCP}} = \mu_0\mathcal{E}_{\mathrm{HCP}}$ with μ_0 the permanent dipole moment, and $a_{\mathrm{L}} = \Delta\alpha\mathcal{E}_{\mathrm{L}}^2/4$ with $\Delta\alpha$ the polarizability anisotropy. Note that $\Delta\alpha$ is positive for linear molecules, which gives positive values for a_{L}, whereas the sign of a_{HCP} is determined by the sign of the HCP amplitude $\mathcal{E}_{\mathrm{HCP}}$. The dynamics of the system is readily determined with the help of the propagator in the impulsive regime, where the duration τ of the pulse is much smaller than the rotational period $\tau_{\mathrm{rot}} = \pi\hbar/B$ [13]. For the process we suggest here, in the dimensionless time $s = t/\tau_{\mathrm{rot}}$ whose origin coincides with the extinction time of the pulse, the propagator reads

PRL 94, 153003 (2005) PHYSICAL REVIEW LETTERS week ending 22 APRIL 2005

$U(s,0) = e^{-i\pi J^2 s} e^{iA_{\rm HCP}\cos\theta} e^{iA_{\rm L}\cos^2\theta}$. The parameters $A_{\rm HCP} = \frac{1}{\hbar}\int dt a_{\rm HCP}(t)$ and $A_{\rm L} = \frac{1}{\hbar}\int dt a_{\rm L}(t)$ are, respectively, the total dimensionless areas of the HCP amplitude and of the laser intensity.

We first consider the case of a cold molecule whose state after the pulse reads $|\phi(s)\rangle = U(s,0)|j=0\rangle$, where $|j\rangle$ stands for the spherical harmonics Y_j^m with $m=0$. The orientation is measured by the expectation value $\langle\cos\theta\rangle(s) = \langle\phi(s)|\cos\theta|\phi(s)\rangle$. It is well known that it is a periodic function (of unit period), which exhibits peaked revivals corresponding to molecular orientation along the field direction [5,6]. The maximal field-free orientation is displayed in Fig. 1 by plotting the maximum of $|\langle\cos\theta\rangle|$ reached over a period as a function of the total areas $A_{\rm L}$ and $A_{\rm HCP}$ at zero rotational temperature, calculated with the above propagator. The case of a single HCP coincides with the ordinate axis. In the absence of the laser pulse, it is seen that the maximal orientation saturates to a value of $\langle\cos\theta\rangle \approx 0.75$. In the presence of a simultaneous pump laser pulse, one observes a wide two-dimensional plateau as well as an island which are both associated with an orientation much higher than the saturation limit of a single high intensity HCP. The plateau is relatively flat in a large two-dimensional region centered approximately around the line $A_{\rm HCP} = 2.5A_{\rm L}$, implying that one can robustly reach a high efficiency for the orientation with a moderate HCP intensity. The island observed around $A_{\rm HCP} = 1.25$ and $A_{\rm L} = 3.7$ indicates that it is also possible to overcome the above saturation by combining a HCP of intensity slightly above unity with a laser pulse of high intensity.

The direction of the orientation can be chosen by the sign of the amplitude of the HCP. Expressing the observable in terms of the projections $c_j = \langle j|\phi(0)\rangle$ of the wave function right after the pulse onto the rotational states $|j\rangle$ leads to $\langle\cos\theta\rangle(s) = \frac{1}{2}\sum c_j^\star c_{j+1} e^{-2i\pi(j+1)s} + \text{c.c.}$ The coefficients c_j can be calculated for the above propagator in the approximation $\langle j|\cos\theta|j\pm1\rangle \simeq 1/2$, which is more accurate for $j \gg 0$ (one has $\langle 0|\cos\theta|1\rangle \approx 0.58$, $\langle 1|\cos\theta|2\rangle \approx 0.52$, $\langle 2|\cos\theta|3\rangle \approx 0.51, \cdots$). This shows that the sign of each product $c_j^\star c_{j+1}$, and hence of $\langle\cos\theta\rangle$, changes with the sign of $A_{\rm HCP}$. For positive $A_{\rm HCP}$, the expectation value corresponding to $\max_s|\langle\cos\theta\rangle|$ is positive on the island and negative on the plateau. We show below that the high orientation efficiency obtained in the region along the line $A_{\rm HCP} = 2.5A_{\rm L}$ has the remarkable property to approach very closely an optimal state as defined in [10], which combines the orientation of high efficiency and of long duration.

The upper panel of Fig. 2 compares the maximal value of $|\langle\cos\theta\rangle|$ as a function of $A_{\rm HCP}$ (i) without the laser and (ii) along the straight line $A_{\rm HCP} = 2.5A_{\rm L}$ seen in Fig. 1. This shows that the saturation of $\langle\cos\theta\rangle \approx 0.75$ obtained

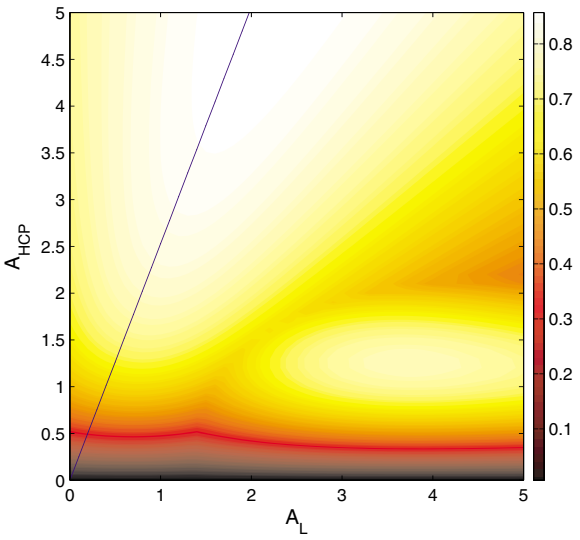

FIG. 1 (color online). Numerical contour plot of $\max_s|\langle\cos\theta\rangle|$ as a function of the total (dimensionless) areas $A_{\rm L}$ and $A_{\rm HCP}$. The straight line $A_{\rm HCP} = 2.5A_{\rm L}$ approximately indicates the maximum for given $A_{\rm HCP}$.

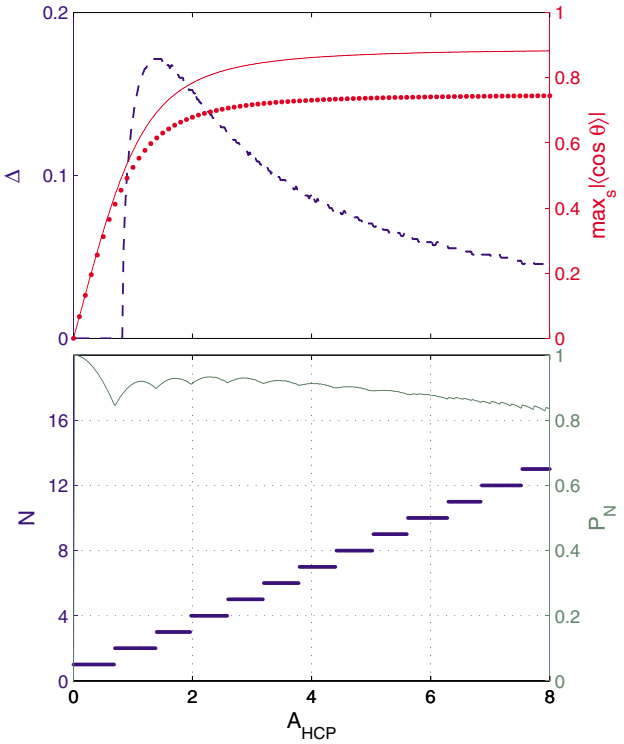

FIG. 2 (color online). As a function of $A_{\rm HCP}$, for $A_{\rm L} = A_{\rm HCP}/2.5$, upper panel: (i) $\max_s|\langle\cos\theta\rangle|$ (solid line, right axis); (ii) for comparison, same quantity with $A_{\rm L} = 0$ (dotted line); (iii) duration Δ for which $|\langle\cos\theta\rangle| > 0.5$ (dashed line, left axis). Lower panel: square modulus $P_N = |\langle\chi_-^{(N)}|\phi(s_{\rm max})\rangle|^2$ of the projection of the state at the time giving the maximum of $|\langle\cos\theta\rangle|$ on the optimal state $|\chi_-^{(N)}\rangle$ (solid line, right axis); dimension N of the corresponding subspace (step function, left axis).

PRL 94, 153003 (2005) PHYSICAL REVIEW LETTERS week ending 22 APRIL 2005

with the HCP alone is significantly overcome (up to $\langle\cos\theta\rangle \approx 0.89$) when the HCP is associated with the laser of appropriate area. The upper panel of Fig. 2 also illustrates the duration of the orientation defined as the time during which $|\langle\cos\theta\rangle| \geq 0.5$ (see also Fig. 3). It is seen that the duration of the revival can be as large as about 18% of the rotational period. The properties displayed in Fig. 2 are robust with respect to the parameters A_{HCP} and A_{L}, which need not be in a strict 2.5 ratio.

The efficiency of the obtained oriented state and its large duration are explained in terms of an optimal state as defined in [10]. We recall that the optimal states correspond to the two states that, respectively, minimize and maximize the projection of $\cos\theta$ in the finite subspace $\mathcal{H}_N$ spanned by the N lowest rotational states $|0\rangle, |1\rangle, \ldots, |N-1\rangle$, namely, $\cos^{(N)}\theta = \Pi_N \cos\theta \Pi_N$ with the projector $\Pi_N = \sum_{j=0}^{N-1} |j\rangle\langle j|$. Considering a finite subspace yields an operator that has a discrete spectrum, whose eigenvectors are readily calculated and for which the duration of the orientation provided by these states can be computed. Furthermore, the controllability of the system can be completely analyzed [14,15]. For a given dimension N, the two optimal states are the eigenvectors associated, respectively, with the smallest and the largest eigenvalues of $\cos^{(N)}\theta$. In the approximation $\langle j|\cos\theta|j \pm 1\rangle \simeq 1/2$ one obtains

$$|\chi_{\pm}^{(N)}\rangle \simeq \sqrt{\frac{2}{N+1}} \sum_{j=0}^{N-1} (\pm 1)^{j+1} \sin\left(\pi \frac{j+1}{N+1}\right) |j\rangle, \quad (2)$$

giving the approximate optimal orientation

$$\langle\chi_{\pm}^{(N)}|\cos^{(N)}\theta|\chi_{\pm}^{(N)}\rangle \simeq \pm\cos\left(\frac{\pi}{N+1}\right). \quad (3)$$

The (relative) duration Δ of the orientation is defined as the time during which $|\langle\cos\theta\rangle| \geq \gamma$ for the revival of maximum efficiency, with γ arbitrarily chosen as $1/2$. We can determine the duration Δ_N for the state $|\chi_{\pm}^{(N)}\rangle$ given in (2) by summing the above expression for $\langle\cos\theta\rangle(s)$ and expanding the result to second order around its extremum, obtaining

$$\Delta_N \approx \frac{2}{\pi}\sqrt{\frac{1}{\Gamma_N}\left[1 - \gamma/\cos\left(\frac{\pi}{N+1}\right)\right]}, \quad (4)$$

where $\Gamma_N = \alpha(N+1)^2 - (N+1)$ with $\alpha = 2/3 - 1/\pi^2$. The shape of Δ_N as a function of N is similar to the dashed curve on the upper panel of Fig. 2, independently of the specific value of γ. In particular, the decrease of this duration for large N is due to the factor Γ_N.

Finding a process that drives the system to an optimal state $\chi_{\pm}^{(N)}$ is of interest since it guarantees an efficient orientation together with a large duration if the dimension N of the subspace $\mathcal{H}_N$ generated by the dynamics is relatively low [10]. The lower panel of Fig. 2 shows that the HCP-laser combination of appropriate areas leads in a single step to a wave function that is remarkably close to the optimal state $|\chi_{-}^{(N)}\rangle$ (more than 90% for $1.5 < A_{\mathrm{HCP}} < 5$). Figure 2 also indicates how the dimension N of the embedding subspace can be chosen by the value of A_{HCP} with $A_{\mathrm{L}} = A_{\mathrm{HCP}}/2.5$. Notice the linear character of this necessarily stepwise function. In the island region of Fig. 1, the dynamics also generates a state close to an optimal one: $|\langle\chi_{+}^{(6)}|\phi(s_{\max})\rangle|^2 \approx 0.86$ for $A_{\mathrm{HCP}} = 1.25$ and $A_{\mathrm{L}} = 3.7$. For comparison, we note that the same optimal states are reached in [10] by a different process involving 15 short HCP kicks sent at specific times and with a low amplitude in order to remain in a given subspace.

Figure 3 shows an example of orientation, measured by $\langle\cos\theta\rangle$, as a function of time for a point on the straight line in Fig. 1 ($A_{\mathrm{HCP}} = 3$). The result is close to that given by the optimal state $\chi_{-}^{(5)}$, whose minimum is taken at the minimum of $\langle\cos\theta\rangle$ generated by the hybrid pulse. In this case, we obtain $|\langle\chi_{-}^{(5)}|\phi(s_{\max})\rangle|^2 \approx 0.93$ (with less than 2% of the total population outside the subspace $\mathcal{H}_5$.) The maximum orientation (in absolute value) $|\langle\cos\theta\rangle| \approx 0.9$ occurs at $s \approx 0.9$. One can observe a relatively large duration of the orientation. In contrast to the case of a sole HCP, the presence of the laser pulse of appropriate area ($A_{\mathrm{L}} = A_{\mathrm{HCP}}/2.5$) allows us to obtain, immediately after the pulse, projections c_j on the rotational states whose moduli are very close to the moduli of the corresponding components of both optimal states. The phases of these projections just after the pulse generally differ from those of the components of the optimal states, but are brought by the free evolution closer to those of one or the other optimal state. In the case of the plateau region, the set of phases after the pulse leads to the state $\chi_{-}^{(N)}$ for positive A_{HCP} and thus yields a minimal value for $\langle\cos\theta\rangle$. This analysis extends to the island region where revivals of opposite sign are observed. As discussed above, by changing the sign of A_{HCP} while keeping A_{L} fixed, one obtains orientation revivals of

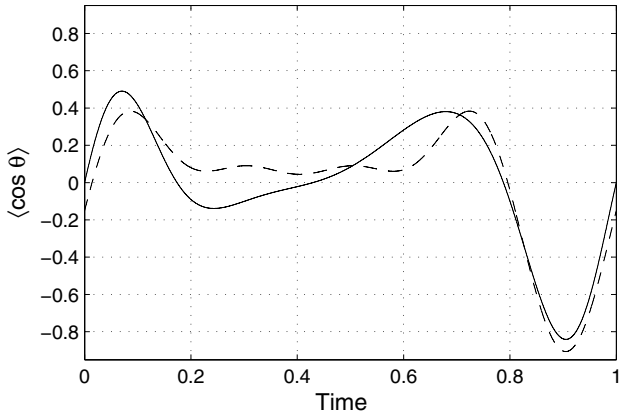

FIG. 3. Orientation as a function of dimensionless time for (i) $A_{\mathrm{HCP}} = 3$ and $A_{\mathrm{L}} = 3/2.5$ (solid line) and (ii) the optimal state $\chi_{-}^{(5)}$ with a time translation (dashed line).

PRL 94, 153003 (2005) PHYSICAL REVIEW LETTERS week ending 22 APRIL 2005

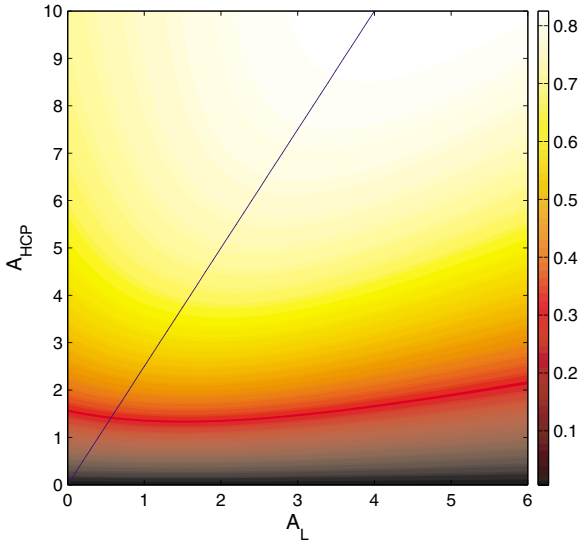

FIG. 4 (color online). Same as Fig. 1 for the dimensionless temperature $\tilde{T} = 5$.

the same absolute values but opposite sign. The direction of the orientation can thus be controlled by the sign of the HCP pulse.

Considering the effect of temperature amounts to statistically averaging over the solutions of the Schrödinger equation with different initial conditions $|j, m\rangle$ weighed by a Boltzmann factor. Figure 4 shows the maximal orientation, measured by the appropriate expectation value of $\cos\theta$, as a function of the field parameters for a dimensionless temperature $\tilde{T} \equiv kT/B = 5$ (which corresponds to $T \approx 5$ K for the LiCl molecule). Notice that the island disappears while the region around the straight line $A_L = A_{HCP}/2.5$ persists. The efficient and long-lived orientation revivals are therefore robust with respect to thermal averaging and to the field parameters. The efficiency is lower than at $T = 0$ K for the same field amplitudes, but one can recover the same value by increasing the amplitudes along the straight line.

In conclusion, we have shown that a combination of a half-cycle pulse and a short nonresonant laser pulse of appropriate amplitudes leads to efficient and long-lived revivals of orientation beyond the known saturation. Furthermore, this is achieved in a controllable manner since the desired target state can be chosen in a set of optimal target states defined in Hilbert subspaces of low dimension and be reached with a projection larger than 90% by a single hybrid pulse. As an illustration, the ground state of a KCl molecule with rotational constant $B \approx 0.13\ \mathrm{cm}^{-1}$ ($\tau_{rot} \approx 128$ ps) and dipole moment $\mu_0 \approx 10.3$ D gives $A_{HCP} \approx 3$ for a pulse duration of 2 ps and a HCP amplitude of 100 kV/cm. To be on the optimal line of Figs. 1 or 4 requires $A_L \approx 1.2$, which corresponds to a peak intensity $I \approx 10^{11}\ \mathrm{W/cm}^2$ for the laser field. These parameters lead to $\max_s|\langle\cos\theta\rangle| \approx 0.85$ and a duration of approximately $1/8$ of the rotational period for a cold molecule (see Fig. 3), and to $\max_s|\langle\cos\theta\rangle| \approx 0.73$ and a duration of approximately $1/20$ of the rotational period for $T = 5$ K. The interest of hybrid pulses is not limited to molecular orientation but extends to optimization issues of a large class of systems where symmetries need to be broken or selectively addressed (e.g., the control of tunneling). The central element consists in using an external field that plays independently on couplings of different symmetries. In order to drive the dynamics even closer to an optimal target state, standard optimization algorithms can be used for trains of these hybrid pulses (with, for instance, the delays and/or the relative amplitudes between the kicks, or even a delay between the HCP and laser pulses) and should require only a low number of hybrid pulses since the first step already brings the system very close to the target state.

This research was supported in part by the *Conseil Régional de Bourgogne* and the *Action Concertée Incitative Photonique* from the French Ministry of Research.

*Electronic address: ddaems@ulb.ac.be
†Electronic address: sguerin@u-bourgogne.fr

[1] H. Stapelfeldt and T. Seideman, Rev. Mod. Phys. **75**, 543 (2003).
[2] B. Friedrich and D. Herschbach, Phys. Rev. Lett. **74**, 4623 (1995).
[3] M. J. J. Vrakking and S. Stolte, Chem. Phys. Lett. **271**, 209 (1997).
[4] S. Guérin, L. P. Yatsenko, H. R. Jauslin, O. Faucher, and B. Lavorel, Phys. Rev. Lett. **88**, 233601 (2002).
[5] C. M. Dion, A. Keller, and O. Atabek, Eur. Phys. J. D **14**, 249 (2001).
[6] M. Machholm and N. E. Henriksen, Phys. Rev. Lett. **87**, 193001 (2001).
[7] L. Cai, J. Marango, and B. Friedrich, Phys. Rev. Lett. **86**, 775 (2001).
[8] H. Sakai, S. Minemoto, H. Nanjo, H. Tanji, and T. Suzuki, Phys. Rev. Lett. **90**, 083001 (2003).
[9] M. Leibscher, I. Sh. Averbukh, and H. Rabitz, Phys. Rev. Lett. **90**, 213001 (2003); Phys. Rev. A **69**, 013402 (2004).
[10] D. Sugny, A. Keller, O. Atabek, D. Daems, C. M. Dion, S. Guérin, and H. R. Jauslin, Phys. Rev. A **69**, 033402 (2004).
[11] J. Ortigoso, Phys. Rev. Lett. **93**, 073001 (2004).
[12] O. Atabek and C. M. Dion, in *Quantum Control: Mathematical and Numerical Challenges*, CRM Proceedings and Lecture Notes Vol. 33 (AMS, Providence, 2003), pp. 1–21.
[13] N. E. Henriksen, Chem. Phys. Lett. **312**, 196 (1999).
[14] V. Ramakrishna, M. V. Salapaka, M. Dahleh, H. Rabitz, and A. Peirce, Phys. Rev. A **51**, 960 (1995).
[15] H. Fu, S. G. Schirmer, and A. I. Solomon, J. Phys. A **34**, 1679 (2001).

Chapter 11

Selective control of rovibrational population transfer in molecules

Adiabatic passage for the rovibrational selective excitation is a promising method. However, except for light molecules such as H_2 or H_F, one cannot achieve this selective population transfer using picosecond chirped pulses, since the population is in general spread into a set of rotational states due to the nanosecond timescale of the rotational motion. It is difficult to construct an experimental setup to generate a direct chirping in a pulse of nanosecond duration, i.e. with a narrow spectrum.

In this paper [194], we show that postpulse rovibrational state selectivity of molecules can be achieved by picosecond chirped adiabatic passage if an additional adiabatic aligning nonresonant laser field is used.

PHYSICAL REVIEW A **71**, 013402 (2005)

State-selective chirped adiabatic passage on dynamically laser-aligned molecules

S. Thomas, S. Guérin,* and H. R. Jauslin
Laboratoire de Physique, UMR 5027 CNRS, Université de Bourgogne, BP 47870, 21078 Dijon, France
(Received 30 July 2002; published 3 January 2005)

We show that rovibrational state selectivity can be achieved by chirped adiabatic passage of molecules that are *adiabatically aligned* by a nonresonant laser field. We develop the tools to design the appropriate frequency and amplitude modulations that allow us to select a given route in the Hilbert space that leads to a final complete excitation of the chosen state, by infrared or by Raman processes. This method allows us to select a given vibrational state in a well-defined rotational J state.

DOI: 10.1103/PhysRevA.71.013402 PACS number(s): 42.50.Hz, 32.80.Bx, 32.80.Lg

I. INTRODUCTION

Selective excitation of the states of atoms and molecules by laser pulses is of considerable importance for the control of processes involving internal and external degrees of freedom [1,2].

A very promising method is the adiabatic passage by sweeping the laser frequency (chirping), which is robust with respect to variations of the field amplitude and frequency. This type of adiabatic passage can be induced by a one-photon infrared chirp [3] or by a Raman chirp [4]. The chirping technique is nowadays well developed in femto- and picosecond time scales (see, e.g., Ref. [5]). The vibrational excitation by adiabatic passage has been widely studied theoretically for models that do not include rotation (e.g., in Refs. [3], [4], [6], and [7]). It is well known that if one uses picosecond chirped pulses, the population is in general spread into a set of rotational states [8–10] due to the nanosecond time scale of the rotational motion. Only for very light molecules (such as H_2 and HF) this rotational time scale is of the order of picoseconds and the rovibrational selectivity can be achieved (see, for instance, Ref. [11], where nonrobust multiphoton π pulses on a picosecond time scale have been used and Ref. [12] for rotational branching in H_2 by Raman chirped adiabatic passage). A rotational model that includes the spontaneous Raman processes has recently been studied [13].

On the other hand, alignment of molecules in their ground vibronic state by laser-induced adiabatic transport along *the pendular dressed states* can be achieved in general during nanosecond time scales [14–17]. This approach needs a strong nonresonant linearly polarized laser field which couples the rotational states (of rotational constant B_0) of the ground vibronic state by two-photon Raman processes through its anisotropic polarizability $\Delta\alpha$. One considers the molecular population initially in the rotational state $|J=0\rangle$, with projection $M=0$ of the rotational angular momentum along the field axis (which is a constant of motion). This leads to an effective rigid rotor dressed by a double-well potential whose minima are in the directions of the field polarization. The wells are deeper and thinner for a stronger field. The eigenvectors of the dressed Hamiltonian are called *pendular states*. Their associated eigenenergies (labeled by a positive integer $\tilde{J}$) as a function of the field amplitude form curves that are continuously connected to the energies associated to the bare states $|J\rangle$. They form two families (even and odd $\tilde{J}$) of near-degenerate eigenvalues. The lowest ones are well localized in the wells and correspond thus to molecular alignment. When the laser field is turned on slowly with respect to the two-photon detuning $6B_0/\hbar$ between the states $|J=2\rangle$ and $|J=0\rangle$, i.e., when [15]

$$6B_0/\hbar \gg 1/T_a, \tag{1}$$

with T_a the duration of the aligning laser pulse, the dressed molecule is *adiabatically* carried along the pendular state $|\tilde{J}=0\rangle$.

In this paper, we show for a model including the vibration and rotation that we can selectively populate a given rovibrational state by chirped adiabatic passage while the molecule is dynamically aligned by an additional nanosecond laser. The mechanism we propose is as follows: The molecule is first adiabatically aligned by a nanosecond pulse. When this pulse is at its maximum, one uses picosecond chirped adiabatic passage to transfer the population to the excited pendular vibrational state, which is adiabatically reconnected to the desired vibrational state when the aligning nanosecond pulse falls down.

A classical-mechanical interpretation could lead to the idea that a well aligned molecule along a given axis would not be subjected to rotation and that the rotational structure could be consequently neglected from the model. We give below a precise quantum-mechanical formulation of this statement.

We develop a systematic procedure to design the appropriate pulse parameters (frequency and amplitude) to achieve the complete transfer to a given allowed rovibrational state. This procedure is based on the topology of the dressed energies as a function of the pulse parameters. It allows us to identify qualitatively the various adiabatic ways to achieve the transfer [18]. The adiabatic passage is quantitatively optimized with the use of specific time-dependent pulse parameters.

We first develop the tools of vibrational selectivity on a rotationless model before considering the complete rovibra-

*Electronic address: Stephane.Guerin@u-bourgogne.fr

tional problem. We illustrate the mechanisms on the example of CO molecules.

II. TOOLS FOR VIBRATIONAL SELECTIVITY BY ADIABATIC PASSAGE: ROTATIONLESS MODEL

In this section we apply the general tools reviewed in Ref. [18] for the vibrational selectivity by adiabatic passage induced by chirped laser fields in rotationless molecules. The rotational degree of freedom is considered in the next section. These tools are based on the adiabatic theorem which states that the dynamics follows approximately the instantaneous eigenvectors associated to eigenvalues continuously connected to the initial one when the Hamiltonian is perturbed sufficiently slowly. When this principle is extended to a quantum system (here a molecule) dressed by a laser field that is pulsed and whose frequency is swept, one has to consider the adiabatic transport, or the so-called adiabatic passage, along eigenvectors of the dressed system molecule + laser field (the so-called Floquet states) as functions of the envelope amplitude and of the instantaneous frequency of the field [6,7]. This leads to surfaces of associated eigenvalues (the so-called quasienergies) as functions of the two field parameters (amplitude and frequency). Inspection of the topology of the surfaces allows us (i) to analyze the various transfers that are permitted by adiabatic transport, and (ii) to design the appropriate laser parameters that will drive the dynamics to a desired state. This has been applied to atomic beam deflection [19], to population transfer in two- and three-level systems [20], and to the production of entangled states [21]. Paths that optimize the nonadiabatic losses have been identified in two-level systems: they correspond to level lines of the eigenenergy surfaces [22]. In this section we extend this study to multilevel systems and show the remarkable efficiency of the process along level lines.

Adiabatic passage is of great interest for state selectivity since it allows population transfers that are robust with respect to fluctuations of the field parameters and with respect to partial knowledge of the system, provided that resonant effects are taken into account. The key of robustness comes from the classification of topologically equivalent curves that connect the same states in the adiabatic limit. In order to study the surfaces of quasienergies, it is therefore generally sufficient to consider effective Hamiltonians that incorporate the resonances. We illustrate below these principles on a few vibrational states that are near-resonant with a chirped laser field.

A. Model

We consider a one-mode vibrational potential $V(x)$ (e.g., the ground electronic state of a diatomic molecule), associated to the vibrational coordinate x, giving the vibrational Hamiltonian

$$H_0(x) = T_{\mathrm{vib}}(\partial_x) + V(x), \tag{2}$$

with T_{vib} the vibrational kinetic energy. We denote by $|n\rangle$ the eigenvectors of $H_0(x)$ associated to the eigenenergies $\hbar\omega_n$. The vibrational mode is coupled to a field of the form $\mathcal{E}(t)\cos[\phi(t)+\theta]$ (where the carrier oscillations and the envelope parts are considered independently) through $\mu_0(x)$, the dipole moment in the ground electronic state of the molecule (permanent dipole moment, nonzero for heteropolar molecule):

$$H(x,t,\phi(t)+\theta) = H_0(x) - \mu_0(x)\mathcal{E}(t)\cos[\phi(t)+\theta], \tag{3}$$

with the amplitude $\mathcal{E}(t)=\mathcal{E}_0\sqrt{\Lambda(t)}$, and $\mathcal{E}_0$, $\Lambda(t)$, $\phi(t)$, respectively, the peak amplitude, the shape (ranging between 0 and 1) of the field intensity, the time-dependent phase, and θ an additional constant phase (that is used to apply conveniently the Floquet theory). We have here considered that the field is linearly polarized, with the polarization axis parallel to the dipole moment of the rotationless molecule. The instantaneous Floquet (or quasienergy) operator characterizing the molecular Hamiltonian dressed by the field reads

$$\begin{aligned} K &= -i\hbar\omega_{\mathrm{eff}}(t)\frac{\partial}{\partial\theta} + H(x,t,\theta) \\ &= -i\hbar\omega_{\mathrm{eff}}(t)\frac{\partial}{\partial\theta} + H_0(x) - \mu_0(x)\mathcal{E}(t)\cos\theta, \end{aligned} \tag{4}$$

where the effective (also called instantaneous) frequency coincides to the derivative of the phase

$$\omega_{\mathrm{eff}}(t) \equiv \frac{d\phi}{dt}(t). \tag{5}$$

The operator $-i\hbar\omega_{\mathrm{eff}}(t)\partial/\partial\theta$ in Eq. (4) characterizes the laser photon field operator in the sense that it can be derived from the photon number associated to a cavity-quantized field when the field is taken outside the cavity in the free space and contains a large average number of photons [23]. Its eigenvectors are denoted by $|k\rangle$ where k is a positive or negative integer that characterizes the relative number of photons with respect to its average. We remark that if we define a time-dependent frequency $\omega(t)$ as $\phi(t)\equiv\omega(t)t$, then the effective frequency reads $\omega_{\mathrm{eff}}(t)=\dot{\omega}(t)t+\omega(t)$, where $\dot{\omega}\equiv d\omega/dt$.

The quasienergy surfaces are formed by the eigenvalues of this Floquet Hamiltonian as functions of the parameters ω_{eff} and $\mathcal{E}$. They can be calculated (at least numerically) for any given potential $V(x)$. One can label the Floquet eigenvectors as $|n;k\rangle$, associated to the quasienergies $\lambda_{n,k}$ with the indices n and k, respectively, related to the free molecule $H_0(x)$ and to the photon field. The quasienergies can be arranged in zones of *quasidegenerate quasienergies*, associated to quasiresonance between the molecule and the field, that are periodic since we have $\lambda_{n,k+\ell}=\lambda_{n,k}+\ell\hbar\omega_{\mathrm{eff}}$ for any positive or negative integer ℓ. For simplicity, one considers the $N+1$ lowest bound states $\{|0\rangle,|1\rangle,\ldots,|N\rangle\}$, associated to the energies $E_0<E_1<\cdots<E_N$ of a Morse potential coupled by a field whose effective frequency is one-photon near-resonant: $\hbar\omega_{\mathrm{eff}}\approx E_1-E_0\approx E_2-E_1\approx\cdots\approx E_N-E_{N-1}$. The effective Hamiltonian in the resonant approximation, that takes into account the one-photon near resonances of one Floquet zone, reads as a tridiagonal matrix:

$$H_{\text{eff}} = \frac{\hbar}{2}\begin{bmatrix} 0 & \Omega_{0,1} & 0 & \cdots & 0 \\ \Omega_{0,1} & 2\Delta_1 & \Omega_{1,2} & \ddots & \vdots \\ 0 & \Omega_{1,2} & 2\Delta_2 & \ddots & 0 \\ \vdots & \ddots & \ddots & \ddots & \Omega_{N-1,N} \\ 0 & \cdots & 0 & \Omega_{N-1,N} & 2\Delta_N \end{bmatrix}, \quad (6)$$

with

$$\Delta_n := \frac{E_n - E_0}{\hbar} - n\omega_{\text{eff}} = n[\omega_0 + (n+1)a - \omega_{\text{eff}}], \quad (7)$$

the Rabi frequency (assumed real and positive without loss of generality)

$$\Omega_{i,j} = -\mathcal{E}(t)\langle i|\mu_0|j\rangle/\hbar, \quad (8)$$

the (constant) anharmonicity

$$a := [(\omega_{n+1} - \omega_n) - (\omega_n - \omega_{n-1})]/2\hbar = -\hbar\omega_0^2/4D, \quad (9)$$

with D the dissociation energy, and the frequency ω_0 related to the energy of the Morse potential: $E_n = \hbar\omega_0\left(n+\frac{1}{2}\right) + \hbar a\left(n+\frac{1}{2}\right)^2$, $n=0,\ldots,N$. This effective Hamiltonian is valid for moderate field intensities $\Omega_{i,j} \ll \omega_0$ (in practice not larger than 10^{13} W/cm^2 to avoid ionization), for small detunings and anharmonicity $|\Delta_n|$, $|a| \ll \omega_0$ and for N significantly smaller than the total number of bound states.

This Hamiltonian can be technically obtained in the Floquet picture as follows: We apply the unitary resonant transformation $R(\theta) \equiv \text{diag}[1, e^{-i\theta}, \ldots, e^{-i(N-1)\theta}]$ to the Floquet operator which allows to write the resonant terms as θ independent plus a nonresonant θ-dependent rest V_2:

$$R^\dagger(\theta)KR(\theta) = -i\hbar\omega_{\text{eff}}(t)\frac{\partial}{\partial\theta} + H_{\text{eff}} + V_2(\theta). \quad (10)$$

The resonant transformation $R(\theta)$ allows to dress the bare states $|0\rangle$ with 0 photon, $|1\rangle$ with minus one photon, $|n\rangle$ with minus n photons, and so on. The state corresponding to a bare state $|n\rangle$ dressed by k photons, when the field is off, reads $|n;k\rangle^{\mathcal{E}=0} = |n\rangle \otimes e^{ik\theta}$. The rest $V_2(\theta)$ contains terms, coupling the Floquet zones, that become of order $\mathcal{O}(\mathcal{E}^2)$ after the application of perturbation theory. Since they are perturbative, their highest-order effects can be incorporated as Stark shifts. However, in the range of intensities considered here, they can be neglected with respect to the coupling Rabi frequency in H_{eff} which is of order $\mathcal{O}(\mathcal{E})$.

B. Surfaces of quasienergy

Figure 1 displays the quasienergy surfaces $\lambda_{n,k}$ in units of $\hbar\omega_0$ connected to the three lowest vibrational states, as functions of the effective frequency ω_{eff} and the field amplitude $\mathcal{E}$ taken as independent parameters. We have chosen the CO molecule for which $a \simeq -6.033\times10^{-5}$ a.u. and $\omega_0 \simeq 0.009\,89$ a.u., using an *ab initio* dipole moment [24]. These surfaces show the different connectivities that are topologically allowed by adiabatic passage. The topology is determined by the resonances characterized by the crossings (labeled as A, B, and A_2) of the curves at $\mathcal{E}=0$ [corresponding to the crossings of the diagonal elements of Eq. (6)].

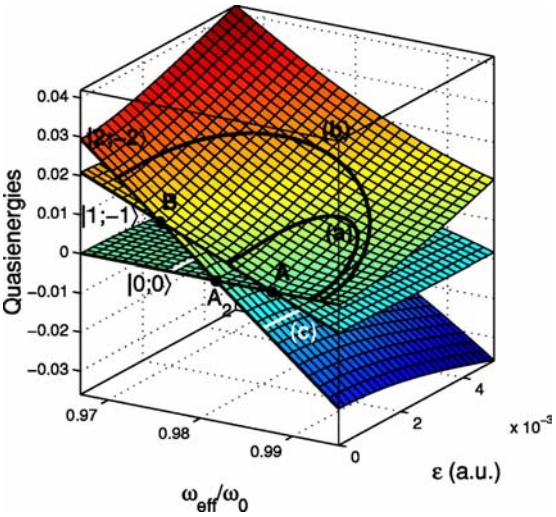

FIG. 1. (Color online) The first three quasienergy surfaces (in units of $\hbar\omega_0$), eigenvalues of H_{eff} (6), as functions of the effective frequency (normalized by ω_0) and the field amplitude $\mathcal{E}$ (in atomic units, with the correspondence amplitude-intensity $\mathcal{E}=5\times10^{-3}$ a.u. $\leftrightarrow I \approx 0.877$ TW/cm^2) calculated from the Hamiltonian (6) for the CO molecule. Paths (a) and (b) correspond to a transition from the state $|0\rangle$ to the states $|1\rangle$ and $|2\rangle$ with absorption of one and two photons, respectively, for decreasing frequency chirp. Path (c) corresponds to a transition from the state $|0\rangle$ to the state $|2\rangle$ with absorption of two photons for increasing frequency chirp.

Intersection A is determined by the crossing between the first and second diagonal elements which occurs at $\omega_{\text{eff}}^{(\text{A})} = \omega_0 + 2a$, intersection B by the crossing between the second and third diagonal elements: $\omega_{\text{eff}}^{(\text{B})} = \omega_0 + 4a$, and intersection A_2 by the crossing between the first and third diagonal elements: $\omega_{\text{eff}}^{(\text{A}_2)} = \omega_0 + 3a$. Thus the crossings A, B, and A_2 characterize, respectively, a one-photon resonance between the bare states $|0\rangle$ and $|1\rangle$, a one-photon resonance between $|1\rangle$ and $|2\rangle$, and a two-photon resonance between $|0\rangle$ and $|2\rangle$. For $\mathcal{E} \neq 0$, the crossings become avoided crossings. The labels $|0;0\rangle$, $|1;-1\rangle$, $|2;-2\rangle$ of Fig. 1 stand for the straight lines in the plane $\mathcal{E}=0$. The slope of these lines labeled by $|n;k\rangle$ corresponds to the relative number of photons: $\partial\lambda_{n,k}/\partial\omega_{\text{eff}}|_{\mathcal{E}=0}/\hbar = k$. Three topologically inequivalent paths are shown in Fig. 1 and give an insight into the state selectivity in this model. Path (a), going around crossing A, allows the population transfer from state $|0;0\rangle$ to $|1;-1\rangle$, i.e., the population transfer from the bare state $|0\rangle$ to $|1\rangle$ with absorption of one photon. Both paths (b) and (c) allow the population transfer from state $|0;0\rangle$ to $|2;-2\rangle$, i.e., the population transfer from the bare state $|0\rangle$ to $|2\rangle$ with absorption of two photons. Since path (b) goes around A and B, it can be described as a succession of two sequential one-photon processes. Since path (3) goes around A_2, it corresponds to a direct two-photon process.

C. Optimization of population transfer using level lines

In addition to the topology, the success of adiabatic passage requires to find parameters that induce negligible nona-

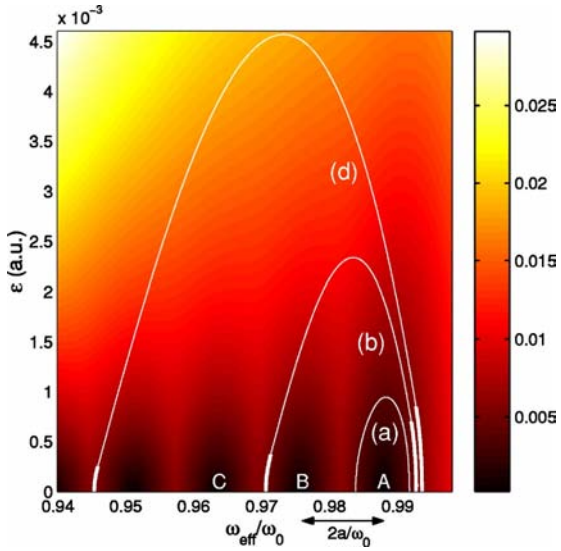

FIG. 2. (Color online) Contour plot of the distance between the upper closest neighbor surfaces of Fig. 1 as a function of the normalized effective frequency and the field amplitude $\mathcal{E}$. Paths (a) and (b) correspond to the ones of Fig. 1.

diabatic losses. The representation of the surfaces as contour plots of level lines allows to guide this search.

1. Sequential one-photon processes

Figure 2 shows the contour plot of the distance between the upper closest neighbor surfaces. Note that we have taken into account in this figure six states and six surfaces. The consecutive one-photon resonances at zero field corresponding to crossings appear in dark zones (one recovers intersections A and B). The crossings are separated at $2a/\omega_0$ in this diagram. For $\mathcal{E}=0$, the line at the right of intersection A corresponds to state $|0;0\rangle$; the segment between A and B corresponds to state $|1;-1\rangle$; the segment between B and C to state $|2;-2\rangle$ and so on for states $|n;-n\rangle$.

Optimal adiabatic passage which gives the minimal nonadiabatic loss for a given peak intensity and a smooth symmetric pulse shape has been shown to follow a level line for two-level systems [22]. This corresponds to parallel quasienergies at all times. This can be applied for population transfer from $|0\rangle$ and $|1\rangle$, using a level line that connects these two states. In this case, the only remaining parameter in the contour diagram is the detuning at the beginning of the process at time t_i: $\Delta_i \equiv \Delta_1(t=t_i)$. The additional condition that guarantees a negligible nonadiabatic loss can be expressed as

$$|\Delta_i| T \gg 1, \tag{11}$$

where T is the characteristic duration of the pulse shape (that is given and assumed to be symmetric for simplicity). For a Gaussian pulse, T can be taken as the full width at half maximum, and it has been shown in Ref. [22] that the condition (11) is more precisely $|\Delta_i| T \gg \sqrt{\ln 2}/2 \approx 0.42$ in this case. Figure 3 displays numerical simulations for a Gaussian pulse, which shows very efficient and monotonic population transfer already for $\Delta_i T = -2.7$.

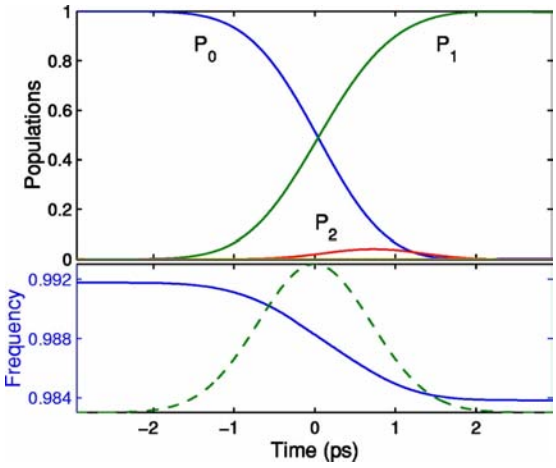

FIG. 3. (Color online) Numerical simulation of the probabilities $P_n = |\langle n|1\rangle|^2$ (upper frame) of the dynamics associated to the path (a) of Figs. 1 and 2 for a Gaussian intensity pulse shape $\Lambda(t) = e^{-4 \ln 2 (t/T)^2}$ (lower frame, dashed line) with $\Delta_i T \approx -2.7$, of peak intensity $I \approx 3.1 \times 10^{10}$ W/cm^2, and the associated effective frequency (lower frame, full line, in units of ω_0).

Population transfer from $|0\rangle$ to states $|N>1\rangle$ cannot be achieved by the following of a single level line with a single pulse by the use of the contour of Fig. 2. One has to connect two pieces of level lines, one connecting the initial state, the other one connecting the final desired state. If the goal is to reach the state $|N\rangle$, one can choose as above $\Delta_i \equiv \Delta_1(t=t_i)$ such that $|\Delta_i| T \gg 1$ and $\Delta_f \equiv \Delta_N(t=t_f)$ at the final time t_f. One has to choose the way in which we leave and reach the level lines and a peak Rabi frequency. One can choose $\Delta_f = \Delta_i$. Adiabatic arguments impose to leave and reach the level lines as slowly as possible, which implies a peak Rabi frequency $\Omega_{\max} = \max_{n \leq N, t} \Omega_{n-1,n}(t)$ such that $\Omega_{\max} > |\Delta_i|$. Figures 4 and 5 show numerics of population transfer to, respectively, the states $|2\rangle$ and $|4\rangle$. The success of the transfer requires a peak Rabi frequency larger than the one used for

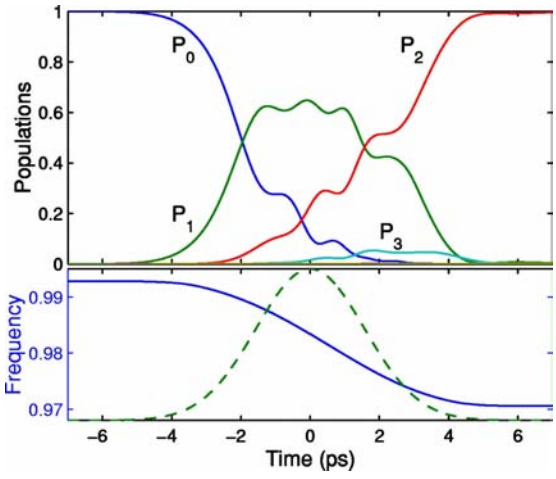

FIG. 4. (Color online) Same as Fig. 3 but with the dynamics associated to the path (b) of Figs. 1 and 2 with $\Delta_i T \approx -7.5$ and the peak intensity $I \approx 0.17 \times 10^{12}$ W/cm^2.

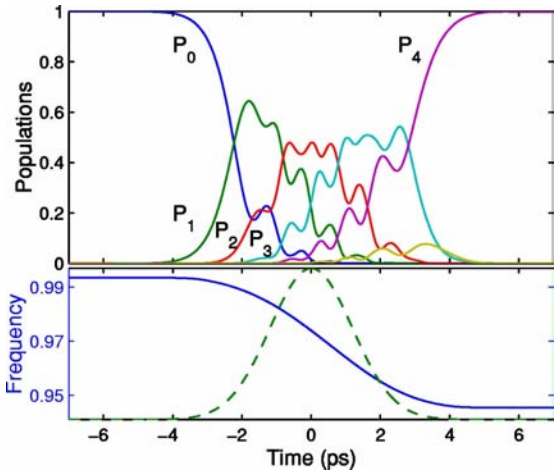

FIG. 5. (Color online) Same as Fig. 3 but with the dynamics associated to the path (d) of Fig. 2 with $\Delta_i T \approx -6.6$ and the peak intensity $I \approx 0.75 \times 10^{12}$ W/cm^2.

the single level line for the transfer to state $|1\rangle$. One notices that all the chirps designed for sequential one-photon processes with a Gaussian envelope have roughly the shape of a hyperbolic tangent curve.

2. Direct multiphoton processes

Figure 1 shows that the path (c) corresponds to a direct two-photon process between the states $|0\rangle$ and $|2\rangle$, in the sense that it goes around the conical intersection A_2, the crossing between the first and third diagonal elements of the effective Hamiltonian (6). Figure 6 shows the contour plot of the distance between the two lowest surfaces of Fig. 1 around crossing A_2. One can see that level lines now connect

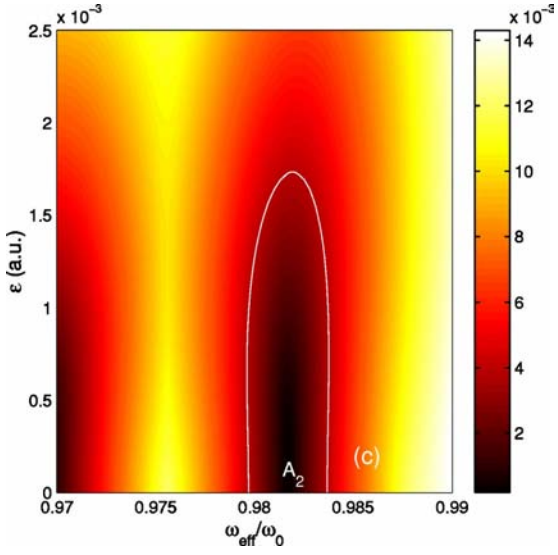

FIG. 6. (Color online) Contour plot of the distance between the lower closest neighbor surfaces of Fig. 1 as a function of the normalized effective frequency and the field amplitude $\mathcal{E}_0$. The paths (c) refer to the ones of Fig. 1.

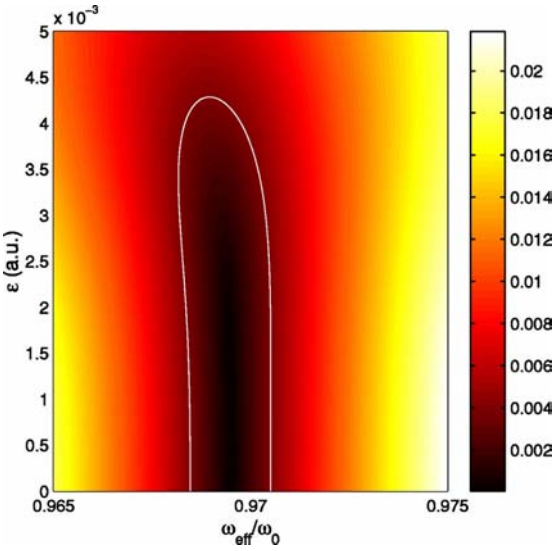

FIG. 7. (Color online) Contour plot of the distance between the two lower closest surfaces, connected to states $|1\rangle$ and $|5\rangle$ at zero field, as a function of the normalized effective frequency and the field amplitude $\mathcal{E}_0$. The white path is an example of a four-photon dynamics.

the states $|0\rangle$ and $|2\rangle$. One remarks that these level lines are slightly *bent*, due to the Stark shifts associated to this direct multiphoton process. Figure 7 shows the contour plot of the distance between the two lower closest surfaces, connected to states $|0\rangle$ and $|4\rangle$ at zero field, corresponding to a four-photon process between these states. The level lines are more bent for this high-order multiphoton process.

Figures 8 and 9 show numerics for population transfer to, respectively, states $|2\rangle$ and $|4\rangle$ by direct multiphoton adiabatic passage. One can see that the population transfer is monotonic unlike their counterparts obtained by sequential one-photon processes. It is more efficient in the sense that smaller duration and field amplitude is required to allow the

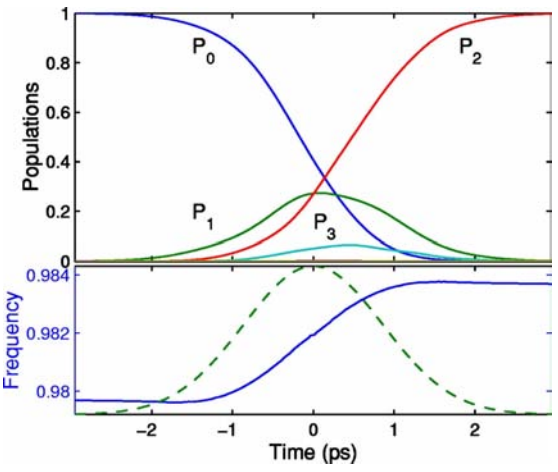

FIG. 8. (Color online) Same as Fig. 3 but with the dynamics associated to the path (c) of Figs. 1 and 6 with $\Delta_i T \approx 3.3$ and the peak intensity $I \approx 0.11 \times 10^{12}$ W/cm^2.

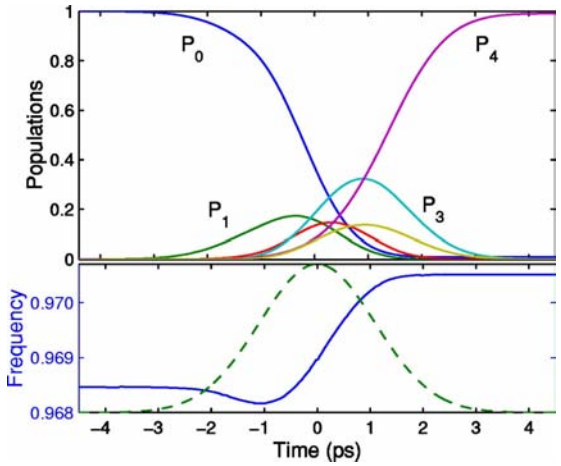

FIG. 9. (Color online) Same as Fig. 3 but with the dynamics associated to the path of Fig. 7 with $\Delta_i T \approx 4.2$ and the peak intensity $I \approx 0.64 \times 10^{12}$ W/cm^2.

transfer by adiabatic passage. This multiphoton process, however, requires in general a nonmonotonic chirp to follow the level line. We remark that numerical calculations for this multiphoton process include second order Stark shifts given by the diagonal (parallel) polarizability [see the diagonal of the Hamiltonian (14)]. The difference of the resulting calculations with and without this Stark effect is nonsignificant (less than 1%). This justifies to use here only the dominant one-photon resonant terms in the Hamiltonian (6).

The two different paths corresponding to the sequential process with twice one-photon and the direct two-photon process have been identified and experimentally tested between electronic atomic states in Ref. [25].

D. Adiabatic passage by Raman chirping

We now investigate the selectivity of adiabatic passage by Raman chirping [4] using the topology tools. We assume that the frequencies of the pump and Stokes pulses of the Raman transitions are far detuned (low frequency) from any excited electronic states and also far detuned from any excited vibrational states. The Hamiltonian that has to be considered reads in this case (with both frequencies chirped)

$$H(x,t,\phi_P(t)+\theta_P,\phi_S(t)+\theta_S) = H_0(x) - \mu_0(x)\mathcal{E} - \frac{\alpha_\parallel(x)}{2}\mathcal{E}^2, \tag{12}$$

with $\alpha_\parallel(x)$ the polarizability parallel to the molecular axis, and the field decomposed in the pump (index P) and Stokes (index S) fields, of time-dependent phase, peak amplitude, and intensity pulse-shape, respectively, $\phi_j(t)$, $\mathcal{E}_{0j}$ and $\Lambda_j(t)$, $j=P,S$:

$$\mathcal{E} := \mathcal{E}_P(t)\cos[\phi_P(t)+\theta_P] + \mathcal{E}_S(t)\cos[\phi_S(t)+\theta_S], \tag{13}$$

$\mathcal{E}_P(t)=\mathcal{E}_{0P}\sqrt{\Lambda_P(t)}$, $\mathcal{E}_S(t)=\mathcal{E}_{0S}\sqrt{\Lambda_S(t)}$. The additional constant phases θ_P and θ_P allow a convenient formulation of the two-mode Floquet theory (see below). The effective Hamiltonian, that takes into account the Raman two-photon near resonances of one Floquet zone in the ground electronic state, is again a tridiagonal matrix:

$$H_{\text{eff}} = \hbar \begin{bmatrix} S_0 & \Omega_{0,1} & 0 & \cdots & 0 \\ \Omega_{0,1} & \Delta_1 + S_1 & \Omega_{1,2} & \ddots & \vdots \\ 0 & \Omega_{1,2} & \Delta_2 + S_2 & \ddots & 0 \\ \vdots & \ddots & \ddots & \ddots & \Omega_{N-1,N} \\ 0 & \cdots & 0 & \Omega_{N-1,N} & \Delta_N + S_N \end{bmatrix} \tag{14}$$

with in this case

$$\Delta_n := \frac{E_0 - E_n}{\hbar} + n\omega_{\text{eff}} = -n[\omega_0 + (n+1)a - \omega_{\text{eff}}], \tag{15}$$

the effective frequency

$$\omega_{\text{eff}}(t) \equiv \frac{d\phi_P}{dt}(t) - \frac{d\phi_S}{dt}(t), \tag{16}$$

the Rabi frequency

$$\Omega_{i,j} = -\mathcal{E}_P(t)\mathcal{E}_S(t)\langle i|\alpha_\parallel|j\rangle/\hbar, \tag{17}$$

and the relative Stark shifts

$$S_i = -[\mathcal{E}_P^2(t) + \mathcal{E}_S^2(t)]\langle i|\alpha_\parallel|i\rangle/\hbar. \tag{18}$$

It is a good approximation to use the static polarizabilities instead of the dynamical ones when the frequencies are far red detuned from any excited electronic states (i.e., low frequencies with respect to the electronic states).

We obtain technically this effective Hamiltonian starting with the two-mode Floquet Born-Oppenheimer Hamiltonian,

$$K = -i\hbar\phi_P(t)\frac{\partial}{\partial\theta_P} - i\hbar\phi_S(t)\frac{\partial}{\partial\theta_S} + H(x,t,\theta_P,\theta_S), \tag{19}$$

which itself results from a static perturbation theory of the full field+molecule (whose axis is assumed parallel to the field polarization) with respect to the electronic coordinates, in the Born-Oppenheimer approximation, up to the second order in field amplitude [18]. We take into account the contribution of the excited electronic states through the parallel polarizability $\alpha_\parallel(x)$ by applying the unitary resonant transformation $R := \text{diag}[1, e^{i(\theta_S-\theta_P)}, \ldots, e^{i(N-1)(\theta_S-\theta_P)}]$, which allows us to write

$$R^\dagger K R = -i\hbar\phi_P\frac{\partial}{\partial\theta_P} - i\hbar\phi_S\frac{\partial}{\partial\theta_S} + H_{\text{eff}} + O(\mathcal{E}_{P,S}^3). \tag{20}$$

In this Raman process with the use of frequencies far blue detuned between vibrational states (e.g., with visible light), the vibrational contribution to the Stark shifts and to the coupling is generally negligible compared to the electronic contribution. The resulting effective Hamiltonian (14) does not depend on the values of the field frequencies as a first approximation.

The tools presented in the preceding subsections can be applied for the selectivity by Raman chirping. The results will be very similar both for sequential Raman two-photon

processes as for direct higher multiphoton processes (such as four,six,… photon processes), since the effective Hamiltonian (14) has the same form as Eq. (6) apart from additional non-negligible Stark shifts, that will bend the level lines of the contour plots of differences of quasienergy surfaces. This will lead in general to a nonmonotonic chirping for efficient following of level lines.

III. ROVIBRATIONAL SELECTIVITY BY ADIABATIC PASSAGE OF AN ADIABATICALLY ALIGNED MOLECULE

In this section we consider the complete rovibrational molecule, and the state selectivity when the molecule is adiabatically aligned. More precisely, we first adiabatically align the molecule with a nonresonant linear polarized nanosecond pulse, apply next a picosecond chirped field that will transfer the population among the resulting dressed vibrational pendular states, and finally switch off the aligning laser adiabatically to reconnect the bare rovibrational states. We first analyze the selection rules of the vibrational pendular states, show the different possibilities of climbing, and construct the Hamiltonian of the model. We next present the state selectivity scenario by one-photon infrared and Raman chirpings.

A. Conditions of selectivity

One considers that the rovibrational structure of the molecule is made as a first approximation of uncoupled rigid rotors (of respective rotational constants B_v), one for each vibrational state $v=0,1,\ldots$. The effective Hamiltonian associated to an isolated vibration v of the molecule dressed by a nonresonant aligning laser of amplitude $\mathcal{E}_a$ reads in the high-frequency limit (with respect to the rotational structure) [14,26]

$$H_{vv}^{\mathrm{nr}} = B_v J^2 + \mathcal{E}_a^2(\Delta\alpha_{vv}\sin^2\Theta - \alpha_{\|,vv})/4, \tag{21}$$

with Θ the polar angle between the molecular axis and the direction of the nonresonant field, $\Delta\alpha_{v'v}=\alpha_{\|,v'v}-\alpha_{\perp,v'v}$, $\alpha_{\perp,v'v}=\langle v'|\alpha_\perp|v\rangle$, $\alpha_{\|,v'v}=\langle v'|\alpha_\||v\rangle$. J is the angular momentum. It consists then of *an effective double well potential for each vibrational state*. The central point is that for an ideally strong aligning field, the pendular eigenenergies of each effective double well potential have a structure of two families labeled by even and odd J, of *doubly near-degenerate pendular ladders* of *large* spacing $E_{v,\tilde{J}+2}-E_{v,\tilde{J}}\sim 2\,(\mathcal{E}_a\sqrt{\Delta\alpha B_v}-B_v\tilde{J})$ [14], which become approximately harmonic $\hbar\omega_v^{(\mathrm{rot-alig})}\sim 2\mathcal{E}_a\sqrt{\Delta\alpha B_v}$ for large amplitude $\mathcal{E}_a$ and low $\tilde{J}$. This is shown in Fig. 10 which displays the pendular energies as a function of the dimensionless quantity characterizing the alignment efficiency

$$\gamma_a = \mathcal{E}_a^2\Delta\alpha_{00}/4B_0. \tag{22}$$

As expected, we can observe for increasing γ_a the states $|\tilde{J}=2k\rangle$ and $|\tilde{J}=2k+1\rangle$, $k=0,1,2,\ldots$, becoming near degenerate by pairs and the formation of an harmonic ladder for the lowest $\tilde{J}$ of increasing spacing.

If one considers infrared one-photon dipolar transitions (for heteronuclear molecules), the selection rules are $\Delta\tilde{J}=\pm1,\pm3,\pm5,\ldots$ [14] with $\Delta v=\pm1$ (if one assumes $B_{v+1}\approx B_v$). For a picosecond chirping applied while the molecule is dynamically aligned, in the ideal situation of a very efficient alignment with infinite spacings $\hbar\omega_v^{(\mathrm{rot-alig})}$, the climbing of the vibrational ladder would occur following the sequence with alternating $\tilde{J}=0$ and $\tilde{J}=1$. We would obtain the following sequence, considering the states at the end of the pulses: $|v=0,J=0\rangle\rightarrow|v=1,J=1\rangle\rightarrow|v=2,J=0\rangle\rightarrow|v=3,J=1\rangle\rightarrow\ldots$, which is the one one would obtain in the rotationless model. The same arguments can be applied for a Raman chirping, with selection rules $\Delta\tilde{J}=0,\pm2,\pm4,\ldots$ and $\Delta v=0,\pm1$, which gives for $\Delta v=\pm1$ the climbing sequence with the same $\tilde{J}$: $|v=0,J=0\rangle\rightarrow|v=1,J=0\rangle\rightarrow|v=2,J=0\rangle\rightarrow\ldots$.

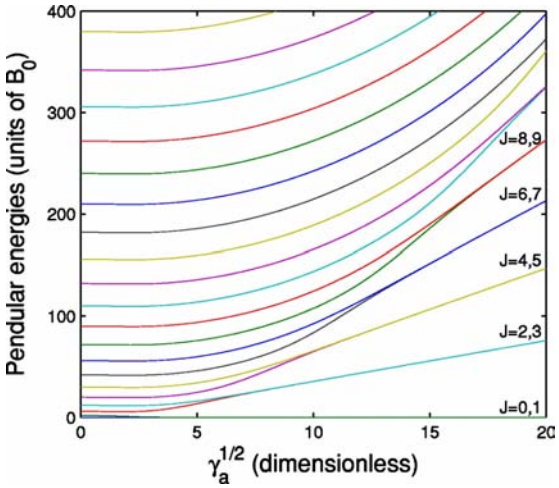

FIG. 10. (Color online) First lowest pendular energies $E_{\tilde{J}}-E_{\tilde{J}=0}$ of the ground vibronic state as functions of $\sqrt{\gamma_a}$ for a nonresonant field. The values of J indicate the connection of the lines when $\gamma_a=0$.

However, the study of a concrete situation requires an aligning nanosecond laser pulse of peak intensity not larger than 10^{13} W/cm^2 to avoid ionization. This peak intensity gives an upper limit for the spacing $\hbar\omega_0^{(\mathrm{rot-alig})}$ of the pendular double harmonic ladder, that has to be characterized. Achieving the rovibrational climbing requires to prevent the rotational spreading, which is possible when the field amplitude satisfies

$$2\mathcal{E}_a\sqrt{\Delta\alpha B_0}/\hbar \gg 1/T_c, \tag{23}$$

where T_c is the pulse duration of the chirped picosecond pulse (the full width half maximum for Gaussian pulses). For instance, for CO, we have $2\sqrt{\Delta\alpha B_0}/\hbar\approx 0.011$ a.u., which already requires $I_a\sim 10^{13}$ W/cm^2 for the intensity of the aligning field to satisfy the condition (23) with $T_c\sim 1$ ps. This condition has to be compared with the intrinsic condition [see Eq. (1)]

$$6B_0/\hbar \gg 1/T_c \tag{24}$$

required to avoid the rotational spreading in absence of aligning laser, which can be satisfied only for very light molecules in the picosecond regime of chirping [12]. The align-

ment can be well quantified by the observable $\langle\cos^2\Theta\rangle$, which reads in the strong-field limit [14]

$$\langle\cos^2\Theta\rangle \to 1 - 1/\sqrt{\gamma_a}. \tag{25}$$

This shows that satisfying the condition (23) will lead to a well aligned molecule $\langle\cos^2\Theta\rangle \sim 0.9$ for a typical rotational constant $B_0 \sim 1$ cm^{-1} of linear molecules (we have for CO: $B_0 \approx 1.92$ cm^{-1}) and $T_c \sim 1$ ps. The use of a rotationless model with $\Theta = 0$ would be in this case a quite good approximation to study the vibrational climbing.

We use in the following a complete model for vibration and rotation to show the feasibility of the state selectivity of an aligned molecule. Four particular strategies can be implemented with such a model: (i) a one-photon chirped infrared scheme with an additional aligning nanosecond laser allowing to climb the vibrational ladder and to end in the isotropic state $J=0$ (for even v) or in $J=1$ (for odd v) at the end of the pulses: $|v=0,J=0\rangle \to |v=1,J=1\rangle \to |v=2,J=0\rangle \to |v=3,J=1\rangle \to |v=4,J=0\rangle \to \cdots$, and (ii) a chirped Raman scheme, with one of the two lasers acting also as the aligning nanosecond laser, allowing us to follow the particular sequences $|v=0,J=0\rangle \to |v=0 \text{ or } 1, J=0 \text{ or } 2\rangle \to |v=0 \text{ or } 2, J=0,2 \text{ or } 4\rangle \to |v=3,J=0,2,\ldots \text{or } 6\rangle \to |v=4,J=0,2,\ldots \text{or } 8\rangle \to \cdots$, i.e., at the end of the pulses (a) to climb the rotational ladder in the same v, (b) to climb the vibrational ladder and to end up in $J=0$, or (c) to climb the vibrational and rotational ladders.

B. Model

The molecule is subjected to an aligning nonresonant field $\varepsilon_a(t)\cos(\omega_a t+\theta_a)$, of fixed carrier frequency ω_a and amplitude $\varepsilon_a(t)=\varepsilon_{0a}\sqrt{\Lambda_a(t)}$, and to a chirped field $\mathcal{E}_c(t)\cos(\phi_c(t)+\theta_c)$, of time-dependent phase $\phi_c(t)$ and amplitude $\mathcal{E}_c(t)=\mathcal{E}_{0c}\sqrt{\Lambda_c(t)}$. The peak amplitudes and the envelopes (taken as Gaussian) for the aligning and chirped fields are respectively denoted $\mathcal{E}_{0a}$, $\Lambda_a(t)$, $\mathcal{E}_{0c}$, $\Lambda_c(t)$. To construct the effective dressed Hamiltonian for the nonresonant aligning field, we will apply a high-frequency contact transformation [18,26] to the Born-Oppenheimer Floquet Hamiltonian,

$$\begin{aligned} K = &- i\hbar\omega_a\frac{\partial}{\partial\theta_a} - i\hbar\phi_c(t)\frac{\partial}{\partial\theta_c} + H_0(x,\Theta,\varphi) \\ &- \mu_0(x)[\mathcal{E}_a(t)\cos\theta_a + \mathcal{E}_c(t)\cos\theta_c]\cos\Theta \\ &+ [\Delta\alpha(x)\sin^2\Theta - \alpha_\parallel(x)]/2 \\ &\times [\mathcal{E}_a(t)\cos\theta_a + \mathcal{E}_c(t)\cos\theta_c]^2, \end{aligned} \tag{26}$$

where

$$H_0(x,\Theta,\varphi) := T_{\text{vib}}(\partial_x) + B(x)T_{\text{rot}}(\Theta,\partial_\Theta,\partial_\varphi) + V(x), \tag{27}$$

with Θ the polar angle between the molecular axis and the direction of the linear polarized fields (in the same direction), φ the azimuthal angle, T_{rot} the rotational kinetic energy, B the rotational constant, and $\Delta\alpha=\alpha_\parallel-\alpha_\perp$. $\alpha_\parallel$ and $\alpha_\perp$ are the static polarizabilities, respectively, parallel and perpendicular to the molecular axis (since we consider low frequencies with respect to the electronic states). We will consider $M=0$, which is invariant for linear polarized fields. We will next use the one-photon resonant approximation for the infrared chirp and the two-photon resonant approximation for the Raman chirp [18]. The effective Hamiltonian between vibrational blocks $H_{v'v}=\langle v'|H|v\rangle$, of energy $\hbar\omega_v$ and of rotational constant $B_v=\langle v|B|v\rangle$, reads thus [18,27]

$$H_{vv} = B_v J^2 + a_{vv}(\mathcal{E}_a^2+\mathcal{E}_c^2) + \hbar\Delta_v(t), \tag{28a}$$

$$H_{v'\neq v} = -\hbar\Omega_{v'v}(t)/2, \tag{28b}$$

with (terms of second order in $1/\hbar\omega$ have been neglected)

$$a_{v'v} = (\Delta\alpha_{v'v}\sin^2\Theta - \alpha_{\parallel,v'v})/4, \tag{29}$$

where we have denoted $\mu_{0,v'v}=\langle v'|\mu_0|v\rangle$. The Stark shifts $a_{vv}(\mathcal{E}_a^2+\mathcal{E}_c^2)$ allow the alignment of the molecule. The quantities $\mu_{0,v'v}$, $\alpha_{\perp,v'v}$, and $\alpha_{\parallel,v'v}$ have been calculated for the CO molecule from the *ab initio* calculations of Ref. [24]. For the one-photon infrared chirp, the Rabi frequencies read

$$\Omega_{v'v}(t) = \mu_{0,v'v}\mathcal{E}_c(t)\cos\Theta/\hbar, \tag{30}$$

and the detunings are $\Delta_v=\omega_v-\omega_0-vd\phi_c/dt=v[\omega_0+(v+1)a-d\phi_c/dt]$ [see Eq. (7)]. For the Raman process, one has

$$\Omega_{v'v}(t) = 2\mathcal{E}_a\mathcal{E}_c a_{v'v}/\hbar, \tag{31}$$

and $\Delta_v=\omega_0-\omega_v+v(w_a-d\phi_c/dt)=-v[\omega_0+(v+1)a-(\omega_a-d\phi_c/dt)]$ [see Eq. (15)].

C. State selectivity by infrared chirping

Considering that the molecule is aligned, we can study the transfer by chirped adiabatic passage between the pendular vibrational states. This is done using the tools described in the preceding section: We consider the surfaces of the stationary dressed energies (of the aligned molecule) as a function of the two parameters: intensity and effective frequency of the chirped laser, and construct in this diagram the path connecting the initial state with the given final one (if the connection exists). This is well visualized using contour plots of differences of some surfaces. We show in Fig. 11, for the CO molecule, the contour plot of the difference of the closest neighboring surfaces, connected to $|v=0,\tilde{J}=0\rangle$, $|v=1,\tilde{J}=1\rangle$, $|v=2,\tilde{J}=0\rangle$, …, $|v=6,\tilde{J}=0\rangle$, $|v=7,\tilde{J}=1\rangle$ when the chirped field is off: $\mathcal{E}_c=0$. We can construct an appropriate path connecting the initial state $|v=0,J=0\rangle$ to a final chosen path. A path (a), as a level line, is shown to go from the vibrational pendular state $|v=0,\tilde{J}=0\rangle$ to $|v=1,\tilde{J}=1\rangle$. This path has been shown to be optimal, in the sense that the nonadiabatic losses are minimized on a level line. To achieve adiabatic passage we have to use a level line satisfying

$$\Delta_1 T_c \gg 1. \tag{32}$$

The appropriate time-dependent chirp is designed from the chosen path in the parameter space and the given pulse envelope.

The path (b) of Fig. 11 connects $|v=0,\tilde{J}=0\rangle$ to $|v=6,\tilde{J}=0\rangle$, which is the final state chosen here. We use a Gaussian

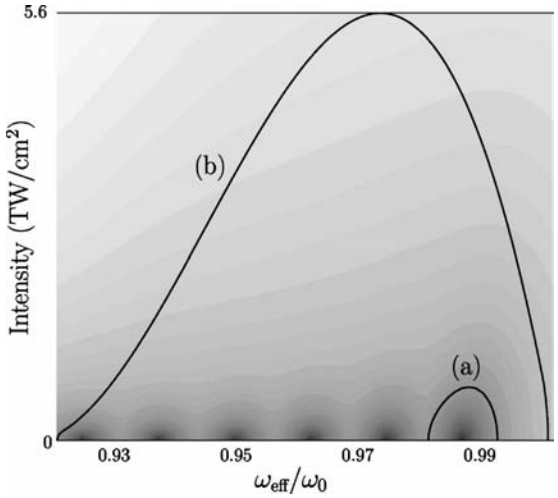

FIG. 11. Contour plot of the difference of the neighboring infrared-laser dressed energy surfaces of the aligned molecule for $\gamma_a=24$ (corresponding to the peak intensity $I_{0a}\approx 8$ TW/cm^2 for CO molecules and giving $\langle\cos^2\Theta\rangle\approx 0.79$). Darker zones characterize closer surfaces. Two appropriate paths connecting $|v=0,\tilde{J}=0\rangle$ with, respectively, (a) $|v=1,\tilde{J}=1\rangle$ and (b) $|v=6,\tilde{J}=0\rangle$ are shown.

intensity envelope of full width at half maximum $T_c\approx 4$ ps. We start at the detuning $\Delta_i=1.6\times10^{-4}$ a.u. and end at $\Delta_f=2.1\times10^{-3}$ a.u. The chirp designed from path (b) with the Gaussian envelope has roughly the shape of a hyperbolic tangent curve (see Sec. II C 1, Figs. 3–5). Figure 12 displays the population history with the complete laser sequence: the nanosecond laser (with a Gaussian intensity envelope of full width at half maximum $T_a\approx 0.4$ ns) is first switched on; while it is at its maximum, the chirping laser with the parameters determined above from path (b) is applied and induces transitions among the pendular vibrational states; finally the nanosecond laser is switched off to reconnect the pendular states to the rotational states. The almost complete transfer from $|v=0,J=0\rangle$ to $|v=6,J=0\rangle$ occurs. The figure shows the projections of the time-dependent state on the molecular bare states. This corresponds to a monotonic adiabatic transfer between the two vibrational pendular states involved in the process.

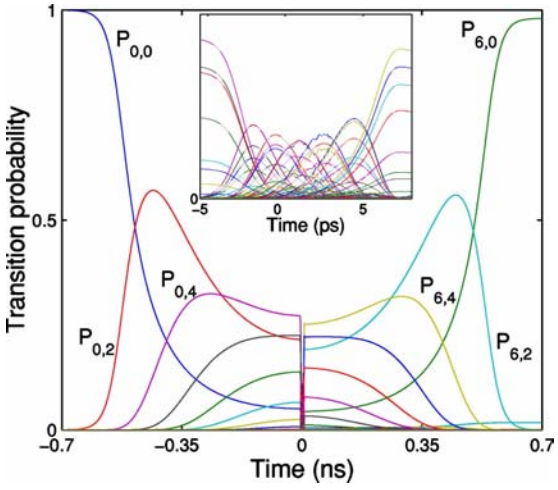

FIG. 12. (Color online) Population history with the peak intensity $I_{0c}=5.6$ TW/cm^2 and the chirp designed from the path (b) of Fig. 11: the curves represent the projections $P_{v,J}=|\langle v,J|\psi(t)\rangle|^2$ of the state $\psi(t)$, solution of the time-dependent Schrödinger equation, on the bare molecular states $|v,J\rangle$. The inset displays details of the population history during the picosecond time scale of the chirped laser.

We remark that the process allowing adiabatic passage from $|v=0,J=0\rangle$ to $|v=1,J=1\rangle$ (not shown) leads to a final non-negligible permanent alignment of the molecule with a value of $\langle\cos^2\theta\rangle=0.6$. Adiabatic passage to higher v and J leads to smaller $\langle\cos^2\theta\rangle$ values ($\gtrsim 0.5$).

It is important to note that climbing the rotational ladder while climbing the vibrational one, following the sequence $|v=0,\tilde{J}=0\rangle$, $|v=1,\tilde{J}=3\rangle$, $|v=2,\tilde{J}=4\rangle$, $|v=3,\tilde{J}=7\rangle$, …, i.e., with alternating $\Delta\tilde{J}=1$ and $\Delta\tilde{J}=3$, is theoretically possible but would require a specific nonmonotonic large chirp for this highly anharmonic sequence of $\tilde{J}$.

We remark that we could have also used a multiphoton chirp instead of sequential one-photon steps, but with a nonmonotonic chirp, as explained in the preceding section for the rotationless model.

D. State selectivity by Raman chirping

The state selective transfer can also be implemented using a Raman process: one of the lasers of the Raman process, of fixed frequency, aligns the molecule and the second laser is chirped to produce the adiabatic passage. We have tested this scheme numerically, choosing a path in parameter space that connects $|v=0,\tilde{J}=0\rangle$ to $|v=6,\tilde{J}=0\rangle$. We have also obtained in this case close to 100% transfer efficiency with $I_{0c}=4.4$ TW/cm^2.

One could also achieve efficiently with a nonmonotonic chirp the selective climbing of v and J: $|v=0,J=0\rangle\rightarrow|v=1,J=2\rangle\rightarrow|v=2,J=4\rangle\rightarrow\ldots\rightarrow|v,J=2v\rangle$.

IV. CONCLUSION

We have developed systematic tools to transfer population by adiabatic passage induced by chirped frequencies using quasienergy surfaces as functions of the field parameters. We have shown that, in a realistic model including rotation, the alignment of molecules during a nanosecond laser pulse can be used for an efficient rovibrational state selectivity. In addition to leading the molecule to a given vibrational state, this method offers the possibility to obtain either an isotropic molecule in $J=0$ or a molecule in a well-defined anisotropic $J>0$ state.

ACKNOWLEDGMENTS

We thank L. P. Yatsenko for stimulating discussions. We acknowledge the financial supports by the *Action Concertée Incitative Photonique* from the French Ministry of Research and by the Conseil Régional de Bourgogne.

[1] J. Karczmarek, J. Wright, P. B. Corkum, and M. Ivanov, Phys. Rev. Lett. **82**, 3420 (1999).
[2] T. Seideman, J. Chem. Phys. **111**, 4397 (1999).
[3] S. Chelkowski, A. D. Bandrauk, and P. B. Corkum, Phys. Rev. Lett. **65**, 2355 (1990).
[4] S. Chelkowski and G. N. Gibson, Phys. Rev. A **52**, R3417 (1995); S. Chelkowski and A. D. Bandrauk, J. Raman Spectrosc. **28**, 459 (1997).
[5] D. J. Maas, C. W. Rella, P. Antoine, E. S. Toma, and L. D. Noordam, Phys. Rev. A **59**, 1374 (1999).
[6] S. Guérin, Phys. Rev. A **56**, 1458 (1997).
[7] K. Drese and M. Holthaus, Eur. Phys. J. D **5**, 119 (1999).
[8] S. Chelkowski and A. D. Bandrauk, J. Chem. Phys. **99**, 4279 (1993).
[9] J. C. Davis and W. S. Warren, J. Chem. Phys. **110**, 4229 (1999).
[10] F. Légaré, S. Chelkowski, and A. D. Bandrauk, Chem. Phys. Lett. **329**, 469 (2000).
[11] I. V. Andrianov and G. K. Paramonov, Phys. Rev. A **59**, 2134 (1999).
[12] S. Sen, S. Ghosh, S. S. Bhattacharyya, and S. Saha, J. Chem. Phys. **116**, 581 (2002).
[13] A. Adelswärd, S. Wallentowitz, and W. Vogel, Phys. Rev. A **67**, 063805 (2003).
[14] B. Friedrich and D. Herschbach, Phys. Rev. Lett. **74**, 4623 (1995).
[15] J. Ortigoso, M. Rodriguez, M. Gupta, and B. Friedrich, J. Chem. Phys. **110**, 3870 (1999).
[16] C. M. Dion, A. Keller, O. Atabek, and A. D. Bandrauk, Phys. Rev. A **59**, 1382 (1999).
[17] T. Seideman, J. Chem. Phys. **115**, 5965 (2001).
[18] S. Guérin and H. R. Jauslin, Adv. Chem. Phys. **125**, 147 (2003).
[19] S. Guérin, L. P. Yatsenko, and H. R. Jauslin, Phys. Rev. A **63**, 031403 (2001).
[20] L. P. Yatsenko, S. Guérin, and H. R. Jauslin, Phys. Rev. A **65**, 043407 (2002).
[21] S. Guérin, R. G. Unanyan, L. P. Yatsenko, and H. R. Jauslin, Phys. Rev. A **66**, 032311 (2002).
[22] S. Guérin, S. Thomas, and H. R. Jauslin, Phys. Rev. A **65**, 023409 (2002).
[23] S. Guérin, F. Monti, J.-M. Dupont, and H. R. Jauslin, J. Phys. A **30**, 7193 (1997).
[24] G. Maroulis, J. Phys. Chem. **100**, 13466 (1996)
[25] B. Broers, H. B. vanLinden van den Heuvell, and L. D. Noordam, Phys. Rev. Lett. **69**, 2062 (1992); P. Balling, D. J. Maas, and L. D. Noordam, Phys. Rev. A **50**, 4276 (1994).
[26] A. Keller, C. M. Dion, and O. Atabek, Phys. Rev. A **61**, 023409 (2000).
[27] S. Guérin, L. P. Yatsenko, H. R. Jauslin, O. Faucher, and B. Lavorel, Phys. Rev. Lett. **88**, 233601 (2002).

Chapter 12

Control of localization and suppression of tunneling by adiabatic passage

In this paper [141], we generalize the idea of orientation of molecules by adiabatic 2+1 processes to generate a state superposition of nearly degenerate states. This is applied to the challenging problem of localization of tunneling starting with a ground state delocalized wavepacket. As opposed to the orientation problem, the field amplitude needs here to be of quite specific value. The process is however robust with respect to the pulse area.

We show that this 2+1 process allows us to control the tunneling dynamics (see Fig. 4).

PRL 93, 223602 (2004) PHYSICAL REVIEW LETTERS week ending 26 NOVEMBER 2004

Control of Localization and Suppression of Tunneling by Adiabatic Passage

N. Sangouard,[1,*] S. Guérin,[1,†] M. Amniat-Talab,[1,2] and H. R. Jauslin[1]

[1]*Laboratoire de Physique de l'Université de Bourgogne, UMR CNRS 5027, BP 47870, 21078 Dijon, France*

[2]*Physics Department, Faculty of Sciences, Urmia University, P.B. 165, Urmia, Iran*

(Received 6 June 2004; published 24 November 2004)

We show that a field of frequency ω combined with its second harmonic 2ω driving a double-well potential allows us to localize the wave packet by adiabatic passage, starting from the delocalized ground state. The relative phase of the fields allows us to choose the well of localization. We can suppress (and restore) the tunneling subsequently by switching on (and off) abruptly the fields at well-defined times. The mechanism relies on the fact that the dynamics is driven to an eigenstate of the Floquet Hamiltonian which is a localized state.

DOI: 10.1103/PhysRevLett.93.223602 PACS numbers: 42.50.Hz, 03.65.Xp, 73.40.Gk

Generating and controlling coherent superpositions of states is of great interest, in particular, for the recent developments of quantum computing [1]. Quantum tunneling is a natural example of superpositions of states, which correspond to spatially localized states. An important goal is to achieve the control of driven tunneling (see, e.g., [2] for a review). Practical realizations can be considered in coupled multiquantum dot systems that can be now built experimentally [3]. Enhancement of tunneling by a nonresonant [4,5] or resonant [6] pulse-shaped field, and the coherent destruction of tunneling (CDT) [7–11] by a cw field are well established. The CDT as shown in [7,8] occurs when the field amplitude allows one to preserve the two bare states $|1\rangle$ and $|2\rangle$ as eigenstates of the Floquet Hamiltonian (dressed by the field) and to make the associated quasienergies cross such that the tunneling time between the two states becomes infinite when the field is on. The CDT has been differently obtained in [10,11], when one of the localized states is an eigenstate of the Floquet Hamiltonian, which requires the coupling to an asymmetric excited electronic surface $|e\rangle$ of similar amplitudes: $|\langle e|\mu|1\rangle| \approx |\langle e|\mu|2\rangle|$ with μ the coupling operator. The CDT by two fields of different frequencies has been investigated in [12]. The CDT proposed so far in the literature is only partially controlled in the sense that one does not know the state of the system, i.e., the phase ξ of the stopped superposition $|1\rangle + e^{i\xi}|2\rangle$, since the initial tunneling state is generally unknown. This can be circumvented if one can also control the localization from the initial unlocalized ground state $|1\rangle$. It has been numerically shown in [13] that the localization is possible by the use of a pulse quasiresonant between the two tunneling states, however, under very restrictive conditions of field amplitudes, frequencies, and also absolute phases.

In this Letter we show a novel mechanism based on adiabatic passage that allows us to control the localization (i.e., with the knowledge of the localization time). This process is robust in the sense that it requires the control of the peak field amplitudes and frequencies but not of the absolute phase of the total field, nor of their pulse areas. Using subsequently the fields but suddenly switched on and off, we propose a consistent scheme of control from localization to suppression of tunneling. The mechanism is formulated as the preparation of one of the coherent superpositions $|\pm\rangle = (|1\rangle \pm |2\rangle)/\sqrt{2}$ in a system of two near-degenerate bare states $\{|1\rangle, |2\rangle\}$ of opposite parity. The key elements of the process are (i) the superpositions $|\pm\rangle$ become *eigenstates* of the Floquet Hamiltonian for specific field amplitudes and (ii) the pulse shapes allow us to reach one of the eigenstates from the ground state $|1\rangle$ by adiabatic passage. Adiabatic passage provides thus a technique to prepare the system in a localized state at a well-defined time. More precisely, a field of an appropriate frequency ω combined with its second harmonic 2ω, coupling the states $|1\rangle$ and $|2\rangle$ by a three-photon process (initially near-resonant, detuned by the energy difference δ between the two states), will induce dynamical Stark shifts that will compensate the detuning δ for specific field amplitudes. Adiabatic passage from the initial delocalized state $|1\rangle$ leads thus to one of the localized states whose localization is controlled by the relative phase of the two fields. The dynamics stays localized as long as the field amplitudes stay subsequently constant.

This localized state can then be used for other controlled manipulations such as the controlled switching on and off of the tunneling. In particular, the tunneling effect can start if the fields are switched off suddenly (more precisely, on a time scale T_{off} satisfying $\delta T_{\text{off}} \ll 1$). The tunneling can be suppressed again if the fields are switched on again but suddenly, at a precisely determined time given by the period of the free tunneling. The wave packet can be alternatively redelocalized by adiabatic passage if the fields are switched off adiabatically.

We first introduce an *effective* model to analyze the qualitative aspects of the mechanism, and then we implement the strategy in a complete model with a double-well potential.

The key to be able to localize with the laser field consists first in noticing that the two localized states $|\pm\rangle$ are eigenstates of the Floquet Hamiltonian. This leads then to a strategy to reach them by adiabatic trans-

port. This can be formulated by considering first the effective two-level system (in a resonant approximation)

$$H_{\rm eff}(t) = \hbar \begin{pmatrix} 0 & \Omega(t)e^{i\varphi} \\ \Omega(t)e^{-i\varphi} & \Delta(t) \end{pmatrix} \quad (1)$$

in the bare basis $\{|1\rangle, |2\rangle\}$, where we assume that the Rabi frequency $\Omega(t)$ and the dynamical detuning (including the relative Stark shift) $\Delta(t)$ are both real such that $\Omega(t) > 0$ and at early times $\Omega(-\infty) = 0$, $\Delta(-\infty) \equiv \delta > 0$, without loss of generality. In the adiabatic limit, the propagator contains on its columns the instantaneous eigenvectors of (1): $|\psi_+\rangle = e^{i\varphi}\cos(\theta/2)|1\rangle + \sin(\theta/2)|2\rangle$, $|\psi_-\rangle = \sin(\theta/2)|1\rangle - e^{-i\varphi}\cos(\theta/2)|2\rangle$, $H_{\rm eff}(t)\psi_\pm = \frac{\hbar}{2} \times [\Delta(t) \pm \sqrt{\Delta^2(t) + 4\Omega^2(t)}]\psi_\pm$. It reads

$$U(t, -\infty) = \begin{pmatrix} e^{-i\eta_-(t)}\sin\frac{\theta(t)}{2} & e^{i[\varphi-\eta_+(t)]}\cos\frac{\theta(t)}{2} \\ -e^{-i[\varphi+\eta_-(t)]}\cos\frac{\theta(t)}{2} & e^{-i\eta_+(t)}\sin\frac{\theta(t)}{2} \end{pmatrix}, \quad (2)$$

$$\tan\theta(t) = -\frac{2\Omega(t)}{\Delta(t)}, \qquad 0 \le \theta(t) < \pi, \quad (3)$$

combined with the dynamical phases

$$\eta_\pm(t) = \frac{1}{2}\int_{-\infty}^{t} ds[\Delta(s) \pm \sqrt{\Delta^2(s) + 4\Omega^2(s)}]. \quad (4)$$

We emphasize that the phases of the eigenvectors have been chosen as usual to satisfy the parallel transport: $\langle\psi_\pm|\partial/\partial t|\psi_\pm\rangle = 0$, leading to a zero geometric phase if one considers a nonclosed trajectory in the parameter space. We can thus generate by adiabatic passage the coherent superposition $|\pm\rangle$ when $\theta = \pi/2$, i.e., for

$$\Omega(t) \gg |\Delta(t)| \quad (5)$$

and for a controllable phase φ. Starting from either state $|1\rangle$ or $|2\rangle$ [with initially $\theta(-\infty) = \pi$ here], we can generate by adiabatic passage the coherent superposition $|-\rangle$ or $|+\rangle$ (i.e., with θ going from π to $\pi/2$) by choosing the phase as $\varphi = 0$ or $\varphi = \pi$. Since $|\pm\rangle$ are eigenstates of the Hamiltonian (1), if Ω is suddenly switched off, the tunneling will start from the well-defined localized state previously prepared. Next, if Ω is suddenly switched on, again the tunneling will stop in the state $|\psi\rangle = a_+|+\rangle + a_-|-\rangle$ in which it is at the switching time. In particular, the tunneling can be stopped in one well if we choose a switching time when $a_+ = 1$ (or $a_- = 1$).

We implement this strategy in a tunneling system driven by two off-resonant pulse-shaped fields, of frequencies ω and its second harmonic 2ω (Fig. 1), of amplitudes $\mathcal{E}_1(t)$ and $\mathcal{E}_2(t)$, respectively, and of relative phase ϕ, leading to the total field $\mathcal{E}(t) = \mathcal{E}_1(t)\cos\omega t + \mathcal{E}_2(t)\cos(2\omega t + \phi)$. The effective Hamiltonian can be written in the three-photon resonant approximation as

$$H_{\rm eff}(t) = \hbar \begin{pmatrix} 0 & |\gamma|\mathcal{E}_2(t)\mathcal{E}_1(t)^2 e^{i\varphi} \\ |\gamma|\mathcal{E}_2(t)\mathcal{E}_1(t)^2 e^{-i\varphi} & \delta + S(t) \end{pmatrix} \quad (6)$$

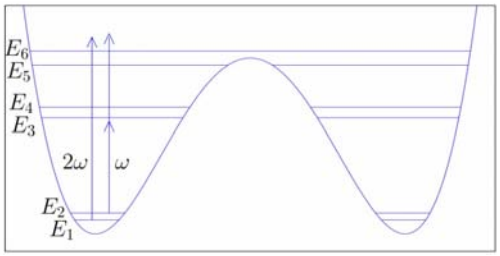

FIG. 1 (color online). Schematic diagram of the energy levels: E_1, E_2 are the energies of the two bare states $|1\rangle$, $|2\rangle$. The arrows represent the fields of frequencies ω and 2ω.

with

$$\varphi = \phi + \arg(\gamma), \qquad \arg(\gamma) = 0 \quad \text{or} \quad \pi, \quad (7)$$

where the energy difference between the states $|2\rangle$ and $|1\rangle$ is denoted by δ and the relative Stark shift $S(t)$ (which is of second order in the field amplitudes) [14]. The off diagonal term $|\gamma|\mathcal{E}_2(t)\mathcal{E}_1(t)^2 e^{i\varphi}$, of third order in field amplitude, is a three-photon coupling between the states $|1\rangle$ and $|2\rangle$. The construction of $H_{\rm eff}(t)$ requires in practice additional states in the model, which are taken into account by standard techniques of partitioning (or adiabatic elimination) [14,15]. This allows one to determine the coefficient γ and the relative Stark shift $S(t)$, which can both be chosen as real without loss of generality (see below for a concrete model). The Stark shifts will depend on the position of these additional states and on their couplings with $|1\rangle$ and $|2\rangle$. For instance, a single additional state $|3\rangle$ of energy E_3 coupled with the state $|2\rangle$ with the coupling element μ_{23}, by the field of frequency ω, with a positive detuning: $\hbar\Delta_{23} := E_3 - E_2 - \hbar\omega > 0$, will repel down the state $|2\rangle$ (of $-|\mu_{23}\mathcal{E}_1|^2/4\Delta_{23}$). Identifying (1) and (6) leads to $\Delta(t) \equiv \delta + S(t)$ and $\Omega(t)e^{i\varphi} \equiv |\gamma|\mathcal{E}_2(t)\mathcal{E}_1(t)^2 e^{i\varphi}$. The condition (5) is well satisfied for the particular field amplitudes such that

$$\Delta \equiv \delta + S = 0 \quad (8)$$

or for strong fields such that $|\gamma|\mathcal{E}_2\mathcal{E}_1^2 \gg |\delta + S|$. This latter condition is not considered in this work since in practice it requires generally very strong fields that would produce destructive processes, such as ionization. The condition (8) is expected to occur for specific values of field amplitudes if the frequency ω is appropriately chosen such that the Stark shift satisfies $S(t) < 0$.

We illustrate the proposed mechanism to manipulate coherently the tunneling in the standard symmetric double-well model potential $\hat{H}_0 = p^2/2 - x^2/2 + x^4/(64D)$ (with $D = 2$ to approximately model the NH_3 tunneling), expressed here in dimensionless units. Choosing the polarization of the lasers in the x direction, we obtain for the driven Hamiltonian $\hat{H}(t) = \hat{H}_0 - x\mathcal{E}(t)$. The $2 + 1$ field shows a bias for $\phi \neq \pi/2$ that allows the breaking of symmetry. Without loss of generality, we can choose a

PRL 93, 223602 (2004) PHYSICAL REVIEW LETTERS week ending 26 NOVEMBER 2004

basis such that $|+\rangle$ and $|-\rangle$ represent the localization in the left and right wells, respectively: $|+\rangle \equiv |L\rangle$, $|-\rangle \equiv |R\rangle$. We choose the appropriate frequency $\omega = 1.71 \times 10^{14}$ Hz which is a one-photon near resonance between states $|2\rangle$ and $|3\rangle$, and a two-photon near resonance between states $|1\rangle$ and $|6\rangle$ (see Fig. 1). The coefficient γ and the Stark shift $S(t)$ can be estimated by partitioning, using the one-photon near resonances for simplification, under the condition $\Omega_{\max} \ll \Delta_{\rm nr}$, where $\Delta_{\rm nr}$ characterizes the minimum detuning associated to the one-photon near resonances and $\Omega_{\max}$ is the peak Rabi frequency. We obtain here that γ is proportional to $\mu_{16}\mu_{23}\mu_{36}$ and $\gamma < 0$; i.e., $\arg(\gamma) = \pi$. The dynamics can be considered as adiabatic inside the subspace spanned by $\{|1\rangle, |2\rangle\}$ if $\Delta_{\rm nr} T \gg 1$, where T stands for a characteristic duration of the pulse [e.g., the full width half maximum (FWHM) for a Gaussian pulse]. The adiabatic dynamics can be characterized by the quasienergy representation (associated to the Floquet Hamiltonian with the double-well driven potential) (see, e.g., [15] for a review of adiabatic dynamics for Floquet Hamiltonians) as a function of the two field amplitudes for a given frequency ω (see Fig. 2). One can see a (dark) region of avoided crossing for moderate field amplitudes, which corresponds approximately to the amplitudes for which the condition (8) is satisfied. This avoided crossing can be intuitively understood as follows: The Stark shifts, which are the elements of lowest order in the field amplitudes, push the two Floquet eigenenergies, connected to the bare states $|1\rangle$ and $|2\rangle$, closer to each other. They subsequently repel since they are coupled (by the three-photon resonance) approximately when the effective Δ becomes zero. A choice of the envelope and peak fields correspond to a specific path in Fig. 2. An additional condition on the speed of the dynamics, which is determined by numerical simulation, has also to be fulfilled to reach adiabatically this avoided crossing.

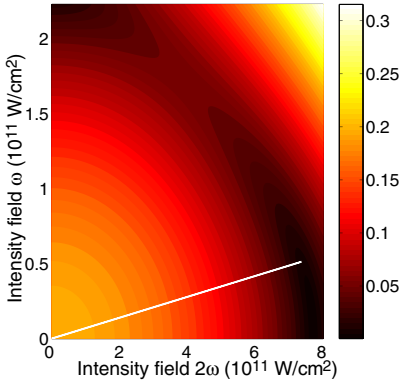

FIG. 2 (color online). Contour plot of the difference of the quasienergies connected to the bare states $|2\rangle$ and $|1\rangle$. The darker region is the considered line of avoided crossings. The white straight line corresponds to the dynamics used to achieve localization.

To achieve localization, we use nanosecond super-Gaussian ramps of shape $\Lambda(t) = \exp[-(t/\tau)^8]$ (here of FWHM 55.8 ns), which include a quasiplateau [see Fig. 4(b), left frame; note that the width of the rising of this super-Gaussian pulse is approximately 15 ns, which gives here for the adiabatic factor $\delta T \approx 565$), and of peak intensities 51 and 740 GW/cm^2 for I_1 and I_2, respectively. They allow (i) the use of the effective Hamiltonian (6) and (ii) adiabatic passage until the avoided crossing. The choice of the relative phase ϕ allows one to choose the well of localization.

As shown in Fig. 3, we obtain the localization of the wave packet from the initial state $|2\rangle$ in the right (left) well for $\phi = 0$ ($\phi = \pi$). The localization is quite robust with respect to the relative phase ϕ: We have observed numerically that the localization probability decreases from 1 to 0.97 when the relative phase is taken as 2.83 instead of π. Figure 4(a) (left frame) shows the localization for a population initially prepared in state $|1\rangle$. The population is localized in the left (right) well for $\phi = 0$ ($\phi = \pi$). Depending on the initial state, we create the target localized state by choosing the relative phase of the two pulses.

To control the subsequent starting and suppression of the tunneling oscillations, we use suddenly switched pulses since the localized states are eigenstates of the Floquet Hamiltonian (see Fig. 4). In practice this is ob-

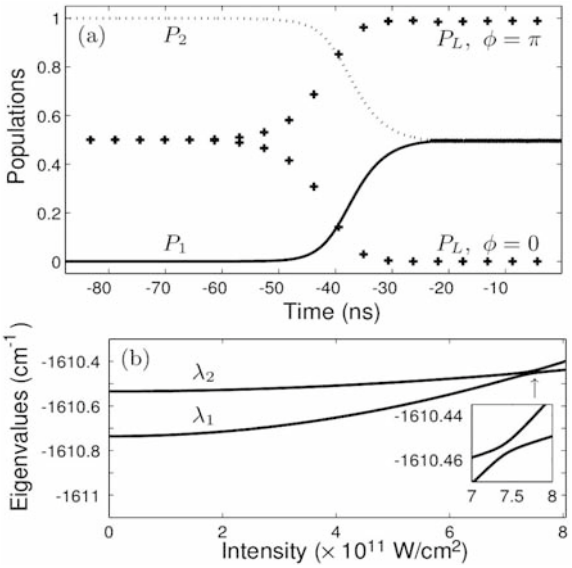

FIG. 3. (a) Numerical simulation of the localization of the populations as a function of time, respectively P_1 (P_2) of the states $|1\rangle$ ($|2\rangle$) in the full (dotted) line with $|2\rangle$ as initial condition. The + lines represent the population P_L localized on the left for the phases $\phi = 0$ and $\phi = \pi$. (b) Floquet eigenvalues λ_1, λ_2, respectively, connected to the bare energies E_1 and E_2, as functions of the intensity of the pulse 2 for a fixed value of the intensity of the pulse 1: $I_1 = 0.51 \times 10^{11}$ W/cm^2. The inset shows an enlargement of the avoided crossing of the Floquet eigenvalues.

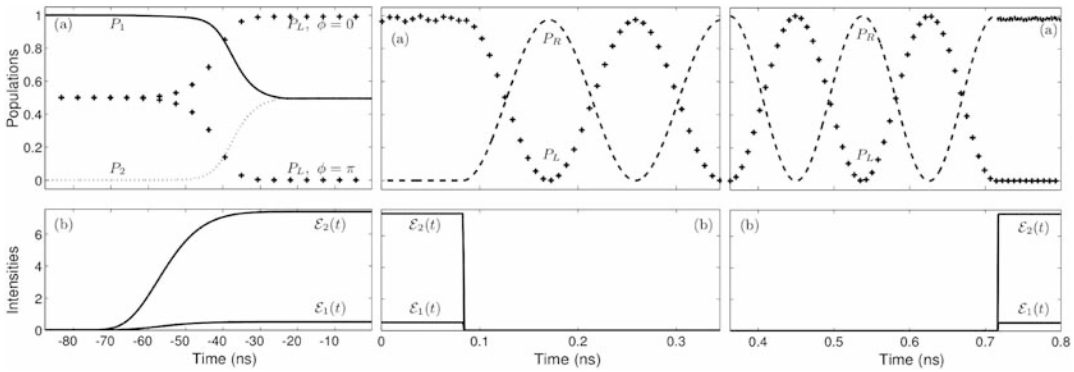

FIG. 4. (a) Left frame: same as Fig. 3(a), but with $|1\rangle$ as the initial condition. Middle and right frames: time continuation of the left frame. The plus (minus) line represents the population localized on the left (right) with the choice $\phi = 0$. (b) Intensities (in 10^{11} W/cm^2) of the pulses as a function of time. The middle (right) frame shows the tunneling starting (suppression) induced by fields suddenly switched off (on).

tained with Gaussian ramps of short FWHM T_s such that $\delta T_s \ll 1$ and $\Delta_{\rm nr} T_s \gg 1$ to avoid the appearance of other resonances. The population is initially prepared in the left well by adiabatic passage (see the left frame of Fig. 4). Tunneling (of period 176 ps) starts when the fields are suddenly switched off ($T_s = 2$ ps is used, which gives here $\delta T_s \approx 0.08$ and $\Delta_{\rm nr} T_s \approx 6$). After three and a half periods, the pulses suddenly switched on (with the same intensities used to localize) induce the suppression of the tunneling and the localization in the right well. This result is in agreement with the CDT by two fields of different frequencies predicted in the context of classical mechanics and with numerical quantum simulations of a localized initial Gaussian wave packet [12]. Since we have localized the wave packet, we have access to the subsequent times of localization, and we can thus start and suppress the tunneling at controlled times. Reversing time in Fig. 3 and in the left frame of Fig. 4 shows that the wave packet can be alternatively redelocalized by adiabatic passage in state $|1\rangle$ or $|2\rangle$ if the fields are switched off adiabatically when the wave packet is in state $|+\rangle$ or $|-\rangle$. The choice of the final state is made by the appropriate choice of the phase $\phi = 0$ or $\phi = \pi$, depending on the state before switching off.

This process of localization by adiabatic passage does not depend on the absolute phase of the total field, nor on the ramp area.

In conclusion, we have shown that it is possible to achieve the localization and suppression of tunneling by adiabatic passage. This controlled switching process can be adapted to the molecular alignment versus orientation. In this context, alignment is obtained by the Stark shifts induced by the two fields and oriented molecules correspond to localized states [16]. The tunneling, which is an oscillation between the two possible orientations, can be obtained by switching off one of the two fields, the other one maintaining the alignment. This scheme of controlled tunneling, reinterpreted as controlled manipulation of superposition of states, can have applications in the context of quantum computing.

We acknowledge the financial support by the ACI Photonique and by the Conseil Régional de Bourgogne.

*Electronic address: nicolas.sangouard@u-bourgogne.fr
†Electronic address: sguerin@u-bourgogne.fr

[1] D. Bouwmeester, A. K. Ekert, and A. Zeilinger, *The Physics of Quantum Information: Quantum Cryptography, Quantum Teleportation, Quantum Computation* (Springer, Berlin, 2000).
[2] M. Grifoni and P. Hänggi, Phys. Rep. **304**, 229 (1998).
[3] R. H. Blick, D. Pfannkuche, R. J Haug, K. von Klitzing, and K. Eber, Phys. Rev. Lett. **80**, 4032 (1998).
[4] W. A. Lin and L. E. Ballentine, Phys. Rev. Lett. **65**, 2927 (1990); Phys. Rev. A **45**, 3637 (1992).
[5] M. Holthaus, Phys. Rev. Lett. **69**, 1596 (1992).
[6] S. Guérin and H. R. Jauslin, Phys. Rev. A **55**, 1262 (1997).
[7] F. Grossmann, T. Dittrich, P. Jung, and P. Hänggi, Phys. Rev. Lett. **67**, 516 (1991).
[8] J. M. Gomez Llorente and J. Plata, Phys. Rev. A **45**, R6958 (1992).
[9] C. E. Creffield, Phys. Rev. B **67**, 165301 (2003).
[10] S. Ya. Kilin, P. R. Berman, and T. M. Maevskaya, Phys. Rev. Lett. **76**, 3297 (1996).
[11] E. Paspalakis, Phys. Lett. A **261**, 247 (1999).
[12] D. Farrelly and J. A. Milligan, Phys. Rev. E **47**, R2225 (1993).
[13] R. Bavli and H. Metiu, Phys. Rev. Lett. **69**, 1986 (1992); Phys. Rev. A **47**, 3299 (1993).
[14] B.W. Shore, *The Theory of Coherent Atomic Excitation* (Wiley, New York, 1990).
[15] S. Guérin and H. R. Jauslin, Adv. Chem. Phys. **125**, 147 (2003).
[16] S. Guérin, L. P. Yatsenko, H. R. Jauslin, O. Faucher, and B. Lavorel, Phys. Rev. Lett. **88**, 233601 (2002).

Part IV

Quantum information by adiabatic passage

Miniaturizing well known processes governed by classical mechanics has the natural obstacles of quantum effects, such as the superposition principle, entanglement, and measurement processes. Another point of view consists in taking advantage of these effects to create new faster processes [195, 196, 197, 198, 199]. This is the starting point of quantum computation, and more generally of quantum information. It has been shown in particular that some classical slow algorithms can be made fast using quantum procedure. This has been first realized by Deutsch and Jozsa (who constructed an algorithm that decides if all possible results of a function are either identical or equally distibuted between two values) [200]. An algorithm of much more practical relevance formulated by P. Shor consists in finding the prime factors of an N-digit number [201]. The Shor's factoring algorithm factorizes in a time of order N^3 , much faster than the known classical counterparts factorizing in a time beyond any powers of N. One can also cite the Grover search algorithm [202], which can find in a database of N items the one that meets a specific criterion in a time of order $\sqrt{N}$, faster than the classical computer, which has been shown to find it in a time of order N.

A quantum computation requires in particular to replace the classical bit by a quantum bit, or qubit, represented by a two-state system $|0\rangle$ and $|1\rangle$. The state of the qubit can be any superposition of the two states and can be represented by a vector on the Bloch sphere. A system composed of two qubits can have the key property of entanglement, such as one of the four Bell States

$$|\psi\rangle = \frac{1}{\sqrt{2}}(|00\rangle - |11\rangle), \tag{12.1}$$

for a two qubit system, where the first (second) qubit stand at the first (second) position. Such superpositions are expected to perform many operations in parallel. The main difficulty is to preserve the coherence of the system during a sufficiently long time to complete the calculation. The qubits should thus be well isolated from the environment.

A quantum computer can be represented as a register, for instance of ions trapped by electromagnetic potentials (radio-frequency Paul trap) [203]. One has to be able to be initialize the register, to execute some specific logic operations, and to have a readout. All these tasks can be achieved by addressing individually the qubits with external fields (see for instance the implementation of the Deutsch-Jozsa algorithm [200] on an ion-trap quantum computer [204]). The logical gate requires a *coupling* between the qubits which should not change the population when the addressing external fields are off. In the case of trapped ions, such a coupling is obtained through the translational collective motion in the trap [205].

Another method to couple separate atoms or ions coherently is to use cavity quantum electrodynamics (CQED) [207]. In the case of atoms, it is very difficult to trap them inside the cavity. It can be however realized using a standing wave dipole-force trap [208]. Instead of free atoms, it has been proposed to use atoms of a specific crystal put in the cavity and combined with magnetic fields [209].

It has been proposed to implement the quantum information protocols by laser manipulation of atomic ensembles containing a large number of identical atoms [210] (using for instance laser-cooled atoms confined in a magnetic optical trap). Such an ensemble is easier to address than a single atom. It allows one to store information with robustness against some practical noise (loss of an atom for instance), and provides strong collective couplings with external fields (such as a quantum cavity fields) with respect to a single atom.

The register could be itself an isolated molecule or an ensemble of molecules with the qubits as some specific states. A well known system is the nuclear spins of a large molecule as qubits, and the computing is realized by nuclear magnetic resonance (NMR) in liquid medium. One

advantage is the weak interaction of the nuclear spins with the environment. The spins interact through J-coupling and the dipole coupling; the latter averages to zero in an isotropic liquid. They are driven by radio frequency pulses of specific areas, giving transitions of π-pulse type. The Shor algorithm has been implemented in a specific molecule with the use of five ^{19}F and two ^{13}C nuclear spins to factorize 15 [211].

One can also mention proposals in solid state systems, such as Cooper pairs [212] or quantum dots as qubits (see for instance [213, 214]).

One could think more generally of each register as a node of a quantum network, with traveling particles that ferry information to communicate between the registers. Such particles can be ideally single photons, where the information is stored in their polarization, for instance $\sigma_{\pm}$, and that can interact with the atoms of the register to encode or decode the information [215, 216].

More generally, quantum communications deals with sending quantum states from one place to another in such a way that they arrive intact. One of the most important applications is quantum cryptography, which deals with the generation and the transmission of a secure key in order to convey a secret message in a quantum way [217]. Typical protocols use single photons as qubits.

The preceding discussion highlights important processes that are required for quantum information, such as entanglement, generation of single photons, and logic quantum gates.

We address in the following chapters these three subjects independently.

Important aspects are the robustness with respect to the external fields and to the details of the model. We explore thus new processes using adiabatic passage techniques.

An important requirement is to avoid the decoherence of the system by decoupling it from the environment. An elegant method consists in using specific decoherence-free subspaces dressed by the external fields [218], for instance made of metastable ground states and thus immune to losses from spontaneous emission. The state carrying the dynamics in such a decoherence-free subspace is known as a dark state. We focus thus on models that possess such properties, and take benefit from adiabatic passage which allows us to control the dynamics using dark states.

In particular, we show in chapter 13 a process to generate photon number states (Fock states) by adiabatic passage. In chapter 14, we show various processes by adiabatic passage that allow us to entangle spins, photons and atoms. Chapter 15 is devoted to quantum gates for single and two qubits.

Chapter 13

Generating multi-photon Fock states by bichromatic adiabatic passage

Many different types of single-photon sources have been proposed and realized using the controlled excitation of single molecules [219, 220] or of single nitrogen-vacancy centers in diamond nanocrystals [221], controlled injection of carriers into a mesoscopic quantum well [222] and using pulsed excitation of semiconductor quantum dots [223, 224].

In the context of cavity QED, single-photon Fock states have been produced by a Rabi π-pulse in a microwave cavity [225, 226] and by the STIRAP technique in an optical cavity [227] based on the scheme proposed in [228] where the Stokes pulse is replaced by a mode of a high-Q cavity. The STIRAP process has also been studied in a system of a four-level atom interacting with a cavity mode and two laser pulses, with a coupling scheme which generates two degenerate dark states [229]. In all these cavity QED schemes one atom interacts with a single-mode high-Q cavity and generates one photon. As the atoms pass through the cavity one by one, more photons can be added to the cavity mode. Recently the generation of two-photon Fock state has been proposed [230] and realized [231] by a single two-level atom interacting with a superconducting cavity which sustains two non-degenerate orthogonally polarized modes. The photons are transferred from the source mode into the target mode of the cavity by a third-order Raman process. However this scheme is not robust with respect to the velocity of the atoms. Also a very recent scheme for producing of Fock states with a large number of photons has been proposed using the Raman excitation of a three-level atom which requires in practice a compensation of a dynamical stark shift and non-robust pulse area techniques [232].

In the article [233] presented below, we extend the resonant STIRAP process with the Stokes pulse as a mode of a high-Q cavity [227, 228], to a bichromatic process (here in two-state systems), similar to the one we presented in chapter 9 with the use of laser pulses, but using a cavity field instead of one of the fields. In this context, this allows us to generate multi-photon Fock states, where the number of photons is controlled in a robust way by the peak amplitude of the fields.

In this process, atoms are used as mediators that extract photons from the maser field to release them to the cavity.

PHYSICAL REVIEW A **70**, 013807 (2004)

Generation of multiphoton Fock states by bichromatic adiabatic passage: Topological analysis

M. Amniat-Talab,* S. Lagrange, S. Guérin,† and H. R. Jauslin‡
Laboratoire de Physique, UMR CNRS 5027, Université de Bourgogne, Boîte Postale 47870, F-21078 Dijon, France
(Received 23 February 2004; published 21 July 2004)

We propose a robust scheme to generate multi-photon Fock states in an atom-maser-cavity system using adiabatic passage techniques and topological properties of the dressed eigenenergy surfaces. The mechanism is an exchange of photons from the maser field into the initially empty cavity by bichromatic adiabatic passage. The number of exchanged photons depends on the design of the adiabatic dynamics through and around the conical intersections of dressed eigenenergy surfaces.

DOI: 10.1103/PhysRevA.70.013807 PACS number(s): 42.50.Dv, 42.50.Pq, 42.50.Ct

I. INTRODUCTION

Over the past few years, new sources of antibunched light that are able to emit a single photon in a given time interval have been the subject of intense theoretical and experimental research. The driving force behind the development of these nonclassical sources is a range of novel applications in quantum information theory which builds on the laws of quantum mechanics to transmit, store, and process information in varied and powerful ways. Advances in this field rely on the ability to manipulate coherently isolated quantum objects while eliminating incoherent interactions with the surrounding environment. Single photon states act as elementary quantum bits (qubits) in quantum cryptography [1–3] and teleportation of a quantum state [4] where their entangled states enable the secure transmission of information.

Many different types of single-photon sources have been proposed and realized using the controlled excitation of single molecules [5,6] or of single nitrogen-vacancy centers in diamond nanocrystals [7], the controlled injection of carriers into a mesoscopic quantum well [8], and using the pulsed excitation of semiconductor quantum dots [9,10].

In the context of cavity QED, single-photon Fock states have been produced by a Rabi π-pulse in a microwave cavity [11,12] and by the stimulated Raman adiabatic passage (STIRAP) technique in an optical cavity [13] based on the scheme proposed in [14] where the Stokes pulse is replaced by a mode of a high-Q cavity. The STIRAP process has also been studied in a system of a four-level atom interacting with a cavity mode and two laser pulses, with a coupling scheme which generates two degenerate dark states [15]. In all these cavity QED schemes one atom interacts with a single-mode high-Q cavity and generates one photon. As the atoms pass through the cavity one by one, more photons can be added to the cavity. Recently the generation of two-photon Fock state has been proposed [16] and realized [17] by a single two-level atom interacting with a superconducting cavity which sustains two nondegenerate orthogonally polarized modes. The photons are transferred from the source mode into the target mode of the cavity by a third-order Raman process. However, this scheme is not robust relative to the velocity of atoms. Also a recent scheme for producing of large Fock states has been proposed using the Raman excitation of a three-level atom which requires in practice a compensation of a dynamical Stark shift and nonrobust pulse area technique [18].

In this paper we propose a robust scheme in which a two-level atom interacts counterintuitively [19] with a single-mode high-Q cavity and a delayed maser field that are both near-resonant with the atomic transition, allowing us to produce a controlled number of photons in the cavity depending on the design of the adiabatic passage. This process is referred to as a bichromatic adiabatic passage since two near-resonant interacting fields act on a single transition. A related work involving exchange of photons between two laser fields through a bichromatic process can be found in Ref. [20]. The transfer of photons from the maser field into the cavity field is based on the adiabatic passage between two dressed states which are the eigenstates of the coupled atom-maser-cavity system. This process is robust because it does not depend on the precise velocity of the atom or on the precise tuning of the maser and the cavity frequencies. The dynamics of the process, under the adiabatic conditions, can be described completely by the topology of the dressed eigenenergy surfaces. This topological aspect is the key to the robustness of the process. Our method is based on the calculation of the dressed eigenenergy surfaces of the effective Hamiltonian as a function of the two Rabi frequencies associated to the maser and the cavity fields, and the application of adiabatic principles to determine the dynamics of the process in view of the topology of the surfaces [21].

The paper is structured as follows. In Sec. II, we use the Floquet formalism and the phase representation of the creation and annihilation operators to construct the effective Hamiltonian of the atom-maser-cavity system. Eigenenergy surfaces of the effective Hamiltonian are displayed in Sec. III as a function of the normalized Rabi frequencies of the cavity and the maser fields. We demonstrate how the analysis of these surfaces allows us to design different adapted adiabatic paths leading to different photon transfers into the cavity field without changing the atomic population at the end of the interaction. Section IV is devoted to the numerical simu-

*Also at the Physics Department, Faculty of Sciences, Urmia University, P. B. 165, Urmia, Iran. Electronic address: amniyatm@u-bourgogne.fr
†Electronic address: sguerin@u-bourgogne.fr
‡Electronic address: jauslin@u-bourgogne.fr

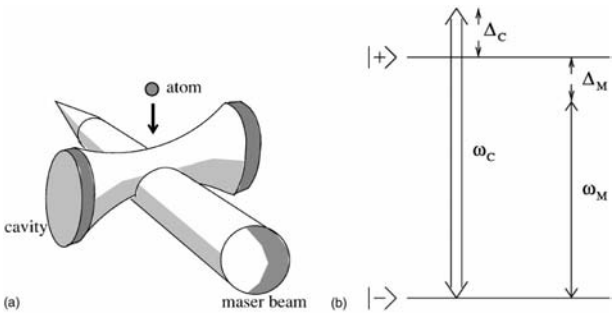

FIG. 1. Experimental configuration and level scheme of the atom.

lation of the evolution governed by the effective Hamiltonian and the final probabilities of the one and two-photon transfer states. Finally, in Sec. V we give some conclusions and indicate conditions for experimental implementation.

II. CONSTRUCTION OF THE EFFECTIVE HAMILTONIAN

We consider a two-level atom of upper and lower states $|+\rangle$ and $|-\rangle$ and of energy difference $E_+ - E_- = \omega_0$ as represented in Fig. 1. We use atomic units in which $\hbar = 1$. The atom in its lower state is released from a source of atoms and falls through a high-Q cavity with velocity v. The atom first encounters the vacuum mode of the cavity with frequency ω_C and waist W_C and then the maser beam with frequency ω_M and waist W_M. Both the maser and the cavity fields are near-resonant with the atomic transition. The distance between the crossing points of the cavity and the maser axis with the atomic trajectory is d. The traveling atom encounters time dependent and delayed Rabi frequencies of the cavity and the maser fields:

$$G(t) = -\mu \sqrt{\frac{\omega_C}{2\epsilon_0 V_{\text{mode}}}} \quad e^{-(vt/W_C)^2},$$

$$\Omega(t) = -\mu \mathcal{E}_M \quad e^{-[(vt-d)/W_M]^2}, \tag{1}$$

where μ, V_{mode}, $\mathcal{E}_M$ are, respectively, the dipole moment of the atomic transition, the effective volume of the cavity mode and the amplitude of the maser field. The detuning of the maser and the cavity fields from the atomic transition are $\Delta_i = \omega_0 - \omega_i$, $i = C, M$. We take the frequencies of the fields such that their difference $\delta = \omega_C - \omega_M$ is positive and very small with respect to ω_C and ω_M. Also we assume

$$\max\{|G(t)|, |\Omega(t)|\} \ll \omega_0. \tag{2}$$

Under these conditions, the counter-rotating terms can be discarded in the rotating-wave approximation (RWA). The semiclassical Hamiltonian of the atom-maser-cavity system can thus be written as

$$H(t, \theta_0 + \omega t) = \omega_C a^\dagger a \mathbb{1}_2 + \begin{pmatrix} \omega_0 & 0 \\ 0 & 0 \end{pmatrix} + G(t) \begin{pmatrix} 0 & a \\ a^\dagger & 0 \end{pmatrix} + \Omega(t)/2 \begin{pmatrix} 0 & e^{-i(\theta_0+\omega t)} \\ e^{i(\theta_0+\omega t)} & 0 \end{pmatrix}, \tag{3}$$

where $a, a^\dagger$ are the annihilation and creation operators of the cavity field, $\mathbb{1}_2$ is the 2×2 identity matrix and the phase θ_0 is the initial phase of the maser field. The periodic time dependence $(\theta_0 + \omega t)$ of the Hamiltonian (3) has been explicitly written for the convenient application of the Floquet theory below. The energy of the lower atomic state has been taken as 0. This Hamiltonian acts on the Hilbert space $\mathcal{H} \otimes \mathcal{F}$ where $\mathcal{H} = \mathbb{C}^2$ is the Hilbert space of the atom generated by $|\pm\rangle$ and $\mathcal{F}$ is the Fock space of the cavity mode generated by the orthonormal basis $\{|n\rangle; n = 0, 1, 2, \ldots\}$ with n the photon number of the cavity field. The dynamics of system is determined by the Schrödinger equation,

$$i \frac{\partial}{\partial t} \phi(t) = H(t, \theta_0 + \omega t) \phi(t), \tag{4}$$

where $\phi(t) \in \mathcal{H} \otimes \mathcal{F}$ with initial condition $\phi_0 = \phi(t_0) = |-\rangle \otimes |n = 0\rangle$. We can think of Eq. (4) as a family of equations parametrized by the phase θ_0. The time-dependent Hamiltonian (3) contains two different time scales: the period $T = 2\pi/\omega$ characterizing fast oscillations of the maser field and $T_{int} \approx W_M/v \approx W_C/v$ characterizing the slow change of the field amplitudes $G(t), \Omega(t)$. The fast periodic time-dependence can be taken into account by use of Floquet theory which consists in *lifting* the dynamics into an enlarged Hilbert space [22],

$$\mathcal{K} := \mathcal{H} \otimes \mathcal{F} \otimes \mathcal{L}, \tag{5}$$

where $\mathcal{L} := L_2(\mathbb{S}^1, d\theta/2\pi)$ denotes the space of square integrable functions of dynamical variable θ on the circle $\mathbb{S}^1$ of length 2π, with a scalar product

$$\langle f_1 | f_2 \rangle_{\mathcal{L}} := \int_0^{2\pi} \frac{d\theta}{2\pi} f_1^*(\theta) f_2(\theta). \tag{6}$$

This space is generated by the orthonormal basis $\{e^{ik\theta}; k \in \mathbb{Z}\}$. One can interpret k as the relative photon number with respect to the (large) average photon number $\bar{k}$ of the maser field. The evolution equation in the enlarged Hilbert space reads as

$$i \frac{\partial}{\partial t} \psi(t; \theta) = K(t; \theta) \psi(t; \theta), \tag{7}$$

with the Floquet Hamiltonian

$$K(t; \theta) = -i\omega_M \frac{\partial}{\partial \theta} \mathbb{1}_2 + H(t; \theta). \tag{8}$$

The operator $-i(\partial/\partial\theta)$ can be interpreted as the relative photon number operator of the maser field [23]. The only time dependence of the Floquet Hamiltonian is from the slow variation of the field amplitudes.

The relation between ϕ and ψ can be established as follows: if $\psi(t;\theta)$ is a solution of (7) with initial condition $\psi(t_0;\theta)=\phi_0\otimes\mathbf{1}_{\mathcal{L}}$, then

$$\phi(t)=\psi(t,\theta_0+\omega t) \tag{9}$$

is a solution of (4) with the initial condition $\phi(t_0)=\phi_0$. $\mathbf{1}_{\mathcal{L}}$ is the basis function $e^{ik\theta}$ with $k=0$. In Eq. (9), taking the fixed value of θ_0 for the dynamical variable θ means *returning* into the original Hilbert space $\mathcal{H}\otimes\mathcal{F}$.

The eigenvectors of the zero-field Floquet Hamiltonian are $|\pm,n,k\rangle=|\pm\rangle\otimes|n\rangle\otimes e^{ik\theta}$ which form an orthonormal basis of the enlarged Hilbert space $\mathcal{K}$. We remark that if at the end of interaction $t=t_f$, the solution of (7) has a form $\psi(t_f;\theta)=\chi\otimes e^{ik\theta}$ then $\phi(t_f)=\chi e^{ik(\theta_0+\omega t_f)}$ and the probability for the solution of (4) to be found in the final states $|\pm,n\rangle$, i.e., $|\langle\phi(t_f)|\pm,n\rangle|^2=|\langle\chi|\pm,n\rangle|^2$, will not depend on the optical phase $\theta_0+\omega t_f$ of the semiclassical Hamiltonian (3).

The evolution of (7) due to slow field amplitudes will be treated in the enlarged Hilbert space by adiabatic principles. We first show that the dynamics of (8) under the bichromatic interaction can be described by an effective Hamiltonian. We start by applying to the Floquet Hamiltonian (8) the unitary transformation,

$$R=\begin{pmatrix} e^{-i\theta} & 0\\ 0 & 1\end{pmatrix}, \tag{10}$$

which yields

$$\begin{aligned} K' &= R^{\dagger}KR\\ &= \omega_C a^{\dagger}a\mathbb{1}_2 - i\omega_M\frac{\partial}{\partial\theta}\mathbb{1}_2+\begin{pmatrix}\Delta_M & \Omega(t)/2\\ \Omega(t)/2 & 0\end{pmatrix}+G(t)\\ &\quad\times\begin{pmatrix}0 & a\,e^{i\theta}\\ a^{\dagger}e^{-i\theta} & 0\end{pmatrix}. \end{aligned} \tag{11}$$

The third term of K', denoted H_{RWA}, is the so-called RWA Hamiltonian, associated to the maser field and the atom. Its eigenvalues are $2\lambda_{\pm}^{(0)}=\Delta_M\pm\sqrt{(\Delta_M)^2+(\Omega)^2}$. To simplify and decouple the Hamiltonian (11), we use the phase representation of a and $a^{\dagger}$ as formulated by Bialynicki-Birula [24]:

$$a\to e^{-i\varphi}\sqrt{-i\frac{\partial}{\partial\varphi}},\quad a^{\dagger}\to\sqrt{-i\frac{\partial}{\partial\varphi}}e^{+i\varphi},\quad a^{\dagger}a\to -i\frac{\partial}{\partial\varphi}, \tag{12}$$

which gives

$$\begin{aligned} K' &= -i\omega_C\frac{\partial}{\partial\varphi}\mathbb{1}_2 - i\omega_L\frac{\partial}{\partial\theta}\mathbb{1}_2+H_{RWA}+G(t)\\ &\quad\times\begin{pmatrix}0 & e^{+i(\theta-\varphi)}\sqrt{-i\frac{\partial}{\partial\varphi}}\\ \sqrt{-i\frac{\partial}{\partial\varphi}}\,e^{-i(\theta-\varphi)} & 0\end{pmatrix}. \end{aligned} \tag{13}$$

Defining the new variables

$$\zeta:=\varphi-\theta,\quad \eta:=\theta, \tag{14}$$

we have

$$\frac{\partial}{\partial\varphi}=\frac{\partial}{\partial\zeta},\quad \frac{\partial}{\partial\theta}=\frac{\partial}{\partial\eta}-\frac{\partial}{\partial\zeta}. \tag{15}$$

The eigenbasis of $(-i(\partial/\partial\varphi)-i(\partial/\partial\theta))$ is $\{e^{in\varphi}e^{ik\theta};n=0,1,2,\ldots,k=0,\pm1,\pm2,\ldots\}$ which can be written as

$$e^{in\varphi}e^{ik\theta}=e^{in(\zeta+\eta)}e^{ik\eta}=e^{in\zeta}e^{i(n+k)\eta}=e^{in\zeta}e^{im\eta}, \tag{16}$$

where $m:=n+k=0,\pm1,\pm2,\ldots$. Substituting (15) in (13) gives

$$\begin{aligned} K' &= -i(\omega_C-\omega_M)\frac{\partial}{\partial\zeta}\mathbb{1}_2 - i\omega_M\frac{\partial}{\partial\eta}\mathbb{1}_2+H_{RWA}+G(t)\\ &\quad\times\begin{pmatrix}0 & e^{-i\zeta}\sqrt{-i\frac{\partial}{\partial\zeta}}\\ \sqrt{-i\frac{\partial}{\partial\zeta}}\,e^{+i\zeta} & 0\end{pmatrix}. \end{aligned} \tag{17}$$

We can define new operators as

$$b:=e^{-i\zeta}\sqrt{-i\frac{\partial}{\partial\zeta}},\quad b^{\dagger}:=\sqrt{-i\frac{\partial}{\partial\zeta}}e^{+i\zeta}, \tag{18}$$

which verify the standard commutation relations $[b,b^{\dagger}]=1$. The new bosonic operator b that corresponds to the process of creation of a cavity photon and associated annihilation of a maser photon can be intuitively interpreted as the transformation of a maser photon into a cavity photon. The Hamiltonian (17) can thus be expressed as

$$K'=-i\omega_M\frac{\partial}{\partial\eta}\mathbb{1}_2+H^{\mathrm{eff}}, \tag{19}$$

where H^{eff} is the reduced effective Hamiltonian,

$$H^{\mathrm{eff}}(t)=\delta b^{\dagger}b\mathbb{1}_2+\begin{pmatrix}\Delta_M & \Omega(t)/2\\ \Omega(t)/2 & 0\end{pmatrix}+G(t)\begin{pmatrix}0 & b\\ b^{\dagger} & 0\end{pmatrix}. \tag{20}$$

K' is defined on the Hilbert space generated by the orthonormal basis $\{|\pm\rangle\otimes e^{in\zeta}\otimes e^{im\eta};n=0,1,2,\ldots;m=0,\pm1,\pm2,\ldots\}$ and H^{eff} is defined on the Hilbert space generated by the orthonormal basis $\{|\pm\rangle\otimes e^{in\zeta};n=0,1,2,\ldots\}$ where n is the number of exchanged photons from the maser field into the cavity field.

III. TOPOLOGY OF THE DRESSED EIGENENERGY SURFACES

The dressed eigenenergy surfaces of K' (19) can be calculated numerically and can be displayed as a function of the normalized Rabi frequencies G/δ and Ω/δ. These surfaces are grouped in families for different values of m, each of which for zero fields consists an infinite set of eigenvalues with equal spacing Δ_M. In what follows, we study the $m=0$ family only which means $k=-n$ ($k\in\mathbb{Z}$ is the relative photon number of the maser field and $n\geqslant 0$ is the photon number of the cavity field). The labeling of the dressed eigenenergy surfaces can be performed in terms of the eigenvectors of the zero-field original Hamiltonian,

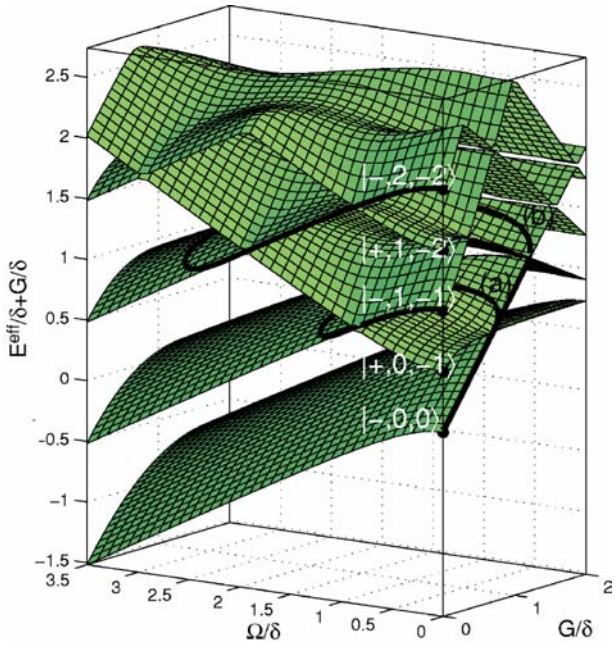

FIG. 2. The first five eigenenergy surfaces (in units of δ) of H^{eff} as functions of G and Ω for $\delta=2\Delta_M=-2\Delta_C$. The term G has been added to E^{eff} for clarity of display. The solid paths (a),(b) correspond to adiabatic evolutions which start from the $|-,0,0\rangle$ state and end at $|-,1,-1\rangle$ and $|-,2,-2\rangle$, respectively.

$$K'(\Omega=0,G=0)=\left(\delta b^{\dagger}b-i\omega_M\frac{\partial}{\partial\eta}\right)\mathbb{1}_2+\begin{pmatrix}\Delta_M & 0\\ 0 & 0\end{pmatrix}, \tag{21}$$

with eigenvalues

$$E'_{+,n,m}(\Omega=0,G=0)=\delta n+m\omega_M+\Delta_M,$$

$$E'_{-,n,m}(\Omega=0,G=0)=\delta n+m\omega_M. \tag{22}$$

Since the eigenvectors of K and K' are related by the transformation (10) as $|\varphi\rangle=R|\varphi\rangle'$, the correspondence between the eigenvalues of the zero-field effective Hamiltonian and the eigenvectors of the original zero-field Hamiltonian are

$$E'(\Omega=0,G=0)_{+,n,m=0}\Leftrightarrow|+,n\rangle'=|+,n,-n-1\rangle,$$

$$E'(\Omega=0,G=0)_{-,n,m=0}\Leftrightarrow|-,n\rangle'=|-,n,-n\rangle. \tag{23}$$

Figure 2 represents the $m=0$ family of the eigenenergy surfaces of K' as a function of the instantaneous normalized Rabi frequencies G/δ and Ω/δ. Any two neighboring surfaces have conical intersections on the plane $G=0$ and also on the plane $\Omega=0$ (except the first surface), corresponding to the situations where only one of the fields (maser or cavity) is interacting with the atom. The topology of these surfaces, determined by the conical intersections, presents insight into the various atomic population and photon transfers from the maser field into the cavity field that can be produced by designing an appropriate path connecting the initial and the chosen final states. Each path corresponds to a choice of the envelope of the pulses. In the adiabatic limit, when the pulses vary sufficiently slowly, the solution of the time-dependent dressed Schrödinger equation follows the instantaneous dressed eigenvectors, following the path on the surface that is continuously connected to the initial state. We start with the dressed state $|-,0,0\rangle$, i.e., the lower atomic state with zero photons in the cavity field. Its energy is shown in Fig. 2 as the starting point of the various paths. The paths shown in Fig. 2 describe accurately the dynamics if the time dependence of the envelopes is slow enough according to the Landau-Zener [25,26] and Dykhne-Davis-Pechukas [27,28] analysis. If two (uncoupled) eigenvalues cross, the adiabatic theorem of Born and Fock [29] shows that the dynamics follows diabatically the crossing. This implies that the various dynamics shown in Fig. 2 are a combination of a global adiabatic passage around the conical intersections and local diabatic evolutions through (or in the neighborhood) of conical intersections of the eigenenergy surfaces [30].

We consider the action of two smooth pulses, associated with the Rabi frequencies $G(t)$ and $\Omega(t)$, which act on the two-level atom with a time delay $\tau=d/v$. Figure 2 shows two examples of the adiabatic paths of different peak amplitudes of the Rabi frequencies and leading to two different photon transfers into the cavity field without changing the atomic population at the end of the interaction. Each of the two black paths [labeled (a) and (b)] corresponds to a sequence of two smooth pulses, shown in Figs. 3(a) and 3(c), of equal length T_{int} and different peak Rabi frequencies $\Omega_{\max},G_{\max}$, separated by a delay such that the cavity pulse interacts before the maser pulse.

For the path (a), the dynamics goes through the first intersection (on the $\Omega=0$ plane) between the first and the second surfaces, but not the second intersection between the second and the third surface. The crossing of the first intersection as G increases with $\Omega=0$, brings the dressed system into the second eigenenergy surface. Turning on and increasing the amplitude Ω (while G decreases) moves the path across this surface. When the maser field decreases, the curve crosses another intersection between the second and the third surface (with $G=0$) that brings the system to the third surface, on which the path (a) stays until the end of the pulse Ω. The transfer state is finally connected to the state $|-,1,-1\rangle$: there is no final transfer of atomic population, but one ω_M photon has been absorbed from the maser field and one ω_C photon has been emitted into the cavity field at the end of the process. The path (b) allows the dynamics (on the $\Omega=0$ plane) to go through the second intersection, but not the third intersection. The next two intersections of the path (b) are located (on the plane $G=0$) between the third and the fourth and between the fourth and the fifth eigenenergy surfaces and the system is finally connected to the state $|-,2,-2\rangle$: there is again no final transfer of atomic population, but two ω_M photons have been absorbed from the maser field and two ω_C photons have been emitted into the cavity field at the end of the process. If the peak amplitudes are taken even larger such that n conical intersections (dynamical resonances) are crossed when G rises with $\Omega=0$ and then n intersection are crossed when Ω decreases with $G=0$, the final state of the system will be $|-,n,-n\rangle$, i.e., the emission of n ω_C photons into the cavity field and the absorbtion of n ω_M

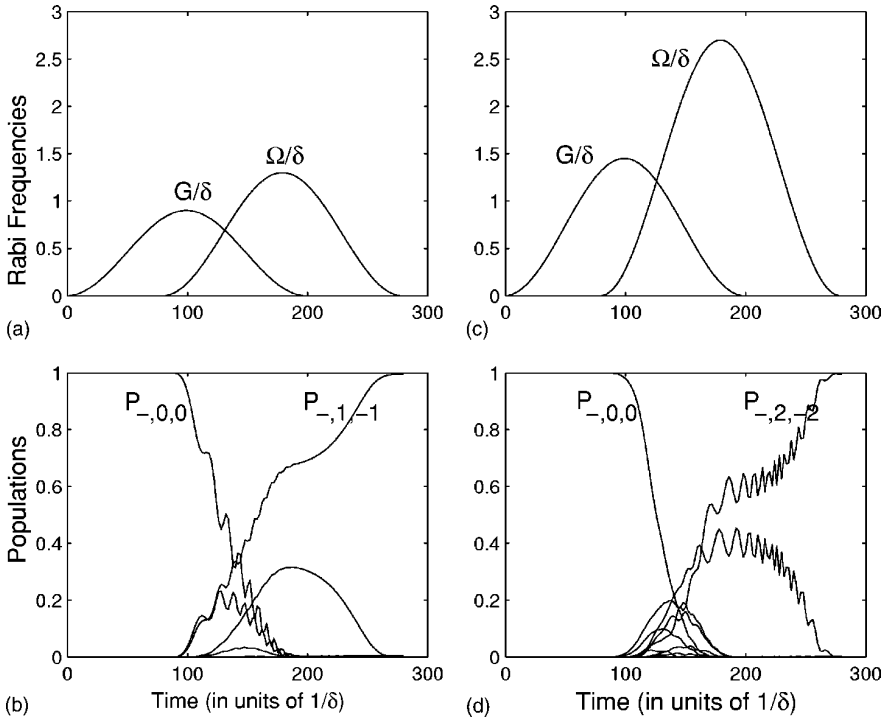

FIG. 3. (a) and (c) Normalized Rabi frequencies with different values of amplitudes for one-photon and two-photon transfers as a function of time. (b) and (d) Time evolution of the populations for one- and two-photon transfers.

photons from the maser field, with no final atomic population transfer. The analysis of the eigenenergy surfaces allows one to determine adapted amplitudes of the Rabi frequencies which will permit to transfer n photons into the cavity field in a robust way.

IV. NUMERICAL SIMULATION

The time evolution of the system for each family of the eigenenergy surfaces is given by the Schrödinger equation

$$i\frac{\partial}{\partial t}\Phi(t) = H^{\text{eff}}(t)\Phi(t). \tag{24}$$

The time dependence of the Rabi frequencies are delayed Gaussians of the form (1). Figures 3(a) and 3(c) show the profile of the Rabi frequencies as functions of time for one-photon and two-photon transfer with an interaction time (full width at half maximum) $T_{\text{int}}=66/\delta$ and a time delay $\tau=57/\delta$. The adapted amplitudes of the Rabi frequencies for n-photon $(n=1,2)$ transfer correspond to the paths (a) and (b) in Fig. 2. The condition for global adiabaticity $|\Delta_{M,C}|T_{\text{int}}=(\delta/2)T_{\text{int}}=33\gg 1$ is well satisfied. Figures 3(b) and 3(d) present the time evolution of populations calculated numerically by solving (24). The atom-maser-cavity system in the initial state $|-,0,0\rangle$ with the suitable forms of Rabi frequencies [Figs. 3(a) and 3(c)] evolves to the finale states $|-,1,-1\rangle$ and $|-,2,-2\rangle$, respectively, with probabilities of $P_{-,1,-1}=|\langle -,1,-1|\Phi(t_f)\rangle|^2=0.99$ and $P_{-,2,-2}=|\langle -,2,-2|\Phi(t_f)\rangle|^2=0.98$.

Figure 4 displays the contour plot of the final population as a function of the normalized Rabi frequencies for one- and two-photon transfers. The white regions represent the adapted values of the Rabi frequencies for which the final probability of one- and two-photon transfers are maximal. This figure shows that the bichromatic adiabatic passage is more robust with respect to the maser Rabi frequency than with respect to the cavity one. The reason comes back to the special structure of the dressed eigenenergy surfaces in Fig. 2. We can see that on the $G=0$ plane, between the first surface and the second one there is not any intersection and between the nth surface and its neighboring surfaces there are $(n-1)$ intersections, i.e., after the $(n-1)$th intersection there are no others. On the other hand on the $\Omega=0$ plane, as the value of G increases, the distance between neighboring intersections decreases. In general, as the distance of conical intersections between neighboring surfaces decreases, the robustness of the adiabatic passage is also decreased.

V. DISCUSSION AND CONCLUSIONS

Using the topological properties of dressed eigenenergy surfaces of the effective Hamiltonian of the atom-maser-cavity system, we have determined adiabatic paths to transfer n photons from the maser field into the cavity field to generate a n-photon Fock state. The realization of parameters satisfying the conditions of the proposed scheme appears feasible with progressive improvements to experiments with high-Q microwave cavities. In this analysis we have assumed that the interaction time between the two-state atom and the fields is short compared to the cavity lifetime T_{cav} and the atom's excited state lifetime T_{at}, i.e., $T_{\text{int}}\ll T_{\text{cav}}, T_{\text{at}}$, which

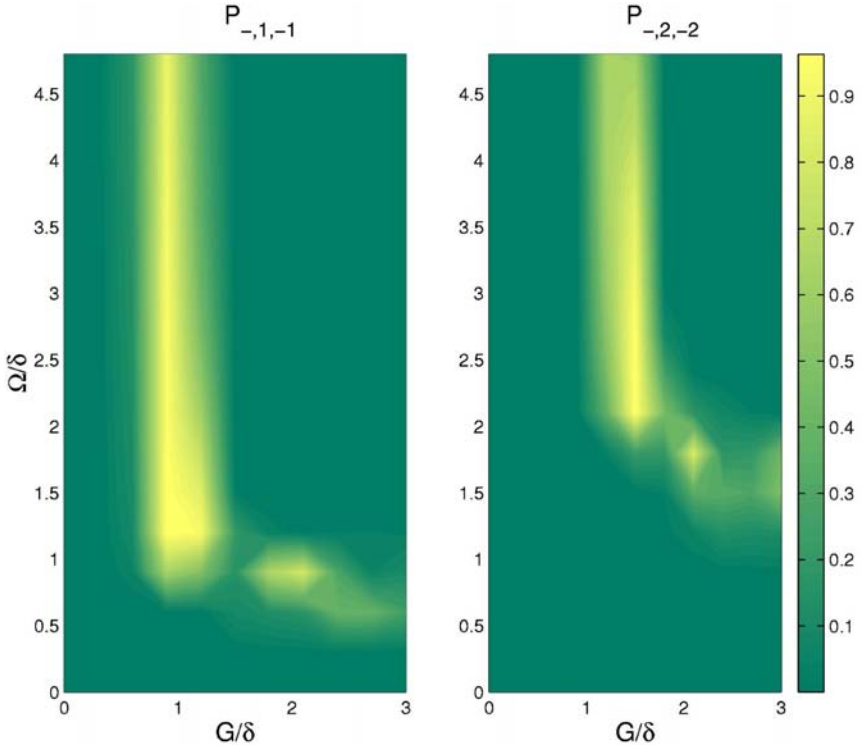

FIG. 4. The contour plot of the populations $P_{-,1,-1}$ and $P_{-,2,-2}$ for one-photon and two-photon transfers as a function of normalized Rabi frequencies. White areas correspond to the approximately complete population transfer.

are essential for an experimental setup and avoiding decoherence effects. In the microwave domain, the radiative lifetime of circular Rydberg states—of the order of $T_{at}=30$ ms—are much longer than those for noncircular Rydberg states. The typical value of the cavity lifetime is of the order of $T_{cav}=1$ ms (corresponding to $Q=3\times10^8$) and the upper limit of interaction time is $T_{int}=100$ μs (atom with a velocity of 100 m/s with the cavity mode waist of $W_C=6$ mm) [31]. The condition of global adiabaticity $G_{max}\,T_{int}\gg1$ for the typical value of $G_{max}\approx0.15$ MHz [31] is well satisfied ($G_{max}\,T_{int}\approx15$). Numerics (Figs. 3 and 4) shows additionally that the diabatic dynamics through the conical intersections of Fig. 2 is also satisfied.

Moreover the decay rate of the cavity is scaled with the number of photons present in the cavity ($T_{int}\ll T_{cav}/n$) which suggests the need to cavities with higher Q factor for producing large Fock states. Closed cavities with $Q=4\times10^{10}$ and longer decay time $T_{cav}=0.3$ s may also be used [32]. The external field can be introduced in these cavities as it is done currently in experiments related to the measurement of the phase diffusion process [33].

ACKNOWLEDGMENTS

M.A-T. gratefully acknowledges the financial support of the French Society SFERE and the MSRT of Iran. We acknowledge support from the Conseil Régional de Bourgogne and the Centre de Ressources Informatiques de l'Université de Bourgogne.

[1] T. Jennewein, C. Simon, G. Weihs, H. Weinfurter, and A. Zeilinger, Phys. Rev. Lett. **84**, 4729 (2000).

[2] D. S. Naik, C. G. Peterson, A. G. White, A. J. Berglund, and P. G. Kwiat, Phys. Rev. Lett. **84**, 4733 (2000).

[3] W. Tittel, J. Brendel, H. Zbinden, and N. Gisin, Phys. Rev. Lett. **84**, 4737 (2000).

[4] D. Bouwmeester, J. W. Pan, K. Mattle, M. Eibl, H. Weinfurter, and A. Zeilinger, Nature (London) **390**, 575 (1997).

[5] C. Brunel, B. Lounis, P. Tamarat, and M. Orrit, Phys. Rev. Lett. **83**, 2722 (1999).

[6] B. Lounis and W. E. Moerner, Nature (London) **407**, 491 (2000).

[7] A. Beveratos, S. Kuhn, R. Brouri, J. P. Poizat, and P. Grangier, Eur. Phys. J. D **18**, 191 (2002).

[8] J. Kim, O. Benson, H. Kan, and Y. Yamamoto, Nature (London) **397**, 500 (1999).

[9] C. Santori, M. Pelton, G. S. Solomon, Y. Dale, and Y. Yamamoto, Phys. Rev. Lett. **86**, 1502 (2001).

[10] P. Michler, A. Kiraz, C. Becher, W. V. Schoenfeld, P. M. Petroff, L. Zhang, E. Hu, and A. Imamoğlu, Science **290**, 2282

(2000).
[11] X. Maître, E. Hagley, G. Nogues, C. Wunderlich, P. Goy, M. Brune, J. M. Raimond, and S. Haroche, Phys. Rev. Lett. **79**, 769 (1997).
[12] B. T. H. Varcoe, S. Brattke, M. Weidinger, and H. Walther, Nature (London) **403**, 743 (2000).
[13] M. Hennrich, T. Legero, A. Kuhn, and G. Rempe, Phys. Rev. Lett. **85**, 4872 (2000).
[14] A. S. Parkins, P. Marte, P. Zoller, O. Carnal, and H. J. Kimble, Phys. Rev. A **51**, 1578 (1995).
[15] S. Q. Gong, R. Unanyan, and K. Bergmann, Eur. Phys. J. D **19**, 257 (2002).
[16] P. Domokos, M. Brune, J. M. Raimond, and S. Haroche, Eur. Phys. J. D **1**, 1 (1998).
[17] P. Bertet, S. Osnaghi, P. Milman, A. Auffeves, P. Maioli, M. Brune, J. M. Raimond, and S. Haroche, Phys. Rev. Lett. **88**, 143601 (2002).
[18] M. F. Santos, E. Solano, and R. L. de Matos Filho, Phys. Rev. Lett. **87**, 093601 (2001).
[19] N. V. Vitanov, T. Halfmann, B. W. Shore, and K. Bergmann, Annu. Rev. Phys. Chem. **52**, 763 (2001).
[20] S. Guérin, L. P. Yatsenko, and H. R. Jauslin, Phys. Rev. A **63**, 031403 (2001).
[21] S. Guérin and H. R. Jauslin, Adv. Chem. Phys. **125**, 147 (2003).
[22] H. Sambe, Phys. Rev. A **7**, 2203 (1973).
[23] S. Guérin, F. Monti, J. M. Dupont, and H. R. Jauslin, J. Phys. A **30**, 7193 (1997).
[24] I. Bialynicki-Birula and Z. Bialynicka-Birula, Phys. Rev. A **14**, 1101 (1976).
[25] L. D. Landau, Phys. Z. Sowjetunion **2**, 46 (1932).
[26] C. Zener, Proc. R. Soc. London, Ser. A **137**, 696 (1932).
[27] A. M. Dykhne, Sov. Phys. JETP **14**, 941 (1962).
[28] J. P. Davis and P. Pechukas, J. Chem. Phys. **64**, 3129 (1976).
[29] M. Born and V. Fock, Z. Phys. **51**, 165 (1928).
[30] L. P. Yatsenko, S. Guérin, and H. R. Jauslin, Phys. Rev. A **65**, 043407 (2002).
[31] J. M. Raimond, M. Brune, and S. Haroche, Rev. Mod. Phys. **73**, 565 (2001).
[32] S. Brattke, B. T. H. Varcoe, and H. Walther, Phys. Rev. Lett. **86**, 3534 (2001).
[33] F. Casagrande, A. Ferraro, A. Lulli, R. Bonifacio, E. Solano, and H. Walther, Phys. Rev. Lett. **90**, 183601 (2003).

Chapter 14

Entangling spins, photons and atoms by adiabatic passage

One of the striking non-classical aspects of a quantum system made of N objects is entanglement, for which the state vector of the system cannot be written, in any basis, as a tensor product of independent substates. The generation and the controlled manipulation of entangled states of N-particle systems is fundamental for the study of basic aspects of quantum theory [234, 235]. The idea is to apply a set of controlled coherent interactions to the particles (atoms, ions, photons) of the system in order to bring them into a tailored entangled state. The physics of entanglement provides the basis of applications such as quantum information processing and quantum communications. Very recently teleportation of quantum states has been realized [236, 237] using atom-atom entanglement following the proposal of Bennett *et al.* [238]. Particles can then be viewed as carriers of quantum bits of information and the realization of engineered entanglement is an essential ingredient of the implementation of quantum gates [239].

Most experimental realizations of entanglement have been implemented with photons. Although the individual polarization states of photons are easily controlled, and their quantum coherence can be preserved over many kilometers of an optical fiber [240], photons cannot be stored for long times, and manipulations of collective entangled states present considerable difficulties even when the photons are confined in the same cavity. The creation of long lived entangled pairs with atoms, on the other hand, is a relatively recent pursuit which may provide reliable quantum information storage. The entangled state of a pair of two-level atoms using pulse area techniques in a microwave cavity has been realized by Hagley *et al.* [241] based on the proposal of Cirac and Zoller [242] (see appendix A). However the pulse area technique is not robust with respect to the velocity of the atoms and the exact-resonance condition. Recently a different scheme has been proposed [229] to entangle two atoms using a tripod STIRAP technique in a four-level atom-cavity-laser system in which one of the pulses corresponds to the field of a cavity-mode. Manipulation of entanglement of two atoms in this scheme, however, requires to control a geometric phase via an integral of Hamiltonian parameters over a closed path in parameter space which is difficult in experimental implementations. The generation of atom-photon entanglement has also been proposed in [243] in a tripod-like laser-atom-cavity system which sustains two cavity modes.

The f-STIRAP is a variation of STIRAP which allows the creation of any preselected coherent superposition of the two degenerate ground states (see Subsection 8.2.2). As in STIRAP, the Stokes pulse linking the initially unpopulated states $|e\rangle$ and $|g_2\rangle$, arrives before the pump pulse linking the initially populated state $|g_1\rangle$ to the excited state $|e\rangle$, but unlike STIRAP where

the Stokes pulse vanishes first, here the two pulses vanish simultaneously while maintaining a constant finite ratio of amplitudes. The advantage of STIRAP is its robustness with respect to the precise tuning of pulse areas, pulse delay, pulse widths, pulse shapes, and detunings. Since f-STIRAP requires a precise ratio of pulse endings, it is not as robust as STIRAP if two different Stokes and pump pulses are used. However in specific circumstances where two laser pulses, one with elliptic polarization and another with σ^- circular polarization are used, f-STIRAP can be made as robust as STIRAP [79]. In f-STIRAP as in STIRAP, if the evolution is adiabatic (for instance with a slow transit of atoms across cw fields), the dynamics of the system follows an adiabatic dark state which does not involve the excited atomic state $|e\rangle$. Therefore this technique is immune to the detrimental consequences of atomic spontaneous emission. The STIRAP technique has interesting applications in the generation of coherent superposition of Fock states [228, 138] and of maximally polarization-entangled photon states [244] in an optical cavity.

14.1 Adiabatic creation of entangled states by a bichromatic field designed from the topology of the dressed eigenenergies

In this section, we propose a simple method for entangling two spins by a bichromatic process [245], using a model introduced in [246]. The bichromatic property is used to show nonintuitive possibilities of entanglement.

PHYSICAL REVIEW A, **66**, 032311 (2002)

Adiabatic creation of entangled states by a bichromatic field designed from the topology of the dressed eigenenergies

S. Guérin,[1,*] R. G. Unanyan,[2,3] L. P. Yatsenko,[4,†] and H. R. Jauslin[1]
[1]*Laboratoire de Physique, UMR CNRS 5027, Université de Bourgogne, Boîte Postale 47870, 21078 Dijon, France*
[2]*Fachbereich Physik, Universität Kaiserslautern, 67653 Kaiserslautern,Germany*
[3]*Institute for Physical Research, Armenian National Academy of Sciences, 378410 Ashtarak, Armenia*
[4]*Institute of Physics of the Ukrainian Academy of Sciences, prospekt Nauky, 46, 252650 Kiev-22, Ukraine*
(Received 28 February 2002; published 18 September 2002)

Preparation of entangled pairs of coupled two-state systems driven by a bichromatic external field is studied. We use a system of two coupled spin-$\frac{1}{2}$ particles that can be translated into a three-state ladder model whose intermediate state represents the entangled state. We show that this entangled state can be prepared in a robust way with appropriate fields. Their frequencies and envelopes are derived from the topological properties of the model.

DOI: 10.1103/PhysRevA.66.032311 PACS number(s): 03.67.−a, 42.50.Hz, 03.65.Ta

I. INTRODUCTION

Entanglement is a key concept in various contemporary areas of active research in quantum physics. It explicitly demonstrates the nonlocal character of quantum theory, having potential applications in quantum communication, cryptography, and computation [1]. The preparation of an entangled state is of great interest for both fundamental and applied reasons. During the last few years various methods for preparation of entangled states of atomic systems have been proposed and some of them experimentally demonstrated [2,3].

Although a quantum system can be manipulated by tailored sequences of resonant pulses of precise area, in particular, π and $\pi/2$ pulses, respectively, for the complete inversion and the equal weight coherent superposition, deviations from the precise pulse area and from resonance can lead to significant errors. Adiabatic passage techniques provide much greater robustness against fluctuations in the interaction parameters. The stimulated Raman adiabatic passage (STIRAP) method [4] has been proposed for the creation of an entangled state of two three-level atoms in a QED cavity [5] and for Λ atomic systems [6].

In this paper we propose a simple method for entangling two subsystems driven by pulse-shaped external fields. For definiteness, we take these to be two identical spins interacting with each other and driven by radio-frequency fields. This system can be translated in a three-level ladder model with the intermediate level corresponding to the entangled state [7]. The goal is to populate completely this entangled state at the end of the pulses by adiabatic passage. The most efficient couplings are obtained with two near one-photon resonant fields. We will show that unlike in the STIRAP process, one- and two-photon detunings are required to populate most efficiently the intermediate level.

We show furthermore that bichromatic effects play an important role, due to the small anharmonicity of the system. The anharmonicity of the equivalent three-level ladder system is determined by the interaction of the spins. It can be in general small enough such that the standard rotating wave approximation (RWA), allowing to assign each field to a unique transition, cannot be applied. In this case one needs to take full account of the bichromatic effects (see, e.g., Ref. [8]). We will show robust regions of field parameters that will generate the entangled state by adiabatic passage below and beyond the standard RWA.

In Sec. II, we describe the model of the two-spin system driven by a bichromatic external field and how it leads to an equivalent three-level system. In Sec. III, we show the result of numerical simulations, for which we develop in later sections a detailed interpretation by constructing adapted effective Hamiltonians that take into account the dominating resonant or quasiresonant effects. In Sec. IV, we derive the Floquet Hamiltonian required to study the system of spins dressed by the external fields. Sections V and VI are devoted to derive relevant effective dressed Hamiltonians for different regions of parameters, respectively, in the weak field regime (below the RWA) and in the strong field regime (beyond the RWA). We finally conclude in Sec. VII.

II. THE MODEL: TWO-SPIN SYSTEM IN EXTERNAL FIELDS

We consider two-spin-$\frac{1}{2}$ particles of the same gyromagnetic ratio μ, coupled by a magnetic dipolar interaction. In a time-dependent magnetic field $\mathbf{B}(t)=[B_x(t),B_y(t),B_z]$, the Hamiltonian of this system reads ($\hbar=1$),

$$\hat{\mathsf{H}}(t)=\hat{\mathsf{H}}_0+\mu\mathbf{B}(t)\cdot(\hat{\mathbf{S}}_1+\hat{\mathbf{S}}_2), \tag{1}$$

where

$$\hat{\mathsf{H}}_0=4\xi\hat{S}_1^z\otimes\hat{S}_2^z-\xi(\hat{S}_{1+}\otimes\hat{S}_{2-}+\hat{S}_{1-}\otimes\hat{S}_{2+}) \tag{2}$$

is the part describing the magnetic dipolar spin-spin interaction, with ξ the magnetic dipolar interaction constant, $\hat{\mathbf{S}}_k=[\hat{S}_k^x,\hat{S}_k^y,\hat{S}_k^z]$ the kth spin operator ($k=1,2$), and $\hat{S}_{k\pm}=\hat{S}_k^x\pm i\hat{S}_k^y$. We assume that the static magnetic field B_z in the z

*Email address: sguerin@u-bourgogne.fr
†Present address: Institute of Physics, National Academy of Sciences of Ukraine, prospekt Nauky, 46, 06350, Kiev-39, Ukraine.

direction is strong enough ($|\mu B_z| \gg |\xi|$) so that the Hamiltonian $\hat{\mathsf{H}}_0$ (2) is justified for this case of identical gyromagnetic ratio μ.

We first construct the general equivalent three-level model driven by external fields and next derive the approximate Hamiltonian that takes into account the bichromatic effects by improving the standard rotating wave approximation.

We remark that the effective Hamiltonian we obtain in Eq. (11) applies also to a spin interaction of the form $\hat{\mathsf{H}}_0' = 4\zeta \hat{S}_1^z \otimes \hat{S}_2^z$.

A. The three-level model

In the spin product state space $\{|m\rangle_1|m\rangle_2\}$ $(m=\downarrow,\uparrow)$, where the states $|\downarrow\rangle_k$ and $|\uparrow\rangle_k$ denote, respectively, the spin-down and spin-up states of the kth spin, a complete basis of orthonormalized eigenstates of $\hat{\mathsf{H}}_0$ is given by

$$|\downarrow\downarrow\rangle \equiv |\downarrow\rangle_1|\downarrow\rangle_2, \tag{3a}$$

$$|\downarrow\uparrow^+\rangle \equiv \frac{1}{\sqrt{2}}[|\downarrow\rangle_1|\uparrow\rangle_2 + |\uparrow\rangle_1|\downarrow\rangle_2], \tag{3b}$$

$$|\uparrow\uparrow\rangle \equiv |\uparrow\rangle_1|\uparrow\rangle_2, \tag{3c}$$

$$|\downarrow\uparrow^-\rangle \equiv \frac{1}{\sqrt{2}}[|\downarrow\rangle_1|\uparrow\rangle_2 - |\uparrow\rangle_1|\downarrow\rangle_2]. \tag{3d}$$

In this basis, the Hamiltonian (1) with $\hat{\mathsf{H}}_0$ of Eq. (2) can be exactly expressed in the block-matrix form

$$\mathsf{H}(t) = \begin{bmatrix} \mathsf{H}_c(t) & \mathbf{0} \\ \mathbf{0} & 0 \end{bmatrix}, \tag{4}$$

where

$$\mathsf{H}_c = \begin{bmatrix} \xi - \beta_z & \frac{1}{\sqrt{2}}(\beta_x + i\beta_y) & 0 \\ \frac{1}{\sqrt{2}}(\beta_x - i\beta_y) & -2\xi & \frac{1}{\sqrt{2}}(\beta_x + i\beta_y) \\ 0 & \frac{1}{\sqrt{2}}(\beta_x - i\beta_y) & \xi + \beta_z \end{bmatrix} \tag{5}$$

with $\beta \equiv [\beta_x, \beta_y, \beta_z] = \mu \mathbf{B}$. The state $|\downarrow\uparrow^-\rangle$ is thus decoupled from the other states; it describes the evolution of a spin-0 singlet in a time-dependent magnetic field. This decoupling justifies our choice of the basis. The other three states $|\downarrow\downarrow\rangle$, $|\downarrow\uparrow^+\rangle$, and $|\uparrow\uparrow\rangle$ are coupled by the transverse (xy) magnetic field. To complete the definition of the problem, we suppose that initially the two-spin system is in the unentangled state $|\downarrow\downarrow\rangle$. Our goal is to establish the conditions leading to the most efficient robust transfer into the entangled state $|\downarrow\uparrow^+\rangle$.

We consider the case when the spin system interacts with a constant magnetic field in the z direction and two radio-frequency fields of respective frequencies ω_1 and ω_2 in the x direction,

$$\beta_z = \text{const}, \tag{6a}$$

$$\beta_x = \Omega_1(t)\cos(\omega_1 t + \theta_1) + \Omega_2(t)\cos(\omega_2 t + \theta_2), \tag{6b}$$

$$\beta_y = 0, \tag{6c}$$

where we assume positive Ω_1 and Ω_2. The state vector $\phi(t)$ is solution of the Schrödinger equation $i(d/dt)\phi(t) = \mathsf{H}_c(t)\phi(t)$ with the Hamiltonian $\mathsf{H}_c(t)$ (5) written in the basis $\{|\downarrow\downarrow\rangle, |\downarrow\uparrow^+\rangle, |\uparrow\uparrow\rangle\}$. When the radio-frequency fields are off ($\beta_x = 0$)), we have thus the following energies $E_{\downarrow\downarrow} \equiv \xi - \beta_z$, $E_{\downarrow\uparrow^+} \equiv -2\xi$, and $E_{\uparrow\uparrow} \equiv \xi + \beta_z$. Without loss of generality we assume $\xi < 0$ and $\beta_z > 0$, leading for a strong enough static magnetic field B_z such that $\beta_z = \mu B_z > 3|\xi|$ to a ladder configuration $E_{\downarrow\downarrow} < E_{\downarrow\uparrow^+} < E_{\uparrow\uparrow}$, whose anharmonicity is given by

$$a \equiv [(E_{\uparrow\uparrow} - E_{\downarrow\uparrow^+}) - (E_{\downarrow\uparrow^+} - E_{\downarrow\downarrow})]/2 = 3\xi. \tag{7}$$

We apply near resonant fields $\omega_1 \approx E_{\downarrow\uparrow^+} - E_{\downarrow\downarrow}$, $\omega_2 \approx E_{\uparrow\uparrow} - E_{\downarrow\uparrow^+}$, i.e., with the detunings Δ_1 and Δ_2,

$$\omega_1 \equiv -3\xi + \beta_z - \Delta_1, \tag{8a}$$

$$\omega_2 \equiv 3\xi + \beta_z - \Delta_2. \tag{8b}$$

B. The bichromatic rotating wave approximation

According to the RWA, one can neglect nonresonant counter-rotating terms under the conditions $\omega_{1,2} \gg \Omega_{1,2}$. The rotating wave transformation

$$\mathsf{R} = \begin{bmatrix} e^{-iE_{\downarrow\downarrow}t} & 0 & 0 \\ 0 & e^{-i(E_{\downarrow\downarrow}+\omega_1)t} & 0 \\ 0 & 0 & e^{-i(E_{\downarrow\downarrow}+\omega_1+\omega_2)t} \end{bmatrix} \tag{9}$$

leads to the state vector $\tilde{\phi}(t) = \mathsf{R}^\dagger \phi(t)$ (whose coefficients have the same absolute values as the ones of ϕ) that satisfies the Schrödinger equation

$$i\frac{d}{dt}\tilde{\phi}(t) = \tilde{\mathsf{H}}_c(t)\tilde{\phi}(t), \tag{10}$$

with the Hamiltonian $\tilde{\mathsf{H}}_c = \mathsf{R}^\dagger \mathsf{H}_c \mathsf{R} - i(\partial \mathsf{R}^\dagger/\partial t)\mathsf{R}$, where only the quasiresonant terms have been kept,

$$\tilde{\mathsf{H}}_c = \frac{1}{2}\begin{bmatrix} 0 & \Omega_1 & 0 \\ \Omega_1 & 2\Delta_1 & \Omega_2 \\ 0 & \Omega_2 & 2(\Delta_1+\Delta_2) \end{bmatrix} + \frac{1}{2}\begin{bmatrix} 0 & e^{-i\delta t}\Omega_2 & 0 \\ e^{i\delta t}\Omega_2 & 0 & e^{i\delta t}\Omega_1 \\ 0 & e^{-i\delta t}\Omega_1 & 0 \end{bmatrix}. \tag{11}$$

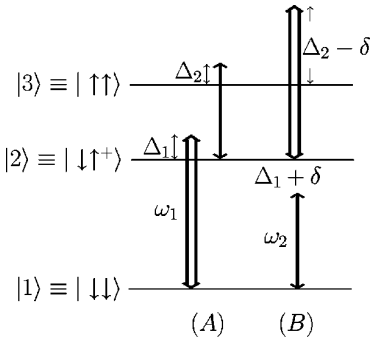

FIG. 1. Diagram of linkage patterns between the three states showing the different couplings. Note that Δ_1 and Δ_2 have been chosen negative here.

The frequency

$$\delta \equiv \omega_1 - \omega_2 = -6\xi + \Delta_2 - \Delta_1 \tag{12}$$

characterizes the *coupling ambiguity* [8]. Note that the standard RWA, for which $\Omega_1, \Omega_2 \ll |\delta|$, corresponds to keeping only the first term in the Hamiltonian (11) if the field 1 (field 2) is resonant with the 1-2 transition (2-3 transition). The full Hamiltonian $\tilde{\mathsf{H}}_c$ allows both fields to couple the two transitions when the field amplitudes Ω_1 and Ω_2 are not small compared to $|\delta|$. The competing coupling schemes are depicted in Fig. 1 . Two limit channels can thus be exhibited, each of which can be given by a standard RWA: the channel A shown in the left part of Fig. 1 (channel B shown in right part of Fig. 1) corresponds to the situation when the field 1 (field 2) couples *only* the 1-2 transition and the field 2 (field 1) couples *only* the 2-3 transition.

The standard RWA can be made if $\Omega_{\max} \ll |a|$, where $\Omega_{\max}$ is the peak Rabi frequency for Ω_i, $i=1,2$. Furthermore, adiabatic passage will require the standard condition $\Omega_{\max}\tau \gg 1$, where τ represents the time of interaction. A standard weak interaction ξ of the order of 100 Hz will thus require a time of interaction of the order of 1 s to satisfy both the RWA and the adiabatic passage condition, which is of the order of the spin relaxation time. Thus a weak interaction requires to take into account the bichromatic effects (with a larger peak Rabi frequency to shorten the time of interaction) in order to avoid the relaxation effects.

We will study more precisely in Secs. V and VI the various regimes that occur in this system. The problem of preparing the entangled state $|2\rangle \equiv |\downarrow\uparrow^{+}\rangle$ is thus reduced to the study of the population transfer into the intermediate level in the ladder system driven by the Hamiltonian $\tilde{\mathsf{H}}_c$ (11).

The populations given by the Schrödinger equation (10) are invariant under the following transformation $\mathcal{T}$:

$$\Delta_1 \rightarrow \Delta_1 + \delta, \tag{13a}$$

$$\Delta_2 \rightarrow \Delta_2 - \delta, \tag{13b}$$

$$\delta \rightarrow -\delta, \tag{13c}$$

$$\Omega_1 \rightleftharpoons \Omega_2 . \tag{13d}$$

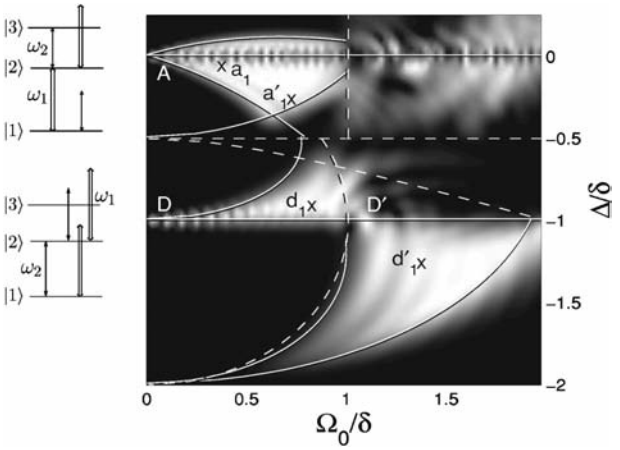

FIG. 2. Contour map of population transfer efficiency $P_2(\infty)$ for varying peak Rabi frequency Ω_0/δ and varying detuning Δ/δ (with $\Delta = \Delta_1 = \Delta_2$) for the sequence 1. White areas correspond to high efficiency transfer (close to 1) to the entangled state. Dark areas correspond to low efficiency transfer (close to 0) to the entangled state $|2\rangle$. The dashed lines separate different regions labeled A, D, and D', associated with different effective Hamiltonians constructed in Secs. V and VI. The regimes of good population transfer are bounded by full lines predicted from the topological analysis. The crosses labeled (a_1), (a'_1), (d_1), and (d'_1) refer to parameters leading to high efficiency. They also refer to the pathways shown, respectively, in Figs. 6, 7, 8, and 9. Besides regions A and D, we have displayed the corresponding linkage patterns, respectively, for $\Delta = 0$ and $\Delta = -\delta$.

We indeed obtain $\tilde{\mathsf{R}}^{\dagger}(\mathcal{T}\tilde{\mathsf{H}}_c)\tilde{\mathsf{R}} - i(\partial\tilde{\mathsf{R}}^{\dagger}/\partial t)\tilde{\mathsf{R}} = \tilde{\mathsf{H}}_c$, with the unitary transformation

$$\tilde{\mathsf{R}} = \begin{bmatrix} 1 & 0 & 0 \\ 0 & e^{-i\delta t} & 0 \\ 0 & 0 & 1 \end{bmatrix}. \tag{14}$$

III. NUMERICAL RESULTS

In this section, we describe the numerical results that are obtained by solving the Schrödinger equation (10), for which we will present a detailed theoretical analysis in the following sections.

Figures 2 and 3 display the population of the state $|2\rangle$ at the end of a sequence of delayed Gaussian pulses of the same lengths and the same peak amplitudes,

$$\Omega_1(t) = \Omega_0 \exp[-(t+\tau)^2/T^2], \tag{15a}$$

$$\Omega_2(t) = \Omega_0 \exp[-(t-\tau)^2/T^2], \tag{15b}$$

for various normalized peak amplitudes Ω_0/δ and detunings Δ/δ, where we have chosen

$$\Delta \equiv \Delta_1 = \Delta_2 . \tag{16}$$

We have considered this restriction of the parameters because it gives preferentially large regions of good population

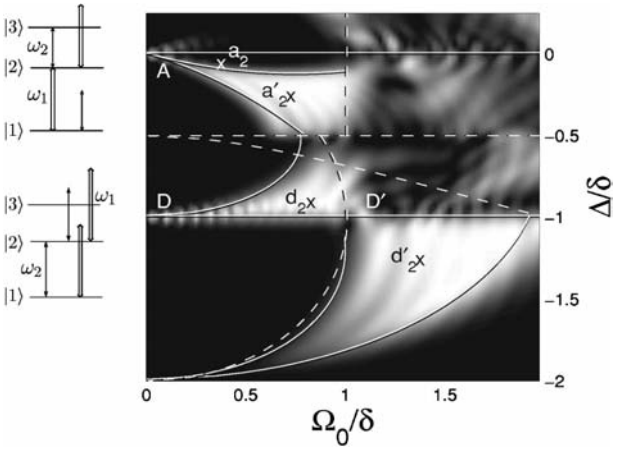

FIG. 3. Contour map of population transfer efficiency $P_2(\infty)$ for varying peak Rabi frequency Ω_0/δ and varying detuning Δ/δ for the sequence 2. The cross labeled (a_2) in one region of low efficiency and the ones labeled (a_2'), (d_2), and (d_2') in the regions of high efficiency refer to the pathways shown, respectively, in Figs. 6, 7, 8, and 9.

transfer. This will be justified in Secs. V and VI. Note that the case $\Delta_1=-\Delta_2$ is irrelevant since it corresponds to a two-photon resonance between the product states $|\downarrow\downarrow\rangle$ and $|\uparrow\uparrow\rangle$. We could have considered equivalently the restriction $\Delta_2=\Delta_1+2\delta$ in accordance with the symmetry (13). The two possible orderings of pulses have been considered: the sequence 1 of Fig. 2 (the sequence 2 of Fig. 3) corresponds to the ω_1 pulse (the ω_2 pulse) being switched on first, with the delay $\tau=1.7T$ ($\tau=-1.7T$). Global adiabaticity is ensured by the choice of a large pulse area $\Omega_0 T=50$.

One can distinguish three islands of robust high transfer (white regions). Specific parameters characterizing these islands are labeled by (a), (a'), (d), and (d'), with the subscript 1 or 2, respectively, for Figs. 2 or 3 [except (a_2) which is outside the regions of high transfer]. These islands of high transfer are analyzed in the following sections by using the dressed Hamiltonian corresponding to $\tilde{\mathsf{H}}_c$ (11) and the adiabatic properties of the dynamics. We will characterize different regimes and associate them with different effective dressed Hamiltonians. We will show that the islands of good transfer can be understood from the topological properties of the appropriate effective dressed Hamiltonian.

We will show the following results.

(i) Regions (a) correspond to a STIRAP-like process associated with the channel A (see Fig. 1) that is perturbed (in the sense of non-resonant perturbation theory) by the channel B. Note that the restriction $\Delta_2=\Delta_1+2\delta$ would have given a STIRAP-like process associated with the channel B perturbed by the channel A.

(ii) Regions (d) (in the weak field regime, i.e., $\Omega_1,\Omega_2<|\delta|$) correspond to an effective two-level SCRAP-like (Stark chirped rapid adiabatic passage) process [9,10].

(iii) Regions (d') (in the strong field regime, i.e., $\Omega_1,\Omega_2\gtrsim|\delta|$) correspond to an effective two-level bichromatic SCRAP process (with additional Stark shifts) as described in Ref. [11].

IV. THE FLOQUET DRESSED HAMILTONIAN

In this section we derive the Floquet Hamiltonian describing the full Hamiltonian of the spin system dressed by the strong fields. It will allow to predict and interpret the various processes occurring in this system by adiabatic passage.

It is convenient to use the adiabatic Floquet theory in order to study the Hamiltonian $\tilde{\mathsf{H}}_c$ (11) since its time dependence contains a characteristic frequency δ. The Floquet Hamiltonian corresponding to $\tilde{\mathsf{H}}_c$ is [8,13]

$$\mathsf{K}^{[\Omega_1,\Omega_2]}=-i\hbar\delta\frac{\partial}{\partial\theta}+\frac{1}{2}\begin{bmatrix}0 & \Omega_1+e^{-i\theta}\Omega_2 & 0\\ \Omega_1+e^{i\theta}\Omega_2 & 2\Delta_1 & \Omega_2+e^{i\theta}\Omega_1\\ 0 & \Omega_2+e^{-i\theta}\Omega_1 & 2(\Delta_1+\Delta_2)\end{bmatrix}. \tag{17}$$

We have formulated this Floquet Hamiltonian in a way which derives naturally from the theory of quantized dressed states in a cavity [12]. The Floquet Hamiltonian allows to take into account the photon exchanges between the atom and the fields. It is formally constructed on the initial phases θ_1 and θ_2 of the fields which are treated as dynamical variables acting on the photonic Hilbert space $\mathcal{L}=\mathcal{L}_2(d\theta_1/2\pi)\otimes\mathcal{L}_2(d\theta_2/2\pi)$, where each $\mathcal{L}_2(d\theta_i/2\pi)$ is the Hilbert space of 2π-periodic functions of the angle θ_i [11]. Since we have applied a bichromatic rotating wave approximation, only the frequency $\delta=\omega_1-\omega_2$, associated with the dynamical variable $\theta\equiv\theta_1-\theta_2$ is left in the effective Hamiltonian. The effective Floquet Hamiltonian K (17) acts thus on the Hilbert space spanned by the three states $\{|1\rangle,|2\rangle,|3\rangle\}$ tensored by the effective photonic Hilbert space $\mathcal{L}_2(d\theta/2\pi)$. This photonic Hilbert space allows to take into account the exchanges of the group of ω_1-ω_2 photons. The eigenstates of K are families of three states denoted $|1;k,-k\rangle$, $|2;k-1,-k\rangle$, and $|3;k-1,-k-1\rangle$ with k a positive or negative integer. The corresponding eigenvalues $\lambda_{1;k,-k}$, $\lambda_{2;k-1,-k}$ and $\lambda_{3;k-1,-k-1}$ have the following periodicity property: $\lambda_{n;k_1,k_2}=\lambda_{n;k_1-1,k_2+1}+\hbar\delta$, for $n=1,2,3$. The notation $|n;k_1,k_2\rangle$ characterizes (when the fields are off) the state $|n\rangle$ dressed by the field of k_1 ω_1 photons and of k_2 ω_2 photons. The integers k_1 and k_2 characterize thus relative photon numbers of the respective fields of frequency ω_1 and ω_2. The initial state is denoted $|1;0,0\rangle$. The problem can be formulated as follows: *we look for robust adiabatic connections between the initial state* $|1;0,0\rangle$ *and the final state* $|2;k-1,-k\rangle$ *for some positive or negative integer k.*

The Floquet Hamiltonian (17) depends parametrically on the pulse shapes and the detunings. The possible connections depend on the *topology* of the eigenenergy surfaces of Eq. (17) as functions of the field envelopes Ω_1 and Ω_2 for given detunings Δ_1 and Δ_2 [11,14]. The topology is characterized by true crossings which occur generically when one of the fields is off. We will study in the following the topology of K using different effective dressed Hamiltonians corresponding

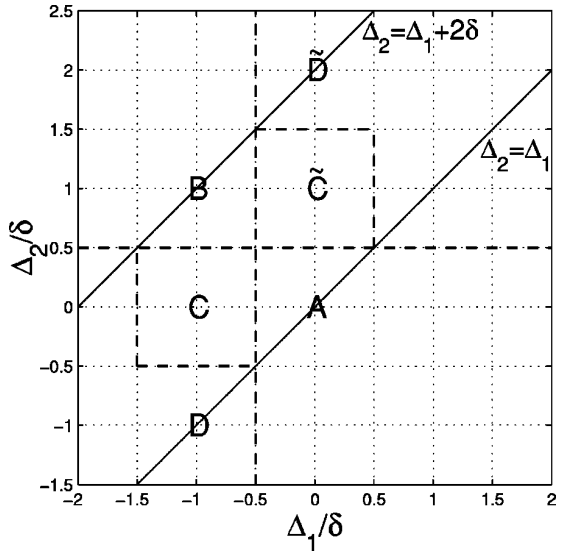

FIG. 4. Schematic diagram of the regimes for a weak-field regime as a function of the normalized detunings Δ_1/δ and Δ_2/δ. The restriction $\Delta_2=\Delta_1$ has been used for Figs. 2 and 3.

to different regimes. These regimes will depend on the ranges of the detunings and of the field amplitudes.

In the next sections we will calculate the eigenenergy surfaces for different relevant cases, using a numerical diagonalization of Eq. (17). This can be done either by discretization of the angle θ or equivalently by using a restricted finite basis of the complete basis $\{e^{ik\theta},k\in\mathbb{Z}\}$ of the photonic Hilbert space $\mathcal{L}_2(d\theta/2\pi)$. Effective Hamiltonians will be determined in the appropriate regions, which give good approximations for these numerical surfaces, and provide an analytic explanation of the different domains where adiabatic transfer is efficient.

We classify the different regimes and construct effective dressed Hamiltonians by determining in the Hamilonian K (17) which terms are *resonant* (or *quasiresonant*) and which are only *perturbative*. The resonant terms are treated by an adapted unitary transformation which allows an explicit diagonalization, whereas the perturbative terms can be treated by stationary pertubation theory. This technique has been presented in Ref. [15]. Note that for a simple RWA two-level system of Rabi frequency Ω and detuning Δ, the perturbative regime is such that $\Omega\ll|\Delta|$ and the resonant regime such that $\Omega\gtrsim|\Delta|$. We classify the different regimes as functions of the ranges of the field amplitudes and of the detunings.

In the following, we have normalized all the quantities with respect to δ.

V. WEAK-FIELD REGIME

The *weak-field regime* occurs when $\Omega_1(t),\Omega_2(t)<\delta$. Note that when one has $\Delta_1=\Delta_2$ additionally, this regime coincides with a *strong spin coupling* since we have then $6|\xi|>\Omega_1(t),\Omega_2(t)$. In this case of weak-field regime, we can intuitively analyze the different regimes with respect to the range of the detunings using the diagram of linkage patterns (Fig. 1). Six relevant regimes (bounded by dashed lines) have been collected in Fig. 4, depending on the quasiresonances.

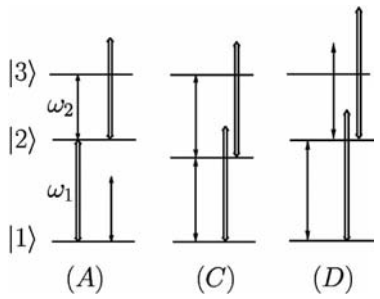

FIG. 5. Diagram of linkage patterns for the three regimes (in the resonant case): A ($\Delta_1=\Delta_2=0$), C ($\Delta_1=-\delta,\Delta_2=0$), and D ($\Delta_1=-\delta,\Delta_2=-\delta$).

(A) The transition 1-2 is quasiresonant with ω_1 and perturbed by ω_2, 2-3 is quasiresonant with ω_2 and perturbed by ω_1.

(B) 1-2 is quasiresonant with ω_2 and perturbed by ω_1, 2-3 is quasiresonant with ω_1 and perturbed by ω_2.

(C) 1-2 and 2-3 are both quasiresonant with ω_2, and perturbed by ω_1.

(D) 1-2 is quasiresonant with ω_2 and perturbed by ω_1, 2-3 is perturbed by ω_2 and ω_1.

($\tilde{C}$) 1-2 and 2-3 are both quasiresonant with ω_1, and perturbed by ω_2.

($\tilde{D}$) 1-2 is quasiresonant with ω_1 and perturbed by ω_2, 2-3 is perturbed by ω_1 and ω_2.

In the exact resonant cases, we have represented the regimes A, C, and D in Fig. 5.

As shown schematically in Fig. 4, the above regimes can be roughly bounded by

$$\Delta_1=\pm\delta/2,\quad \Delta_1=-3\delta/2,\quad \Delta_2=\pm\delta/2,\quad \Delta_2=3\delta/2. \tag{18}$$

By the symmetry (13), we recover the regime B from the regime A, $\tilde{C}$ from C, $\tilde{D}$ from D (exchanging additionally Ω_1 and Ω_2).

The regimes A and B are STIRAP-like regimes; D and $\tilde{D}$ are SCRAP-like regimes.

We do not consider other regimes where the state $|1\rangle$ is almost not depopulated by adiabatic passage.

The line $\Delta=-\delta/2$ appears as a dashed line in Figs. 2 and 3, where the restriction $\Delta_1=\Delta_2$ has been considered.

A. Regime *A*

When the transition 1-2 is quasiresonant with the frequency ω_1 and the transition 2-3 quasiresonant with the frequency ω_2, the process can be analyzed as the channel A *perturbed* (in the sense nonresonant perturbation theory) by the channel B. We refer to it as the regime A as shown in Figs 2 and 3, where it is roughly bounded by the dashed lines $\Delta=-\delta/2$, $\Delta=\delta/2$ (not shown), and $\Omega_0=\delta$. This regime is approximately characterized by the following effective Hamiltonian in the basis $\{|1;0,0\rangle,\ |2;-1,0\rangle,\ |3;-1,-1\rangle\}$ [13]:

$$\tilde{H}_c^A=\frac{1}{2}\begin{bmatrix} -\frac{(\Omega_2)^2}{2(\delta+\Delta_1)} & \Omega_1 & 0 \\ \Omega_1 & 2\Delta_1+\frac{(\Omega_2)^2}{2(\delta+\Delta_1)}+\frac{(\Omega_1)^2}{2(\delta-\Delta_2)} & \Omega_2 \\ 0 & \Omega_2 & 2(\Delta_1+\Delta_2)-\frac{(\Omega_1)^2}{2(\delta-\Delta_2)} \end{bmatrix}, \tag{19}$$

which corresponds to the Hamiltonian characterizing the channel A with additional time dependent Stark shifts (on the diagonal) induced by the channel B. Note that this effective Hamiltonian is less precise for bigger Ω_1 or Ω_2 approaching δ.

1. Topology of the channel A in the RWA limit

Before analyzing the dynamics given by this Hamiltonian (19), we recall the results in the limit case of a very weak-field $\Omega_1(t),\Omega_2(t)\ll\delta$ obtained in Ref. [14]. In this case the perturbative terms can be neglected and the Hamiltonian becomes

$$\tilde{H}_c^A\rightarrow\frac{1}{2}\begin{bmatrix} 0 & \Omega_1 & 0 \\ \Omega_1 & 2\Delta_1 & \Omega_2 \\ 0 & \Omega_2 & 2(\Delta_1+\Delta_2) \end{bmatrix}. \tag{20}$$

This resulting effective Hamiltonian corresponds to the channel A alone. The topology of the energy surfaces of this Hamiltonian has been analyzed in Ref. [14]. It has been shown that the adiabatic transfer to state $|2\rangle$ is topologically allowed for

$$\Delta_1\Delta_2>0. \tag{21}$$

The topological analysis shows moreover that for the sequence 1 the region of this process is bounded in the parameter space by the curves

$$\Omega_0=2\sqrt{\Delta_1(\Delta_1+\Delta_2)} \tag{22}$$

and for the sequence 2 by the curves (22) and

$$\Omega_0=2\sqrt{\Delta_2(\Delta_1+\Delta_2)}. \tag{23}$$

2. Topology of the channel A perturbed by the channel B

Taking now into account the perturbation by the channel B [Hamiltonian (19)] leads to two kinds of topology as shown in Figs. 6 and 7, where the surfaces of quasienergies as functions of the normalized Rabi frequencies Ω_1/δ and Ω_2/δ, respectively, for $\Delta=\Delta_1=\Delta_2=-\delta/20$ and $\Delta=\Delta_1=\Delta_2=-\delta/4$ have been displayed. The eigenvalues of Eq. (19) (not shown) fit these surfaces well except in Fig. 7 when $\Omega_1\sim\delta$ and $\Omega_2\sim\delta$ because of an additional dynamical resonance (i.e., a resonance occuring beyond a threshold of the field amplitudes) [15,8] which involves the surface connected with $|3;0,-2\rangle$ (which corresponds to the surface connected to $|3;-1,-1\rangle$ and translated of δ) and the surface right below.

Figure 6 shows that the two conical intersections, one occurring for $\Omega_1=0$, the other one for $\Omega_2=0$, determine the boundary of the adiabatic connection between the initial state $|1;0,0\rangle$ and the target state $|2;-1,0\rangle$. A detailed analysis of the dynamics through the conical intersections can be found in Ref. [14]. We summarize here the main results using an example of a crossing occurring for $\Omega_1=0$: if the dynamics goes *exactly* through the crossing, where Ω_1 is exactly zero, then adiabatic passage through the intersection occurs along

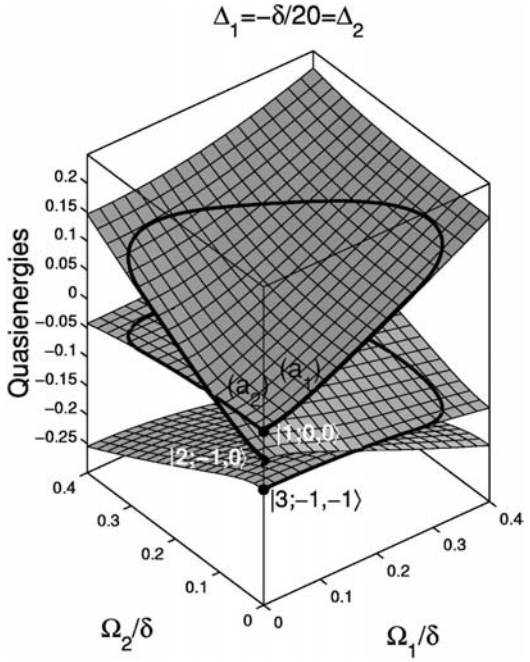

FIG. 6. Quasienergy surfaces (in units of δ) as functions of Ω_1/δ and Ω_2/δ for $\Delta_1=\Delta_2=-\delta/20$. The path denoted a_1 (sequence 1), for $\Omega_0=0.35\delta$, connects the states $|1\rangle$ and $|2\rangle$ with the absorption of one ω_1 photon. The path denoted a_2 (sequence 2), for $\Omega_0=0.35\delta$, connects the states $|1\rangle$ and $|3\rangle$ with the absorptions of one ω_1 photon and of one ω_2 photon.

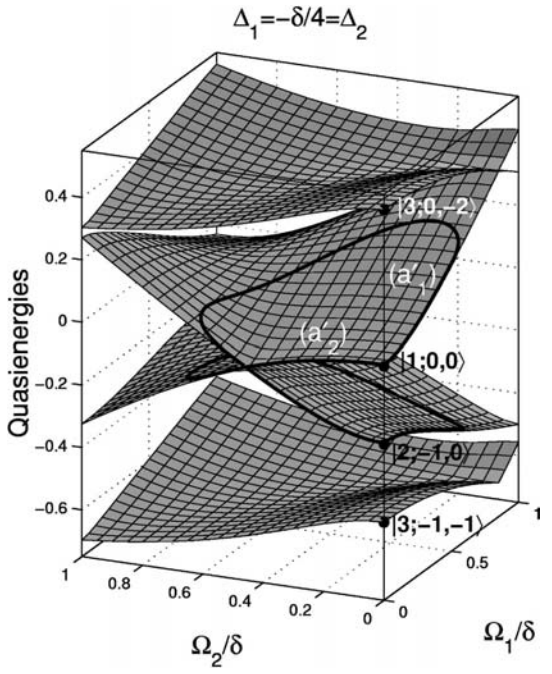

FIG. 7. Quasienergy surfaces as functions of Ω_1/δ and Ω_2/δ for $\Delta_1=\Delta_2=-\delta/4$. The two different paths, denoted a_1' and a_2' (for $\Omega_0=0.7\delta$) depending on the sequence of the pulses connect the states $|1\rangle$ and $|2\rangle$ with the absorption of one ω_1 photon.

a smooth line. If the dynamics slightly misses the crossing, i.e., for a specific $\Omega_1\neq 0$, it encounters instead a thin avoided crossing. It is expected to be passed *diabatically*, i.e., with a jump from one branch to the other, for a sufficiently small Ω_1 with respect to the speed of the passage, according to a local Landau-Zener analysis. Thus the Landau-Zener analysis provides the matching between the adiabatic evolution far from the conical intersection and the diabatic behavior near the intersection. Note that a too large Ω_1 with respect to the speed of the passage would lead either (i) to an undesirable splitting of the population along the two surfaces near the intersection, followed by an adiabatic evolution of these two states, or (ii) for a larger Ω_1, to an adiabatic evolution staying on the initial surface.

For the sequence 1, the conical intersection occurring for $\Omega_1=0$ is favorable for this adiabatic connectivity. The path denoted a_1 (also corresponding to the cross a_1 of Fig. 2) is an example for the complete transfer. However, for the sequence 2, the conical intersection occurring for $\Omega_1=0$ is also favorable but the one occurring for $\Omega_2=0$ is detrimental since it makes $|1;0,0\rangle$ connect to $|3;-1,-1\rangle$. The path denoted a_2 is an example for the complete transfer to $|3;-1,-1\rangle$ (also corresponding to the cross a_2 of Fig. 3).

For a bigger detuning (in absolute value), the topology is different as shown in Fig. 7. The previous conical intersection occurring for $\Omega_2=0$ has now disappeared and another one involving the surfaces connected to $|1;0,0\rangle$ and $|3;0,-2\rangle$ has appeared. The two conical intersections, the one occurring for $\Omega_1=0$ and the other one for $\Omega_2=0$, are involved for the adiabatic connection between the initial state $|1;0,0\rangle$ and the target state $|2;-1,0\rangle$. More precisely, for the sequence 1, these two conical intersections determine the boundary of this adiabatic connection; the path denoted a_1' (also corresponding to the cross a_1' of Fig. 2) is an example for the complete transfer. However, for the sequence 2 only the conical intersection occurring for $\Omega_1=0$ binds now the adiabatic connection; the path denoted a_2' is an example for the complete transfer (also corresponding to the cross a_2' of Fig. 3).

Using the effective Hamiltonian (19), the position of the previous conical intersections, for $\Omega_1=0$ and $\Omega_2=0$, respectively, lead to the three boundaries for the sequence 1,

$$\Delta=\frac{\Omega_2}{16\delta}[-5\Omega_2\pm\sqrt{9(\Omega_2)^2+32\delta^2}], \tag{24a}$$

$$\Omega_1=\sqrt{2(\delta-\Delta)[2(\delta+\Delta)-\sqrt{2(\delta+\Delta)}]}. \tag{24b}$$

The delay between the pulses has been chosen sufficiently large such that it is a good approximation to consider that the adiabatic connectivity is quite well described by the value of the peak amplitudes. Thus we have displayed these boundaries in Fig. 2 as full lines, with $\Omega_2=\Omega_0$ for Eq. (24a) and with $\Omega_1=\Omega_0$ for Eq. (24b). They globally determine the boundary of the lower and upper part of the island of good transfer of the regime A observed in the numerical computation. This island is crossed by the line of resonance $\Delta=0$ around which the transfer to $|2\rangle$ depends on the pulse areas, as shown by small oscillating islands.

For the sequence 2, the conical intersections involved give the following boundaries:

$$\Delta=\frac{\Omega_2}{16\delta}[-5\Omega_2-\sqrt{9(\Omega_2)^2+32\delta^2}], \tag{25a}$$

$$\Omega_1=\sqrt{(\delta-\Delta)[4\Delta+\delta\pm\sqrt{\delta(\delta+8\Delta)}]},\quad \text{for}\quad \Delta<0. \tag{25b}$$

These curves are displayed in Fig. 3, with $\Omega_2=\Omega_0$ for Eq. (25a) and with $\Omega_1=\Omega_0$ for Eq. (25b). They give a good prediction of the island of good transfer of the regime A observed numerically.

For the two sequences, the islands of good transfer to the state $|2\rangle$ of the regime A occur with absorption of one ω_1 photon.

B. Regime *B*

This regime is characterized by the transition quasiresonant 1-2 with the frequency ω_2 and the quasiresonant transition 2-3 with the frequency ω_1. This process can be analyzed as the channel B *perturbed* (in the sense of nonresonant perturbation theory) by the channel A and is described by the effective Hamiltonian $\tilde{H}_c^B=\mathcal{T}\tilde{H}_c^A$,

$$\tilde{\mathsf{H}}_c^{\mathrm{B}}=\frac{1}{2}\begin{bmatrix} -\frac{(\Omega_1)^2}{2\Delta_1} & \Omega_2 & 0 \\ \Omega_2 & 2(\Delta_1+\delta)+\frac{(\Omega_1)^2}{2\Delta_1}-\frac{(\Omega_2)^2}{2\Delta_2} & \Omega_1 \\ 0 & \Omega_1 & 2(\Delta_1+\Delta_2)+\frac{(\Omega_2)^2}{2\Delta_2} \end{bmatrix}. \tag{26}$$

The regions of high transfer efficiency to the state $|2\rangle$ are bounded in the same manner as in the regime A by the lines (24) and (25) to which we apply the transformation $\mathcal{T}$ (13).

C. Regime *C*

The regime *C* is characterized by a mixture of regimes *A* and *B* for which the transitions 1-2 and 2-3 are both quasiresonant with the same frequency ω_2. As long as the ω_1 field is perturbative for both transitions, we have the following effective Hamiltonian:

$$\tilde{\mathsf{H}}_c^{C}=\frac{1}{2}\begin{bmatrix} -\frac{(\Omega_1)^2}{2\Delta_1} & \Omega_2 & 0 \\ \Omega_2 & 2(\Delta_1+\delta)+\frac{(\Omega_1)^2}{2\Delta_1}-\frac{(\Omega_1)^2}{2(\Delta_2-\delta)} & \Omega_2 \\ 0 & \Omega_2 & 2(\Delta_1+\Delta_2+\delta)+\frac{(\Omega_1)^2}{2(\Delta_2-\delta)} \end{bmatrix}, \tag{27}$$

in the basis $\{|1;0,0\rangle, |2;0,-1\rangle, |3;0,-2\rangle\}$. No efficient transfer is observed in this regime.

D. Regime *D*

This regime is such that the only quasiresonance is between the states 1 and 2 with ω_2. In this case, in the basis $\{|1;0,0\rangle, |2;0,-1\rangle, |3;0,-2\rangle\}$ we can construct an effective Hamiltonian from the previous one [Eq. (27)] considering that the ω_2 field is perturbative for the transition 2-3,

$$\tilde{\mathsf{H}}_c^{D}=\frac{1}{2}\begin{bmatrix} -\frac{(\Omega_1)^2}{2\Delta_1} & \Omega_2 & 0 \\ \Omega_2 & 2(\Delta_1+\delta)+\frac{(\Omega_1)^2}{2\Delta_1}-\frac{(\Omega_1)^2}{2(\Delta_2-\delta)}-\frac{(\Omega_2)^2}{2\Delta_2} & 0 \\ 0 & 0 & 2(\Delta_1+\Delta_2+\delta)+\frac{(\Omega_1)^2}{2(\Delta_2-\delta)}+\frac{(\Omega_2)^2}{2\Delta_2} \end{bmatrix}. \tag{28}$$

We can remark that this Hamiltonian is valid for the field amplitude Ω_2 below the position of the resonance occurring between the transition 2-3 and the ω_2 field that can be estimated by

$$\Omega_2^r\equiv 2\sqrt{\Delta_2(\Delta_1+\Delta_2+\delta)} \quad \text{and} \quad \Delta_1+2\Delta_2+\delta\leqslant 0. \tag{29}$$

This limit is represented as the bent dashed line crossing the figure horizontally in Figs. 2 and 3 (with $\Omega_0=\Omega_2^r$). Below this limit, one is allowed to decouple the states $|2;0,-1\rangle$ and $|3;0,-2\rangle$ from the Hamiltonian (27). A more detailed analysis of this regime shows that a *dynamical resonance* between the transition 1-2 and the ω_1 field, induced by the ω_2 field occurs approximately for

$$\Omega_2=\Omega_2^{\mathrm{dr}}\equiv\sqrt{-\Delta_1(\Delta_1+2\delta)}. \tag{30}$$

It is obtained when the difference of the dressed eigenvalues connected to $|1;0,0\rangle$ and $|2;0,-1\rangle$ (calculated without the Stark shifts) compensates the difference of the frequencies δ. This additional resonance is described as dynamical since it occurs beyond a threshold of the ω_2 field amplitude. It is represented as the bent dashed line crossing the figure vertically (which separates the regimes *D* and *D'*) in Figs. 2 and 3 with $\Omega_0=\Omega_2^{\mathrm{dr}}$. The Hamiltonian (28) is thus approximately valid *before* the dynamical resonance (30).

Below this dynamical resonance, this Hamiltonian (28) is very similar to the one describing the Stark chirped rapid adiabatic passage between the states $|1;0,0\rangle$ and $|2;0,-1\rangle$ [9]. The pump of this process is here Ω_2 and the Stark pulse Ω_1. We have here Ω_2 acting additionally as a Stark pulse.

It is important to note that when $\Delta_1=-\delta$, the field ω_2 is exactly in resonance with the transition 1-2, and it cannot induce any complete population transfer from $|1\rangle$ to $|2\rangle$.

Below this boundary (plotted as a full line in Figs. 2 and 3), i.e., for $\Delta_1 < -\delta$, the topology does not allow the transfer from $|1\rangle$ to $|2\rangle$. Above this boundary ($\Delta_1 > -\delta$), the transfer is possible as shown by the surfaces of quasienergies (for $\Delta = \Delta_1 = \Delta_2 = 9\delta/10$) in Fig. 8. The eigenvalues of Eq. (28) (not shown) fit well these surfaces below the dynamical resonances $\Omega_2 < \Omega_2^r$. Figure 8 shows that the conical intersection for $\Omega_2 = 0$ between the surfaces connected to $|1;0,0\rangle$ and the target state $|2;0,-1\rangle$ determines the boundary of the adiabatic connection between these states. This characterizes a transfer to the state $|2\rangle$ with absorption of one ω_2 photon. This boundary is calculated from the effective Hamiltonian (28),

$$\Omega_1 = 2\sqrt{\Delta \frac{\Delta^2 - \delta^2}{2\delta - \Delta}}. \tag{31}$$

It is plotted in Figs. 2 and 3 as a full line in the region D and determines the boundary of the upper island of good transfer of this region.

The cases beyond the dynamical resonance are studied in the following section.

VI. STRONG-FIELD REGIMES

The *strong-field regime* occurs when $\Omega_1(t), \Omega_2(t) \gtrsim \delta$. For $\Delta_1 = \Delta_2$, this corresponds to a *weak spin coupling* since one has then $6|\xi| \lesssim \Omega_1(t), \Omega_2(t)$. More resonances occur in this case and the previous effective Hamiltonians are no longer valid. We will study in detail the interesting regime D' which gives quite large areas of transfer to state $|2\rangle$.

This regime is located below the resonance (29) and beyond the dynamical resonance (30), when the transition 1-2 is quasiresonant with both the ω_1 and ω_2 fields and when the transition 2-3 is not resonant with either the ω_1 field or the ω_2 field. This regime is thus characterized by the effective dressed Hamiltonian,

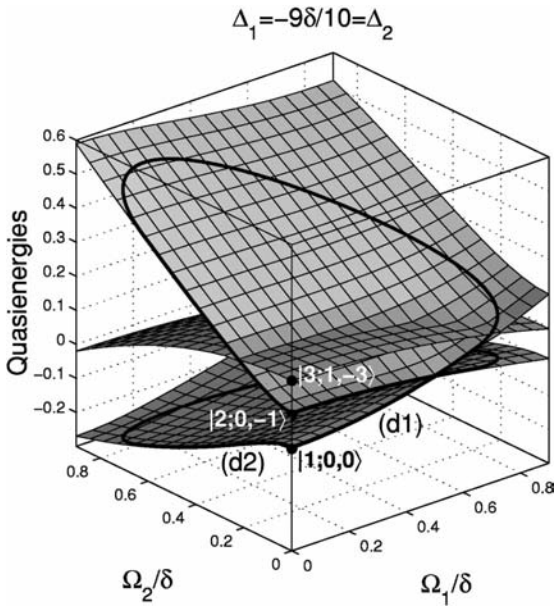

FIG. 8. Quasienergy surfaces as functions of Ω_1/δ and Ω_2/δ for $\Delta_1 = \Delta_2 = -9\delta/10$. Two different paths (denoted d_1 and d_2) for $\Omega_0 = 0.8\delta$ connect the states $|1\rangle$ and $|2\rangle$ with the absorption of one ω_2 photon.

$$\mathsf{K}^{D'} = -i\delta\frac{\partial}{\partial\theta} + \frac{1}{2}\begin{bmatrix} 0 & \Omega_2 + e^{i\theta}\Omega_1 & 0 \\ \Omega_2 + e^{-i\theta}\Omega_1 & 2(\Delta_1+\delta) - \dfrac{(\Omega_1)^2}{2(\Delta_2-\delta)} - \dfrac{(\Omega_2)^2}{2\Delta_2} & 0 \\ 0 & 0 & 2(\Delta_1+\Delta_2+\delta) + \dfrac{(\Omega_1)^2}{2(\Delta_2-\delta)} + \dfrac{(\Omega_2)^2}{2\Delta_2} \end{bmatrix}. \tag{32}$$

It is equivalent to a two-level system driven by a bichromatic field [11] with additional Stark shifts. The surfaces of quasienergies as functions of the normalized Rabi frequencies Ω_1/δ and Ω_2/δ (for $\Delta = \Delta_1 = \Delta_2 = -7\delta/5$) are displayed in Fig. 9. This figure shows that the two conical intersections, one for $\Omega_1 = 0$ and one for $\Omega_2 = 0$, determine the boundary of the adiabatic connection between the initial state $|1;0,0\rangle$ and the target state $|2;1,-2\rangle$. We calculate the boundaries using the effective Hamiltonian (32), which are plotted as full lines in Figs. 2 and 3,

$$\Omega_1 = 2\sqrt{(\Delta-\delta)[2\delta - \Delta - 2\sqrt{\delta(2\delta-\Delta)}]}, \tag{33a}$$

$$\Omega_2 = 2\sqrt{\Delta[\delta - \Delta - \sqrt{\delta(\delta - 4\Delta)}]}. \tag{33b}$$

This process corresponds to a multiphoton transfer to the state $|2\rangle$, with absorption of two ω_2 photons and emission of one ω_1 photon.

The analysis of the topology allows to improve the transfer efficiency. It shows indeed that a ω_1 field amplitude weaker than the ω_2 field amplitude is better in this regime since the conical intersection for $\Omega_1 = 0$ occurs for a smaller value than the one for $\Omega_2 = 0$.

This process of a two-level system driven by a bichromatic field studied in Ref. [11] shows that the transfer can still occur for a stronger field (i.e., for a weaker spin coupling), but with absorption of more than two ω_2 photons and emission of more than one ω_1 photon. This result is shown in Fig. 10 where strong field white islands can be observed. The

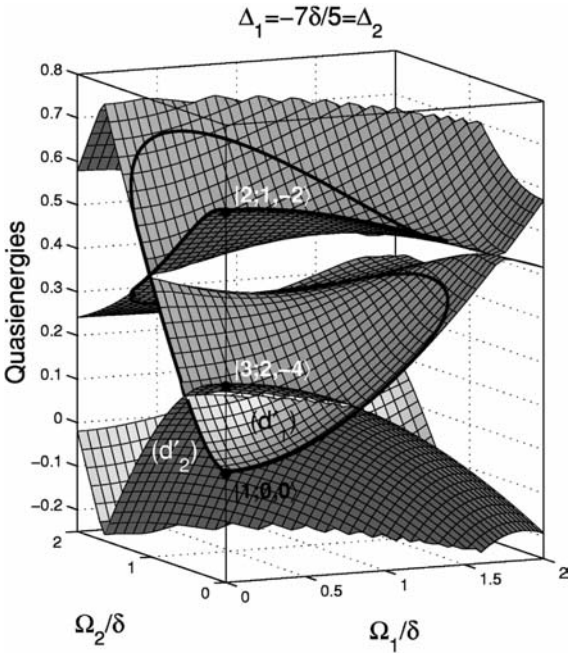

FIG. 9. Quasienergy surfaces as functions of Ω_1/δ and Ω_2/δ for $\Delta_1=\Delta_2=-7\delta/5$. Two different paths (denoted d_1' and d_2') for $\Omega_0=3\delta/2$ connect the states $|1\rangle$ and $|2\rangle$ with the absorption of two ω_2 photons and the emission of one ω_1 photon.

lower white islands correspond to good population transfer to the entangled state $|2;k-1,-k\rangle$, with $k=1,2,3,4$ from left to right.

VII. CONCLUSION

In a system of two interacting identical spins in an external bichromatic field, we have determined the choices of laser pulses which can give a maximal final population in the entangled state. The proposed strategies are robust with respect to the external parameters. We have found that in the parameter space it is possible to find large regions where the quantum system can be transferred to the entangled state with a high efficiency. These regions of good transfer have been characterized by the topology of the surfaces of dressed states as functions of the parameters.

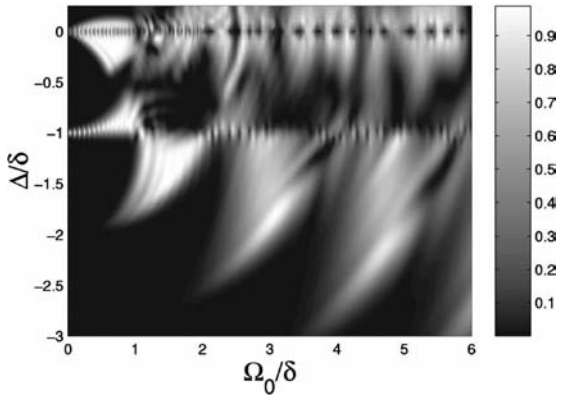

FIG. 10. Contour map of population transfer efficiency $P_2(\infty)$ as in Fig. 2, but for stronger field amplitudes.

The implementation of the scheme we propose in this paper can be realized for different physical systems. An example could be of the type similar to the one used in Ref. [16] for the realization of two-qubit phase gates. The similarity of our model with the nuclear magnetic resonance scheme of Ref. [16] is the adiabatic evolution. The Berry adiabatic phase gate operation was, however, realized for different nuclei i.e. with different gyromagnetic constants. In this case the two-particle states are represented through a four-level quantum system (see, e.g., Ref. [17]). In the present paper we propose instead to use identical spins to generate an entangled state through a simpler effective three-level system.

The methods employed here are quite general and can be applied for a large variety of systems. We anticipate interesting applications of this method in quantum computing and quantum communication.

ACKNOWLEDGMENTS

We acknowledge support by INTAS 99-00019 and the Conseil Régional de Bourgogne. S.G. acknowledges support from a CNRS project ''jeunes chercheurs'' and thanks the Institute of Physics of the National Academy of Sciences of Armenia in Ashtarak for kind hospitality. R.U. thanks for support by the Alexander Von Humboldt Foundation and l'Université de Bourgogne for kind hospitality. The authors thank N. Vitanov for useful discussions.

[1] C. Williams and S. Clearwater, *Explorations in Quantum Computing* (Springer-Verlag, New York, 1998).

[2] E.S. Fry, T. Walther, and S. Li, Phys. Rev. A **52**, 4381 (1995); J.I. Cirac and P. Zoller, Phys. Rev. Lett. **74**, 4091 (1995); E. Hagley, X. Maitre, G. Nogues, C. Wunderlich, M. Brune, J.M. Raimond, and S. Haroche, *ibid.* **79**, 1 (1997); B.E. King, C.S. Wood, C.J. Myatt, Q.A. Turchette, D. Leibfried, W.M. Itano, C. Monroe, and D.J. Wineland, *ibid.* **81**, 1525 (1998); Q.A. Turchette, C.S. Wood, B.E. King, C.J. Myatt, D. Leibfried, W.M. Itano, C. Monroe, and D.J. Wineland, *ibid.* **81**, 3631 (1998).

[3] A. Sørensen and K. Mølmer, Phys. Rev. Lett. **82**, 1971 (1999); C.A. Sackett, D. Kielpinski, B.E. King, C. Langer, C.J. Myatt, M. Rowe, Q.A. Turchatte, W.M. Itano, D.J. Wineland, and C. Monroe, Nature (London) **404**, 256 (2000).

[4] N.V. Vitanov, M. Fleischhauer, B.W. Shore, and K. Bergmann, Adv. At., Mol., Opt. Phys. **46**, 55 (2001).

[5] T. Pellizzari, S.A. Gardiner, J.I. Cirac, and P. Zoller, Phys. Rev. Lett. **75**, 3788 (1995).

[6] I.V. Bargatin, B.A. Grishanin, and V.N. Zadkov, Phys. Rev. A **61**, 052305 (2000).

[7] R. Unanyan, N.V. Vitanov, and K. Bergmann, Phys. Rev. Lett.

87, 137902 (2001).
[8] R.G. Unanyan, S. Guérin, B.W. Shore, and K. Bergmann, Eur. Phys. J. D **8**, 443 (2000).
[9] L.P. Yatsenko, B.W. Shore, T. Halfmann, K. Bergmann, and A. Vardi, Phys. Rev. A **60**, R4237 (1999).
[10] T. Rickes, L.P. Yatsenko, S. Steuerwald, T. Halfmann, B.W. Shore, N.V. Vitanov, and K. Bergmann, J. Chem. Phys. **113**, 534 (2000).
[11] S. Guérin, L.P. Yatsenko, and H.R. Jauslin, Phys. Rev. A **63**, 031403 (2001).
[12] S. Guérin, F. Monti, J.M. Dupont, and H.R. Jauslin, J. Phys. A **30**, 7193 (1997).
[13] S. Guérin, R.G. Unanyan, L.P. Yatsenko, and H.R. Jauslin, Opt. Express **4**, 84 (1999).
[14] L.P. Yatsenko, S. Guérin, and H.R. Jauslin, Phys. Rev. A **65**, 043407 (2002).
[15] H.R. Jauslin, S. Guérin, and S. Thomas, Physica A **279**, 432 (2000).
[16] J.A. Jones, V. Vedral, A. Ekert, and G. Castagnoli, Nature (London) **403**, 869 (2000).
[17] R.G. Unanyan, B.W. Shore, and K. Bergmann, Phys. Rev. A **63**, 043405 (2001).

14.2 Preparation of atom-photon, atom-atom and photon-photon entanglement by adiabatic passage – Decoherence-free entanglement

In subsection 14.2.1, we first review various entanglements between atom and photons that can be generated by traveling atoms or photons when they interact with cavities adiabatically. This can be viewed as the counterpart of processes already known but with the use of non-robust π-pulse techniques, as reviewed in appendix A.

The adiabatic techniques offer the additional feature of decoherence-free processes when the fields (laser and cavity fields) have appropriate sequences. This is shown in subsection 14.2.2 for the preparation of atom-atom entanglement.

14.2.1 Preparation of atom-photon, atom-atom and photon-photon entanglement by adiabatic passage [247]

PHYSICAL REVIEW A **71**, 023805 (2005)

Atom-photon, atom-atom, and photon-photon entanglement preparation by fractional adiabatic passage

M. Amniat-Talab,[1,2,*] S. Guérin,[1,†] N. Sangouard,[1] and H. R. Jauslin[1]
[1]*Laboratoire de Physique, UMR CNRS 5027, Université de Bourgogne, B.P. 47870, F-21078 Dijon, France*
[2]*Physics Department, Faculty of Sciences, Urmia University, P.B. 165, Urmia, Iran*
(Received 28 July 2004; published 10 February 2005)

We propose a relatively robust scheme to generate maximally entangled states of (i) an atom and a cavity photon, (ii) two atoms in their ground states, and (iii) two photons in two spatially separate high-Q cavities. It is based on the interaction via fractional adiabatic passage of a three-level atom traveling through a cavity mode and a laser beam. The presence of optical phases is emphasized.

DOI: 10.1103/PhysRevA.71.023805 PACS number(s): 42.50.Dv, 03.65.Ud, 03.67.Mn

I. INTRODUCTION

One of the nonclassical aspects of a quantum system made of N parts is entanglement, for which the state vector of the system cannot be written, in any basis, as a tensor product of independent substates. The generation and the controlled manipulation of entangled states of N-particle systems is fundamental for the study of basic aspects of quantum theory [1,2]. The idea is to apply a set of controlled coherent interactions to the particles (atoms, ions, photons) of the system in order to bring them into a tailored entangled state. The physics of entanglement provides the basis of applications such as quantum information processing and quantum communications. Very recently teleportation of quantum states has been realized [3,4] using atom-atom entanglement following the proposal of Bennett *et al.* [5]. Particles can then be viewed as carriers of quantum bits of information and the realization of engineered entanglement is an essential ingredient of the implementation of quantum gates [6].

Most experimental realizations of entanglement have been implemented with photons. Although the individual polarization states of photons are easily controlled, and their quantum coherence can be preserved over many kilometers of an optical fiber [7], photons cannot be stored for long times, and manipulations of collective entangled states present considerable difficulties even when photons are confined in the same cavity. The creation of long-lived entangled pairs with atoms, on the other hand, is a relatively recent pursuit which may provide reliable quantum information storage. The entangled state of a pair of two-level atoms using pulse area technique in a microwave cavity has been realized by Hagley *et al.* [8] based on the proposal of Cirac and Zoller [9]. However, the pulse area technique is not robust with respect to the velocity of the atoms and the exact-resonance condition. Recently a different scheme has been proposed [10] to entangle two atoms using a tripod stimulated Raman adiabatic passage (STIRAP) technique in a four-level atom-cavity-laser system in which one of the pulses corresponds to the field of a cavity mode. Manipulation of entanglement of two atoms in this scheme, however, requires to control a geometric phase via an integral of Hamiltonian parameters over a closed path in parameter space which is difficult in experimental implementations. The generation of atom-photon entanglement has also been proposed in Ref. [11] in a tripodlike laser-atom-cavity system which sustains two cavity modes.

In Λ-type systems, fractional STIRAP (f-STIRAP) is a variation of STIRAP [12] which allows the creation of any preselected coherent superposition of the two degenerate ground states [13]. As in STIRAP, the Stokes pulse linking the initially unpopulated states $|e\rangle$ and $|g_2\rangle$, arrives before the pump pulse linking the initially populated state $|g_1\rangle$ to the excited state $|e\rangle$, but unlike STIRAP where the Stokes pulse vanishes first, here the two pulses vanish simultaneously while maintaining a constant finite ratio of amplitudes. The f-STIRAP has been shown to increase the coherence between the lower states of Λ systems in nonlinear optics experiments [14]. The advantage of STIRAP is the robustness of its control with respect to the precise tuning of pulse areas, pulse delay, pulse widths, pulse shapes, and detunings. Since f-STIRAP requires a precise ratio of pulse endings, it is not as robust as STIRAP if two different pulses are used. However, in specific circumstances where a laser of elliptic polarization can be used, f-STIRAP can be made as robust as STIRAP [13]. In f-STIRAP as in STIRAP, if the evolution is adiabatic (for instance with a slow transit of atoms across cw fields), the dynamics of the system follows an adiabatic dark state which does not involve the excited atomic state $|e\rangle$. Therefore this technique is immune to the detrimental consequences of atomic spontaneous emission. The STIRAP technique has interesting applications in the generation of coherent superposition of Fock states [15,16] and of maximally polarization-entangled photon states [17] in an optical cavity.

In this paper we consider neutral three-level Λ-type atoms with twofold degenerate ground states $|g_1\rangle$, $|g_2\rangle$ and an excited state $|e\rangle$. The qubits are stored in the two ground states of the atoms. Our scheme to create the entangled states is based on the resonant interaction of the atoms with an optical cavity mode and a laser field as follows:

(i) Atom-photon entanglement: the first atom initially in the ground state $|g_1\rangle$ interacts with the cavity mode (initially

*Electronic address: amniyatm@u-bourgogne.fr
†Electronic address: sguerin@u-bourgogne.fr

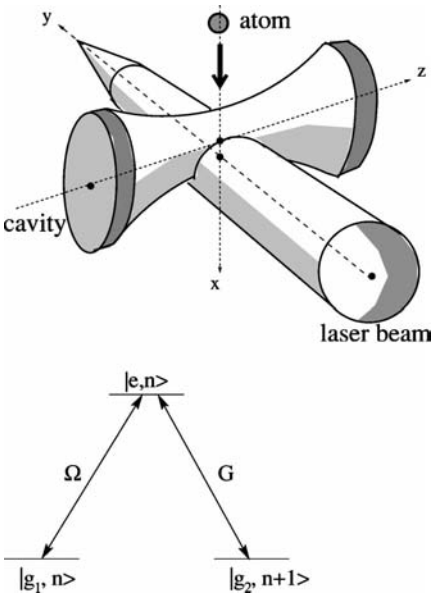

FIG. 1. Experimental configuration and the linkage pattern of atom-cavity-laser system with a two-photon resonance between states $|g_1,n\rangle$ and $|g_2,n+1\rangle$.

in the vacuum state) and the laser field in the frame of f-STIRAP with the cavity-laser sequence (meaning that the atom meets first the cavity).

(ii) Atom-atom entanglement: when the first atom has left the interaction region, the second atom initially in the ground state $|g_2\rangle$ interacts with the laser-cavity sequence in the frame of STIRAP. After the creation of an entangled state of the atoms, the cavity mode is left in the vacuum state which is not entangled with the two atoms. Therefore the decoherence effect of the cavity damping does not affect the atom-atom entanglement before and after the interaction. The cavity damping must be negligible only during the time of entanglement preparation.

(iii) Photon-photon entanglement: after the interaction of the atom with the first cavity and the laser field in the frame of f-STIRAP, the same atom interacts with the same laser field and the second cavity in the frame of STIRAP. At the end of the interaction, the atomic state factorizes and is left in the ground state $|g_2\rangle$.

II. CONSTRUCTION OF THE EFFECTIVE HAMILTONIAN

Figure 1 represents the linkage pattern of the atom-cavity-laser system. The laser pulse associated to the Rabi frequency $\Omega(t)$ couples the states $|g_1\rangle$ and $|e\rangle$, and the cavity mode (Stokes pulse) with Rabi frequency $G(t)$ couples the states $|e\rangle$ and $|g_2\rangle$. The Rabi frequencies $\Omega(t)$ and $G(t)$ are chosen real and positive without loss of generality. These two fields interact with the atom with a time delay, each of the fields is in one-photon resonance with the respective transition. The semiclassical Hamiltonian (i.e., with a classical laser field) of this system in the rotating-wave approximation can be written in the atomic basis $\{|g_1\rangle,|e\rangle,|g_2\rangle\}$ (in units of $\hbar$) as

$$H(t)=\omega_C a^\dagger a+\begin{bmatrix}0 & \Omega(t)e^{i(\omega_L t+\varphi_L)} & 0\\ \Omega(t)e^{-i(\omega_L t+\varphi_L)} & \omega_e & G(t)a\\ 0 & G(t)a^\dagger & 0\end{bmatrix}, \tag{1}$$

where $a(a^\dagger)$ is the annihilation (creation) operator for the cavity mode, ω_e is the energy of the atomic excited state ($\omega_{g_1}=\omega_{g_2}=0$), ω_C, ω_L are the carrier frequencies of the cavity mode and the laser field respectively $\omega_C=\omega_L=\omega_e$, and φ_L is the initial phase of the laser field. The time dependence of $\Omega(t)$ and $G(t)$ comes from the motion of the atom across the laser and cavity fields and the time origin is defined below.

The Hamiltonian $H(t)$ is block diagonal in the manifolds $\{|g_1,n\rangle,|e,n\rangle,|g_2,n+1\rangle;\ n=0,1,2,\ldots\}$, where n is the number of photons in the cavity mode, $|e,n\rangle\equiv|e\rangle\otimes|n\rangle$ and $|n\rangle$ is a n-photon Fock state. The vector $|g_2,0\rangle$ is not coupled to any other ones, i.e., $|g_2,0\rangle$ is a *stationary state* of the system. One can thus restrict the problem to the projection of the Hamiltonian in the subspace $\{|g_1,0\rangle,|e,0\rangle,|g_2,1\rangle\}$:

$$H_P:=PHP, \tag{2a}$$

$$P=|g_1,0\rangle\langle g_1,0|+|e,0\rangle\langle e,0|+|g_2,1\rangle\langle g_2,1|, \tag{2b}$$

if one considers the initial state $|g_1,0\rangle$. The associated dynamics is determined by the Schrödinger equation $i(\partial/\partial t)|\Psi(t)\rangle=H_P(t)|\Psi(t)\rangle$. The effective Hamiltonian can be written as

$$H^{\text{eff}}=R^\dagger H_P R-iR^\dagger\frac{\partial R}{\partial t}, \tag{3a}$$

$$R(t)=|g_1,0\rangle\langle g_1,0|+e^{-i\omega_L t}(|e,0\rangle\langle e,0|+|g_2,1\rangle\langle g_2,1|), \tag{3b}$$

which reads in the basis $\{|g_1,0\rangle,|e,0\rangle,|g_2,1\rangle\}$

$$H^{\text{eff}}(t)=\begin{bmatrix}0 & \Omega(t)e^{i\varphi_L} & 0\\ \Omega(t)e^{-i\varphi_L} & 0 & G(t)\\ 0 & G(t) & 0\end{bmatrix}, \tag{4}$$

with the corresponding dynamics $i(\partial/\partial t)|\Phi(t)\rangle=H^{\text{eff}}(t)|\Phi(t)\rangle$. The relation between $|\Psi\rangle$ and $|\Phi\rangle$ is established by unitary transformation R as $|\Psi\rangle=R|\Phi\rangle$.

III. ATOM-PHOTON ENTANGLEMENT

The system is taken to be initially in the state $|g_1,0\rangle$,

$$|\Phi(-\infty)\rangle=|g_1,0\rangle=|\Psi(-\infty)\rangle \tag{5}$$

and we will transform it at the end of interaction into the atom-photon entangled state

$$|\Phi(t\to+\infty)\rangle=\cos\vartheta|g_1,0\rangle-e^{-i\varphi_L}\sin\vartheta|g_2,1\rangle, \tag{6a}$$

$$|\Psi(t\to+\infty)\rangle=\cos\vartheta|g_1,0\rangle-e^{-i(\omega_L t+\varphi_L)}\sin\vartheta|g_2,1\rangle, \tag{6b}$$

where ϑ is a constant mixing angle ($0\leq\vartheta\leq\pi/2$). It is important to notice the presence of the generally unknown ab-

solute phase $\omega_L t+\varphi_L$ in the resulting entangled state (6b). This optical phase factor was not taken into account by Parkins *et al.* in the generation of an arbitrary superpositions of Fock states [15]. This phase that changes rapidly as a function of the time, is expected to be uncontrollable in practice.

One of the instantaneous eigenstates (the dark state) of $H^{\text{eff}}(t)$ which corresponds to a zero eigenvalue, and therefore to a zero dynamical phase, is

$$|D(t)\rangle = \frac{1}{\sqrt{\Omega^2(t)+G^2(t)}}[G(t)|g_1,0\rangle - \Omega(t)e^{-i\varphi_L}|g_2,1\rangle]. \tag{7}$$

As in f-STIRAP, the cavity-mode pulse comes first and is followed after a certain time delay by the laser pulse, but the two pulses vanish simultaneously, that can be asymptotically formulated as

$$\lim_{t\to-\infty}\frac{\Omega(t)}{G(t)}=0, \quad \lim_{t\to+\infty}\frac{\Omega(t)}{G(t)}=\tan\vartheta. \tag{8}$$

The dark state (7) has consequently the limits $|D(-\infty)\rangle = |g_1,0\rangle$ and $|D(+\infty)\rangle = \cos\vartheta|g_1,0\rangle - e^{-i\varphi_L}\sin\vartheta|g_2,1\rangle$ with such a pulse sequence and allows thus one to generate a coherent superposition of states by adiabatic passage. It should be emphasized that this formulation in terms of asymptotics (8) does not describe correctly what occurs at the beginning and the ending of f-STIRAP for a concrete realization which is not strictly adiabatic. In particular, using this asymptotics would give a failure of f-STIRAP for Gaussian pulses (considered below), which do not asymptotically give a constant ending ratio for any delay and pulse width. The inspection of the nonadiabatic couplings [13] shows that what matters is that the Rabi frequency amplitudes end in a constant ratio *in a time interval where they are non-negligible*, and Eq. (8) has to be understood in this sense. The goal in the following is to show that such a pulse sequence can be designed in a cavity by an appropriate choice of the parameters.

In an optical cavity, the spatial variation of the atom-field coupling for a Hermite-Gauss TEM_{mn} mode is given by

$$G_{mn}(x,y,z) = G_0 H_m\left(\frac{\sqrt{2}x}{W_C}\right)H_n\left(\frac{\sqrt{2}y}{W_C}\right) \times e^{-(x^2+y^2)/W_C^2}\cos\left(\frac{2\pi z}{\lambda}\right), \tag{9}$$

where $G_0=\mu\sqrt{\omega_C/(2\epsilon_0 V_{\text{mode}})}$ with μ, V_{mode} respectively the dipole moment of the atomic transition and the effective volume of the cavity mode. The transverse distribution is determined by Hermite polynomials H_m, H_n and the cavity waist W_C [18]. The standing wave along the cavity z axis gives rise to a $\cos(2\pi z/\lambda)$ dependence of the mode with the wavelength λ. A particular transverse mode is selected by adjusting the cavity length. We consider the maximum coupling mode TEM_{00} resonant with the $|e\rangle\leftrightarrow|g_2\rangle$ transition of the atom

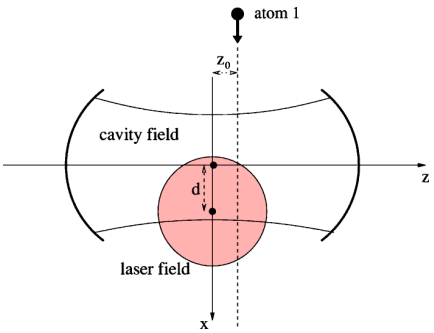

FIG. 2. The geometry of the cavity mode and the laser fields in the xy plane with different waists ($W_C > W_L$), and the trajectory of the first atom. The specific values of z_0 and d are chosen such that the atom interacts with the fields via f-STIRAP with the sequence cavity-laser.

$$G(x,y,z) = G_0 e^{-(x^2+y^2)/W_C^2}\cos\left(\frac{2\pi z}{\lambda}\right). \tag{10}$$

Figure 2 shows a situation where an atom initially in the state $|g_1\rangle$ falls with velocity v (on the $y=0$ plane and $z=z_0$ line) through an optical cavity initially in the vacuum state $|0\rangle$ and then encounters the laser beam, which is parallel to the y axis (orthogonal to the cavity axis and the trajectory of the atom). The laser beam of waist W_L is resonant with the $|e\rangle\leftrightarrow|g_1\rangle$ transition. The distance between center of the cavity and the laser axis is d. The traveling atom encounters the time dependent and delayed Rabi frequencies of the cavity and the laser fields as follows:

$$G(t) = G_0 e^{-(vt)^2/W_C^2}\cos\left(\frac{2\pi z_0}{\lambda}\right), \tag{11a}$$

$$\Omega(t) = \Omega_0 e^{-z_0^2/W_L^2}\, e^{-(vt-d)^2/W_L^2}, \tag{11b}$$

where the time origin is defined when the atom meets the center of the cavity $x=0$. The appropriate values of z_0 and d that lead to the f-STIRAP process can be extracted from a contour plot of the final population $P_{|g_1,0\rangle} := |\langle g_1,0|\Phi(+\infty)\rangle|^2$ as a function of z_0 and d that we calculate numerically (see Fig. 3). The white dot in Fig. 3 shows values of z_0 and d to obtain a f-STIRAP process with $\vartheta\simeq\pi/4$ (called half-STIRAP). It has been chosen such that at the end of interaction $P_{|g_1,0\rangle}\simeq P_{|g_2,1\rangle}\simeq 0.5$ and $P_{|e,0\rangle}\simeq 0$.

Figure 4 shows (a) the cavity-laser pulse sequence of half-STIRAP for the first atom, and (b) the time evolution of populations which shows half-half population for the states $|g_1,0\rangle$, $|g_2,1\rangle$ and zero population for the state $|e,0\rangle$ at the end of the interaction. This case corresponds to the generation of the maximally atom-photon entangled state $1/\sqrt{2}(|g_1,0\rangle - e^{-i(\omega_L t+\varphi_L)}|g_2,1\rangle)$ by adiabatic passage. Assuming Gaussian pulse profiles for $\Omega(t)$ and $G(t)$ of widths $T_L = W_L/v$ and $T_C = W_C/v$, respectively, we have the sufficient condition of adiabaticity [13]:

$$\Omega_0 T_L, G_0 T_C \gg 1. \tag{12}$$

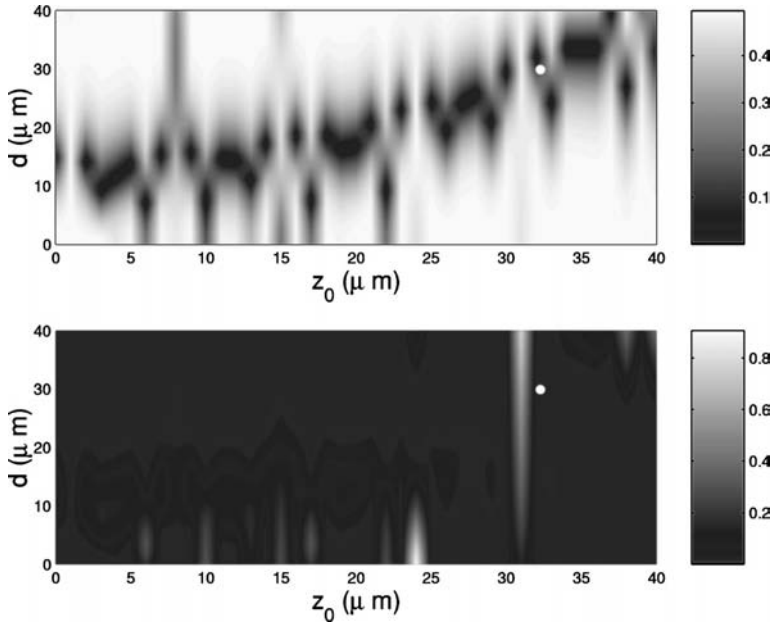

FIG. 3. Top panel: contour plot of the final population $\left|\frac{1}{2}-P_{|g_1,0\rangle}\right|$ as a function of z_0 and d (black areas correspond to approximately half population transfer) with the pulse parameters as $W_L=20\ \mu$m, $W_C=30\ \mu$m, $v=2$ m/s, $\lambda=780$ nm, $\Omega_0=50(v/W_L)$, $G_0=50(v/W_C)$. Bottom panel: the same plot for the population of the excited state $P_{|e,0\rangle}:=|\langle e,0|\Phi(+\infty)\rangle|^2$ where black areas correspond to approximately zero population transfer. The white dot shows specific values of z_0 and d used in Fig. 4 to obtain a half-STIRAP process.

We remark that the case $\vartheta=\pi/2$ corresponds to the standard STIRAP with the final state $|\Psi(t\rightarrow+\infty)\rangle=-e^{-i(\omega_L t+\varphi_L)}|g_2,1\rangle$, i.e., to the generation of a single-photon Fock state in the cavity mode without population transfer to the atomic excited state at the end of interaction. Here the optical phase factor appears as an irrelevant global phase factor. A one-photon Fock state has been produced in such a way in an optical cavity via STIRAP by Hennrich *et al.* [19] based on the proposal of Refs. [15,20]. A robust scheme for the generation of multiphoton Fock states in a microwave cavity via bichromatic adiabatic passage has been proposed in Ref. [21].

IV. ATOM-ATOM ENTANGLEMENT

In this section we consider a situation where the first atom has been entangled with the cavity mode via f-STIRAP as described by Eq. (6b), and the second atom initially in the ground state $|g_2^{(2)}\rangle$ is going to interact with the *same* laser and cavity-mode fields but through a STIRAP process (see Fig. 5). The superscript labels the two atoms. The state of the atom$^{(2)}$-atom$^{(1)}$-cavity system after entanglement of the atom$^{(1)}$ reads

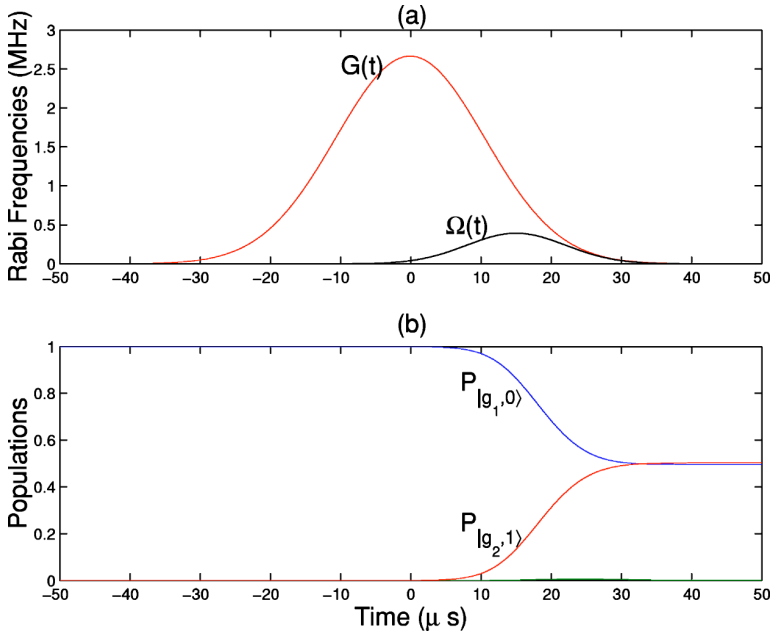

FIG. 4. (a) Rabi frequencies of the cavity mode and the laser field for the first atom corresponding to the same pulse parameters and the specific values $z_0=31.9\ \mu$m, $d=30.2\ \mu$m of the white dot in Fig. 3. (b) Time evolution of the populations for the trajectory of the first atom which represents a half-STIRAP.

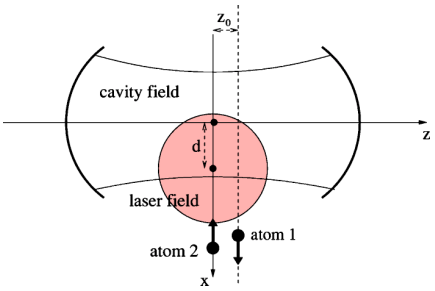

FIG. 5. The proposed geometry of the cavity and the laser fields in xz plane as well as the trajectory of the atoms for generation of atom-atom entanglement. The second atom initially in the ground state $|g_2\rangle$ arrives at the center of the cavity with a time delay τ. This atom encounters the sequence laser cavity on the line $z=0$.

$$|\Psi(t)\rangle = |g_2^{(2)}\rangle(\cos\vartheta|g_1^{(1)},0\rangle - e^{-i(\omega_L t+\varphi_L)}\sin\vartheta|g_2^{(1)},1\rangle). \tag{13}$$

The second atom moves on the line $z=0$ in the same plane (see Fig. 5) as the first one such that the two atoms experience the same optical phase $e^{i\omega t}$ of the laser field. It encounters time-dependent and delayed Rabi frequencies given by

$$G^{(2)}(t) = G_0 e^{-[v(t-\tau)]^2/W_C^2}, \tag{14a}$$

$$\Omega^{(2)}(t) = \Omega_0 e^{-[v(t-\tau)+d]^2/W_L^2}, \tag{14b}$$

where τ is the time delay between the two atoms. By standard STIRAP, with the sequence of laser-cavity (see Fig. 6), we can transfer the population from the initial state $|g_2^{(2)},1\rangle$to the final state $|g_1^{(2)},0\rangle$. On the other hand the state $|g_2^{(2)},0\rangle$ is stationary with respect to this STIRAP process. Using the transformation $R^{(2)}(t)=|g_1^{(2)},0\rangle\langle g_1^{(2)},0|+e^{-i\omega_L t}(|e^{(2)},0\rangle\langle e^{(2)},0|+|g_2^{(2)},1\rangle\langle g_2^{(2)},1|)$, this results in

$$|g_2^{(2)},0\rangle \to |g_2^{(2)},0\rangle, \quad -e^{-i(\omega_L t+\varphi_L)}|g_2^{(2)},1\rangle \to |g_1^{(2)},0\rangle. \tag{15}$$

Hence if the second atom encounters the laser field before the cavity field in the frame of a standard STIRAP, the final state of the atom$^{(2)}$-atom$^{(1)}$-cavity system will be

$$\begin{aligned}|\Psi(+\infty)\rangle &= \cos\vartheta|g_2^{(2)},0\rangle|g_1^{(1)}\rangle + \sin\vartheta|g_1^{(2)},0\rangle|g_2^{(1)}\rangle \\ &= |0\rangle(\cos\vartheta|g_2^{(2)}\rangle|g_1^{(1)}\rangle + \sin\vartheta|g_1^{(2)}\rangle|g_2^{(1)}\rangle).\end{aligned} \tag{16}$$

Since the cavity-mode state factorizes and is left in the vacuum state, there is no projection noise when one traces over the unobserved cavity field, and the cavity is ready to prepare another entanglement. We can manipulate this entanglement coherently to reach the maximal atom-atom entanglement by tuning the ratio of fields such that $\tan\vartheta=1$ in the f-STIRAP stage, as shown in Figs. 3 and 4.

Figure 6 shows the successful STIRAP process for the second atom (moving along the line $z=0$) that allows one to generate the entangled state (16).

The generation of atom-atom entanglement with the two atoms interacting simultaneously ($\tau=0$ in Fig. 5) with the cavity mode, that can be described by a two-atom dark state presented in Ref. [22], will be discussed elsewhere.

V. PHOTON-PHOTON ENTANGLEMENT

In Refs. [23–25] among many others, different schemes have been proposed to entangle two and three microwave

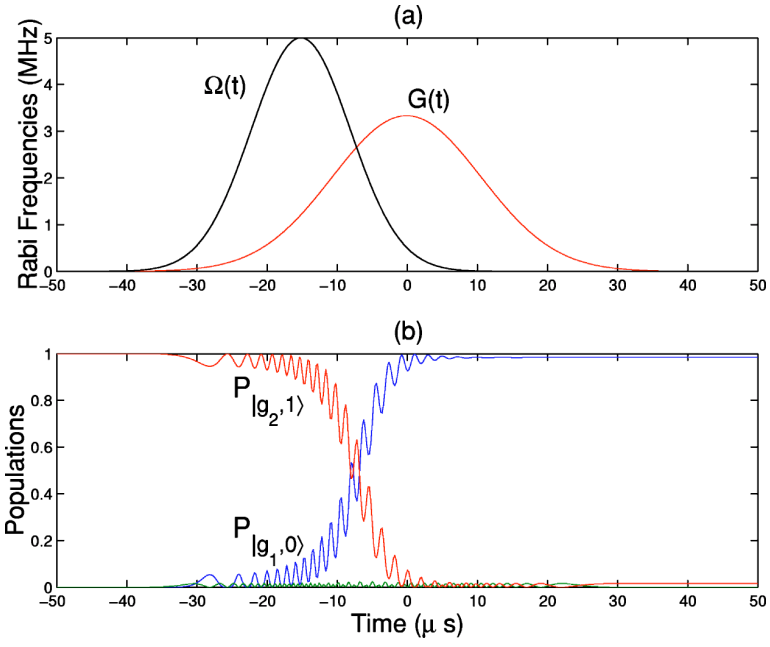

FIG. 6. (a) Rabi frequencies of the fields for the second atom traveling on the line $z=0$ with the same parameters of Fig. 4. (b) Time evolution of the populations.

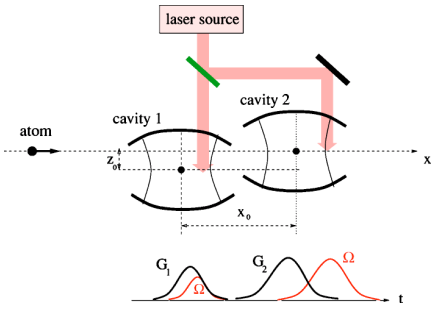

FIG. 7. Proposed setup for entangling of two photons generated in two optical cavities interacting with a three-level atom and a laser field, and the schematic pulse sequences. The atom interacts with the first cavity via f-STIRAP in the same conditions of Fig. 2 and next with the second cavity via standard STIRAP with the sequence cavity laser in each one. The propagation direction of the laser beams are perpendicular to the plane *xz* as in Fig 1.

cavities through the interaction with a Rydberg atom. A method of generating particular entangled states of two cavities appeared as an intermediate step in the teleportation procedure proposed by Davidovich *et al.* [26]. Here we propose another scheme to entangle two optical cavities interacting with an atom. We consider a situation where an atom has been entangled with the first single-mode cavity via a f-STIRAP technique as described in Sec. II, and it interacts next with another single-mode optical cavity, initially in the vacuum state, and the same laser field (see Fig. 7). The distance z_0 between the axis of motion of the atom and the center of the first cavity, ensures having an f-STIRAP process for the first cavity. Hence the state of the cavity$^{(2)}$-atom-cavity$^{(1)}$ system after the f-STIRAP process is

$$|\Psi(t)\rangle = |0^{(2)}\rangle(\cos\vartheta|g_1,0^{(1)}\rangle - e^{-i(\omega_L t+\varphi_L)}\sin\vartheta|g_2,1^{(1)}\rangle), \tag{17}$$

where the superscripts denote the number of cavities. If the atom interacts with the second cavity in the frame of a standard STIRAP and the atom encounters the cavity mode before the laser pulse, since the state $|g_1,0^{(2)}\rangle$ evolves to $|g_2,1^{(2)}\rangle$ and the state $|g_2,0^{(2)}\rangle$ does not change during the interaction:

$$|g_1,0^{(2)}\rangle \rightarrow -e^{-i(\omega_L t+\varphi_L)}|g_2,1^{(2)}\rangle,$$

$$|g_2,0^{(2)}\rangle \rightarrow |g_2,0^{(2)}\rangle, \tag{18}$$

the final state of the system will be (up to an irrelevant common phase factor)

$$|\Psi(+\infty)\rangle = |g_2\rangle(\cos\vartheta|1^{(2)},0^{(1)}\rangle + e^{i\alpha}\sin\vartheta|0^{(2)},1^{(1)}\rangle), \tag{19}$$

where $\alpha = 2\pi(x_0^2+z_0^2)^{1/2}/\lambda$ is the phase shift of the laser field due to the optical path difference between the two cavities. Since the atomic state factorizes and is left in the ground state $|g_2\rangle$, the atom does not have spontaneous emission and it could be used to prepare another entanglement.

VI. DISCUSSIONS AND CONCLUSIONS

We have proposed a robust scheme to generate atom-photon, atom-atom, and photon-photon entanglement, using a combination of f-STIRAP and STIRAP techniques in Λ systems. This scheme is robust with respect to variations of the velocity of the atom v, of the peak Rabi frequencies G_0, Ω_0 and of the pulse detunings, but not with respect to the parameters d, z_0. For given values of W_C, W_L, the adapted values of d and z_0 in the f-STIRAP process can be determined from a contour plot of the final populations as explained in Sec. III.

The presence of optical phases in the case of atom-photon entanglement, expected to be uncontrollable, was emphasized. In the case of atom-atom entanglement the optical phase is not present, as long as the two atoms move in the same plane perpendicular to the propagation direction of the laser beam.

Dissipation in the form of spontaneous emission and cavity damping is another important practical issue. The adiabatic passage technique is robust against the effects of spontaneous emission, as the excited atomic state is never appreciably populated. Cavity damping is certainly a problem as its effects come into play as soon as the cavity mode is excited, leading to a degradation of the adiabatic transfer. In this analysis we have assumed that the interaction time between the atom and the fields $T_{\rm int} \approx W_C/v \approx W_L/v$ is short compared to the cavity lifetime $T_{\rm cav}$, which are essential for an experimental realization.

Since the decay rate of the cavity scales with the number of photons present in the cavity ($T_{\rm int} \ll T_{\rm cav}/n$), our scheme involving only one cavity photon requires $T_{\rm int} \ll T_{\rm cav}$. In a real experiment, it is desirable that the entangled states are as long-lived as possible. This requires in the optical domain, where $T_{\rm int} \approx 15$ μs, a cavity lifetime of $T_{\rm cav} \gg 15$ μs. This is beyond the currently available optical cavities where $T_{\rm cav} \approx 1$ μs. One could still consider the generation of atom-atom entanglement in an optical cavity using a two-atom dark state of the type presented in Ref. [22] which does not require such a stringent constraint for the cavity lifetime. In the microwave domain, cavities with a photon lifetime of 1 ms [27] and of 0.3 s [28] have been made. The upper limit of interaction time is $T_{\rm int} = 100$ μs (atom with a velocity of 100 m/s with the cavity mode waist of $W_C = 6$ mm). The condition of global adiabaticity $G_0\, T_{\rm int} \gg 1$ for the typical value of $G_0 \approx 0.15$ MHz [27] is well satisfied $G_0 T_{\rm int} \approx 15$. The proposed schemes of entanglement generation could be implemented in a microwave cavity by using a maser field and atomic Rydberg states.

ACKNOWLEDGMENTS

M.A.-T. wishes to acknowledge the financial support of the MSRT of Iran and SFERE. We acknowledge support from the Conseil Régional de Bourgogne.

[1] A. Einstein, B. Podolski, and N. Rosen, Phys. Rev. **47**, 777 (1935).
[2] J. S. Bell, Physics (Long Island City, N.Y.) **1**, 195 (1964).
[3] M. Riebe *et al.*, Nature (London) **429**, 734 (2004).
[4] M. D. Barrett *et al.*, Nature (London) **429**, 737 (2004).
[5] C. H. Bennett, G. Brassard, C. Crépeau, R. Jozsa, A. Peres, and W. K. Wootters, Phys. Rev. Lett. **70**, 1895 (1993).
[6] A. Ekert and R. Jozsa, Rev. Mod. Phys. **68**, 733 (1996).
[7] W. Tittel, J. Brendel, B. Gisin, T. Herzog, H. Zbinden, and N. Gisin, Phys. Rev. A **57**, 3229 (1998).
[8] E. Hagley, X. Maître, G. Nogues, C. Wunderlich, M. Brune, J. M. Raimond, and S. Haroche, Phys. Rev. Lett. **79**, 1 (1997).
[9] J. I. Cirac and P. Zoller, Phys. Rev. A **50**, R2799 (1994).
[10] S. Q. Gong, R. Unanyan, and K. Bergmann, Eur. Phys. J. D **19**, 257 (2002).
[11] B. Sun, M. S. Chapman, and L. You, Phys. Rev. A **69**, 042316 (2004).
[12] N. V. Vitanov, T. Halfmann, B. W. Shore, and K. Bergmann, Annu. Rev. Phys. Chem. **52**, 763 (2001).
[13] N. V. Vitanov, K. A. Suominen, and B. W. Shore, J. Phys. B **32**, 4535 (1999).
[14] V. A. Sautenkov, C. Y. Ye, Y. V. Rostovtsev, G. R. Welch, and M. O. Scully, Phys. Rev. A **70**, 033406 (2004).
[15] A. S. Parkins, P. Marte, P. Zoller, and H. J. Kimble, Phys. Rev. Lett. **71**, 3095 (1993).
[16] A. S. Parkins, P. Marte, P. Zoller, O. Carnal, and H. J. Kimble, Phys. Rev. A **51**, 1578 (1995).
[17] W. Lange and H. J. Kimble, Phys. Rev. A **61**, 063817 (2000).
[18] M. Keller, B. Lange, K. Hayasaka, W. Lange, and H. Walther, J. Phys. B **36**, 613 (2003).
[19] M. Hennrich, T. Legero, A. Kuhn, and G. Rempe, Phys. Rev. Lett. **85**, 4872 (2000).
[20] A. Kuhn, M. Hennrich, T. Bondo, and G. Rempe, Appl. Phys. B: Lasers Opt. **69**, 373 (1999).
[21] M. Amniat-Talab, S. Lagrange, S. Guérin, and H. R. Jauslin, Phys. Rev. A **70**, 013807 (2004).
[22] T. Pellizzari, S. A. Gardiner, J. I. Cirac, and P. Zoller, Phys. Rev. Lett. **75**, 3788 (2001).
[23] C. C. Gerry, Phys. Rev. A **54**, R2529 (1996).
[24] J. A. Bergou and M. Hillery, Phys. Rev. A **55**, 4585 (1997).
[25] D. E. Browne and M. B. Plenio, Phys. Rev. A **67**, 012325 (2003).
[26] L. Davidovich, N. Zagury, M. Brune, J. M. Raimond, and S. Haroche, Phys. Rev. A **50**, R895 (1994).
[27] J. M. Raimond, M. Brune, and S. Haroche, Rev. Mod. Phys. **73**, 565 (2001).
[28] S. Brattke, B. T. H. Varcoe, and H. Walther, Phys. Rev. Lett. **86**, 3534 (2001).

14.2.2 Decoherence-free creation of atom-atom entanglement in cavity via fractional STIRAP [248]

PHYSICAL REVIEW A **72**, 012339 (2005)

Decoherence-free creation of atom-atom entanglement in a cavity via fractional adiabatic passage

Mahdi Amniat-Talab,[1,2,*] Stéphane Guérin,[1,†] and Hans-Rudolf Jauslin[1,‡]
[1]*Laboratoire de Physique, UMR CNRS 5027, Université de Bourgogne, Boîte Postale 47870, F-21078 Dijon, France*
[2]*Physics Department, Faculty of Sciences, Urmia University, P.B. 165, Urmia, Iran*
(Received 23 March 2005; published 28 July 2005)

We propose a robust and decoherence insensitive scheme to generate controllable entangled states of two three-level atoms interacting with an optical cavity and a laser beam. Losses due to atomic spontaneous transitions and to cavity decay are efficiently suppressed by employing fractional adiabatic passage and appropriately designed atom-field couplings. In this scheme the two atoms traverse the cavity-mode and the laser beam in opposite directions and become entangled in the free space outside the cavity. We also show that the coherence of a traveling atom can be transferred to the other one without populating the cavity mode.

DOI: 10.1103/PhysRevA.72.012339 PACS number(s): 03.67.Mn, 32.80.Qk, 42.50.Dv, 03.65.Ud

I. INTRODUCTION

The physics of entanglement provides the basis of applications such as quantum information processing and quantum communications. Particles can then be viewed as carriers of quantum bits of information and the realization of engineered entanglement is an essential ingredient of the implementation of quantum gates [1], cryptography [2], and teleportation [3]. The creation of long-lived entangled pairs of atoms may provide reliable quantum information storage. The idea is to apply a set of controlled coherent interactions to the atoms of the system in order to bring them into a tailored entangled state. The problem of controlling entanglement is thus directly connected to the problem of coherent control of population transfer in multilevel systems.

In the context of cavity QED, one of the main obstacles to realize atom-atom entanglement is the decoherence resulting from the cavity decay. Additionally, the cavity couples to an excited state of the atom that undergoes spontaneous emission. Regarding these considerations, in recent years several schemes to entangle atoms [4,5] and to implement quantum gates [6–10] using optical cavities have been proposed. Very recently another scheme to entangle two traveling atoms in the atoms-cavity-laser system via adiabatic passage has been proposed in Ref. [11]. However, this scheme requires one to turn off the laser field when the two atoms have equal coupling with the cavity mode, which is very difficult from the experimental point of view. Moreover, this scheme requires one to compensate a dynamical Stark shift which is also very difficult in a real experiment. To avoid decoherence effects, it is most convenient to design transfer strategies that do not populate the decoherence channels during the time evolution of the system.

In this paper we propose an alternative way to entangle two traveling atoms interacting with an optical cavity and a laser beam, based on three-level interactions in a Λ configuration. This method is based on the coherent creation of superposition of atom-atom-cavity states via fractional stimulated Raman adiabatic passage (f-STIRAP) [12] that keeps the cavity mode and the excited atomic states unpopulated during the whole interaction. In Ref. [13], using f-STIRAP and a one-atom dark state, a robust scheme to generate atom-atom entanglement was proposed, where the two traveling atoms encounter the cavity mode one by one. Here, the two atoms enter simultaneously into the cavity in such a way that the system follows a two-atom dark state that allows us to keep additionally the cavity mode empty.

II. CONSTRUCTION OF THE MODEL

We consider the situation described in Fig. 1, where the two atoms move in planes orthogonal to the z axis as follows:

$$z_1 = z_0,\ x_1 = -x_0 + v_1 t\cos\theta_1, \quad y_1 = -y_0 + v_1 t\sin\theta_1,$$

$$z_2 = 0,\ x_2 = x_0 + v_2(t-\tau)\cos\theta_2,$$

$$y_2 = -y_0 + v_2(t-\tau)\sin\theta_2, \tag{1}$$

where $(x_i, y_i, z_i), i=1,2$ are the coordinates of the ith atom $(x_0, y_0 > 0)$, τ is the time delay of the second atom with re-

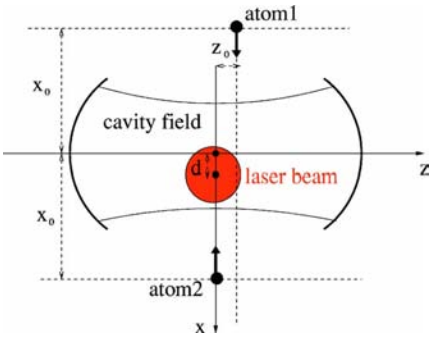

FIG. 1. (Color online) Geometrical configuration of the atoms-cavity-laser system in the proposed scheme. The propagation direction of the laser beam is parallel to the y axis and perpendicular to the page.

*Electronic address: amniyatm@u-bourgogne.fr
†Electronic address: sguerin@u-bourgogne.fr
‡Electronic address: jauslin@u-bourgogne.fr

spect to the first one, θ_i is the angle that the ith atom constructs with the positive direction of the x axis ($\theta_1 \in [0, \pi/2[, \theta_2 \in]\pi/2, \pi]$), and v_i is the velocity of the ith atom. Since the laser field propagates in the direction of the y axis, the time-dependent optical phase of the laser field, taking into account the Doppler shift, seen by each atom is

$$\varphi_1(t) = \omega_L t - k v_1 t \sin\theta_1, \quad \varphi_2(t-\tau) = \omega_L t - k v_2 (t-\tau) \sin\theta_2, \tag{2}$$

where k is the wave-vector magnitude of the laser field. Figure 2 represents the linkage pattern of the atom-cavity-laser system. The laser pulse associated with the Rabi frequency $\Omega(t)$ couples the states $|g_1\rangle$ and $|e\rangle$, and the cavity-mode with Rabi frequency $G(t)$ couples the states $|e\rangle$ and $|g_2\rangle$. The Rabi frequencies $\Omega(t)$ and $G(t)$ are chosen real without loss of generality. These two fields interact with the atom with a time delay, each of the fields is in one-photon resonance with the respective transition. The semiclassical Hamiltonian of this system in the resonant approximation where

$$|\Omega_0|, |G_0| \ll \omega_e, \omega_C, |\partial\varphi_1/\partial t|, |\partial\varphi_2/\partial t|, \tag{3}$$

with Ω_0, G_0 the peak values of the Rabi frequencies, can then be written as ($\hbar = 1$)

$$H(t) = \sum_{i=1,2} \{\omega_e |e\rangle_{ii}\langle e| + [G_i(t) a |e\rangle_{ii}\langle g_2| + \text{H.c.}] + [\Omega_i(t) e^{i\varphi_i(t)} |g_1\rangle_{ii}\langle e| + \text{H.c.}]\} + \omega_C a^\dagger a, \tag{4}$$

where the subscript i on the states denotes the two atoms, a is the annihilation operator of the cavity mode, ω_e is the energy of the atomic excited state ($\omega_{g_1} = \omega_{g_2} = 0$), and ω_C is the frequency of the cavity mode taking resonant $\omega_C = \omega_L = \omega_e$ which implies $k v_i \sin\theta_i \ll \omega_L$. In the following we consider the state of the atom1-atom2-cavity system as $|A1, A2, n\rangle$ where $\{A1, A2 = g_1, e, g_2\}$, and $\{n = 0, 1\}$ is the number of photons in the cavity mode.

Regarding Fig. 2, the subspace $\mathcal{S}$ generated by the states $\{|g_1, g_2, 0\rangle, |e, g_2, 0\rangle, |g_2, g_2, 1\rangle, |g_2, e, 0\rangle, |g_2, g_1, 0\rangle\}$ is decoupled under H from the rest of the Hilbert space of the system. If we consider the initial state of the system as $|g_1, g_2, 0\rangle$, the Hamiltonian of the system in the subspace $\mathcal{S}$ will be

$$H_P(t) := PHP = \begin{pmatrix} 0 & \Omega_1(t) e^{+i\varphi_1(t)} & 0 & 0 & 0 \\ \Omega_1(t) e^{-i\varphi_1(t)} & \omega_e & G_1(t) & 0 & 0 \\ 0 & G_1(t) & \omega_C & G_2(t-\tau) & 0 \\ 0 & 0 & G_2(t-\tau) & \omega_e & \Omega_2(t-\tau) e^{-i\varphi_2(t-\tau)} \\ 0 & 0 & 0 & \Omega_2(t-\tau) e^{+i\varphi_2(t-\tau)} & 0 \end{pmatrix}, \tag{5}$$

where P is the projector on the subspace $\mathcal{S}$. The effective Hamiltonian is thus given by

$$H^{\text{eff}} := R^\dagger H_P R - i R^\dagger \frac{\partial R}{\partial t} = \begin{bmatrix} 0 & \Omega_1(t) & 0 & 0 & 0 \\ \Omega_1(t) & k v_1 \sin\theta_1 & G_1(t) & 0 & 0 \\ 0 & G_1(t) & k v_1 \sin\theta_1 & G_2(t-\tau) & 0 \\ 0 & 0 & G_2(t-\tau) & k v_1 \sin\theta_1 & \Omega_2(t-\tau) \\ 0 & 0 & 0 & \Omega_2(t-\tau) & k(v_1 \sin\theta_1 - v_2 \sin\theta_2) \end{bmatrix}, \tag{6}$$

where the unitary transformation R is

$$R = \begin{pmatrix} 1 & 0 & 0 & 0 & 0 \\ 0 & e^{-i\varphi_1(t)} & 0 & 0 & 0 \\ 0 & 0 & e^{-i\varphi_1(t)} & 0 & 0 \\ 0 & 0 & 0 & e^{-i\varphi_1(t)} & \\ 0 & 0 & 0 & 0 & e^{-i[\varphi_1(t) - \varphi_2(t-\tau)]} \end{pmatrix}. \tag{7}$$

The dynamics of the system is governed by the Schrödinger equation $i\partial/\partial t |\Phi(t)\rangle = H^{\text{eff}}(t) |\Phi(t)\rangle$.

An essential condition for the STIRAP and f-STIRAP processes is the four-photon resonance between the states $|g_1, g_2, 0\rangle$ and $|g_2, g_1, 0\rangle$ which means:

$$|\Delta := k(v_1 \sin\theta_1 - v_2 \sin\theta_2)| \ll |\Omega_0|, |G_0|. \tag{8}$$

This condition can be achieved by control of the velocity of atoms, and of the deflection angles of the atoms $\theta_{i=1,2}$. Numerics shows that, in practice, the condition (8) is satisfied for $\Delta \lesssim \{\Omega_0, G_0\}/100$. Assuming this condition allows one to consider $\Delta \sim k v_1 \sin\theta_1 \sim 0$ in Eq. (8), if we additionally assume $v_1 \sim v_2 \equiv v$. In this case τ is the delay of arrival at the center of the cavity ($x = y = 0$) of the second atom with respect to the first one.

III. ATOM-ATOM ENTANGLEMENT

The system is taken to be initially in the state $|g_1, g_2, 0\rangle$,

$$|\Phi(t_i)\rangle = |g_1, g_2, 0\rangle. \tag{9}$$

The goal is to transform it at the end of interaction into an atom-atom entangled state

$$\begin{aligned}|\Phi(t_f)\rangle &= \cos\vartheta|g_1, g_2, 0\rangle + \sin\vartheta|g_2, g_1, 0\rangle \\ &= (\cos\vartheta|g_1, g_2\rangle + \sin\vartheta|g_2, g_1\rangle)|0\rangle,\end{aligned} \tag{10}$$

where ϑ is a constant mixing angle ($0 \leqslant \vartheta \leqslant \pi/2$), and the cavity-mode state factorizes and is left in the vacuum state. The qubits are stored in the two degenerate ground states of the atoms. The decoherence due to atomic spontaneous emission is produced if the states $\{|e, g_2, 0\rangle, |g_2, e, 0\rangle\}$ are populated, and the cavity decay occurs if the state $|g_2, g_2, 1\rangle$ is populated during the adiabatic evolution of the system. Therefore we will design the Rabi frequencies $\{\Omega_1(t), G_1(t), \Omega_1(t), G_2(t)\}$ in our scheme such that these states are not populated during the dynamics. We remark that we will use a resonant process without any adiabatic elimination.

One of the instantaneous eigenstates (the two-atom dark state) of $H^{\text{eff}}(t)$ which corresponds to a zero eigenvalue is [10]

$$|D(t)\rangle = C(G_1\Omega_2|g_1, g_2, 0\rangle - \Omega_1\Omega_2|g_2, g_2, 1\rangle + G_2\Omega_1|g_2, g_1, 0\rangle), \tag{11}$$

where C is a normalization factor. The possibility of decoherence-free generation of atom-atom entanglement arises from the following behavior of the dark state:

$$\lim_{t \to t_i} \frac{\Omega_1(t)}{\Omega_2(t)} = 0, \quad |D(t_i)\rangle \sim |g_1, g_2, 0\rangle, \tag{12a}$$

$$\lim_{t \to t_f} \frac{\Omega_1(t)}{\Omega_2(t)} = \tan\vartheta,$$

$$|D(t_f)\rangle \sim \cos\vartheta|g_1, g_2, 0\rangle + \sin\vartheta|g_2, g_1, 0\rangle, \tag{12b}$$

$$t_i < t < t_f, \quad G_1(t) \sim G_2(t) \gg \Omega_1(t), \Omega_2(t),$$

$$|D(t)\rangle \sim \Omega_2(t)|g_1, g_2, 0\rangle + \Omega_1(t)|g_2, g_1, 0\rangle. \tag{12c}$$

Equations (12a) and (12b) are known as f-STIRAP conditions [12,13], and the condition (12c) guarantees the absence of population in the state $|g_2, g_2, 1\rangle$ during the time evolution of the system [14,15]. Equation (12b) means that the Rabi frequencies fall off in a constant ratio, during the time interval where they are non-negligible. We remark that this formulation opens up the possibility to implement f-STIRAP with Gaussian pulses. The goal in the following is to show that such a pulse sequence can be designed in a cavity by an appropriate choice of the parameters.

In an optical cavity, the spatial variation of the atom-field coupling for the maximum coupling TEM_{00} mode, resonant with the $|e\rangle \leftrightarrow |g_2\rangle$ atomic transition, is given by

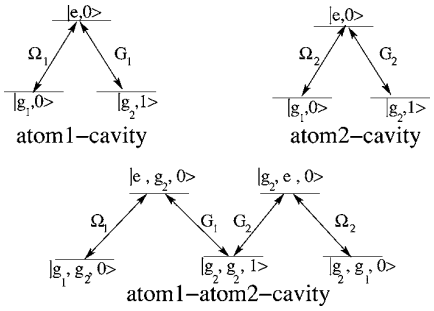

FIG. 2. Linkage pattern of the system corresponding to the effective Hamiltonian.

$$G(x, y, z) = G_0 e^{-(x^2+y^2)/W_C^2} \cos\left(\frac{2\pi z}{\lambda}\right), \tag{13}$$

where W_L is the waist of the cavity mode, and $G_0 = -\mu\sqrt{\omega_C/(2\epsilon_0 V_{\text{mode}})}$ with μ and V_{mode}, respectively, the dipole moment of the atomic transition and the effective volume of the cavity mode. The spatial variation of the atom-laser coupling for the laser beam of Fig. 1 is

$$\Omega(x, z) = \Omega_0 e^{-(x^2+z^2)/W_L^2}, \tag{14}$$

where W_L is the waist of the laser beam, and $\Omega_0 = -\mu\mathcal{E}/2$ with $\mathcal{E}$ the amplitude of the laser field. Figure 1 shows a situation where the first atom, initially in the state $|g_1\rangle$, goes with velocity v (on the $y=0$ plane at the $z=z_0$ line) through an optical cavity initially in the vacuum state $|0\rangle$ and then encounters the laser beam, which is parallel to the y axis (orthogonal to the cavity axis and the trajectory of the atom). The laser beam is resonant with the $|e\rangle \leftrightarrow |g_1\rangle$ transition. The distance between the center of the cavity and the laser axis is d. The second atom, synchronized with the first one $\tau=0$, moves with the same velocity v on the $y=0$ plane at $z=0$ in the opposite direction with respect to the first atom. The traveling atoms encounter the time-dependent and delayed Rabi frequencies of the cavity mode and the laser fields as follows:

$$G_1(t) = G_0 e^{-(vt)^2/W_C^2} \cos\left(\frac{2\pi z_0}{\lambda}\right), \tag{15a}$$

$$\Omega_1(t) = \Omega_0 e^{-z_0^2/W_L^2} e^{-(vt-d)^2/W_L^2}, \tag{15b}$$

$$G_2(t) = G_0 e^{-(vt)^2/W_C^2}, \tag{15c}$$

$$\Omega_2(t) = \Omega_0 e^{-(vt+d)^2/W_L^2}, \tag{15d}$$

where the time origin is defined when the atoms meet the center of the cavity at $x=y=0$. The appropriate values of z_0 and d that lead to the f-STIRAP process can be extracted from a contour plot of the final population $P_{|g_1,g_2,0\rangle}(t_f) := |\langle g_1, g_2, 0|\Phi(t_f)\rangle|^2$ as a function of z_0 and d that we calculated numerically (see Fig. 3). The white dot in Fig. 3 shows values of z_0 and d to obtain an f-STIRAP process with $\vartheta \simeq \pi/4$ (called half-STIRAP). It has been chosen such that at the end of interaction $P_{|g_1,g_2,0\rangle}(t_f) \simeq P_{|g_2,g_1,0\rangle}(t_f) \simeq 0.5$, and the

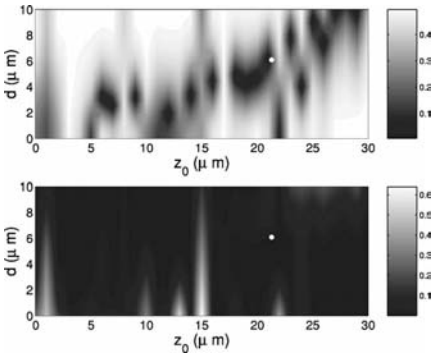

FIG. 3. Top panel: contour plot at the final time t_f of $|\frac{1}{2} - P_{|g_1,g_2,0\rangle}(t_f)|$ as a function of z_0 and d (black areas correspond to approximately half population transfer) with the pulse parameters as $W_L=20\ \mu$m, $W_C=40\ \mu$m, $v=2$ m/s, $\lambda=780$ nm, $\Omega_0=20(v/W_L)$, and $G_0=100(v/W_C)$. Bottom panel: The same plot for the sum of the final populations in intermediate states $P_{|e,g_2,0\rangle}(t_f)+P_{|g_2,g_2,1\rangle}(t_f)+P_{|g_2,e,0\rangle}(t_f)$ where black areas correspond to approximately zero population. The white dot shows specific values of z_0 and d used in Fig. 4 to obtain a half-STIRAP process.

populations of the other states of the subspace $\mathcal{S}$ are zero.

Figure 4 shows for parameter values associated to the white dot in Fig. 3, (a) the time dependence of the Rabi frequencies of half-STIRAP for two atoms, and (b) the time evolution of the populations which shows that the population is split at 50% among the states $|g_1,g_2,0\rangle,|g_2,g_1,0\rangle$ and is almost zero for the other states of $\mathcal{S}$ during the interaction for $G_0\sim 3\Omega_0$. This case corresponds to the generation of the maximally atom-atom entangled state $1/\sqrt{2}(|g_1,g_2,0\rangle + |g_2,g_1,0\rangle)$ by adiabatic passage. We see in Fig. 4 that the overall time for entanglement to be completed is approximately the duration of the crossing of the first atom with the laser field. Assuming Gaussian pulse profiles for $\Omega(t)$ and $G(t)$ of widths $T_L=W_L/v$ and $T_C=W_C/v$, respectively, the sufficient condition of adiabaticity is

$$\Omega_0 T_L, G_0 T_C \gg 1. \tag{16}$$

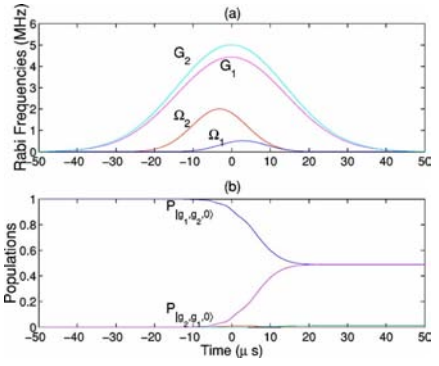

FIG. 4. (Color online) (a) Rabi frequencies of the cavity-mode and the laser field for two atoms. (b) Time evolution of the populations which represents a two-atom half-STIRAP. The population of the states $\{|e,g_2,0\rangle,|g_2,e,0\rangle|g_2,g_2,1\rangle\}$ is almost zero during the whole dynamics.

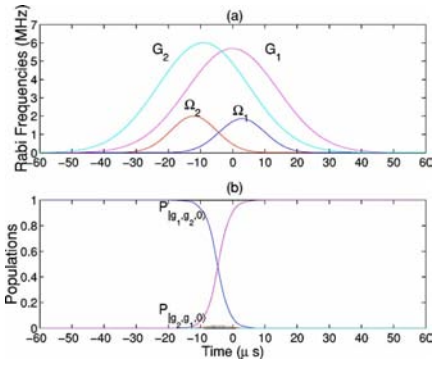

FIG. 5. (Color online) (a) Rabi frequencies of the cavity-mode and the laser field for two atoms with the pulse parameters as $v=2$ m/s, $W_L=20\ \mu$m, $W_C=40\ \mu$m, $\lambda=780$ nm, $\Omega_0=2$ MHz, $G_0=6.5$ MHz, $z_0=5.5\ \mu$m, $d=6\ \mu$m, and $\tau=-9\ \mu$s. (b) Time evolution of the populations which represents a two-atom STIRAP. We observe that the states $\{|e,g_2,0\rangle,|g_2,e,0\rangle|g_2,g_2,1\rangle\}$ are not populated during the whole dynamics.

The state $|g_2,g_2,0\rangle$ is the stationary state of the system. If the second atom enters inside the cavity before the first one ($\tau<0$), we can transfer completely the population from the state $|g_1,g_2,0\rangle$ to $|g_2,g_1,0\rangle$ *without populating the other states of* $\mathcal{S}$ *during the dynamics* (see Fig. 5). In particular, given that the first atom initially is prepared in a coherent superposition of the ground states $\alpha|g_1\rangle+\beta|g_2\rangle$, that the second atom is initially in the state $|g_2\rangle$, and that the cavity-mode is initially in the vacuum state, a two-atom STIRAP will coherently map this superposition onto the second atom:

$$\alpha|g_1,g_2,0\rangle+\beta|g_2,g_2,0\rangle \rightarrow \alpha|g_2,g_1,0\rangle+\beta|g_2,g_2,0\rangle. \tag{17}$$

IV. CONCLUSIONS

In summary, we have proposed a robust and decoherence-free scheme to generate atom-atom entanglement, using the f-STIRAP technique in Λ systems. This scheme is robust with respect to variations of the velocity of the atoms v, of the peak Rabi frequencies G_0,Ω_0, and of the field detunings, but not with respect to the parameters d,z_0, describing the relative positions of the laser beam and the cavity, shown in Fig. 1. Our scheme can be implemented in an optical cavity with $G_0\sim\kappa\sim\Gamma$. The necessary condition to suppress the cavity decoherence is $G_0\gg\Omega_0$ which is satisfied in practice for $G_0\sim 3\Omega_0$ (see Figs. 4 and 5). For given values of W_C,W_L, the adapted values of d and z_0 in the f-STIRAP process can be determined from a contour plot of the final populations. Decoherence channels are suppressed during the whole evolution of the system. In this scheme, as opposed to other schemes [4–10], we do not need to fix the atoms inside the optical cavity nor to apply two laser beams for each of the individual atoms.

ACKNOWLEDGMENTS

M. A.-T. wishes to acknowledge the financial support of the MSRT of Iran and SFERE. We acknowledge support from the Conseil Régional de Bourgogne.

[1] A. Ekert and R. Jozsa, Rev. Mod. Phys. **68**, 733 (1996).
[2] A. K. Ekert, Phys. Rev. Lett. **67**, 661 (1991).
[3] C. H. Bennett, G. Brassard, C. Crépeau, R. Jozsa, A. Peres, and W. K. Wootters, Phys. Rev. Lett. **70**, 1895 (1993).
[4] M. B. Plenio, S. F. Huelga, A. Beige, and P. L. Knight, Phys. Rev. A **59**, 2468 (1999).
[5] A. S. Sørensen and K. Mølmer, Phys. Rev. Lett. **90**, 127903 (2003).
[6] A. Beige, D. Braun, B. Tregenna, and P. L. Knight, Phys. Rev. Lett. **85**, 1762 (2000).
[7] J. Pachos and H. Walther, Phys. Rev. Lett. **89**, 187903 (2002).
[8] E. Jané, M. B. Plenio, and D. Jonathan, Phys. Rev. A **65**, 050302(R) (2002).
[9] X. X. Yi, X. H. Su, and L. You, Phys. Rev. Lett. **90**, 097902 (2003).
[10] T. Pellizzari, S. A. Gardiner, J. I. Cirac, and P. Zoller, Phys. Rev. Lett. **75**, 3788 (1995).
[11] C. Marr, A. Beige, and G. Rempe, Phys. Rev. A **68**, 033817 (2003).
[12] N. V. Vitanov, K. A. Suominen, and B. W. Shore, J. Phys. B **32**, 4535 (1999).
[13] M. Amniat-Talab, S. Guérin, N. Sangouard, and H. R. Jauslin, Phys. Rev. A **71**, 023805 (2005).
[14] N. V. Vitanov, Phys. Rev. A **58**, 2295 (1998).
[15] A. M. Steane and D. M. Lucas, Fortschr. Phys. **48**, 839 (2000).

Chapter 15

Quantum gates by adiabatic passage

Quantum information (QI) processing requires the construction of specific quantum logic gates in a controllable way [195]. A universal set of gates, which can generate all possible operations, is not unique [198]. A convenient set consists of the general single-qubit gate corresponding to a transition matrix of the $U(2)$ group, or more precisely, if we discard an irrelevant global phase factor, to a transition matrix of the $SU(2)$ group, and a two-qubit gate, such as the controlled-NOT or the controlled-phase gates [195, 249].

Experimental implementations of QI algorithms suffer from inaccuracies in the gate operations originating from imperfect knowledge of the system and the interaction parameters, which reduce the fidelity of QI processing. Adiabatic passage techniques provide powerful, efficient and robust tools for overcoming these uncertainties. A particularly successful example is stimulated Raman adiabatic passage (STIRAP) [71], which has been used for complete or partial population transfer between the two lower states in Λ systems, or more generally between two metastable states. Another concern in QI processing is the decoherence that may occur, for instance, through spontaneous emission from intermediate excited states. STIRAP again is an elegant solution since it allows one to transfer the population between the two lower states (supposed to be ground or long lived metastable states) without transiently populating the excited state. This is possible because the population is trapped at all times in a dark state, confining the quantum dynamics to a spontaneous-emission-free subspace. It is thus natural to construct a qubit from two such metastable states and use STIRAP for QI processing.

Various generalizations and extensions of STIRAP have been proposed and demonstrated. One of these extensions, tripod-STIRAP [149], has been considered for realizations of quantum gates using geometric phases [150, 250]. Such schemes allow one to generate a geometric phase without fragile dynamical phases [251], which are sensitive to all interaction parameters. However, this holonomy process requires the control of the area bounded by a curve in the parameter space that defines the geometric phase, and hence it is not as robust as STIRAP. Recently a general SU(2) gate has been proposed [151] that uses the relative phase of the driving fields, which can be controlled very precisely (see Section 8.2.1, paragraph "Implementation of one-qubit phase gates"). An extension to two-qubit gates has been proposed [206] by using a cavity to couple the qubits [207]. Such proposals feature robust processes without dynamical and geometric phases and make use of spontaneous-emission-free dark states.

In Section 15.1, we describe a realistic experimental situation with elliptically polarized pulsed laser fields and real atomic systems with Zeeman sublevels, where one-qubit quantum gates can be operated [252]. We also propose an alternative implementation of a generalized rotation gate constructed by using a combination of two non-resonant f-STIRAP processes with elliptically polarized laser fields. This combination allows one to compensate the dynamical

phase produced by one f-STIRAP.

In Section 15.2, we describe the construction of two qubit quantum gates, with the particular example of the SWAP gate, which interchanges the values of the two qubits [253]. The system is constituted of atoms trapped in CQED with strong couplings [207, 206]. Such a system represents a challenging technology, but has the advantages of (i) clean and strong (since resonant) qubit coupling, without additional detrimental Stark shifts, and of (ii) allowing a decoherence-free adiabatic dynamics in specific dark states.

The construction of the SWAP gate that we present does not require a composition of elementary gates from a universal set. We propose to employ direct techniques adapted to the preparation of this specific gate.

We have extended this process in such a system to construct an entangling CNOT gate [254], and generalized CU gate [255].

15.1 Single qubit quantum gates [252]

Available online at www.sciencedirect.com
SCIENCE DIRECT®
Optics Communications 264 (2006) 362–367
OPTICS COMMUNICATIONS
www.elsevier.com/locate/optcom

Implementation of single-qubit quantum gates by adiabatic passage and static laser phases

X. Lacour [a], S. Guérin [a,*], N.V. Vitanov [b], L.P. Yatsenko [c], H.R. Jauslin [a]

[a] Laboratoire de Physique, Université de Bourgogne, UMR CNRS 5027, BP 47870, 21078 Dijon Cedex, France
[b] Department of Physics, Sofia University, James Bourchier 5 Blvd., 1164 Sofia, Bulgaria
[c] Institute of Physics, Ukrainian Academy of Sciences, Prospect Nauki 46, Kiev-22, 252650, Ukraine

Received 28 October 2005; accepted 19 January 2006

Abstract

We propose and analyse experimentally feasible implementations of single-qubit quantum gates based on stimulated Raman adiabatic passage (STIRAP) between magnetic sublevels in atoms coupled by elliptically polarized pulsed laser fields, in part based on a proposal by Kis and Renzoni [Z. Kis, F. Renzoni, Phys. Rev. A 65 (2002) 032318]. These techniques require only the control of the relative phase of the driving fields but do not involve any dynamical or geometric phases, which makes it independent of the other interaction details: detuning, pulse shapes, pulse areas and pulse durations. The suggested techniques are immune to spontaneous emission since the qubit manipulation proceeds through non-absorbing dark states. We also propose an alternative technique using compensation of dynamical Stark shifts by two consecutive non-resonant fractional-STIRAP processes.

PACS: 03.67.Lx; 03.65.Vf; 32.80.Qk

1. Introduction

Quantum information (QI) processing requires the construction of specific quantum logic gates in a controllable way [2]. A universal set of gates, which can generate all possible operations, is not unique [3]. A convenient set consists of the general single-qubit gate corresponding to a transition matrix of the U(2) group, or more precisely, if we discard an irrelevant global phase factor, to a transition matrix of the SU(2) group, and a two-qubit gate, such as the controlled-NOT or the controlled-phase gates [2,4].

Experimental implementations of QI algorithms suffer from inaccuracies in the gate operations originating from imperfect knowledge of the system and the interaction parameters, which reduce the fidelity of QI processing. Adiabatic passage techniques [5,6] provide powerful, efficient and robust tools for overcoming these uncertainties. A particularly successful example is stimulated Raman adiabatic passage (STIRAP) [7], which has been used for complete or partial population transfer between the two lower states in Λ systems, or more generally between two metastable states. Another concern in QI processing is the decoherence that may occur, for instance, through spontaneous emission from intermediate excited states. STIRAP again is an elegant solution since it allows to transfer the population between the two lower states (supposed to be ground or long lived metastable states) without transiently populating the excited state. This is possible because the population is trapped at all times in a dark state, confining the quantum dynamics to a spontaneous-emission-free subspace. It is thus natural to construct a qubit from two such metastable states and use STIRAP for QI processing.

Various generalizations and extensions of STIRAP have been proposed and demonstrated [7]. One of these extensions, tripod-STIRAP [8], has been considered for

* Corresponding author.
E-mail address: sguerin@u-bourgogne.fr (S. Guérin).

0030-4018/$ - see front matter © 2006 Elsevier B.V. All rights reserved.
doi:10.1016/j.optcom.2006.01.059

realizations of quantum gates using geometric phases [9,10]. Such schemes allow one to generate a geometric phase without fragile dynamical phases [11], which are sensitive to all interaction parameters. However, this holonomy process requires the control of the area bounded by a curve in the parameter space that defines the geometric phase, and hence it is not as robust as STIRAP. Recently a general SU(2) gate has been proposed [1] that uses the relative phase of the driving fields, which can be controlled very precisely. An extension to two-qubit gates has been suggested [12] by using a cavity to couple the qubits [13]. Such proposals feature robust processes without dynamical and geometric phases and make use of spontaneous-emission-free dark states.

In this paper, we describe a realistic experimental situation with elliptically polarized pulsed laser fields and real atomic systems with Zeeman sublevels, where one-qubit quantum gates can be operated. We also suggest an alternative implementation of a generalized rotation gate constructed by using a combination of two non-resonant fractional-STIRAP (f-STIRAP [14]) processes with elliptically polarized laser fields. This combination allows one to compensate the dynamical phase produced by one f-STIRAP.

This paper is organised as follows. In Section 2 we describe the implementation of the Kis–Renzoni gate [1] in a tripod system formed by the magnetic sublevels of the $j = 1 - j = 0$ transition. In Section 3 we propose an experimentally feasible realisation of the phase gate. In Section 4 we suggest a novel implementation of the rotation gate. In Section 5 we discuss the feasibility of the experimental implementations. Finally, a summary of our results is presented in Section 6.

2. Implementation of the Kis–Renzoni gate with Zeeman sublevels

The qubit is composed of two degenerate states $|0\rangle$ and $|1\rangle$ of the same parity, which are coupled to each other by a two-photon transition via some excited state $|e\rangle$. For the construction of the proposed quantum gates, we consider an additional, ancillary state $|a\rangle$, which is degenerate with the qubit states $|0\rangle$ and $|1\rangle$ and has the same parity. Such a system can be formed most conveniently by coupling two atomic levels with angular momenta $j = 1$ and $j = 0$ by three laser fields of linear (π) and circular (σ_+ and σ_-) polarizations. The four Zeeman sublevels provide the necessary states for the gate operations. The axis of quantization has been selected by the preparation of the initial state. To be specific, we shall assume that states $|0\rangle$ and $|1\rangle$ are the $m = -1$ and $m = 1$ sublevels of the $j = 1$ level, respectively, and state $|a\rangle$ is the $m = 0$ sublevel, as shown in Fig. 1. We remark that one can use for the qubit alternatively any other pair of the three $j = 1$ sublevels, as shown below.

In the basis $\{|0\rangle,|1\rangle,|a\rangle,|e\rangle\}$, the Hamiltonian reads in the rotating wave approximation [15]

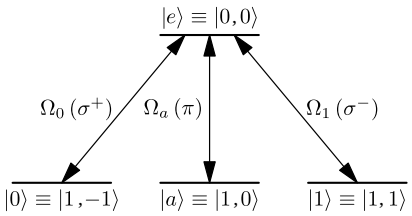

Fig. 1. Symbolic representation of a Zeeman system used for the implementation of a single-qubit gate with the states denoted by $|j,m\rangle$. For each transition the Rabi frequencies of the fields and their polarisations are displayed.

$$H = \frac{\hbar}{2}\begin{bmatrix} 0 & 0 & 0 & \Omega_0 \\ 0 & 0 & 0 & \Omega_1 \\ 0 & 0 & 0 & \Omega_a \\ \Omega_0^* & \Omega_1^* & \Omega_a^* & 2\Delta \end{bmatrix}, \tag{1}$$

where Δ is the one-photon detuning.

A robust implementation of the general single qubit gate by adiabatic passage has been proposed by Kis and Renzoni [1]. It requires in particular identical time dependencies of two pulse shapes that we implement by a single specific elliptically polarized pulse. This gate allows one to transfer the qubit state onto any desired point of the Bloch sphere by using two consecutive STIRAPs with Rabi frequencies

$$\Omega_0(t) = \Omega(t)\cos\chi, \tag{2a}$$

$$\Omega_1(t) = \Omega(t)e^{i\eta}\sin\chi, \tag{2b}$$

$$\Omega_a^{(j)}(t) = \Omega_a(t-\tau^{(j)})e^{-i\varphi^{(j)}} \tag{2c}$$

with $\Omega(t) = \Omega_0\sqrt{\Lambda(t)}$. In the present implementation the laser pulses $\Omega_0(t)$ and $\Omega_1(t)$ are, respectively, σ^+ and σ^- polarized. Because they must have the same time dependence, they can be produced by just one elliptically polarized laser pulse of intensity envelope $\Lambda(t)$ and amplitude Ω_0; then the mixing angle χ is related to the ellipticity of this pulse and η to the angle of rotation of the polarization ellipse. This allows both to reduce the number of pulsed fields required (which makes it easier to implement) and to fulfill automatically the requirement for the same time dependence of $\Omega_0(t)$ and $\Omega_1(t)$. Then $\tau^{(j)}$ is the delay between the elliptically polarized pulse and the linearly polarized pulse $\Omega_a^{(j)}$ (of peak amplitude Ω_a), and $\varphi^{(j)}$ is the phase of the linearly polarized pulse at step j ($j = 1,2$). $\Omega(t)$ and $\Omega_a(t)$ are assumed real and positive without loss of generality.

The system is initially in a given superposition of the two states $|0\rangle$ and $|1\rangle$ of the qubit. The elliptically polarized pulse allows us to connect the bare-state basis $\{|0\rangle,|1\rangle,|a\rangle,|e\rangle\}$ to the basis $\{|C\rangle,|NC\rangle,|a\rangle,|e\rangle\}$, where

$$|C\rangle = \cos\chi|0\rangle + e^{i\eta}\sin\chi|1\rangle, \tag{3a}$$

$$|NC\rangle = -\sin\chi|0\rangle + e^{i\eta}\cos\chi|1\rangle \tag{3b}$$

are states that are, respectively, coupled and non-coupled to the excited state $|e\rangle$. In this latter basis, the first STIRAP with the linearly polarized pulse first ($\tau^{(1)} > 0$) transfers the

364 X. Lacour et al. / Optics Communications 264 (2006) 362–367

population of the coupled state to the ancillary state. This population comes back to the coupled state with a reverse STIRAP ($\tau^{(2)} < 0$). In the adiabatic limit, the overall evolution matrix is

$$U(\varphi,\chi,\eta) = \mathrm{e}^{\mathrm{i}\varphi/2}\begin{bmatrix} \mathrm{e}^{\mathrm{i}\varphi/2}\cos^2\chi + \mathrm{e}^{-\mathrm{i}\varphi/2}\sin^2\chi & -\mathrm{i}\mathrm{e}^{-\mathrm{i}\eta}\sin\chi/2\sin\eta/2 \\ -\mathrm{i}\mathrm{e}^{\mathrm{i}\eta}\sin\chi/2\sin\eta/2 & \mathrm{e}^{-\mathrm{i}\varphi/2}\cos^2\chi + \mathrm{e}^{\mathrm{i}\varphi/2}\sin^2\chi \end{bmatrix} \tag{4}$$

with $\varphi = \varphi^{(2)} - \varphi^{(1)}$, which represents a general matrix of SU(2) up to an irrelevant global phase factor, producing thus the general one-qubit quantum gate. The process is most efficient for an exact single-photon resonance ($\Delta = 0$), but it is not required, as long as the pulse areas are sufficiently large to enforce adiabatic evolution, as in standard STIRAP.

The important feature of this scheme is that it requires only the control of the relative laser phases $\varphi^{(j)}$ and η and it is thus robust with respect to the field amplitudes, the interaction duration, and the single-photon detuning Δ.

The Rabi frequencies (2) are particularly suitable for the choice of the qubit to implement the gate in a robust way. Other choices of the qubit require to adapt the direction of propagation and the polarization of the fields to preserve the robustness. Using the spherical coordinates (of unit vectors $\mathbf{e_r}, \mathbf{e_\theta}, \mathbf{e_\varphi}$), we decompose the electric field (in complex notation), orthogonal to the direction of propagation defined along $\mathbf{e_r}$, as $\mathbf{E} = E_+\boldsymbol{\varepsilon}_+ + E_-\boldsymbol{\varepsilon}_- + E_z\mathbf{e_z} = E_\theta \mathbf{e}^{i(\phi_\theta-\omega t)}\mathbf{e_\theta} + E_\varphi \mathbf{e}^{i(\phi_\varphi-\omega t)}\mathbf{e_\varphi}$, where E_+, E_- and E_z are, respectively, associated to the σ_+, σ_-, and π polarizations, with

$$E_+ = -\frac{\mathrm{e}^{-\mathrm{i}\varphi}}{\sqrt{2}}\left(E_\theta \mathrm{e}^{\mathrm{i}\phi_\theta}\cos\theta - \mathrm{i}E_\varphi \mathrm{e}^{\mathrm{i}\phi_\varphi}\right)\mathrm{e}^{-\mathrm{i}\omega t}, \tag{5a}$$

$$E_- = \frac{\mathrm{e}^{\mathrm{i}\varphi}}{\sqrt{2}}\left(E_\theta \mathrm{e}^{\mathrm{i}\phi_\theta}\cos\theta + \mathrm{i}E_\varphi \mathrm{e}^{\mathrm{i}\phi_\varphi}\right)\mathrm{e}^{-\mathrm{i}\omega t}, \tag{5b}$$

$$E_z = -E_\theta \mathrm{e}^{\mathrm{i}(\phi_\theta-\omega t)}\sin\theta. \tag{5c}$$

One can see that a single pulse can be used to produce any combination (E_+/E_-) (setting $\theta = 0$), (E_+/E_z) (setting $E_\theta \cos\theta = E_\varphi$ and $\phi_\varphi = \phi_\theta + \pi/2$), (E_-/E_z) (setting $E_\theta\cos\theta = E_\varphi$ and $\phi_\varphi = \phi_\theta - \pi/2$).

3. The phase gate

As an example of the general unitary transformation (4) described above, we consider the *phase gate* Ph(φ), which corresponds to a rotation on the Bloch sphere around the z-axis. Applied to the qubit $\{|0\rangle,|1\rangle\}$ the phase gate rotates the phase of state $|1\rangle$ by an angle φ, as described by the matrix

$$\mathrm{Ph}(\varphi) = \begin{bmatrix} 1 & 0 \\ 0 & \mathrm{e}^{\mathrm{i}\varphi} \end{bmatrix}. \tag{6}$$

The phase gate is a particular case of the general one-qubit quantum gate (4): $\mathrm{Ph}(\varphi) = U(\varphi,\pi/2,0)$. It can therefore be implemented by using a sequence of two STIRAP processes, each involving a linearly polarized pulse and a circularly polarized pulse, and operating on the three-state subsystem $\{|a\rangle,|e\rangle,|1\rangle\}$. State $|0\rangle$ is unaffected by the phase gate (6). Within the subsystem $\{|a\rangle,|e\rangle,|1\rangle\}$ only state $|1\rangle$ is populated before the gate operation, partly or completely, depending on the state of the qubit. The first STIRAP, with the π-field (Stokes) preceding the σ_--field (pump), transfers the population of state $|1\rangle$ to $|a\rangle$. Then the second STIRAP, with now the σ_--field (Stokes) preceding the π-field (pump), returns the population from state $|a\rangle$ to $|1\rangle$. This pulse sequence is depicted in the upper frame of Fig. 2.

The associated phases φ_π, φ_{σ_-} are defined such that the π and σ_- electric-field amplitudes read $\mathscr{E}_i(t) = \mathscr{E}_{i,\max}\sqrt{\Lambda(t)}\cos(\omega_i t - \varphi_i)$ $(i = \pi,\sigma_-)$, with $\Lambda(t)$ the intensity pulse shape and $\mathscr{E}_{i,\max}$ the peak amplitude of the field i. The π and σ_- fields are exactly in two-photon resonance. The adiabatic condition is satisfied when $\Omega_{i,\max}T \gg 1$, where $\Omega_{i,\max}$ is the peak Rabi frequency of the field i and T is the characteristic duration of the pulse [e.g. the full-width-at-half-maximum (FWHM) for Gaussian pulses].

The combination of the two STIRAPs leads to the phase gate (6) between states $|0\rangle$ and $|1\rangle$ with the phase

$$\varphi = \varphi_\pi^{(2)} - \varphi_{\sigma_-}^{(2)} + \varphi_{\sigma_-}^{(1)} - \varphi_\pi^{(1)}. \tag{7}$$

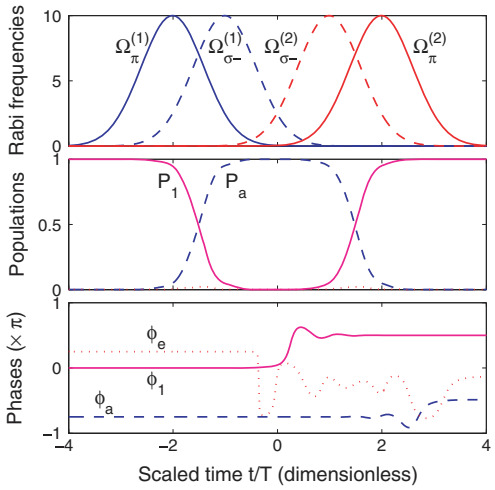

Fig. 2. Numerical simulation of the double-STIRAP process (using pulses of Gaussian intensity of FWHM T, a pump–Stokes delay $T/2$, and a delay $1.5T$ between the two STIRAPs) for the generation of the phase $\varphi = \pi/2$ in state $|1\rangle$, initially and finally fully populated, with $\Omega_{\max}T = 10$ (where $\Omega_{\max}$ is the peak Rabi frequency, which is here the same for all fields), $\varphi_\pi^{(1)} = \pi/2$, $\varphi_\pi^{(2)} = \pi$, and $\varphi_{\sigma_-}^{(1)} = \varphi_{\sigma_-}^{(2)} = -\pi/4$. Upper frame: pump (full lines) and Stokes (dashed lines) Rabi frequencies (in units of $1/T$). Middle frame: Populations $P_j := |\langle j|\psi\rangle|^2$ with $|\psi\rangle$ the state of the dynamics, $j = 1$ (full line), a (dashed line), e (dotted line) (P_e could be reduced for larger $\Omega_{\max}T$). Lower frame: Phases $\phi_j := \arg(\langle j|\psi\rangle)$, with $\varphi \equiv \phi_1(+\infty)$.

Fig. 2 shows a numerical simulation for the generation of the phase $\varphi = \pi/2$. This scheme requires π fields that do not overlap with each other, whereas the σ_- fields can overlap if they have the same phases, $\varphi^{(2)}_{\sigma_-} = \varphi^{(1)}_{\sigma_-}$. We obtain numerically $\varphi \approx 0.4998\pi$.

As shown in Fig. 3, we can obtain this phase gate using only three fields instead of four, with a single σ_- field and two π fields in the sequence $\pi - \sigma_- - \pi$; then the σ_- will serve as pump in the first STIRAP and as Stokes in the second STIRAP. This requires a longer σ_- field since it has to overlap with both π fields, which are not allowed to overlap with each other. In this case, $\varphi = \varphi^{(2)}_{\pi} - \varphi^{(1)}_{\pi}$, independently of the σ_- phase. We obtain here $\varphi \approx 0.4999\pi$.

Such a use of a single elliptically polarized pulse instead of two intermediate pulses applies also to the generation of the general single-qubit gate (4).

Following Ref. [12], one can interpret this phase gate in terms of a geometric phase using the scheme of Ref. [10], which involves time-dependent phases making a closed loop in the parameter space. This requires to reinterpret the two π fields of Fig. 2 as a *single* field of bipulse shape [associated to the Rabi frequency $\Omega_b(t)$] with a time-dependent phase $\Phi(t)$. It takes the constant value $\varphi^{(1)}_{\pi}$ during the first STIRAP, next changes to $\varphi^{(2)}_{\pi}$ while the amplitude of $\Omega_b(t)$ is zero, and stays constant during the second STIRAP. Then the phase associated to this process reads

$$\varphi^{(2)}_{\pi} - \varphi^{(1)}_{\pi} - \int \mathrm{d}t \frac{\mathrm{d}\Phi}{\mathrm{d}t} \sin^2\theta(t), \tag{8}$$

with $\tan\theta(t) = \Omega_b(t)/\Omega_{\sigma_-}(t)$. In the case of a closed loop of the parameters, requiring $\varphi^{(2)}_{\pi} = \varphi^{(1)}_{\pi}$, only the geometric phase $\oint \mathrm{d}\Phi \sin^2\theta$ is left, requiring the control of the closed curve $\theta(\Phi)$ [10]. In the proposed double-STIRAP phase gate, we have instead static phases $\varphi^{(2)}_{\pi} \neq \varphi^{(1)}_{\pi}$ and $\int \mathrm{d}t \frac{\mathrm{d}\Phi}{\mathrm{d}t} \sin^2\theta(t) = 0$, since the phase Φ of the $\Omega_b(t)$ field jumps (virtually) only when its amplitude is zero.

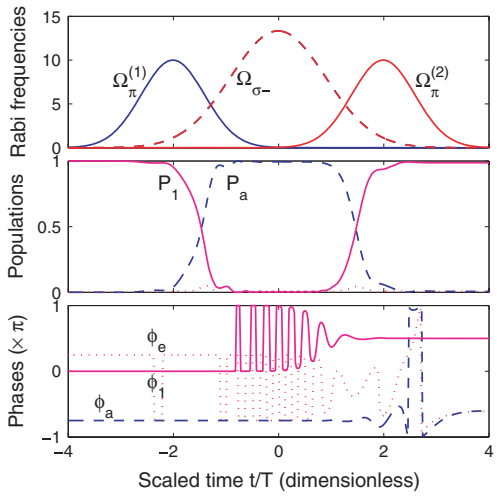

Fig. 3. Same as Fig. 2, but with a single σ_- pulse 50% longer and 33% higher.

This double-STIRAP phase gate has therefore a considerable advantage over the previous proposals because experimentally it will be easier to control the static relative phase between the two π polarized fields than a closed curve $\theta(\Phi)$ in the parameter space. The proposed realization with magnetic sublevels is particularly suitable for this static phase control because all laser pulses can be delivered from the same laser pulse by beam splitters, polarizers and delay lines. Hence, owing to the robustness of STIRAP against variations in pulse areas and the single-photon detuning, intensity and frequency fluctuations of the laser cannot affect the gates appreciably.

4. The generalized rotation gate by non-resonant fractional STIRAP

We consider now the construction of the generalized rotation gate, defined as

$$R(\alpha,\phi) = \begin{bmatrix} \cos\alpha & \mathrm{e}^{\mathrm{i}\phi}\sin\alpha \\ -\mathrm{e}^{-\mathrm{i}\phi}\sin\alpha & \cos\alpha \end{bmatrix}. \tag{9}$$

It generalizes the ordinary rotation gate with the additional phase parameter ϕ. We propose to use two consecutive fractional STIRAP processes [14], the second one compensating the dynamical phase resulting from the first one (of reversed sequence). For the realization of this gate, we couple only the three states $|0\rangle$, $|1\rangle$ and $|e\rangle$ by elliptically polarized fields (see Fig. 1), i.e. $\Omega_a = 0$ in Eq. (1). We first recall the f-STIRAP process and calculate the associated propagator: If the population is initially in state $|0\rangle$, f-STIRAP allows a partial adiabatic transfer of the population between the states $|0\rangle$ and $|1\rangle$ if the pulses are switched on counterintuitively (Stokes–pump sequence, with in this case the Rabi frequencies for the pump and Stokes fields, respectively, denoted $\Omega_{P\equiv\sigma_+}$ and $\Omega_{S\equiv\sigma_-}$) and switched off in a given constant ratio: $\Omega_P/\Omega_S \underset{t\to+\infty}{\to} \tan\alpha$ [14]. In order to obtain a robust process, one can use a variation of this procedure with the following polarizations [14]: one laser is σ_- polarized and the other one is elliptically polarized: $\sigma_-\cos\alpha + \sigma_+\sin\alpha$, such that the Rabi frequencies for the resulting pump and Stokes fields now read, respectively,

$$\Omega_{\sigma_+}(t) = \mathrm{e}^{-\mathrm{i}\phi}\sqrt{\Lambda_{\mathrm{el.}}(t-\tau)}\Omega_0 \sin\alpha, \tag{10a}$$

$$\Omega_{\sigma_-}(t) = \sqrt{\Lambda_{\sigma_-}(t)}\Omega_0 + \sqrt{\Lambda_{\mathrm{el.}}(t-\tau)}\Omega_0 \cos\alpha, \tag{10b}$$

with $\Lambda_{\sigma_-}(t)$ and $\Lambda_{\mathrm{el.}}(t)$ being the intensity envelopes of the σ_- and elliptically polarized pulses respectively, $\tau > 0$ the delay between them, and ϕ the relative static phase. The elliptically polarized pulse starting and finishing after the σ_- polarized pulses, produces the falling off of the effective pump and Stokes fields in the prescribed ratio. The robustness of such a process has been extensively studied in Ref. [14].

To construct the rotation gate (9), we consider a large detuning Δ for the Hamiltonian (1) such that the excited state can be adiabatically eliminated. Under the conditions [16]

$$(\Omega_0 T)^2 \gg \Delta T \gg \Omega_0 T \gg 1, \tag{10c}$$

the propagator between the beginning and the end of the process (times t_i and t_f, respectively) reads thus in the basis $\{|0\rangle,|1\rangle\}$

$$U(t_f,t_i)=\begin{bmatrix}\cos\alpha & e^{i\phi}e^{-iA_-}\sin\alpha\\ -e^{-i\phi}\sin\alpha & e^{-iA_-}\cos\alpha\end{bmatrix}, \tag{11}$$

with the dynamical phase

$$A_-=\int_{t_i}^{t_f}\frac{dt}{2}\left(\Delta-\sqrt{\Delta^2+\Omega_{\sigma_+}^2(t)+\Omega_{\sigma_-}^2(t)}\right). \tag{12}$$

Eq. (11) shows that a generalized rotation gate between states $|0\rangle$ and $|1\rangle$ with a single f-STIRAP would require $A_-=0$, i.e. to cancel the dynamical phase A_-. This cannot be implemented in a robust manner. We show below that the compensation of the dynamical phase can be achieved in a robust manner by combining two f-STIRAPs as follows: The first pulse sequence is in fact a reversed f-STIRAP with the elliptic and σ_- pulses starting with the constant ratio $\Omega_{\sigma_+}/\Omega_{\sigma_-}\underset{t\to-\infty}{\to}\cot\alpha$ and ending such that the σ_- pulse vanishes first. Then the propagator at the end of this reversed f-STIRAP (starting and ending at times respectively t_i and t_f) reads in the basis $\{|0\rangle,|1\rangle\}$

$$U_1(t_f,t_i)=\begin{bmatrix}e^{-iA_-} & 0\\ 0 & 1\end{bmatrix}R(\alpha,\phi). \tag{13}$$

The second pulse sequence is the standard f-STIRAP described above. The propagator of this f-STIRAP reads (with variables denoted with primes)

$$U_2(t_f',t_i')=R(\alpha,\phi)\begin{bmatrix}1 & 0\\ 0 & e^{-iA_-'}\end{bmatrix}. \tag{14}$$

The resulting operation is associated to the propagator

$$U(t_f',t_i)=U_2U_1=R(\alpha,\phi)\begin{bmatrix}e^{-iA_-} & 0\\ 0 & e^{-iA_-'}\end{bmatrix}R(\alpha,\phi), \tag{15}$$

which is the rotation gate $R(2\alpha,\phi)$ (up to an irrelevant global phase) under the condition $A_-=A_-'$. This condition is satisfied if the f-STIRAP and reversed f-STIRAP have the same characteristics, i.e. the same pulse shapes, peak amplitudes, pulse durations, and a reversed delay with the same absolute values. Fig. 4 shows a numerical simulation for the generation of the Hadamard gate $R(2\alpha=\pi/4,\ \phi=0)$.

5. Experimental implementation

As a realistic atomic level scheme, we consider the 2^3S_1–2^3P_0 transition in metastable helium, of linewidth $\Gamma=10^7\ s^{-1}$ (see for instance [17]). The Rabi frequencies are $\Omega\sim10^8\sqrt{I}\ s^{-1}$ with the field intensities I in W/cm^2. We obtain beyond the resonant approximation using the polarizability an upper estimate for the relative Stark shifts (in absolute value) as $S\sim100I\ s^{-1}$. Taking into account the loss of the intermediate state requires for adiabatic passage $\Omega_0T_p\gg1$ and $(\Omega_0T_p)^2\gg\Gamma T_p$, satisfied for $\Omega_0\gg\Gamma$.

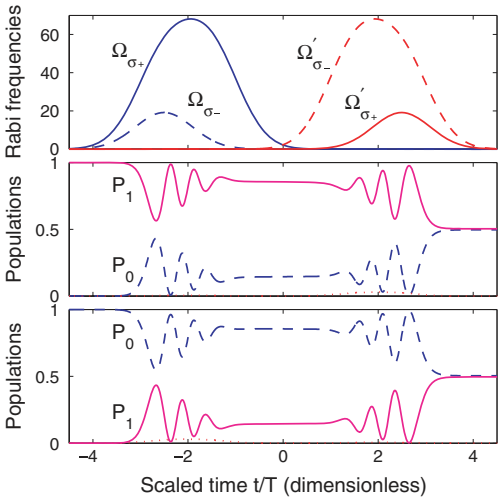

Fig. 4. Numerical simulation of the double f-STIRAP process (using elliptically polarized pulses of Gaussian intensity of FWHM T and a circular-σ_- delay $T/2$, and a delay $2T$ between the two f-STIRAPs) for the generation of the Hadamard gate, with $\Omega_0T=50$, $\Delta T=350$ [satisfying at best the condition (10c)], $\phi_{\sigma_+}=\phi_{\sigma_-}$, $\phi'_{\sigma_+}=\phi'_{\sigma_-}$. Upper frame: pump (full lines) and Stokes (dashed lines) Rabi frequencies (in units of $1/T$). Middle frame: Populations $P_j:=|\langle j|\psi\rangle|^2$, $j=1$ (full line), 0 (dashed line), e (dotted line) for the initial state $|\psi(-\infty)\rangle=|1\rangle$. We obtain $P_0\approx0.496$. Lower frame: Populations for the initial state $|\psi(-\infty)\rangle=|0\rangle$. We obtain $P_1\approx0.496$.

For the resonant processes, we can for instance consider $T_p=1\ \mu s$ (typical in beam experiments) with $I=100$ W/cm^2 which gives $\Omega_0\sim10^9\ s^{-1}$, $\Omega_0T_p=10^3$ and an estimate of the phases $S_{max}T_p\sim10^{-2}\ll2\pi$. They can therefore be neglected.

The preceding scheme with a robust dynamical compensation $A_-=A_-'$ could be realistically tested for instance in an atomic beam experiment with cw laser fields and mirrors, as the one described in Ref. [18], allowing a counter-propagation of the first sequence (see Fig. 5). In such a beam experiment the field amplitude and the speed of the beam have to stay constant between the two sequences. The angle 2α of the rotation requires only the control of the polarization of the fields.

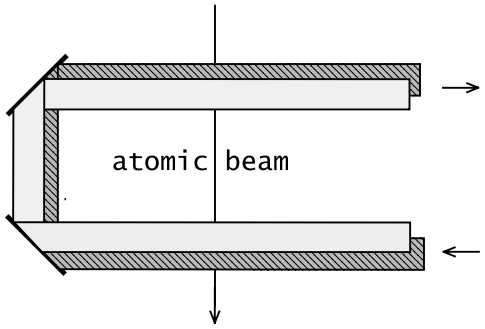

Fig. 5. Scheme of fields of circular (light) and elliptic (shaded) polarization used with an atomic beam to implement the rotation gate.

As opposed to the preceding configuration, the general single qubit gate of Ref. [1] requires a three-dimensional scheme in beam experiments, since the π-linear pulse has to propagate orthogonally to the σ fields.

6. Conclusion

In conclusion, we have described and discussed robust techniques to generate the single-qubit phase and rotation gates in the same system using sequences of two STIRAPs (for the phase gate) and two f-STIRAPs (for the rotation gate). The phase of the phase gate is generated by the static relative phase of two pump laser fields of the two STIRAPs, which is readily controllable experimentally. The angle of the rotation gate is constructed by maintaining a constant ratio of the field amplitudes of standard and reversed f-STIRAP, either at the beginning or at the end of the process, which can be achieved in a robust manner by using elliptically polarized fields.

Acknowledgments

This paper is in honor of Bruce Shore's recent 70th birthday. The main ideas in this study are based on his pioneering work on adiabatic passage. We acknowledge support from the Conseil Régional de Bourgogne. N.V.V. acknowledges support from the European Union's Transfer of Knowledge Project CAMEL (Grant No. MTKD-CT-2004-014427). L.P.Y. and N.V.V. thank l'Université de Bourgogne for invited professorships during which this work has been accomplished.

References

[1] Z. Kis, F. Renzoni, Phys. Rev. A 65 (2002) 032318.
[2] M.A. Nielsen, I.L. Chuang, Quantum Computation and Quantum Information, Cambridge University Press, Cambridge, 2000.
[3] A. Galindo, M.A. Delgado, Rev. Mod. Phys. 74 (2002) 347.
[4] A. Barenco, C.H. Bennett, R. Cleve, D.P. DiVincenzo, N. Margolus, P. Shor, T. Sleator, J.A. Smolin, H. Weinfurter, Phys. Rev. A 52 (1995) 3457.
[5] N.V. Vitanov, M. Fleischhauer, B.W. Shore, K. Bergmann, Adv. Atom. Mol. Opt. Phys. 46 (2001) 55.
[6] S. Guérin, H.R. Jauslin, Adv. Chem. Phys. 125 (2003) 147.
[7] K. Bergmann, H. Theuer, B.W. Shore, Rev. Mod. Phys. 70 (1998) 1003.
[8] R.G. Unanyan, M. Fleischhauer, B.W. Shore, K. Bergmann, Opt. Commun. 155 (1998) 144;
H. Theuer, R.G. Unanyan, C. Habschied, K. Klein, K. Bergmann, Opt. Express 4 (1999) 77.
[9] R.G. Unanyan, B.W. Shore, K. Bergmann, Phys. Rev. A 59 (1999) 2910.
[10] L.-M. Duan, J.I. Cirac, P. Zoller, Science 292 (2001) 1695.
[11] R.G. Unanyan, M. Fleischhauer, Phys. Rev. Lett. 69 (2004) 050302.
[12] H. Goto, K. Ichimura, Phys. Rev. A 70 (2004) 012305.
[13] T. Pellizzari, S.A. Gardiner, J.I. Cirac, P. Zoller, Phys. Rev. Lett. 75 (1995) 3788.
[14] N.V. Vitanov, K.-A. Suominen, B.W. Shore, J. Phys. B 32 (1999) 4535.
[15] B.W. Shore, The Theory of Coherent Atomic Excitation, Wiley, New York, 1990.
[16] N.V. Vitanov, S. Stenholm, Opt. Commun. 135 (1997) 394.
[17] J. Lawall, M. Prentiss, Phys. Rev. Lett. 72 (1994) 993.
[18] F. Vewinger, M. Heinz, R.G. Fernandez, N.V. Vitanov, K. Bergmann, Phys. Rev. Lett. 91 (2003) 213001.

15.2 Two qubit quantum gates: The swap gate [253]

PHYSICAL REVIEW A **72**, 062309 (2005)

Fast SWAP gate by adiabatic passage

N. Sangouard,* X. Lacour, S. Guérin, and H. R. Jauslin
Laboratoire de Physique, Université de Bourgogne, UMR CNRS 5027, BP 47870, 21078 Dijon Cedex, France
(Received 26 January 2005; revised manuscript received 20 May 2005; published 6 December 2005)

We present a process for the construction of a SWAP gate which does not require a composition of elementary gates from a universal set. We propose to employ direct techniques adapted to the preparation of this specific gate. The mechanism, based on adiabatic passage, constitutes a decoherence-free method in the sense that spontaneous emission and cavity damping are avoided.

DOI: 10.1103/PhysRevA.72.062309 PACS number(s): 03.67.Lx, 32.80.Qk

I. INTRODUCTION

The perspective of a high computational power generates intense efforts to build quantum computers. The quantum logical gates, which are one of the essential building blocks of a quantum computer, have received a lot of attention. They act on qubits, whose states ideally should be insensitive to decoherence, easily prepared and measured. Moreover, the construction of logical gates requires a robust mechanism with respect to fluctuations of experimental parameters. The usual approach consists in creating a set of universal gates [1] such that all logical quantum gates can, in principle, be obtained from the composition of gates belonging to this set. The universal sets $\{U_2\}$ [2] and $\{U_1, \text{CNOT}\}$ [3] where U_N is a general unitary matrix in SU(2^N) have played a central role in quantum computation. However, this generic construction usually requires compositions of many elementary gates. This entails an accumulation of decoherence and of other detrimental effects, which become a considerable obstacle for a practical implementation.

In this paper, we propose a technique to build a fast SWAP gate obtained by a scheme based on adiabatic passage with an optical cavity. It does not use the composition of gates but aims instead at the construction of a specific gate in such a way that losses and decoherence effects remain as small as possible. This direct method is faster, i.e., it involves considerably fewer individual steps than the composition of elementary gates build independently. It is thus less exposed to losses and decoherence processes.

We chose a representation of qubits by atomic states driven by adiabatic fields in a configuration that is particularly insensitive to decoherence. Indeed, the decoherence due to spontaneous emission can be avoided if the dynamics follows a dark state, i.e., a state without components on lossy excited states. Moreover, the adiabatic principles provide the robustness of the method with respect to partial knowledge of the model and against small variations of field parameters. To implement the gates in a robust manner, one has to control precisely the parameters that determine the action of the gates. We therefore do not use dynamical phases, requiring controllable field amplitudes, nor geometrical phases, requiring a controllable loop in the parameter space [4–7]. We use instead static phase differences of lasers, which can be easily controlled experimentally.

In this context of atomic qubits manipulated by adiabatic laser fields, a mechanism has been proposed in Ref. [8] to implement by four pulses all one-qubit gates, i.e., a general unitary matrix U_1 in SU(2) in a tripod system [4,5]. In Ref. [9], five-level atoms are fixed in a single-mode optical cavity and are addressed individually by a set of laser pulses [10]. The authors proposed sequences of seven pulses to build a two-qubit controlled-phase gate [C-phase(θ)] and a two-qubit controlled-NOT gate (CNOT). The configuration of the five-level atoms is defined by adding a second excited state to the tripod system [see Fig. 2(a)]. Since in the tripod, all one-qubit gates can be constructed [8], one thus has a mechanism to implement the universal set $\{U_1, \text{C-phase}(\theta)\}$ [11] from which all quantum gates can be deduced. For instance, the SWAP gate, which interchanges the values of two qubits, requires three CNOT gates [12], or can be decomposed into six *Hadamard* gates and three C-phase(π) gates (see Fig. 1), which corresponds to at least 21 pulses in this system.

Since in the experimental implementation of each gate there are always losses, due to uncontrolled interactions or decoherence, it is useful to design direct implementations of specific gates instead of relegating them to a superposition of many elementary gates.

II. SYSTEM

We propose an alternative mechanism based on adiabatic passage along dark states for the construction of the SWAP gate, which compared to the composition into C-phase and Hadamard gates, or into CNOT gates of Ref. [9], has the advantage to involve a much smaller number of pulses and thus to operate in a shorter time. This mechanism is

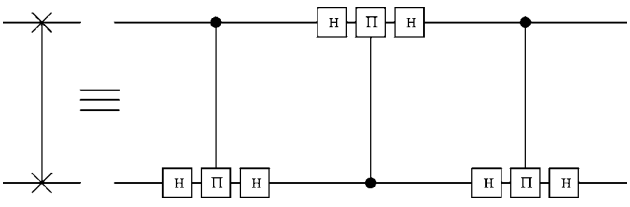

FIG. 1. Decomposition of the SWAP gate from C-phase(π) gates and Hadamard (H) gates on the two qubits.

*Electronic address: nicolas.sangouard@u-bourgogne.fr

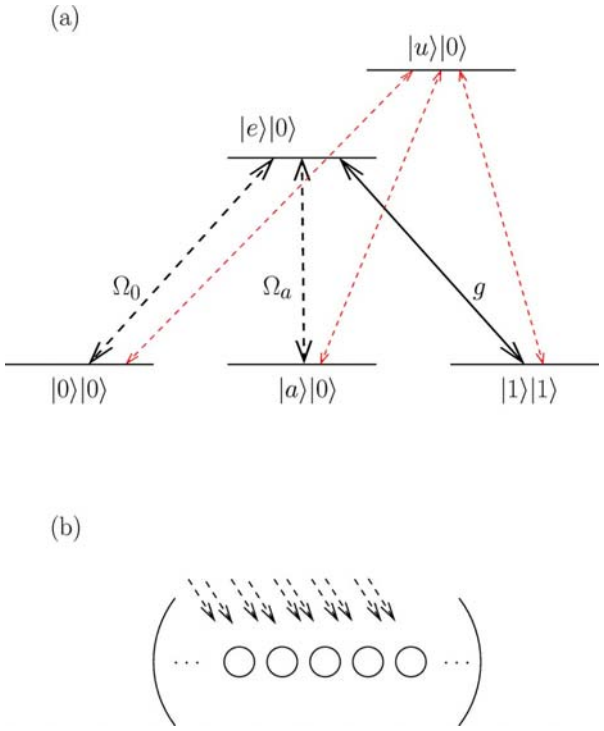

FIG. 2. (Color online) (a) Schematic representation of the five-level atom. Arrows show the laser (full arrows) and cavity (dashed arrows) couplings to perform the swap gate (thick arrows) and the general one qubit gate (thin arrows). (b) Representation of the atomic register trapped in a single-mode optical cavity. The atoms are represented by circles, the laser fields by dashed arrows.

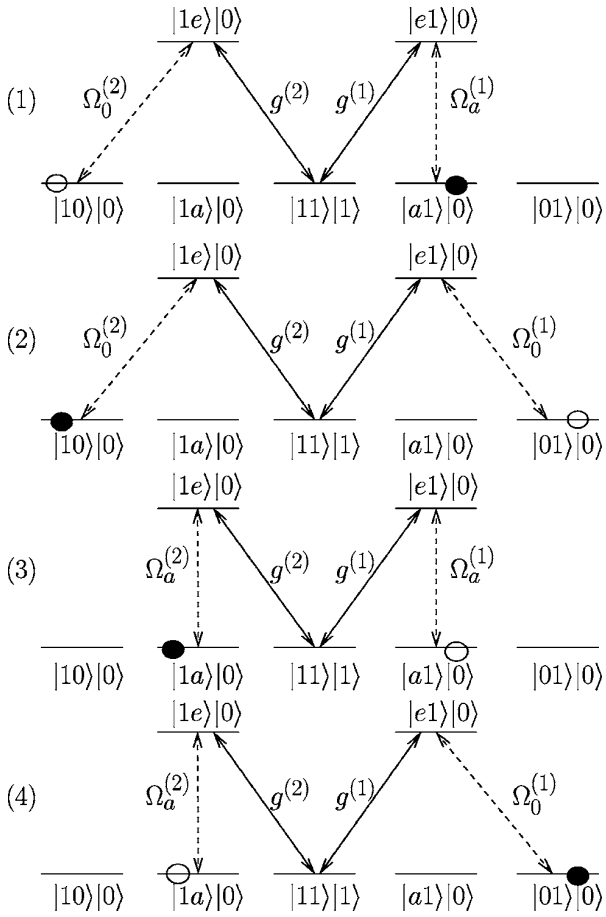

FIG. 3. Schematic representation of the four steps of the construction of the SWAP gate. For each step, the intial state is represented by an empty circle, whereas the final state is symbolized by a full black circle.

decoherence-free in the sense that, in the adiabatic limit and under the condition of a cavity Rabi frequency much larger than the laser Rabi frequency, the excited atomic states and the cavity mode are not populated during the dynamics. We emphasize that the goal here is not to create an alternative universal set of gates offering the possibility to construct an arbitrary gate, but to prepare specific logical quantum gates in a fast way.

We assume that the atoms are fixed inside an optical cavity [Fig. 2(b)]. The proposed mechanism is implemented in the five-level extension of the tripod-type system in which the universal gate of Refs. [8,9] can be implemented [Fig. 2(a)].

We will use a notation, e.g., in Figs. 2 and 3, involving two kets: the left one labels the state of the atoms (a single or a pair) and the right one the photon number of the cavity field. The three ground states (for instance Zeeman levels) $|0\rangle|0\rangle$, $|a\rangle|0\rangle$, and $|1\rangle|1\rangle$ are coupled to the excited state $|e\rangle|0\rangle$, respectively, by two lasers associated to the Rabi frequencies Ω_0 and Ω_a, and by a single mode cavity associated to the Rabi frequency g. The upper state $|u\rangle$ is only used to implement a general one-qubit gate. We assume that the polarizations and the frequencies are such that each field drives a unique transition by a one-photon resonant process. As a consequence, the Stark shifts, which would add detrimental phases, can be neglected here. (Some estimates are presented below.) The atomic states $|0\rangle$ and $|1\rangle$ represent the computational states of the qubit. The ancillary state $|a\rangle$ will be used for the swap operation. The atomic register is fixed in the single-mode optical cavity [see Figs. 2(a) and 2(b)]. Each atom (labelled by k) of the register is driven by a set of two pulsed laser fields [$\Omega_0^{(k)}(t)$ and $\Omega_a^{(k)}(t)$] and by the cavity mode $g^{(k)}$ which is time independent.

III. MECHANISM

We propose a mechanism to prepare a SWAP gate with the help of a simple interaction scheme. The SWAP gate acts on two qubits as follows. The initial state $|\psi_i\rangle$ of the atoms in the cavity, before interaction with the lasers, is defined as

$$|\psi_i\rangle = \alpha|00\rangle|0\rangle + \beta|01\rangle|0\rangle + \gamma|10\rangle|0\rangle + \delta|11\rangle|0\rangle, \qquad (1)$$

where the indices s_1, s_2 of the states of the form $|s_1 s_2\rangle|0\rangle$ denote, respectively, the state of the first and second atom, and $|0\rangle$ is the initial vacuum state of the cavity-mode field. $\alpha, \beta, \gamma, \delta$ are complex coefficients. The swap gate exchanges the values of the two qubits leading to the output state

$$|\psi_o\rangle = \alpha|00\rangle|0\rangle + \gamma|01\rangle|0\rangle + \beta|10\rangle|0\rangle + \delta|11\rangle|0\rangle. \quad (2)$$

The main idea to construct this gate is represented in Fig. 3. It consists of exchanging the values of the qubits by the use of an ancillary ground state. Adiabatic passage along dark states (i.e., with no components in the atomic excited states and a negligible component in the excited cavity states) will be used.

The four steps can be summarized as follows:

(1) The population of $|10\rangle|0\rangle$ is completely transferred into $|a1\rangle|0\rangle$ by the use of two resonant pulses $\Omega_a^{(1)}$, $\Omega_0^{(2)}$ switched on and off in a counterintuitive pulse sequence [i.e., $\Omega_a^{(1)}$ before $\Omega_0^{(2)}$]. After the interaction, the state becomes

$$|\psi_1\rangle = \alpha|00\rangle|0\rangle + \beta|01\rangle|0\rangle + \gamma|a1\rangle|0\rangle + \delta|11\rangle|0\rangle. \quad (3)$$

(2) With a similar technique, the population of $|01\rangle|0\rangle$ is transferred into $|10\rangle|0\rangle$ by the use of the counterintuitive sequence of two pulses $\Omega_0^{(2)}$, $\Omega_0^{(1)}$ leading to the state

$$|\psi_2\rangle = \alpha|00\rangle|0\rangle + \gamma|a1\rangle|0\rangle + \beta|10\rangle|0\rangle + \delta|11\rangle|0\rangle. \quad (4)$$

(3) The population of $|a1\rangle|0\rangle$ is transferred into $|1a\rangle|0\rangle$ by the use of the sequence $\Omega_a^{(2)}$, $\Omega_a^{(1)}$ giving

$$|\psi_3\rangle = \alpha|00\rangle|0\rangle + \gamma|1a\rangle|0\rangle + \beta|10\rangle|0\rangle + \delta|11\rangle|0\rangle. \quad (5)$$

(4) The population of $|1a\rangle|0\rangle$ is transferred into $|01\rangle|0\rangle$ by the use of the sequence $\Omega_0^{(1)}$, $\Omega_a^{(2)}$. As a result, the system is in the state

$$|\psi_4\rangle = \alpha|00\rangle|0\rangle + \gamma|01\rangle|0\rangle + \beta|10\rangle|0\rangle + \delta|11\rangle|0\rangle, \quad (6)$$

which coincides with the output state of the SWAP gate.

In what follows, we give the instantaneous eigenvectors connected with the initial condition and that are thus adiabatically followed by the dynamics for the four steps. We show that they are associated with dark states with no component in the atomic excited states and a negligible component in the excited cavity states.

Since the lasers do not couple the atomic state $|1\rangle$, the state $|11\rangle|0\rangle$ of the initial condition (1) is decoupled from the other ones. The other states of (1) are connected to two orthogonal decoupled subspaces denoted $\mathcal{H}_7$ and $\mathcal{H}_{16}$ of dimension 7 and 16, respectively. For each step, one ground state $|0\rangle$ or $|a\rangle$ of each atom is coupled by a laser field to the excited state, and the other one is not coupled to the excited state. To summarize the calculation of the instantaneous eigenstates for the four steps, we introduce the following notation: the state coupled by a laser field is labeled $|L^{(i)}\rangle$ ($|0^{(i)}\rangle$ or $|a^{(i)}\rangle$) and the noncoupled state $|N^{(i)}\rangle$ [$|a^{(i)}\rangle$ or $|0^{(i)}\rangle$]. The index $i=1,2$ labels the atom i. The instantaneous eigenstates in each subspace $\mathcal{H}_7$ and $\mathcal{H}_{16}$ can be characterized as follows: in $\mathcal{H}_7$, the states $|N^{(1)}1\rangle|0\rangle$ and $|1N^{(2)}\rangle|0\rangle$ are not coupled by the lasers and thus do not participate to the dynamics. Only the atomic dark state (i.e., without component in the excited atomic states) [10],

$$|\phi_7\rangle \propto g^{(1)}\Omega^{(2)}|L^{(1)}1\rangle|0\rangle + g^{(2)}\Omega^{(1)}|1L^{(2)}\rangle|0\rangle - \Omega^{(1)}\Omega^{(2)}|11\rangle|1\rangle, \quad (7)$$

(where the normalization coefficient has been omitted) participates in the dynamics. The first step, associated with $L^{(1)}\equiv a$, $L^{(2)}\equiv 0$, $\Omega^{(1)}\equiv\Omega_a^{(1)}$, $\Omega^{(2)}\equiv\Omega_0^{(2)}$ leads to the initial and final connections symbolically written as $|10\rangle|0\rangle\rightarrow|\phi_7\rangle\rightarrow|a1\rangle|0\rangle$ (see Fig. 3). The second, third, and fourth steps give, respectively, the connections $|01\rangle|0\rangle\rightarrow|\phi_7\rangle\rightarrow|10\rangle|0\rangle$, $|a1\rangle|0\rangle\rightarrow|\phi_7\rangle\rightarrow|1a\rangle|0\rangle$, and $|1a\rangle|0\rangle\rightarrow|\phi_7\rangle\rightarrow|01\rangle|0\rangle$. We determine four atomic dark states in the subspace $\mathcal{H}_{16}$ connected to the state $|00\rangle|0\rangle$ of the initial condition (1),

$$|\phi_{16(1)}\rangle \propto \Omega^{(2)}|N^{(1)}1\rangle|1\rangle - g^{(2)}|N^{(1)}L^{(2)}\rangle|0\rangle, \quad (8a)$$

$$|\phi_{16(2)}\rangle \propto g^{(1)}g^{(2)}\sqrt{2}|L^{(1)}L^{(2)}\rangle|0\rangle - g^{(2)}\Omega^{(1)}\sqrt{2}|1L^{(2)}\rangle|1\rangle - g^{(1)}\Omega^{(2)}\sqrt{2}|L^{(1)}1\rangle|1\rangle + \Omega^{(1)}\Omega^{(2)}|11\rangle|2\rangle, \quad (8b)$$

$$|\phi_{16(3)}\rangle = |N^{(1)}N^{(2)}\rangle|0\rangle, \quad (8c)$$

$$|\phi_{16(4)}\rangle \propto \Omega^{(1)}|1N^{(2)}\rangle|1\rangle - g^{(1)}|L^{(1)}N^{(2)}\rangle|0\rangle. \quad (8d)$$

The state $|00\rangle|0\rangle$ is connected initially and finally to the dark state $|\phi_{16(n)}\rangle$ at the nth step. The phase term of the final state is equal to one: (i) the optical phase is null since the populated atomic states are degenerate, (ii) the dynamical phase is reduced to zero since the eigenvalues associated to each dark state are null, and (iii) the geometric phase is equal to zero. Indeed, at every time ($\langle\phi_d'(s)|d/ds|\phi_d(s)\rangle=0$ $|\phi_d'(s)\rangle$ and $|\phi_d(s)\rangle$ being two different or identical dark eigenstates) since for $|\phi_d'(s)\rangle=|\phi_d(s)\rangle$, the phase of the lasers is constant during each step and for $|\phi_d'(s)\rangle\neq|\phi_d(s)\rangle$, the dark states belong to orthogonal subspaces.

Since the dynamics follows atomic dark states, the excited atomic state is never populated (in the adiabatic limit). Moreover, the projections of the dark states into the excited cavity photon states can be made negligible if $g^{(i)}\gg\Omega^{(i)}$ [15]. In this case, the mechanism we propose is a decoherence-free method in the sense that the process is not sensitive to spontaneous emission from the atomic excited states and to the lifetime of photons in the optical cavity.

We present the numerical validation of the mechanism proposed for the construction of the SWAP gate. We show in Fig. 4, the time evolution of four initial states: in (a) and (d) the population of the initial states $|00\rangle|0\rangle$ and $|11\rangle|0\rangle$, respectively, stays in these states after the interaction with the eight pulses, in (b) and (c) the population of the initial states $|01\rangle|0\rangle$ and $|10\rangle|0\rangle$ are exchanged. In (e), we show the Rabi frequencies associated to each pulses. The laser Rabi frequencies are all chosen of the form $\Omega(t)=\Omega_{\max}e^{-(t/T_p)^2}$. Since the four steps of the mechanism can be seen as double-STIRAPs [13,14], each STIRAP involving one laser and the cavity, the amplitudes of the coupling must satisfy $\Omega_{\max}T_p, gT_p\gg 1$ to fulfill the adiabatic conditions. The delay between two pulses of the same step is chosen equal to $2\times 0.6T_p$ to minimize the nonadiabatic losses [16]. Moreover, the condition $g\gg\Omega_{\max}$ guarantees that the cavity mode is negligibly populated during the interaction with the pulses.

IV. DISCUSSION

We notice that the two identical pulses $\Omega_0^{(2)}$ used successively in the first and second step can be replaced by a single

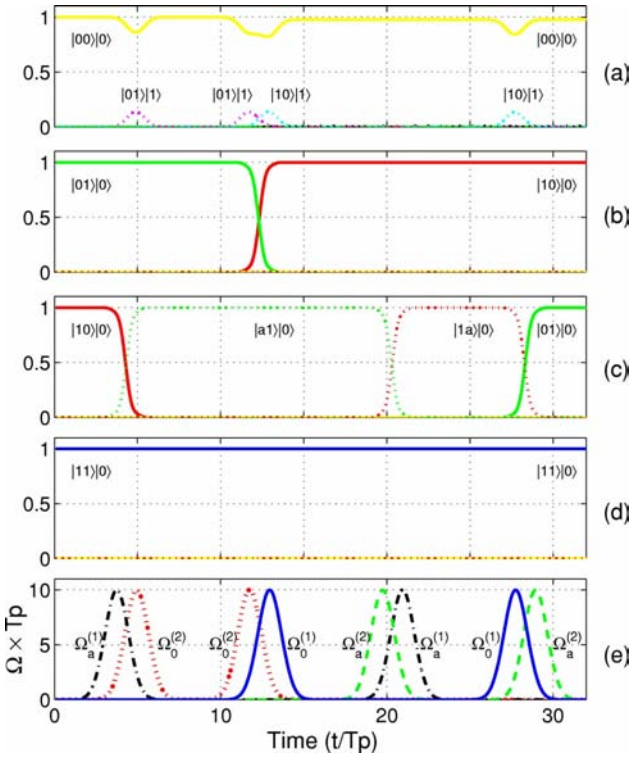

FIG. 4. (Color online) Numerical simulation exhibiting the populations for the initial conditions: (a) $|00\rangle|0\rangle$, (b) $|01\rangle|0\rangle$, (c) $|10\rangle|0\rangle$, and (d) $|11\rangle|0\rangle$. The states which are populated during the interaction with the pulses or between two steps are indicated. (e) Rabi frequencies. The parameters used are $\Omega_{\max}T_p=10$, $gT_p=25$. The delay between two pulses of the same steps is $1.2T_p$.

pulse. The process we propose then requires the use of only seven adiabatic pulses.

As a realistic atomic level scheme, we consider the $2\,^3S_1$-2^3P_0 transition in metastable helium, of linewidth $\Gamma=10^7$ s^{-1} (see for instance [17]). The Rabi frequencies are $\Omega\sim 10^8\sqrt{I}$ s^{-1} with the field intensities I in W/cm^2. We obtain beyond the resonant approximation using the polarizability an upper estimate for the Stark shifts (in absolute value) as $S\sim 100I$ s^{-1}. Taking into account the loss of the intermediate state requires $(\Omega_{\max}T_p)^2\gg\Gamma T_p$ for adiabatic passage, which is satisfied for $\Omega_{\max}T_p\gg 1$ and $\Omega_{\max}\gg\Gamma$. We use $\Omega_{\max}T_p=10$ corresponding to, e.g., $I=10^4$ W/cm^2 and $T_p=1$ ns, which gives $\Omega_{\max}\sim 10^{10}$ s^{-1} and an estimate of the phases $S_{\max}T_p\sim 10^{-3}\ll 2\pi$. They can therefore be neglected.

The swap method we have presented can be extended to build a CNOT gate. The process is composed of six steps: We first transfer the population of the state $|1\rangle$ of the second atom in the ancillary state $|a\rangle$ by STIRAP using two additional resonant laser fields with the upper state $|u\rangle$. The next four steps allow us to interchange the populations of the states $|10\rangle|0\rangle$ and $|1a\rangle|0\rangle$ by a similar swap method like the one shown in this paper. The last step transfers back the population of the ancillary state $|a\rangle$ of the second atom in state $|1\rangle$. The population transfers are realized by adiabatic passage along dark states. We thus obtain a direct and decoherence-free method for the creation of the CNOT gate that requires the use of 11 pulses. In comparison to the method proposed in Ref. [9], this technique does not use f-STIRAP (in which the ratio of two pulses has to be controlled [16]). A specific system (such as Zeeman states) is not necessarily required to guarantee the robustness of the technique.

V. CONCLUSION

In conclusion, we have proposed to use a mechanism adapted to the construction of a specific gate instead of relying on compositions of a large number of elementary gates. We have illustrated this idea by the construction of a SWAP gate in a system where all one-qubit gates and the C-phase gate can be built. This technique requires the use of a cavity and seven pulses in a double-STIRAP configuration instead of 21 pulses when the SWAP gate is created from the composition of elementary gates. It is robust against variations of amplitude and duration of the pulses and of the delay between the pulses. Moreover, it constitutes a decohence-free method in the sense that the excited states with short lifetimes are not populated and the cavity mode has no photon during the process. We conclude by noticing that this technique allows one to entangle the qubits on which it acts by manipulating the phase of the pulses. In this case, we get the composition of gates that could offer interesting possibilities to execute rapid quantum algorithms in which this composition is required.

Work is in progress to generalize this fast method to other gates. This requires other pulse sequences and involves different dark states.

[1] A. Galindo and M. A. Martin-Delgado, Rev. Mod. Phys. **74**, 347 (2002).
[2] D. P. DiVincenzo, Phys. Rev. A **51**, 1015 (1995).
[3] A. Barenco C. H. Bennett, R. Cleve, D. P. DiVincenzo, N. Margolus, P. Shor, T. Sleator, J. A. Smolin, and H. Weinfurter,Phys. Rev. A **52**, 3457 (1995).
[4] R. Unanyan, M. Fleischhauer, B. W. Shore, and K. Bergmann, Opt. Commun. **155**, 144 (1998).
[5] R. G. Unanyan, B. W. Shore, and K. Bergmann, Phys. Rev. A **59**, 2910 (1999).
[6] L.-M. Duan, J. I. Cirac, and P. Zoller, Science **292**, 1695 (2001).
[7] R. G. Unanyan and M. Fleischhauer, Phys. Rev. A **69**, 050302(R) (2004).
[8] Z. Kis and F. Renzoni, Phys. Rev. A **65**, 032318 (2002).
[9] H. Goto and K. Ichimura, Phys. Rev. A **70**, 012305 (2004).
[10] T. Pellizzari, S. A. Gardiner, J. I. Cirac, and P. Zoller, Phys.

Appendix A

π-pulse technique in microwave cavity

In this Appendix we review the π-pulse technique in a microwave cavity [242, 225, 241] in order to explain by a simple method the ideas of:

1 Generation of single-photon Fock state,
2 Creation of atom-photon entanglement,
3 Transfer of coherence from atom into a cavity mode,
4 Transfer of coherence between two atoms,
5 Creation of atom-atom entanglement,
6 Creation of photon-photon entanglement.

The experimental realization of these ideas is not easy due to the non-robust character of the π-pulse technique.

The Hamiltonian of a two-level atom (corresponding e.g. to circular Rydberg states) interacting with a single-mode high-Q cavity is given by the Jaynes-Cummings Hamiltonian in the rotating-wave approximation (in units such that $\hbar = 1$):

$$H(t) = \omega_C a^\dagger a \ \mathbf{1}_2 + \begin{pmatrix} \omega_e & 0 \\ 0 & \omega_g \end{pmatrix} + G(t) \begin{pmatrix} 0 & a \\ a^\dagger & 0 \end{pmatrix}, \tag{A.1}$$

where $G(t)$ is the Rabi frequency of the cavity mode. (The Rabi frequency is often alternatively defined as twice the G factor in the literature.) This Hamiltonian is block-diagonal in the subspaces $\mathcal{S}_n$ with $n = 0, 1, 2, \cdots$ spanned by vectors $\{|e, n\rangle, |g, n+1\rangle\}$. The state $|g, 0\rangle$ is a stationary state of the system. If the initial state of the system is $|e, 0\rangle$ or $|g, 1\rangle$, then the effective Hamiltonian of the system in the subspace $\mathcal{S}_0$ will be

$$H^{\text{eff}}(t) = \begin{pmatrix} \delta & G(t) \\ G(t) & 0 \end{pmatrix}, \tag{A.2}$$

where we have shifted the reference of energy to $\omega_C + \omega_g$, and δ is the detuning from the one-photon resonance $\delta = \omega_e - \omega_g - \omega_C$. An essential condition for the π-pulse technique is the exact one-photon resonance $\delta = 0$. In this case, the propagator corresponding to $H^{\text{eff}}(t)$ is given by

$$U(t) = \cos A(t) \ \mathbf{1}_2 - i \sin A(t) \ \sigma_x, \tag{A.3}$$

where σ_x is the pauli matrix, and

$$A(t) := \int_0^t G(s) ds, \tag{A.4}$$

is the pulse area. Hence, the time evolution of the system for $A(t_f) = \pi/2$ and with different initial conditions will be as follows:

$$|e,0\rangle \xrightarrow{A_1(t_f)=\pi/2} -i|g,1\rangle, \tag{A.5}$$

$$|g,1\rangle \xrightarrow{A_1(t_f)=\pi/2} -i|e,0\rangle. \tag{A.6}$$

1 Equation (A.5) indicates that if the atom, initially in the excited state $|e\rangle$, enters into a microwave cavity initially in the vacuum state and if we control the velocity of the atom such that the pulse area equals $\pi/2$, then we can transfer the atomic excitation to the cavity field by generating a single-photon Fock state.

2 For $A(t_f) = \pi/4$ the final state of the system will be a maximally entangled atom-photon state:

$$|e,0\rangle \xrightarrow{A_1(t_f)=\pi/4} \frac{1}{\sqrt{2}}(|e,0\rangle - i|g,1\rangle). \tag{A.7}$$

3 If the atom is initially in a coherent superposition $\alpha|e\rangle + \beta|g\rangle$, the final state of the system for $A(t_f) = \pi/2$ will be

$$(\alpha|e\rangle + \beta|g\rangle)|0\rangle \xrightarrow{A(t_f)=\pi/2} |g\rangle(-i\alpha|1\rangle + \beta|0\rangle), \tag{A.8}$$

since $|g,0\rangle \rightarrow |g,0\rangle$. This means that the interaction has transferred the coherence from the two-level atom to a cavity-mode field by a $\pi/2$-pulse technique.

4 This coherence can then be transferred to a second two-level atom initially in the state $|g\rangle$ (with the same velocity as the first atom) which crosses the cavity after a time delay with the reverse process of the one performed on the first atom:

$$\begin{aligned} |g,g\rangle(-i\alpha|1\rangle + \beta|0\rangle) &\xrightarrow{A(t_f)=\pi/2} -\alpha|g,e,0\rangle + \beta|g,g,0\rangle \\ &= |g\rangle(-\alpha|e\rangle + \beta|g\rangle)|0\rangle. \end{aligned} \tag{A.9}$$

5 To create atom-atom maximal entanglement [242] we suppose that the initial state of the combined system is $|e,g,0\rangle$. Two atoms enter successively into the cavity with different pulse areas. The combined system is left in the final state

$$\begin{aligned} |e,g,0\rangle &\xrightarrow{A_1(t_f)=\pi/4} \frac{1}{\sqrt{2}}(|e,g,0\rangle - i|g,g,1\rangle) \\ &\xrightarrow{A_2(t_f)=\pi/2} \frac{1}{\sqrt{2}}(|e,g,0\rangle - |g,e,0\rangle), \end{aligned} \tag{A.10}$$

which corresponds to a pair of atoms in a maximally entangled atomic state with an empty cavity. The cavity field which starts and ends up in the vacuum state and remains at the end of the process uncorrelated from the atoms, acts as a *catalyst* for the atom-atom entanglement.

6 One can also entangle two photons in two spatially separate microwave cavities by an atom, initially in the state $|e\rangle$, which enters successively into two empty cavities. Hence the

initial state of the combined system is $|e,0,0\rangle$, where the second (third) symbol in the ket refers to the photon number in the first (second) cavity. If the duration of the interaction of the atom with the first and the second cavity is controlled such that $A_1(t_f) = \pi/4$ and $A_2(t_f) = \pi/2$, the state of the combined system will evolve as follows:

$$\begin{aligned} |e,0,0\rangle &\xrightarrow{A_1(t_f)=\pi/4} \frac{1}{\sqrt{2}}(|e,0,0\rangle - i|g,1,0\rangle) \\ &\xrightarrow{A_2(t_f)=\pi/2} \frac{1}{\sqrt{2}}(-i|g,0,1\rangle - i|g,1,0\rangle) \\ &= \frac{-i}{\sqrt{2}}|g\rangle(|0,1\rangle + |1,0\rangle), \end{aligned} \tag{A.11}$$

which represents a pair of photons maximally entangled in two cavities in the presence of an atom in its ground state.

Conclusion - Outlook

In this manuscript, we have presented in a self-contained way tools and strategies for the control of atomic and molecular processes by external fields with parameters specifically designed to achieve particular goals. Control of selective population transfer, of the external degrees of freedom (atomic deflection, tunneling localization, and alignment of molecule), and applications to quantum information processing have been studied.

The techniques can be divided in two classes: adiabatic passage, adapted for moderately short pulses and that leads to specific processes while the field is on or right after the pulse, and processes induced by short pulses that yield specific postpulse effects. For adiabatic passage, geometric analysis of the eigenenergies of the complete system (quasienergies) as functions of the parameters allows one to establish robust strategies of population transfer. On the other hand, short pulses allow one to prepare a specific superposition that subsequently evolves inducing desirable properties, such as revivals of alignment.

In these two classes it is required (i) to define a target state that has the desired properties, and (ii) to construct a process that allows one to reach the target state. For the adiabatic regime, the target state can be in general easily related to a dressed potential, in terms of eigenstates (e.g. for the state selectivity) or in geometric terms (alignment or tunneling effect for instance). In the sudden regime, the target state is not directly connected to the potential, but rather related to an observable that characterizes the goal to achieve (for instance $\cos^2\Theta$ for the alignment, where Θ is the angle between the molecular axis and a reference axis).

One of the main points to construct strategies in the adiabatic regime consists in inducing in the system resonances by choosing appropriate frequencies. These resonances determine indeed the essential aspects of the geometry and the topology of the quasienergies, that determine the possible strategies. Particular care must be taken to construct effective Hamiltonians that incorporate the relevant resonances. The perturbative effects that slightly modify the resonances are not so important since they do not change the final effect provided that adiabaticity is preserved.

The global perspective of this work consists in extending these tools for more complex systems, especially the adiabatic techniques, taking benefits of its robustness.

In particular, the extension of the adiabatic techniques to *open quantum systems*, i.e. to quantum systems coupled to an external environment, is of interest since adiabatic processes require relatively long times, where decoherence, such as dephasing (i.e. loss of phase) and spontaneous emission may take place. These decoherence effects are of importance in particular in quantum information processings.

The passage to open systems is made by replacing the Schrödinger equation by a master equation which depends on the environment. A widely studied class is the linear Lindblad equation, which assumes a Markovian bath with small correlation times [256]. It is associated to a Lindblad generator (LG) which generalizes the Hamiltonian to open systems, and the adiabatic passage is expected to occur along a set of eigenvectors of this LG. It has been argued that this is not generally the case, when the LG is not diagonalizable, and that the Jordan blocks take then the role of the eigenvectors [257]. However it is not yet clear whether this occurs for relevant physical situations.

An other extension of our tools can be made when a continuum of the field-free spectrum is considered. In this case, the natural construction consists in applying a complex-scaling rotation of the quasienergy operator that will allow one to describe the resonances in the continuum with squared integrable functions (see for instance [258]).

Concerning quantum information, robust adiabatic techniques that avoid geometrical phases, have not been fully exploited in particular to construct logical gates and algorithms. They could

be applied for instance in trapped ion systems, where a particular control of Stark shifts is required.

Alignment by strong fields of molecules will be analyzed for more complex systems, such as asymmetric top molecules (see for instance [259] and [260]), molecules interacting with its environment (e.g. through collision [261]), and molecules trapped in solids [262].

Bibliography

[1] S. Guérin and H. R. Jauslin, *Control of quantum dynamics by laser pulses: Adiabatic Floquet theory*, Adv. Chem. Phys. **125**, 147 (2003).

[2] J.H. Shirley, *Solution of the Schrödinger equation with a Hamiltonian periodic in time*, Phys. Rev. **138**, B979 (1965).

[3] H. Sambe, *Steady states and quasi-energies of a quantum-mechanical system in an oscillating field*, Phys. Rev. A **7**, 2203 (1973).

[4] J. Howland, *Stationary scattering theory for time-dependent Hamiltonians*, Math. Ann. **207**, 315 (1974).

[5] J.Bellissard, *Stability and Instability in Quantum Mechanics*, in "Trends and developments in the eighties", S.Albeverio, Ph.Blanchard (Eds), World Scientific, Singapore 1985.

[6] S. I. Chu, *Recent developments in semiclassical Floquet theories for intense-field multiphoton processes* Adv. At. Mol. Phys. **21**, 197 (1985).

[7] S. I. Chu, *Generalized Floquet theoretical approaches to intense field multiphoton and non-linear optical processes*, Adv. Chem. Phys. **73**, 739 (1987).

[8] I. Bialynicki-Birula and Z. Bialynicka-Birula, *Quantum electrodynamics of intense photon beams. New approximation method*, Phys. Rev. A **14**, 1101 (1976).

[9] I. Bialynicki-Birula and C. L. Van, Acta Physica Polonica A **57**, 599 (1980).

[10] S. Guérin, F. Monti, J.-M. Dupont, H. R. Jauslin, *On the relation between cavity dressed states, Floquet states, RWA approximation and semiclassical models*, J. Phys. A **30**, 7193 (1997).

[11] C. Cohen-Tannoudji, J. Dupont-Roc and G. Grynberg, *Atom-Photon Interactions* (John Wiley and Sons, New York, 1992).

[12] G. Compagno, R. Passante, and F. Persico, *Atom-Field Interactions and Dressed Atoms* (Cambridge University Press, Cambridge, 1995).

[13] P. Carruthers and M. M. Nieto, *Phase and Angle Variables in Quantum Mechanics*, Rev. Mod. Phys. **40**, 411 (1968).

[14] J. M. Lévy-Leblond, *Who is afraid of nonhermitian operators? A quantum description of angle and phase*, Ann. Phys. **101**, 319 (1976).

[15] P. A. M. Dirac, *The Principles of Quantum Mechanics* 4th Ed (Clarendon Press, London, 1958).

[16] J. Von Neumann, *Mathematische Grundlagen der Quantenmechanik* (Springer,Berlin, 1932).

[17] G. A. Raggio and S. Zivi, *On the semiclassical description of N-level systems interacting with radiation fields*, J. Math. Phys. **26**, 2529 (1985).

[18] T. S. Ho and S. I. Chu, *Semiclassical many-mode Floquet theory: II. Non-linear multi-photon dynamics of a two-level system in a strong bichromatic field*, J. Phys. B **17**, 2101 (1984).

[19] H. R. Jauslin and J. L. Lebowitz, *Spectral and stability aspects of quantum chaos*, Chaos **1**, 114 (1991).

[20] P. Blekher, H. R. Jauslin and J. L. Lebowitz, *Floquet spectrum for two-level systems in quasiperiodic time-dependent fields*, J. Stat. Phys. **68**, 271 (1992).

[21] H. R. Jauslin in *II Granada Lectures in Computational Physics* edited by P. L. Garrido and J. Marro (World Scientific, Singapore,1993).

[22] G. Casati et L. Molinari, *Quantum chaos with time-periodic Hamiltonians*, Prog. Theor. Phys. (Suppl.), **98**, 286 (1989).

[23] D. Daems, A. Keller, S. Guérin, O. Atabek, and H.R. Jauslin, *Unitary time-dependent superconvergent technique for pulse-driven quantum dynamics*, Phys. Rev. A **67**, 052505 (2003).

[24] U. Peskin and N. Moiseyev, *The solution of the time-dependent Schrödinger equation by the (t, t') method: theory, computational algorithm and applications*, J. Chem. Phys. **99**, 4590 (1993).

[25] R.H. Young and W.J Deal, *Adiabatic response to an oscillatory field*, J. Math. Phys. **11**, 3298 (1970).

[26] H. P. Breuer and M. Holthaus, *Quantum phases and Landau-Zener transitions in oscillating fields*, Phys. Lett. A **140**, 507 (1989).

[27] S. Guérin, *Complete dissociation by chirped laser pulses designed by adiabatic Floquet analysis*, Phys. Rev. A **56**, 1458 (1997).

[28] K. Drese and M. Holthaus, *Floquet theory for short laser pulses*, Eur. Phys. J. D **5**, 119 (1999).

[29] M. V. Berry, *Quantal phase factors accompanying adiabatic changes*, Proc. R. Soc. London A **392**, 45 (1984).

[30] M. Born and V. Fock, *Beweis des Adiabatensatzes*, Z. Phys. **51**, 165 (1928).

[31] T. Kato, *On the adiabatic theorem of quantum mechanics*, Phys. Soc. Jap. **5**, 435 (1958).

[32] G. Nenciu, *On the adiabatic theorem of quantum mechanics*, J. Phys. A **13**, L15-L18 (1980).

[33] G. Hagedorn, *Adiabatic Expansions near Eigenvalue Crossings*, Ann. Phys. **196**, 278-295 (1989).

[34] *Adiabatic evolution for systems with infinitely many eigenvalue crossings* A. Joye, F. Monti, S. Guérin, and H. R. Jauslin, J. Math. Phys. **40**, 5456 (1999).

[35] J.E. Avron, A. Elgart, *Adiabatic theorem without a gap condition: Two-level system coupled to quantized radiation field*, Phys. Rev. A **58**, 4300 (1998).

[36] J.E. Avron, A. Elgart, *Adiabatic theorem without a gap condition*, Commun. Math. Phys. **203**, 445 (1999).

[37] F. Wilczek and A. Zee, *Appearance of Gauge Structure in Simple Dynamical Systems*, Phys. Rev. Lett. **52**, 2111 (1984).

[38] D. J. Moore and G. E. Stedman, *Non-adiabatic Berry phase for periodic Hamiltonians*, J. Phys. A **23**, 2049 (1990).

[39] Y. Aharanov and J. Anandan, *Phase change during a cyclic quantum evolution*, Phys. Rev. Lett. **58**, 1593 (1987).

[40] A. N. Seleznyova *Cyclic states, Berry phases and the Schrodinger operator*, J. Phys. A **26**, 981 (1993).

[41] J. Samuel and R. Bhandari, *General Setting for Berry's Phase*, Phys. Rev. Lett. **60**, 2339 (1988).

[42] A. Ceulemans and M. Szopa, *The Berry phase for a threefold degenerate state*, J. Phys. A **24**, 4495 (1991).

[43] B. W. Shore, *The Theory of Coherent Atomic Excitation* (Wiley, New York, 1990).

[44] L. Allen and J. H. Eberly, *Optical Resonance and Two-Level Atoms* (Dover, New York, 1987).

[45] A. M. Dykhne, *Quantum transitions in the adiabatic approximation* , Sov. Phys. JETP **11**, 411 (1960); *Adiabatic perturbation of discrete spectrum states*, Sov. Phys. JETP **14**, 941 (1962).

[46] J. P. Davis and P. Pechukas, *Nonadiabatic transitions induced by a time-dependent Hamiltonian in the semiclassical/adiabatic limit: The two-state case*, J. Chem. Phys. **64**, 3129 (1976).

[47] J.-T. Hwang and P. Pechukas, *The adiabatic theorem in the complex plane and the semiclassical calculation of nonadiabatic transition amplitudes*, J. Chem. Phys. **67**, 4640 (1977).

[48] A. Joye, H. Kuntz, and C.-Ed. Pfister, *Exponential Decay and Geometric Aspect of Transition Probabilities in the Adiabatic Limit*, Ann. Phys. **208**, 299 (1991).

[49] A. Joye, G. Mileti, and C.-Ed. Pfister, *Interferences in adiabatic transition probabilities mediated by Stokes lines*, Phys. Rev. A **44**, 4280 (1991).

[50] M. V. Berry, *Histories of adiabatic quantum transitions*, Proc. R. Soc. London A **429**, 61 (1990).

[51] M. V. Berry, *Quantum phase corrections from adiabatic iteration*, Proc. R. Soc. London A **414**, 31 (1987).

[52] A. Joye and C.-E. Pfister, *Superadiabatic Evolution and Adiabatic Transition Probability between two non-degenerate Levels isolated in the Spectrum*, J. Math. Phys. **34**, 454 (1993).

[53] A. Joye, *Non-trivial Prefactors in Adiabatic Transition Probabilities Induced by High Order Complex Degeneracies*, J. Phys. A **26**,6517 (1993).

[54] K. Drese and M. Holthaus, *Perturbative and nonperturbative processes in adiabatic population transfer*, Eur. Phys. J. D **3**, 73 (1998).

[55] S. Guérin, S. Thomas and H. R. Jauslin, *Optimization of population transfer by adiabatic passage*, Phys. Rev. A **65**, 023409 (2002).

[56] L.P. Yatsenko, S. Guérin, and H. R. Jauslin, *Pulse-driven near-resonant quantum adiabatic dynamics: Lifting of quasidegeneracy*, Phys. Rev. A **70**, 043402 (2004).

[57] P. R. Berman, L. Yan, K.-H. Chiam and R. Sung, *Nonadiabatic transitions in a two-level quantum system: Pulse-shape dependence of the transition probability for a two-level atom driven by a pulsed radiation field*, Phys. Rev. A **57**, 79 (1998).

[58] M. Holthaus and B. Just, *Generalized π pulses*, Phys. Rev. A **49**, 1950 (1994).

[59] M. V. Korolkov, J. Manz, G. K. Paramonov, *Theory of ultrafast laser control for state-selective dynamics of diatomic molecules in the ground electronic state: vibrational excitation, dissociation, spatial squeezing and association*, Chem. Phys. **217**, 341 (1997).

[60] S. Guérin and H. R. Jauslin, *Laser-enhanced tunneling through resonant intermediate levels*, Phys. Rev. A **55**, 1262 (1997).

[61] L. P. Yatsenko, N. V. Vitanov, B. W. Shore, T. Rickes, and K. Bergmann, *Creation of coherent superpositions using Stark-chirped rapid adiabatic passage*, Opt. Commun. **204**, 413 (2002).

[62] N. V. Vitanov and B.M. Garraway, *Landau-Zener model: Effects of finite coupling duration*, Phys. Rev. A **53**, 4288 (1996); *Erratum: Landau-Zener model: Effects of finite coupling duration* , Phys. Rev. A **54**, 5458 (1996).

[63] N. Rosen and C. Zener, *Double Stern-Gerlach Experiment and Related Collision Phenomena*, Phys. Rev. **40**, 502 (1932).

[64] Yu. N. Demkov, *Charge transfer at small resonance defects*, Sov. Phys. JETP **18**, 138 (1964).

[65] G.S. Vasilev and N.V. Vitanov, *Coherent excitation of a two-state system by a Gaussian field*, Phys. Rev. A **70**, 053407 (2004).

[66] L. D. Landau, *Zur Theorie der Energiebertragung II*, Phys. Z. Sowjetunion **2**, 46 (1932).

[67] C. Zener, *Non-adiabatic crossing of energy levels*, Proc. R. Soc. London A **137**, 696 (1932).

[68] C. E. Carrol and F. T. Hioe, *Transition probabilities for the three-level Landau-Zener model*, J. Phys. A **19**, 2061 (1986).

[69] S. Guérin, L. P. Yatsenko and H. R. Jauslin, *Dynamical resonances and the topology of the multiphoton adiabatic passage*, Phys. Rev. A **63**, R031403 (2001).

[70] L. P. Yatsenko, S. Guérin and H. R. Jauslin, *Topology of adiabatic passage*, Phys. Rev. A **65**, 043407 (2002).

[71] N. V. Vitanov, M. Fleischhauer, B. W. Shore, and K. Bergmann, *Coherent manipulation of atoms and molecules by sequential pulses*, Adv. At. Mol. Opt. Phys. **46**, 55 (2001); N. V. Vitanov, T. Halfmann, B. W. Shore, and K. Bergmann, Annu. Rev. Phys. Chem. *Laser-induced population transfer by adiabatic passage techniques*, **52**, 763 (2001).

[72] S. Chelkowski and A. D. Bandrauk, *Raman chirped adiabatic passage: A new method for selective excitation of high vibrational states*, J. Raman Spectroscopy **28**, 459 (1997).

[73] L. P. Yatsenko, B. W. Shore, T. Halfmann, K. Bergmann, and A. Vardi, *Source of metastable H(2s) atoms using the Stark chirped rapid-adiabatic-passage technique*, Phys. Rev. A **60**, R4237 (1999).

[74] T. Rickes, L. P. Yatsenko, S. Steuerwald, T. Halfmann, B. W. Shore, N. V. Vitanov and K. Bergmann, *Efficient adiabatic population transfer by two-photon excitation assisted by a laser-induced Stark shift*, J. Chem. Phys. **113**, 534 (2000).

[75] M. V. Danileiko, V. I. Romanenko, and L. P. Yatsenko, *Landau-Zener transitions and population transfer in a three-level system driven by two delayed laser pulses*, Opt. Commun. **109**, 462 (1994).

[76] *Stimulated hyper-Raman adiabatic passage. II. Static compensation of dynamic Stark shifts*, S. Guérin, L. P. Yatsenko, T. Halfmann, B. W. Shore, and K. Bergmann, Phys. Rev. A **58**, 4691 (1998).

[77] D. Grischkowsky, M. M. T. Loy, P. F. Liao, *Adiabatic following model for two-photon transitions: Nonlinear mixing and pulse propagation*, Phys. Rev. A **12**, 2514 (1975).

[78] N. Sangouard, S. Guérin, L. P. Yatsenko, and T. Halfmann, *Preparation of coherent superposition in a three-state system by adiabatic passage*, Phys. Rev. A **70**, 013415 (2004).

[79] N. V. Vitanov, K.-A. Suominen, and B. W. Shore, *Creation of coherent atomic superpositions by fractional stimulated Raman adiabatic passage*, J. Phys. B **32**, 4535 (1999).

[80] I. I. Rabi, *Space Quantization in a Gyrating Magnetic Field*, Phys. Rev. 51, 652 (1937).

[81] N. V. Vitanov, *Transition times in the Landau-Zener model*, Phys. Rev. A **59**, 988 (1999).

[82] Yu. N. Demkov and M. Kunike, Vestn. Leningr. Univ. Fiz. Khim. **16**, 39 (1969).

[83] F. T. Hioe and C. E. Carroll, *Two-state problems involving arbitrary amplitude and frequency modulations*, Phys. Rev. A **32**, 1541 (1985); J. Zakrzewski, *Analytic solutions of the two-state problem for a class of chirped pulses*, ibid. **32**, 3748 (1985); K.-A. Suominen and B. M. Garraway, *Population transfer in a level-crossing model with two time scales*, ibid. **45**, 374 (1992).

[84] F. T. Hioe, *Solution of Bloch equations involving amplitude and frequency modulations*, Phys. Rev. A 30, 2100 (1984).

[85] A. Bambini and P. R. Berman, *Analytic solutions to the two-state problem for a class of coupling potentials*, Phys. Rev. A 23, 2496 (1981).

[86] E. E. Nikitin, *The probability of nonadiabatic transitions in the case of nondivergent terms*, Optika Spectr. 13, 431 (1962); *Resonance and nonresonance intermolecular energy exchange in molecular collisions*, Discuss. Faraday Soc. 33, 14 (1962); *The theory of nonadiabaic transitions. Recent development with the exponential model*, Adv. Quantum Chem. 5, 135 (1970).

[87] M. S. Child, *Semiclassical Mechanics with Molecular Applications* (Clarendon, Oxford, 1991).

[88] W. Scherer, *Quantum averaging I: Poincaré-von Zeipel is Rayleigh-Schrödinger*, J. Phys. A **27**, 8231 (1994).

[89] W. Scherer, *Quantum averaging II: Kolmogorov's algorithm*, J. Phys. A **30**, 2825 (1997).

[90] W. Scherer, *Quantum averaging III: Time-dependent systems*, J. Math. Phys. **39**, 2597 (1998).

[91] W. Scherer, *New perturbation algorithms for time-dependent quantum systems*, Phys. Lett. **A 233**,1 (1997).

[92] W. Scherer, *Superconvergent perturbation method in quantum mechanics*, Phys. Rev. Lett. **74**, 1495 (1995).

[93] C. Chandre, H.R. Jauslin, *A version of Thirring's approach to the KAM theorem for quadratic Hamiltonians with degenerate twist*, J. Math. Phys. **39**, 5856 (1998).

[94] C. Chandre, H. R. Jauslin, *Renormalization-group analysis for the transition to chaos in Hamiltonian systems*, Phys. Rep. **365**, 1 (2002).

[95] J.H. Van Vleck, *On σ-Type Doubling and Electron Spin in the Spectra of Diatomic Molecules*, Phys. Rev. **33**, 467 (1929).

[96] H. R. Jauslin, S. Guérin and S. Thomas, *Quantum averaging for driven systems with resonances*, Physica A **279**, 432 (2000).

[97] H. Primas, *Generalized Perturbation Theory in Operator Form*, Rev. Mod. Phys. **35**, 710 (1963).

[98] V.G. Tyuterev, V.I. Perevalov, *Generalized contact transformations of a Hamiltonian with quasi-degenerate zero-order approximation. Application to accidental vibration-rotation resonances in molecules*, Chem. Phys. Lett. **74**, 494 (1980).

[99] H. Feshbach, *A unified theory of nuclear reactions. II*, Ann. Phys. **19**, 287 (1962).

[100] A. Messiah, *Quantum Mechanics* (Wiley, N.Y., 1962).

[101] P.-O. Löwdin, *Studies in perturbation theory. IV. solution of eigenvalue problem by projection operator formalism*, J. Math. Phys. **3**, 969 (1962); *Perturbation theory. I. An elementary iteration-variation procedure for solving the Schrödinger equation by partitioning technique*, J. Mol. spec. **10**, 12 (1963).

[102] L. Mower, *Projection-operator approach to perturbation theory*, Phys. Rev. A **22**, 882 (1980).

[103] A. Keller, C. M. Dion, and O. Atabek, *Laser-induced molecular rotational dynamics: A high-frequency Floquet approach*, Phys. Rev. A **61**, 023409 (2000).

[104] L.H. Eliasson, *Floquet solutions for the 1-dimensional quasiperiodic Schrödinger equation*, Commun. Math. Phys. **146**, 447 (1992).

[105] L.H. Eliasson, *Ergodic skew systems on* $\mathbb{T}^d \times SO(3,\mathbb{R})$*,* Preprint ETH Zürich, (1991).

[106] R. Krikorian, *Réductibilité presque partout des systèmes quasipériodiques dans le cas* $SO(3)$, C. R. Académie des Sciences, Paris, Serie I **321**, 1039 (1995).

[107] R. Krikorian, C^0*-densité globale des systèmes produits-croisés réductibles sur le cercle*, Ergodic Th. Dyn. Syst. **19**, 61 (1999).

[108] H.R. Jauslin, *Small divisors in driven quantum systems*; in *Stochasticity and Quantum Chaos*, Z. Haba, W. Cegla, L. Jakóbczyk (eds.), Kluwer Publ. 1995.

[109] S. Guérin, R. Unanyan, L. Yatsenko, H.R. Jauslin, *Floquet perturbative analysis for STIRAP beyond the rotating wave approximation*, Optics Express **4**, 84 (1999).

[110] E.T. Jaynes and F. Cummings, *Comparison of quantum and semiclassical radiation theories with application to beam maser*, Proc. IEEE **51**, 89 (1963).

[111] M. Amniat-Talab, S. Guérin, and H. R. Jauslin, *Quantum averaging and resonances: two-level atom in a one-mode quantized field*, J. Math. Phys. **46**, 042311 (2005).

[112] N.V. Vitanov, Z. Kis, and B.W. Shore, *Coherent excitation of a degenerate two-level system by an elliptically polarized laser pulse*, Phys. Rev. A **68**, 063414 (2003).

[113] L.P. Yatsenko, S. Guérin, T. Halfmann, K. Böhmer, B.W. Shore, and K. Bergmann, *Stimulated hyper-Raman adiabatic passage. I. The basic problem and examples*, Phys. Rev. A **58**, 4683 (1998).

[114] P.S. Pershan, J.P. van der Ziel, and L.D. Malmstrom, *Theoretical discussion of the inverse Faraday effect, Raman scattering and related phenomena*, Phys. Rev. **143**, 574 (1966).

[115] M. Born and E. Wolf, *Principles of Optics* , 7^{th} (reprinted) edition (Cambridge University Press, 2002).

[116] V.S. Malinovsky and I.R. Sola, Phys. Rev. Lett. **93**, 190502 (2004); *Quantum control of entanglement by phase manipulation of time-delayed pulse sequences. I*, Phys. Rev. A **70**, 042304 (2004); *Quantum control of entanglement by phase manipulation of time-delayed pulse sequences. II*, Phys. Rev. A **70**, 042305 (2004).

[117] V.S. Malinovsky and I.R. Sola, *Phase-Controlled Collapse and Revival of Entanglement of Two Interacting Qubits*, Phys. Rev. Lett. **96**, 050502 (2006).

[118] G. Herzberg, *Molecular Spectra and Molecular Structure I. Spectra of Diatomic Molecules* (Van Nostrand Reinhold, New-York, 1950).

[119] H. Lefebvre-Brion, R.W. Field *The Spectra and Dynamics of Diatomic Molecules* (Elsevier, 2004).

[120] R. N. Zare, *Angular Momentum* (Wiley, New-York, 1988).

[121] P. Rabl, D. DeMille, J. M. Doyle, M. D. Lukin, R. J. Schoelkopf, and P. Zoller, *Hybrid Quantum Processors: molecular ensembles as quantum memory for solid state circuits*, eprint quant-ph/0604140

[122] J. T. Hougen, *The Calculation of Rotational Energy Levels and Rotational Line Intensities in Diatomic Molecules* (version 1.0), http://physics.nist.gov/DiatomicCalculations. National Institute of Standards and Technology, Gaithersburg, MD (2001).

[123] P. Atkins, R. Friedman, *Molecular Quantum Mechanics* (Oxford University Press, 2005).

[124] M. Hippler, *Interference in two-photon rotational line strengths of diatomic molecules*, Mol. Phys. **97**, 105 (1999).

[125] B. Friedrich and D. Herschbach, *Alignment and Trapping of Molecules in Intense Laser Fields*, Phys. Rev. Lett. **74**, 4623 (1995).

[126] D. Daems, S. Guérin, E. Hertz, H.R. Jauslin, B. Lavorel, and O. Faucher, *Field-free two-direction alignment alternation of linear molecules by elliptic laser pulses*, Phys. Rev. Lett. **95**, 063005 (2005).

[127] J. Karczmarek, J. Wright, P. Corkum, and M. Ivanov, *Optical centrifuge for molecules*, Phys. Rev. Lett. **82**, 3420 (1999).

[128] D.M. Villeneuve, S.A. Aseyev, P. Dietrich, M. Spanner, M.Yu. Ivanov, and P.B. Corkum, *Forced molecular rotation in an optical centrifuge*, Phys. Rev. Lett. **85**, 542 (2000).

[129] M. Spanner and M.Yu. Ivanov, *Angular trapping and rotational dissociation of a diatomic molecule in an optical centrifuge*, J. Chem. Phys. **114**, 3456 (2001).

[130] M. Spanner, K.M. Davitt, and M.Yu. Ivanov, *Stability of angular confinement and rotational acceleration of a diatomic molecule in an optical centrifuge*, J. Chem. Phys. **115**, 8403 (2001).

[131] D. Daems, S. Guérin, H.R. Jauslin, A. Keller and O. Atabek, *Optimized time-dependent perturbation theory for pulse-driven quantum dynamics in atomic or molecular systems*, Phys. Rev. A **68**, 051402(R) (2003); *Publisher's Note*, Phys. Rev. A **68**, 069902 (2003).

[132] D. Daems, S. Guérin, H.R. Jauslin, A. Keller and O. Atabek, *Pulse-driven quantum dynamics beyond the impulsive regime*, Phys. Rev. A **69**, 033411 (2004).

[133] D. Sugny, A. Keller, O. Atabek, D. Daems, S. Guérin and H.R. Jauslin, *Time-dependent unitary perturbation theory for intense laser driven molecular orientation*, Phys. Rev. A **69**, 043407 (2004).

[134] P. Brumer and M. Shapiro, *Laser Control of Molecular Processes*, Annu. Rev. Phys. Chem., **43**, 257, (1992).

[135] P. Marte, P. Zoller, and J.L. Hall, *Coherent atomic mirrors and beam splitters by adiabatic passage in multilevel systems*, Phys. Rev. A, **44**, R4118, (1991).

[136] M. Weitz, T. Heupel, and T.W. Hänsch, *Multiple Beam Atomic Interferometer*, Phys. Rev. Lett. **77**, 2356 (1996).

[137] T. Esslinger, F. Sander, M. Weidemüller, A. Hemmerich, and T.W. Hänsch, *Subrecoil Laser Cooling with Adiabatic Transfer*, Phys. Rev. Lett. **76**, 2432 (1996).

[138] A.S. Parkins, P. Marte, P. Zoller, O. Carnal, and H.J. Kimble, *Quantum-state mapping between multilevel atoms and cavity light fields*, Phys. Rev. A **51**, 1578 (1995).

[139] J. Javanainen and M. Mackie, *Probability of photoassociation from a quasicontinuum approach*, Phys. Rev. A **58**, R789 (1998).

[140] D. Bouwmeester, A.K. Ekert, and A. Zeilinger. *The Physics of Quantum Information: Quantum Cryptography, Quantum Teleportation, Quantum Computation*. Springer, Berlin, 2000.

[141] N. Sangouard, S. Guérin, M. Amniat-Talab, and H.R. Jauslin, *Control of localization and suppression of tunneling by adiabatic passage*, Phys. Rev. Lett. **93**, 223602 (2004).

[142] M. Holthaus, *Pulse-shape-controlled tunneling in a laser field*, Phys. Rev. Lett. **69**, 1596 (1992).

[143] M. Grifoni, P. Hänggi, *Driven quantum tunneling*, Phys. Rep. **304**, 229 (1998).

[144] M. A. Daleh, A. M. Peirce, and H. Rabitz, *Optimal control of quantum-mechanical systems: Existence, numerical approximation, and applications*, Phys. Rev. A **37**, 4950 (1988).

[145] A. Bartana, R. Kosloff, and D. J. Tannor, *Laser cooling of molecules by dynamically trapped states*, Chem. Phys. **267**, 195 (2001).

[146] I.R. Sola, V.S. Malinovsky, and D.J. Tannor, *Optimal pulse sequences for population transfer in multilevel systems*, Phys. Rev. A **60**, 3081 (1999).

[147] A. Isidori, *Nonlinear Control Systems* (Springer Verlag, New York, 1995).

[148] U. Boscain, G. Charlot, J.-P. Gauthier, S. Guérin, and H. R. Jauslin, *Optimal Control in Laser Induced Population Transfer for two- and three-level quantum System*, J. Math. Phys. **43**, 2107 (2002).

[149] R. Unanyan, M. Fleischhauer, B.W. Shore, and K. Bergmann, *Robust creation and phase-sensitive probing of superposition states via stimulated Raman adiabatic passage (STIRAP) with degenerate dark states*, Opt. Commun. **155**, 144 (1998); H. Theuer, R.G. Unanyan, C. Habschied, K. Klein, and K. Bergmann, *Novel laser controlled variable matter wave beamsplitter*, Opt. Express **4**, 77 (1999).

[150] R.G. Unanyan, B.W. Shore, and K. Bergmann, *Laser-driven population transfer in four-level atoms: Consequences of non-Abelian geometrical adiabatic phase factors*, Phys. Rev. A **59**, 2910 (1999).

[151] Z. Kis and F. Renzoni, *Qubit rotation by stimulated Raman adiabatic passage*, Phys. Rev. A **65**, 032318 (2002).

[152] V.A. Sautenkov, C.Y. Ye, Y.V. Rostovtsev, G.R. Welch, and M.O. Scully, *Enhancement of field generation via maximal atomic coherence prepared by fast adiabatic passage in Rb vapor*, Phys. Rev. A **70**, 033406 (2004).

[153] R. G. Unanyan, S. Guérin, B. W. Shore, and K. Bergmann, *Efficient population transfer by delayed pulses despite coupling ambiguity*, Eur. Phys. J. D **8**, 443 (2000).

[154] L.P. Yatsenko, B. W. Shore, N.V. Vitanov, and K. Bergmann, *Retroreflection-induced bichromatic adiabatic passage*, Phys. Rev. A **68**, 043405 (2003).

[155] A.P. Conde, L.P. Yatsenko, J. Klein, M. Oberst, and T. Halfmann, *Experimental demonstration of population inversion driven by retroreflection-induced bichromatic adiabatic passage*, Phys. Rev. A **72**, 053808 (2005).

[156] R. G. Unanyan, S. Guérin, and H. R. Jauslin, *Coherent population trapping under bichromatic fields*, Phys. Rev. A **62**, 043407 (2000).

[157] V. I. Romanenko, L. P. Yatsenko, *Scattering of atoms in a bichromatic field of oppositely propagating light pulses* , Sov. Phys. JETP **90**, 407 (2000).

[158] S. Guérin, H. R. Jauslin and R. Unanyan, *Multiphoton processes in lambda three-level systems* in *Multiphoton Processes 1999* (L. F. DiMauro, R. F . Freeman and K. C. Kulander Eds), AIP Conf. Proc. **525**, 571 (2000).

[159] H. Stapelfeldt and T. Seideman, *Colloquium: Aligning molecules with strong laser pulses*, Rev. Mod. Phys. **75**, 543 (2003).

[160] J. Ortigoso, M. Rodriguez, M. Gupta, and B. Friedrich, *Time evolution of pendular states created by the interaction of molecular polarizability with a pulsed nonresonant laser field*, J. Chem. Phys. **110**, 3870 (1999).

[161] J. J. Larsen, H. Sakai, C. P. Safvan, I. Wendt-Larsen and H. Stapelfeldt, *Aligning molecules with intense nonresonant laser fields* J. Chem. Phys. **111**, 7774 (1999).

[162] T. Seideman, *Revival Structure of Aligned Rotational Wave Packets*, Phys. Rev. Lett. **83**, 4971 (1999).

[163] T. Seideman, *On the dynamics of rotationally broad, spatially aligned wave packets*, J. Chem. Phys. **115**, 5965 (2001).

[164] F. Rosca-Pruna and M. J. J. Vrakking, *Experimental Observation of Revival Structures in Picosecond Laser-Induced Alignment of I_2*, Phys. Rev. Lett. **87**, 153902 (2001); *Revival structures in picosecond laser-induced alignment of I_2 molecules. I. Experimental results*, J. Chem. Phys. **116**, 6567 (2002); *II. Numerical modeling*, J. Chem. Phys. **116**, 6579 (2002).

[165] V. Renard, M. Renard, S. Guérin, Y.T. Pashayan, B. Lavorel, O. Faucher, and H.R. Jauslin, *Postpulse Molecular Alignment Measured by a Weak Field Polarization Technique*, Phys. Rev. Lett. **90**, 153601 (2003).

[166] V. Renard, M. Renard, A. Rouzée, S. Guérin, H.R. Jauslin, B. Lavorel, and O. Faucher, *Nonintrusive monitoring and quantitative analysis of strong laser-field-induced impulsive alignment*, Phys. Rev. A **70**, 033420 (2004).

[167] H. J. Loesch, *Orientation and Alignment in Reactive Beam Collisions: Recent Progress*, Annu. Rev. Phys. Chem. **46**, 555 (1995).

[168] T. D. Hain, R. M. Moision, and T. J. Curtis, *Hexapole state-selection and orientation of asymmetric top molecules: CH_2F_2*, J. Chem. Phys. **111**, 6797 (1999).

[169] B. Friedrich and D. Herschbach, *Enhanced orientation of polar molecules by combined electrostatic and nonresonant induced dipole forces*, J. Chem. Phys. **111**, 6157 (1999); *Manipulating Molecules via Combined Static and Laser Fields*, J. Phys. Chem. A **103**, 10280 (1999); L. Cai, J. Marango, and B. Friedrich, *Time-Dependent Alignment and Orientation of Molecules in Combined Electrostatic and Pulsed Nonresonant Laser Fields*, Phys. Rev. Lett. **86**, 775 (2001).

[170] R. Baumfalk, N.H. Nahler, and U. Buck, *Photodissociation of oriented HXeI molecules in the gas phase*, J. Chem. Phys. **114**, 4755 (2001); H. Sakai, S. Minemoto, H. Nanjo, H. Tanji, and T. Suzuki, *Controlling the Orientation of Polar Molecules with Combined Electrostatic and Pulsed, Nonresonant Laser Fields*, Phys. Rev. Lett. **90**, 083001 (2003); S. Minemoto, H. Nanjo, H. Tanji, T. Suzuki, and H. Sakai, *Observation of molecular orientation by the combination of electrostatic and nonresonant, pulsed laser fields*, J. Chem. Phys. **118**, 4052 (2003).

[171] C. M. Dion, A. Keller, and O. Atabek, *Orienting molecules using half-cycle pulses*, Eur. Phys. J. D **14**, 249 (2001).

[172] M. Maccholm and N. E. Henriksen, *Field-Free Orientation of Molecules*, Phys. Rev. Lett. **87**, 193001 (2001).

[173] R. R. Jones, D. You, and P. H. Bucksbaum, *Ionization of Rydberg atoms by subpicosecond half-cycle electromagnetic pulses*, Phys. Rev. Lett. **70**, 1236 (1993).

[174] N. E. Tielking and R. R. Jones, *Coherent population transfer among Rydberg states by subpicosecond, half-cycle pulses*, Phys. Rev. A **52**, 1371 (1995).

[175] R. B. Vrijen, G. M. Lankhuijzen, and L. D. Noordam, *Delayed Electron Emission in the Ionization of Rydberg Atoms with Half-Cycle THz Pulses*, Phys. Rev. Lett. **79**, 617 (1997).

[176] S. Guérin, L.P. Yatsenko, H.R. Jauslin, O. Faucher and B. Lavorel, *Orientation of Polar Molecules by Laser Induced Adiabatic Passage*, Phys. Rev. Lett. **88**, 233601 (2002).

[177] M. J. J. Vrakking and S. Stolte, *Coherent control of molecular orientation*, Chem. Phys. Lett. **271**, 209 (1997).

[178] C.M. Dion, A.D. Bandrauk, O. Atabek, A. Keller, H. Umeda, Y. Fujimura, *Two-frequency IR laser orientation of polar molecules. Numerical simulations for HCN*, Chem. Phys. Lett. **302**, 215 (1999).

[179] D. Sugny, A. Keller, O. Atabek, D. Daems, C.M. Dion, S. Guérin and H.R. Jauslin, *Reaching optimally oriented molecular states by laser kicks*, Phys. Rev. A **69**, 033402 (2004).

[180] D. Sugny, A. Keller, O. Atabek, D. Daems, C.M. Dion, S. Guérin and H.R. Jauslin, *Laser control for the optimal evolution of pure quantum states*, Phys. Rev. A **71**, 063402 (2005).

[181] M. Leibscher, I.S. Averbukh, and H. Rabitz, *Molecular Alignment by Trains of Short Laser Pulses*, Phys. Rev. Lett. **90**, 213001 (2003); M. Leibscher, I.S. Averbukh, and H. Rabitz, *Enhanced molecular alignment by short laser pulses*, Phys. Rev. A **69**, 013402 (2004).

[182] J.G. Underwood, M. Spanner, M.Yu. Ivanov, J. Mottershead, B.J. Sussman, and A. Stolow, *Switched Wave Packets: A Route to Nonperturbative Quantum Control*, Phys. Rev. Lett. **90**, 223001 (2003).

[183] C.M. Dion, A. Keller, and O. Atabek, *Optimally controlled field-free orientation of the kicked molecule*, Phys. Rev. A, **72**, 023402 (2005).

[184] D. Daems, S. Guérin, D. Sugny and H.R. Jauslin, *Efficient and Long-Lived Field-Free Orientation of Molecules by a Single Hybrid Short Pulse*, Phys. Rev. Lett. **94**, 153003 (2005).

[185] G. Granucci, P. Van Leuven and M. Persico, *Alignment of molecules in pulsed resonant laser fields*, J. Chem. Phys. **120**, 7438 (2004).

[186] D. Sugny, A. Keller, O. Atabek, D. Daems, C.M. Dion, S. Guérin and H.R. Jauslin, *Control of mixed-state quantum systems by a train of short pulses*, Phys. Rev. A **72**, 032704 (2005).

[187] N.E. Henriksen, *Molecular alignment and orientation in short pulse laser fields*, Chem. Phys. Lett. **312**, 196 (1999).

[188] T. Seideman, *Rotational excitation and molecular alignment in intense laser fields*, J. Chem. Phys. **103**, 7887 (1995).

[189] V. Renard, E. Hertz, S. Guérin, H.R. Jauslin, B. Lavorel, and O. Faucher, *Control of field-free molecular alignment by phase-shaped laser pulses*, Phys. Rev. A **72**, 025401 (2005).

[190] D. Normand, L. A. Lompré, and C. Cornaggia, *Laser-induced molecular alignment probed by a double-pulse experiment*, J. Phys. B **25**, L497 (1992); J. H. Sanderson, R. V. Thomas, W. A. Bryan, W. R. Newell, A .J. Langley and P. F. Taday, *Alignment and bending of CO_2 by intense femtosecond laser pulses*, J. Phys. B **31**, L599 (1998); G. R. Kumar, P. Gross, C. P. Safvan, F. A. Rajgara, and D. Mathur, *Pendular motion of linear CS_2 in intense laser fields*, J. Phys. B **29**, L95 (1996); L. J. Frasinski, J. Plumridge, J. H. Posthumus, K. Codling, P. F. Taday, E. J. Divall, and A. J. Langley, *Counterintuitive Alignment of H_2^+*

in Intense Femtosecond Laser Fields, Phys. Rev. Lett. **86**, 2541 (2001); J. H. Posthumus, J. Plumridge, M. K. Thomas, K. Codling, L. J. Frasinski, A. J. Langley and P. F. Taday, *Dynamic and geometric laser-induced alignment of molecules in intense laser fields*, J. Phys. B **31**, L553 (1998); Ch. Ellert and P. B. Corkum, *Disentangling molecular alignment and enhanced ionization in intense laser fields*, Phys. Rev. A **59**, R3170 (1999).

[191] B. Lavorel, O. Faucher, M. Morgen, and R. Chaux, *Analysis of femtosecond Raman-induced polarization spectroscopy (RIPS) in N_2 and CO_2 by fitting and scaling laws*, J. Raman Spectroscopy. **31**, 77 (2000).

[192] V. Renard, O. Faucher, and B. Lavorel, *Measurement of laser-induced alignment of molecules by cross defocusing*, Opt. Lett. **30**, 70 (2005).

[193] G. Maroulis, *Electric Polarizability and Hyperpolarizability of Carbon Monoxide*, J. Phys. Chem. **100**, 13466 (1996).

[194] S. Thomas, S. Guérin, and H.R. Jauslin, *State-selective chirped adiabatic passage on dynamically laser-aligned molecules*, Phys. Rev. A **71**, 013402 (2005).

[195] M.A. Nielsen and I.L. Chuang, *Quantum Computation and Quantum Information* (Cambridge University Press, Cambridge, 2000).

[196] A.M. Steane and D.M. Lucas, *Quantum computing with trapped ions, atoms and light*, Fortschr. Phys. **48**, 9 (2000). Preprint quant-ph/0004053.

[197] D.P. DiVincenzo, *The Physical Implementation of Quantum Computation*, Fortschr. Phys. **48**, 771 (2000). Preprint quant-ph/0002077.

[198] A. Galindo and M.A. Martin-Delgado, *Information and computation: Classical and quantum aspects*, Rev. Mod. Phys. **74**, 347 (2002).

[199] J. Stolze and D. Suter, *Quantum Computing: A short Course from Theory to Experiment* (Wiley-VCH, Weinheim, 2004).

[200] D. Deutsch and R. Jozsa, *Rapid solution of problems by quantum computation*, Proc. Roy. Soc. London A **439**, 553 (1992).

[201] P. Shor, *Polynomial-time algorithms for prime factorization and discrete logarithms on a quantum computer*. In Proceedings, 35th Annual Symposium on Foundations of Computer Science, pp 124-134, edited by S. Goldwasser (1994). IEEE Press.

[202] Lov K. Grover, *A fast quantum mechanical algorithm for database search*. In Proceedings, 28th Annual ACM Symposium on the Theory of Computation, pp 212-219, New York, 1996. ACM Press.

[203] J.I. Cirac and P. Zoller, *Quantum Computations with Cold Trapped Ions*, Phys. Rev. Lett. **74**, 4091 (1995).

[204] S. Gulde, M. Riebe, G.P.T. Lancaster, C. Becher, J. Eschner, H. Häffner, F. Schmidt-Kaler, I.L. Chuang, and R. Blatt, *Implementation of the Deutsch-Jozsa algorithm on an ion-trap quantum computer*, Nature **421**, 48 (2003).

[205] K. Mølmer and A. Sørensen, *Multiparticle Entanglement of Hot Trapped Ions*, Phys. Rev. Lett. **82**, 1835 (1999); A. Sørensen and K. Mølmer, *Quantum Computation with Ions in Thermal Motion*, Phys. Rev. Lett. **82**, 1971 (1999).

[206] H. Goto and K. Ichimura, *Multiqubit controlled unitary gate by adiabatic passage with an optical cavity*, Phys. Rev. A **70**, 012305 (2004).

[207] T. Pellizzari, S. A. Gardiner, J. I. Cirac and P. Zoller, *Decoherence, Continuous Observation, and Quantum Computing: A Cavity QED Model*, Phys. Rev. Lett. **75**, 3788, (1995).

[208] S. Nussmann, M. Hijlkema, B. Weber, F. Rohde, G. Rempe, and A. Kuhn, *Submicron Positioning of Single Atoms in a Microcavity*, Phys. Rev. Lett. **95**, 173602 (2005).

[209] K. Ichimura, *A simple frequency-domain quantum computer with ions in a crystal coupled to a cavity mode*, Opt. Commun. **196**, 119 (2001); *Erratum to "A simple frequency-domain quantum computer with ions in a crystal coupled to a cavity mode"*, Opt. Commun. **199**, 453 (2001).

[210] M.D. Lukin, S.F. Yelin, M. Fleischhauer, *Entanglement of Atomic Ensembles by Trapping Correlated Photon States*, Phys. Rev. Lett. **84**, 4232 (2000).

[211] L. Vandersypen, M. Steffen, G. Breyta, C.S. Yannoni, M.H. Sherwood, and I.L. Chuang, *Experimental realization of Shor's quantum factoring algorithm using nuclear magnetic resonance*, Nature **414**, 883 (2001).

[212] Y. Makhlin, G. Schön, and A. Shnirman, *Quantum-state engineering with Josephson-junction devices*, Rev. Mod. Phys. **73**, 357 (2001).

[213] D. Loss and D.P. DiVincenzo, *Quantum computation with quantum dots*, Phys. Rev. A **57**, 120 (1998).

[214] M. Bayer, P. Hawrylak, K. Hinzer, S. Fafard, M. Korkusinski, Z.R. Wasilewski, O. Stern, and A. Forchel, *Coupling and entangling of quantum states in quantum dot molecules*, Science **291**, 451 (2001).

[215] I. Cirac, P. Zoller, H.J. Kimble, and H. Mabuchi, *Quantum state transfer and entanglement distribution among distant nodes of a quantum network*, Phys. Rev. Lett. **78**, 3221 (1997).

[216] N. Sangouard, *Decoherence-free manipulation of photonic memories for quantum computation*, Phys. Rev. A **73**, 022304 (2006).

[217] N. Gisin, G. Ribordy, W. Tittel, and H Zbinden, *Quantum cryptography*, Rev. Mod. Phys. **74**, 145 (2002).

[218] D.A. Lidar, I.L. Chuang, and K.B. Whaley, *Decoherence-Free Subspaces for Quantum Computation*, Phys. Rev. Lett. **81**, 2594 (1998).

[219] C. Brunel, B. Lounis, P. Tamarat, and M. Orrit, *Triggered Source of Single Photons based on Controlled Single Molecule Fluorescence*, Phys. Rev. Lett. **83**, 2722 (1999).

[220] B. Lounis and W.E. Moerner, *Single photons on demand from a single molecule at room temperature*, Nature **407**, 491 (2000).

[221] A. Beveratos, S. Kuhn, R. Brouri, J. P. Poizat, and P. Grangier, *Room temperature stable single-photon source* , Eur. Phys. J. D **18**, 191 (2002).

[222] J. Kim, O. Benson, H. Kan, and Y. Yamamoto, *A single-photon turnstile device*, Nature **397**, 500 (1999).

[223] C. Santori, M. Pelton, G.S. Solomon, Y. Dale, and Y. Yamamoto, *Triggered Single Photons from a Quantum Dot*, Phys. Rev. Lett. **86**, 1502 (2001).

[224] P. Michler, A. Kiraz, C. Becher, W.V. Schoenfeld, P.M. Petroff, L. Zhang, E. Hu, and A. Imamoglu, *A quantum dot single-photon turnstile device*, Science **290**, 2282 (2000).

[225] X. Maître, E. Hagley, G. Nogues, C. Wunderlich, P. Goy, M. Brune, J.M. Raimond, and S. Haroche, *Quantum Memory with a Single Photon in a Cavity*, Phys. Rev. Lett. **79**, 769 (1997).

[226] B.T.H. Varcoe, S. Brattke, M. Weidinger, and H. Walther, *Preparing pure photon number states of the radiation field*, Nature **403**, 743 (2000).

[227] M. Hennrich, T. Legero, A. Kuhn, and G. Rempe, *Vacuum-Stimulated Raman Scattering Based on Adiabatic Passage in a High-Finesse Optical Cavity*, Phys. Rev. Lett. **85**, 4872 (2000).

[228] A.S. Parkins, P. Marte, P. Zoller, and H.J. Kimble, *Synthesis of arbitrary quantum states via adiabatic transfer of Zeeman coherence*, Phys. Rev. Lett. **71**, 3095 (1993).

[229] S.Q. Gong, R. Unanyan, and K. Bergmann, *Preparation of Fock states and quantum entanglement via stimulated Raman adiabatic passage using a four-level atom*, Eur. Phys. J. D **19**, 257 (2002).

[230] P. Domokos, M. Brune, J.M. Raimond, and S. Haroche, *Photon-number-state generation with a single two-level atom in a cavity: a proposal*, Eur. Phys. J. D **1**, 1 (1998).

[231] P. Bertet, S. Osnaghi, P. Milman, A. Auffeves, P. Maioli, M. Brune, J.M. Raimond, and S. Haroche, *Generating and Probing a Two-Photon Fock State with a Single Atom in a Cavity*, Phys. Rev. Lett. **88**, 143601 (2002).

[232] M. França Santos, E. Solano, and R.L. de Matos Filho, *Conditional Large Fock State Preparation and Field State Reconstruction in Cavity QED*, Phys. Rev. Lett. **87**, 093601 (2001).

[233] M. Amniat-Talab, S. Lagrange, S. Guérin, and H. R. Jauslin, *Generation of multiphoton Fock states by bichromatic adiabatic passage: Topological analysis*, Phys. Rev. A **70**, 013807 (2004).

[234] A. Einstein, B. Podolski, and N. Rosen, *Can Quantum-Mechanical Description of Physical Reality Be Considered Complete?*, Phys. Rev. **47**, 777 (1935).

[235] J.S. Bell, *On the Einstein-Podolsky-Rosen paradox*, Physics **1**, 195 (1964).

[236] M. Riebe, H. Haffner, C.F. Roos, W. Hansel, J. Benhelm, G.P.T. Lancaster, T.W. Korber, C. Becher, F. Schmidt-Kaler, D.F.V. James, R. Blatt , *Deterministic quantum teleportation with atoms*, Nature **429**, 734 (2004).

[237] M.D. Barrett, J. Chiaverini, T. Schaetz, J. Britton, W.M. Itano, J.D. Jost, E. Knill, C. Langer, D. Leibfried, R. Ozeri, D.J. Wineland, *Deterministic quantum teleportation of atomic qubits*, Nature **429**, 737 (2004).

[238] C.H. Bennett, G. Brassard, C. Crépeau, R. Jozsa, A. Peres, and W.K. Wootters, *Teleporting an unknown quantum state via dual classical and Einstein-Podolsky-Rosen channels*, Phys. Rev. Lett. **70**, 1895 (1993).

[239] A. Ekert and R. Jozsa, *Quantum computation and Shor's factoring algorithm*, Rev. Mod. Phys. **68**, 733 (1997).

[240] W. Tittel, J. Brendel, H. Zbinden, and N. Gisin, *Quantum Cryptography Using Entangled Photons in Energy-Time Bell States*, Phys. Rev. Lett. **84**, 4737 (2000).

[241] E. Hagley, X. Maître, G. Nogues, C. Wunderlich, M. Brune, J.M. Raimond, and S. Haroche, *Generation of Einstein-Podolsky-Rosen Pairs of Atoms*, Phys. Rev. Lett. **79**, 1 (1997).

[242] J.I. Cirac and P. Zoller, *Preparation of macroscopic superpositions in many-atom systems*, Phys. Rev. A **50**, R2799 (1994).

[243] B. Sun, M.S. Chapman, and L. You, *Atom-photon entanglement generation and distribution*, Phys. Rev. A **69**, 042316 (2004).

[244] W. Lange and H.J. Kimble, *Dynamic generation of maximally entangled photon multiplets by adiabatic passage* , Phys. Rev. A **61**, 063817 (2000).

[245] S. Guérin, R. G. Unanyan, L. P. Yatsenko, H. R. Jauslin, *Adiabatic creation of entangled states by a bichromatic field designed from the topology of the dressed eigenenergies*, Phys. Rev. A **66**, 032311 (2002).

[246] R. G. Unanyan, N. V. Vitanov, and K. Bergmann, Phys. Rev. Lett. **87**, 137902 (2001).

[247] M. Amniat-Talab, S. Guérin, N. Sangouard and H. R. Jauslin, *Atom-photon, atom-atom, and photon-photon entanglement preparation by fractional adiabatic passage*, Phys. Rev. A **71**, 023805 (2005).

[248] M. Amniat-Talab, S. Guérin, and H. R. Jauslin, *Decoherence-free creation of atom-atom entanglement in a cavity via fractional adiabatic passage*, Phys. Rev. A **72**, 012339 (2005).

[249] A. Barenco, C.H. Bennett, R. Cleve, D.P. DiVincenzo, N. Margolus, P. Shor, T. Sleator, J.A. Smolin, and H. Weinfurter, *Elementary gates for quantum computation*, Phys. Rev. A **52**, 3457 (1995).

[250] L.-M. Duan, J.I. Cirac, P. Zoller, *Geometric manipulation of trapped ions for quantum computation*, Science **292**, 1695 (2001).

[251] R.G. Unanyan and M. Fleischhauer, *Geometric phase gate without dynamical phases*, Phys. Rev. A **69**, 050302 (2004).

[252] X. Lacour, S. Guérin, N.V. Vitanov, L.P. Yatsenko and H.R. Jauslin, *Implementation of single-qubit quantum gates by adiabatic passage and static laser phases*, Opt. Commun. **264**, 362 (2006).

[253] N. Sangouard, X. Lacour, S. Guérin, and H. R. Jauslin, *Fast quantum logical gate by adiabatic passage*, Phys. Rev. A **72**, 062309 (2005).

[254] N. Sangouard, X. Lacour, S. Guérin, and H. R. Jauslin, *CNOT gate by adiabatic passage with an optical cavity*, Eur. Phys. J. D **37**, 451 (2006).

[255] X. Lacour, N. Sangouard, S. Guérin, and H. R. Jauslin, *Arbitrary state controlled-unitary gate by adiabatic passage*, Phys. Rev. A **73**, 042321 (2006).

[256] H.-P. Breuer and F. Petruccione, *The Theory of Open Quantum Systems* (Oxford University Press, Oxford, 2002).

[257] M.S. Sarandy and D.A. Lidar, *Adiabatic quantum computation in open quantum systems*, Phys. Rev. Lett. **95**, 250503 (2005); *Adiabatic approximation in open quantum systems*, Phys. Rev. A **71**, 012331 (2005).

[258] N. Ben-Tal, N. Moiseyev, R. Kosloff, *Harmonic generation in ionizing systems by the complex scaled adiabatic-switch method*, Phys. Rev. A. **48**, 2437 (1993).

[259] J.J. Larsen, K. Hald, N. Bjerre, H. Stapelfeldt and T. Seideman, *Three Dimensional Alignment of Molecules Using Elliptically Polarized Laser Fields*, Phys. Rev. Lett. **85**, 2470 (2000).

[260] J.G. Underwood, B.J. Sussman, and A. Stolow, *Field-Free Three Dimensional Molecular Axis Alignment*, Phys. Rev. Lett. **94**, 143002 (2005).

[261] S. Ramakrishna and T. Seideman, *Intense Laser Alignment in Dissipative Media as a Route to Solvent Dynamics*, Phys. Rev. Lett. **95**, 113001 (2005).

[262] T. Kiljunen, B. Schmidt, and N. Schwentner, *Intense-Field Alignment of Molecules Confined in Octahedral Fields*, Phys. Rev. Lett. **94**, 123003 (2005); *Aligning and orienting molecules trapped in octahedral crystal fields*, Phys. Rev. A **72**, 053415 (2005); *Time-dependent alignment of molecules trapped in octahedral crystal fields* , J. Chem. Phys. **124**, 164502 (2006).

Part V

Curriculum Vitæ